

TOPICS IN
HETEROCYCLIC CHEMISTRY

24

Series Editor Bert U. W. Maes
Volume Editors Philip A. Gale • Wim Dehaen

Anion Recognition in Supramolecular Chemistry

 Springer

24

Topics in Heterocyclic Chemistry

Series Editor: Bert U. W. Maes

Editorial Board:

**D. Enders • S.V. Ley • G. Mehta • K.C. Nicolaou •
R. Noyori • L.E. Overman • A. Padwa • S. Polanc**

Topics in Heterocyclic Chemistry

Series Editor: Bert U.W. Maes

Recently Published and Forthcoming Volumes

Anion Recognition in Supramolecular Chemistry

Volume Editors: P.A. Gale, W. Dehaen
Volume 24, 2010

Synthesis of Heterocycles via Multicomponent Reactions I

Volume Editors: R.V.A. Orru, E. Ruijter
Volume 23, 2010

Heterocyclic Scaffolds I: β -Lactams

Volume Editor: B. Banik
Volume 22, 2010

Phosphorous Heterocycles II

Volume Editor: R.K. Bansal
Volume 21, 2009

Phosphorous Heterocycles I

Volume Editor: R.K. Bansal
Volume 20, 2009

Aromaticity in Heterocyclic Compounds

Volume Editors: T. Krygowski, M. Cyrański
Volume 19, 2009

Heterocyclic Supramolecules I

Volume Editor: K. Matsumoto
Volume 17, 2008

Bioactive Heterocycles VI

Flavonoids and Anthocyanins in Plants,
and Latest Bioactive Heterocycles I

Volume Editor: N. Motohashi
Volume 15, 2008

Heterocyclic Polymethine Dyes

Synthesis, Properties and Applications

Volume Editor: L. Strekowski
Volume 14, 2008

Synthesis of Heterocycles via Cycloadditions II

Volume Editor: A. Hassner
Volume 13, 2008

Synthesis of Heterocycles via Cycloadditions I

Volume Editor: A. Hassner
Volume 12, 2008

Bioactive Heterocycles V

Volume Editor: M.T.H. Khan
Volume 11, 2007

Bioactive Heterocycles IV

Volume Editor: M.T.H. Khan
Volume 10, 2007

Bioactive Heterocycles III

Volume Editor: M.T.H. Khan
Volume 9, 2007

Bioactive Heterocycles II

Volume Editor: S. Eguchi
Volume 8, 2007

Heterocycles from Carbohydrate Precursors

Volume Editor: E.S.H. ElAshry
Volume 7, 2007

Bioactive Heterocycles I

Volume Editor: S. Eguchi
Volume 6, 2006

Marine Natural Products

Volume Editor: H. Kiyota
Volume 5, 2006

QSAR and Molecular Modeling Studies in Heterocyclic Drugs II

Volume Editor: S.P. Gupta
Volume 4, 2006

QSAR and Molecular Modeling Studies in Heterocyclic Drugs I

Volume Editor: S.P. Gupta
Volume 3, 2006

Anion Recognition in Supramolecular Chemistry

Volume Editors:
P.A. Gale, W. Dehaen

With contributions by

E. Alcalde · P. Anzenbacher · P.D. Beer · C.W. Bielawski ·
J.T. Davis · W. Dehaen · I. Dinarès · A.H. Flood · P.A. Gale ·
Y. Hua · K.-S. Jeong · H. Juwarker · N.L. Kilah · C.-H. Lee ·
H. Maeda · K.P. McDonald · N. Mesquida · B.M. Rambo ·
J.L. Sessler · E.S. Silver · J. Suk

 Springer

The series *Topics in Heterocyclic Chemistry* presents critical reviews on "Heterocyclic Compounds" within topic-related volumes dealing with all aspects such as synthesis, reaction mechanisms, structure complexity, properties, reactivity, stability, fundamental and theoretical studies, biology, biomedical studies, pharmacological aspects, applications in material sciences, etc. Metabolism will also be included which will provide information useful in designing pharmacologically active agents. Pathways involving destruction of heterocyclic rings will also be dealt with so that synthesis of specifically functionalized non-heterocyclic molecules can be designed.

The overall scope is to cover topics dealing with most of the areas of current trends in heterocyclic chemistry which will suit to a larger heterocyclic community.

As a rule, contributions are specially commissioned. The editors and publishers will, however, always be pleased to receive suggestions and supplementary information. Papers are accepted for *Topics in Heterocyclic Chemistry* in English.

In references, *Topics in Heterocyclic Chemistry* is abbreviated *Top Heterocycl Chem* and is cited as a journal.

Springer www home page: springer.com
Visit the THC content at springerlink.com

Topics in Heterocyclic Chemistry ISSN 1861-9282
ISBN 978-3-642-15443-0 e-ISBN 978-3-642-15444-7
DOI 10.1007/978-3-642-15444-7
Springer Heidelberg Dordrecht London New York

Library of Congress Control Number: 2010933516

© Springer-Verlag Berlin Heidelberg 2010

This work is subject to copyright. All rights are reserved, whether the whole or part of the material is concerned, specifically the rights of translation, reprinting, reuse of illustrations, recitation, broadcasting, reproduction on microfilm or in any other way, and storage in data banks. Duplication of this publication or parts thereof is permitted only under the provisions of the German Copyright Law of September 9, 1965, in its current version, and permission for use must always be obtained from Springer. Violations are liable to prosecution under the German Copyright Law.

The use of general descriptive names, registered names, trademarks, etc. in this publication does not imply, even in the absence of a specific statement, that such names are exempt from the relevant protective laws and regulations and therefore free for general use.

Cover design: WMXDesign GmbH, Heidelberg, Germany

Printed on acid-free paper

Springer is part of Springer Science+Business Media (www.springer.com)

Series Editor

Prof. Dr. Bert U.W. Maes
Organic Synthesis
Department of Chemistry
University of Antwerp
Groenenborgerlaan 171
B-2020 Antwerp
Belgium

Volume Editors

Prof. Philip A. Gale
School of Chemistry
University of Southampton
Southampton
SO17 1BJ, UK
philip.gale@soton.ac.uk

Prof. Wim Dehaen
Department of Chemistry
University of Leuven
Celestijnenlaan 200 F
3001 Leuven
Belgium
wim.dehaen@chem.kuleuven.be

Editorial Board

Prof. D. Enders
RWTH Aachen
Institut für Organische Chemie
52074, Aachen, Germany
enders@rwth-aachen.de

Prof. Steven V. Ley FRS
BP 1702 Professor
and Head of Organic Chemistry
University of Cambridge
Department of Chemistry
Lensfield Road
Cambridge, CB2 1EW, UK
svl1000@cam.ac.uk

Prof. G. Mehta FRS
Director
Department of Organic Chemistry
Indian Institute of Science
Bangalore 560 012, India
gm@orgchem.iisc.ernet.in

Prof. K.C. Nicolaou
Chairman
Department of Chemistry
The Scripps Research Institute
10550 N. Torrey Pines Rd.
La Jolla, CA 92037, USA
kcn@scripps.edu
and
Professor of Chemistry
Department of Chemistry and Biochemistry
University of CA
San Diego, 9500 Gilman Drive
La Jolla, CA 92093, USA

Prof. Ryoji Noyori NL

President

RIKEN (The Institute of Physical
and Chemical Research)

2-1 Hirosawa, Wako

Saitama 351-0198, Japan

and

University Professor

Department of Chemistry

Nagoya University

Chikusa, Nagoya 464-8602, Japan

noyori@chem3.chem.nagoya-u.ac.jp

Prof. Larry E. Overman

Distinguished Professor

Department of Chemistry

516 Rowland Hall

University of California, Irvine

Irvine, CA 92697-2025

leoverma@uci.edu

Prof. Albert Padwa

William P. Timmie Professor of Chemistry

Department of Chemistry

Emory University

Atlanta, GA 30322, USA

chemap@emory.edu

Prof. Slovenko Polanc

Professor of Organic Chemistry

Faculty of Chemistry and Chemical

Technology

University of Ljubljana

Askerceva 5

SI-1000 Ljubljana

Slovenia

slovenko.polanc@fkkt.uni-lj.si

Topics in Heterocyclic Chemistry

Also Available Electronically

Topics in Heterocyclic Chemistry is included in Springer's eBook package *Chemistry and Materials Science*. If a library does not opt for the whole package the book series may be bought on a subscription basis. Also, all back volumes are available electronically.

For all customers who have a standing order to the print version of *Topics in Heterocyclic Chemistry*, we offer the electronic version via SpringerLink free of charge.

If you do not have access, you can still view the table of contents of each volume and the abstract of each article by going to the SpringerLink homepage, clicking on "Chemistry and Materials Science," under Subject Collection, then "Book Series," under Content Type and finally by selecting *Topics in Heterocyclic Chemistry*.

You will find information about the

- Editorial Board
- Aims and Scope
- Instructions for Authors
- Sample Contribution

at springer.com using the search function by typing in *Topics in Heterocyclic Chemistry*.

Color figures are published in full color in the electronic version on SpringerLink.

Aims and Scope

The series *Topics in Heterocyclic Chemistry* presents critical reviews on "Heterocyclic Compounds" within topic related volumes dealing with all aspects such as synthesis, reaction mechanisms, structure complexity, properties, reactivity, stability, fundamental and theoretical studies, biology, biomedical studies, pharmacological aspects, applications in material sciences etc. Metabolism is also included which provides information useful in designing pharmacologically active agents. Pathways involving destruction of heterocyclic ring are also dealt with so that synthesis of specifically functionalized non-heterocyclic molecules can be designed.

Overall scope is to cover topics dealing with most of the areas of current trends in heterocyclic chemistry which suits a larger heterocyclic community.

The individual volumes of *Topics in Heterocyclic Chemistry* are thematic. Review articles are generally invited by the volume editors.

In references *Topics in Heterocyclic Chemistry* is abbreviated *Top Heterocycl Chem* and is cited as a journal.

Preface

This edition of Topics in Heterocyclic Chemistry concerns the use of heterocycles as components of anion receptors and sensors. Initially, an area restricted to pyrrole alone, a much wider range of heterocycles have now been used as hydrogen bond donors and as other components in synthetic anion receptor systems. The pioneer of this area, Jonathan L. Sessler from the University of Texas at Austin, who first employed expanded porphyrin systems, such as sapphyrin, as anion receptors provides the first chapter with Brett Rambo, Eric Silver and Chris Bielawski on covalent polymers containing discrete heterocyclic anion receptors. Keeping with the topic of pyrrolic macrocycles, Chang-Hee Lee and Phil Gale discuss recent advances in the anion complexation chemistry of calixpyrroles (flexible pyrrole macrocycles in which the pyrrole rings are linked by sp³ hybridised carbon atoms), while Wim Dehaen covers the related area of calixphyrin macrocycles (macrocycles which combine the properties of calixpyrroles and porphyrins). Moving from macrocyclic pyrrole-based anion receptors, Hiromitsu Maeda reviews progress in the design and synthesis of acyclic pyrrole-based anion receptor systems. The prodigiosins are a class of tripyrrolic natural products that have been shown to have a range of useful biological activities which have been linked to their anion complexation and membrane transport properties. The chemistry of this fascinating family of compounds is surveyed by Jeff Davis. We then begin to move away from pyrrole with an account of the recent blossoming of indole-based anion receptors by Hemraj Juwarker, Jae-min Suk and Kyu-Sung Jeong. Finally, in the pyrrole arena Pavel Anzenbacher Jr discusses the role pyrrole-based anion receptors can play in sensing anions. Ermitas Alclade, Immaculada Dinarès and Neus Mesquida discuss how CH hydrogen bonds and electrostatic interactions are key non-covalent interactions in the complexation of anions by imidazolium based anion receptors, while Nathan Kilah and Paul Beer discuss the role of pyridinium and pyridine in hosts for anions. Finally, recent advances in the use of triazoles as components of anion receptors are surveyed by Kevin McDonald, Yuran Hua and Amar Flood. Our aim in editing this book was to illustrate the wide range of structures both simple and complex, acyclic and cyclic, charged and neutral that function as effective anion receptor systems.

Southampton, UK
Leuven, Belgium
July 2010

Phil Gale
Wim Dehaen

Contents

Covalent Polymers Containing Discrete Heterocyclic Anion Receptors ...	1
Brett M. Rambo, Eric S. Silver, Christopher W. Bielawski, and Jonathan L. Sessler	
Calix[n]pyrroles as Anion and Ion-Pair Complexants	39
Philip A. Gale and Chang-Hee Lee	
Calix[n]phyrins: Synthesis and Anion Recognition	75
Wim Dehaen	
Acyclic Oligopyrrolic Anion Receptors	103
Hiromitsu Maeda	
Anion Binding and Transport by Prodigiosin and Its Analogs	145
Jeffery T. Davis	
Indoles and Related Heterocycles	177
Hemraj Juwarker, Jae-min Suk, and Kyu-Sung Jeong	
Pyrrole-Based Anion Sensors, Part I: Colorimetric Sensors	205
Pavel Anzenbacher Jr.	
Pyrrole-Based Anion Sensors, Part II: Fluorescence, Luminescence, and Electrochemical Sensors	237
Pavel Anzenbacher Jr.	
Imidazolium-Based Receptors	267
Ermitas Alcalde, Immaculada Dinarès, and Neus Mesquida	
Pyridine and Pyridinium-Based Anion Receptors	301
Nathan L. Kilah and Paul D. Beer	

1,2,3-Triazoles and the Expanding Utility of Charge Neutral CH•••Anion Interactions	341
Kevin P. McDonald, Yuran Hua, and Amar H. Flood	
Index	367

Covalent Polymers Containing Discrete Heterocyclic Anion Receptors

Brett M. Rambo, Eric S. Silver, Christopher W. Bielawski,
and Jonathan L. Sessler

Abstract This chapter covers recent advances in the development of polymeric materials containing discrete heterocyclic anion receptors, and focuses on advances in anion binding and chemosensor chemistry. The development of polymers specific for anionic species is a relatively new and flourishing area of materials chemistry. The incorporation of heterocyclic receptors capable of complexing anions through noncovalent interactions (e.g., hydrogen bonding and electrostatic interactions) provides a route to not only sensitive but also selective polymeric materials. Furthermore, these systems have been utilized in the development of polymers capable of extracting anionic species from aqueous media. These latter materials may lead to advances in water purification and treatment of diseases resulting from surplus ions.

Keywords Anion complexation · Molecular receptors · Polymers · Sensing

Contents

1	Introduction	2
2	Anion Receptors as Polymer Additives	4
3	Side-Chain Polymers Containing Anion Responsive Heterocycles	14
4	Polymers Containing Neutral, Anion Receptors	20
5	Polymers Containing Anion Receptors Conjugated to Their Main Chains	26
6	Conclusions	34
	References	35

Abbreviations

AIBN	2,2'-Azobisisobutyronitrile
ATP	Adenosine triphosphate
BSA	Bovine serum albumin
CTAB	Cetyltriethylammonium bromide
CV	Cyclic voltammetry
DIQ	Diindolylquinoxaline
DMF	Dimethylformamide
DPQ	Dipyrrolylquinoxaline
DPV	Differential pulse voltammetry
ESIPT	Excited-state intramolecular proton transfer
GMP	Guanosine monophosphate
GPC	Gel permeation chromatography
HEPES	(4-(2-Hydroxyethyl)-1-piperazineethanesulfonic acid
IL	Ionic liquid
IPT	Intermolecular-proton transfer
ISE	Ion-selective electrode
MeCN	Acetonitrile
MeOH	Methanol
nbd	Norbornadiene
NMR	Nuclear magnetic resonance
PCA	Principal component analysis
PDI	Polydispersity index
PET	Photo-induced electron transfer
PLAS	Plasma-like aqueous solution
PMMA	Poly(methyl methacrylate)
PPA	Polyphenylacetylene
PVC	Polyvinyl chloride
SBS	Polystyrene-block-polybutadiene-block-polystyrene
SCE	Standard calomel electrode
TBA	Tetrabutylammonium
TEA	Triethylamine
THF	Tetrahydrofuran

1 Introduction

The field of polymer chemistry has made tremendous progress since Staudinger first pioneered various polymerization methods in the early 1920s [1, 2]. Staudinger proposed structural formulae for natural rubber, polystyrene, and polyoxymethylene, and is also credited with coining the term “macromolecule” which is still

commonly used today. The field of synthetic polymers was advanced further in the 1930s when Carothers developed two widely used synthetic polymers, neoprene, and nylon [3, 4]. The importance of these materials cannot be overstated. For example, nylon and other polyamides are excellent fiber forming materials, and were initially used to make ropes, parachutes, and tents, but applications have since greatly expanded and these and other synthetic polymers can now be seen in almost all aspects of everyday life. This ubiquity has spawned wide-spread efforts to develop new and improved materials. A few areas of advanced focus within this general paradigm include creating synthetic replacements for biological tissues [5, 6] and developing macromolecular materials suitable for use in diagnostic and array technologies [7, 8].

Another major thrust in polymer chemistry has come from the field of “supramolecular chemistry,” a term coined by Lehn to mean chemistry beyond the molecule [9, 10]. As chemists began to exploit the weak noncovalent interactions (which represent the foundation of supramolecular chemistry) to create new molecular receptors and chemosensors, it soon became apparent that the same principles could lead to advances in the field of polymer chemistry [11–14]. A major subset of this latter effort has been devoted to the synthesis of so-called main-chain supramolecular polymers, where reversible/dynamic noncovalent interactions within the polymer backbone are used to assemble monomers into larger polymeric structures [15]. Separate from this, a number of researchers began to realize the potential benefits of incorporating small molecule supramolecular receptors into polymeric structures. The vast majority of these latter systems consist of conjugated polymers containing receptors for positively charged or neutral species. One highly utilized approach involves the incorporation of crown ether species for metal ion recognition and sensing [16]. For example, Swager reported how an appropriately designed, conjugated polymer chemosensor containing crown ethers would undergo recognizable changes as the result of potassium induced aggregation [17].

In spite of the above advances, it was only recently that the number of polymers that incorporate receptors for anionic species began to increase. This tardiness in terms of materials development is somewhat surprising given the role anionic species play in the environment and in biological processes. It is now well recognized that many anionic species, such as fluoride, nitrate, phosphate, and cyanide, constitute major environmental pollutants; there is thus a clear, widely appreciated need for materials capable of recognizing, capturing, and detecting these and other anionic species. Furthermore, excesses in phosphate anion levels in patients suffering from end-stage renal failure is a frequent complication that can lead to a disease state known as hyperphosphatemia [18, 19]. In most cases dialysis in combination with ingestible anion exchange resins is used to control the level of phosphate in the blood. However, neither of these methods is fully satisfactory, in part because the underlying methodologies are not phosphate selective. The authors thus believe that new materials, such as anion-specific dialysis membranes, could be used to control phosphate anion concentrations for patients on dialysis and lead to clinical advances. The incorporation of supramolecular receptors specific to anionic species into polymeric frameworks represents a first step towards achieving

this long-range goal. Related anion binding macromolecules could also see application in the recognition and sensing of anions of environmental concerns and in the areas of separation and purification. Taken in concert, these various potential benefits provide an incentive to prepare anion receptor-modified polymers. The goal of this chapter is to provide a summary of recent work in the area.

To the best of our knowledge, no reviews have appeared that cover the chemistry of macromolecular systems targeting the problem of anion recognition. The focus of this chapter will be on polymeric systems that incorporate heterocycle-based anion receptors into polymeric structures. Heterocyclic receptors as additives to polymers (Fig. 1a) for applications such as polyelectrolyte development, will be covered, as will be polymers that contain anion receptors either as pendant side-chains (Fig. 1b) or incorporated directly into the polymer main-chain (Fig. 1c). As will become apparent from the present review, the majority of the systems that exist today are conjugated polymers that have been applied as so-called chemosensors. However, it is our hope and expectation that a detailed description of these and related systems will inspire the synthesis of new and improved systems for anion detection, sequestration, extraction, and separations, among other conceivable applications.

2 Anion Receptors as Polymer Additives

According to the principle of Occam's Razor, "entities must not be multiplied beyond necessity," which one can interpret to mean that often the simplest

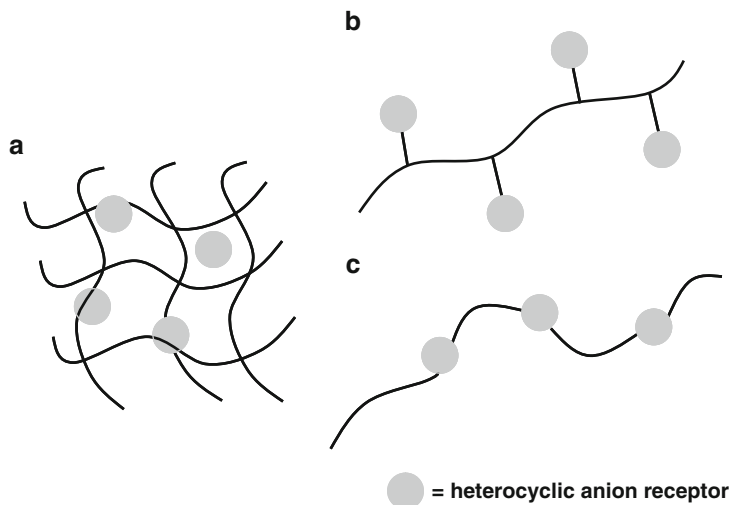


Fig. 1 Schematic representation of heterocyclic anion receptors incorporated into polymeric materials (a) as additives in polymers (b), via attachment as appendages on the side-chains of polymers, and (c) by direct incorporation into the main-chain of the polymer backbone

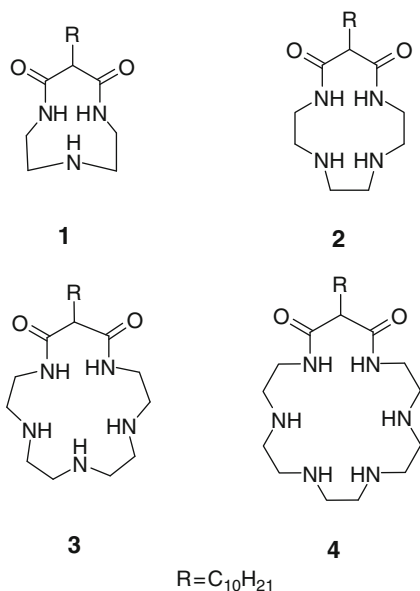
explanation is the correct one. Analogously, in engineering and materials science, one attempts to get the biggest bang for one's buck by using cheap and simple materials to build up complexity and solve pressing problems. Over-complicated syntheses or expensive starting materials can lead to greatly diminished returns and harpoon the chances that the molecule or material will ever see wide-spread application. Such appreciations may well have inspired early researchers working at the interface of anion recognition and polymer research. This is because most initial efforts in the area were focused on integrating heterocyclic anion receptors into polymeric systems by simply blending various anion receptors into the polymers. Such approaches, which are akin to blending chocolate chips into cookie dough, are markedly different from synthetic strategies that involve attaching recognition units to the polymer backbone or creating receptors that are functionalized in such a way that they may act as precursors for polymer synthesis. These approaches are thus treated separately in this chapter, with the focus of this particular section being on polymeric materials whose properties have been modified via the blending in of anion receptors.

Arguably the most important area where the blending strategy has been successfully applied involves the development of ion-selective electrodes (ISEs). Such analytical tools derive their selectivities from the specificities of the constituent ionophores and their abilities to form stable complexes with analytes that are subsequently transported into electrode membranes. Ideally, an ISE should respond to a specific ion and should not be affected by the presence of other ions in solution. A number of ISEs utilizing polymer matrix liquid membranes have been developed and investigated. As detailed below, the incorporation of appropriately chosen receptors for a target ion into the electrode membrane represents a particularly valuable approach to anion-specific ISE development.

Early work in the development of ISEs for anionic species utilized polyamines. One such example was reported by Carey and Riggan who incorporated cyclic azoethers (**1–4**) into polyvinyl chloride (PVC) membranes for construction of phosphate-selective electrodes (Fig. 2) [20]. The chemical inertness of PVC, combined with its adsorptivity and stability features, has traditionally made it an ideal choice for electrode development. In the particular case of the Carey and Riggan study, ISEs were constructed by dipping an electrode into a membrane-forming “cocktail” which consisted of 20 wt % ionophore (i.e., **1–4**), 45 wt % PVC, and 35 wt % dibutyl sebacate in tetrahydrofuran (THF). This resulted in the formation of a PVC matrix with a thickness of 15–30 μm over the open end of the electrode.

The electrode produced using **1** as the enmeshed ionophore showed excellent selectivity for dibasic phosphate (HPO_4^{2-}), exhibiting a near-Nernstian slope of ~ 29 mV per activity decade and a linear range of 10^{-7} – 10^{-1} M at $\text{pH} = 7.2$. Ionophores **1–4** demonstrated an inverse relationship between ring size and the linear range of the electrodes made with each ionophore. The electrode developed with **1** was also shown to respond to varying pHs, a finding that led the authors to suggest that this electrode responds specifically to dibasic phosphate anions. Furthermore, the electrode demonstrated selectivity over other interfering anions (e.g., $\text{HPO}_4^{2-} > \text{SCN}^- \approx \text{Cl}^- > \text{NO}_3^- > \text{SO}_4^{2-}$). The selectivity of the electrode is

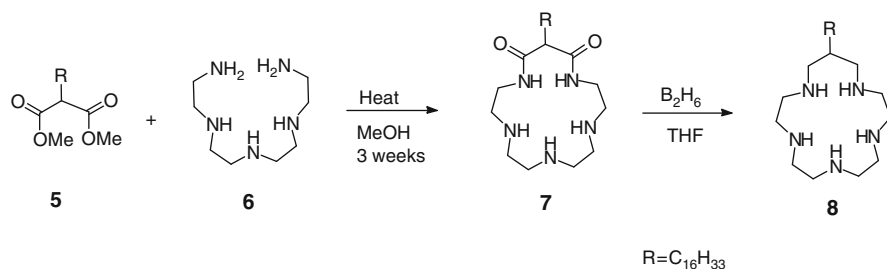
Fig. 2 Cyclic polyamines of varying sizes that have been used as ionophores for phosphate-selective electrodes



consistent with the so-called Hofmeister bias [21], with the exception that Cl^- gives rise to a greater response than NO_3^- . The authors postulate that possible interactions between chloride and membrane components, such as PVC, could account for this observation. Carey and Riggan reasoned that the inherent selectivity of **1** could be attributed to preferential conformational changes upon binding, according to preliminary modeling results. Gratifyingly, the electrode showed great durability, retaining selectivity and usability over a period of 9 months while being repeatedly used in tests of human saliva and phosphate standards.

Umezawa et al. developed a similar ISE based on modified aza-crown ether, **8** [22], which was obtained by treating $\text{C}_{16}\text{H}_{33}$ -substituted malonate (**5**) with tetraethylenepentamine (**6**) in absolute methanol for 3 weeks under conditions of reflux. This produced macrocycle **7** (Scheme 1). The amide linkages were then reduced to amines using $\text{BH}_3 \cdot \text{THF}$. This procedure allowed receptor **8** to be isolated in 40% yield after purification involving recrystallization from a mixture of MeCN and MeOH. The receptor was then used to create a PVC-based ISE. As above, good anion selectivity was seen with this system, in this case toward adenosine triphosphate (ATP^{4-}) in comparison to phosphate and other biologically ubiquitous anions. In HEPES buffer at pH 6.7, a linear response to ATP^{4-} was found from 10^{-3} to 10^{-7} M with a response slope of -14.5 mV. Additionally, the electrode did not appear to exhibit any memory effect (hysteresis) corresponding to changes in concentration.

At physiological pH, the aza-crown ether derivative **8** was believed to be triply protonated (i.e., existing as a tri-cation). The use of such a charged receptor, as opposed to a neutral receptor, was thought to account for the observed selectivity



Scheme 1 Synthesis of aza-crown ether derivative **8** developed by Umezawa et al.

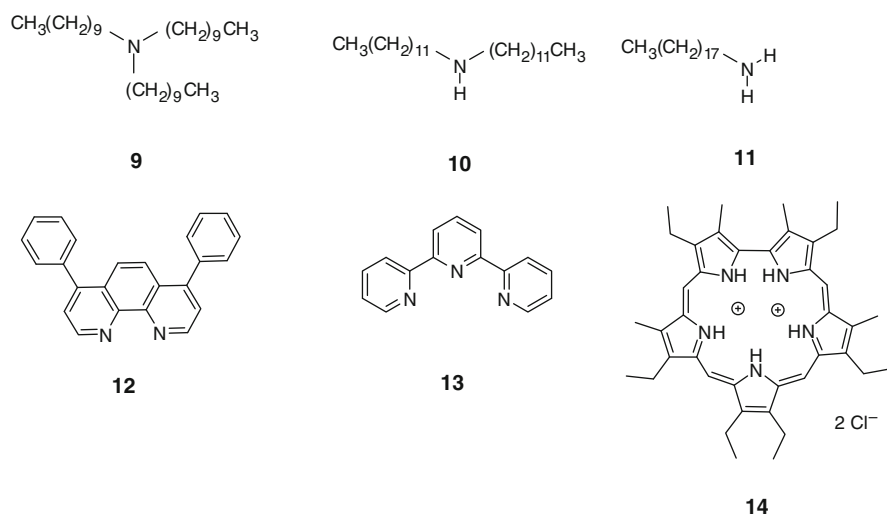


Fig. 3 Aliphatic and heteroaromatic amines used as ionophores to construct ISEs

for ATP^{4-} and/or its monoprotinated form, HATP^{3-} . This finding was considered to be unique at the time since it meant that the neutral form of the receptor (as used to prepare the modified electrode) undergoes protonation at the surface of the ISE, thus producing a more effective, charged receptor. This finding inspired the construction of yet additional ISEs.

In 1998 Umezawa, Sessler, and coworkers conducted a comprehensive study of a variety of aliphatic and heteroaromatic lipophilic amines (Fig. 3) and their potentiometric anionic response to neutral phenols [23]. The amines used in this study included the aza-crown ether derivative discussed above (**8**), tri(decyl)amine (**9**), 4,7-diphenyl-1,10-phenanthroline (**12**), terpyridine (**13**), and sapphyrin (**14**) [24].

The electrodes developed by Umezawa and Sessler utilized PVC matrix membranes. Membranes that incorporated aliphatic amines (**9–11**) exhibited potentiometric selectivities that correspond to the acidity (hydrogen donor activity) as well as the lipophilicity (extractability) of the phenols. The authors explained the anionic

response on the basis of a decrease in the amount of charge separated by the protonated amines and counteranions across the membrane. The pH profiles of heteroaromatic amines **12**, **13**, and **14** led the authors to suggest that protonation of these latter species is less facile, but still leads to charge separation across the membrane interface generating a membrane potential. Interestingly, the membrane developed using sapphyrin (**14**) as the ionophore showed selectivity for catechol, reflecting an innate geometrical discrimination.

In a separate study, Umezawa and Sessler studied the potentiometric response of membranes containing expanded porphyrins towards carboxylate anions and inorganic anions [25]. The expanded porphyrins used in this study included sapphyrin (**14**), rubyrin (**15**), and triphenylrosarin (**16**). Prior to using these particular species as ISE elements, Sessler and coworkers had shown that various expanded porphyrins are capable of binding anionic species in their protonated forms through a combination of hydrogen bonding and electrostatic interactions [26]. Specifically, sapphyrin was demonstrated to be an efficient receptor for fluoride, phosphate, and phenylphosphate [27, 28]. Rubyrin [29], which is a 26 π -electron species, was shown to demonstrate an affinity for chloride and GMP, whereas triphenylrosarin [30], a fully conjugated 24 π -electron macrocycle, was likewise shown to recognize the chloride anion. In both cases, prior protonation of the macrocycle was deemed necessary to achieve efficient anion binding (Fig. 4).

Umezawa and coworkers prepared PVC membranes containing expanded porphyrins **14–16** using a procedure similar to that used to obtain the previously described systems. In this case, pH titrations involving the resulting electrodes served to demonstrate that protonation of the expanded porphyrins at the surface of the electrode is required for uptake of the targeted anions and to obtain a potentiometric response. This set of electrodes demonstrated a strong response to the benzoate anion, but did not respond well to inorganic anions or saturated aliphatic carboxylate anions. Interestingly, the electrode developed from sapphyrin (**14**)

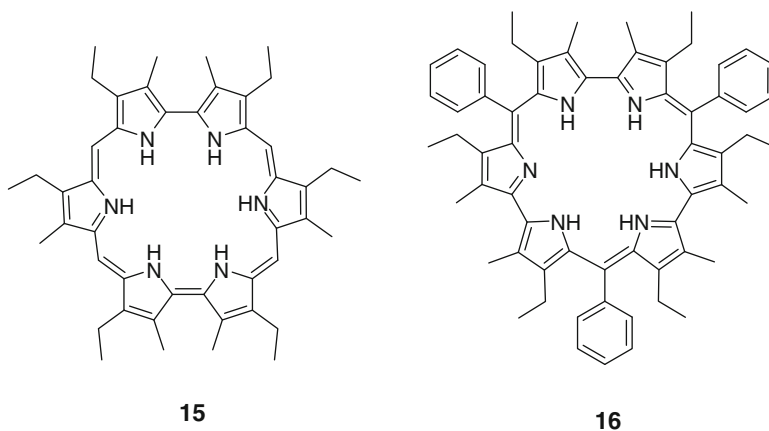


Fig. 4 Expanded porphyrins rubyrin (**15**) and triphenylrosarin (**16**)

deviated from the Hofmeister series, and showed selectivity for fluoride – a much more hydrophilic anion – over chloride and bromide. The sapphyrin-based electrode in this study appeared to discriminate for fluoride based on size, the specificity of the charge–charge interactions, and via hydrogen bond formation. At the time of the work, a selective potentiometric response based on size represented a new approach to developing analyte-specific ISEs.

In 1999, Král, Sessler, and Gale developed PVC-derived ISEs from neutral anion receptors [31]. This study utilized *meso*-octamethylcalix[4]pyrrole (**17**) and its pyridine containing analogs dichlorocalix[2]pyrrole[2]pyridine (**18**) as well as tetrachlorocalix[4]pyridine (**19**). This series of macrocyclic receptors represents a matched set, wherein it was considered that if the pyridine moieties remain unprotonated they should act as strong (**17**), intermediate (**18**), and weak anion receptors (**19**), respectively. Calix[4]pyrrole is a known neutral macrocycle that binds anionic species through hydrogen bonding interactions, showing selectivity for $F^- > Cl^- > H_2PO_4^-$ when studied as the TBA salts in dichloromethane [32] (Fig. 5).

ISEs developed from **17** displayed a strong anionic response (negative slope) at lower pH values (i.e., 3.5 and 5.5) in the case of Br^- , Cl^- , and $H_2PO_4^-$. A correspondingly lower response was observed with F^- . However, at higher pH (i.e., 9.0) electrodes derived from **17** displayed a cationic response (positive slope) toward Cl^- and Br^- . Non-Hofmeister selectivity was also seen in the case of an ISE produced from **17** (i.e., $Br^- < Cl^- < OH^- \approx F^- < HPO_4^{2-}$). The authors rationalized this finding by suggesting that **17** acts as a direct anion binding agent at low pH, whereas at higher pH this same receptor acts, at least in part, as a hydroxide anion-complexing receptor. ISEs based on receptors **18** and **19** displayed selectivities in accordance with the Hofmeister series at pH 9.0. The authors also reported that at lower pH values ISEs derived from **18** and **19** displayed increased anionic responses and improved selectivities for hydrophilic anions (e.g., F^- and $H_2PO_4^-$); this observation was rationalized in terms of protonation of the pyridine containing receptors, which led to the higher anion binding effects. These results, when considered in concert, provide initial support for the notion that calixpyrroles, as

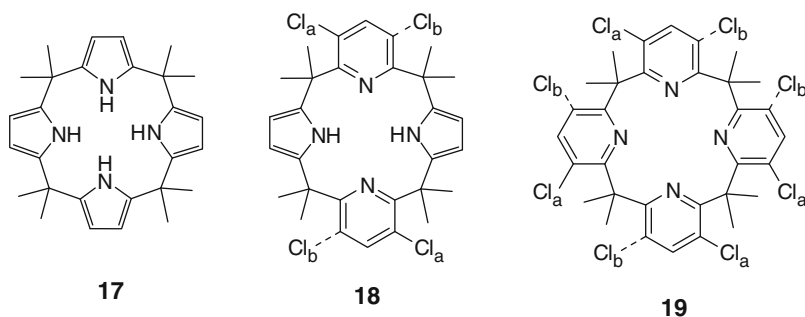


Fig. 5 Calix[4]pyrrole (**17**), dichlorocalix[2]pyrrole[2]pyridine (**18**), and tetrachlorocalix[4]pyridine (**19**). As described in the text, these anion receptors were incorporated into ISE membranes

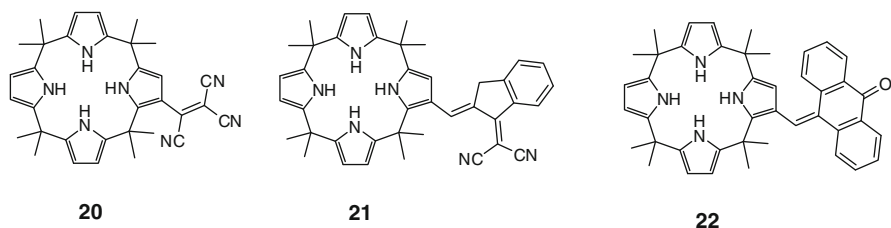


Fig. 6 Calix[4]pyrrole derived chemosensors from nonchromogenic dye precursors

well as other neutral receptors, may be used in the development of anion-specific ISEs and, more broadly, polymeric systems capable of interacting specifically with negatively charged analytes.

The incorporation of heterocyclic receptors into polymeric materials has not been limited to the development of selective electrodes. For example, Anzenbacher and Nishiyabu designed chromogenic anion chemosensors based on calix[4]pyrrole (**17**) that were produced by attaching nonchromophoric dye precursors to the macrocyclic framework [33]. The ease and high yield of the underlying preparation offer obvious advantages over attaching pre-existing chromophores to calixpyrroles. The calixpyrrole derivatives **20–22** produced by these researchers were found to display dramatic color changes upon the addition of the fluoride, acetate, pyrophosphate, and phosphate anions (Fig. 6).

In an effort to demonstrate the relevance of chemosensors **20–22** to health care applications, studies were performed using carboxylates of medical interest (salicylate, ibuprofen, naproxen). Toward this end, Anzenbacher and his group developed a new assay utilizing polyurethane films that contained receptors **20–22** embedded noncovalently within macromolecular matrices. According to the authors, the polyurethane support served two purposes. First, the polymer physically acted to screen off various blood plasma protein carboxylates from the active sites. Second, its hydrophobic nature prevented hydrophilic anions (e.g., HCO_3^-) from penetrating into the matrix and biasing the embedded sensor. The actual test experiments involved the use of a multiwell assay that contained the functionalized polyurethane. It was found that relatively lipophilic aromatic carboxylates were able to penetrate films containing **20**, bind with the chemosensor, and produce a response. This response takes the form of a characteristic change in the color of the polymer film (Fig. 7). The affinity for the carboxylate anions was as follows: naproxen \approx ibuprofen \geq salicylate $>$ laurate $>$ acetate (prepared in plasma-like aqueous solution (PLAS)).

A follow up article in 2007 by Anzenbacher et al. was concerned with the development of easy to use chemosensors and arrays for anions in water [34]. The low charge to radius ratio and high energy of solvation of various anions (e.g., F^- has an ionic radius of 1.33 Å and $\Delta G_{\text{hydration}} = -465 \text{ kJ mol}^{-1}$ [21]) makes sensing in water a particularly challenging task. Anzenbacher utilized eight pyrrole hydrogen bond donor motifs as the chemosensor elements (Fig. 8). These motifs

Fig. 7 Polyurethane films in which chemosensor **20** is embedded. PLAS solutions of anions (10 mM), bovine serum albumin (BSA), and blood plasma were applied to polymer films at pH = 7.4. This figure, which originally appeared in *J Am Chem Soc* 2005, 127, 8270–8271 (copyright Am Chem Soc), is reproduced with permission [33]

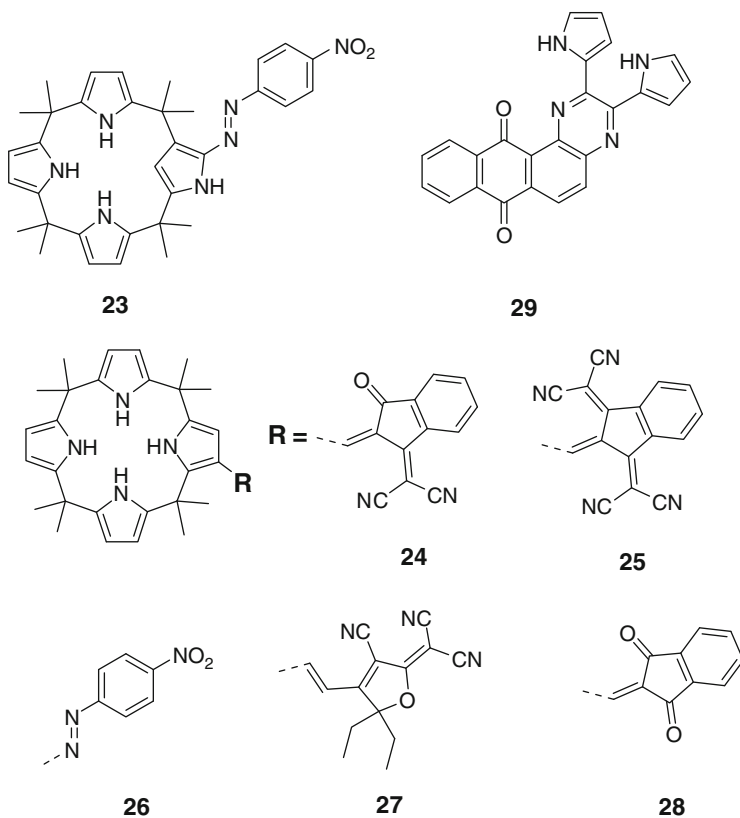
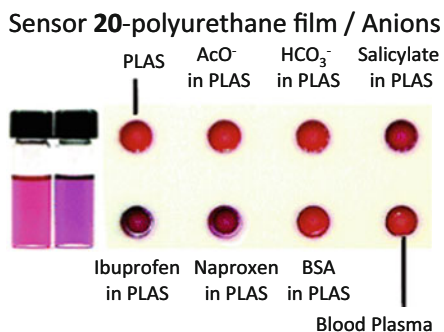


Fig. 8 Hydrogen bonding chemosensors for anions based on pyrrole hydrogen bond donor motifs

included N-confused calix[4]pyrrole (**23**), calix[4]pyrrole **21** and its derivatives **24–28**, as well as the anthraquinone based dipyrrolylquinoxaline (DPQ) **29**.

As in the previous study, Anzenbacher blended sensing elements **21** and **23–29** with a polyurethane hydrogel, and cast the resulting modified polymer into a microwell array. Individual wells were filled with 400 nl of polymer-sensor mixture (approximately 0.08% sensor in polyurethane w/w) in a tectophilic THF solution (5% w/w) and dried to form polymer films (10 μm thick). The use of a hydrogel in these studies lends mechanical support to the sensor ensemble and presumably helps draw the bulk analyte into the matrix and partially remove the hydrate from the anion (all anions were applied in aqueous solutions). Wells prepared in this way produced a naked-eye detectable color change upon exposure to the fluoride, pyrophosphate, and acetate anions. Anions were typically added as aqueous solutions (200 nl) of their corresponding TBA salts. The authors observed that the magnitude and dynamic range of the colorimetric response corresponded well with the affinity displayed by the chemosensor molecule in organic solution. Furthermore, multivariate analysis, specifically principal component analysis (PCA), was used to distinguish between ten different brands of fluoride-containing toothpaste.

The final study considered in this section involves work reported by Ebdon and coworkers in 2004. They were able to improve upon the findings of Carey and Riggan (*vide supra*) by developing an improved phosphate-selective electrode containing receptors as both additives to polymers and as covalently linked side-chain functional elements [35]. This study is important in that it allowed the relative benefits of receptors incorporated as additives into preformed polymers to be compared with those where the receptors are covalently attached to polymers. In prior work, Ebdon et al. demonstrated immobilization of quaternary ammonium species containing allyl groups via a free radical cross-linking reaction [36]. The resulting membranes were used as receptors for nitrates. They thus employed similar methods as were used by Carey and Riggan to immobilize derivatives of receptor **1** (*vide supra*); this was done by substituting a terminal allyl-bearing alkyl group to the macrocyclic core. However, in contrast to these earlier researchers, Ebdon et al. utilized monomers **30** and **31** (Fig. 9) whose syntheses were based on previously reported procedures [20, 36]. These monomers were added to

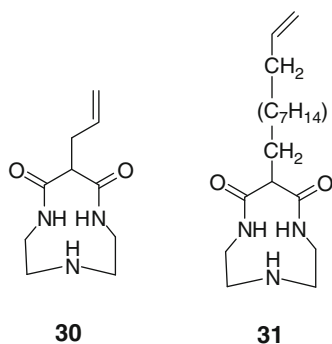


Fig. 9 Cyclic amine monomers **30** and **31**

membranes composed of the relatively heat resistant polystyrene-block-polybutadiene-block-polystyrene (SBS); subsequent cross-linking was achieved via a hot-pressing process using a Bytec industrial heated press (obtained from Bytec, London, UK) [37].

To test the efficacy of a trapped ionophore in a polymer blend versus an ionophore covalently bound to a polymer, Ebdon and coworkers constructed two electrodes. One of these was a PVC-based membrane akin to that used by Carey and Riggan; the second electrode consisted of the previously mentioned SBS-based membrane containing covalently bound ionophores. Under the conditions of analysis, receptor **30** was found to be too hydrophilic for use as an embedded (i.e., not cross-linked) probe. Specifically, it was found to leach out of the PVC-based membrane during processing, such that no response to phosphate could be detected. On the other hand, the SBS-based electrode incorporating **30** worked well, as long as a hot-pressing process was used to ensure covalent cross-linking between **30** and the SBS backbone. This electrode gave a response slope of -16 ± 3 mV, had a linear range of 2.2×10^{-3} to 5×10^{-6} mol dm $^{-3}$ H $_2$ PO $_4^-$ and a limit of detection of 1.0×10^{-6} mol dm $^{-3}$ H $_2$ PO $_4^-$. While these results compared favorably to those obtained by Carey and Riggan the nature of the comparison was not identical. Therefore to permit a more accurate assessment of the trapped versus covalently bound ionophore approaches, Ebdon and coworkers synthesized a more hydrophobic monomer, **31**, which showed improved performance in the PVC matrix electrode. The PVC-**31** electrode showed detection abilities comparable to those of electrodes created using **1** embedded in PVC. Specifically, a response slope of -34.0 ± 2.0 mV, a linear range of 2.2×10^{-3} – 5×10^{-6} mol dm $^{-3}$ H $_2$ PO $_4^-$, and a limit of detection of 5×10^{-6} mol dm $^{-3}$ H $_2$ PO $_4^-$ was seen. Due to **31** being simply embedded in the PVC matrix, the electrode had a response lifetime of merely 4 days, compared to the SBS-**30** electrode. In the latter case, where the ionophore was covalently bound, a lifetime of 20 days was observed.

With these results in hand, Ebdon and coworkers sought to extend further the lifetime and improve the response of their phosphate-selective electrodes. To do this, they turned to clay composites, an approach known for improving stability, as well as altering the backfilling of electrolytes which resulted in significant improvement in the limit of detection in electrode systems [38, 39]. By blending in 23.8% (m/m) PoleStarTM 200R (clay-based filler), Ebdon and coworkers found that the lifetime of the electrode could be extended from 20 days to 40 days for the bound electrode. That comparable response behavior was seen for the ISEs based on mobile and bound ionophores is consistent with the notion that ionophore mobility is not necessary to get a working ISE. Nevertheless, it is important to appreciate that the ISEs based on covalently bound ionophores exhibit significantly increased robustness and stability as compared to analogous PVC-membranes containing “trapped” ionophores.

The work of Ebdon and coworkers thus provides an important demonstration of the potential advantages that can accrue from appending receptors covalently to polymeric materials. Taking this a step further, the formation of well-defined polymers with precisely placed receptors can be expected to enhance the performance of

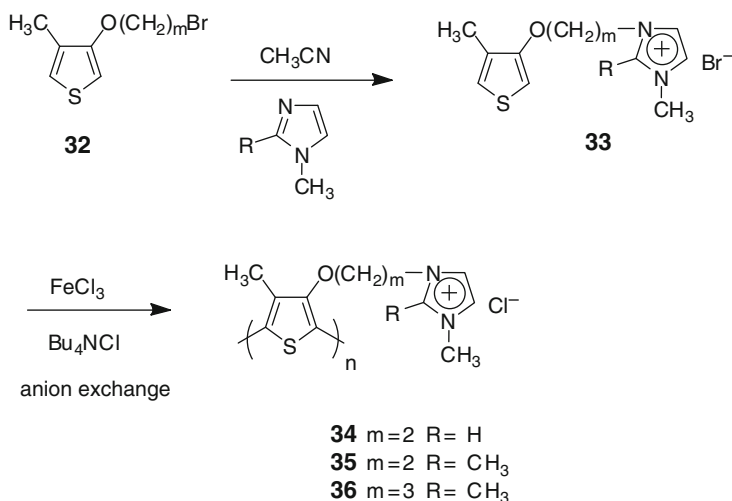
the aforementioned devices (and other applications) even further. Along these lines, the following sections will highlight two classes of such receptor functionalized polymers, specifically those where receptors are (1) attached as side-chain appendages to polymeric frameworks and (2) incorporated directly into polymer backbones.

3 Side-Chain Polymers Containing Anion Responsive Heterocycles

The incorporation of anionic receptors into well-defined polymers and other macromolecules is expected to produce materials that offer a number of advantages as compared to their small molecule analogs. For example, polymers often have significantly different solubilities than small molecules, a feature that is likely to be particularly useful in the areas of anion extraction and separation. Attachment to a polymer provides a method for immobilizing anionic receptors and chemosensors and can prevent “leaching,” or loss of the receptor, which can be advantageous in applications involving the use of mixed phases. The use of polymers can also lead to beneficial matrix effects that can serve to decrease the solvation of a targeted anion or its counteranion. Again, this can be useful in any application involving transfer of an anionic species from an aqueous to hydrophobic environment. Finally, polymeric materials can often be used to create mechanically-robust thin films; where the films contain anion receptors, new and practical applications in the areas of *inter alia* membrane technology, filter devices, and sensors can be easily envisioned.

In this section the focus will be on polymeric materials wherein anion receptors are incorporated as pendant side-chains. As will be detailed below, several basic strategies have been used to prepare such materials. The use of differing synthetic methods, and the choice of the receptor system in question, has allowed a degree of affinity and selectivity to be designed into polymeric systems. However, the hope and expectation is that yet-improved systems can be obtained. Indeed, as implied in the introductory remarks, one objective of this review is to stimulate additional effort along these lines.

Early functionalized polymer systems targeting the problem of selective anion recognition relied on the use of secondary electrostatic interactions for the detection of anionic species. Indeed, rather than incorporating an anion receptor per se, these systems relied on cationic species that would then attract anions as the result, presumably to maintain charge balance. This strategy is elegantly embodied in the work of Leclerc and coworkers who in 2002 reported a polythiophene derivative containing a pendant imidazolium salt [40]. This polymer was prepared by an oxidative polymerization procedure using FeCl_3 as the oxidizing agent (Scheme 2) [41]. The polymer was soluble in aqueous solution and at 55°C (0.1 M NaCl or 10 mM tris(hydroxymethyl)aminomethane (Tris) buffer/0.1 M NaCl) the solutions were yellow in color ($\lambda_{\text{max}} = 397 \text{ nm}$). The red-shifted absorption maxima was



Scheme 2 Synthesis of cationic polythiophene derivatives containing imidazolium salts

attributed to the random-coil conformation and subsequent decrease in effective conjugation [42].

Polymer **34** was initially used for the colorimetric and fluorometric detection of nucleic acids. The cationic polymer displayed an ability to transduce oligonucleotide hybridization easily, with the specific capture of a 20-mer probe translating into a clear optical output. In a separate study, Ho and Leclerc used the related polymers **35** and **36** as colorimetric and fluorometric chemosensors for the specific detection of the iodide anion [43]. The impetus for this latter study derives in part from the fact that iodide is a biologically relevant anion, mostly known for its role in thyroid functions. In the study itself, electrostatic interactions were thought to result in a conformational change of the polythiophene derivatives causing a change in the effective conjugation of the polymer chain. Iodide anions promote the aggregation and planarization of polymer **35** causing a red-shift in absorbance as well as fluorescence quenching. The optical effects monitored using absorption and emission spectroscopies were shown to be independent of the corresponding counter cation (e.g., Na^+ vs. K^+). The authors also demonstrated that these systems were dependant on the length and nature of the side chain; for instance, they found that polymer **36** displayed reduced sensitivity under conditions similar to those used to analyze polymer **35**.

In a more recent study Tang et al. employed a different approach towards creating polymers with positively charged appendages [44]. Specifically, with the goal of exploiting the so-called “molecular wire effect” noted for conjugated polymers, these researchers synthesized polyphenylacetylenes (PPAs) containing imidazole moieties attached to the backbone (i.e., as pendant side-chains). These materials were prepared via postpolymerization functionalization, wherein substitution with imidazole was used to generate polymer **37** (Fig. 10). Polymer **37**

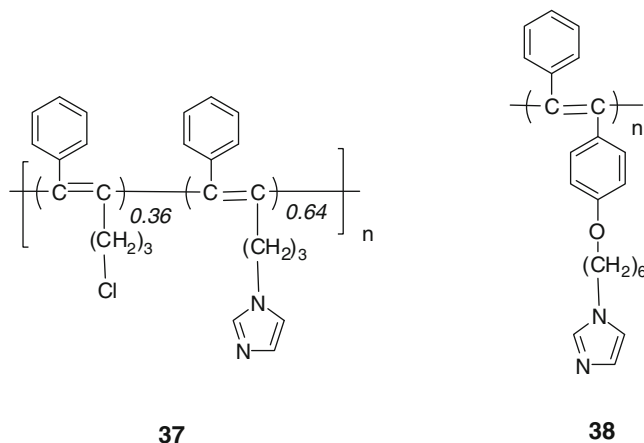


Fig. 10 Polyphenylacetylenes functionalized with imidazole moieties

displayed poor solubility in THF, chloroform, and dimethylformamide (DMF) but was readily soluble in ethanol. This material demonstrated both the strong luminescence (i.e., blue fluorescence) characteristic of disubstituted polyacetylenes, as well as the metal ion-coordinating ability of imidazoles. As such, it was proposed that polymer **37** would provide a new kind of potentially efficient chemosensor.

It was shown that Cu^{2+} could quench the fluorescence of polymer **37** (1.06×10^{-4} M solution in ethanol) completely at very low concentration (1.48 ppm) with the corresponding Stern–Volmer constant determined to be 3.7×10^5 M. Tang and coworkers were then able to take advantage of a “turn on” method of anion sensing by employing species that competitively bound Cu^{2+} . In particular, low concentrations of CN^- (i.e., 7.0×10^{-5} M $^{-1}$ of sodium cyanide) served to “turn on” the fluorescence of the polymer **37**· Cu^{2+} complex. The reactivation of the fluorescence signal was not observed in the presence of other anionic species. The detection of CN^- is highly important given its inherent toxicity to mammals and its common use in industrial applications such as gold mining, electroplating, and metallurgy [45, 46].

In 2009, Tang and coworkers utilized polymer **37** to sense α -amino acids via a similar “turn on” fluorescence approach [47]. The use of a normal UV lamp allowed histidine to be differentiated from other α -amino acids; in particular, histidine allowed for the visual observation of a restored blue fluorescence at concentrations as low as 4.0×10^{-5} M. Using fluorescence spectroscopy to monitor the “turned on” fluorescence signal after exposure of the polymeric complex **37**· Cu^{2+} allowed histidine to be detected at concentrations as low as 2.1 ppm.

Recognizing that the human eye is not generally as sensitive to the blue fluorescence produced by **37** as it is to green light, Tang et al. generated a second generation imidazole-pendant PPA (e.g., polymer **38**) [48]. In this polymer the residual halogen groups were completely converted to imidazole substituents (effected synthetically by converting **37** to the corresponding bromide); this yielded

Fig. 11 PPA containing naphthalimide as a pendant side-chain

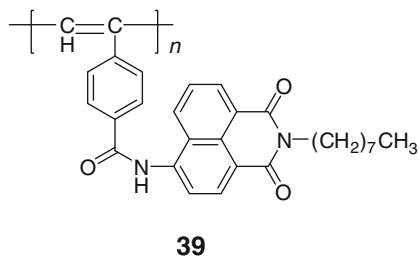
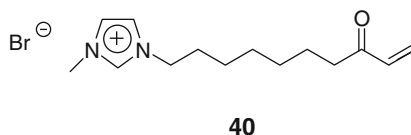


Fig. 12 Photonic ionic liquid monomer based on imidazolium salts



a polymer with strong green fluorescence (**38**). The chemosensing behavior of **38** could be observed visually or with the help of a normal UV lamp. This material was capable of detecting copper and cyanide at concentrations as low as 0.85 and 1.38 ppm, respectively.

A novel PPA containing naphthalimide subunits in the side-chain was developed by Tian and coworkers in 2009 [49]. Previous work with naphthalimides demonstrated that these systems act as chemosensors for fluoride ions based on a unique intermolecular proton transfer (IPT) signaling mechanism (Fig. 11) [50, 51]. Polymer **39** was synthesized using $[\text{Rh}(\text{nbd})\text{Cl}]_2$ as a catalyst, resulting in a material that was soluble in most common organic solvents.

On addition of tetrabutylammonium fluoride (TBAF) to an acetonitrile solution of **39**, a drastic color change from colorless to yellow was observed. The change in the absorption and emission spectra of **39** allowed for a ratiometric detection of fluoride anions in solution. Titrations with other anionic species lead to no spectral changes. Ratiometric fluorescent probes allow for improved reliability and a greater effective dynamic range by providing a built-in correction for environmental effects [52, 53]. While there has been a number of ratiometric fluorescent probes developed for cationic species [54, 55], there are few reports of ratiometric fluorescent polymers for F^- anions [56]. Interest in the detection and recognition of the fluoride anion is of growing interest given its association with nerve gas (it is, for instance, a hydrolysis product of Sarin) and the role that UF_6 plays in the enrichment of uranium-235.

Taking a more materials based approach to anion sensing, Li and coworkers developed a novel photonic ionic liquid (IL) system for the detection of various anions (Fig. 12) [57]. Utilizing an imidazolium-based IL monomer (**40**), these investigators performed a photopolymerization of this monomer in 1:1 feed ratio with methylmethacrylate in the presence of the cross-linker ethylene glycol dimethacrylate, and the initiator 2,2'-azoisobutyronitrile (AIBN). The polymerization itself

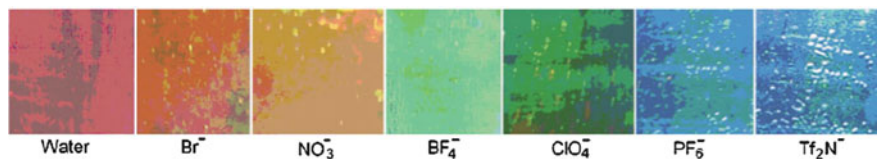


Fig. 13 Photonic IL polymer shifts its stop gap as a function of counter anion leading from a shift from *pink* to *blue*. This figure, which originally appeared in *Adv Mater* 2008, 20, 4074–4078 (Copyright Wiley-VCH GmbH & Co. KGaA), is reproduced with permission [57]

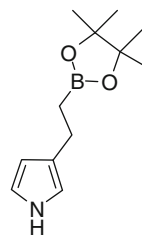
was effected in the presence of silica colloidal crystals in a mixed solvent system consisting of a 1:1 mixture of methanol and chloroform. The silica colloidal crystals were then etched away with 1% HF solution to yield a photonic IL film with an inverse opal structure. The resulting 3D ordered photonic IL was utilized in the naked-eye detection of anions (*vide infra*).

It is well known that the hydrophobicity and hydrophilicity of ILs can be tuned by counteranion exchange [58]. In the case of macromolecules containing such species, such tuning was expected to be characteristic of the material. The use of appropriate solvents leads to swelling or shrinking of the films, which should result in a change in the stop gap of the photonic ILs. Similar effects were expected from counteranion exchange. As can be seen from an inspection of Fig. 13, such effects were observed for exposure of the photonic IL films to nitrate (NO_3^-), tetrafluoroborate (BF_4^-), perchlorate (ClO_4^-), phosphorous hexafluoride (PF_6^-), bis(trifluoromethylsulfonyl)imide (Tf_2N^-), and bromide (Br^-). Subsequent monitoring by FTIR served to confirm adsorption of the anions to the films. The most hydrophobic anion, Tf_2N^- , results in the largest shift in absorbance, 76 nm, while the most hydrophilic, NO_3^- , led to a relatively modest shift of only 18 nm.

Boron-based heterocyclic receptors have also been appended to polymers. Fabre and coworkers in 1999 reported one of the first examples of an immobilized boronate anion receptor [59]. In particular, Fabre et al. detail a polypyrrole functionalized with pendant boronate pinacol ester derivatives (**41**) that can function as an electrochemical chemosensor for anions when electrodeposited onto a platinum electrode via anodic oxidation performed in acetonitrile. The concentration of anionic analyte was then monitored via shifts in the cyclic voltammograms. To synthesize the pyrrolic monomer, Fabre and coworkers began with 1-(phenylsulfonyl)-3-vinylpyrrole. Hydroboration by diisopinocampheylborane yielded the intermediate diethyl boronate derivative. Reaction with pinacol then gave the pinacol boronate derivative. Subsequent deprotection of the phenylsulfonyl group by electrochemical reduction gave monomer **41** in 13% overall yield. Electropolymerization of **41** was achieved in anhydrous MeCN using 10^{-1} M Bu_4NPF_6 as the supporting electrolyte (Fig. 14).

In water/acetonitrile mixtures, the polymer-coated platinum electrode based on **41** exhibited a reversible redox process at -0.11 V versus a standard calomel electrode (SCE). Upon addition of a 2 mM solution of potassium fluoride (KF) to the system, a cathodic shift to -0.37 V versus SCE was observed – a result that is

Fig. 14 Pinacol-based boronate derivatized pyrrole monomer



41

consistent with the expectation that the polymer would be easier to oxidize when fluoride is bound. Fabre et al. also reasoned that the negative charge of the fluoride anion might be stabilized by the positive charge created on the polymer backbone as the result of oxidation. Presumably, this adds to the signal response. In contrast to fluoride, very little response was seen when the boronate functionalized polypyrrole was exposed to the chloride or bromide anions, requiring a minimum concentration of 20 mM before a recognizable response was seen in the cyclic voltammetry (CV) traces.

A different set of electrochemical sensors for anion detection was developed by Royal and coworkers, who relied on ferrocene–viologen (4,4′-bipyridinium) based redox active receptors, as well as related polymer films [60]. The stated long-range goal of this research was to develop a sensor for ATP^{2-} that would function in biological milieus. This is a particularly challenging objective given the ubiquity and relatively high concentrations of other anionic species in the human body, including in particular chloride and inorganic phosphate. Cognizant of this challenge, Royal et al. first synthesized the small molecule receptors **42** and **43**. These compounds were made so as to test the sensing abilities of the ferrocene–viologen receptors per se. Here, it is to be noted that receptor **42** represents a ferrocene with viologens bound at the 1 and 1′ positions, while **43** is an *ansa* system wherein two viologens are connected through two ferrocenes to form a macrocycle that is formally analogous to the cyclobis(paraquat-*p*-phenylene) “blue box” made famous by Stoddart [61]. Films of polymer-**44** were deposited onto an electrode surface via oxidative electrochemical polymerization of the pyrrole fragment (0.9 V vs. Ag/Ag^+ 10^{-2} M in MeCN + TBA salts of perchlorate (TBAP) (Fig. 15).

These investigators chose CV and differential pulse voltammetry (DPV) as the probe methods used to investigate the binding affinities of **42**, **43** and polymer-**44**. In the case of the redox active receptors **42** and **43**, exposure to H_2PO_4^- , SO_4^{2-} , HPO_4^{2-} , CF_3COO^- , F^- , and Cl^- produced no significant shifts in the CV or DPV curves. However, the $\text{Fc}^{0/+}$ couple in **42** was found to undergo a shift of -10 mV when exposed to HSO_4^- , $\text{S}_2\text{O}_4^{2-}$, and ATP^{2-} , while a shift of -10 mV in this wave was seen when **43** was exposed to PhPO_4^{2-} and $\text{S}_2\text{O}_4^{2-}$. Of particular note is that the ferrocene linked system **43** experienced a shift in the $\text{Fc}^{0/+}$ wave of -25 mV when titrated with two molar equivalents of ATP^{2-} , thus revealing a selectivity for this all-important biological analyte. Royal et al. argued that this selectivity can be

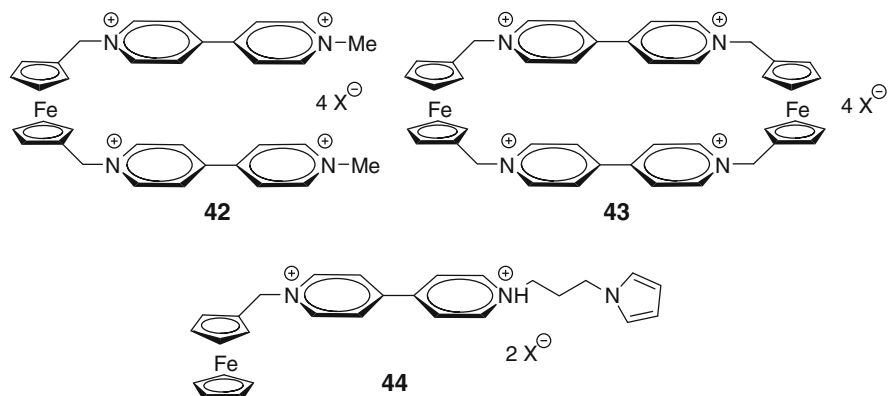


Fig. 15 Ferrocene–viologen based receptors developed for polypyrrole-based ATP²⁻ sensing

attributed to **43** forming a hexacationic receptor upon oxidation, increasing the electrostatic interactions with ATP²⁻. Charge-transfer interactions between the electron rich adenosine ring system and the viologens are also thought to contribute to the anion binding process.

On oxidative electropolymerization of monomer **44** in MeCN, an ATP²⁻ selective electrode was produced. When the polymer-coated electrode was titrated against H₂PO₄⁻, PhPO₄²⁻ and halide anions, which had previously caused no shifts or only modest shifts in the CV peaks of receptors **42** and **43**, little in the way of response was likewise observed. On the other hand, exposure to ATP²⁻ over a concentration range of 10⁻⁵–10⁻³ M produced a cathodic shift in the Fe^{0/+} peak that increased to a maximum ΔE_p of -35 mV (i.e., from $E_p = 460$ mV to $E_p = 425$ mV vs. SCE). This was considered an excellent result that highlights the possible detection of ATP in aqueous media polymeric, which could in due course allow for the use of these electrodes in more biologically-oriented environments.

In this section we have covered polymeric materials that incorporate anion receptors as pendant side-chains. These systems have been applied as chemosensors for species such as CN⁻, F⁻, and phosphate derivatives. This approach toward material development is attractive because it allows the beneficial features of various monomeric receptors (e.g., specificity and signal output) to be combined with those of polymers (e.g., solubility and stability). In this section, the receptors discussed derived their selectivity from electrostatic interactions or subsequent deprotonation on exposure to anionic species. In contrast, the ensuing section will focus on incorporation of neutral heterocyclic receptors with strong affinity for anionic species.

4 Polymers Containing Neutral, Anion Receptors

The previous section provides an introduction into polymeric materials containing receptors capable of recognizing anionic species. The aforementioned systems incorporate anion responsive or sensing moieties as side-chain appendages.

However, the innate functionality of these materials was typically derived from electrostatic interactions or deprotonation after exposure to anionic species. This often resulted in a colorimetric or fluorometric response. In this section, we will look at neutral receptors capable of binding anions with high affinity, often through multiple hydrogen bonding interactions. In particular, the structural incorporation of calix[4]pyrrole into polymeric systems will be covered, as well as other molecular receptors [e.g., crown ether, DPQ, and diindolylquinoxaline (DIQ)]. Earlier in this chapter, polymer matrices containing calix[n]pyrrole, and derivatives thereof, were described. These materials not only represent a creative approach to ISE development, but also are exemplary of initial progress in the development of polymers containing neutral anion receptors. One advantage of the strategies described below is the ability to tune material properties based on choice of receptor as well as polymer design (e.g., alteration of polymer type, cross-linking, or monomer loading levels).

Early progress in this field is represented by two sets of resins prepared by Kaledkowski [62, 63]. In the first of these, calix[4]pyrrole (**45**) and calix[4]pyrrole [2]thiophene (**47**) were attached to cross-linked vinylbenzene chloride/divinylbenzene copolymer beads. A condensation of phenol-substituted calix[4]pyrrole with formaldehyde (**46**) was used to synthesize the second set of resins. Both these materials displayed an ability to “capture” halides and cyanide anions from MeCN (i.e., nonaqueous media). Furthermore, resins that contained the “expanded” calix [4]pyrrole[2]thiophene unit demonstrated an enhanced affinity for larger anionic species, such as iodide. This result correlates well with the selectivities observed for the stand-alone receptor [64] (Fig. 16).

In a more recent study, Sessler, Bielawski, and coworkers reported poly(methyl methacrylate)s (PMMA)s containing pendant calix[4]pyrroles [65]. As mentioned in the chapter on calix[n]pyrroles by Gale and Lee, these new polymeric materials were utilized in the extraction of TBAF and TBACl from aqueous media. The calix [4]pyrrole methacrylate monomer (**48**) was prepared in 84% yield from treatment of a hydroxymethyl calixpyrrole derivative with methacryloyl chloride in the presence of triethylamine (TEA). Homopolymer (**49**) was prepared via treatment of monomer **48** with 1 mol% AIBN in THF solution. The reaction was then stirred at 70°C for 17 h under nitrogen atmosphere. The resulting viscous polymer solution was precipitated by drop-wise addition into excess cold methanol, and recovered in 66% yield. Analysis using gel permeation chromatography (GPC) revealed a number-average molecular weight (M_n) of 23,600 Da (relative to PMMA standards) and a polydispersity index (PDI) of 2.3. Furthermore, this conventional free radical polymerization technique was also used to generate a calixpyrrole containing PMMA copolymer (**50**). Using GPC analysis, copolymer **50** was found to possess a M_n of 85,500 Da and a PDI of 2.1. Sessler and Bielawski concluded from the high molecular weight of **50**, compared to **49**, that the steric bulk of the calixpyrrole negatively impacted the growth of the polymer (**48**) (Fig. 17).

In an effort to explore the anion binding ability of copolymer **50** under interfacial conditions, Sessler and Bielawski utilized NMR spectroscopic techniques. Toward this end, a D₂O solution of TBAF (90 mM) was exposed to a CD₂Cl₂ solution of

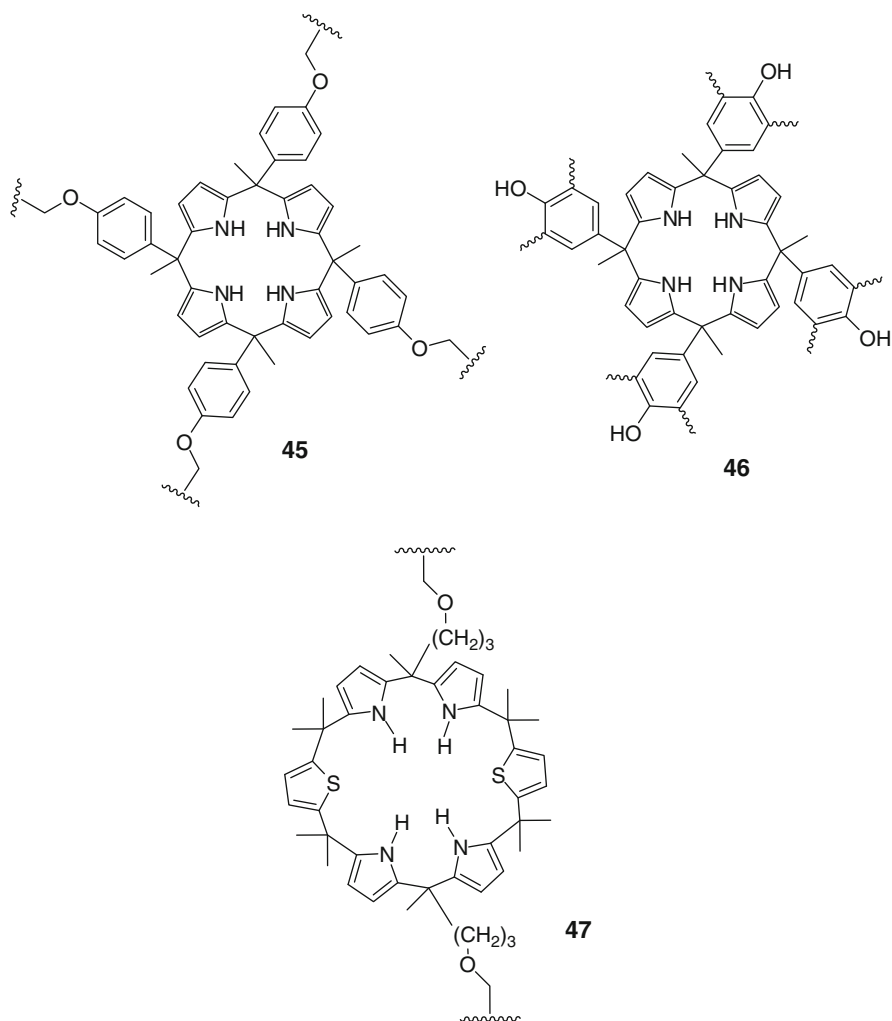


Fig. 16 Polymer resins containing calix[4]pyrrole (**45** and **46**) and calix[4]pyrrole[2]thiophene (**47**) receptors

polymer **50** (effective concentration of calixpyrrole repeat unit = 6.5 mM). The layered mixture was shaken for 20 min and then centrifuged to separate the organic and aqueous layers. Analysis of the organic layer (CD_2Cl_2) via ^1H NMR spectroscopy revealed substantial downfield shift in the pyrrole NH protons ($\Delta\text{ppm} = 0.32$ ppm), which is typically observed upon anion binding. Furthermore, peaks corresponding to the TBA^+ counter cation (at $\delta = 3.2$ ppm) were observed, confirming that both the anion (F^-) and the cation (TBA^+) were present in the organic phase. A greater downfield shift in the NH pyrrole proton signal was

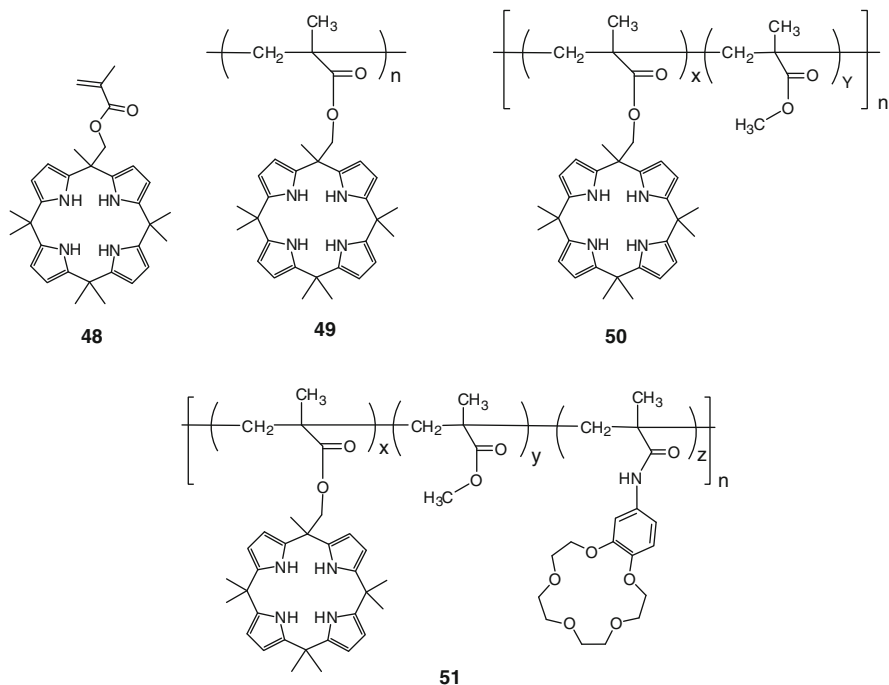


Fig. 17 Calix[4]pyrrole methacrylate monomer (**48**), calix[4]pyrrole methacrylate homopolymer (**49**), calix[4]pyrrole-*co*-methylmethacrylate polymer (**50**), and the calix[4]pyrrole-*co*-benzo-crown[5]-*co*-methylmethacrylate polymer (**51**) developed by Sessler, Bielawski, and coworkers

observed on exposure to TBACl under analogous extraction conditions and concentrations. These results are consistent with the ability of polymer **50** to extract chloride over fluoride. This selectivity runs counter to the anion affinities displayed by calix[4]pyrrole in dichloromethane [32]. However, the observed affinities are in agreement with the so-called Hofmeister bias, as chloride is a more hydrophobic anion ($\Delta G_{\text{h}} = -340 \text{ KJ mol}^{-1}$) than fluoride anion ($\Delta G_{\text{h}} = -465 \text{ KJ mol}^{-1}$) [21, 66]; chloride anion was thus expected to be extracted more readily than this latter, more hydrophilic species. Support for this rationalization came from the finding that octamethylcalix[4]pyrrole and PMMA were both capable of extracting TBACl, but 35% less efficiently than polymer **50**. In the case of TBAF only polymer **50** was capable of removing fluoride from the aqueous layer.

The results described above represent one of the first examples of a molecular receptor functionalized polymer capable of extracting anionic species from aqueous media. However, polymer **50** displayed low affinity for “hard” salts containing hydrophilic cations (e.g., K^+ and Na^+). In 2008, Sessler, Bielawski, and coworkers addressed this issue by appending benzo-[15]-crown-5-ether, a subunit known for its ability to complex cationic species [67], as a pendant group to the calix[4]pyrrole functionalized PMMA polymer backbone [68]. The resulting copolymer (i.e., **51**)

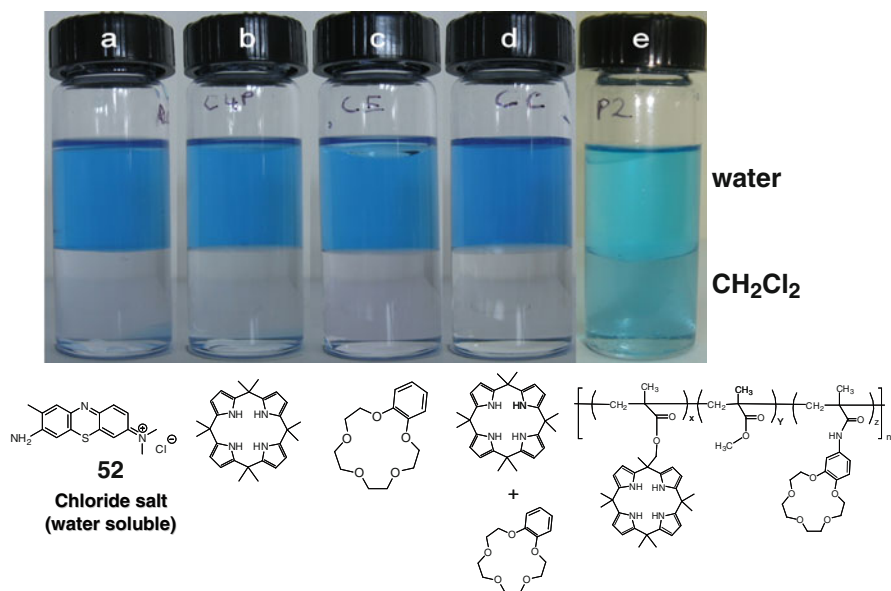


Fig. 18 Aqueous solutions of water-soluble chloride salt (**52**) after extraction with CH_2Cl_2 (bottom layer) solutions of: (a) blank with CH_2Cl_2 , (b) octamethylcalix[4]pyrrole, (c) benzo-[15]-crown-5-ether, (d) a mixture of octamethylcalix[4]pyrrole, and benzo-15-crown[5]ether (e) and polymer **51**. This figure, which originally appeared in *Angew Chem Int Ed* 2008, 47, 9648–9652 (Copyright Wiley-VCH GmbH & Co. KGaA), is reproduced with permission [68]

was prepared by the previously described free radical polymerization. Initial quantitative evidence that copolymer **51** could extract chloride salts came from a visual extraction test utilizing water-soluble dye **52** (Fig. 18). An aqueous solution of **52** was extracted with a CH_2Cl_2 solution of copolymer **51**, as well as control solutions of octamethylcalix[4]pyrrole (Fig. 18b), benzo-[15]-crown-5-ether (Fig. 18c), and a mixture of both receptors (Fig. 18d). Only the organic layer containing copolymer **51** displayed evidence of successful extraction of dye **52**, as observed by a light blue colored organic phase.

The amount of dye (**52**) removed from the aqueous layer, on exposure to copolymer **51** and control compounds, was quantified with the use of UV–Vis spectroscopy. Analysis of the aqueous layer, postextraction, confirmed that copolymer **51** was able to extract dye **52** into the organic phase 54% more effectively than octamethylcalixpyrrole, benzo-[15]-crown-5-ether, or the mixture of receptors.

The promise of the results described above led Sessler and Bielawski to explore whether or not copolymer **51** was capable of extracting two hard ions, namely KF . Thus, a 3.4 M D_2O solution of KF was exposed to a CD_2Cl_2 solution of copolymer **51** (effective concentration of the calix[4]pyrrole and crown ether repeat units 6.25 and 4.86 mM, respectively) and extracted via the previously described procedure. This resulted in the appearance of a signal at $\delta = -121.7$ ppm in the ^{19}F NMR

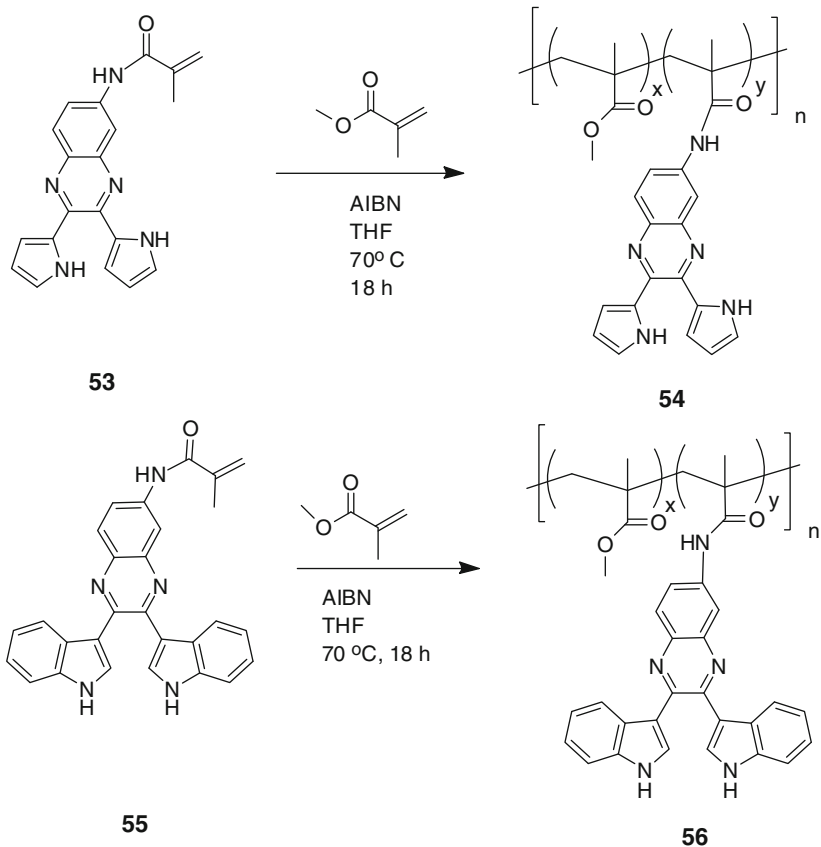
spectrum of the organic phase. The fluoride anion concentration in this phase was quantified via addition of fluorobenzene (final concentration: 14.21 mM) as an internal standard ($\delta = -114.3$ ppm) to the aforementioned extraction experiment. Comparative integration showed copolymer **51** was capable of extracting KF (7.55 ± 0.04 mM) more efficiently than copolymer **50** (5.71 ± 0.03 mM). The extraction efficiencies determined by ^{19}F NMR were further supported by flame emission spectroscopy (FES), which was used to quantify the amount of potassium extracted into the organic phase (6.84 ± 0.05 mM).

In more recent collaborative work involving the Sessler and Bielawski groups, the above strategy was applied to the development of polymeric chemosensors. In this work, quinoxaline derivatives known as DPQ and DIQ were utilized as the anion chemosensor elements. DPQs contain pyrroles appended through an α -pyrrolic position to the 5 and 6 positions of the quinoxaline. First developed by Oddo [69] in the early twentieth century, DPQs were later “rediscovered” by Sessler and coworkers in 1999 as an efficient fluorometric and colorimetric small molecule chemosensors for anions, e.g., fluoride (F^-), dihydrogen phosphate (H_2PO_4^-), etc. [70]. The 6-nitro derivative (nitro-DPQ) showed remarkable affinity and selectivity for the fluoride anion, exhibiting a binding constant of $118,000 \text{ M}^{-1}$ in dichloromethane. It also produced an easily discernible yellow-to-red color change. On the other hand, DIQ demonstrated high affinity and selectivity for dihydrogen phosphate, with the nitro derivative exhibiting a binding constant of $20,000 \text{ M}^{-1}$ in dichloromethane [71].

A two step modification was used to synthesize methacrylamide monomers of DPQ (**53**) and DIQ (**55**). Subsequently, free radical polymerization, using the previously described synthetic method, resulted in methylmethacrylate copolymers of DPQ (**54**) and DIQ (**56**) (Scheme 3). The resulting copolymers showed relatively high molecular weights (ca. 40,000 Da) and polydispersities in the order of 2.1–2.5, similar to previously observed systems.

Thin films of the DPQ polymer **54** (ratio of DPQ to MMA repeat units = 1:10; unpublished results) were prepared using Langmuir–Blodgett techniques. On exposure to HF vapors (generated from a 48% aqueous solution of HF) a colorimetric response from bright yellow to red was observed (cf. Fig 19b). After 2 min the red color began to fade (Fig. 19c), and was no longer observable after 10 min.

Likewise, thin films of copolymer **54** were prepared and used as a “dip-stick” test (i.e., direct exposure to solutions of HF). Exposure to a 48% solution of aqueous HF resulted in a drastic colorimetric change from yellow to dark purple (Fig. 19e). On exposure to a 25% aq. solution of HF a change from yellow to red was observed. However, control studies using HCl as the acid solution showed similar colorimetric changes, suggesting that the observed color changes are a result of protonation of the imine in the DPQ, rather than binding of the F^- anion. Incorporating DPQ and DIQ sensing moieties into polymeric systems allows for potential application in material-based devices, and demonstrates the tunability of this approach based on monomer selection.



Scheme 3 Free radical polymerization of DPQ (**53**) and DIQ (**55**) acrylamide monomers used to generate DPQ (**54**) and DIQ (**56**) methyl methacrylate copolymers

5 Polymers Containing Anion Receptors Conjugated to Their Main Chains

As previously mentioned, polymeric materials often provide advantages beyond those generally displayed by their constituent monomers. One such advantage, displayed by certain polymers (particularly conjugated polymers), is their ability to conduct charge. This type of conductive polymer can be used to transform a chemical signal into an easily detectable optical or electrical event [72]. The incorporation of anion receptors into such materials should facilitate sensing applications via signal amplification. With this goal in mind, it was considered useful to incorporate discrete receptors into the main-chain of covalent polymers. An excellent example of this strategy was reported by Lee et al., who in 2007 succeeded in incorporating quinoxaline receptors into a set of derivatized polyfluorene

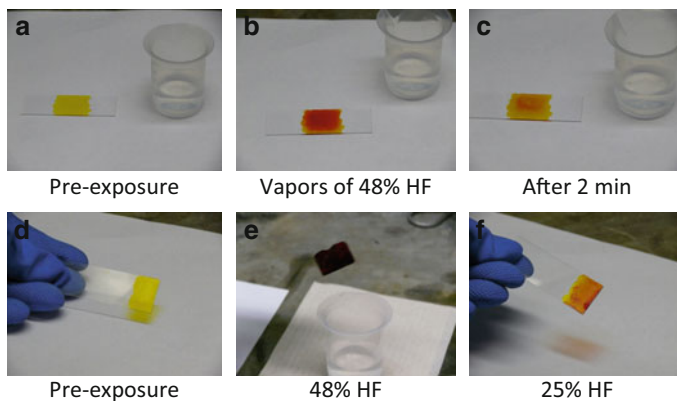
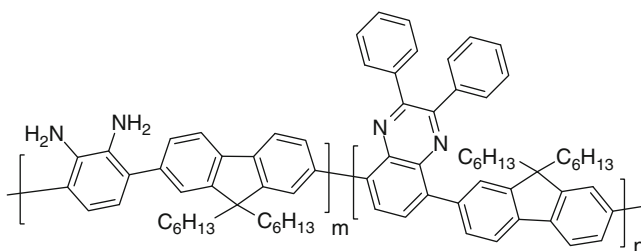


Fig. 19 Thin films of DPQ copolymer **54** as they appear upon: (a) Pre-exposure to HF vapors, (b) postexposure to 48% aq. HF vapors, (c) 2 min after exposure to 48% aq. HF vapors, (d) pre-exposure to aqueous solutions of HF (i.e., “dip-stick” method), (e) after dipping film of copolymer **54** into 48% aq. HF, and (f) after dipping a film of copolymer **54** into 25% aq. HF



57

Fig. 20 Poly[*ortho*-diaminophenylene-fluorene]-*co*-(quinoxaline-fluorene)]

copolymers (Fig. 20) [73]. The polymer in question, poly[*ortho*-diaminophenylene-fluorene]-*co*-(quinoxaline-fluorene)] (**57**), was prepared by effecting polymerization of 4,7-dibromo-2,1,3-benzothiadiazole, 9,9-dihexylfluorene-2,7-bis(trimethyleneborate), and 5,8-dibromo-2,3-diphenylquinoxaline through Suzuki coupling, followed by reduction to the *ortho*-diamino group using lithium aluminum hydride. The authors suggested that a selective interaction between the *ortho*-diamino group and the fluoride anion results not only in a colorimetric change, observable by the naked-eye, but also in fluorescence quenching as the result of a photo-induced electron transfer process (PET).

In 2008, Lee and coworkers reported a new set of azomethine-containing conjugated polymers containing fluorene and/or quinoxaline units that are closely attached to their main chains; as above, these systems, represented by canonical structures **58** and **59**, were synthesized by Suzuki-coupling reactions followed by hydrogenation and condensation with cyclohexanone (Fig. 21) [74].

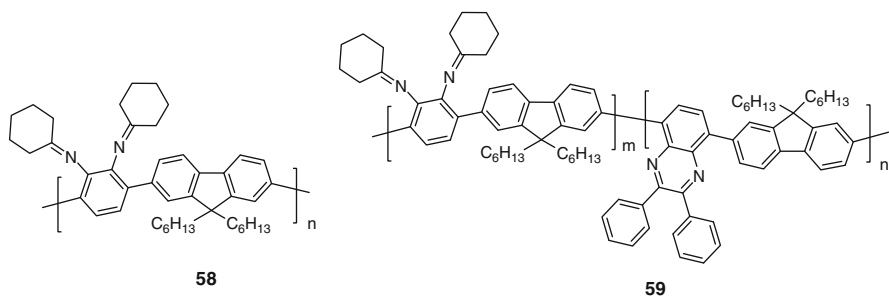


Fig. 21 Azomethine-containing conjugated polymers containing linked fluorene and quinoxaline subunits

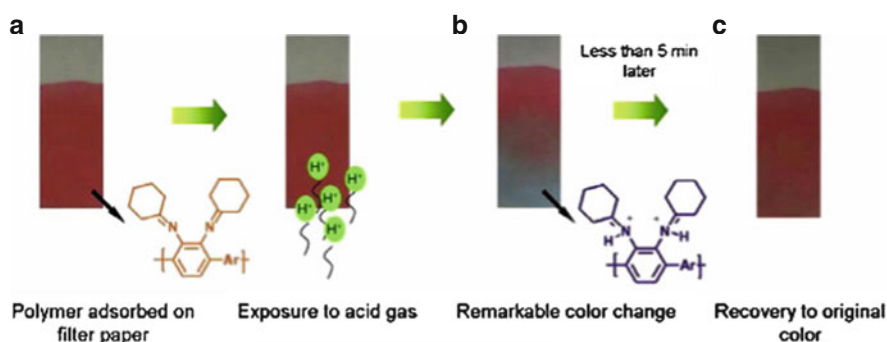


Fig. 22 Changes of polymer **58** upon exposure to acid gas in the solid state; (a) polymer **58** embedded onto filter paper (b) after exposure to acid vapors for 10 s and (c) regeneration after exposure to air for 5 min. This figure, which originally appeared in *React Funct Polym* 2008, 68, 1696–1703 (Copyright, Elsevier) is reproduced with permission [74]

Polymers **58** and **59** were used in the naked-eye detection of acid vapors. Towards this end, the polymers were deposited onto filter paper and exposed to acid vapors. This led to a dramatic color change from bright red to bluish violet (Fig. 22). This color change, which is thought to result from protonation of the imine unit, as opposed to a structural alteration, was found to be reversible, with the color fading when the deposited polymer was left exposed to air for 5 min. Protonated versions of polymers **58** and **59**, obtained by pre-exposure to TFA, were also used to prepare a set of anion-induced colorimetric sensors. Specifically, exposure of these TFA-treated polymers to iodide and acetate ions resulted in drastic chromatic changes, which allowed for naked-eye detection of these particular negatively charged species.

As previously mentioned, DPQ is a highly effective receptor for the fluoride anion, thus several groups have developed polymeric systems that rely on this quinoxaline derivative as the anion chemosensor element. Sun and coworkers

Fig. 23 DPQ-based poly(phenylene ethynylene)

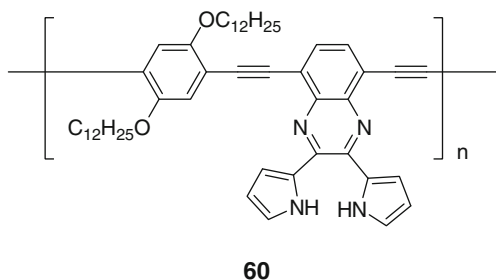
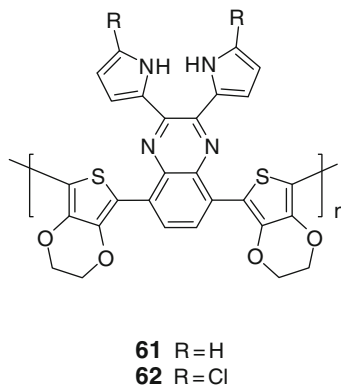


Fig. 24 Structure of DPQ-based polymers used as sensors



prepared a DPQ-containing poly(phenylene ethynylene) backbone via palladium-catalyzed Sonagashira cross-coupling reactions, producing polymer **60** (Fig. 23) [75]. These systems were found to undergo a bathochromic shift in the UV–Vis absorption spectra when exposed to TBAF in CH_2Cl_2 solution. A quenching of the fluorescence intensity was also seen.

Based on careful ^1H NMR spectroscopic titrations, Sun et al. attributed the bathochromic shift in the UV–Vis absorption spectra, as well as the fluorescence quenching, to deprotonation of one of the pyrrolic units, rather than hydrogen bonding of the pyrrolic N–H protons. From UV–Vis absorbance titrations, they were able to calculate an effective binding constant (per DPQ subunit) of $2.52 \times 10^3 \text{ M}^{-1}$ for I^- and $1.44 \times 10^3 \text{ M}^{-1}$ for pyrophosphate ($\text{HP}_2\text{O}_7^{3-}$).

Anzenbacher et al., have also prepared conjugated polymers containing DPQs. These systems were prepared from monomers of DPQ functionalized with ethylenedioxythiophenes (EDOTs) which were then electropolymerized and subsequently doped (Fig. 24) [76]. The polymeric systems prepared in this way (**61** and **62**) allow for two forms of anion sensing, namely by following the anion-induced color changes via UV–Vis absorption spectroscopy, or using a bipotentiostat to monitor the changes in current produced by the addition of anions. Polymer **61** demonstrated good affinities for the fluoride and pyrophosphate anions, yielding

effective binding constants of 48,000 and 61,100 M^{-1} , respectively. Polymer **62** is similar to **61** but contains chlorides in the α pyrrolic position of the pyrrolic subunits. The chloride modified polymer showed selectivity toward dihydrogen phosphate, exhibiting an effective per DPQ binding constant of 90,000 M^{-1} . This polymer also displayed an affinity for fluoride and pyrophosphate, although reduced compared to that displayed by the dihydrogen phosphate anion (the effective affinity constants were 24,000 and 11,000 M^{-1} for fluoride and pyrophosphate, respectively).

A somewhat different class of conjugated polymers containing neutral heterocycles as anion chemosensors was reported by Wang et al.; these researchers produced polyphenylenes copolymerized with phenol-substituted oxadiazoles (systems **65** and **66**) as efficient fluorescent sensors for fluoride anions [77]. Wang and coworkers began by first synthesizing the small molecule model compounds 2,5-bis(2-hydroxyphenyl)-1,3,4-oxadiazole (**63**) and 2-(2-hydroxyphenyl)-5-phenyl-1,3,4-oxadiazole (**64**), systems that they found to act as colorimetric and fluorescent chemosensors of F^{-} and $H_2PO_4^{-}$ (Fig. 25) [78].

It was demonstrated that **63** exhibited a high affinity for dihydrogen phosphate and fluoride anions ($K_a = 7.9 \times 10^5$ and $8.6 \times 10^4 M^{-1}$, respectively) in DMF, while **64** exhibited a slightly higher affinity for dihydrogen phosphate ($K_a = 1.8 \times 10^6$ and $4.1 \times 10^4 M^{-1}$ for $H_2PO_4^{-}$ and F^{-} ; studied as the respective TBA salts in DMF). The ability of the small molecule model systems to bind dihydrogen phosphate in organic media led to the assumption that polymeric systems would follow suit. However, contrary to this expectation, Wang et al. reported that polymers **65** and **66** (Fig. 26) exhibited higher affinities for fluoride over dihydrogen phosphate when studied in chloroform solutions (5 μM concentrations). The emission intensity of polymer **65** decreased up to 380-fold on exposure to F^{-} , which was accompanied by an emission red-shift of up to 15 nm. However, the addition of $H_2PO_4^{-}$ led to only a sixfold reduction in emission intensity (both anions studied as the respective TBA salts). The anion binding properties of **66** were similar to **65** but

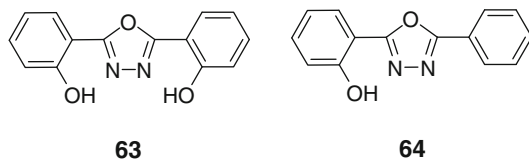


Fig. 25 Structures of oxadiazole-based small molecule chemosensors

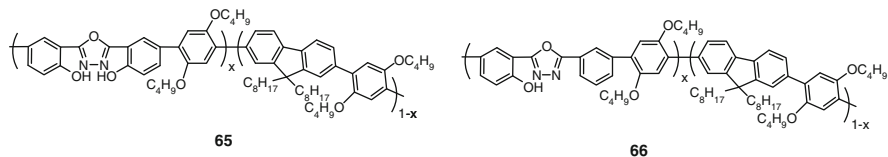


Fig. 26 Polyphenylenes containing phenol-substituted oxadiazole moieties

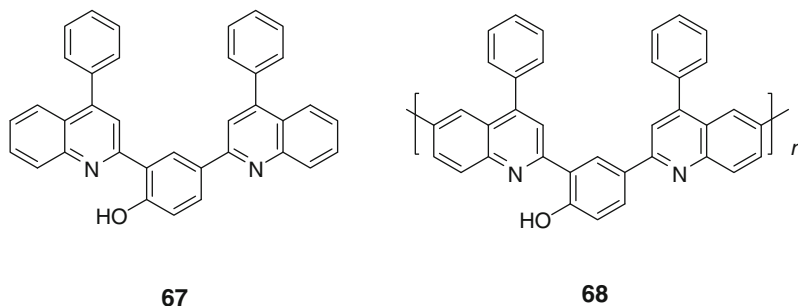


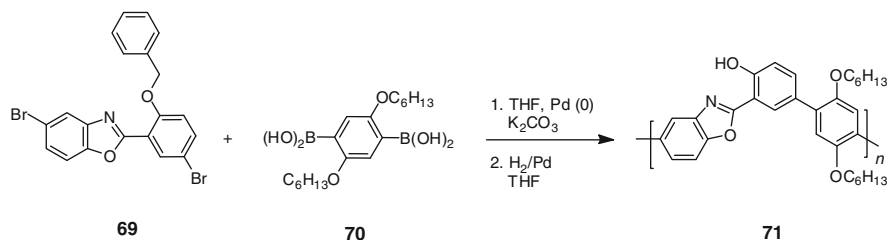
Fig. 27 Small molecule model hydroxylated diquinoline control and corresponding polymer system

significant reduction in sensitivity for F^- was observed. This latter finding was attributed to the different number of hydroxyl binding sites in each repeat unit. The more global change in affinity, namely selectivity of fluoride over dihydrogen phosphate, was ascribed to the fact that the polymers exist in coil conformations. Such structures were expected to limit access to the hydroxyl sites in the case of bulky anions such as dihydrogen phosphate, while still permitting smaller, more charge dense anions, such as fluoride, to bind. Based in part on further studies (*vide infra*) from the Wang group, it is likely that this “binding” involves at least partial deprotonation of the hydroxyl protons.

In a separate study involving conjugated fluorescent polymers as anion sensors, Wang et al. prepared hydroxyl-functionalized polyquinoline-derived macromolecules (PQOH, **68**; cf. Fig. 27) [79]. Polymer **68** was prepared via a nickel-catalyzed coupling of a methoxy-protected precursor followed by demethylation (BBr_3 followed by water) [80]. A hydroxyl-containing quinoline, **67**, was synthesized as a small molecule control.

The model compound **67** and the polymer **68** (Fig. 22) were both found to undergo naked-eye detectable color changes, as well as fluorescence “turn-on” in the presence of TBAF in DMSO. On addition of this fluoride anion salt, solutions of **67** were found to change from colorless to yellow, with even larger changes, from colorless to red, being seen in the case of polymer **68**. Other anionic species, namely chloride, bromide, and dihydrogen phosphate (all studied as their TBA salts), did not produce color changes in the case of polymer **68**. Exposure of polymer **68** to TBAF, but not to other anions, was also found to engender a new fluorescent emission peak at 620 nm. This observation is most easily rationalized in terms of the hydroxyl groups undergoing deprotonation when exposed to F^- (an anion recognized for its basicity in organic milieus) a chemical change that was expected to give rise to an intramolecular charge-transfer interaction.

Deprotonation also likely accounts for the efficacy of a set of polyhydroxybenzoxazole-based colorimetric and fluorometric chemosensors for fluoride (cf. structure **71**) introduced by the Lee group, whose other contributions are featured elsewhere in this chapter [81]. In this case, a Suzuki cross-coupling polymerization



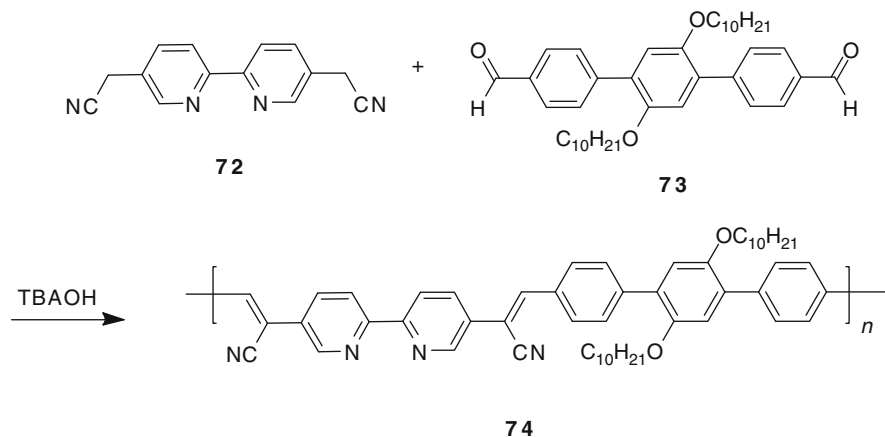
Scheme 4 Suzuki cross-coupling reaction to yield poly[2-(2'-hydroxyphenyl)benzoxazole] (**71**)

strategy was employed (Scheme 4). Specifically, palladium-catalyzed polymeric coupling of the dibromo-benzoxazole monomer (**69**) with a dialkoxyphenylene diboron acid precursor (**70**), followed by deprotection of the benzyl groups, gave rise to the desired polymer, namely poly[2-(2'-hydroxyphenyl)benzoxazole] (**71**). This polymer, a grayish-white powder with $M_n = 5,090$ Da and polydispersity of 1.56, proved soluble in most organic solvents.

Polymer **71** exhibited UV–Vis absorbance maximum at 331 nm, and on excitation at 330 nm, was characterized by fluorescence emission maxima at 414 and 518 nm (both spectra being observed in chloroform). The unique fluorometric results are attributed to excited-state intramolecular proton transfer (ESIPT) of the enol form and the excited state of a polar tautomeric keto form [82, 83]. Furthermore, naked-eye and spectroscopic analysis of polymer **71** in DMF in the presence of various anionic salts demonstrated the use of this macromolecular system as a fluoride chemosensor. Specifically, on the addition of TBAF, DMF-polymer solutions were found to undergo a naked-eye detectable shift from colorless to yellow. This process, when followed by UV–Vis spectroscopy, is characterized by the emergence of a new maximum at 420 nm. Unfortunately, Lee et al. did not quantify these results to determine binding selectivities or limits of detection.

A different class of polymeric anion chemosensors containing receptors within the main-chain is those that rely on the use of bipyridyl moieties as the anion recognition motif. An excellent example of this type of material was reported by Lee and coworkers [84]. These researchers carried out a Knoevenagel condensation of 5,5'-bis(cyanomethyl)-2,2'-bipyridine (**72**), and 2',5'-didecyloxy-*p*-terphenyl-4,4''-dialdehyde (**73**); this gave rise to a bipyridine polymer linked by cyanostyryl groups (**74**, cf. Scheme 5). This polymer proved to be a dark yellow solid with $M_w = 12,500$ Da and polydispersity of 1.47.

Lee et al. tested a number of anions against polymer **74**, including chloride, sulfate, and dihydrogen phosphate (all anions tested as their corresponding TBA salts using DMF as the solvent). However, only the hydroxide anion appeared to induce any significant colorimetric shift in the UV–Vis spectrum or fluorescent amplification. Initial fluorescence spectral analyses of polymer **74** in DMF revealed a broad emission peak at 535 nm when excitation was effected at 404 nm. On addition of TBAOH, the photoluminescence intensity increased with a strong new



Scheme 5 Bipyridine containing polymer synthesized via Knoevenagel condensation

emission peak at 480 nm and bright, blue–green fluorescence visible to the naked-eye was also observed. In the case of the UV–Vis absorption spectrum, the initial absorption maximum at 404 nm seen for **74** was found to disappear as TBAOH was titrated into the DMF solution. A blue-shift in the absorption maximum (to 354 nm) takes place, resulting in a color shift from orange to colorless. These results were rationalized in terms of changes in the electronics of the system that occur as the hydroxide anion binds to the bipyridine subunits. The authors did not report having tested fluoride or cyanide; both of these anions are relatively basic and may be capable of being bound by the bipyridine recognition sites present in polymer **74** as well.

Valijaveettil and coworkers developed a series of poly(*p*-phenylene carbazole) copolymers that enabled the colorimetric and fluorometric detection of iodide anions (Fig. 28) [85]. Carbazole is an interesting functional group for incorporating into polymers given its high thermal stability and moderately high oxidation potential [86, 87]. The polymerization reactions used to produce polymers **75–79** relied on the use of a Suzuki polycondensation process carried out in the presence of potassium carbonate, a palladium catalyst, and cetyltriethylammonium bromide (CTAB) used as the chain transfer reagent (40 mol%). Thermal gravimetric analyses of **75–79** revealed that these polymers were stable up to 390°C.

Polymers **75–79** proved to be highly fluorescent displaying quantum yields in the range of 0.58–0.78 when studied in THF; these values are significantly higher than those of typical polycarbazoles [88], and led to the consideration that these polymers could be used as fluorometric anion chemosensors. In fact, spectral changes were only observed when these systems were exposed to iodide (e.g., TBAI, LiI, NaI, and KI) among other common anions, including fluoride, chloride, bromide, nitrate, perchlorate, dihydrogen phosphate, and hydrogen sulfate (all studied as the TBA salts in THF solution). The polymers were colorless in solution; however, on addition of iodide salts a change to yellow was observed. A red shift in

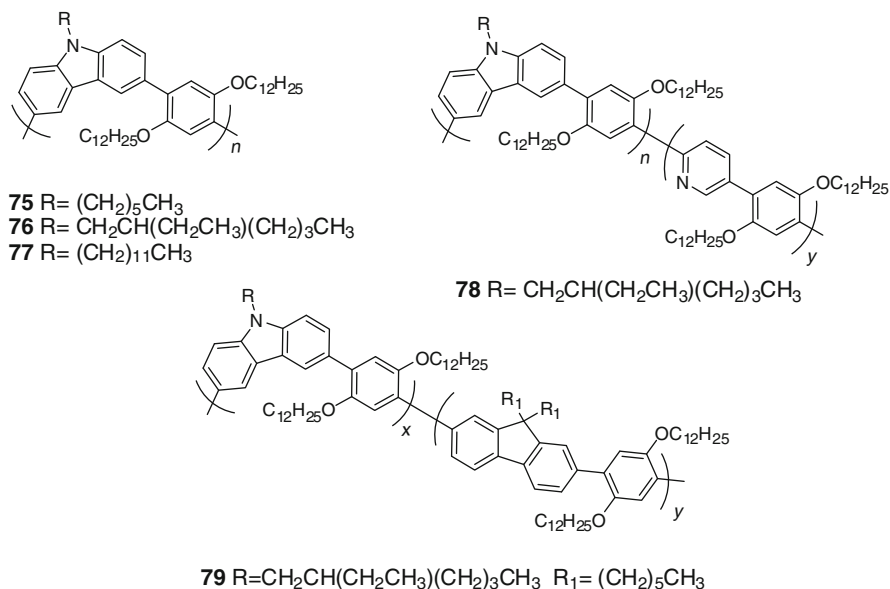


Fig. 28 Carbazole containing conjugated polymers

absorbance and emission was also observed on addition of iodide salts. The red shift in absorbance is attributed to the lower level of carbazole loading present in polymers **78** and **79**. In all cases, the nature of the iodide counter cation was found to have no influence on the observed color change.

6 Conclusions

This chapter provides a summary of polymeric systems that contain heterocyclic anion receptors. The polymeric materials covered within this chapter are diverse and cover a broad range of applications. The ability to incorporate neutral receptors (and/or charged species) into different varieties of polymers is beginning to be translated into a corresponding ability to tune the anion recognition properties of macromolecules to meet specific needs. A number of these needs were discussed, including applications involving the use of receptor-polymer combinations as additives for ion-selective membrane development, in the extraction of ions from aqueous media, and the selective sensing of anionic species. Likewise, a broad range of anion receptors, including aza-crown ethers, calix[4]pyrrole, carbazole, and quinoxalines were reviewed in the context of highlighting these applications. The anion-specific receptors can be directly blended with existing polymers as so-called “additives” to enhance material properties. Furthermore, synthetic design also allows for the incorporation of anion receptors into the polymers themselves,

either as pendant side-chains or directly included as part of the main-chain polymer backbone. The examples given in this chapter are meant to provide a general overview of the field of anion-specific polymers and provide a summary of the current state-of-the art. As such, it is expected that the present review will make it clear to the reader that there is much left to do within this fast-evolving area of materials chemistry.

Acknowledgments This work was supported by the National Institute of Health (grant GM 58907 to J.L.S.) and the Robert A. Welch Foundation (grants F-1018 and F-1621 to J.L.S. and C.W.B., respectively).

References

1. Staudinger H (1920) *Ber Dtsch Chem Ges* 53B:1073–1085
2. Staudinger H (1924) *Ber Dtsch Chem Ges* 57B:1203–1208
3. Carothers WH, Coffman DD (1932) *J Am Chem Soc* 54:4071–4076
4. Carothers WH (1934) *J Ind Eng Chem* 26:30–33
5. Urry DW, Parker TM, Reid MC, Gowda DC (1991) *J Bioact Compat Polym* 3:263–282
6. Barrera DA, Zylstra E, Lansbury PT, Langer R (1993) *J Am Chem Soc* 115:11010–11011
7. Fodor SP, Read JL, Pirrung MC, Stryer L, Lu AT, Solas D (1991) *Science* 251:767–773
8. Haab BB, Dunham MJ, Brown PO (2001) *Genome Biol* 2:1–13
9. Lehn J-M (1985) *Science* 227:849–856
10. Lehn J-M (2007) *Chem Soc Rev* 36:151–160
11. Brunsveld L, Folmer BJB, Meijer EW, Sijbesma RP (2001) *Chem Rev* 101:4071–4097
12. Bouteiller L (2007) *Adv Polym Sci* 207:79–112
13. Rieth S, Baddeley C, Badjic JD (2007) *Soft Matter* 3:137–154
14. Shimizu LS (2007) *Polym Int* 56:444–452
15. Fox JD, Rowan SJ (2009) *Macromolecules* 42:6823–6835
16. Liu H, Wang S, Luo Y, Tang W, Yu G, Li L, Chen C, Liu Y, Xi F (2001) *J Mater Chem* 11:3063–3067
17. Kim J, McQuade DT, McHugh SK, Swager TM (2000) *Angew Chem Int Ed* 39:3868–3872
18. Charra B, Calemard E, Ruffet M, Chazot C, Terrat J-C, Vanel T, Laurent G (1992) *Kidney Int* 41:1286–1291
19. Gutzwiller JP, Schneditz D, Huber AR, Schindler C, Gutzwiller F, Zehnder CE (2002) *Nephrol Dial Transplant* 17:1037–1044
20. Carey CM, Riggan WB (1994) *Anal Chem* 66:3587–3591
21. Hofmeister F (1888) *Arch Exp Pathol Pharmacol* 24:247–260
22. Umezawa Y, Kataoka M, Takami W, Kimura E, Koike T, Nada H (1988) *Anal Chem* 60:2392–2396
23. Ito T, Radecka H, Umezawa K, Kimura T, Yashiro A, Lin XM, Kataoka M, Kimura E, Sessler JL, Odashima K, Umezawa Y (1998) *Anal Sci* 14:89–98
24. Král V, Furuta H, Shreder HK, Lynch V, Sessler JL (1996) *J Am Chem Soc* 118:1595–1607
25. Lin XM, Umezawa K, Tohda K, Furuta H, Sessler JL, Umezawa Y (1998) *Anal Sci* 14:99–108
26. Sessler JL, Cyr MJ, Furuta H, Kral V, Mody T, Morishima M (1993) *Pure Appl Chem* 65:393–398
27. Shionoya M, Furuta H, Lynch V, Harriman A, Sessler JL (1992) *J Am Chem Soc* 114:5714–5722
28. Furuta H, Cyr MJ, Sessler JL (1991) *J Am Chem Soc* 113:6677–6678
29. Sessler JL, Morishima T, Lynch V (1991) *Angew Chem Int Ed Engl* 30:977–980

30. Sessler JL, Weghorn SJ, Morishima T, Rosingana M, Lynch V, Lee V (1992) *J Am Chem Soc* 114:8306–8307
31. Král V, Sessler JL, Shishkanova TV, Gale PA, Volf R (1999) *J Am Chem Soc* 121:8771–8775
32. Gale PA, Sessler JL, Král V, Lynch V (1996) *J Am Chem Soc* 118:5140–5141
33. Nishiyabu R, Anzenbacher P Jr (2005) *J Am Chem Soc* 127:8270–8271
34. Palacios MA, Nishiyabu R, Marquez M, Anzenbacher P Jr (2007) *J Am Chem Soc* 129:7538–7544
35. Le Goff T, Braven J, Ebdon L, Scholefield D (2004) *Anal Chim Acta* 510:175–182
36. Ebdon L, Braven J, Frampton NC (1990) *Analyst* 115:189–193
37. Le Goff T, Braven J, Ebdon L, Scholefield D (2002) *Anal Chem* 74:2596
38. Le Goff T, Marsh J, Braven J, Ebdon L, Scholefield D (2002) *Green Chem* 4:486–491
39. Mi Y, Mathison S, Goines R, Logue A, Bakker E (1999) *Anal Chim Acta* 397:103–111
40. Ho H-A, Boissinot M, Bergeron MG, Corbeil G, Doré K, Boudreau D, Leclerc M (2002) *Angew Chem Int Ed* 41:1548–1551
41. Chayer M, Faïd K, Leclerc M (1997) *Chem Mater* 9:2902–2905
42. Leclerc M (1999) *Adv Mater* 11:1491–1498
43. Ho HA, Leclerc M (2003) *J Am Chem Soc* 125:4412–4413
44. Zeng Q, Cai P, Li Z, Qin J, Tang BZ (2008) *Chem Commun*:1094–1096
45. Jin WJ, Fernández-Argüelles MT, Costa-Fernández JM, Pereiro R, Sanz-Medel A (2005) *Chem Commun* 883–885
46. Anzenbacher P Jr, Tyson DS, Jursíková K, Castellano FN (2002) *J Am Chem Soc* 124:6232–6233
47. Zeng Q, Zhang L, Li Z, Qin J, Tang BZ (2009) *Polymer* 50:434–440
48. Zeng Q, Lam JWY, Jim CKW, Qin A, Qin J, Li Z, Tang BZ (2008) *J Polym Sci A Polym Chem* 46:8070–8080
49. Qu Y, Hua J, Jiang Y, Tian H (2009) *J Polym Sci A* 47:1544–1552
50. Liu B, Tian H (2005) *J Mater Chem* 15:2681–2686
51. Li Y, Cao LF, Tian H (2006) *J Org Chem* 71:8279–8282
52. Kubo Y, Yamamoto M, Ikeda M, Takeuchi M, Shinkai S, Tamao K (2003) *Angew Chem Int Ed Engl* 42:2036–2040
53. Takakusa H, Kikuchi K, Urano Y, Sakamoto S, Yamaguchi K, Nagano T (2002) *J Am Chem Soc* 124:1653–1657
54. Taki M, Wolfor JL, O'Halloran TV (2004) *J Am Chem Soc* 126:712–713
55. Yang R-H, Chan W-H, Lee AWM, Xia P-F, Zhang H-K, Li K (2003) *J Am Chem Soc* 125:2884–2885
56. Coskun A, Akkaya E (2004) *Tetrahedron Lett* 45:4947–4949
57. Hu X, Huang J, Zhang W, Li M, Tao C, Li G (2008) *Adv Mater* 20:4074–4078
58. Fei Z, Geldbach TJ, Zhao D, Dyson PJ (2006) *Chem Eur J* 12:2122–2130
59. Nicolas M, Fabre B, Simonet J (1999) *Chem Commun*:1881–1882
60. Reynes O, Bucher C, Moutet J-C, Royal G, Saint-Aman E (2004) *Chem Commun*:428–429
61. Bernardo AR, Stoddart JF, Kaifer AE (1992) *J Am Chem Soc* 114:10624–10631
62. Kaledkowski A, Trochimczuk AW (2006) *React Polym* 66:740–746
63. Kaledkowski A, Trochimczuk AW (2006) *React Polym* 66:957–966
64. Sessler JL, An D, Cho WS, Lynch V (2003) *J Am Chem Soc* 125:13646–13647
65. Aydogan A, Coady DJ, Lynch VM, Akar A, Marquez M, Bielawski CW, Sessler JL (2008) *Chem Commun*:1455–1457
66. Custelcean R, Moyer BA (2007) *Eur J Inorg Chem* 1321–1340
67. Pedersen CJ (1967) *J Am Chem Soc* 89:7017–7036
68. Aydogan A, Coady DJ, Kim SK, Akar A, Bielawski CW, Marquez M, Sessler JL (2008) *Angew Chem Int Ed* 47:9648–9652
69. Oddo B (1911) *Gazz Chim Ital* 41:248–255
70. Black CB, Andrioletti B, Try AC, Ruiperez C, Sessler JL (1999) *J Am Chem Soc* 121:10438–10439

71. Sessler JL, Cho D-G, Lynch V (2006) *J Am Chem Soc* 128:16518–16519
72. McQuade DT, Pullen AE, Swager TM (2000) *Chem Rev* 100:2537
73. Kim HJ, Lee JH, Kim TH, Lyoo WS, Kim DW, Lee C, Lee TS (2007) *J Polym Sci A Polym Chem* 45:1546–1556
74. Kim HJ, Lee JH, Lee M, Lee TS (2008) *React Funct Polym* 68:1696–1703
75. Wu C-Y, Chen M-S, Lin C-A, Lin S-C, Sun S-S (2006) *Chem Eur J* 12:2263–2269
76. Aldakov D, Anzenbacher P Jr (2004) *J Am Chem Soc* 126:4752–4753
77. Zhou G, Chen Y, Wang L, Jing X, Wang F (2005) *Macromolecules* 38:2148–2153
78. Tong H, Zhou G, Wang L, Jing X, Wang F, Zhang J (2003) *Tetrahedron Lett* 44:131–134
79. Tong H, Wang L, Jing X, Wang F (2003) *Macromolecules* 36:2584–2586
80. Ma H, Jen AK-Y, Wu J, Wu X, Liu S, Shu C, Dalton LR, Marder SR, Thayumanavan S (1999) *Chem Mater* 11:2218–2225
81. Lee JK, Na J, Kim TH, Kim Y-S, Park WH, Lee TS (2004) *Mater Sci Eng C* 24:261–264
82. Ikegami M, Arai T (2000) *Chem Lett*:996
83. Tanaka K, Kumagai T, Aoki H, Deguchi M, Iwata S (2001) *J Org Chem* 66:7328
84. Kim Y-S, Lee JK, Park WH, Lee TS (2005) *Thin Solid Films* 477:100–103
85. Vetrichelvan M, Rajagopal N, Valiyaveetil S (2006) *Macromolecules* 39:8303–8310
86. Kuwabara Y, Ogawa H, Inada H, Nona N, Shirota Y (1994) *Adv Mater* 6:667–669
87. Li J, Liu D, Li Y, Lee CS, Kwong HL, Lee S (2005) *Chem Mater* 17:1208–1212
88. Iraqi A, Wataru I (2004) *J Polym Sci A Polym Chem* 42:6041–6051

Calix[n]pyrroles as Anion and Ion-Pair Complexants

Philip A. Gale and Chang-Hee Lee

Abstract This chapter covers advances in calixpyrrole chemistry and specifically in the application of these species as anion and ion-pair complexation agents over the last 5 years. Over this time, the chemistry of these easy-to-make macrocycles advanced with the discovery of the ion-pair complexation properties of calixpyrroles, in addition to the development of strapped calixpyrroles that incorporate extra hydrogen bond donors and possess higher affinities for anions than the parent macrocycle. Calixpyrroles have also been employed as anion complexants in solvent–solvent extraction and in polymers. They have also been shown to function as lipid bilayer transport agents for salts and as organocatalysts.

Keywords Anion complexation · Hydrogen bonding · Pyrrole · Receptor

Contents

1	Introduction	40
2	Synthesis	42
3	Anion and Ion-Pair Complexation	45
4	Strapped Systems	54
5	Extraction and Transport	64
6	Catalysis	68
7	Conclusions	70
	References	70

P.A. Gale (✉)

School of Chemistry, University of Southampton, Southampton SO17 1BJ, UK
e-mail: philip.gale@soton.ac.uk

C.-H. Lee

Department of Chemistry, Kangwon National University, Chun-Chon 200-701, Korea
e-mail: chhlee@kangwon.ac.kr

Abbreviation

NMR Nuclear magnetic resonance

1 Introduction

Calix[4]pyrroles (*meso*-octaalkylporphyrinogens) are a class of tetrapyrrolic macrocycle first synthesized in the late nineteenth century by Baeyer via the acid (HCl)-catalysed condensation of pyrrole and acetone [1]. Contemporaneously with Bayer, Dennstedt and Zimmermann studied this reaction using ‘Chlorzink’ as the acid catalyst [2–4]. The structure of the molecule was correctly assigned by Chelintzev and Tronov in 1916 [5–7] as a cyclic tetramer consisting of four pyrrole rings linked in the 2- and 5-positions by sp^3 -hybridized carbon atoms. These authors carried out a variety of condensation reactions with other ketones illustrating the generality of the synthesis. The synthesis was refined by Rothmund and Gage who obtained improved yields with the use of methanesulfonic acid in the synthesis in 1955 [8]. The metal complexation chemistry of porphyrinogens has been extensively explored in seminal work by Floriani and co-workers [9]. This elegant work is outside the scope of this chapter, which focuses on anion and ion-pair complexation. In 1996, Sessler and co-workers reported that *meso*-octamethylcalix[4]pyrrole **1** and tetraspirocyclohexylcalix[4]pyrrole **2** form complexes with anion both in organic solution and in the solid state [10]. Single crystal X-ray studies showed that in the absence of anions, receptor **1** adopts a so-called ‘1,3-alternate’ conformation in the solid state with pyrrole rings oriented alternatively ‘up’ and ‘down’ relative to the plane of the macrocycle. However, in the presence of tetrabutylammonium chloride, the macrocycle adopts a ‘cone’ conformation with all the four pyrrole rings directed towards the anion, binding it via four hydrogen bonds (Fig. 1). The similarity of the conformations adopted by compounds **1** and **2** in the absence and presence of anions to those adopted by the calix[4]arenes [11–13] led the authors to propose renaming the compounds ‘calix[*n*]pyrroles’

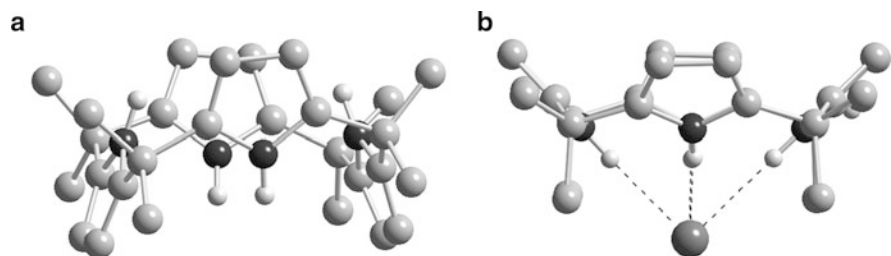
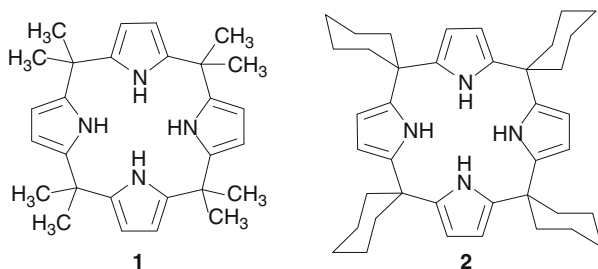


Fig. 1 The X-ray crystal structures of (a) compound **1** and (b) the tetrabutylammonium chloride complex of compound **1**. Counter cations, solvent and non-acidic hydrogen atoms have been omitted for clarity

where n is the number of pyrrole rings in the macrocycle. This analogy to calixarenes emphasized that octaalkylporphyrinogens have little chemistry in common with porphyrins with the presence of two alkyl groups on each linking *meso*-carbon rendering them relatively stable to oxidation. Indeed, quite unlike planar aromatic porphyrin macrocycles that are deeply coloured, the calixpyrroles are white colourless materials possessing a ‘three-dimensional’ coordination chemistry.



Initial solution studies with compound **1** in dichloromethane- d_2 by ^1H NMR titration techniques revealed that this compound bounds fluoride (added as the trihydrate of the tetrabutylammonium salt) selectively with a stability constant of $17,170 \text{ M}^{-1}$. Chloride and dihydrogen phosphate were also bound albeit with lower affinity (350 and 97 M^{-1} respectively).

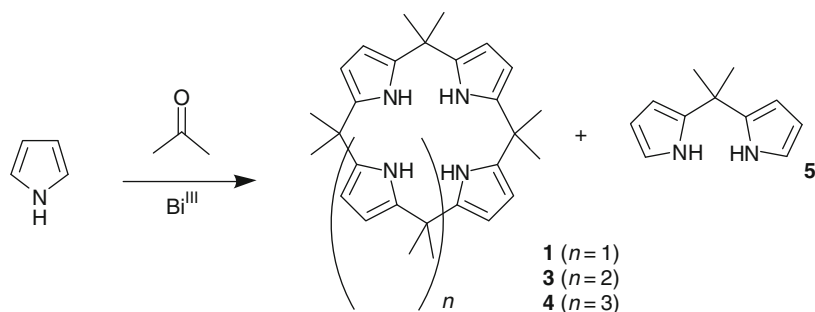
The cyclic tetramer is the thermodynamic product of the condensation reaction. Various strategies have been employed in order to access calixpyrroles containing >4 pyrrole rings. The first successful report was in 1997, in which a calix[5]arene was functionalized with five ketone groups at the lower rim and subsequent reaction with five equivalents of pyrrole in the presence of $\text{BF}_3 \cdot \text{OEt}_2$ afforded a calix[5]arene–calix[5]pyrrole pseudo-dimer in 10% yield [14]. In an elegant work, Kohnke and co-workers have converted *meso*-dodecamethylcalix[6]furan to *meso*-dodecamethylcalix[6]pyrrole by reaction with *m*-CPBA followed by zinc/acetic acid to ring open the furan rings producing α,δ -diketones which can then be ring closed with ammonium acetate to afford the cyclic pyrrolic macrocycle [15]. Other approaches include Eichen and co-workers’ use of bulky ketones to afford calix [6]pyrroles [16] and Sessler and co-workers’ use of 3,4-difluoropyrrole to allow the isolation of kinetic products including fluorinated calix[5 and 8]pyrroles [17]. The synthesis of expanded systems is still an area of interest.

Early work on the anion complexation properties of calixpyrroles has been reviewed elsewhere [18, 19]. This chapter will concentrate on the progress over the last 5 years and, in particular, on the discovery of the ion-pair complexation properties of these macrocycles, on the development of strapped systems, on the immobilization of calixpyrroles and the properties of the new materials produced and on the extraction and transport ability of these systems. We will also look at the roles calixpyrroles can play in catalysis. Hybrid calixpyrroles [20–23] containing other heterocycles or bipyroles as part of the ligand framework are outside the scope of this chapter whilst the roles calixpyrroles can play as anion sensors are covered by Pavel Anzenbacher Jr. in his chapter in this book.

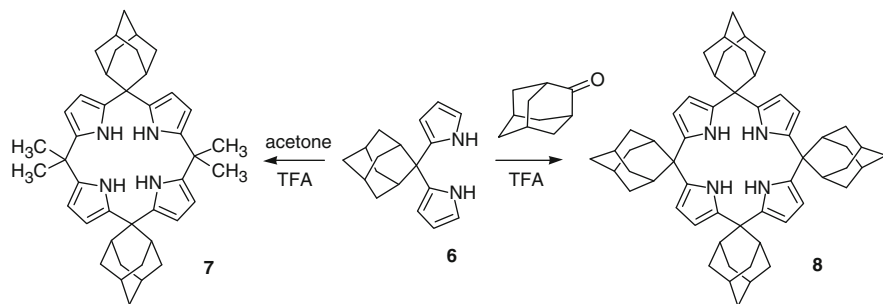
2 Synthesis

The synthesis of *meso*-octamethylcalix[4]pyrrole has been used by Shriver and Westphal as the basis for an undergraduate organic chemistry experiment [24] illustrating both the straightforward synthesis of the macrocycle and its anion-binding properties via the formation of a colourless complex with the yellow 4-nitrophenolate anion [25]. Recent advances in the synthesis of this macrocycle include microwave-assisted synthesis of calix[4]pyrroles containing hydroxamic acids [26] and azo-functionalized derivatives [27]. AmberlystTM-15 has been employed by Chauhan and co-workers as a solid acid catalyst, which can be removed from the reaction conveniently by filtration [28] whilst Kulkarni and co-workers have used molecular sieve MCM-41 as a heterogeneous catalyst for calixpyrrole synthesis [29]. Kumar and co-workers have used 1-butyl-3-methylimidazolium tetrafluoroborate ionic liquids as a medium for ytterbium(III) triflate catalysed synthesis of calix[4]pyrroles, a method that works cleanly and in high yield for a variety of alkyl and aryl functionalized systems [30]. In 2009, Chacón-García and co-workers have investigated the use of a variety of Lewis acids in the synthesis including bismuth nitrate, which affords a mixture of *meso*-octamethylcalix[4]pyrrole and *meso*-dodecamethylcalix[5]pyrrole in a 1:2 ratio (Scheme 1) [31].

Adamantane-derived calix[4]pyrroles have been reported by Mlinarić and co-workers in addition to a number of adamantane functionalized calix[4]pyrroles [32]. Calixpyrroles **7** and **8** were prepared from adamantane-dipyromethane **6** by acid-catalysed condensation with acetone or 2-adamantanone with compound **7** only being formed in low yield but macrocycle **8** formed in 38% yield (Scheme 2). Solid-state grinding with tetrabutylammonium chloride and subsequent IR and powder X-ray diffraction provided evidence for chloride complexation in the solid state. Addition of tetrabutylammonium chloride in DMSO increased the solubility of the macrocycle and an NMR comparison in DMSO-*d*₆ showed a downfield shift of the NH groups upon addition of chloride consistent with the formation of a solution complex. Unfortunately, solubility problems prevented the determination of stability constants via ¹H NMR titration methods.



Scheme 1 Products obtained by the reaction of pyrrole and acetone in the presence of a range of bismuth (III) salts



Scheme 2 Synthesis of calix[4]pyrroles **7** and **8**

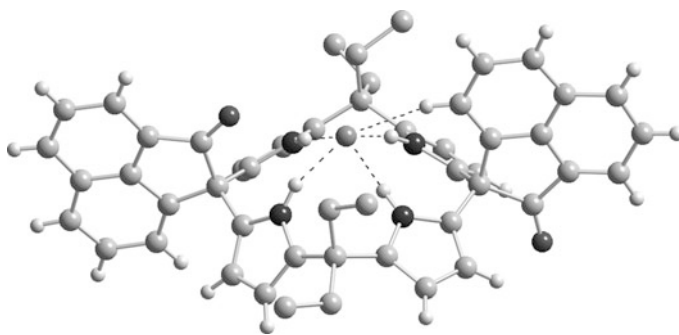
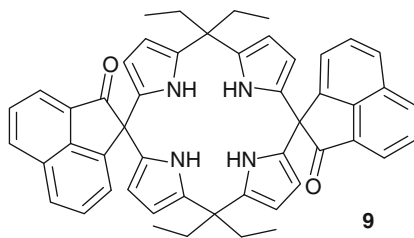
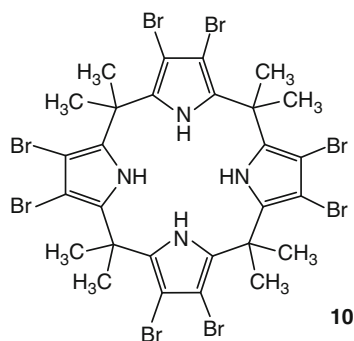


Fig. 2 X-ray crystal structure of the fluoride complex of compound **9**. Counter cations and certain non-acidic hydrogen atoms have been removed for clarity

Cheng and co-workers have also published the synthesis of calix[4]pyrroles containing bulky substituents at the *meso* position with the synthesis of an acenaphthenequinone-based macrocycle **9** [33]. The authors crystallized the tetrabutylammonium fluoride complex of this receptor and elucidated the crystal structure (Fig. 2). Interestingly, the authors found an aromatic $\text{CH}\cdots\text{F}^-$ hydrogen bond from one of the acenaphthenequinone groups in addition to the four pyrrole $\text{NH}\cdots\text{F}^-$ interactions. Stability constant determinations using UV/vis titration techniques in dichloromethane showed that receptor **9** binds fluoride with a stability constant of $6.6 \times 10^4 \text{ M}^{-1}$ and chloride with a stability constant of $5.4 \times 10^3 \text{ M}^{-1}$.

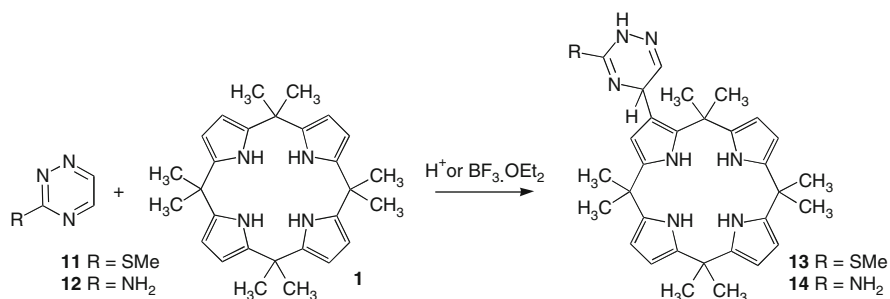


Calix[4]pyrroles functionalized at a pyrrole CH position [34] are attractive synthetic goals as the substituents can modulate the affinity of the calixpyrrole for anionic guests [35], act as a reporter group [36] or provide a point of attachment for immobilization of the macrocycle [37]. One of the first examples studied in terms of the effect of the substituents on anion-binding affinity was octabromo-*meso*-octamethylcalix[4]pyrrole **10** [38]. This compound was shown to have an enhanced affinity for anions in CD_2Cl_2 as compared to parent macrocycle **1**. Sarker and co-workers have refined Sessler's method of preparation [38] with a route that circumvents the need for purification of this material by column chromatography [39, 40].



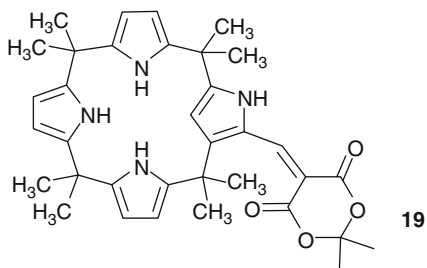
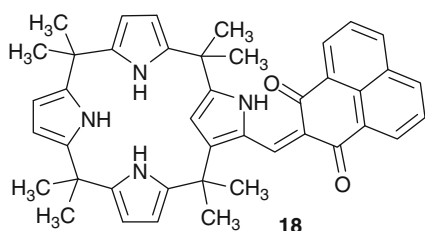
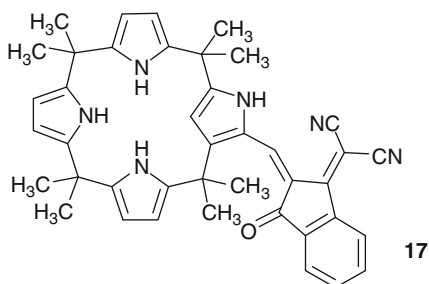
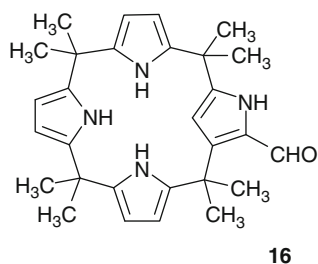
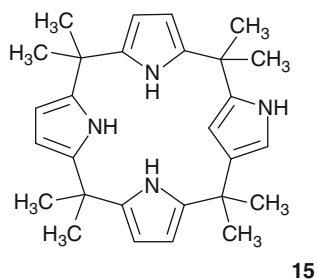
Chupakhin and co-workers have reported the first example of direct heterylation of a calix[4]pyrrole. Reaction of protonated 3-methylthio- (**11**) and 3-amino-1,2,4-triazines (**12**) with compound **1** in CF_3COOH gave adducts **13** and **14** (Scheme 3) [41].

The synthesis of *N*-confused calix[4]pyrrole **15** was first reported by Dehaen and co-workers in 1999 [42, 43]. Confused calixpyrroles are calixpyrrole macrocycles in which one or more of pyrrole rings are linked via the 2- and 4- positions rather than the 2- and 5- positions. They are formed during the condensation reaction and can be separated from 'regular' calixpyrroles via column chromatography. In 2007, Dehaen, Gale and co-workers reported the formylation of compound **15** with the



Scheme 3 Synthesis of calix[4]pyrroles **13** and **14**

Vilsmeier reagent. The resulting aldehyde **16** can undergo reactions with active methylenes, leading to coloured derivatives **17–19** [44]. In another elegant work, Dehaen and co-workers have shown that azo-functionalized *N*-confused calix[4]pyrroles can function as anion sensors via changes in their UV/vis spectrum [45], whilst Anzenbacher and co-workers have synthesized chromogenic *N*-confused calix[4]pyrroles with azo and tricyanoethenyl derivatives at the α -position for use as colorimetric anion sensors [46].



3 Anion and Ion-Pair Complexation

The discovery reported in 1996 [10] that calix[4]pyrroles bind anionic species has led on to a renaissance in the chemistry of these easy-to-make macrocycles with reports of the use of these compounds in a variety of anion receptors, sensors

and transport agents. In 2005, Moyer, Sessler, Gale and co-workers reported that *meso*-octamethylcalix[4]pyrrole **1** functions as an ion-pair receptor in solution and in the solid state [47]. The authors crystallized solid-state complexes of compound **1** with a variety of caesium salts (fluoride, chloride, bromide). Additionally, carbonate and ethyl carbonate complexes were obtained by crystallizing the receptor from a solution of caesium hydroxide in ethanol/dichloromethane. In all the cases, the caesium cation was observed to reside in the ‘cup’ of the calix[4]pyrrole–anion complex. The authors also crystallized a number of commercially available 1,3-dialkylimidazolium halide salts with compound **1** and found again that the large charge diffuse cation resides in the calix[4]pyrrole–anion complex cup in the solid state (Fig. 3). Initial studies in solution by ^1H NMR in a variety of different solvents also provided evidence for cation inclusion in solution, in the case of both the caesium and imidazolium salts.

Gale and co-workers subsequently showed that *N*-ethylpyridinium (EtPy) salts bind to compound **1** in a similar fashion with the pyridinium cation residing in the calixpyrrole–anion complex cup [48, 49] and that ^1H NMR titrations in dichloromethane- d_2 with a variety of chloride and bromide salts (tetra-*n*-butylammonium (TBA), 1-ethyl-3-methylimidazolium (EMIM), 1-butyl-3-methylimidazolium (BMIM) and EtPy) gave very different results as the cation was changed with NH shifts increasing in the order TBA < EMIM < BMIM < EtPy. The authors attributed these findings to compound **1** acting as an ion-pair receptor in solution. Similar behaviour has been observed with *N*-confused calixpyrroles [50].

The finding that calix[4]pyrrole can function as an ion-pair receptor, coupled with apparent disparities in solution phase binding data acquired by different groups [51], led Sessler, Schmidtchen, Gale and co-workers to re-examine the chloride-binding properties of compound **1** in solution using a combination of ^1H and isothermal titration calorimetry (ITC) techniques [52]. The previous

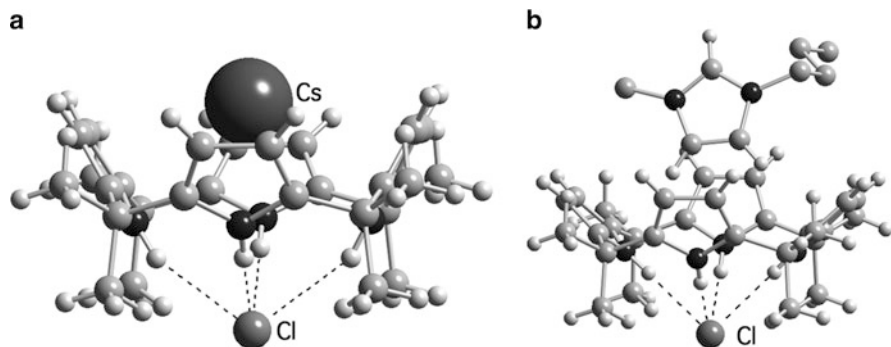
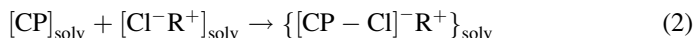


Fig. 3 The X-ray crystal structures of the CsCl (*left*) and 1-butyl-3-methylimidazolium chloride (*right*) complexes of compound **1**. Certain hydrogen atoms and solvent molecules have been omitted for clarity

assumption that calix[4]pyrrole acts as a simple anion receptor (**1**) was re-examined and the authors considered solvation and ion-pairing effects (2).



The authors studied the interaction of **1** with a variety of different chloride salts (tetraethylammonium (TEA), tetrapropylammonium (TPA), TBA, tetrabutylphosphonium (TBP) and tetraphenylphosphonium (TPhP)). The authors found that stability constants were dependent on the solvent used; however, a correlation between the binding behaviour and the permittivity, polarizability, dielectric constant, donicity or acceptor strength of the solvent could not be found. The authors found that the effect of the counter cation was generally small but in some cases can be significant. This was particularly true in dichloromethane in which TBA Cl is not well behaved in terms of clean 1:1 receptor:anion complex formation. NMR titration in dichloromethane- d_2 showed a 100-fold decrease in affinity when switching from TEA to TBA Cl. The authors proposed that in this solvent the size and charge density of the counter cation have a substantial effect on the stability of the ion pair formed by the cation binding to the calixpyrrole cup-shaped cavity formed by the chloride complex. These effects would be masked when moving to a more highly solvating solvent and hence would not be reflected in observable changes in the stability constant for anion complexation. This was found to be the case in DMSO solution by both NMR and ITC. A further study by the same groups showed that methyltrialkylammonium salts are bound especially strongly in halogenated solvents [53]. Crystal structure analysis of a number of such complexes including the complex of compound **1** with methyltributylammonium (MTBA) chloride (Fig. 4) showed the methyl group oriented into the calix[4]pyrrole cup. Stability constant determinations by ITC with MTBA Cl in dichloromethane at 298 K revealed a stability constant of $1.5 \times 10^5 \text{ M}^{-1}$ as compared to 4.3×10^2 for TBA Cl.

As mentioned above, Sessler and co-workers have synthesized fluorinated calix [4,5 and 8]pyrroles [17]. By using tetrabutylammonium chloride as a template and

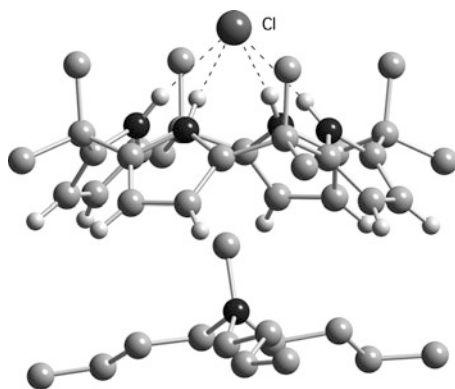
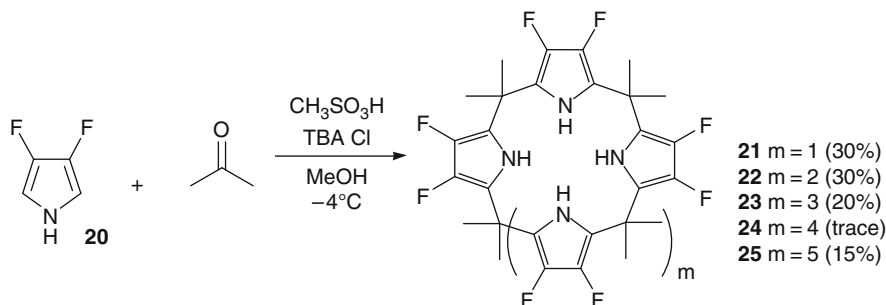
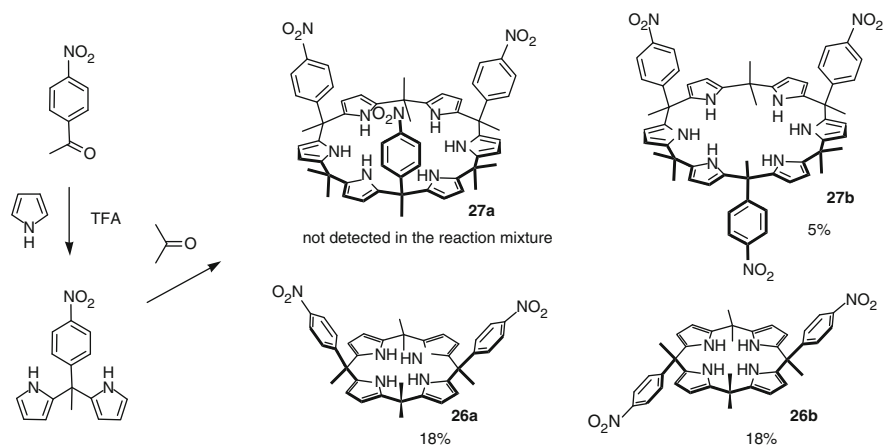


Fig. 4 The X-ray crystal structure of **1**. MTBA-Cl. Dichloromethane, certain hydrogen atoms and disorder have been removed for clarity



Scheme 4 Synthesis of fluorinated calix[n]pyrroles ($n = 4$ –8). The numbers in parentheses are isolated yields



Scheme 5 Synthesis of nitrophenyl-functionalized calix[4]pyrroles **26a** and **26b** and calix[6]pyrrole **27b**

conducting the condensation at low temperature, Sessler was able to isolate the range of fluorinated calix[n]pyrroles with $n = 4$ –8 (Scheme 4) and determine their stability constants with a range of anionic guests [54]. Sessler found that the octafluorinated calix[4]pyrrole **21** shows higher affinities for a range of anions than compound **1** in acetonitrile or DMSO as determined by ITC, presumably because of the presence of the electron-withdrawing substituents increasing the acidity of the pyrrole NH groups. Receptor **25** showed significantly higher affinity for larger anions than receptor **21**. For example, bromide was bound by receptor **25** with a stability constant of $1,10,000 \text{ M}^{-1}$ in acetonitrile whilst compound **21** binds this anion with a stability constant of $3,400 \text{ M}^{-1}$. Similarly, acetate is bound with a stability constant of $10,00,000 \text{ M}^{-1}$ by compound **25** and $3,50,000 \text{ M}^{-1}$ by compound **21**.

Kohnke and co-workers have reported the synthesis of 4-nitrophenyl-functionalized calix[4]pyrroles and a calix[6]pyrrole as shown in Scheme 5 by cyclization of 5-methyl-5-(4-nitrophenyl)dipyrromethane with acetone in the presence of

trifluoroacetic acid to afford the $\alpha\alpha$ -calix[4]pyrrole isomer **26a** in 18% yield, the $\alpha\beta$ -isomer **26b** in 18% yield and calix[6]pyrrole **27b** in 5% yield [55]. The authors found that compounds **26a** and **26b** showed modulated affinities for chloride and fluoride compared to compound **1**. For example, in dry CD_2Cl_2 compounds **1**, **26a** and **26b** bound fluoride with stability constants of $1.7 \times 10^4 \text{ M}^{-1}$, $8.4 \times 10^5 \text{ M}^{-1}$ and $1.2 \times 10^5 \text{ M}^{-1}$, respectively whilst chloride was bound with stability constants of 350, 2,300 and 163 M^{-1} , respectively. NMR studies with calix[6]pyrrole **27b** showed that the receptor has a lower affinity for chloride than the parent *meso*-dodecamethylcalix[6]pyrrole **4** with stability constants ca. $2 \times 10^5 \text{ M}^{-1}$ for **27b** and Cl^- and ca. 10^7 M^{-1} with compound **4**. However, interestingly, ^1H NMR experiments at -50°C in dry CD_2Cl_2 show two sets of peaks in a 1:2 ratio corresponding to chloride binding to the two faces of the receptor with stronger binding to the face containing the two nitroaromatic groups.

The authors also studied the complexation properties of compound **26a** with a variety of hydroxybenzoic acids and benzenedicarboxylic acids **28–33** as potential components of pH-controlled molecular switches or as templates that could (in bis-anionic form) induce the assembly of molecular capsules [56]. For example, ^1H NMR studies of **26a** in CD_3CN were conducted in the presence of one equivalent of 3-hydroxybenzoic acid **29** in the absence, presence of one equivalent and presence of ten equivalents of DBU. NMR studies indicated that in the presence of one equivalent of DBU, deprotonation of the carboxylate group would occur which would bind to the calixpyrrole NH hydrogen-bonding array. However, in the presence of ten equivalents of DBU, deprotonation of the less acidic phenolate group would occur and the phenolate O-atom would then hydrogen bond to the NH groups (Fig. 5), so switching the orientation of the anionic guest in the receptor. When a similar experiment was conducted with 4-hydroxybenzoic acid **28**, in the presence of excess base, a molecular capsule would form with the dianion bridging between two calixpyrroles. The crystal structure of such a capsule formed by isophthalate **31** complexation by receptor **26a** was elucidated (Fig. 6).

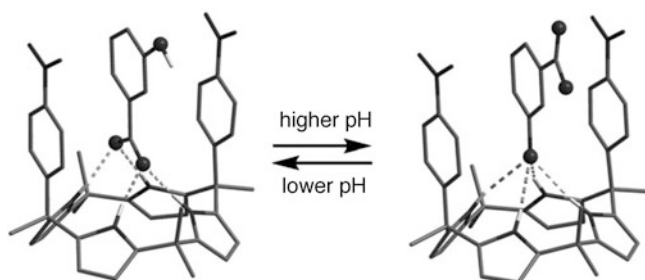


Fig. 5 The topological switch for binding 3-hydroxybenzoic acid anions as a function of pH. Reproduced with permission from Chem Eur J 2008, 14, 11593. Copyright 2008 Wiley-VCH

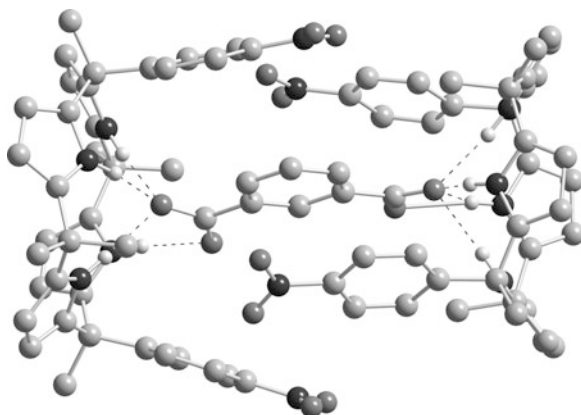
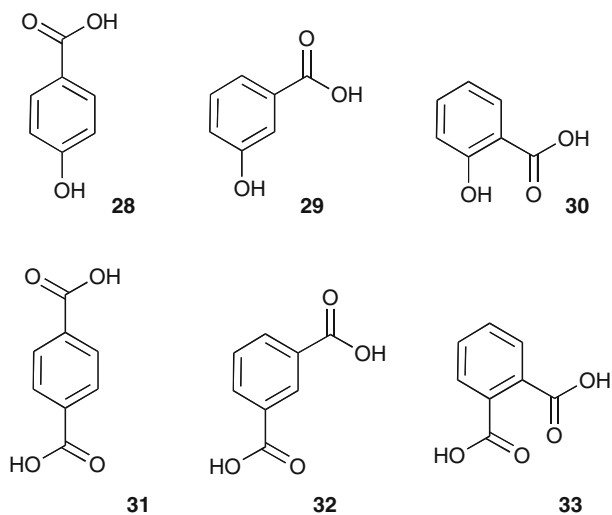
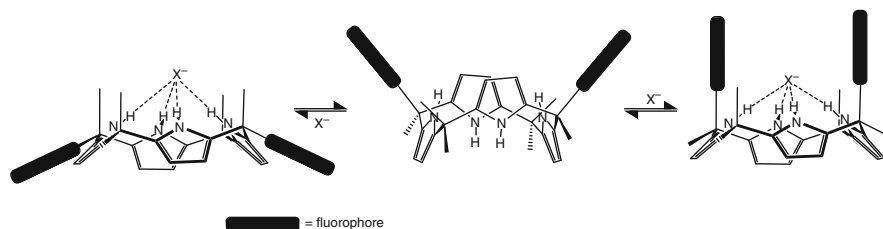


Fig. 6 The X-ray crystal structure of the isophthalate complex of receptor **26a**

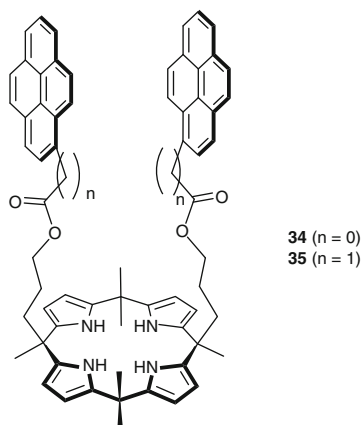


Lee and co-workers have synthesized and studied the anion-binding behaviour of calix[4]pyrroles bearing appended fluorophores at the *meso* positions on one side of the calix[4]pyrrole [57]. The spatial orientation of the *meso* substituents undergoes a dramatic change upon anion complexation (Scheme 6).

If two or more fluorophores are introduced at the *meso* positions of the calix[4]pyrrole (**34** and **35**), the conformational rearrangement could potentially be used to change the fluorescence properties of the molecule as a whole. The effect will be enhanced when auxiliary hydrogen-bonding donor sites are introduced into the linker arm.



Scheme 6 Idealized conformational changes of fluorophore-appended calix[4]pyrrole that are expected to occur upon anion binding



The study indicated that these receptors act as hosts that exhibit a selective increase in their fluorescence intensity upon the addition of Pb^{2+} or Cu^{2+} . When excess chloride anion is added after subjecting the host to pre-complexation with Pb^{2+} , the cation-induced enhancement in fluorescence is sustained. No changes in fluorescence are observed when the calix[4]pyrrole host is first treated with chloride anion, followed by the addition of Pb^{2+} . These results are consistent with pre-complexation of Pb^{2+} not serving to inhibit the binding of chloride anion, while in contrast the initial interaction between a chloride anion and the calix[4]pyrrole cavity acts to inhibit the subsequent binding of Pb^{2+} , possibly due to anion binding based constraints on the conformational flexibility of the receptors.

Sessler and co-workers have described the synthesis of a calix[4]pyrrole–crown-6-calix[4]arene pseudo-dimer **36** and studied its caesium fluoride ion-pair complexation properties [58]. Crystals of the CsF complex of **36** were obtained by slow evaporation of a chloroform/methanol solution of the receptor in the presence of excess caesium fluoride. The structure (shown in Fig. 7) reveals the caesium cation bound to the calix-crown group whilst the calix[4]pyrrole complexes fluoride. A methanol molecule is hydrogen bonded to the bound fluoride. There is a significant separation between the bound solvent-separated ion pair of 10.92 Å. In CDCl_3 solution, addition of tetrabutylammonium fluoride caused changes in the ^1H NMR

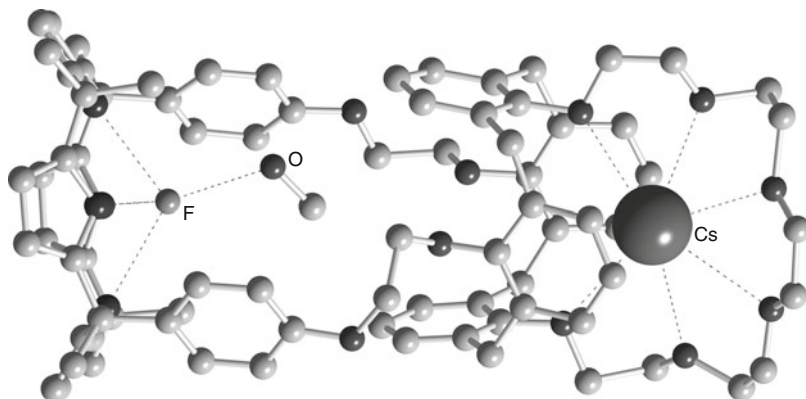
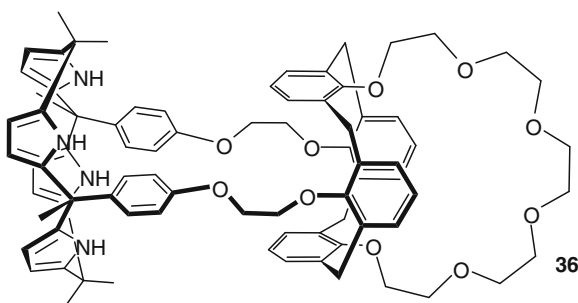
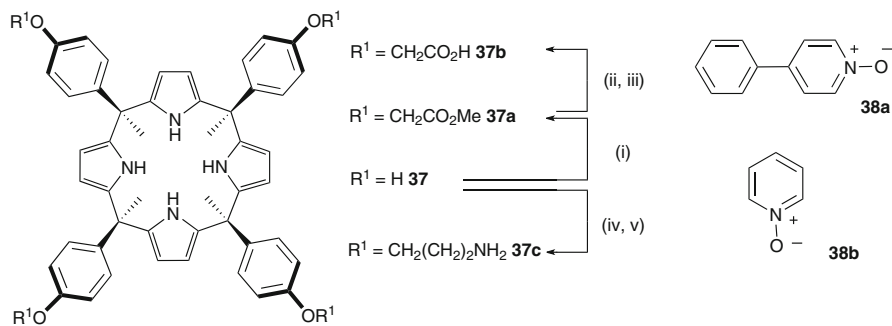


Fig. 7 A view of the **36** CsF complex showing fluoride bound to the calixpyrrole moiety and caesium bound in the calix crown with an anion–cation separation of 10.92 Å

spectrum consistent with fluoride complexation. Other tetrabutylammonium halide salts had no effect. Presumably, this selectivity is due to the less accessible and more rigid calix[4]pyrrole binding site as compared to compound **1**. Very different behaviour was observed in 10% (v/v) CD₃OD in CDCl₃. No change in the NMR spectrum was observed upon addition of five equivalents of tetrabutylammonium fluoride to the receptor in this solvent mixture. This is due to the higher degree of solvation of fluoride by methanol under these conditions. However, addition of CsF lead to significant changes to the NMR spectrum consistent with Cs⁺ binding to the calix crown and F⁻ binding to the calixpyrrole. Thus, fluoride binding is influenced by the presence of Cs⁺.



In an elegant work, Ballester and co-workers have shown that extended cavity calix[4]pyrroles **37a–37c** function as receptors for pyridine *N*-oxides **38a** and **38b**. By appending carboxylate and amine groups to extended cavity calixpyrrole **37**, (Scheme 7) Ballester rendered derivatives **37b** and **37c** water-soluble. Stability constants with 4-phenylpyridine *N*-oxide and pyridine *N*-oxide were measured in CD₃CN and D₂O by a combination of ¹H NMR and UV/vis titration techniques. The results (Table 1) show that compounds **37b** and **37c** form particularly stable complexes with both pyridine *N*-oxides in water, driven by a combination of



Scheme 7 Synthesis of receptors **37a–37c** and structures of pyridine *N*-oxide guests **38a** and **38b**. Reaction conditions: (i) $\text{BrCH}_2\text{COOMe}$, K_2CO_3 , DMF; (ii) LiOH , H_2O ; (iii) H^+ ; (iv) 3-bromopropylphthalimide, NaH ; (v) NH_2NH_2

Table 1 Stability constants (M^{-1}) for 1:1 complexes of pyridine *N*-oxides **38a** and **38b** with receptors **37a**, **37b** and **37c**. Determined in D_2O and CD_3CN

Receptor	K_a (M^{-1}) in CD_3CN	K_a (M^{-1}) in D_2O
Guest	38a ; 4-Phenylpyridine <i>N</i> -Oxide	
37a	$>10^{4a}/(1 \pm 0.4) \times 10^{4b}$	– ^c
37b	$(2.9 \pm 0.3) \times 10^{3a}/(2 \pm 0.4) \times 10^{3b}$	$(2.4 \pm 1.3) \times 10^{3a}$
37c	– ^c	$(1.5 \pm 0.2) \times 10^{3a}$
Guest	38b ; Pyridine <i>N</i> -Oxide	
37a	$>10^{4a}/(2.9 \pm 0.2) \times 10^{4b}$	– ^c
37b	$>10^{4a}/(2.5 \pm 0.2) \times 10^{4b}$	$>10^{4a}/(1.6 \pm 0.2) \times 10^{4b}$
37c	– ^c	$>10^{4a}/(2.0 \pm 0.2) \times 10^{4b}$

^a¹H NMR titration

^bUV–vis titration

^cNot soluble

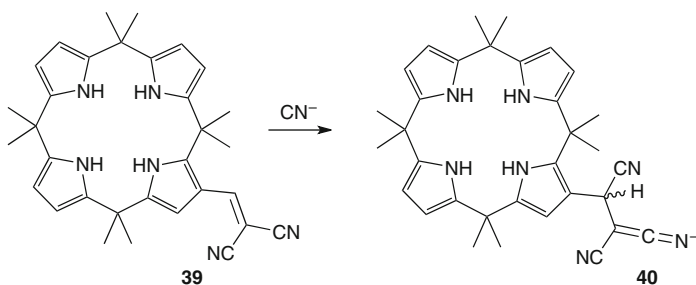
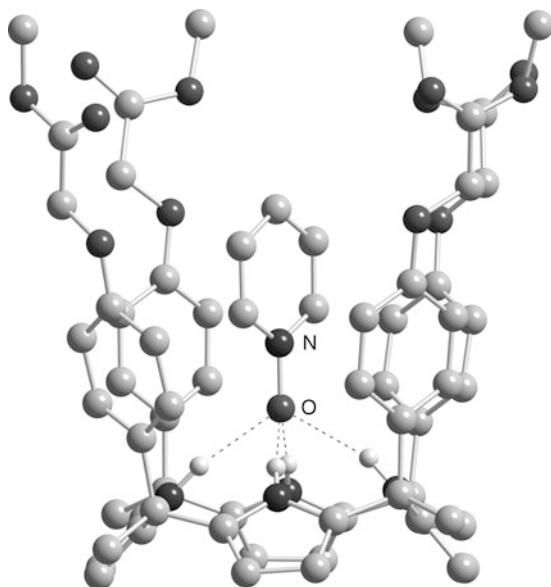
hydrogen-bonding and hydrophobic interactions. The crystal structure of the complex between receptor **35a** and pyridine *N*-oxide was elucidated confirming inclusion of the zwitterionic guest in the calixpyrrole extended cavity (Fig. 8). Ballester and co-workers have also recently reported the assembly of a calix[4]pyrrole resorcinarene hybrid into a hexameric capsule with TMA Cl [59].

Danil de Namor and co-workers have also studied the anion and ion-pair complexation properties of extended cavity calix[4]pyrroles in a series of detailed studies [60–64].

Most recently, Lee and co-workers have found that the dicyanovinyl-substituted calix[4]pyrrole **39** position is an excellent ratiometric sensor for cyanide anion in the presence of other anions [65]. The yellow colour of the receptor **39** is completely bleached only upon the addition of cyanide anion forming the adduct **40** (Scheme 8).

This result shows that a calixpyrrole-based chemodosimeter can be designed and that such systems are selective for the cyanide anion. The anion-binding sites present in **39** could play a role in reducing the effective concentration of inhibitory anions during the ratiometric detection of cyanide anion (Fig. 9).

Fig. 8 X-ray crystal structure of the inclusion complex **38b** **37a**. Non-acidic hydrogen atoms are omitted for clarity



Scheme 8 Cyanide sensing by compound **39**

4 Strapped Systems

Until 2002, most of the modifications of calix[4]pyrrole skeleton focused on the functionalization of the β -pyrrolic or *meso* positions. Although such peripheral modifications are easy to achieve, the compounds produced have inherent limitations in the enhancement of binding affinity and selectivity. Even the introduction of highly electron-withdrawing fluorine substituents at the eight β -pyrrolic positions, improves the binding affinity by less than a factor of 10 [17, 54]. Thus, new

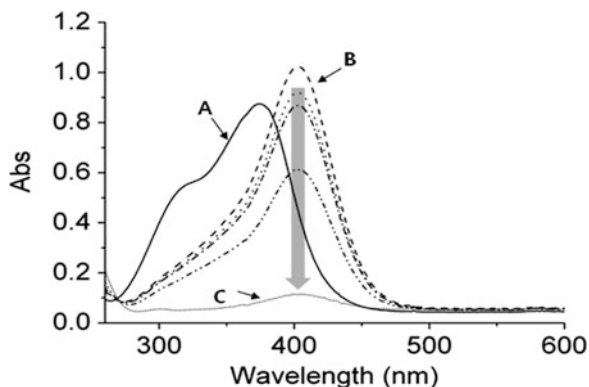
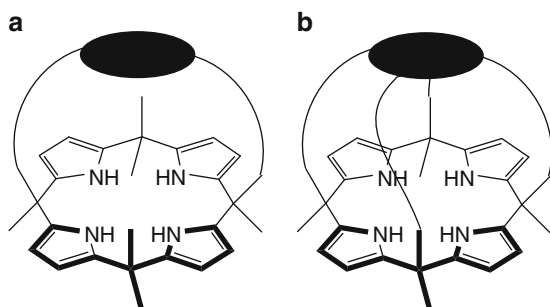


Fig. 9 Time dependent UV–vis spectral changes of host **39** (41.2 μM) seen upon the addition of 20 equivalents of cyanide anion in $\text{CH}_3\text{CN}/\text{DMSO}$ (3%). (A) free host **39** only, (B) after 10 s upon addition of 20 equiv. of cyanide anion, (C) after 19 min. upon addition of 20 equiv. of cyanide anion

Fig. 10 Schematic representations of (a) strapped calixpyrrole and (b) capped calixpyrrole



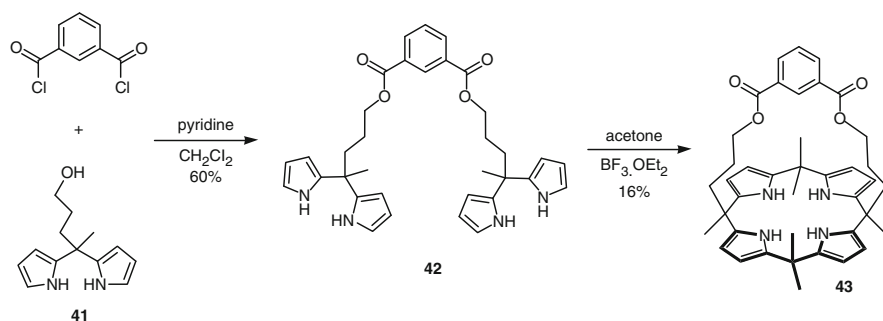
methods are necessary to access calixpyrrole-based receptors with improved affinity and selectivity. As shown in Fig. 10, one of the most effective ways of achieving these goals is to impose spatial isolation of binding domain by introducing various straps on one side of the calixpyrrole macrocycle. The partially protected cavity can effectively inhibit guest–solvent interactions.

The isolation of the binding domain from the solvent matrix imparts a number of advantages in terms of substrate recognition. Firstly, it can serve to enhance the affinity for a targeted guest or substrate by reducing guest–solvent interactions. Secondly, the modifications needed to effect such isolation usually produce binding domains of controlled size and shape that generally give rise to greater inherent selectivity. Thirdly, these structural variations can be used to lock the conformation of calixpyrroles into those that are favourable for anion binding. Such conformational ‘locking’ would, thus, be expected to contribute to enhance the binding affinities. Strapped or capped systems have an inherent advantage over deep cavity

systems in that the pre-organization of the central binding domain may be better controlled. In particular, the use of a diametrically crossed strap is expected to create a well-defined binding domain, while manipulation of the strap length allows the size of the resulting ‘pocket’ to be adjusted more completely. This should translate into enhanced selectivity.

The first pre-organized calix[4]pyrrole system, so-called ‘strapped calixpyrroles’, appeared in 2002 [66] and the new receptors indeed exhibited enhanced affinities and selectivities for anions.

The synthesis of host **43** was accomplished in three steps (Scheme 9). The condensation of 5-hydroxy-2-pentanone with pyrrole in the presence of an acid catalyst afforded the corresponding dipyrromethane **41**. The reaction of isophthaloyl dichloride with two equivalents of **41** gave **42**. Subjecting this latter acyclic precursor to acid-catalysed condensation with acetone then afforded desired product **43** in 16% yield. A crystallographic analysis of **43** revealed that the calix[4]pyrrole core exists in a twisted, 1,3-alternate conformation (Fig. 11).



Scheme 9 Synthesis of diester-strapped calix[4]pyrrole **43**

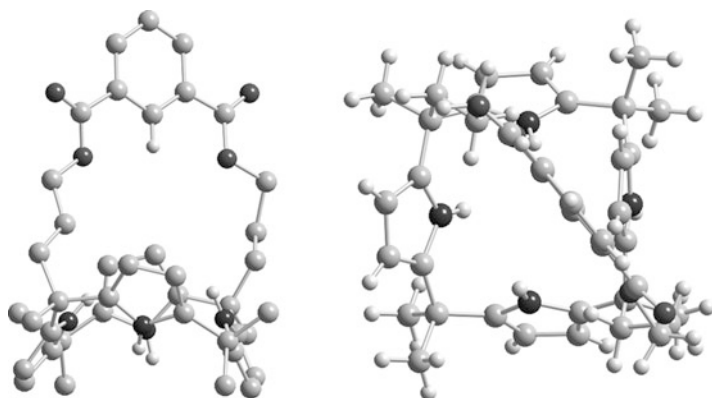
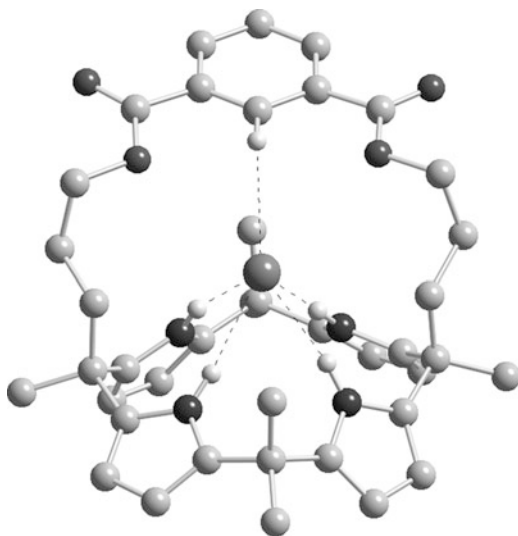


Fig. 11 Two views of the single crystal X-ray structure of diester-strapped calix[4]pyrrole **43**. Certain hydrogen atoms have been omitted from the side view for clarity

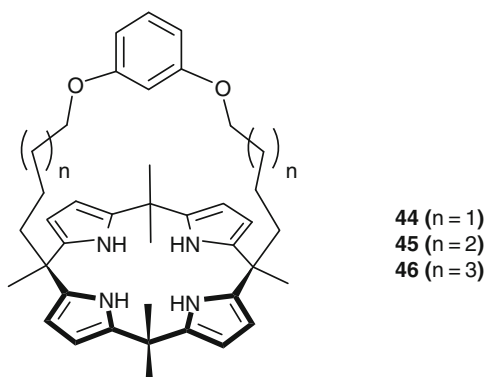
Fig. 12 Single crystal X-ray structure of diester-strapped calix[4]pyrrole **43** binding chloride. Counter cation and non-acidic hydrogen atoms have been omitted for clarity



A single crystal X-ray structure of the chloride complex of **43** revealed that the anion resides within the cavity (Fig. 12) [67]. The calix[4]pyrrole portion of the receptor exists in a cone conformation. Careful analysis of the structure showed that the central Ar–H is involved in anion recognition through medium-strength hydrogen bonding. The distance between the Ar–C and the bound chloride anion was 2.92 Å, a value consistent with a medium strength of CH–Cl hydrogen bond.

Anion binding studies, carried out in DMSO-*d*₆, using ¹H NMR spectroscopic techniques and ITC, revealed that chloride anion and fluoride anions are bound essentially irreversibly to the cavity. The stability constant, *K*_a, for chloride was found to be $1.0 \times 10^5 \text{ M}^{-1}$ with 1/1 binding stoichiometry. The stability constant for fluoride was estimated to be $3.9 \times 10^6 \text{ M}^{-1}$ from a competition experiment.

In order to see the effect of the length of the strap, a series of strapped calix[4]pyrroles **44–46** containing ether-containing bridges with different lengths, were synthesized. This series of receptors was expected to provide insight into the effect of the cavity size on the anion binding affinity [67].



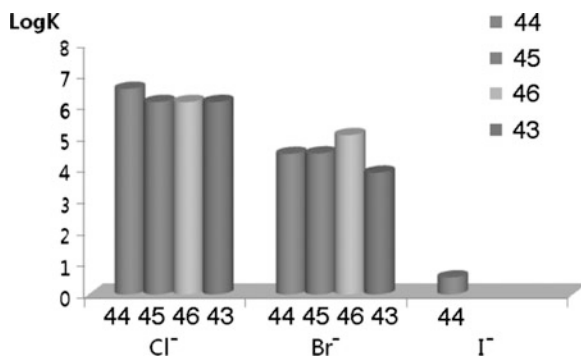
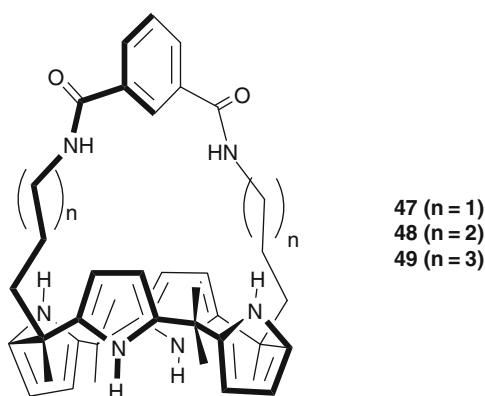


Fig. 13 Stability constants of diether strapped calix[4]pyrroles **44**, **45**, **46** and ester strapped calix [4]pyrrole **43**

The anion-binding affinities of the receptors **44–46** determined by ITC in dry acetonitrile are shown in Fig. 13. The data revealed that the receptors did not discriminate between chloride and bromide and that iodide anion is too big to fit to the cavity.

The highest chloride anion affinity was observed with receptor **44** and the highest affinity for bromide anion was observed in the case of the receptor containing the longest strap i.e. **46**. The chloride anion-bound receptor **44** is stable even in the presence of excess CsB(Ph)₄, evidence which led the authors to suggest that the binding domain is protected from an appreciable interaction with a counter cation.

Since the incorporation of additional hydrogen-bonding donor sites on the strap could serve to increase the affinity further, the strapped systems bearing isophthalate-derived diamides **47–49** were synthesized [68].



The anion-binding behaviour of these receptors, investigated by proton NMR spectroscopy and ITC, were found to display similar affinities to those of compounds

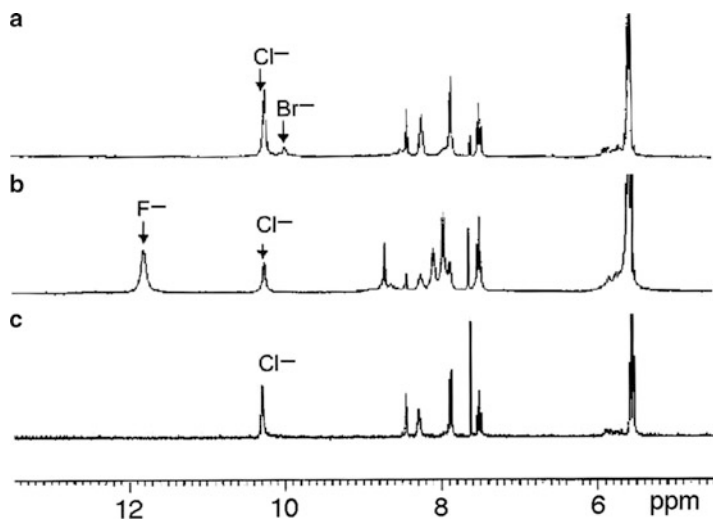


Fig. 14 300 MHz ^1H NMR spectra of (a) diamide-strapped calix[4]pyrrole **48** (1 mM) + TBABr (1 mM) + TBACl (1 mM), (b) (**48**) (1 mM) + TBABr (1 mM) + TBACl (1 mM) + TBAF (1 mM) in CD_3CN , (c) (**48**) (1 mM) in 495 μL of CD_3CN + 5 μL of sea water

44–46. However, no size-dependent selectivity for these anions was observed when the length of the bridging strap was varied [68].

The chemical shifts of the pyrrolic NH protons in the ^1H NMR spectrum of **48** were found to be correlated uniquely with the nature of the anions (e.g. $\text{F}^- = 11.9$, $\text{Cl}^- = 10.3$, $\text{Br}^- = 10.0$ ppm). Thus, by using the relative integral of anion-bound NH peak, it is possible to determine semi-quantitatively the concentration of chloride anion in both sea water and drinking water as shown in Fig. 14.

A strapped calix[4]pyrrole, **50**, containing a fluorophore as a part of the strap, was also synthesized [67] in order to check the reliability of the stability constants obtained by different methods. The anion affinity was determined using both fluorescence titration and ITC. The stability constants obtained by these two different methods were found to be in good agreement with one another. An interesting feature of receptor **50** is that its fluorescence emission properties could be controlled via the addition of appropriate cations and anions. In particular, it was found that the fluorescence intensity could be enhanced via the addition of sodium cations (Fig. 15). Presumably, this reflects the fact that these latter species bind to the carbonyl moiety in coumarin, thereby turning off an inherent photoinduced electron transfer (PET) quenching process. In contrast, the fluorescence intensity of **50** could be reduced via the addition of anions that are known to bind within the calix [4]pyrrole core [69]. Such systematic, substrate-dependent changes in fluorescence emission intensity means this receptor acts as a rudimentary supramolecular logic device.

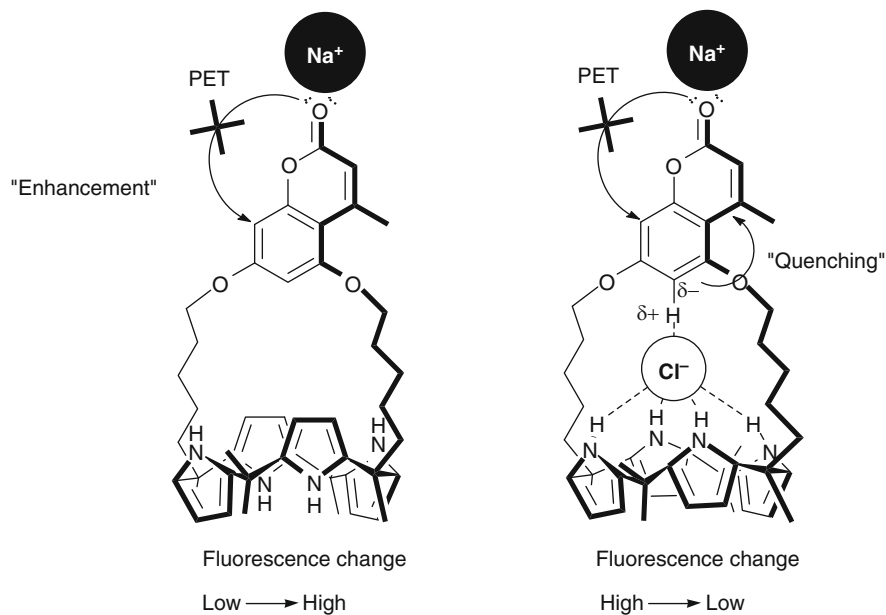
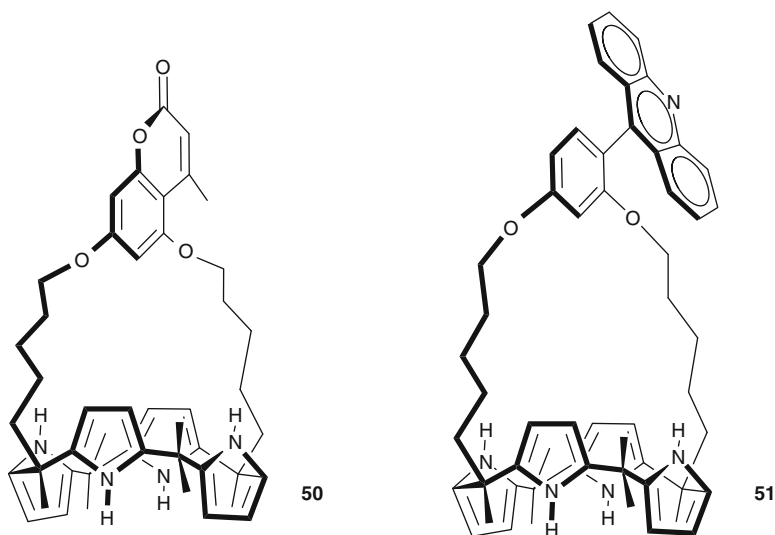


Fig. 15 Schematic representation of the interactions of **50** with cation and anions. (a) The Na^+ cation is thought to bind to the coumarin carbonyl oxygen atom, thereby inhibiting an inherent PET quenching process. (b) In contrast, the binding of chloride anion (Cl^-) activates a different PET mode and serves to quench the fluorescence

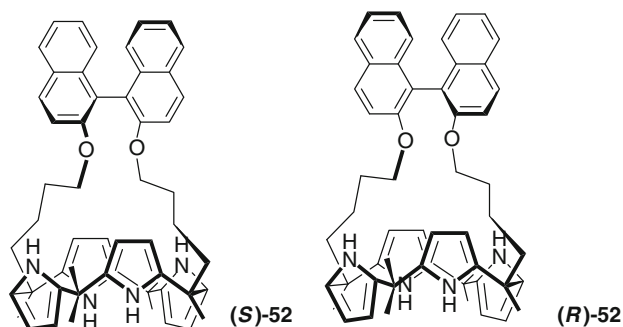


Acridine-strapped calix[4]pyrrole **51** was synthesized [70] and quantitative analyses of the solution-phase chloride and bromide anion binding properties of

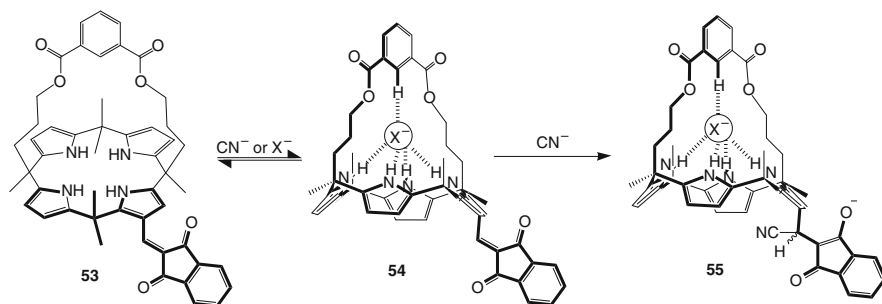
51 were conducted using ITC [70]. The resulting stability constants, determined in CH_3CN at 30°C , for the formation of the chloride and bromide complexes of **51** were $2.41 \times 10^7 \text{ M}^{-1}$ and $6.81 \times 10^4 \text{ M}^{-1}$, respectively. Receptor **51** shows a relatively high selectivity factor of ~ 350 for chloride over bromide.

Effort has been devoted to the preparation of chiral, non-racemic calix[4]pyrroles. Such systems would be potentially useful in the recognition and, potentially, separation of various anion-containing enantiomeric species, including amino acids. With these regards, a pair of chiral calix[4]pyrroles, (**S**)-**52** and (**R**)-**52**, was prepared [71].

The CD spectra of the two enantiomeric BINOL-strapped calix[4]pyrroles (**S**)-**52** and (**R**)-**52** were found to be nearly mirror images of one another. The resulting systems show significant selectivity to selected chiral carboxylate anions (*R*)-2-phenylbutyrate or (*S*)-2-phenylbutyrate in acetonitrile. The stability constants (K_a) were found to be ca. 10 times larger for the (*S*)-guest–(*S*)-host pair than in the case of the corresponding (*R*)-guest–(*S*)-host combination.



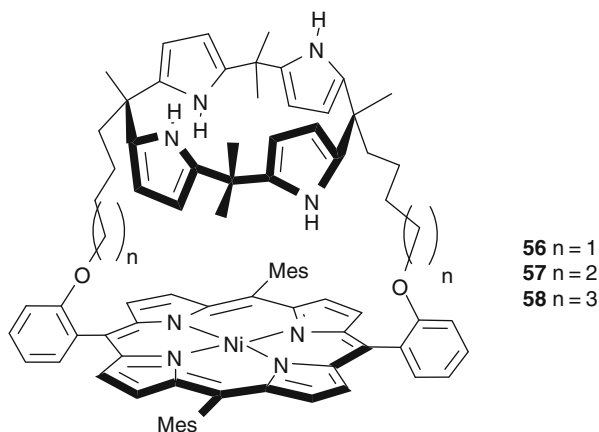
A strapped calix[4]pyrrole bearing an 1,3-indanedione group at a β -pyrrolic position have shown that the system is a good ratiometric cyanide-selective chemosensor (Scheme 10) [72]. A concentration-dependent bleaching of the initial yellow colour was observed upon addition of the cyanide anion. The bleaching was



Scheme 10 Formation of a cyanide adduct **55**

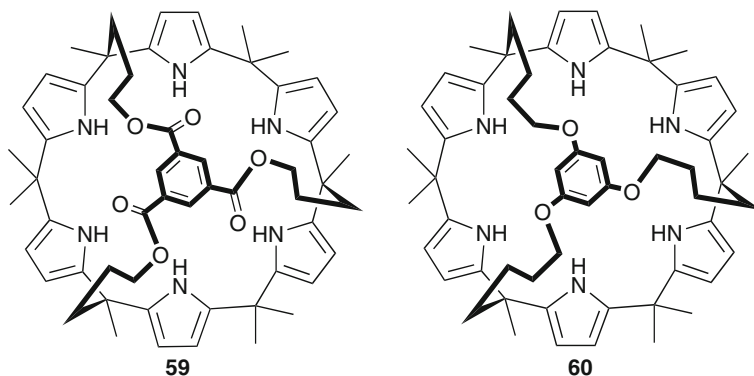
observed exclusively with the cyanide anion and the selectivity maintained even in the presence of excess of other anions. Since the receptor **53** is inherently chiral, two diastereomeric cyanide adducts **55** were formed. Spectroscopic studies provides support for a mechanistic interpretation wherein the cyanide anion forms a complex with the receptor ($K_a = 2.78 \times 10^4 \text{ M}^{-1}$) through a fast equilibrium, which is followed by slow nucleophilic addition to the β -position of the 1,3-indanedione group. A minimum inhibitory effect from other anions was observed, a feature that could be beneficial in the selective sensing of the cyanide anion.

Construction of a pre-organized receptor containing both hydrogen-bonding donor sites and a Lewis acidic metal ion centre is also something that can be conceived within the strapped calixpyrrole paradigm. Since the putative metal centre could act as an electron-pair acceptor or as a redox-active site, the ensuing combination of anion recognition and metal cation coordination could lead to enhancements in substrate binding or selectivity. These potential benefits provided the incentive to prepare the calix[4]pyrrole-metalloporphyrin conjugates (**52**)–(**54**) [73].

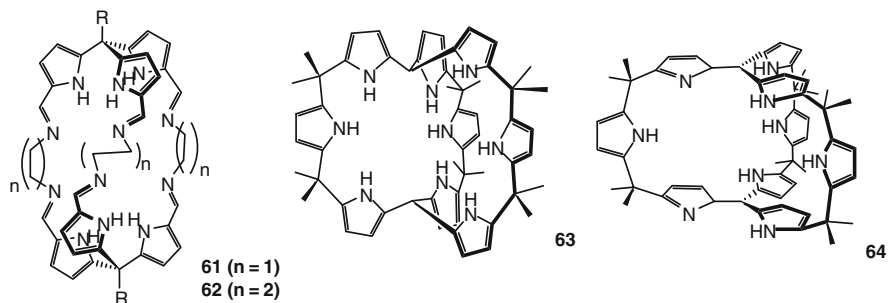


Anion-binding studies revealed that receptors (**56**–**58**) bound fluoride anion strongly in organic solvents, with neither compounds displaying any appreciable affinity for Cl^- , Br^- , and I^- . The ^1H NMR spectroscopic titrations and associated Job plots provided support to the fact that the bound fluoride anion resides within the cavity. Presumably, this strong size selectivity is imposed by the combination of the Lewis acid and hydrogen-bonding recognition functionality present within what is an overall pre-organized receptor [74].

The examples described so far all provide support for the proposal that proper encapsulation of the anion-binding domain within a calixpyrrole-type system can lead to receptors with high affinity and selectivity. In an effort to extend this principle beyond the realm of simple calix[4]pyrroles, the capped calix[6]pyrroles (**59**–**60**), were synthesized [75]. Interestingly, these larger systems also showed appreciable selectivity for the fluoride anion, at least in organic media.

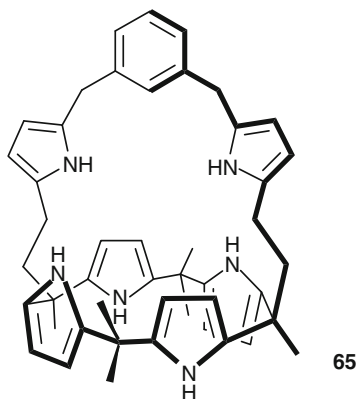


A different approach to achieving non-planar topographies involves constructing cryptand-like systems. The first such system to be characterized structurally was the imine-linked tripyrromethane dimers **61** and **62** reported by P.D. Beer [76]. In this case, the neutral substrate, ethylenediamine, was found within the cavity, with the corresponding solution phase binding affinity being $1,500 \text{ M}^{-1}$ in CDCl_3 . Slightly thereafter, the Sessler group reported the synthesis and structure of a ‘3-D calixpyrrole’ **63** and its oxidized analogue **64** [77, 78]. Neither of these systems contains a cavity-like void space. As a result, only solvent molecules, such as water and dichloromethane, were found trapped inside. However, in the case of **63**, anions were observed to bind on the exterior of the receptor.



A system that, in some respects, is closer to being a real cryptand-like calix[4]pyrrole **65** was recently synthesized by the Lee group [79]. This system was designed so as to incorporate additional pyrrolic NH donor functionality within a strapped calix[4]pyrrole framework. Quantitative analyses of the solution-phase fluoride anion binding properties of **65** were performed using ITC in DMSO. It was found that for K_a values measured were substantially larger and the titration isotherms also revealed the presence of a second event after the initial heat-evolving process. The ^1H NMR titration indicates the existence of anion- π interaction between the bound fluoride anion and the two pyrrole rings on the strap. This second event is ascribed to the binding of two pyrrole N-Hs on the strap with

additional fluoride anion. Such ancillary binding interactions were not seen in the case of chloride or acetate anion. The calculated K_{a1} value for fluoride anion binding was $1.28 \times 10^8 \text{ M}^{-1}$, while the calculated K_{a2} , corresponding to the putative secondary fluoride anion binding event, was $1.35 \times 10^5 \text{ M}^{-1}$, both in DMSO at 25°C. The stability constants for chloride and acetate anion binding in the same solvent were $3.27 \times 10^7 \text{ M}^{-1}$ and $9.35 \times 10^6 \text{ M}^{-1}$, respectively. These values are noteworthy for being substantially larger than those seen for any other neutral pyrrolic anion receptor, especially in light of the fact that the solvent (spectral grade DMSO) was not subject to any special drying. It thus appears as if the use of pyrrole-bearing straps provides a particularly effective way to enhance anion-binding affinities.

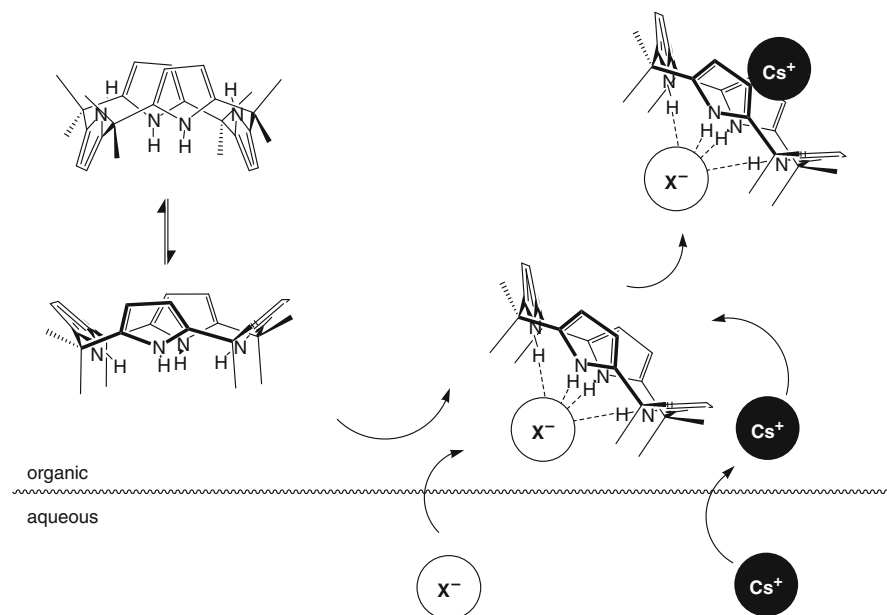


5 Extraction and Transport

The ion-pair complexation properties of calix[4]pyrroles make them suitable as ion-pair extractants (from the aqueous to the organic phase) and also as transport agents for ion pairs across lipid bilayer membranes.

For example, Moyer, Sessler, Delmau and co-workers have demonstrated that *meso*-octamethylcalix[4]pyrrole **1** is capable of extracting caesium bromide and chloride salts from water into nitrobenzene (Scheme 11) [80]. The extraction results were modelled in order to shed light on the equilibria present in the extraction process. The binding energy of the halide was found to be 7 kJ mol^{-1} larger for caesium chloride than for caesium bromide whilst the ion-pairing free energies between the calixpyrrole-anion complexes and caesium were found to be about the same for the chloride and bromide complexes suggesting that caesium is binding to the calixpyrrole's bowl-shaped cavity.

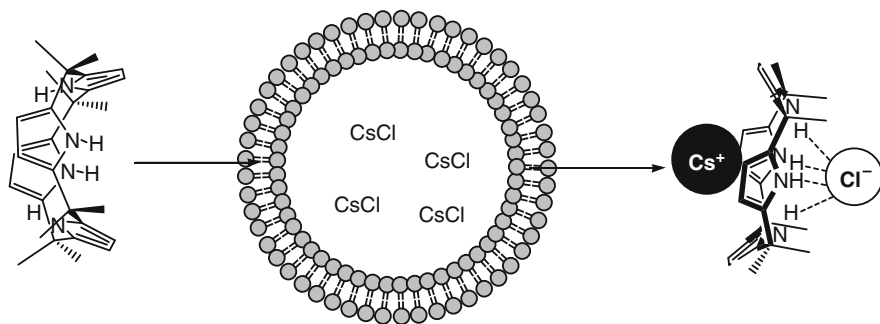
Quesada, Gale and co-workers have shown that compound **1** is capable of transporting ion pairs across lipid bilayer membranes [81]. POPC (1-palmitoyl-2-oleoyl-*sn*-glycero-3-phosphocholine) vesicles were prepared encapsulating caesium chloride solution buffered to pH 7.2. These were suspended in sodium nitrate solution at the same pH and a solution of compound **1** added in DMSO. A chloride-selective



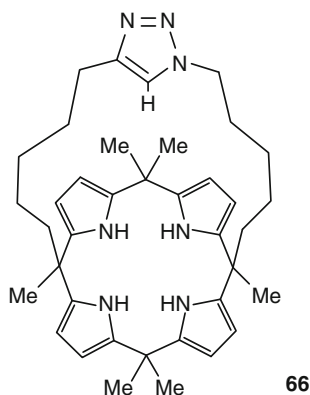
Scheme 11 Proposed steps in caesium salt extraction

electrode was used to monitor the release of this anion from the vesicles. It was found that under these conditions compound **1** functioned as an effective chloride transport agent. However, when vesicles were prepared encapsulating sodium, potassium or rubidium chloride and the experiment repeated no chloride transport was observed. The authors hypothesized that compound **1** functions as a caesium chloride membrane co-transporter rather than a chloride nitrate antiporter. To confirm this, the external anion was changed from nitrate to sulphate and the experiment repeated with caesium chloride encapsulated vesicles. Sulphate is particularly hydrophilic and cannot be transported through the bilayer. Under these conditions, chloride was again released from the vesicles, thus ruling out a potential chloride nitrate antiport mechanism and confirming the caesium chloride co-transport process (Scheme 12).

Gale and co-workers continued their studies on the membrane transport properties of calix[4]pyrroles and synthesized the strapped system **66** which contains a 1,2,3-triazole group [82]. Triazole groups have been shown by Flood and others to be excellent hydrogen bond donor groups for complexing anionic guests [83–85]. This receptor proved to have a higher affinity for chloride (added as the TEA salt) in acetonitrile ($K_a = 2.6 \times 10^6 \text{ M}^{-1}$) than the parent calix[4]pyrrole **1** ($K_a = 1.9 \times 10^5 \text{ M}^{-1}$) as measured by ITC. The receptor was shown to transport CsCl across lipid bilayers in a similar fashion to compound **1**. However, unlike **1**, the receptor was shown to be able to facilitate the release of chloride from vesicles containing NaCl presumably via a Cl^-/NO_3^- antiport process.



Scheme 12 Proposed mechanism for chloride efflux from vesicles containing caesium chloride

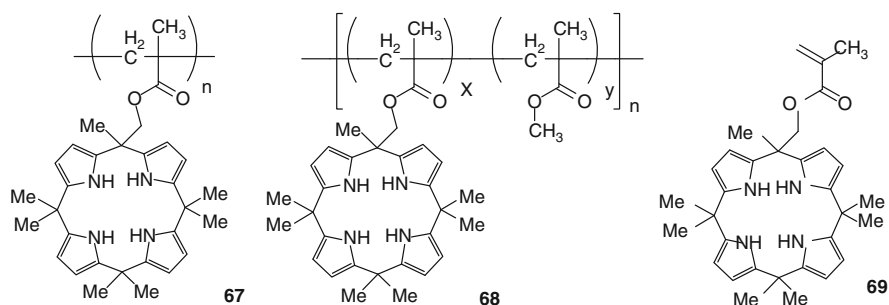


66

Shamsipur and co-workers have shown that calix[4]pyrrole **1** and analogues with different length alkyl chains at the *meso* position can facilitate selectively the transport of silver ions across a supported liquid membrane from a solution containing a variety of transition metal salts as part of a silver picrate ion-paired complex [86].

Immobilized calixpyrrole-based systems have been shown to be particularly effective for the extraction of anions and ion pairs from aqueous to organic solution. Akar, Bielawski, Sessler and co-workers have prepared poly(methyl methacrylate) polymers containing pendant calix[4]pyrrole subunits [87]. Both homopolymer **67** and copolymer **68** were prepared from monomer **69** using free radical methods. Copolymer **68** was shown to be capable of extracting tetrabutylammonium chloride and fluoride from aqueous solution as evidenced by an ^1H NMR downfield shift of the pyrrole NH resonances in the polymer upon the addition of either the fluoride or chloride salt in D_2O to a CD_2Cl_2 solution of the polymer. Greater downfield shifts were observed with chloride than fluoride. Model studies using compound **1** showed no downfield shifts of the pyrrole NH resonances under identical conditions. The polymer did not extract tetrabutylammonium dihydrogen phosphate which suggests that the polymer is extracting anions according to the Hofmeister bias such that the

more hydrophobic anions are extracted more efficiently than the more hydrophilic ones (Cl^- : $\Delta G_{\text{h}} = 340 \text{ kJ mol}^{-1}$; F^- : $\Delta G_{\text{h}} = -465 \text{ kJ mol}^{-1}$; H_2PO_4^- : $\Delta G_{\text{h}} = -465 \text{ kJ mol}^{-1}$). Anzenbacher and co-workers have also prepared acrylate and acrylamide calixpyrrole monomers for inclusion in polymerized films [88].



By combining 15-crown-5 moieties into an analogous copolymer **70** containing calix[4]pyrrole, Akar, Bielawski, Sessler and co-workers have produced a polymer that can extract potassium fluoride efficiently from aqueous solution to CD_2Cl_2 . A comparison with polymers containing only benzo-15-crown-5 **71** or only calix[4]pyrrole **72** as receptors shows extracted potassium concentrations of 6.84, 4.73 and $0.65 \pm 0.05 \text{ mM}$ for polymers **70**, **71** and **72**, respectively. Receptor **73**, which contains both crown and calixpyrrole binding sites, did not extract KF under these conditions (Table 2). As was observed previously, KCl was extracted by **70** more efficiently than KF because of the more hydrophobic nature of chloride.

Table 2 Summary of KF extraction efficiencies^a

Cmpd ^b	calix/crown ^c	eff. (%) (total) ^{d,e}	eff. (%) (calix) ^{d,f}	eff. (%) (total) ^{e,g}	eff. (%) (crown) ^{g,h}
70	1.0:0.8	67	121	61	137
71	1.0:0.0	88	88	73	n.d. ⁱ
72	0.0:1.0	6	n.d. ⁱ	12	12
73	1.0:1.0	0	0	0	0

^aExtraction efficiencies (eff.) are reported as the percent (%) of extractant populated with KF upon exposure to a saturated aqueous solution of KF

^bSee above for structures of compounds studied

^cRelative molar ratios of the calixpyrrole (calix) to crown ether (crown) units in the extractant

^dCalculated from total fluoride extracted

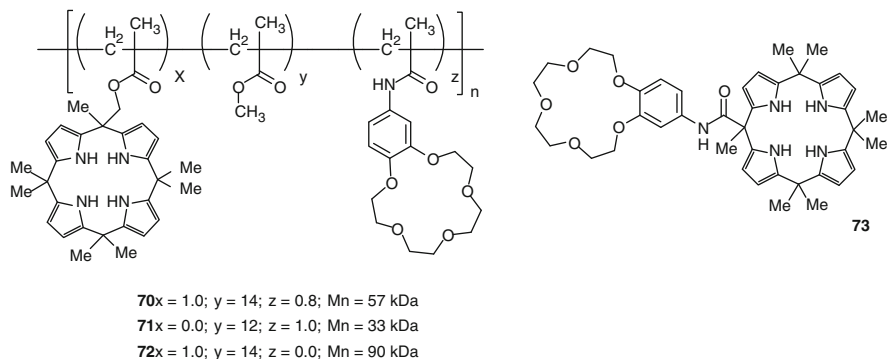
^eBased on the total number of ion receptors (calixpyrrole + crown ether) in the extractant

^fBased on the total number of calixpyrrole units in the extractant

^gCalculated from the total potassium extracted

^hBased on the total number of crown ether units in the extractant

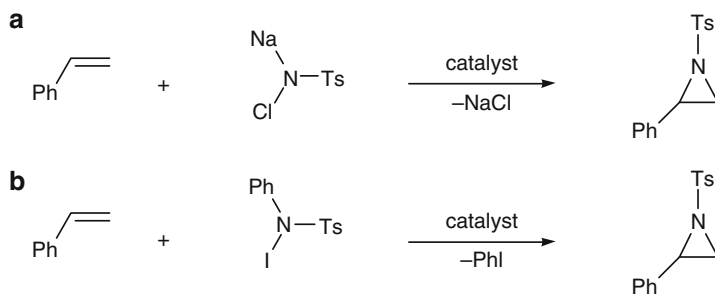
ⁱn.d. = not determined



Other work on immobilized calixpyrroles includes the preparation of resins containing the macrocycle for anion or metal extraction [89, 90] and the immobilization of compound **1** in cellulose acetate films and subsequent study of the transport of solutes through these materials [91].

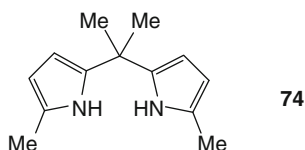
6 Catalysis

The use of un-metallated calix[4]pyrroles as catalysts has recently begun to be explored. Pérez, Bielawski, Sessler and co-workers have discovered that calix[4]pyrrole **1** acts as a promoter of the cuprous chloride-catalysed aziridination of styrene by the nitrene source chloramine-T in acetonitrile (Scheme 13a) [92]. They found that the calix[4]pyrrole interacts with the chlorine atom in CuCl as the addition of compound **1** and CuCl also promotes the reaction when PhI = NTs is used as the nitrene source (Scheme 13b). Additionally, compound **1** had no effect on the reaction when CuI was used as the catalyst. Interestingly, when compound **74**

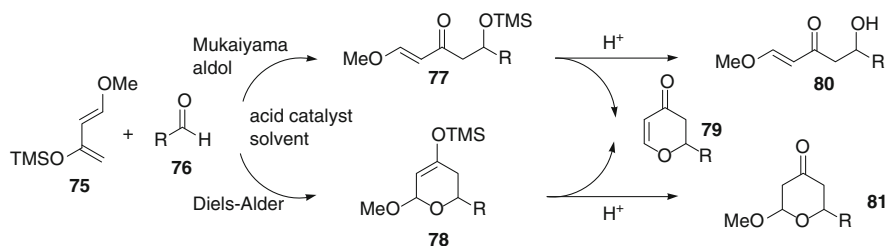


Scheme 13 Calixpyrrole mediated catalysis

was used instead of calix[4]pyrrole no appreciable quantity of aziridine product was observed.



Kohnke, Soriente and co-workers have explored the use of macrocycles **26a** and **26b** as organocatalysts for the hetero Diels–Alder reaction of Danishefsky's diene with aromatic aldehydes (Scheme 14) [93]. Compound **26a** and model compound **82** were found to be catalytically inactive despite the former receptor having a higher affinity for anions than compound **26b**. Compound **26b** was found to catalyse the reaction, with the distribution of products under various conditions shown in Table 3.



Scheme 14 The reaction of Danishefsky's diene with aldehydes. In this study, R = *p*-NO₂C₆H₄, macrocycles **26a** or **26b** or dipyrromethane **82** were used as the acid catalysts in dichloromethane

Table 3 Conversion data for the cycloaddition of silyloxydiene **75** to the *p*-nitrobenzaldehyde **76** in the presence of **26a**, **26b** and **82**^a

Entry	75 : 76 ^b	Solv. ^c	Catalyst ^d	Conv. ^e	79 ^f	80 ^f	81 ^f
1	2	2	–	–	–	–	–
2	5	2	26a (20)	–	–	–	–
3	2	2	26b (10)	36	–	11	25
4	2	4	26b (10)	25	–	20	5
5	2	2	26b (20)	60	–	3	57
6	5	2	26b (20)	90	33	7	50
7	5	4	26b (20)	51	47	4	–
8	5	2	82 (20)	–	–	–	–

^aAll reactions were performed with 0.67 mmol of diene **75**

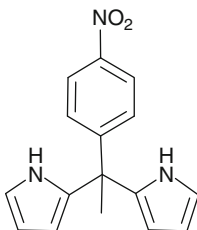
^bMolar ratio of the reagents

^cVolume of solvent (mL)

^dAmount of catalyst (mol %)

^eConversion (mol %) determined on the isolated compounds

^fYield based on isolated product



82

Theoretical studies by Hæffner and co-workers have demonstrated the possibility of activating C–F bonds using an amine-functionalized octafluorocalix[4]pyrrole [94]. The authors show that the reaction between the calixpyrrole and CH₃F via a Menshutkin displacement reaction is favourable from a thermochemical perspective.

7 Conclusions

The discovery reported in 1996 [10] that calix[4]pyrroles could bind anions led on to a new rich vein of molecular recognition chemistry. Similarly, the discovery that calixpyrroles actually function as ion-pair receptors [47] has led on to important chemistry in the area of metal salt extraction and membrane transport. Strapped calixpyrroles possess particularly high affinities for anions and offer the possibility of customizing the hydrogen-bonding array with additional hydrogen bond donor groups or sensing moieties to produce new molecular devices. There is still much new chemistry to explore with this old class of macrocycle.

References

1. Baeyer A (1886) *Ber Dtsch Chem Ges* 19:2184–2185
2. Dennstedt M, Zimmerman J (1886) *Ber Dtsch Chem Ges* 19:2189
3. Dennstedt M, Zimmermann J (1887) *Ber Dtsch Chem Ges* 20:850–857
4. Dennstedt M (1890) *Ber Dtsch Chem Ges* 23:1370–1374
5. Chelintzev VV, Tronov BV (1916) *J Russ Phys Chem Soc* 48:105
6. Chelintzev VV, Tronov BV (1916) *J Russ Phys Chem Soc* 48:1197–1209
7. Chelintzev VV, Tronov BV, Karmanov SG (1916) *J Russ Phys Chem* 48:1210–1221
8. Rothmund P, Gage CL (1955) *J Am Chem Soc* 77:3340–3342
9. Floriani C (1996) *Chem Commun*: 1257
10. Gale PA, Sessler JL, Král V, Lynch V (1996) *J Am Chem Soc* 118:5140–5141
11. Gutsche CD, Stewart DR (1993) *Org Prep Proced Int* 25:137–139
12. Gutsche CD, Iqbal M (1990) *Org Synth* 68:234–237
13. Gutsche CD, Dhawan B, Leonis M, Stewart D (1990) *Org Synth* 68:238–242
14. Gale PA, Genge JW, Kral V, McKervey MA, Sessler JL, Walker A (1997) *Tetrahedron Lett* 38:8443–8444

15. Cafeo G, Kohnke FH, Torre GLL, White AJP, Williams DJ (2000) *Angew Chem Int Ed Engl* 39:1496–1498
16. Turner B, Botoshansky M, Eichen Y (1998) *Angew Chem Int Ed Engl* 37:2475–2478
17. Sessler JL, Anzenbacher P, Shriver JA, Jursikova K, Lynch VM, Marquez M (2000) *J Am Chem Soc* 122:12061–12062
18. Gale PA, Sessler JL, Král V (1998) *Chem Commun*:1–8
19. Gale PA, Anzenbacher P, Sessler JL (2001) *Coord Chem Rev* 222:57–102
20. Sessler JL, An DQ, Cho WS, Lynch V, Yoon DW, Hong SJ, Lee CH (2005) *J Org Chem* 70:1511–1517
21. Piatek P, Lynch VM, Sessler JL (2004) *J Am Chem Soc* 126:16073–16076
22. Sessler JL, An DQ, Cho WS, Lynch V, Marquez J (2005) *Chem Eur J* 11:2001–2011
23. Cafeo G, Kohnke FH, White ALP, Garozzo D, Messina A (2007) *Chem Eur J* 13:649–656
24. Shriver JA, Westphal SG (2006) *J Chem Educ* 83:1330–1332
25. Gale PA, Twyman LJ, Handlin CI, Sessler JL (1999) *Chem Commun*:1851–1852
26. Jain VK, Mandalia HC, Suresh E (2008) *J Inc Phenom* 62:167–178
27. Jain VK, Mandalia HC (2009) *J Inc Phenom* 63:27–35
28. Chauhan SMS, Garg B, Bisht T (2007) *Molecules* 12:2458–2466
29. Kishan MR, Rani VR, Kulkarni SJ, Raghavan KV (2005) *J Mol Catal A* 237:155–160
30. Kumar A, Ahmad I, Rao MS (2008) *Can J Chem* 86:899–902
31. Chacón-García L, Chavez L, Cacho DR, Altamirano-Hernández J (2009) *Beilstein J Org Chem* 5(2)
32. Alešković M, Halasz I, Basarić N, Mlinaric-Majerski K (2009) *Tetrahedron* 65:2051–2058
33. Yang WZ, Yin ZM, Li Z, He JQ, Cheng JP (2008) *J Mol Struct* 889:279–285
34. Anzenbacher P, Jursikova K, Shriver JA, Miyaji H, Lynch VM, Sessler JL, Gale PA (2000) *J Org Chem* 65:7641–7645
35. Anzenbacher P, Try AC, Miyaji H, Jursikova K, Lynch VM, Marquez M, Sessler JL (2000) *J Am Chem Soc* 122:10268–10272
36. Miyaji H, Anzenbacher P, Sessler JL, Bleasdale ER, Gale PA (1999) *Chem Commun*: 1723–1724
37. Sessler JL, Gale PA, Genge JW (1998) *Chem Eur J* 4:1095–1099
38. Gale PA, Sessler JL, Allen WE, Tvermoes NA, Lynch V (1997) *Chem Commun*:665–666
39. Dey S, Pal K, Sarkar S (2006) *Tetrahedron Lett* 47:5851–5854
40. Dey S, Pal K, Sarkar S (2008) *Tetrahedron Lett* 49:960–964
41. Chupakhin ON, Rusinov GL, Itsikson NA, Beresnev DG, Ya I (2004) *Russ Chem Bull (Translation of Izvestiya Akademii Nauk, Seriya Khimicheskaya)* 53:1351–1352
42. Depraetere S, Smet M, Dehaen W (1999) *Angew Chem Int Ed Engl* 38:3359–3361
43. Anzenbacher P, Nishiyabu R, Palacios MA (2006) *Coord Chem Rev* 250:2929–2938
44. Dehaen W, Gale PA, Garcia-Garrido SE, Kostermans M, Light ME (2007) *New J Chem* 31:691–696
45. Gu R, Depraetere S, Kotek J, Budka J, Wagner-Wysiecka E, Biernat JF, Dehaen W (2005) *Org Biomol Chem* 3:2921–2923
46. Nishiyabu R, Palacios MA, Dehaen W, Anzenbacher P (2006) *J Am Chem Soc* 128: 11496–11504
47. Custelcean R, Delmau LH, Moyer BA, Sessler JL, Cho WS, Gross D, Bates GW, Brooks SJ, Light ME, Gale PA (2005) *Angew Chem Int Ed* 44:2537–2542
48. Bates GW, Gale PA, Light ME (2006) *CrystEngComm* 8:300–302
49. Bates GW, Gale PA, Light ME (2008) *Supramol Chem* 20:23–28
50. Bates GW, Kostermans M, Dehaen W, Gale PA, Light ME (2006) *CrystEngComm* 8:444–447
51. Schmidtchen FP (2002) *Org Lett* 4:431–434
52. Sessler JL, Gross DE, Cho WS, Lynch VM, Schmidtchen FP, Bates GW, Light ME, Gale PA (2006) *J Am Chem Soc* 128:12281–12288
53. Gross DE, Schmidtchen FP, Antonius W, Gale PA, Lynch VM, Sessler JL (2008) *Chem Eur J* 14:7822–7827

54. Sessler JL, Cho WS, Gross DE, Shriver JA, Lynch VM, Marquez M (2005) *J Org Chem* 70:5982–5986
55. Bruno G, Cafeo G, Kohnke FH, Nicolo F (2007) *Tetrahedron* 63:10003–10010
56. Cafeo G, Kohnke FH, Valenti L, White AJP (2008) *Chem Eur J* 14:11593–11600
57. Yoo JD, Jeoung EH, Lee CH (2009) *Supramol Chem* 21:164–172
58. Sessler JL, Kim SK, Gross DE, Lee CH, Kim JS, Lynch VM (2008) *J Am Chem Soc* 130:13162–13166
59. Gil-Ramirez G, Benet-Buchholz J, Escudero-Adan EC, Ballester P (2007) *J Am Chem Soc* 129:3820–3821
60. de Namor AFD, Abbas I, Hammud HH (2007) *J Phys Chem B* 111:3098–3105
61. de Namor AFD, Khalife R (2008) *J Phys Chem B* 112:15766–15774
62. de Namor AFD, Shehab M, Khalife R, Abbas I (2007) *J Phys Chem B* 111:12177–12184
63. de Namor AFD, Shehab M, Abbas I, Withams MV, Zvietcovich-Guerra J (2006) *J Phys Chem B* 110:12653–12659
64. de Namor AFD, Shehab M (2005) *J Phys Chem B* 109:17440–17444
65. Hong S-J, Yoo J, Kim S-H, Kim J-S, Yoon J, Lee C-H (2008) *Chem Commun*:189–191
66. Yoon DW, Hwang H, Lee CH (2002) *Angew Chem Int Ed* 41:1757–1759
67. Lee CH, Na HK, Yoon DW, Won DH, Cho WS, Lynch VM, Shevchuk SV, Sessler JL (2003) *J Am Chem Soc* 125:7301–7306
68. Lee CH, Lee JS, Na HK, Yoon DW, Miyaji H, Cho WS, Sessler JL (2005) *J Org Chem* 70:2067–2074
69. Miyaji H, Kim HK, Sim EK, Lee CK, Cho WS, Sessler JL, Lee CH (2005) *J Am Chem Soc* 127:12510–12512
70. Jeong SD, Yoo J, Na HK, Chi DY, Lee CH (2007) *Supramol Chem* 19:271–275
71. Miyaji H, Hong SJ, Jeong SD, Yoon DW, Na HK, Hong J, Ham S, Sessler JL, Lee CH (2007) *Angew Chem Int Ed* 46:2508–2511
72. Kim SH, Hong SJ, Yoo JD, Kim SK, Sessler JL, Lee CH (2009) *Org Lett* 11. doi: 10.1021/ol901361h
73. Panda PK, Lee CH (2004) *Org Lett* 6:671–674
74. Panda PK, Lee CH (2005) *J Org Chem* 70:3148–3156
75. Lee CH, Yoon DW, Sohn HY, Song MY (2007) *Supramol Chem* 19:265–270
76. Fox OD, Rolls TD, Beer PD, Drew MGB (2001) *Chem Commun*:1632–1633
77. Bucher C, Zimmerman RS, Lynch V, Sessler JL (2001) *J Am Chem Soc* 123:9716–9717
78. Bucher C, Zimmerman RS, Lynch V, Sessler JL (2003) *Chem Commun*:1646–1647
79. Lee CH, Miyaji H, Yoon DW, Sessler JL (2008) *Chem Commun*:24–34
80. Wintergerst MP, Levitskaia TG, Moyer BA, Sessler JL, Delmau LH (2008) *J Am Chem Soc* 130:4129–4139
81. Tong CC, Quesada R, Sessler JL, Gale PA (2008) *Chem Commun*:6321–6323
82. Fisher MG, Gale PA, Hiscock JR, Hursthouse MB, Light ME, Schmidtchen FP, Tong CC (2009) *Chem Commun*:3017–3019
83. Li Y, Flood AH (2008) *Angew Chem Int Ed Engl* 47:2649–2652
84. Jumarker H, Lenhardt JM, Pharm DM, Craig SL (2008) *Angew Chem Int Ed Engl* 47:3740–3743
85. Meudtner RM, Hecht S (2008) *Angew Chem Int Ed* 47:4926–4930
86. Amiri AA, Safavi A, Hasaninejad AR, Shrghi H, Shamsipur M (2008) *J Memb Sci* 325:295–300
87. Aydogan A, Coady DJ, Lynch VM, Akar A, Marquez M, Bielawski CW, Sessler JL (2008) *Chem Commun*:1455–1457
88. Zyryanov GV, Kinstle TH, Anzenbacher P (2008) *Synlett*:1171–1174
89. Kaledkowski A, Trochimczuk AW (2006) *Sep Sci Technol* 41:3431–3447
90. Kaledkowski A, Trochimczuk AW (2006) *React Funct Polym* 66:957–966
91. Valente AJM, Jimenez A, Simoes AC, Burrows HD, Polishchuk AY, Lobo VMM (2007) *Eur Polym J* 43:2433–2442

92. Martínez-García H, Morales D, Pérez J, Coady DJ, Bielawski CW, Gross DE, Cuesta L, Marquez M, Sessler JL (2007) *Organometallics* 26:6511–6514
93. Cafeo G, De Rosa M, Kohnke FH, Neri P, Soriente A, Valenti L (2008) *Tetrahedron Lett* 49:153–155
94. Hæffner F, Marquez M, Gonzalez C (2007) *J Phys Chem A* 111:268–272

Calix[n]phyrins: Synthesis and Anion Recognition

Wim Dehaen

Abstract This chapter covers advances in calix[n]phyrin chemistry since 2001, focusing on their synthesis and properties as anion complexants. Over the last 8 years, the structural variety of calixphyrins has significantly increased, and several applications as anion complexants were reported.

Keywords Anion complexation · Chromophore · Pyrrole · Receptor

Contents

1	Introduction	76
2	Synthesis	77
2.1	Synthesis of Calixphyrins Starting from Porphyrins	77
2.2	Synthesis of Calix[4]phyrins Starting from Calix[4]pyrroles	80
2.3	Synthesis of Calixphyrins Starting from Acyclic (Oligo)pyrrole Building Blocks	80
3	<i>N</i> -Confused Calixphyrins	89
4	Calixphyrins Incorporating Other Rings	92
5	Anion Complexation	96
6	Conclusion	99
	References	100

Abbreviations

DDQ	4,5-Dichloro-3,6-dioxo-1,2-benzonitrile
NCP	<i>N</i> -confused porphyrin
NMR	Nuclear magnetic resonance

W. Dehaen

Department of Chemistry, University of Leuven, Celestijnenlaan 200F, 3001 Leuven, Belgium
e-mail: wim.dehaen@chem.kuleuven.be

OEP	β -Octaethylporphyrin
PTSA	4-Methylphenylsulphonic acid
PVC	Poly(vinyl chloride)
TBA	Tetrabutylammonium
TFA	Trifluoroacetic acid
TPP	<i>meso</i> -Tetraphenylporphyrin

1 Introduction

The name “calix[n]phyrin” was proposed by Sessler and co-workers [1] for a certain class of pyrrole-containing macrocycles. This name contains parts of both porphyrins and calixpyrroles, suggesting a hybrid structure for calixphyrins. Whereas the former two classes of compounds have, respectively, only sp^2 or sp^3 -hybridised *meso*-carbon atoms separating the pyrrole units, calixphyrins are characterised by having both types of *meso*-atoms. In the case of systems with four pyrroles, the calix[4]phyrins, this means that one, two, or three sp^2 -hybridised atoms may be present next to the complementing sp^3 -hybridised centres. Furthermore, in the case of two sp^2 -centres two different isomers, *cis* or *trans*-like or 5,10 versus 5,15-fashion across the macrocycle, are possible. Therefore, this nomenclature needed to be refined by adding a set of numbers between brackets as known from the expanded porphyrin and calix[n]pyrrole literature. The number of numerals refers to the number of pyrroles in the macrocycle. Each individual number indicates the amount of *meso*-atoms; for calixphyrins treated in this chapter, this is mainly 1. One starts with the highest order sp^2 -centre and continues in the direction in which the nearest sp^2 -centre lies. Bold numbers designate sp^2 -hybridised *meso*-carbons, whereas italicised numbers refer to the sp^3 -centres. In this way, a systematic name can be given to all types of calixphyrins, including those that historically were named differently, such as porpho(mono)methenes, (5,10 and 5,15) porphodimethenes, phlorins (porphotrimethenes) and their more oxidised isoporphyrin analogues, as well as higher-order derivatives (Fig. 1).

The calix[4]phyrins are quite different from the fully conjugated porphyrin analogues from the viewpoint of their chemical and conformational stability. Many calixphyrins were first isolated as the metal complexes and the coordination chemistry is quite rich and significantly different from that of the porphyrin analogues. On the other hand, the calixphyrins, although they have less hydrogen bonding sites, share the possibility of anion binding with their more reduced calixpyrrole analogues.

Sessler et al. covered the earlier calix[n]phyrin literature until 2000–2001 and for discussion on the historic origin of calix[n]phyrin chemistry the reader is referred to this excellent and seminal review [1]. We will focus on the more recent examples, comparing with earlier results only when they are of importance for the discussion.

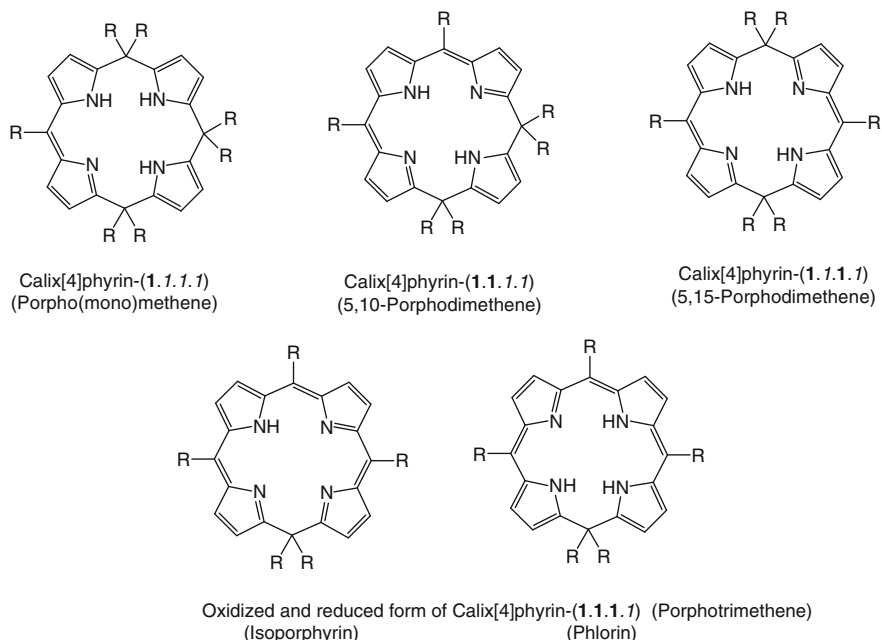


Fig. 1 “Historic” and systematic names and structures of some calix[4]phyrins

2 Synthesis

Three main strategies are possible for the synthesis of calixphyrins: (a) starting from porphyrins or expanded analogues; (b) oxidation of metallated calixpyrroles and (c) starting from acyclic (oligo)pyrrole building blocks. The three methods are complementary and each gives access to differently substituted calixphyrins.

2.1 Synthesis of Calixphyrins Starting from Porphyrins

Senge et al. have carried out a detailed study concerning the addition of organolithium reagents to porphyrins and metalloporphyrins [2–9]. Different products may be formed depending on the (metallo)porphyrin, the organolithium and the reaction circumstances that are used.

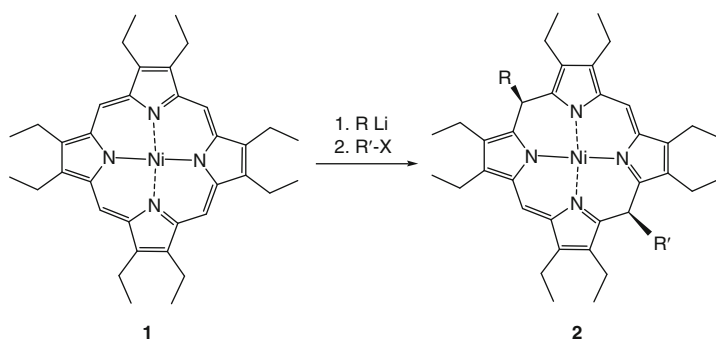
For instance, addition of organolithium reagents to Ni(II) complexes of β -octaethylporphyrin (OEP) **1** and alkylation of the resulting anions afford highly substituted calix[4]phyrins-(1.1.1.1) **2** in a one-pot procedure [2]. The yields are reasonable (50–80%) and the reactions are stereospecific. These calixphyrins **2**, that have a roof-like structure, could not be readily oxidised to the corresponding

porphyrins by DDQ as it was possible for the monoadducts of OEP and organolithiums (without the alkylation step; Scheme 1) [3].

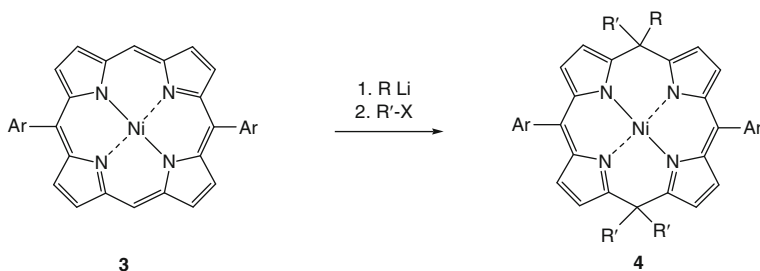
5,15-Diarylporphyrins **3** react in a different way if alkyllithiums and small alkylating agents (e.g. MeI) are used and completely substituted Ni(II) complexes **4** may be obtained in yields up to 80% [2]. The use of aryllithiums on the other hand results in the formation of tetrasubstituted porphyrins as reported earlier by Senge [5] (Scheme 2).

The palladium-catalysed reaction of free-base *meso*-tetrasubstituted porphyrins **5** (R = aryl, alkyl) affords hydrochlorins, e.g. chlorins **6** and isomeric calix[4]phyrins-(1.1.1.1) **7**. The yields of compounds **7** are dependent on the lithium reagent and type of palladium catalyst used and in some cases (e.g. linear alkyllithiums), the monosubstituted or 2,3-disubstituted chlorin derivatives **6** may be formed as the only products. Sterically hindered alkyllithiums or aryllithiums favour the products **7** (Scheme 3) [5, 6].

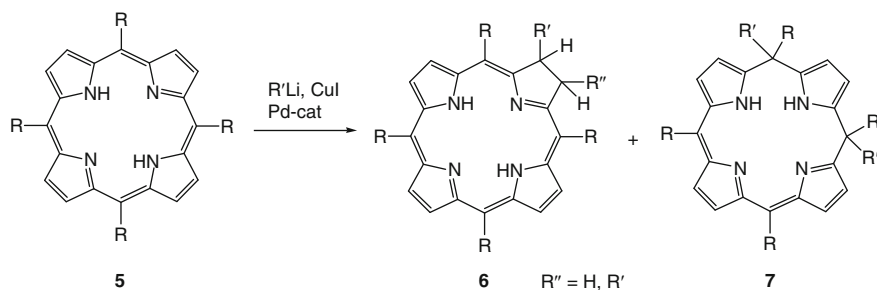
Earlier work, for instance by Callot and co-workers [1, 10–12], had shown that the uncatalysed reactions of (metallo)porphyrins and their *N*-alkylated analogues with organolithiums lead to the formation of phlorins, chlorins and porphodimethenes in very low yields (1–5%). In more recent work [6], Senge showed a



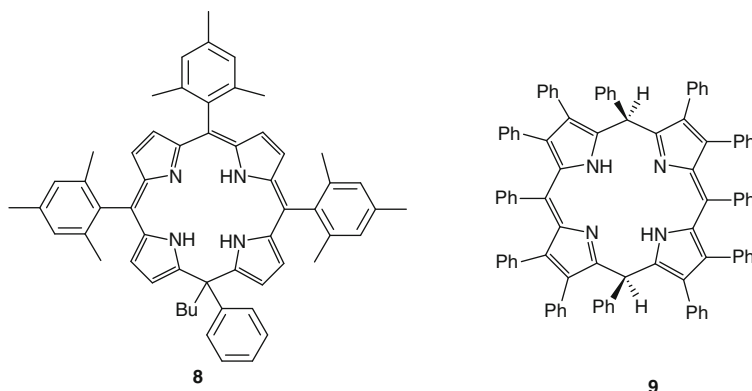
Scheme 1 Reductive dialkylation of Ni-OEP



Scheme 2 Reductive peralkylation of 5,15-diarylporphyrins



Scheme 3 Catalysed addition of organolithiums to *meso*-tetrasubstituted porphyrins



Scheme 4 Calix[4]phyrins stabilised by steric hindrance

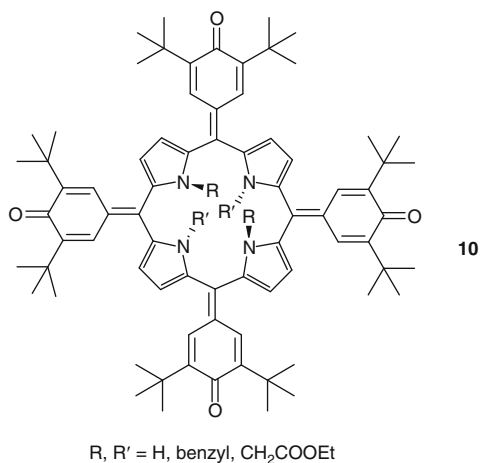
yield of 40% of hexaphenylcalixphyrin **7** ($\text{R} = \text{R}' = \text{Ph}$) in uncatalysed reactions starting from *meso*-tetraphenylporphyrin (TPP) and phenyllithium.

Geier and co-workers reported the increased stability of phlorin products with *meso*-mesityl substituents after uncatalysed addition of BuLi to *meso*-tetraarylporphyrins. The best light and air stability are obtained for product **8** when all sp^2 -hybridised *meso*-positions bear a bulky mesityl substituent [13].

The sterically hindered dodecaphenylporphyrin (DPPH₂) can be diprotonated, facilitating reduction by SnCl₂ to the roof shaped calix[4]phyrin-(1.1.1.1) **9** (structure analogous to **2**). The latter compound is stable and cannot be oxidised back to DPPH₂ (Scheme 4) [14].

The interesting oxoporphyrinogens or porphotetramethenes **10** [15–28] that are derived from *meso*-phenolic porphyrins by oxidation strictly speaking do not belong to the calixphyrin family because they have sp^2 -hybridised *meso*-carbon atoms only and therefore will not be treated in detail here. However, the *N*-alkylated analogues have a 1,3-alternating calix-like structure and some derivatives have been involved in anion sensing (Fig. 2).

Fig. 2 Oxoporphyrinogens



2.2 Synthesis of Calix[4]phyrins Starting from Calix[4]pyrroles

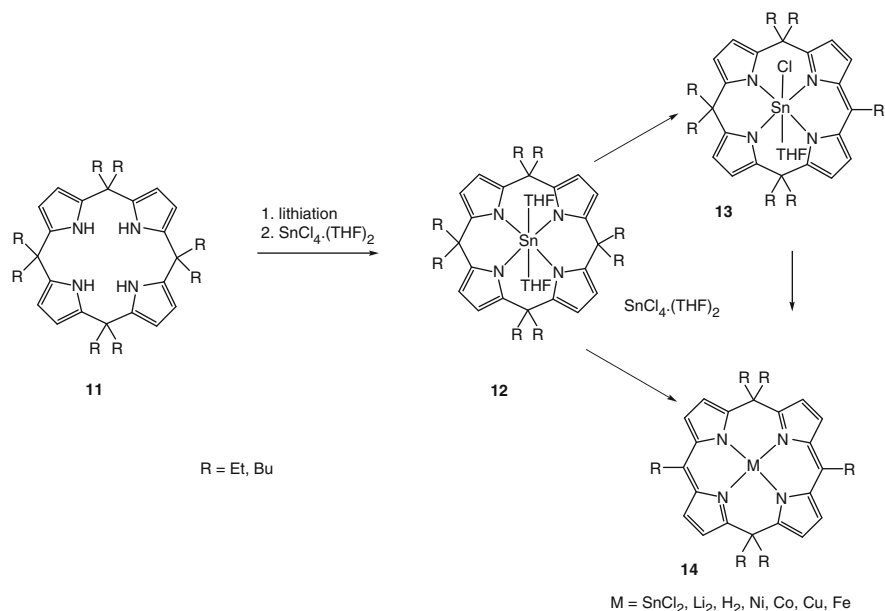
This way to prepare calix[4]phyrins has been mainly investigated by Floriani and co-workers and their work has been covered in the earlier review [1, 29–32]. In recent years, no new data were reported.

The easily available octaalkylcalix[4]pyrroles **11** (“porphyrinogens”) can be tetralithiated and converted to the tin(IV) complexes **12**. Addition of oxidising agent (e.g. the THF complex of SnCl₄) affords multigram amounts of either the porphomethene (calix[4]phyrin-(1.1.1.1)) (**13**) or the porphodimethene-(1.1.1.1) (**14**) analogues. The Sn complex of the calixphyrin-(1.1.1.1) **14** was demetallated via conversion to the lithium or magnesium salt and working up with water. Alternatively, the intermediate dilithium salt may be treated with the THF complexes of other metal salts (e.g. MCl₂ in which M = Ni, Fe, Co, Cu) to afford a variety of metallated calix[4]phyrins-(1.1.1.1) (Scheme 5) [29–32].

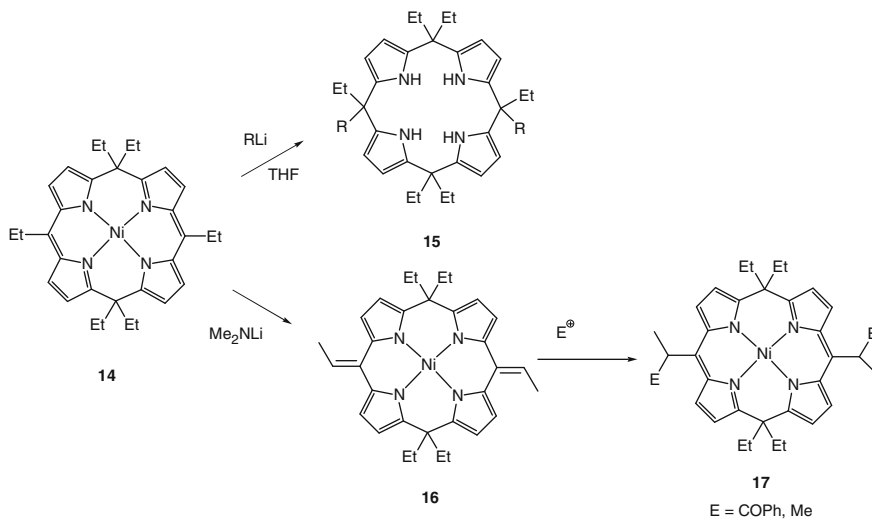
The Ni analogue of **14** (R = Et) was converted to substituted calix[4]pyrroles **15** after addition of different nucleophiles (H, Bu, CH₂CN) or to its isomer **16** with exocyclic double bonds after treatment with dimethylamide anion. This compound **16** with enamine character can be functionalised with electrophiles, affording C-benzoylated or methylated calix[4]phyrin-(1.1.1.1) **17** (Scheme 6) [29].

2.3 Synthesis of Calixphyrins Starting from Acyclic (Oligo)pyrrole Building Blocks

In the last few years, most calixphyrins have been prepared according to this method. Several variants are possible including synthesis (a) from dipyrromethanes



Scheme 5 Heptaalkyl and hexaalkylcalix[4]phyrins by oxidation, starting from calix[4]pyrroles



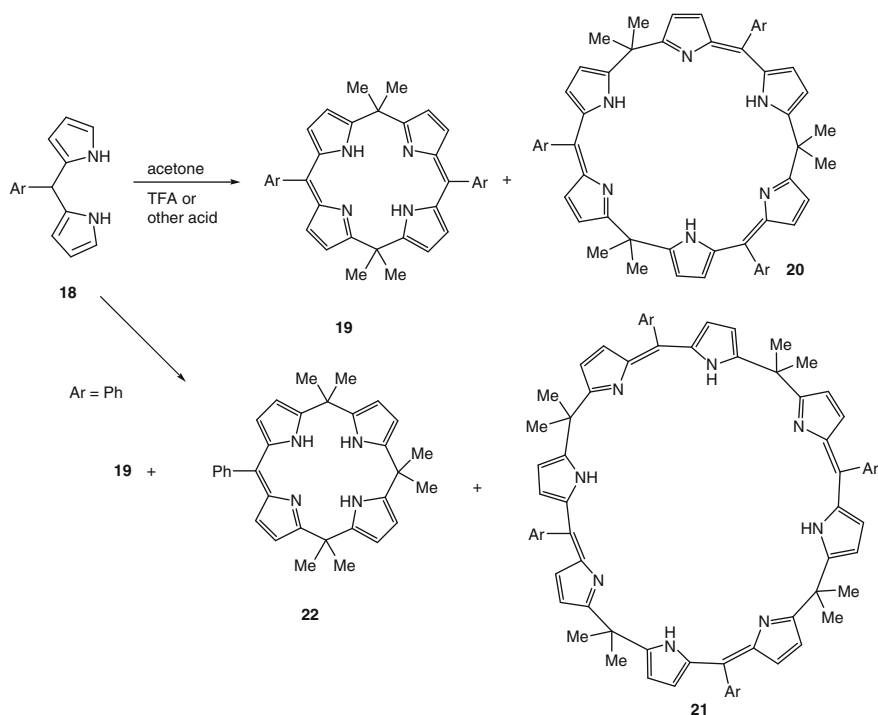
Scheme 6 Formation of unsymmetrical calix[4]pyrroles and functionalisation of calixphyrins-*(1.1.1.1)*

and carbonyl compounds (aldehydes, ketones), (b) from tripyrranes or higher pyrranes and (c) from monocyclic pyrrole building blocks.

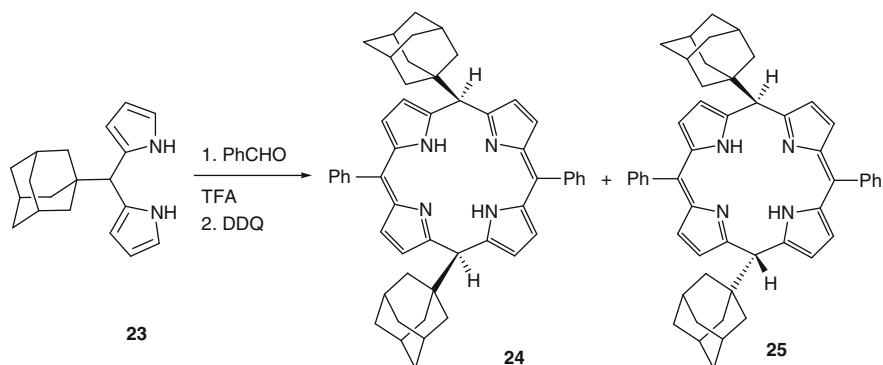
A quite successful synthesis of calix[n]pyrins was reported by Sessler and co-workers starting from mesityldipyrromethane **18** (Ar = 2,4,6-Me₃C₆H₂) and acetone, using different acid catalysts followed by DDQ oxidation. The calix[n]pyrins **19–21** of sizes $n = 4, 6$ and 8 were isolated in 44, 23 and 9% yield, respectively, when acetone was the solvent and TFA the catalyst. However, the calix[4]pyrin **19** was formed nearly exclusively when dichloromethane was employed as the solvent [33]. Similar results were obtained starting from the dipyrromethane **18** (90% yield of **19**, Ar = C₆F₅) derived from pentafluorobenzaldehyde [34].

The less stable phenyldipyrromethane (Ar = Ph [35]) apparently decomposed during the reaction and different calixpyrin products **19** and “scrambled” calixpyrin-(1.1.1.1) **22** were obtained back in poor yield (5% each) (Scheme 7).

Mlinarić-Majerski et al. reported the condensation of the very stable (1-adamantyl)-dipyrromethane **23** with benzaldehyde, followed by DDQ oxidation. The bulky adamantyl group prevents complete oxidation to the porphyrin, resulting in 12% yield of the *syn*-isomer of calixpyrin-(1.1.1.1) **24** while the *anti*-isomer **25** was not found. Analogous calix[4]pyrroles containing 1-adamantyl substituents could not be



Scheme 7 Different calix[n]pyrins starting from aryldipyrromethanes and acetone



Scheme 8 Formation of *syn*-isomer of 5,15-bis(1-adamantyl) calixphyrin

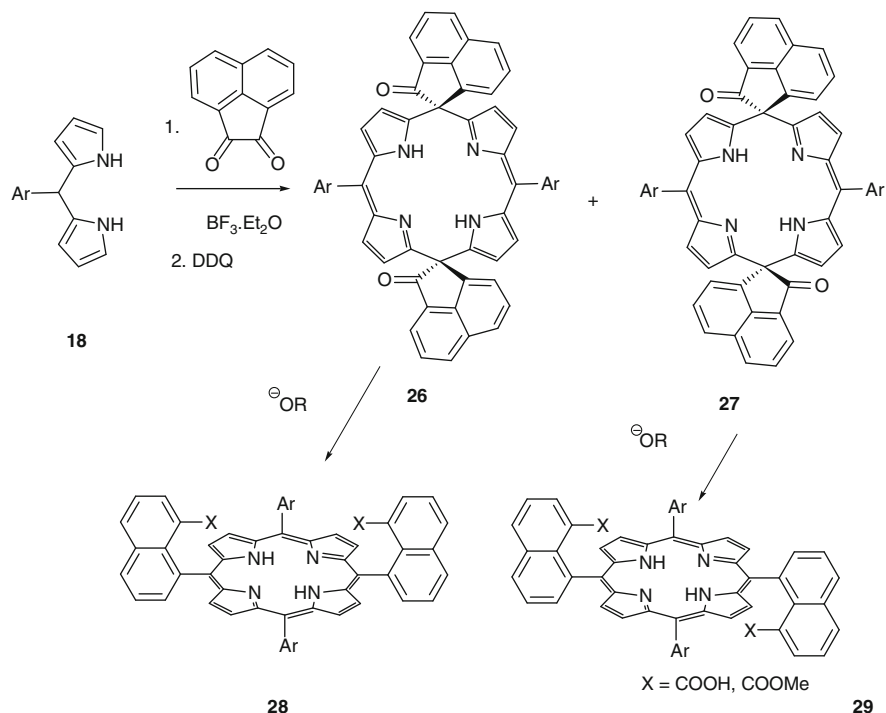
oxidised to the corresponding calix[4]phyrins [36]. These findings are similar to earlier reports from Senge et al. in which pivalaldehyde or other sterically hindered aldehydes were condensed with an arylaldehyde, resulting in the formation of porphomethenes and porphodimethenes in low yield (<1%) rather than the corresponding fully aromatised porphyrins (Scheme 8) [4].

Scott and co-workers reported the synthesis of a 1:2 *syn/anti* mixture of isomeric spirocalix[4]phyrins **26** and **27** in 26% combined yield from the BF_3 -catalysed condensation of mesityldipyrromethane **18** and acenaphthenequinone [37, 38]. This work was reported around the same time as and independent from Sessler's first publications on calixphyrins [33].

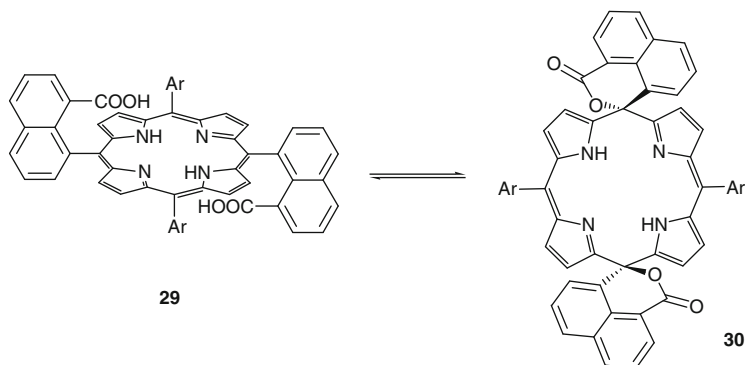
Heating of the spiro compounds **26** and **27** in the presence of 30% KOH or NaOMe results in the formation of the respective porphyrins **28** and **29**. The work was expanded to other benzaldehydes, and other vicinal diketones such as aceanthrenequinone, phenanthrenequinone and pyrene-4,5-dione (Scheme 9) [39].

Further synthetic transformations of the porphyrins of type **29** include the electrochemical interconversion to calix[4]phyrins-(1.1.1.1) **30** containing spiro-lactone groups [40]. The metallated derivatives of porphodimethenes **27** can undergo a facile oxidative rearrangement in two steps to non-planar and sheet-like porphyrins **31** and **32** (only the major *cis*-isomer shown, selectivity *cis/trans* about 2:1) (Schemes 10 and 11) [41].

Alternatively, 5,5-disubstituted dipyrromethanes **33** can be used in combination with benzaldehydes to prepare calix[4]phyrins. These dialkylated dipyrromethanes **33** are rather prone to acid-catalysed decomposition; therefore, even when using a very reactive aldehyde, e.g. pentafluorobenzaldehyde, for the condensation with **33** (R = Me) in the presence of TFA a relatively low yield (15%) only of the corresponding calix[4]phyrin-(1.1.1.1) **34** can be obtained after oxidation with DDQ. In other conditions (NH_4Cl , $\text{BF}_3 \cdot \text{Et}_2\text{O}$ in propionitrile), the "scrambled" product **35** is the major one (35% yield) with only 6% of the expected **34** (for Ar = C_6F_5 ; for Ar = 3- $\text{NO}_2\text{C}_6\text{H}_4$ the yields were 28/9%). Adding Florisil to the TFA catalyst resulted in the formation of **34** (Ar = C_6F_5) in a reasonable 41% yield [42, 43].

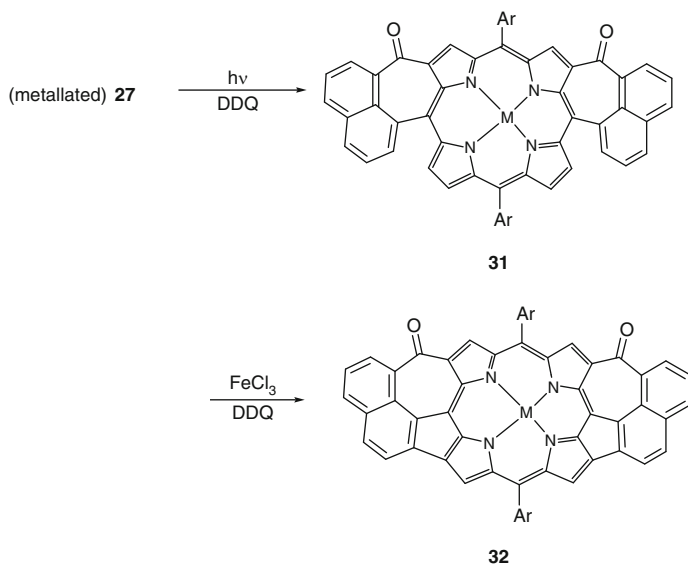


Scheme 9 Formation of two isomeric spirocalix[4]pyrins and ring opening to the corresponding porphyrins

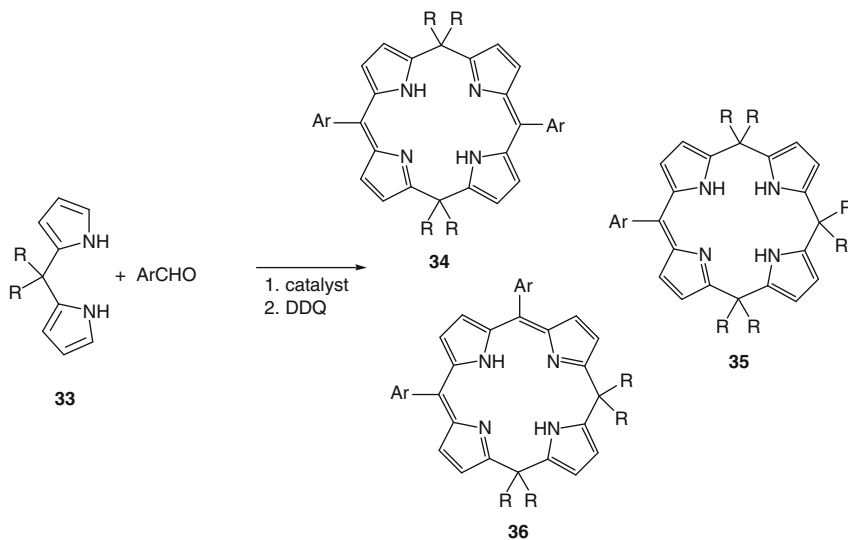


Scheme 10 Interconversion of porphyrins and spirocalixpyrins

With less reactive aldehydes (Ar = 4-hexadecyloxyphenyl) and dipyrroheptane **33** (R = Pr), using TFA catalysis, we observed the formation of the expected calixpyrin-(1.1.1.1) **34** (12%) and a small amount (3%) of the isomeric product **36** [44]. The use of ferrocene-carboxaldehyde with dimethyldipyrromethane **33**



Scheme 11 Sheetlike porphyrins starting from calixpyrins



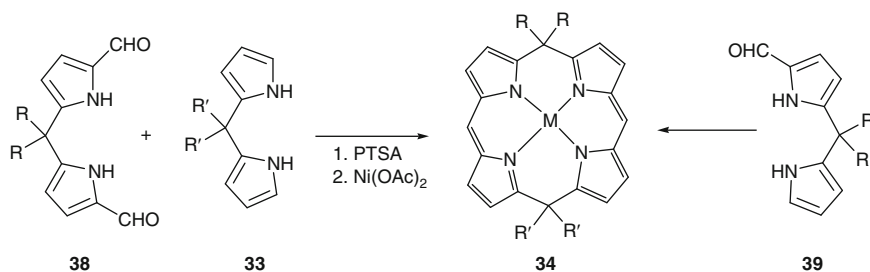
Scheme 12 Different calixpyrins from 5,5'-dialkyldipyromethanes and aromatic aldehydes

(R = Me) in similar conditions affords the three products of type **34–36** in yields of 16, 12 and 5%, respectively [45]. The phlorin **35** (R = Me) was the only product (35% yield) when 4-nitrophenylbenzaldehyde was used (Scheme 12) [46].

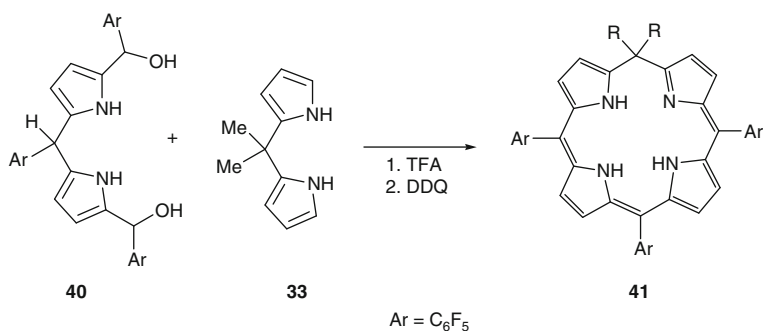
Condensing diformylated 5,5-dipyrromethanes **37** together with the parent compounds **33** under PTSA catalysis is a possibility to obtain low yields (1.5–3%) of unsymmetrically substituted calixphyrins-(1.1.1.1) **38**. The yield of this modular synthesis could be significantly improved (to 18–28%) by adding Ni(OAc)₂ to the reaction mixture, resulting in the formation of the Ni(II) complexes of **38**. Alternatively, the monoformylated dipyrromethane analogue **39** can be used in the same way to get symmetrical calix[4]phyrins (Scheme 13) [47].

A similar [2+2] procedure was reported by Geier and co-workers to obtain a 45% yield of calixphyrin-(1.1.1.1) **41** starting from dipyrromethane **33** and a dipyrromethanedicarbinol **40**. Different acid catalysts were tried but again TFA was found to be superior [48]. Lindsey reported the synthesis of a calixphyrin of type **34** (Pd complex) from two equivalents of a monophenylcarbinol analogue of **33** (Scheme 14) [49].

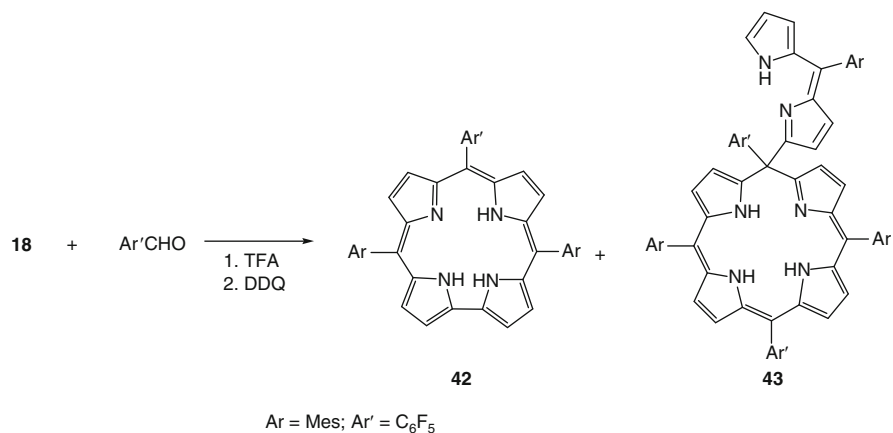
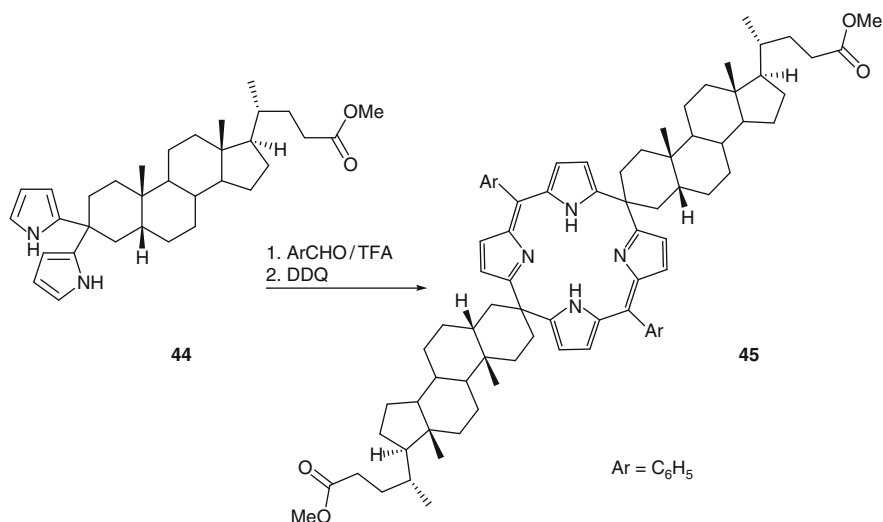
A remarkable phlorin–dipyrin conjugate **43** was reported by Gryko and Koszarna as a side-product of the acid-catalysed (TFA) condensation of aryldipyrromethanes **18** (Ar = mesityl) and pentafluorobenzaldehyde (2:1 ratio). The major product in this reaction is the corrole **42** (27% yield), along with the calixphyrin-(1.1.1.1) **43** (up to 16% yield). Combinations of other aldehydes and aryldipyrromethanes gave even lower yields of the analogues of **43** (Scheme 15) [50].



Scheme 13 Templated McDonald type synthesis of calixphyrins

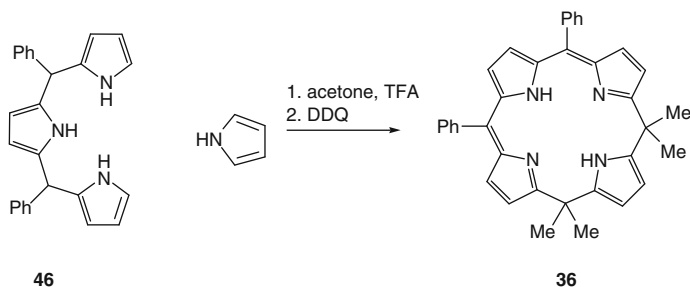


Scheme 14 Calixphyrins from dipyrromethanes and dipyrromethanedicarbinols

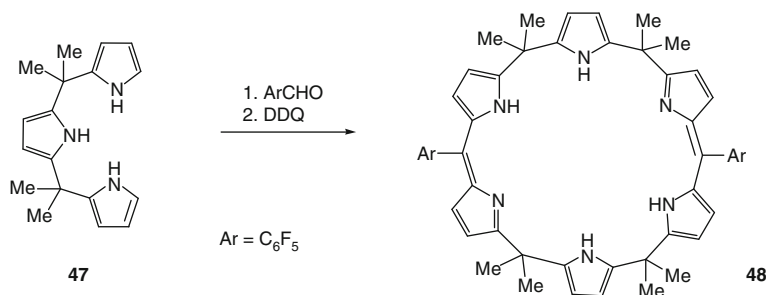
**Scheme 15** Phlorin-dipyrrin conjugate**Scheme 16** Steroidal spiroannulated calixphyrins derived from lithocholate ester

An interesting steroidal spiroannulated calixphyrin-(1.1.1.1) **45** was prepared as a mixture of diastereoisomers in very low yield (2%) from a dipyrromethane **44**, derived of a lithocholate ester after oxidation and combination of the keto derivative with pyrrole, and pentafluorobenzaldehyde (Scheme 16) [51].

Tripyrrane **46** was condensed with pyrrole and acetone (TFA catalysis) to afford the calixphyrin-(1.1.1.1) **36** (R = C₆H₅) in 15% yield [36]. A tetramethylated tripyrrane **47** was combined with pentafluorobenzaldehyde (without acid catalyst) to afford a calix[6]phyrin **48** in about 10% yield. The use of compound **47**, benzaldehyde and TFA catalysis was unproductive (Schemes 17 and 18) [52, 53].

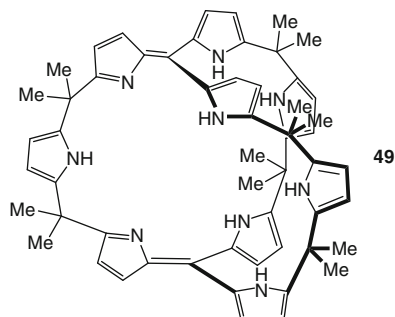


Scheme 17 Synthesis of calix[4]phyrins starting from tripyrranes



Scheme 18 Synthesis of calix[6]phyrins starting from tripyrranes

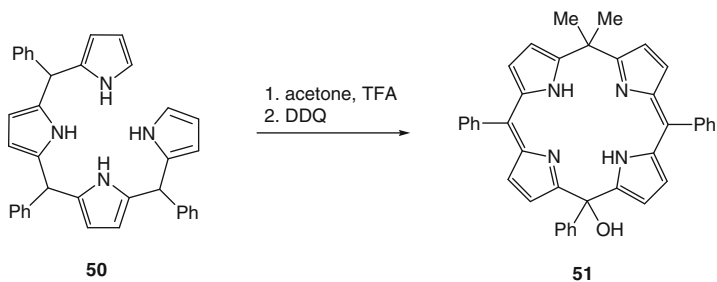
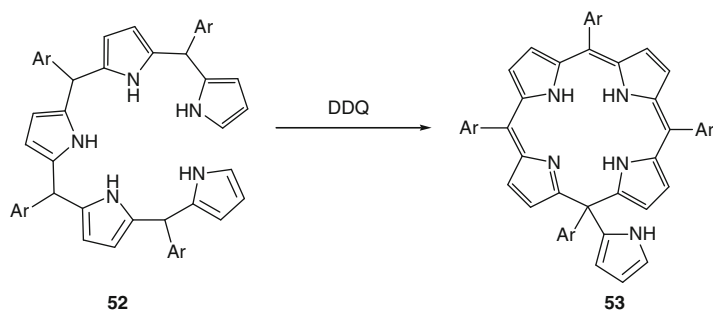
Fig. 3 Three-dimensional calixphyrin-like structure



The three-dimensional, cryptand-like calix[6]phyrin analogue **49** was prepared from **47**, orthoformate and TFA after DDQ oxidation [54].

The tetrapyrane **50** was condensed with acetone but did not afford the expected calixphyrin **41** (R = Me, Ar = Ph). Instead, a hydroxy analogue **51** was isolated (35% yield). Complexation of compound **51** with Zn(II) resulted in the formation of the porphodimethene **41** (Ar = Ph, R = Me) (Fig. 3; Scheme 19) [33].

The oxidative cyclisation of pentapyrrane **52** did not give a sapphyrin, as expected, but rather 22% of the *meso*-(2-pyrrolyl) calixphyrin **53**. The latter is transformed to the corresponding *meso*-tetraarylporphyrin after elimination of pyrrole on treatment with TFA (Scheme 20) [55].

**Scheme 19** Hydroxylated calix[4]phyrin**Scheme 20** Pyrrolylcalix[4]phyrin

Using a modified Lindsey protocol, “calix[3]dipyrriins” **54** were prepared in modest yield (0–15%) from a series of benzaldehydes and pyrrole. The products were metallated with $[\text{Ni}(\text{acac})_2]$ and often the corresponding porphyrin was isolated as a by-product, or even as the main product in some cases. Starting from 4-methoxycarbonylbenzaldehyde, the highest yield (15%) of **54** was obtained in combination with 8% of porphyrin. The reaction works only if the nickel salt is added after the condensation. Paramagnetic copper (II) salts of **54** also could be prepared [56]. Small amounts (2% yield) of calix[5]phyrins-(1.1.1.1.1) **55** were obtained as by-products from the acid-catalysed condensation reaction of 2-(2,2,2-trifluoro-1-hydroxyethyl)pyrrole, next to a variety of other macrocyclic polypyrroles. A slightly higher yield (4–5%) of calix[5]phyrin is obtained from the [2+2]-condensation of the corresponding tripyrrane and dipyrrenedicarbinol building blocks (Fig. 4) [57].

3 *N*-Confused Calixphyrins

The *N*-confused porphyrin (NCP) **56** ($\text{R} = \text{H}$) was combined with an in situ formed ketene, leading to the regio- and diastereoselective formation of the corresponding calix[4]phyrins **57** rather than the expected azetidinone [2+2] products [58].

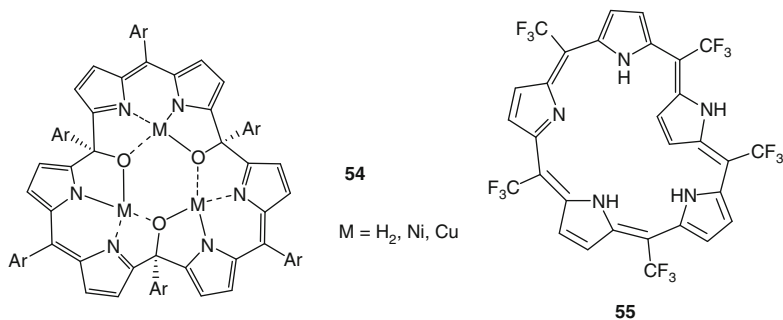
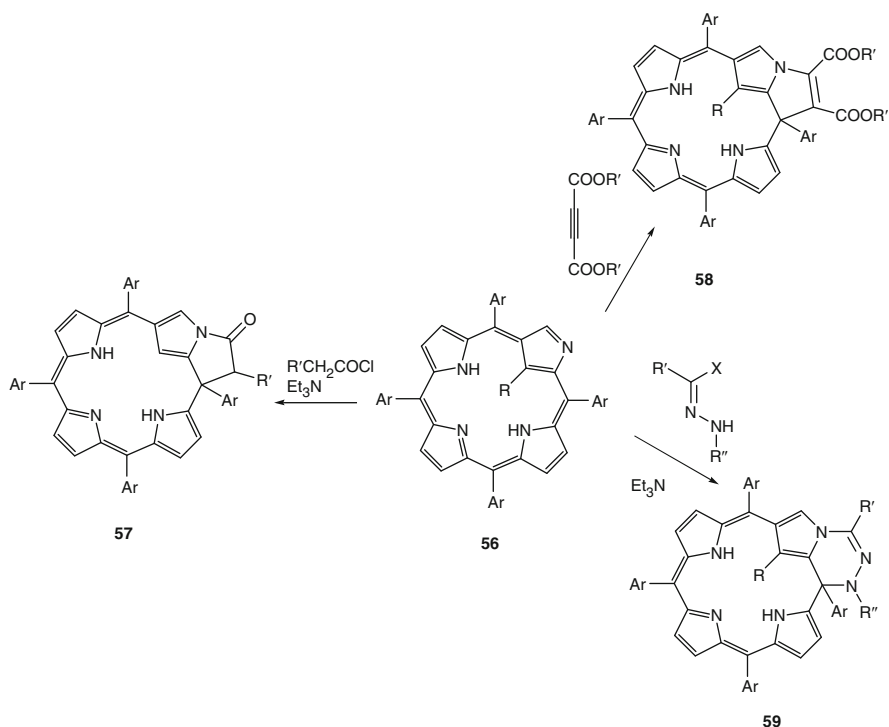


Fig. 4 Calix[3]dipyrins and calix[5]phyrins



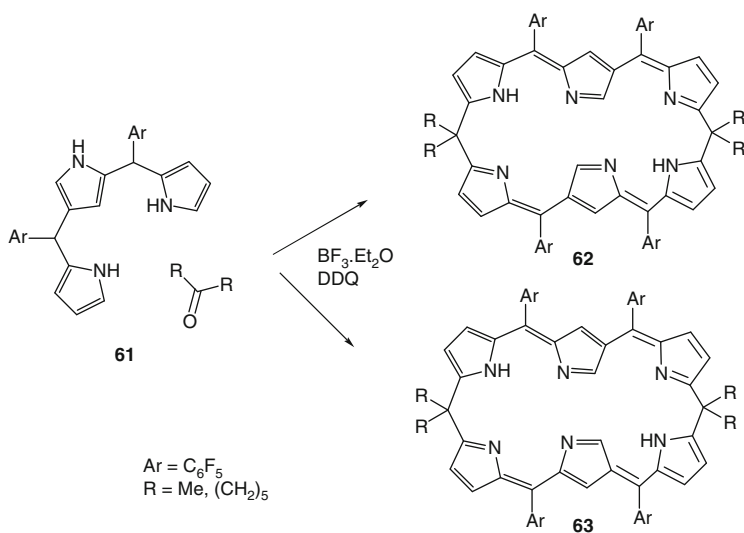
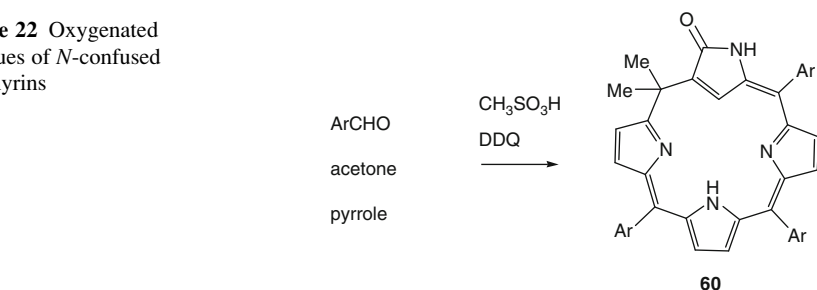
Scheme 21 Cycloaddition to *N*-confused porphyrins leading to calix[4]phyrins

Similarly, porphyrinoid **56** (R = H, NO₂), was reacted with either nitrilimines or diethyl acetylenedicarboxylate, affording respectively the fused calixphyrins **58** and **59** via zwitterionic intermediates, proceeding through an addition/cyclisation pathway [59]. Nitration of free-base NCP **56** (Ar = Ph) results in the formation of *meso*-dihydroxylated calixphyrin-(1.1.1.1) (Scheme 21) [60].

The condensation of an aromatic aldehyde, acetone and pyrrole in the presence of methanesulphonic acid, followed by DDQ oxidation gives the corresponding NCP analogue **56** (17% yield, R = H) and a small amount (3%) of an *N*-confused calixphyrin **60** with an amide group. The latter compound **60** was converted in good yields to Ni(II) and Cu(II) complexes with a metal-C bond [61]. The Zn complex did not have a metal-C bond (Scheme 22) [62].

Doubly *N*-confused calix[6]phyrins **62–63** were prepared by the condensation of an *N*-confused tripyrrane **61** with ketones. The condensation is catalysed by BF₃ etherate and can occur head-to-head or head-to-tail, affording two isomeric calix[6]phyrins-(1.1.1.1.1.1) **62** and **63** in fair combined yields (19–33%) [63]. The corresponding bis-Pt(II) complexes were prepared and their near-IR emission was studied (Scheme 23).

Scheme 22 Oxygenated analogues of *N*-confused calixphyrins



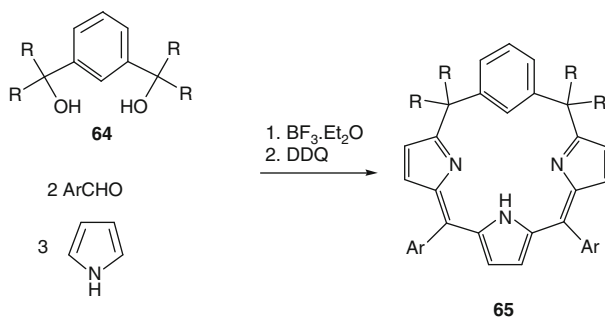
Scheme 23 Doubly *N*-confused calix[6]phyrins

4 Calixphyrins Incorporating Other Rings

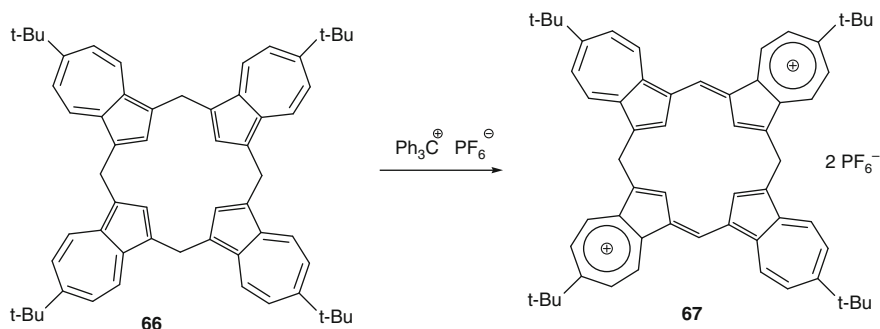
Some of the pyrrole rings in the calixphyrin structure may be substituted by carbocyclic or heterocyclic rings. *m*-Benziporphomethenes **65** with a *meta*-substituted benzene ring were prepared by Latos-Grażyński et al. by a mixed condensation of a dialcohol **64** (R = Ph), pyrrole and 4-nitrobenzaldehyde in 14% yield. The corresponding ZnCl, NiCl and CdCl complexes of **65** were prepared. From the NMR spectrum and X-ray studies of the paramagnetic NiCl complex, it can be seen that there is a weak agostic metal-arene bond [64]. A *m*-benzporphodimethene analogue **65** (R = Me, Ar = Ph) was prepared in a similar way (27% yield) and proposed as a long-wavelength Zn²⁺-specific chemosensor. Upon Zn²⁺-binding, the fluorescence ($\lambda_{\text{max}} = 672$ nm, quantum yield 0.34) is switched on, while **65** by itself is non-fluorescent. The corresponding Cd and Hg complexes are less stable complexes that are less fluorescent at a longer wavelength. Other metal ions, even if they bind, do not induce fluorescence (Scheme 24) [65].

An all-carbocyclic, dicationic calix[4]phyrin-(1.1.1.1) analogue **67** was prepared by hydride abstraction of a calix[4]azulene **66** [66] with trityl hexafluorophosphate. Oxidation of **66** with DDQ did not lead to identifiable products. The product **67** could be isolated by precipitation. Other calixphyrin analogues (the (1.1.1.1) monocationic, (1.1.1.1) dicationic and (1.1.1.1) tricationic analogues) may be present but they could not be isolated in the pure form. The authors commented that further stabilisation by *gem*-dimethyl groups would be needed to allow these systems to achieve their full potential (Scheme 25) [67].

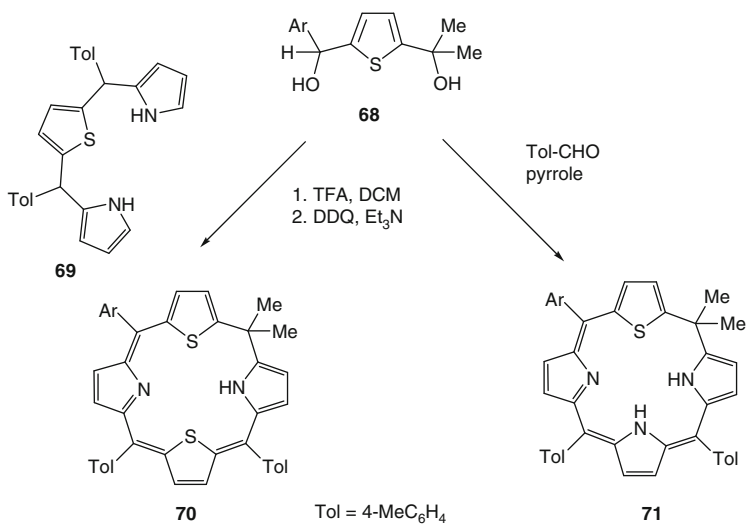
Thia analogues of calix[4]phyrin-(1.1.1.1) (thiaphlorins) were prepared starting from thiophene dialcohols **68**. In a first approach, **68** is combined with a “tripyrane” analogue **69** to afford the N₂S₂ core calixphyrin analogue **70** in low to fair yield (5–21%). The N₃S core analogue **71** is available in generally lower yields (3–9%) after a mixed condensation of **68**, pyrrole and an aromatic aldehyde. The thiaphlorin **70** (Ar = 4-iodophenyl) was covalently linked to other macrocyclic chromophores, such as porphyrins and thiaporphyrins, using the Sonogashira coupling reaction, affording the dyads **72** in fair yields [68, 69].



Scheme 24 *meta*-Benziporphodimethenes



Scheme 25 Azulenyl analogues of calix[4]phyrins



Scheme 26 Thiacalixphyrins and dithiacalixphyrins

Matano et al. reported compounds similar to **70** and **71** using a 2+2 approach, including also N₂SO core when the furan analogues of **68** were used [70].

Thia and selenacalix[5]phyrin analogues were reported by Chandrasekar et al. from tetrapyranes and analogues of **68** (Scheme 26; Fig. 5) [71].

In a series of recent articles [72–76], Matano et al. reported on the synthesis and properties of P,S-containing hybrid calix[4]phyrins **75**. The compounds **75** were prepared (24% yield) starting from triheterocyclic building blocks **73** and dialcohols **74**, together with a small amount (5%) of the reduced form **76**. The sulphur of **75** can be removed by treatment with excess P(NMe₂)₃. The palladium complexes **77** can be prepared in high yield from both the reduced or oxidised forms by treatment with Pd(II) or Pd(0) complexes, respectively. Also rhodium(I) and

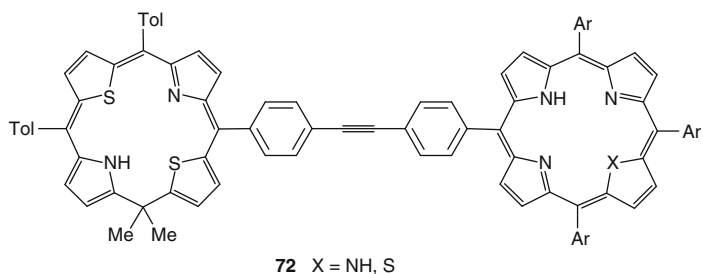
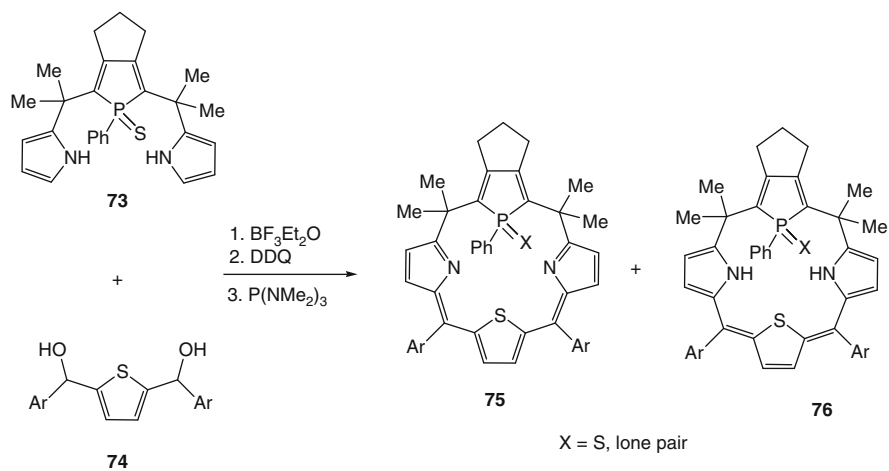


Fig. 5 Dyads of thiacalixphyrin and (thia)porphyrin



Scheme 27 P,S-containing hybrid calixphyrins

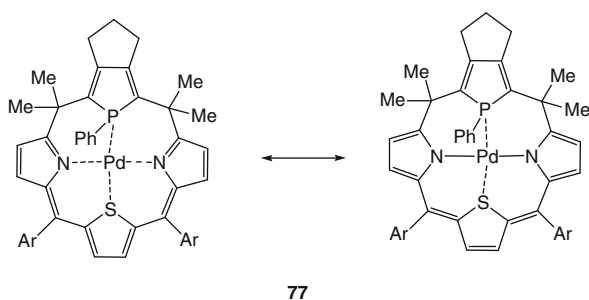
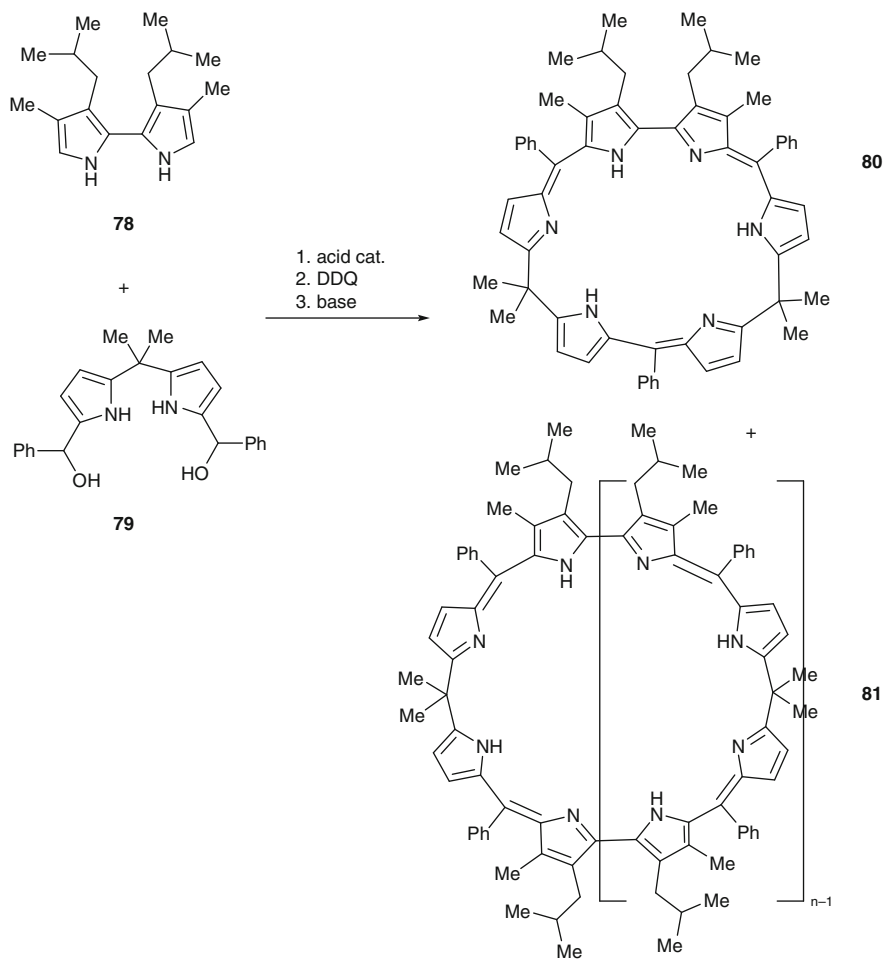


Fig. 6 Resonance structures of Pd complexes of P,S-containing hybrid calixphyrins

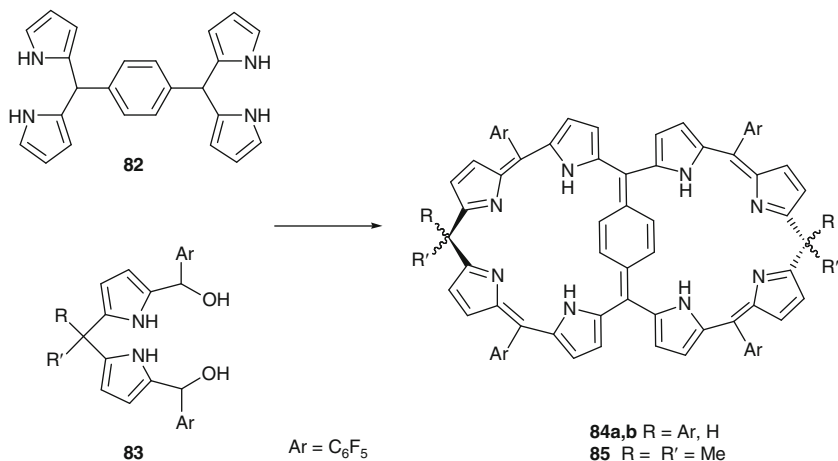
Au(I) complexes were obtained. The hybrid calixphyrins behave as neutral, anionic, or dianionic tetradentate ligands with electronic structures that are varying widely (Scheme 27; Fig. 6) [76].

Hybrid compounds that are related to calixphyrins are the cyclohexapyrroles **80** with C_2 -symmetry that are on the basis of 2,2'-bipyrrole units **78** and dipyrromethanediols **79**. The cyclohexapyrroles **80** bear some analogy to the calix[3]bipyrroles [77, 78] but also incorporate sp^2 -hybridised *meso*-carbons. The optimum yield of **80** is 15% when a 0.22 ratio of TFA to **78** is used. With other acid catalysts or other relative concentrations of reagents, more of the different cyclic oligomers **81** ($n = 1-7$) corresponding to the "normal" condensation reaction are formed (Scheme 28) [79].

Osuka et al. reported internally 1,4-phenylene-bridged calixphyrins analogues. Condensation of 1,4-phenylene bis-dipyrromethane **82** with dipyrromethanediol **83** ($R =$ pentafluorophenyl, $R' = H$) in the presence of methanesulphonic acid followed by *p*-chloranil oxidation gave the expected porphyrin dimer (2% yield),



Scheme 28 Calixphyrins-(1.1.1.1.0) and cyclic oligomers ($n = 1-7$)



Scheme 29 Internally 1,4-phenylene bridged calixpyrrolin analogues

together with an even lower yield (0.6 and 0.5%) of two isomeric octapyrroles **84a, b**. The compound **85** was prepared in a similar way from **82** and **83** (R = R' = Me) in 3% yield (Scheme 29) [80].

5 Anion Complexation

In fact, many reports have not appeared on the anion binding properties of calix[n]pyrrolins, certainly in comparison with the calix[n]pyrroles. This may be explained by the fact that the more reduced calixpyrrolins have less N–H bonds to interact via electrostatic hydrogen bonds with anions. However, protonation of the basic di or oligopyrrolin units in the macrocycle significantly increases the anion binding. An advantage of calixpyrrolins is that they (and certainly their protonated forms) contain a strong chromophore that helps in carrying out the binding experiments.

In their first report on calix[n]pyrrolins, Sessler et al. mentioned that all three calixpyrrolins **19–21** bind anions, as judged from changes in the UV–Vis spectrum when dichloromethane solutions of **19–21** are treated with tetrabutylammonium (TBA) salts of various anions [33]. However, these initial findings were not followed up by more detailed reports.

The “deep cavity” calix[6]pyrrolin **48** does not bind anions unless it is protonated. In the solid phase, a complex $[\mathbf{48}.\text{H}^+]\text{Cl}^-$ was formed that was analysed by X-ray crystallography, showing the chloride counterion firmly located into the cavity. In solution-phase (acetone), the diprotonated form of **48** can be generated by treatment with excess of oleum (90 molar equivalents $\text{H}_2\text{SO}_4.30\%\text{SO}_3$). It was calculated that iodide and $\mathbf{48}.\text{2H}^+$ show a K_a for 1:1 complexation of $8 \times 10^7 \text{ M}^{-1}$ [52].

The sterically congested adamantane calixphyrin **24** does not bind tetrabutylammonium salts (fluoride, chloride, bromide), as no changes could be seen in either the UV–Vis or the NMR (CDCl_3) spectra on addition of excess of the salt [36]. Apparently, no experiments were carried out with the protonated form of **24**.

A chiral calixphyrin-(1.1.1.1) dimer **86** was prepared starting from **35** ($\text{Ar} = 3\text{-NO}_2\text{C}_6\text{H}_4$) by reduction of the nitro function and coupling of the anilino derivative to a binaphthyl moiety. The resulting chiral receptor **86** exhibits moderate enantio-recognition towards D-malic acid as determined by potentiometry, using liquid membrane ion-selective electrodes with PVC membranes, incorporating **86**. With the same technique, the corresponding monomeric calixphyrins **34–35** ($\text{Ar} = \text{pentafluorophenyl}, 3\text{-NO}_2\text{C}_6\text{H}_4$) were shown to possess oxoanion (benzoate, salicylate, nitrate) affinity at pH 9, while halides were poorly bound. UV–Vis and electrochemical titrations of **34–35** and these anions showed a 1:1 binding ratio (Fig. 7) [42].

An isothiocyanato-substituted calix[4]phyrin-(1.1.1.1) **87** was prepared from the corresponding macrocycle **35** ($\text{Ar} = 4\text{-nitrophenyl}$) via reduction and treatment of the aniline derivative of **35** with 1,1'-dithiocarbonyl-2,2'-pyridone. This product **87** is of use to prepare anion sensors. Thus, the isothiocyanato function has been used for the attachment of the calixphyrin moiety to solid support (Tentagel S NH_2). Alternatively, the NCS function can be used to functionalise the calixphyrin group with amines or amino acids. The binding of fluoride to the functionalised solid support **88** was evaluated by following the shifts in the ^1H magic angle spinning spectra.

Binding of the monocalixphyrin **35** ($\text{Ar} = 4\text{-nitrophenyl}$) to fluoride (TBA salts, in dichloromethane) was shown by ^1H NMR and UV–Vis spectroscopy to be relatively weak, but still two orders of magnitude stronger than to chloride, bromide or hydrogen sulphate. Iodide showed no response at all to **35** (Scheme 30) [46].

Bucher et al. described electrochemical sensing of the protonated form of calixphyrin–ferrocene conjugate **35** ($\text{Ar} = 2\text{-ferrocenyl}$). The electrochemical recognition properties of the protonated form of **35**, which could be obtained by addition of one equivalent of perchloric acid, were studied towards various anionic substrates, but every attempt to electrochemically sense a binding event between 35H^+ and any anionic substrate proved unsuccessful. The failure was not attributed

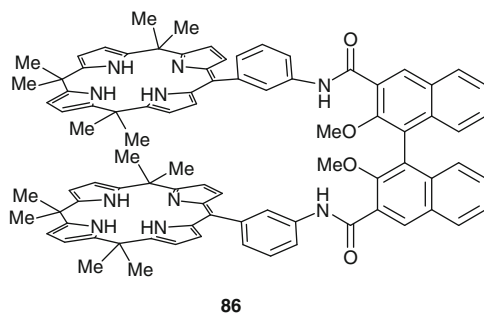
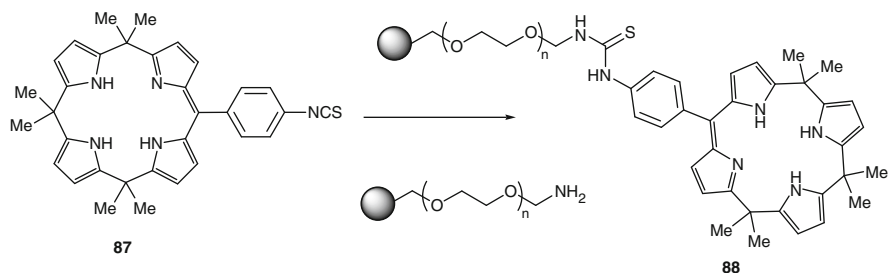


Fig. 7 Chiral calixphyrin-(1.1.1.1) dimer



Scheme 30 Isothiocyanato functionalised calixphyrin for functionalisation of a solid support

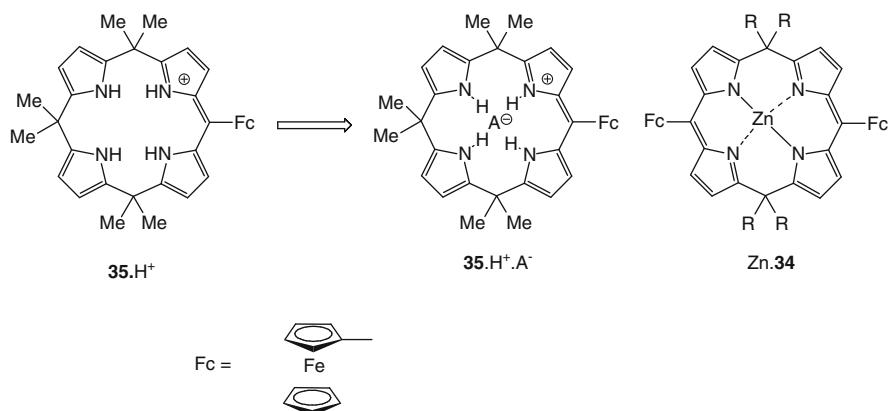


Fig. 8 Anion binding to protonated form or zinc complex of calix[4]phyrin–ferrocene conjugates

to the absence of binding but rather as the consequence of a too weak perturbation effect on the redox probe. However, the Zn complex of the calix[4]phyrin-(1.1.1.1) **34** in its neutral reduced state binds fluoride, chloride and bromide (as the TBA salt) with constants of 8,200, 3,500 and 3,000 M^{-1} , respectively [45, 81]. In comparison with the binding to the Zn tetratolylporphyrin-chloride (250 M^{-1}) [82], the binding to the former receptor is quite higher (Fig. 8).

The phlorins **53** bind fluoride anions as monitored by UV–Vis spectroscopy. The stoichiometry of receptor to fluoride is 1:2 as indicated by the Job plot, with binding constants 3.4×10^4 and $1.2 \times 10^5 \text{ M}^{-1}$. No detectable colour change is found with the other halide anions [55, 83].

The protonated forms of thiaphlorin **70** show strong absorptions in their 800–860 nm regions. A fit for a 1:1 binding profile with TBA salts was found, and the highest affinities of 70.H^+ were for bromide and iodide rather than chloride, thiocyanate or hydrogensulphate. In the case of dyad **72** ($\text{X} = \text{S}$), the thiocalix[4]phyrin part can be selectively protonated without protonating the thiaporphyrin subunit, and the changes in the strong fluorescence of the latter unit on addition of TBA salts were used for the anion binding study in dichloromethane. The binding

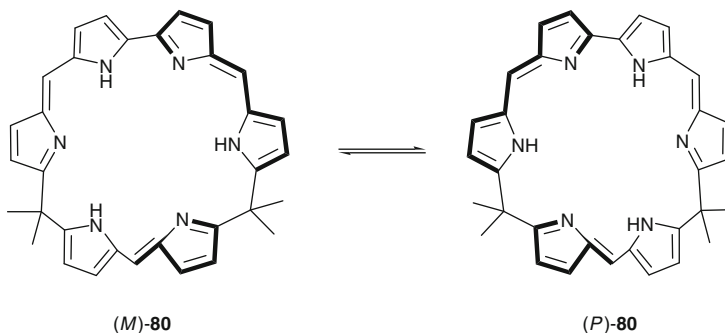


Fig. 9 Helical structures **80**

constant K_a for protonated dyad **72.H⁺** was obtained by fluorescence spectroscopy, observing the enhancement in the fluorescence in the conjugated thiaporphyrin unit ($\lambda_{em} = 692$ nm).

The hybrid calix[6]phyrin **80** forms complexes with (S)-(+)- or (R)-(-)- mandelic acid inducing a CD Cotton effect in the visible region at 461 and 650 nm. The π -conjugated tetrapyrrolic structural unit in compound **80** is helical, and therefore this C_2 -symmetrical cyclic hexapyrrole can be applied as a chirality sensing device. On the other hand, as the pyrroles in **80** are not convergent, this calixphyrin analogue may not be suitable as an anion host (Fig. 9) [79].

The anion binding behaviours of the related N,N' -dialkylated oxoporphyrinogens **10** or even the non-alkylated derivatives have been studied extensively by Hill, D'Souza et al. [21–28]. X-ray and computational studies show a rigid structure and saddle ring puckering with opposite hydrogens pointing in the same direction, away from the plane of the macrocycle. Two 1,3-alternating pyrrole hydrogens are on the same side, ideally placed for binding of a variety of anions. These intensively coloured oxoporphyrinogens may be used to distinguish fluoride chromogenically from other anions [23]. Solvatochromism was combined with anion binding in an attempt to provide more selective tests for anions. Derivatives of **10** are highly effective in electrochemical anion sensing, using the redox activity of the hemiquinoid *meso*-substituents. Cathodic shifts up to 600 mV (for fluoride) were observed upon anion binding (solvent: *o*-dichlorobenzene) and this correlated well with the anion binding constants [26]. Recently, a sophisticated oligochromophoric system based on **10**, peripheral porphyrin and C_{60} units has been used to show anion complexation induced stabilisation of charge separation [28].

6 Conclusion

In the last decade, several research groups have reported on the synthesis and properties of calix[n]phyrins. Different synthetic methods were explored in detail. As a result, a large variety of calixphyrins is now available, including calixphyrins

of different ring sizes, *N*-confused derivatives and analogues containing other rings than pyrrole. Calixphyrins, especially calix[4]phyrins are ligands that can be metallated with different (mainly transition) metals.

The anion binding properties of calix[n]phyrins have been less explored in comparison to those of the corresponding calix[n]pyrroles. In many cases, protonation of the dipyrromethene unit(s) is needed to get significant binding.

Further development of the anion binding properties of calix[n]phyrins may involve conjugation of additional anion binding groups to the ring structure. Moreover, the properties of calix[n]phyrins in anion transport remain unexplored.

References

1. Sessler JL, Zimmerman RS, Bucher C, Král V, Andrioletti B (2001) *Pure Appl Chem* 73:1041–1057
2. Bischoff I, Feng X, Senge MO (2001) *Tetrahedron* 57:5573–5583
3. Senge MO, Kalisch WW, Bischoff I (2000) *Chem Eur J* 6:2721–2738
4. Senge MO, Runge S, Speck M, Ruhlandt-Senge K (2000) *Tetrahedron* 56:8927–8932
5. Sergeeva NN, Senge MO (2006) *Tetrahedron Lett* 47:6169–6172
6. Sergeeva NN, Shaker YM, Finnigan EM, McCabe T, Senge MO (2007) *Tetrahedron* 63:12454–12464
7. Senge MO, Bischoff I (2001) *Eur J Org Chem*:1735–1751
8. Kalisch WW, Senge MO (1998) *Angew Chem Int Ed* 37:1107–1109
9. Senge MO (2005) *Acc Chem Res* 38:733–743
10. Krattinger B, Callot HJ (1996) *Tetrahedron Lett* 37:7699–7702
11. Krattinger B, Callot HJ (1998) *Tetrahedron Lett* 39:1165–1168
12. Krattinger B, Callot HJ (1999) *Eur J Org Chem*:1857–1867
13. LeSaulnier TD, Graham BW, Geier GR (2005) *Tetrahedron Lett* 46:5633–5637
14. Kojima T, Hanabusa K, Ohkubo K, Shiro M, Fukuzumi S (2008) *Chem Commun*:6513–6515
15. Milgrom LR (1983) *Tetrahedron* 39:3895–3898
16. Milgrom LR, Mofidi N, Jones CC, Harriman A (1989) *J Chem Soc Perkin Trans* 2:301–309
17. Milgrom LR, Nolan KB, Povey DC (1989) *Chem Commun*:1751–1753
18. Milgrom LR, Hill JP, Dempsey PF (1994) *Tetrahedron* 37:13477–13484
19. Milgrom LR, Hill JP, Yahioğlu G (1995) *J Heterocycl Chem* 32:97–101
20. Dolušić E, Toppet S, Smeets S, Van Meervelt L, Tinant B, Dehaen W (2003) *Tetrahedron* 59:395–400
21. Hill JP, Hewitt IJ, Anson CE, Powell AL, McCarty PA, Karr PA, Zandler ME, D'Souza F (2004) *J Org Chem* 69:5861–5869
22. Hill JP, Schmitt W, McCarty AL, Ariga K, D'Souza F (2005) *Eur J Org Chem*:2893–2902
23. Hill JP, Schumacher AL, D'Souza F, Labuta J, Redshaw C, Elsegood MRJ, Aoyagi M, Nakanishi T, Ariga K (2006) *Inorg Chem* 45:8288–8296
24. Hill JP, Sandanayaka ASD, McCarty AL, Karr PA, Zandler ME, Charvet R, Ariga K, Araki Y, Ito O, D'Souza F (2006) *Eur J Org Chem*:595–603
25. Schumacher AL, Sandanayaka ASD, Hill JP, Ariga K, Karr PA, Araki Y, Ito O, D'Souza F (2007) *Chem Eur J* 13:4628–4635
26. Schumacher AL, Hill JP, Ariga K, D'Souza F (2007) *Electrochem Commun* 9:2751–2754
27. Xie Y, Hill JP, Schumacher AL, Sandanayaka ASD, Araki Y, Karr PA, Labuta J, D'Souza F, Ito O, Anson CE, Powell AK, Ariga K (2008) *J Phys Chem C* 112:10559–10572
28. D'Souza F, Subbaiyan NK, Xie Y, Hill JP, Ariga K, Ohkubo K, Fukuzumi S (2009) *J Am Chem Soc* 134:16138–16146

29. Da Silva C, Bonomo L, Solari E, Scopelliti R, Floriani C, Re N (2000) *Chem Eur J* 6:4518–4531
30. Bonomo L, Solari E, Scopelliti R, Floriani C, Re N (2000) *J Am Chem Soc* 122:5312–5326
31. Re N, Bonomo L, Da Silva C, Solari E, Scopelliti R, Floriani C (2001) *Chem Eur J* 7:2536–2546
32. Floriani C, Floriani-Moro R (2000) *Porphyrin handbook*, vol 3, pp 405–420
33. Král V, Sessler JL, Zimmerman RS, Seidel D, Lynch V, Andrioletti B (2000) *Angew Chem Int Ed* 39:1055–1058
34. Dolenský B, Kroulík J, Král V, Sessler JL, Dvořáková H, Bouř P, Bernátkova M, Bucher C, Lynch V (2004) *J Am Chem Soc* 126:13714–13722
35. Bucher C, Seidel D, Lynch V, Král V, Sessler JL (2000) *Org Lett* 2:3103–3106
36. Alešković M, Halasz I, Basarić N, Mlinarić-Majerski K (2009) *Tetrahedron* 65:2051–2058
37. Harmjanž M, Scott MJ (2000) *Chem Commun*:397–398
38. Harmjanž M, Gill HS, Scott MJ (2001) *J Org Chem* 66:5374–5383
39. Harmjanž M, Božidarević I, Scott MJ (2001) *Org Lett* 3:2281–2284
40. Harmjanž M, Gill HS, Scott MJ (2000) *J Am Chem Soc* 122:10476–10477
41. Gill HS, Harmjanž M, Santamaria J, Finger I, Scott MJ (2004) *Angew Chem Int Ed* 43:485–490
42. Bernátkova M, Andrioletti B, Král V, Rose E, Vaissermann J (2004) *J Org Chem* 69:8140–8143
43. Bernátkova M, Dvořáková H, Andrioletti B, Král V, Bouř P (2005) *J Phys Chem A* 109:5518–5526
44. Orlewska C, Toppet S, Dehaen W (2005) *Synth Commun* 35:1953–1959
45. Bucher C, Devillers CH, Moutet J-C, Pécaut J, Royal G, Saint-Aman E, Thomas F (2005) *Dalton Trans*:3620–3631
46. Jha SC, Lorch M, Lewis RA, Archibald SJ, Boyle RW (2007) *Org Biomol Chem* 5:1970–1974
47. Orlewska C, Maes W, Toppet S, Dehaen W (2005) *Tetrahedron Lett* 46:6067–6070
48. O'Brien AY, McGann JP, Geier GR (2007) *J Org Chem* 72:4084–4092
49. Sharada DS, Muresan AZ, Muthukumaran K, Lindsey JS (2005) *J Org Chem* 70:3500–3510
50. Gryko DT, Koszarna B (2005) *Eur J Org Chem*:3314–3318
51. Huang NTT, Klímková P, Sorrenti A, Mancini G, Drašar P (2009) *Steroids* 74:715–720
52. Bucher C, Zimmerman RS, Lynch V, Král V, Sessler JL (2001) *J Am Chem Soc* 123:2099–2100 (Erratum *ibid.* 123:12744)
53. Chen W, Liu TJ (2008) *Chinese Chem Lett* 19:1199–1201
54. Bucher C, Zimmerman RS, Lynch V, Sessler JL (2003) *Chem Commun*:1646–1647
55. Ka J-W, Lee C-H (2001) *Tetrahedron Lett* 42:4527–4529
56. Inoue M, Ikeda C, Kawata Y, Venkatraman S, Furukuwa K, Osuka A (2007) *Angew Chem Int Ed* 46:2306–2309
57. Shimizu S, Aratani N, Osuka A (2006) *Chem Eur J* 12:4909–4918
58. Li X, Chmielewski P, Xiang J, Xu J, Jiang L, Li Y, Liu H, Zhu D (2006) *Org Lett* 8:1137–1140
59. Li X, Chmielewski P, Xiang J, Xu J, Jiang L, Li Y, Liu H, Zhu D (2006) *J Org Chem* 71:9739–9742
60. Hung C-H, Liaw C-C, Chin M-W, Chang G-F, Chuang C-H (2006) *J Porphyr Phthalocyan* 10:953–961
61. Furuta H, Ishizuka T, Osuka A, Uwatoko Y, Ishikawa Y (2001) *Angew Chem Int Ed* 40:2323–2325
62. Furuta H, Ishizuka T, Osuka A (2003) *Inorg Chem Commun*:398–401
63. Won DH, Toganoh M, Terada Y, Fukatsu S, Uno H, Furuta H (2008) *Angew Chem Int Ed* 47:5438–5441
64. Stepien M, Latos-Grazynski L, Szterenberg L, Panek J, Latajka Z (2004) *J Am Chem Soc* 126:4566–4580
65. Hung C-H, Chang G-F, Kumar A, Lin GF, Luo L-Y, Chin W-M, Diao EW-G (2008) *Chem Commun*:978–980

66. Colby DA, Lash TD (2002) *J Org Chem* 67:1031–1033
67. Lash TD, El-Beck JA, Dolby DA (2009) *J Org Chem* 74:8830–8833
68. Gupta I, Fröhlich R, Ravikanth M (2006) *Chem Commun*:3726–3728
69. Gupta I, Fröhlich R, Ravikanth M (2008) *Eur J Org Chem*:1884–1900
70. Matano Y, Miyajima T, Ochi N, Nakao Y, Sakaki S, Imahori H (2008) *J Org Chem* 73:5139–5142
71. Gokulnath S, Chandrashekar TK (2008) *Org Lett* 10:637–640
72. Matano Y, Miyajima T, Nakabuchi T, Imahori H, Ochi N, Nakao Y, Sakaki S (2006) *J Am Chem Soc* 128:11760–11761
73. Matano Y, Miyajima T, Ochi N, Nakabuchi T, Shiro M, Nakao Y, Sakaki S, Imahori H (2008) *J Am Chem Soc* 130:990–1002 (Erratum *ibid.* 130:14123)
74. Ochi N, Nakao Y, Sato H, Matano Y, Imahori H, Sakaki S (2009) *J Am Chem Soc* 131:10955–10963
75. Matano Y, Fujita M, Miyajima T, Imahori H (2009) *Organometallics* 28:6213–6217
76. Matano Y, Imahori H (2009) *Acc Chem Res* 42:1193–1204
77. Sessler JL, An D, Cho W-S, Lynch V (2003) *Angew Chem Int Ed* 42:2278–2281
78. Sessler JL, An D, Cho W-S, Lynch V, Marquez M (2005) *Chem Commun*:540–542
79. Setsune J, Tsukajima A, Watanabe J (2007) *Tetrahedron Lett* 48:1531–1535
80. Anand VG, Saito S, Shimizu S, Osuka A (2005) *Angew Chem Int Ed* 44:7244–7248
81. Rhee SW, Na YH, Do Y, Youngkyu K, Kim J (2000) *Inorg Chim Acta* 309:49–56
82. Bucher C, Devillers CH, Moutet J-C, Royal G, Saint-Aman E (2004) *New J Chem* 28:1584–1587
83. Ka J-W, Won DH, Lee C-H (2003) *Bull Korean Chem Soc* 24:661–663

Acyclic Oligopyrrolic Anion Receptors

Hiromitsu Maeda

Abstract Recent progress in the guest-binding and supramolecular chemistry of anion-responsive acyclic oligopyrroles is summarized here in this chapter. The hydrogen-bonding properties of the pyrrole NH sites determine anion binding in acyclic oligopyrroles such as guanidinocarbonyl and amidopyrroles, dipyrrens and their analogs, dipyrrolylquinoxalines, and boron complexes of dipyrrolyldiketones. Linear oligopyrroles can be incorporated as subunits in various macromolecules and complexes by means of covalent and noncovalent interactions; in fact, boron complexes of dipyrrolyldiketones form assembled structures and, with the appropriate substituents, soft materials such as anion-responsive supramolecular gels.

Keywords Anion receptors · Open-chain systems · Pyrrole derivatives · Supramolecular assemblies

Contents

1	Introduction	104
2	Guanidinocarbonylpyrrole-Based and Amidopyrrole-Based Anion Receptors	106
2.1	Guanidinocarbonylpyrrole-Based Anion Receptors	106
2.2	Amidopyrrole-Based Anion Receptors	111
3	Dipyrrens and Their Analogs as Anion Receptors	115
4	Dipyrrolylquinoxalines and Related Aryl-Bridged Bispyrroles	119
4.1	Dipyrrolylquinoxalines	119
4.2	Anion-Responsive Aryl-Bridged Bispyrroles	126
5	Boron Complexes of Dipyrrolyldiketones as Acyclic Anion Receptors with Planar Geometries	129
5.1	Boron Complexes of Dipyrrolyldiketones	129

H. Maeda (✉)

College of Pharmaceutical Sciences, Institute of Science and Engineering, Ritsumeikan University, Kusatsu 525–8577, Japan

PRESTO, Japan Science and Technology Agency (JST), Kawaguchi 332–0012, Japan

e-mail: maedahir@ph.ritsumeai.ac.jp

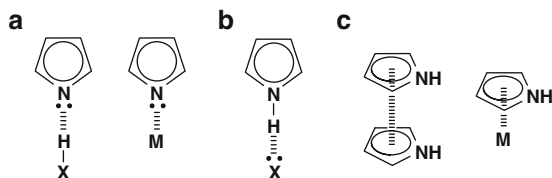
5.2 Aryl-Substituted Anion Receptors	133
5.3 Supramolecular Structures Consisting of Acyclic Anion Receptors	135
6 Summary	139
References	140

1 Introduction

The electrostatic hydrogen-bonding interactions between anions and polarized hydrogen-bonding donor sites are exploited in various receptor–anion complexes that conduct anion exchange in equilibrium. In biotic systems, we have ClC chloride channels that selectively conduct Cl[−] ions across cell membranes to regulate electrical excitation in skeletal muscle and salt and water exchange across epithelial barriers [1, 2]. The X-ray structures of two prokaryotic ClC Cl[−] channels were solved in 2002 and revealed much information about their functioning on a molecular level. Both structures revealed dimeric proteins forming individual subunits. Each subunit comprised two halves in an antiparallel alignment to create a selectivity filter in which Cl[−] ions were stabilized by electrostatic interactions with α -helix dipoles and by chemical interaction with NH and OH sites [3]. Together with such studies, considerable efforts have also been devoted to the development of artificial anion receptors and carriers, and various binding motifs have been synthesized in recent years [4–20]. Of particular interest are electronically neutral π -conjugated planar receptors, which form “planar anions” with spherical halide anions. This is because negatively charged planar units, in combination with appropriate counter cations, are essential building blocks for supramolecular assemblies and functional materials.

Pyrrole, one building block for planar anion receptors, is a well-known π -conjugated aromatic heterocyclic molecule [21] found in not only biotic dyes such as heme and chlorophyll but also artificial porphyrin derivatives [22]. In contrast to the relatively “inert” benzene, pyrrole has more electrons (six) than atoms (five) in the framework, and therefore, pyrrole moieties are reactive and stabilized by, for example, incorporation into aromatic macrocycles such as porphyrins or substitution by electron-withdrawing moieties. Pyrrole exhibits “duality” at its nitrogen moiety, which behaves both as a hydrogen-bonding acceptor or a metal coordination ligand due to the N site (Fig. 1a) and a hydrogen-bonding donor

Fig. 1 Possible interactions of pyrrole as (a) a hydrogen-bonding acceptor and a metal coordination site, (b) a hydrogen-bonding donor, and (c) a π -plane for stacking and metal coordination. The structures with the “aromatic circle” represent various types of pyrrole units



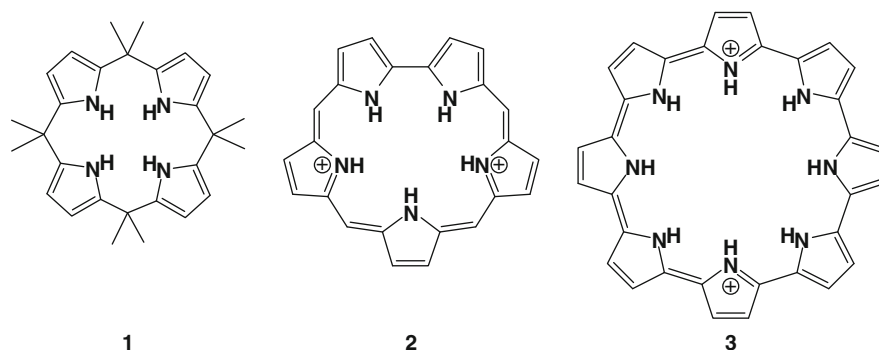


Fig. 2 Representative cyclic oligopyrrole-based anion receptors: calix[4]pyrrole **1**, protonated sapphyrin **2**, and cyclooctapyrrole **3**. Expanded porphyrins **2** and **3** are represented as their skeleton forms

due to the NH site (Fig. 1b). Further, as the π -planes of the pyrrole unit also enable stacking and the formation of π -ligands for metal complexing (Fig. 1c), pyrrole rings can act as potential building blocks for nanoscale supramolecular structures. However, pyrrole rings are often in preorganized macrocycles such as porphyrins and their analogs, wherein their N sites are located on the inside of fairly rigid closed structure and consequently cannot exhibit their potential as interaction sites. Therefore, new aspects of pyrrole rings may be revealed by exploring novel *acyclic* oligopyrrolic systems, which may find application in functional supramolecular materials that exploit new properties and phenomena.

The pyrrole NH site is an efficient hydrogen-bonding donor. In fact, thus far, macrocycles consisting of pyrroles are considered particularly attractive as essential binding units due to the presence of polarized NH sites, as seen in calixpyrroles (e.g., calix[4]pyrrole **1**) [23–26] and expanded porphyrins, [27–30] including diprotonated sapphyrins (e.g., β -alkyl-substituted sapphyrin **2**) [31–33] and cyclooligopyrroles (e.g., cyclooctapyrrole **3**) [34] (Fig. 2). Multiple NH sites in macrocycles efficiently bind the desired anion in a cooperative fashion to form receptor–anion complexes and although less extensively studied, acyclic pyrrole derivatives have potentially even greater advantages [10, 14, 20, 35, 36]. This is because they can incorporate additional recognition units for hydrogen bonding, metal coordination, and van der Waals interactions, or simply because they easily form various macrocyclic systems. Receptors with linear geometries must often change conformation to fit the volume and shape of the negatively charged species. Therefore, for a linear receptor, the essential factor that determines the binding affinity to a guest species would be the existence of temporal preorganization, along with other factors such as the strength of the induced effect required to polarize the association site(s) and the steric and electrostatic interference from peripheral substituents. The balance between flexibility and rigidity is a key issue for controlling the anion-binding behavior of acyclic oligopyrroles and, essentially,

for forming supramolecular structures with and without anions. The variety of linear oligopyrroles available, itself, increases the potential for finding novel supramolecular materials.

This chapter summarizes linear oligopyrrole systems as anion-binding receptors and explores their application to supramolecular chemistry. Note that, in sharp contrast to closed systems such as regular porphyrins, the pyrrole ring strongly determines the characteristics of open-chain oligopyrroles that constitute the building blocks of supramolecular assemblies.

2 Guanidinocarbonylpyrrole-Based and Amidopyrrole-Based Anion Receptors

The pyrrole ring, with its polarized NH site, acts as an anion receptor by itself (Fig. 3), though obviously not an efficient receptor in solution due to the absence of supplementary interaction sites and cooperative binding sites among multiple pyrrole rings. In fact, the binding constant (K_a) of 2,5-dimethylpyrrole for F^- in CD_2Cl_2 was estimated to be only $\sim 9 M^{-1}$ [23]. However, pyrrole can form an anion complex in the crystal state: Gale et al. reported the first single-crystal X-ray structure of a pyrrole–anion complex using single crystals fabricated by the addition of a tetramethylammonium salt of Cl^- to pyrrole solvent [37]. Although anion-responsive monomeric pyrrole derivatives are interesting, this review is limited to oligopyrrolic systems.

2.1 Guanidinocarbonylpyrrole-Based Anion Receptors

The representative “supplementary” interaction sites on pyrrole rings are guanidine and amide NH moieties: guanidine has positively charged and polarized NH sites, [17, 38, 39] whereas the amide NH is well-known as a polarized hydrogen-bonding donor site due to the neighboring carbonyl unit [14, 16]. In 1999, Schmuck reported the synthesis of 2-(guanidinocarbonyl)pyrrole **4**, which selectively binds *N*-acetyl- α -amino acid carboxylates in aqueous media (Fig. 4a). In $DMSO-d_6$, **4** associates with acetate ($CH_3CO_2^-$) with a binding constant (K_a) of $>10^6 M^{-1}$. Even in 40% water/ $DMSO-d_6$, **4** binds $CH_3CO_2^-$ and *N*-acetyl-L-alanine carboxylate at 2,790 and 770 M^{-1} , respectively. The corresponding phenylalanine carboxylate is bound much stronger ($1,700 M^{-1}$) than those including alanine, tryptophan

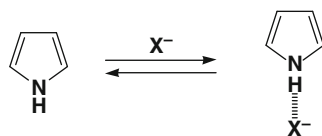


Fig. 3 Anion-binding mode of pyrrole

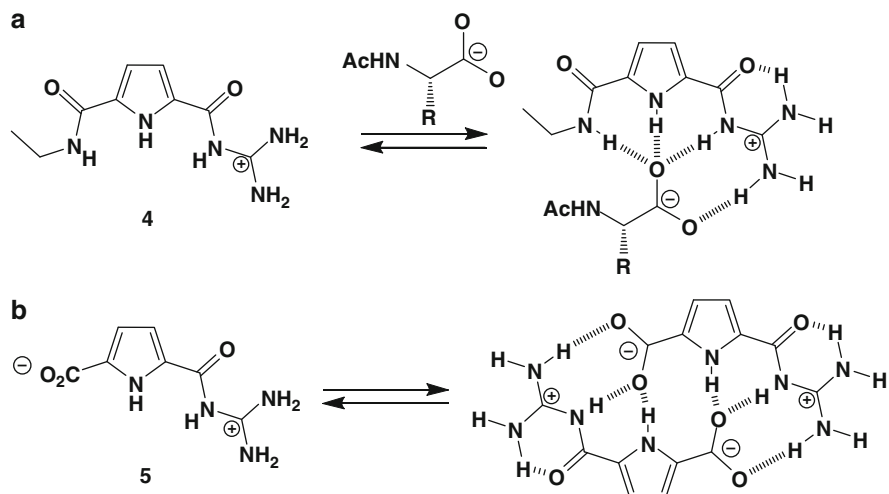


Fig. 4 (a) Amino acid carboxylate binding of guanidinocarbonylpyrrole **4**; (b) self-assembled dimerization of guanidinocarbonylpyrrole **5**

(810 M^{-1}), and lysine (360 M^{-1}) because of the effective π -stacking between the phenyl group of phenylalanine and the acylguanidinium unit of **4** [40]. Because of the carboxylate binding property of guanidinocarbonylpyrrole derivatives, receptors bearing a carboxylate unit should self-assemble to form dimer and oligomer structures. In fact, 5-(guanidinocarbonyl)-1*H*-pyrrole-2-carboxylate **5** (Fig. 4b) is converted to an intermolecular self-assembled dimer, without the formation of dispersed oligomers, in DMSO. The dimer is very stable with a dimerization constant of ca. 10^{12} M^{-1} [41]. Schmuck summarized the chemistry of a variety of derivatives with the guanidinocarbonylpyrrole moiety in a review [42]; therefore, hereafter, this section/chapter covers only oligopyrrolic systems bearing the guanidinocarbonyl moiety.

Schmuck has reported self-assembled molecules formed with bispyrrole zwitterions bearing both carboxylate and guanidinium moieties (**6–8**, Fig. 5a). In DMSO, zwitterion **6** forms a specifically folding monomer in which the carboxylate group on one end of the molecule interacts with the guanidinocarbonylpyrrole moiety on the other end (Fig. 5b). In sharp contrast, zwitterion **7**, with a shorter spacer, cannot form such a folding structure. The concentration-independent behavior of **6** excludes the possibility of dimerization and higher oligomerization by self-assembly [43]. Another zwitterion **8** also forms a self-folding structure in methanol [44].

Apart from zwitterions such as **6–8**, bis-zwitterion **9** (Fig. 6a), which has a long oxyethylene spacer, forms a self-folding monomer and a self-assembled dimer in concentration-dependent equilibrium in $\text{DMSO-}d_6$ and $\text{DMSO-}d_6/\text{D}_2\text{O}$ mixtures (0.5–50 mM) (Fig. 6b). This was the first example of homodimerization based solely on hydrogen-bond-enforced ion pair formation that led to stable nanometer-sized discrete particles in DMSO–water mixtures even without any structural bias within

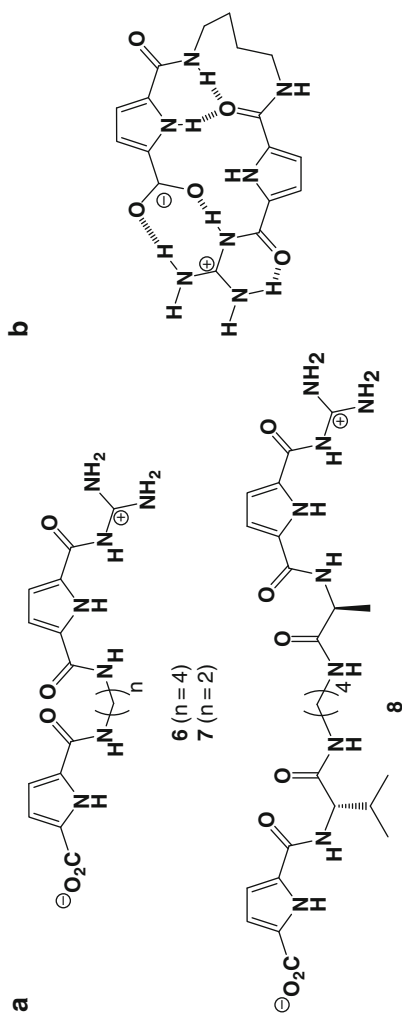


Fig. 5 (a) Guanidincarbonylpyrrole-based zwitterions **6–8**; (b) self-folding mode of **6**

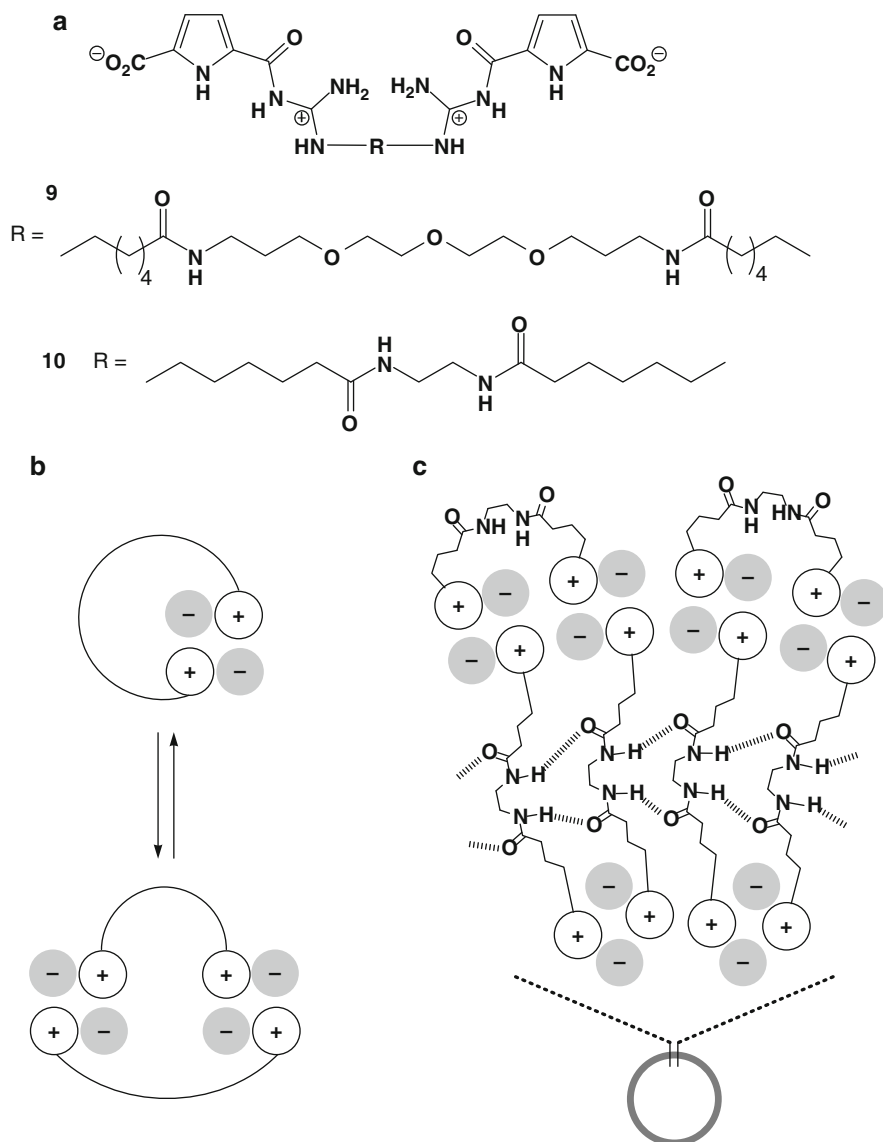


Fig. 6 (a) Guanidinoacetylpyrrole-based bis-zwitterions **9** and **10**; (b) schematic representation of self-folding monomer and self-assembled dimer of bis-zwitterions; (c) schematic representation of self-assemblies to form vesicle

the molecule. The formation of nanometer-sized discrete particles by self-assembly was confirmed by DOSY NMR, FAB-MS, dynamic light scattering (DLS), and small-angle neutron scattering (SANS) studies [45]. Further, in DMSO (0.5–50 mM), bis-zwitterion **10** (Fig. 6a), wherein two charged binding sites are bridged by a

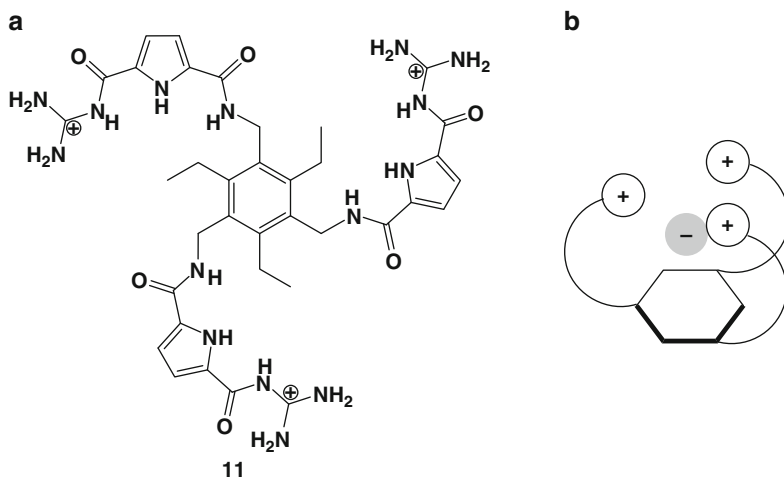


Fig. 7 (a) Guanidinocarbonylpyrrole trimer **11**; (b) anion-binding mode resembling a “molecular flytrap”

bisamide lipophilic spacer, forms larger vesicular structures of ca. 150 nm under concentrated conditions (Fig. 6c) along with monomer and dimer. The formation of larger aggregates was verified by atomic force microscopy (AFM) as well as DLS and SANS [46].

An efficient binding motif for guest species, especially trianions, is a tripodal host molecule based on 1,3,5-trisubstituted benzene [47]. Schmuck and Schwegmann also prepared a tripodal guanidinocarbonylpyrrole receptor **11** (Fig. 7a), that binds trianionic species such as trimesic acid tricarboxylate and citrate with unprecedented high association constants of $>10^5 \text{ M}^{-1}$ in pure aqueous solutions. This makes receptor **11** one of the most efficient tricarboxylate receptors in aqueous media ($K_a = 3.4 \times 10^5 \text{ M}^{-1}$ and $1.6 \times 10^5 \text{ M}^{-1}$ for trimesic acid (benzene-1,3,5-tricarboxylate) and citrate, respectively, as indicated by UV/vis spectral changes). This is because of the formation of an anion-binding complex resembling a “molecular flytrap,” as elucidated from ^1H NMR and theoretical studies (Fig. 7b) [48]. Further, Schmuck and Schwegmann used the tripodal receptor **11** as a “naked-eye” sensor assembly for an indicator displacement assay with carboxyfluorescein for the selective detection of citrate [49].

Zwitterionic guanidinocarbonylpyrrole can form supramolecular polymers [50, 51] via additional metal coordination interactions [52–54]. Schmuck and coworkers reported the assembly behavior of terpyridyl-appended zwitterion **12** (Fig. 8a), which dimerizes into hydrogen-bonding ion pairs in aqueous solution and, upon the addition of Fe(II), forms single-stranded supramolecular polymers in DMSO (Fig. 8b). Polymerization by Fe(II) complexation was initially detected through DOSY NMR spectral changes and also by AFM – on a highly oriented pyrolytic graphite (HOPG) substrate, highly ordered molecular adlayers of individual polymer strands, each several hundred nanometers long, were observed [55].

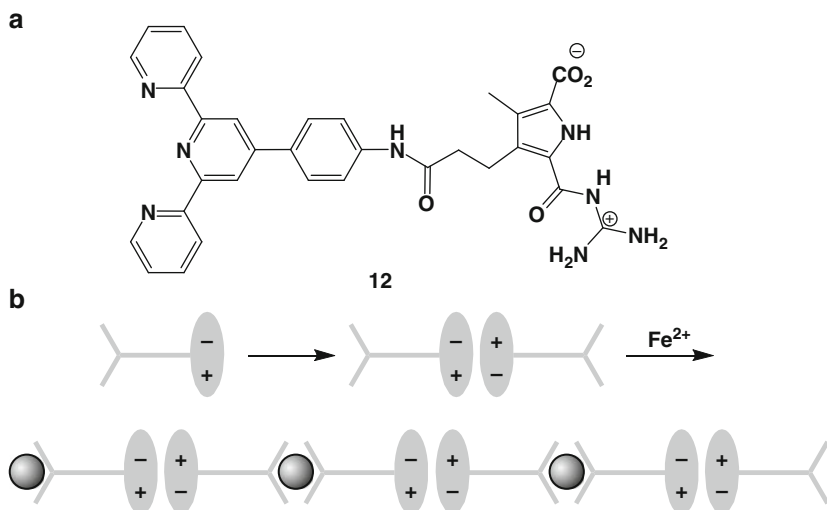


Fig. 8 (a) Terpyridine-guanidinocarbonylpyrrole hybrid **12**; (b) formation pathway for supramolecular polymers by self-assembled dimerization and metal coordination

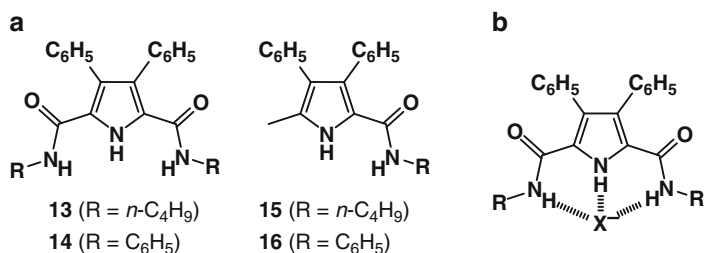


Fig. 9 (a) Amidopyrroles **13**–**16**; (b) anion-binding mode of amidopyrroles **13** and **14**

2.2 Amidopyrrole-Based Anion Receptors

In 2001, Gale et al. reported 2,5-diamidopyrroles and 2-amidopyrroles (**13**–**16**, Fig. 9a) as simple anion-binding receptors. Amidopyrroles provide convergent binding sites (Fig. 9b), which enable them to efficiently bind anions, especially oxoanions in CD₃CN and 0.5% H₂O/DMSO. For example, **13** shows a K_a value of 2,500 M⁻¹ for benzoate in CD₃CN [56, 57]. Gale reviewed the various derivatives comprising the amidopyrrole moiety [13]; hence, this section focuses on the amidopyrrole-based oligopyrroles.

Gale et al. prepared phenylene-bridged amidopyrrole-dimers **17** and **18** (Fig. 10a), which have chlorine moieties at the β -positions, which enhance the polarity of the pyrrole NH. Crystals of **17** and **18**, obtained by slow evaporation of CH₃CN solutions in the presence of excess tetrabutylammonium fluoride (TBAF), exhibit interlocked chains of deprotonated **17** and **18** anions linked via N–H⋯N

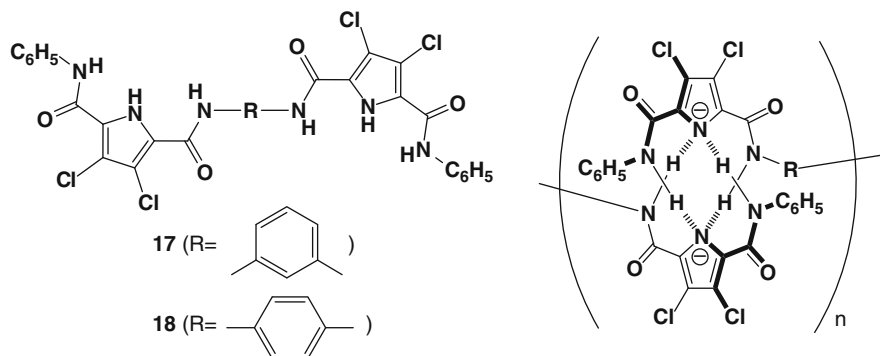


Fig. 10 (a) Phenylene-bridged amidopyrrole-dimers **17** and **18**; (b) schematic representation of hydrogen-bonding chain structures of deprotonated **17** and **18**

hydrogen bonds (Fig. 10b). In the solid state, the two half molecules are essentially planar, whereas the complete molecule is twisted such that the angle between the pyrrole rings is $61.79(5)^\circ$ [58]. Further, single-crystal X-ray analysis of the Cl^- complex of *p*-phenylene-bridged **18** as a TBA salt shows a [1 + 2]-type binding mode [59]. The molecular structures of protonated and Cl^- complexes were also supported by the theoretical studies of Navakhun and Ruangpornvisuti [60, 61].

Incorporation of additional pyrrole NH units to the monomeric amidopyrroles **13** and **14** would enhance the affinity for anion binding and modify the binding selectivity. Sessler et al. prepared amide-bridged tripyrrolyl derivative **19** (Fig. 11a). Single-crystal X-ray analysis has shown that tripyrrolyl **19** forms intermolecular hydrogen bonds in the solid state. In $\text{DMSO-}d_6$, **19** shows anion binding toward H_2PO_4^- and $\text{C}_6\text{H}_5\text{CO}_2^-$ with K_a values of 5,500 and $10,300 \text{ M}^{-1}$, higher than those of **14** (1,450 and 560 M^{-1} , respectively), but no binding toward Cl^- , Br^- , and HSO_4^- [62]. Sessler et al. replaced the core pyrrole ring of **19** with pyridyl and phenyl moieties to afford bispyrrole derivatives **20–22** (Fig. 11b). The solid-state structure of **20** shows a slightly distorted conformation with intramolecular hydrogen bonding, for example, between the pyrrole-NH and amide-C=O. The bispyrroles **20–22** exhibit anion binding in nonpolar solvents such as $\text{CH}_2\text{ClCH}_2\text{Cl}$, wherein **20** binds CH_3CO_2^- ($K_a = 19,000 \text{ M}^{-1}$), but do not interact with Cl^- and Br^- . Interestingly, **23**, an isomeric form of **20** with different amide linkages, does bind Cl^- ($K_a = 805 \text{ M}^{-1}$) under similar conditions [63]. Further, Cheng and coworkers reported the similar receptors **24** and **25** as reference molecules of **26** and **27** (Fig. 11c), which have $\text{sp}^3 \text{CH}_2$ moieties between pyrrole rings. Among **24–27**, receptor **26** binds anions more efficiently in $\text{DMSO-}d_6$, wherein K_a values for F^- are 102 (**24**), 73 (**25**), 1,266 (**26**), and 138 (**27**) M^{-1} . In **24** and **25**, the bulky Boc groups at the terminal positions inhibit the formation of U-type structures appropriate for efficient anion binding [64].

In 2004, Cheng and coworkers prepared 1,2-phenylene-bridged bisamidopyrrole **28** (Fig. 12), which forms a CH_3OH -assisted helical assembly via intermolecular

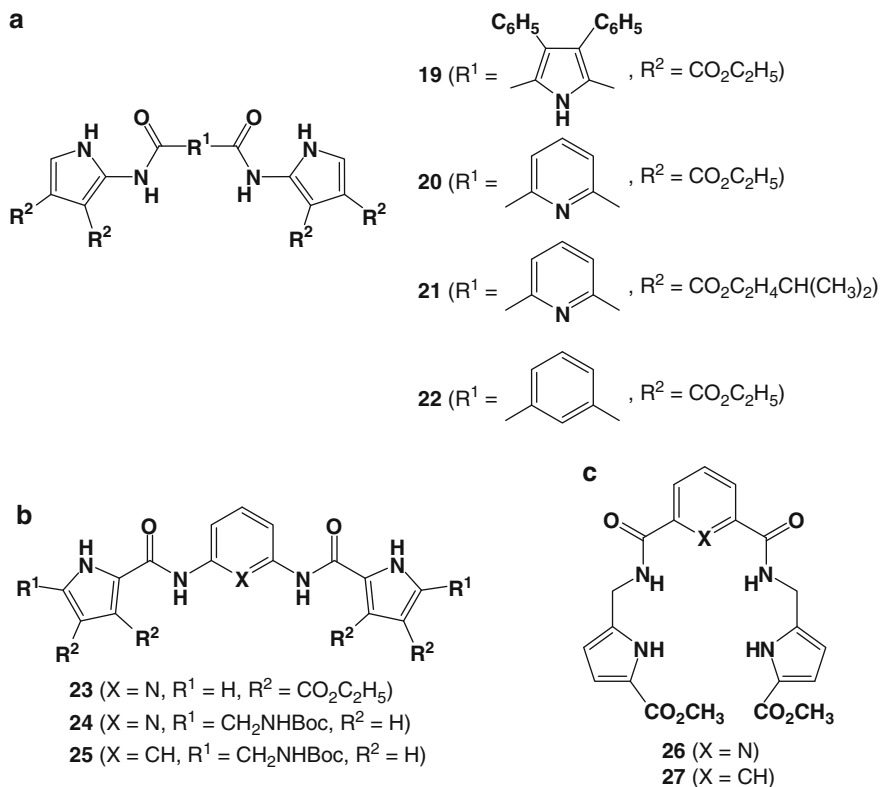


Fig. 11 (a–c) Bis- and trisamidopyrrole-based anion receptors 19–27

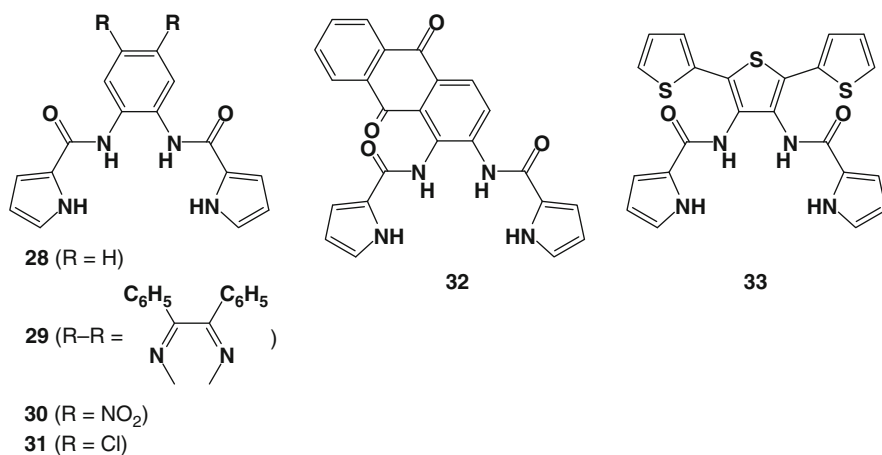


Fig. 12 Bisamidopyrrole-based anion receptors 28–33

hydrogen bonding when crystallized from $\text{CH}_3\text{OH}/\text{EtOAc}$ and a knot-like dimer structure when crystallized from $\text{CHCl}_3/\text{DMSO}$ or $\text{H}_2\text{O}/\text{DMSO}$. In $\text{DMSO}-d_6$, **28** binds F^- , Cl^- , and H_2PO_4^- with K_a values of 320, <10 , and 100 M^{-1} , respectively [65]. Sun and coworkers modified the skeleton structure of **28** to obtain derivatives **29–33** from pyrrole-2-carbonyl chloride and various diamino-substituted aryl units. In $\text{CH}_3\text{CN}/\text{H}_2\text{O}$ (9:1, v/v), both **29** and **30** respond to CN^- but not to F^- , Cl^- , Br^- , I^- , NO_3^- , CH_3CO_2^- , $\text{C}_6\text{H}_5\text{CO}_2^-$, $\text{HP}_2\text{O}_7^{3-}$, H_2PO_4^- , HSO_4^- , or ClO_4^- . Upon the addition of CN^- , the absorption bands of **29** at 291 and 378 nm decrease while three new bands at 299, 372, and 428 nm appear. Concomitantly, the fluorescence maximum at 425 nm shifts to 554 nm. The binding constant for [1 + 2]-type stoichiometry is estimated as $\log K = 5.91$. Similarly, **30** shows absorption spectral changes with $\log K = 9.20$. The colorimetric response of **30** to CN^- persists up to 50% water content. As seen in the ^1H NMR spectral changes of **30** in $\text{DMSO}-d_6$, formation of a CN^- adduct, a cyanohydrin, enables the sensing behavior to this anion. In contrast, **29** shows interactions between its pyrrole moieties and CN^- [66]. A detailed examination of the interactions between receptors **29–33** and anions in CH_3CN or DMSO suggests efficient sensing behaviors via association, deprotonation, and cyanohydrin formation [67].

In 2007, Anzenbacher and coworkers demonstrated that the tripodal sensor molecules **34–37** based on 1,3,5-triaminomethylbenzene (Fig. 13) can bind and sense anions in hydrophilic polymer matrices, despite their inability to bind anions in water. Proton NMR titration suggests the formation of [1 + 1] complexes with C_3 symmetry. The anion-binding affinities of **35–37** follow the general order $\text{H}_2\text{PO}_4^- > \text{HP}_2\text{O}_7^{3-} > \text{CH}_3\text{CO}_2^- \gg \text{Cl}^- > \text{Br}^-$; for example, the K_a (M^{-1}) range of **35–37** are within the values of 10–100 for Cl^- , $1.0\text{--}5.0 \times 10^6$ for CH_3CO_2^- , $2.3\text{--}5.0 \times 10^6$ for H_2PO_4^- , and $1.0\text{--}5.0 \times 10^6$ for $\text{HP}_2\text{O}_7^{3-}$ in DMSO . To lower selectivity of receptors **35–37** to anions compelled the authors to examine the possibility of sensor arrays including other anion receptors, that is, arrays to detect changes in fluorescence intensity from sensor-polyurethane films upon the addition of aqueous solutions containing anions [68].

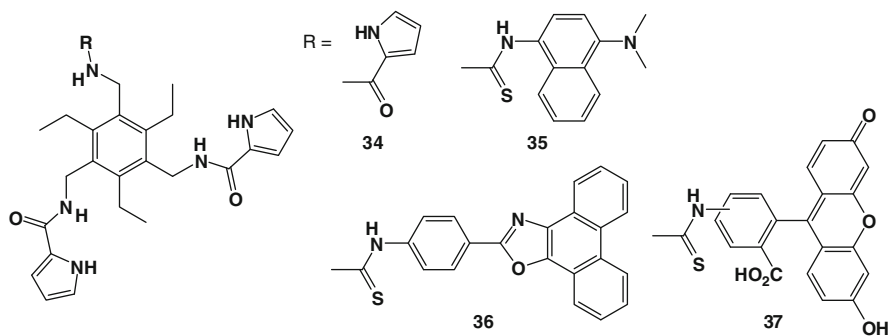


Fig. 13 Amidopyrrole-based tripodal receptors **34–37**

3 Dipyrrens and Their Analogs as Anion Receptors

Dipyrrens (dipyrromethenes) **38**, partial structures of porphyrins, are well-known parts of bile pigment structures and consisting of two pyrroles with an sp^2 -*meso* position; they are essential π -conjugated bidentate monoanionic ligands for metal ions in natural and artificial systems [69, 70]. Dipyrrens have only one pyrrole NH; therefore, the protonated form can act as an anion receptor (Fig. 14a). As observed in the pioneering works by Fischer and Orth, β -alkyl-substituted dipyrrens can be prepared and “stored” as hydrohalogenated salts [21]; however, few investigations have been conducted on the nature of protonated dipyrrens as anion receptors, whose anion complexes are usually observed in solid-state structures. In 1978, Sheldrick reported the first example of the crystal structure of a protonated dipyrren of a Br^- salt **39** (Fig. 14b) [71]. Sessler et al. also demonstrated a similar anion complex, a Cl^- salt of protonated **40**. In CH_3CN , the K_a values of **40** and **41**, after protonation by HI, for Cl^- as a TBA salt are 8.8×10^5 and $3.0 \times 10^5 \text{ M}^{-1}$, respectively, as determined by isothermal titration calorimetry (ITC) (Fig. 14c) [72]. Dolphin and coworkers reported anion complexes of *meso*-aryl-substituted dipyrren as protonated forms **42** and **43**. Based on the conformation with two pyrrole rings facing the “outside,” perfluorophenyl dipyrren forms [2 + 1 (= receptors + anion)] complexes with dianion ZnBr_4^{2-} and ZnCl_4^{2-} (**42**) in the solid state, whereas the dipyrren forms a 1-D supramolecular chain structure with Br^- (**43**) (Fig. 14d). This is in sharp contrast to **39** and **40**, in which two pyrrole NH in the corresponding dipyrren molecule cooperatively bind an anion [73].

The flexibility observed in pyrrole inversion by protonation might be one of the reasons why the anion-binding chemistry of dipyrrens has not been well investigated. In contrast to dipyrrens, dipyrinones such as **44** reported by Huggins and

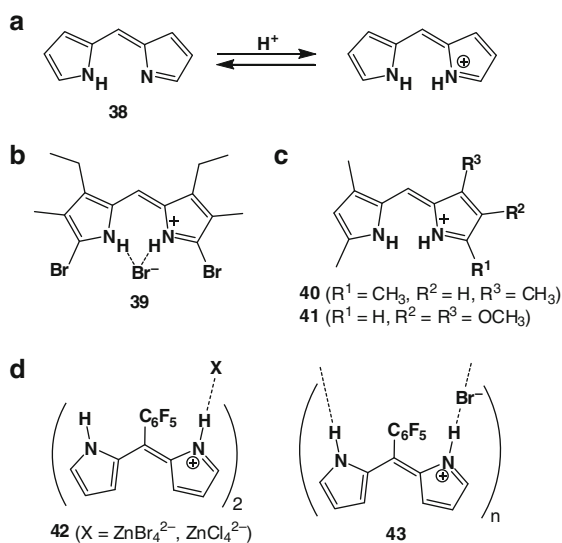
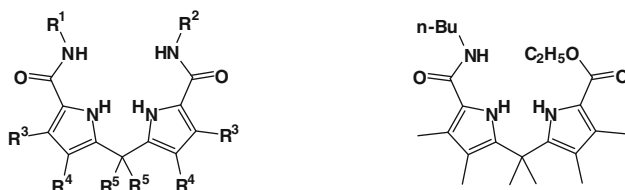
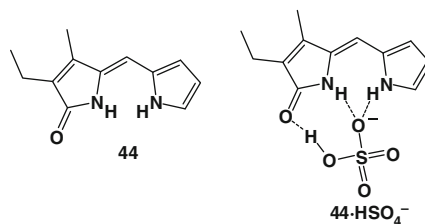


Fig. 14 (a) Skeleton structure of dipyrren (dipyrromethene) **38**; (b) first structure-solved Br^- -complex of protonated dipyrren **39**; (c) protonated dipyrrens **40** and **41**; (d) anion complexes of *meso*-perfluorophenyl dipyrren in a protonated form (**42** and **43**)

Fig. 15 Dipyrinone **44** and HSO_4^- complex



- 45** ($R^1 = R^2 = \text{Ph}$, $R^3 = \text{CH}_3$, $R^4 = \text{CH}_2\text{CH}_3$, $R^5 = \text{H}$)
46 ($R^1 = R^2 = n\text{-Bu}$, $R^3 = \text{CH}_3$, $R^4 = \text{CH}_2\text{CH}_3$, $R^5 = \text{H}$)
47 ($R^1 = R^2 = \text{Ph}$, $R^3 = R^4 = R^5 = \text{CH}_3$)
48 ($R^1 = R^2 = n\text{-Bu}$, $R^3 = R^4 = R^5 = \text{CH}_3$)
49 ($R^1 = \text{Ph}$, $R^2 = n\text{-Bu}$, $R^3 = R^4 = R^5 = \text{CH}_3$)

50

Fig. 16 Amide-substituted dipyrromethanes **45–50**

coworkers, wherein one of the pyrrole α -positions is oxidized (Fig. 15), can behave as neutral bidentate anion receptors. Dipyrinone **44** binds Cl^- , Br^- , NO_3^- , and HSO_4^- with binding constants (K_a) of 122, <10, 94, and $1,680 \text{ M}^{-1}$, respectively, in CDCl_3 . The preference for HSO_4^- over other anions stems from the additional interaction between the amide-oxygen of **44** and protonic OH of the anion; this is also revealed by single-crystal X-ray analysis of **44**· HSO_4^- [74].

Dipyrromethanes comprising two pyrrole rings bridged by an sp^3 meso carbon can be used as building units for π -conjugated porphyrin-related macrocycles as well as dipyrins, as discussed above. Dipyrromethanes can also be considered as partial structures of calix[4]pyrroles. The weak cooperative interactions of the pyrrole NH due to the open-chain structures suggest that anion-binding properties of dipyrromethane are fairly insignificant. However, supplementary interaction sites would enhance the binding affinities for anions, as observed in monopyrrolic anion receptor systems. Gale and coworkers reported the synthesis of 2,2-bisamidodipyrrolylmethanes: less stable **45** and **46** and relatively stable **47–49**, and hemiamide derivative **50** (Fig. 16). Single-crystal X-ray analysis of **45–49** and hemiamide **50** revealed the formation of various hydrogen-bonding assemblies using pyrrole and amide NH sites and amide–CO moieties. In fact, **45–50** can bind, for example, F^- with K_a values of 8,990, 7,560, 124, 89, and 429 M^{-1} in 5% $\text{H}_2\text{O}/\text{DMSO}-d_6$ and $1,450 \text{ M}^{-1}$ in 0.5% $\text{H}_2\text{O}/\text{DMSO}-d_6$, respectively. Significantly, **45** binds F^- and H_2PO_4^- (114 and 234 M^{-1} , respectively) even in the extremely competitive solvent mixture 25% $\text{H}_2\text{O}/\text{DMSO}-d_6$. Efficient binding to H_2PO_4^- is also supported by DFT geometry optimization, showing that the receptor adopts a

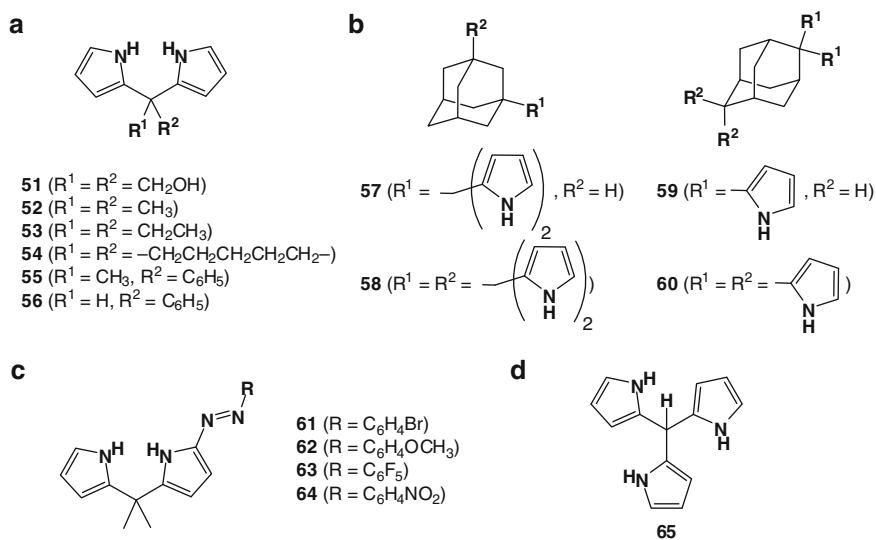


Fig. 17 (a) *Meso*-disubstituted dipyrromethanes **51–60**; (b) adamantane-based dipyrromethanes **57–60**; (c) 1-aryldipyrromethanes **61–64**; (d) tripyrrolemethane **65**

cleft conformation wherein the receptor binds two oxygen atoms in H_2PO_4^- , each by hydrogen bonding with the pyrrole and amide NH site [75, 76].

Another strategy for enhancing the binding affinities of dipyrromethanes is via the formation of charge-transfer (CT) complexes. Jiang and coworkers examined the complexation between dipyrromethanes **51–55** (Fig. 17a) and tetracyanoquinodimethane (TCNQ) in $\text{CH}_3\text{CN}/\text{H}_2\text{O}$ (1:1, v/v). TCNQ complexes of **52–55** do not show any changes in color and absorption spectra on the addition of anions. However, **51**·TCNQ can serve as a highly selective colorimetric sensor (from blue to pale purple) for anions, especially PO_4^{3-} and CO_3^{2-} . In this case, the anion-binding and sensing motifs are quite different: presumably, *meso*-hydroxymethyl units for binding and electron-rich properties, essential for CT complexation, for sensing [77]. On the other hand, Sessler et al. examined the anion-binding properties of **52** in a nonpolar solvent without electron deficient components; the K_a values in CD_2Cl_2 are 2,100, 110, 19, <10, <10, 310, 11, and <10 M^{-1} for F^- , Cl^- , Br^- , I^- , HSO_4^- , H_2PO_4^- , NO_3^- , and ClO_4^- , respectively [78]. Further, incorporation of bulky units at the *meso* position would hinder the rotational mobility of the pyrrole moieties and thus increase the stability of anion complexes. In fact, Mlinarić-Majerski and coworkers prepared adamantane-based dipyrromethanes **57–60** (Fig. 17b), which show greater K_a values for anions (e.g., 80 M^{-1} for Cl^- with **57**) than *meso*-phenyldipyrromethane **56** (e.g., 22 M^{-1} for Cl^-) in CDCl_3 . Binding to F^- , especially by “dimers” **58** and **60**, involves slightly complicated [2 + 1], [1 + 1], and [1 + 2] modes [79]. Attachment of a chromogenic moiety to dipyrromethane is another method for anion sensing. Chauhan et al. prepared 1-aryldipyrromethanes (**61–64**, Fig. 17c), which bind anions with

K_a values of, for example, $>10^6 \text{ M}^{-1}$ for F^- with **64** in DMSO. In particular, **64** shows a dramatic color change from orange to blue on F^- binding, corresponding to the absorption changes from $\lambda_{\text{max}} = 438 \text{ nm}$ to $\lambda_{\text{max}} = 575 \text{ nm}$ [80]. Denekamp, Suwinska, and Eichen reported the anion-binding behavior of the simple tripyrrole molecule **65** (Fig. 17d). Tripyrrolemethane **65** shows efficient [1 + 1] and [1 + 2] F^- binding in CD_3CN ($K_1 = 41,000 \text{ M}^{-1}$ and $K_2 = 17,000 \text{ M}^{-1}$) and wet $\text{DMSO}-d_6$ ($K_1 = 5,000 \text{ M}^{-1}$ and $K_2 = 2,000 \text{ M}^{-1}$ in 0.25% $\text{D}_2\text{O}/\text{DMSO}-d_6$; $K_1 = 1,400 \text{ M}^{-1}$ and $K_2 = 1,000 \text{ M}^{-1}$ in 1% $\text{D}_2\text{O}/\text{DMSO}-d_6$; $K_1 = 220 \text{ M}^{-1}$ and $K_2 = 200 \text{ M}^{-1}$ in 5% $\text{D}_2\text{O}/\text{DMSO}-d_6$). Receptor **65** exhibits [1 + 1] binding for H_2PO_4^- with K_a values of 300, 60, <50 , and $<50 \text{ M}^{-1}$ in CD_3CN , 0.25, 1, and 5% $\text{D}_2\text{O}/\text{DMSO}-d_6$, respectively. The addition of halide anions as TBA salts to **65** results in significantly smaller guest-induced shifts in the ^1H NMR spectra. Further, single-crystal X-ray analysis of the Br^- complex of **65** reveals the formation of six crystallographically independent structures, some of which use the pyrrole β -CH site for Br^- binding [81].

Sessler et al. also examined the anion-binding properties of a directly bridged bispyrrole, bipyrrole **66** (Fig. 18). Bipyrrole **66** shows K_a values of 246, 4,090, and $3,650 \text{ M}^{-1}$ for Cl^- , $\text{C}_6\text{H}_5\text{CO}_2^-$, and CH_3CO_2^- by ITC (30°C) and 53 and 35 M^{-1} for Br^- and HSO_4^- by ^1H NMR titrations (25°C) in CH_3CN , respectively [82]. Further, Fang and coworkers reported bis(pyreno[2,1-*b*]pyrrole) (**67**, Fig. 18), one of the derivatives including π -fused “pyrrole” rings, which displays excellent selectivity and sensitivity to F^- in comparison with other anions such as Cl^- . Excess F^- as a TBA salt causes deprotonation at one of the pyrrole NH of **67** in DMSO, resulting in remarkable colorimetric and fluorescent changes in the visible region. ^1H NMR spectral changes using 2,2'-bisindole instead of **67** suggest that the *anti* form twisted conformation with and without the presence of 1 equiv of F^- is transformed to *syn* conformation with presumably planar structure by deprotonation [83].

Prodigiosin, a naturally occurring oligopyrrole, is characterized by a common pyrrolylpyrromethene skeleton consisting of dipyrryn and bipyrrole [84]. Davis provides a good review of the anion-binding chemistry of prodigiosin in this book [85], and so a detailed discussion is excluded in this section. As a π -conjugated pyrrole oligomer with methyne bridges and direct α - α linkages, the hexapyrrolic “prodigiosin dimer” **68**, which is protonated by HCl, was reported by Sessler et al. (Fig. 19a). Single-crystal X-ray analysis of the Cl^- complex of the hexapyrryn **68** in protonated form reveals the formation of a fairly planar [1 + 2]-type complex with an S-shaped conformation. NOE supports the S-shaped conformation in solution state [86]. Sessler and coworkers also prepared higher linear oligopyrroles **69–71**

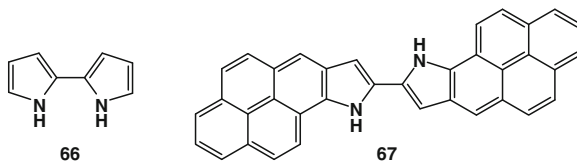


Fig. 18 Bipyrrole **66** and bispyrenopyrrole **67**

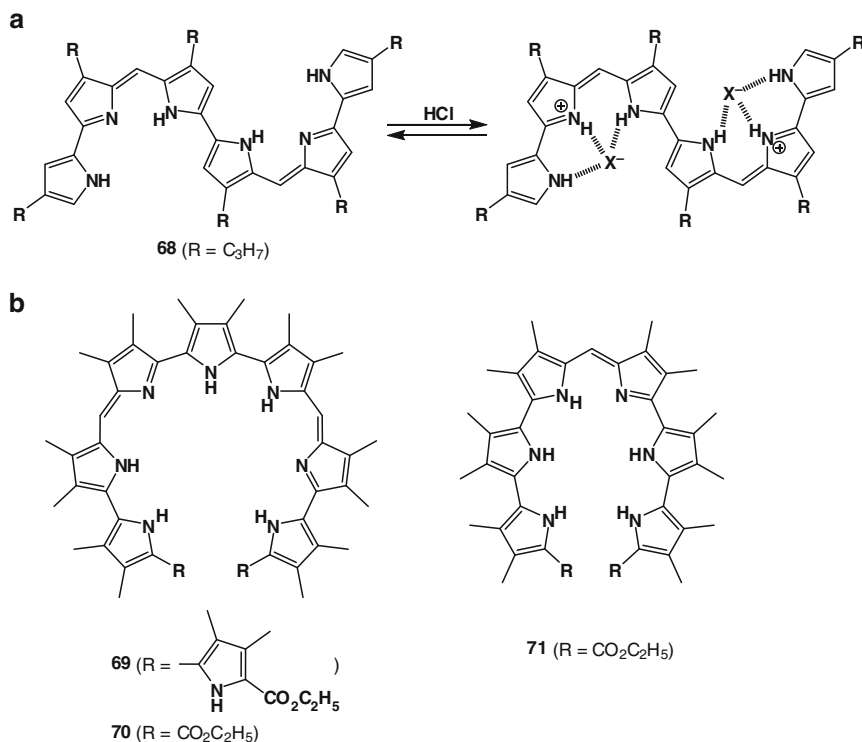


Fig. 19 (a) Hexapyrrin **68** and anion-binding mode in protonated form; (b) nona-, hepta-, and hexapyrrolic open-chain systems **69–71**

(Fig. 19b), which show absorption maxima in the visible region like that of **68**. The oligopyrroles **69–71** exhibit absorption spectral changes in the adduct forms with acetic acid [87].

4 Dipyrrolylquinoxalines and Related Aryl-Bridged Bispyrroles

4.1 Dipyrrolylquinoxalines

Oddo and Dainotti, in 1911, first synthesized 2,3-dipyrrol-2-ylquinoxaline (**72**, Fig. 20a), a fluorescent dye directly connected to the pyrrole ring, by the acid-catalyzed condensation of 1,2-dipyrrol-2-ylethanedione (**73**, Fig. 20b) and *o*-phenylenediamine [88]; the process was later refined by Behr et al. [89] Since the first synthesis, the anion-binding properties of dipyrrolylquinoxaline (DPQ), among the open-chain pyrrole derivatives, has not been investigated for a long time. In 1999, Sessler and coworkers found that the DPQ **72** undergoes a change in color

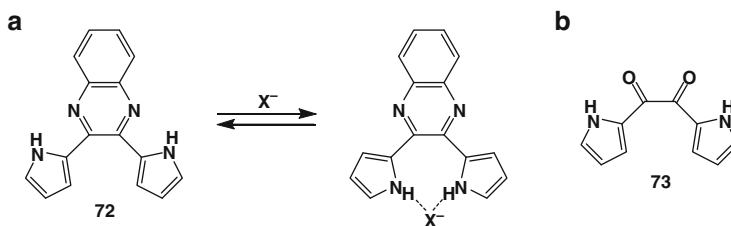


Fig. 20 (a) Skeleton structure of dipyrrolylquinoxaline (DPQ) **72** and the anion-binding mode; (b) 1,2-dipyrrol-2-ylethanedione **73**

and quenching of emission in the presence of certain anions. It contains two pyrrole NH groups that can function as anion-binding moieties and has a built-in quinoxaline ring that might serve as a colorimetric receptor for anions. As illustrated in Fig. 20a, this putative sensing system is expected to operate through a combination of electronic and conformational effects. DPQ **72** shows binding affinities (K_a), estimated by UV/vis absorption spectral changes upon the addition of anions, of 18,200, 50, and 60 M^{-1} for F^- , Cl^- , and $H_2PO_4^-$ as TBA salts in CH_2Cl_2 , respectively, comparable to those of **73** at 23,000, 170, and $<50 M^{-1}$, respectively. And although DPQ is an electronically neutral acyclic oligopyrrole system, attachment of the electron-withdrawing moiety quinoxaline enhances the polarity of the pyrrole NH, further promoting efficient binding to anions [90, 91].

The individual building blocks of DPQ **72** can be replaced with other pyrrole and quinoxaline moieties to afford the derivatives **74–80**, which possess various electron-withdrawing or electron-donating groups (Fig. 21a). For example, mono-*N*-substituted **74** shows the smaller K_a values of 120, <50 , and $<50 M^{-1}$ for F^- , Cl^- , and $H_2PO_4^-$. And 6-nitroquinoxaline-containing **75** exhibits a higher K_a value (118,000 M^{-1} in CH_2Cl_2) for F^- and comparable values (50 and 65 M^{-1}) for Cl^- and $H_2PO_4^-$, [90] whereas 3,4-difluoropyrrole-substituted **76** shows higher anion binding (61,600, 180, and 17,300 M^{-1} for F^- , Cl^- , and $H_2PO_4^-$, in CH_2Cl_2) than **72** [92]. Diamino-substituted **78**, prepared from dinitro **77**, can be transformed to the phenanthroline derivative **81** by condensation with 1,10-phenanthroline-5,6-diketone. Ru(II) and Co(III) complexes (**81-Ru**, **81-Co**) in the form of ClO_4^- salts (Fig. 21b) show higher K_a values for F^- (12,000 and 54,000 M^{-1} in DMSO) than **72** ($<100 M^{-1}$) and **81** (440 M^{-1}). The trend in K_a values observed in **81**, **81-Ru**, and **81-Co** is correlated with the increasing total charge of the receptor. The redox properties of the metal complex can be used to detect the anion-binding behavior of **81-Co** with electrochemical techniques: differential pulse voltammetry (DPV) on **81-Co** in DMSO shows a reversible redox signal at 160 mV (vs SHE) assignable to Co^{III}/Co^{II} , which disappears (or significantly shifts) on the addition of F^- . Addition of Cl^- and $H_2PO_4^-$ also shifts the higher reduction signals because of the “electron-donating” properties of the bound anions [93]. As extended derivatives of dialkoxy-substituted **79** and **80**, “crowned” DPQs **82–85** (Fig. 21c) were also reported. Single-crystal X-ray structures of **79**, **82**, and **83** show hydrogen-bonding molecular assemblies. The pyrrole NH sites of **79** and **83**, in particular,

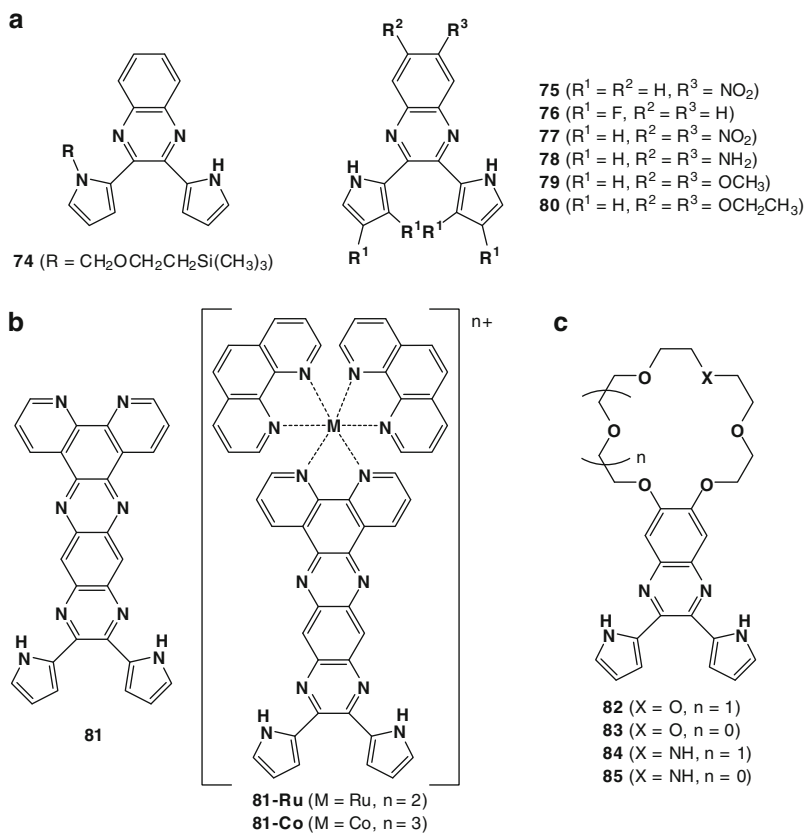


Fig. 21 (a) DPQ derivatives **74–80**; (b) phenanthroline-substituted DPQ **81** and metal complexes (**81-Ru**, **81-Co**); (c) crown-appended DPQs **82–85**

form hydrogen bonds with methoxy- and crown-oxygen moieties. The cation-binding properties of **82–85** have been examined, and a K^+ -bridged dimer structure has been observed in solid-state **83**. And although attempts have not yet proved successful, crown-substituted anion receptors are considered potential motifs for cooperatively binding cations and anions [94].

The modification of pyrrole α -positions also provides useful anion receptor molecules. Several α -formyl-substituted derivatives **86–88** (Fig. 22a), prepared from **72**, **79**, and **80**, can be converted into [2 + 2]-type Schiff-base macrocycles **89–91** (Fig. 22b) by condensation with 1,8-diaminoanthracene. These macrocycles have two “pseudo” cavities; **89** exhibits homotropic positive allosteric effects for F^- and H_2PO_4^- binding in CH_2Cl_2 . The binding constants ($\log K$) and the Hill coefficients are estimated to be 11.0 and 2.2 for F^- and 3.8 and 1.9 for H_2PO_4^- , respectively. This is the first example of an artificial allosteric system for H_2PO_4^- ; once an anion is captured in one cavity, the other cavity “shrinks” to the point where its size is better optimized for anion binding [95]. Further, tetrapyrrole and

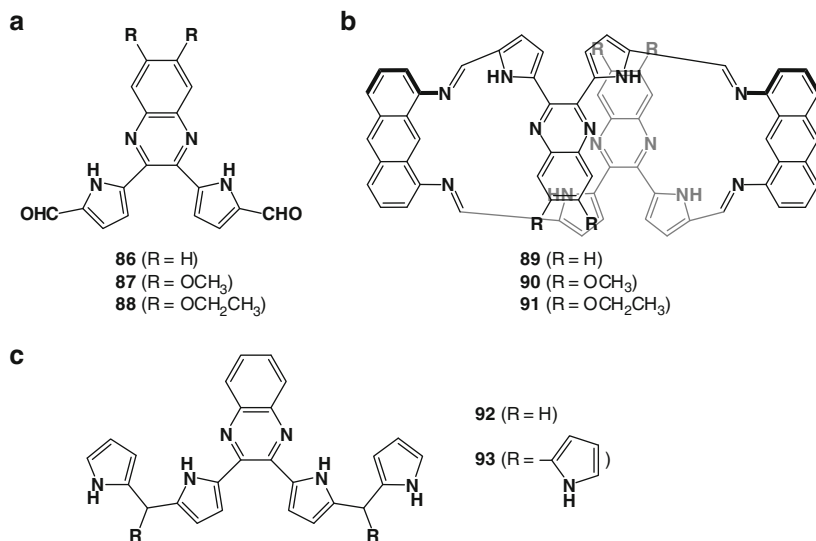


Fig. 22 (a) Formyl-substituted DPQs **86–88**; (b) DPQ-bridged macrocycles **89–91**; (c) oligopyrrolyl-substituted DPQs **92** and **93**

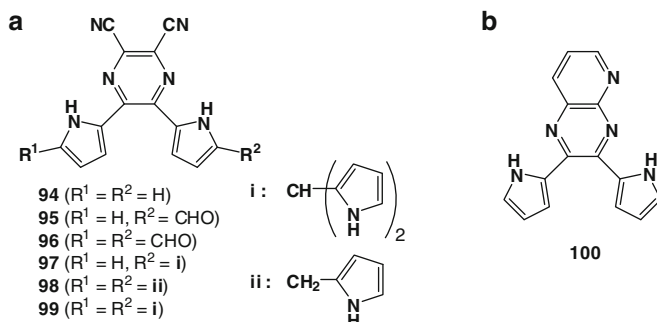


Fig. 23 (a) Dipyrrolylpyrazine derivatives **94–99**; (b) dipyrrolyl-substituted pyrido[2,3-*b*]-pyrazine **100**

hexapyrrole derivatives **92** and **93** (Fig. 22c) were obtained by acid-catalyzed condensation of the biscarbinol form of **86** and **86**, itself, with excess pyrrole. The receptors **92** and **93** have claw-like multiple binding NH sites; they show higher K_a values, 32,000, 550, and 4,300 M⁻¹ (**92**) and >1,000,000, 5,800, and 300,000 M⁻¹ (**93**) in CH₂Cl₂, for F⁻, Cl⁻, and H₂PO₄⁻, respectively [96].

Pyrazine analogs **94–99** (Fig. 23a) were also prepared from dipyrrolyldiketone and diaminomaleonitrile and subsequent formylation of **95** and **96**. A similar synthetic protocol for **92** and **93** affords oligopyrrolic **97–99**; **99** shows higher K_a values for Cl⁻, 48,000 M⁻¹, than **93**. The hexapyrrolic analogous receptors **93** and **99** also efficiently bind dicarboxylates such as oxalate, malonate, and succinate as

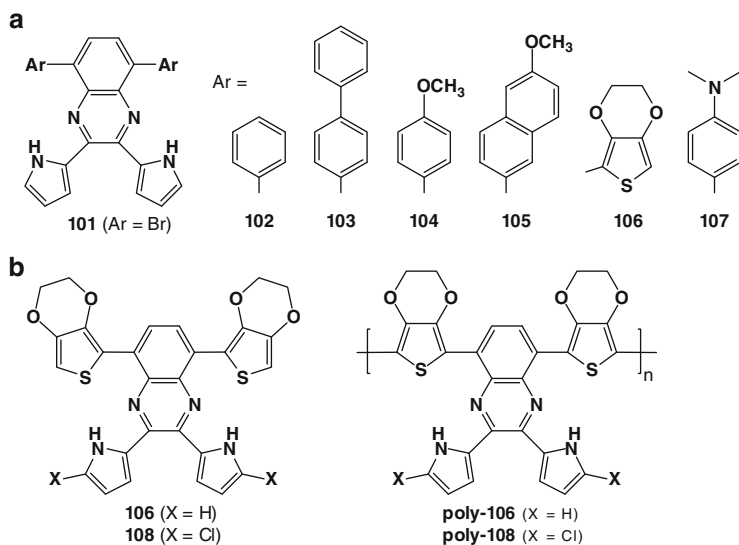


Fig. 24 (a) 5,8-Dibromo- and 5,8-diaryl-substituted dipyrrolylquinoxalines **101**–**107**; (b) thienyl-substituted dipyrrolylquinoxalines **106** and **108** and their polymers

TBA salts in CH_2Cl_2 (e.g., 30,000 (**93**) and 24,000 (**99**) M^{-1} for oxalate) [97]. In addition, Smanta and coworkers reported dipyrrolyl-substituted pyrido[2,3-*b*]pyrazine **100** (Fig. 23b), which has both anion-binding and metal coordination sites, is responsive to F^- (4,900 M^{-1} in CH_3CN) in the metal-free form [98].

The scope for the formation of functional materials based on a DPQ structure has also been examined. Anzenbacher and coworkers introduced aryl moieties at the 5- and 8-positions of the DPQ skeleton in an attempt to enhance and tune the fluorescence output. Stille coupling or Suzuki coupling was used to prepare 5,8-diaryl-substituted receptors **102**–**107** from the dibromo derivative **101** (Fig. 24a). The presence of 5,8-diaryl substituents results in both a dramatic increase in emission intensity and a shift in emission maximum from that of parent **72** ($\lambda_{\text{em}} = 490$ nm, $\Phi_{\text{F}} = 0.15$ in CH_2Cl_2). That is, $\lambda_{\text{em}} = 500$ nm, $\Phi_{\text{F}} = 0.25$ for **102**; $\lambda_{\text{em}} = 506$ nm, $\Phi_{\text{F}} = 0.38$ for **103**; $\lambda_{\text{em}} = 514$ nm, $\Phi_{\text{F}} = 0.24$ for **104**; $\lambda_{\text{em}} = 520$ nm, $\Phi_{\text{F}} = 0.13$ for **105**; $\lambda_{\text{em}} = 595$ nm, $\Phi_{\text{F}} = 0.22$ for **106**; and $\lambda_{\text{em}} = 610$ nm, $\Phi_{\text{F}} = 0.26$ for **107**. The K_{a} values of **102**–**107** in CH_2Cl_2 are in the range of 10,200 (**105**) to 51,300 (**102**) M^{-1} for F^- and 24,300 (**105**) to 93,700 (**102**) M^{-1} for $\text{HP}_2\text{O}_7^{3-}$ (14,300 M^{-1} for **72**). Significant changes in color and fluorescence emission are observed by the addition of F^- and $\text{HP}_2\text{O}_7^{3-}$. Therefore, polyurethane-embedded sensors exhibit color response in the presence of aqueous solutions of specific anions [99, 100]. Further, thienyl-substituted **106** and α -chloro **108** yield conductive materials poly-**106** and poly-**108**, whose band gaps were estimated at 1.39 and 1.36 eV, respectively (Fig. 24b). Upon treatment with aqueous solutions containing $\text{HP}_2\text{O}_7^{3-}$ as TBA salts, the sensor films exhibited gradual changes in their vis–NIR absorption spectra due to anion binding; the results were also supported by

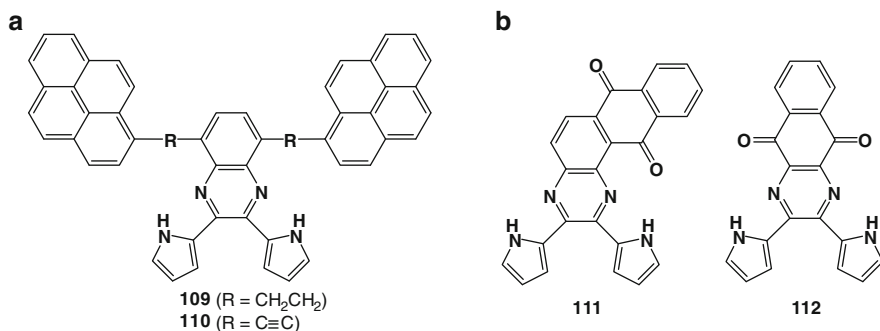


Fig. 25 (a) Pyrene-substituted dipyrrylquinoxalines **109** and **110**; (b) quinone-substituted dipyrrylquinoxalines **111** and **112**

tests using the electrochemical quartz crystal microbalance method (EQCM). Sensing devices containing poly-**108** and interdigitated ITO electrodes show dramatic changes on exposure to anion ($\text{HP}_2\text{O}_7^{3-}$) in both the vis–NIR spectra and drain current. The low-level p-doping and corresponding positive charge in the polymer result in a dramatic increase in the anion affinity [101, 102].

Pyrene-attached **109** and **110** (Fig. 25a) exhibit fluorescence quenching through efficient binding of F^- ($K_a = 17,300$ and $19,600 \text{ M}^{-1}$, respectively) and $\text{HP}_2\text{O}_7^{3-}$ ($K_a = 18,000$ and $29,500 \text{ M}^{-1}$, respectively), comparable to parent **72**. The sensor **110** achieves signal amplification through effective excited state localization, whereas **109** shows Förster resonance energy transfer (FRET)-based light harvesting from the pyrene moieties to the DPQ moiety. Excitation of **109** at 320 nm, the absorption wavelength of pyrene moieties, results in tenfold amplification of fluorescence compared to **72**. This means that **109** can be easily used for anion sensing at concentrations ten times lower than for **72** [103]. Anzenbacher et al. also reported that sensors **111** and **112** comprise a chromophore capable of undergoing an intensive change in color and a redox-active quinone moiety that generate strong colorimetric and electrochemical signals (Fig. 25b). The UV/vis absorption spectral changes of **111** and **112** show efficient binding to F^- ($K_a = 482,200$ and $150,700 \text{ M}^{-1}$, respectively) and $\text{HP}_2\text{O}_7^{3-}$ ($K_a = 316,000$ and $626,000 \text{ M}^{-1}$, respectively) in 0.5% $\text{H}_2\text{O}/\text{CH}_3\text{CN}$. The electrochemical reduction waves of **111** and **112** in square-wave voltammetry (SWV) show cathodic shifts because the electron-rich sensor–anion complex is difficult to reduce. Binding constants estimated from SWV show considerable agreement with those obtained from UV/vis absorption spectral changes [104]. Anzenbacher and coworkers also used receptor **111** as one of the sensor molecules in arrays that can detect anions in aqueous solutions [105]. Wong and coworkers also examined optical and electrochemical sensing via anion binding and conducted a theoretical study on **94** and **111** [106].

Other extended and polymeric systems **113**–**115** (Fig. 26) were reported by Sun and coworkers. Monomer **113** exhibits stronger F^- and $\text{HP}_2\text{O}_7^{3-}$ “binding” ($K_a = 2,520$ and $1,440 \text{ M}^{-1}$, respectively) than for CN^- (310 M^{-1}), CH_3CO_2^-

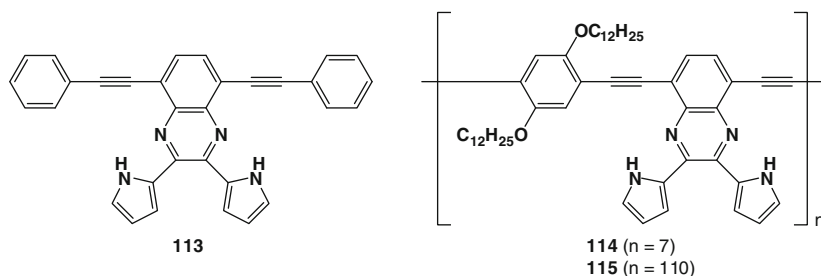


Fig. 26 Monomeric and polymeric forms of phenylethynyl-substituted dipyrrolylquinoxalines **113–115**

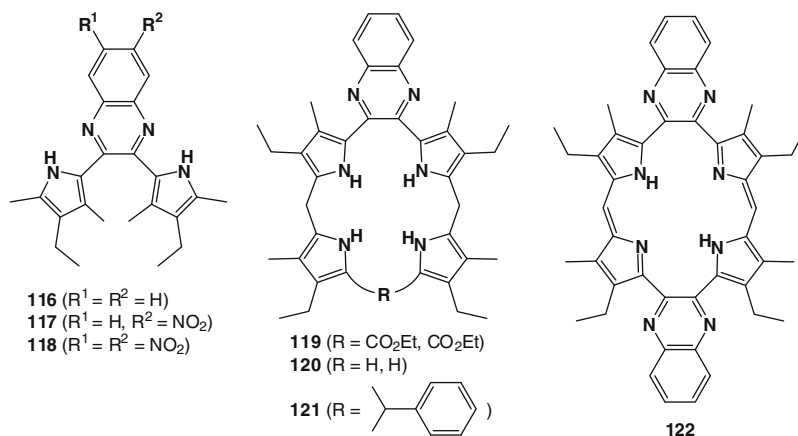


Fig. 27 Alkyl-substituted DPQs **116–120** and macrocycles **121** and **122**

(50 M^{-1}), and other anions such as Cl^- and H_2PO_4^- ($<10 \text{ M}^{-1}$) in CH_2Cl_2 ; here, F^- and $\text{HP}_2\text{O}_7^{3-}$ are associated with a pyrrole NH while the other pyrrole NH is deprotonated under ambient conditions. The sensitivity of a DPQ-based chemosensor can be easily enhanced by incorporation into conjugated polymers **114** and **115**. The quenching constants derived from the Stern–Volmer plots, 16,800 (**113**), 70,200 (**114**), and 52,000 (**115**) M^{-1} for F^- and 11,200 (**113**), 49,300 (**114**), and 38,000 (**115**) M^{-1} for $\text{HP}_2\text{O}_7^{3-}$, respectively, demonstrated that a conjugated polymer with about ten repeating recognition sites can induce a substantial quenching effect with a 34-fold increase in sensitivity over the corresponding monomeric sensor [107].

Andrioletti and coworkers synthesized peralkyl-substituted DPQ **116–118**, which, however, cannot be further modified to obtain derivatives. Therefore, from the precursory diketone of **116**, tetrapyrrole derivatives **119** and **120**, similar to **91**, were obtained. Note that **120** is a good starting material for macrocycles such as **121** and **122** (Fig. 27). π -Conjugated **122** can be considered as a quinoxaline-bridged dipyrrolic cyclic oligomers with a boat-like conformation [108].

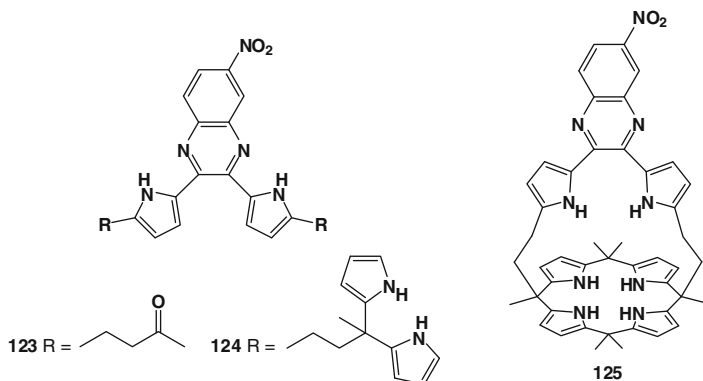


Fig. 28 DPQ-calix[4]pyrrole hybrid **125** and starting **123** along with intermediate **124**

Lee, Sessler, and coworkers reported DPQ-strapped calix[4]pyrrole **125**, which is prepared from **123** via the dipyrromethane derivative **124** (Fig. 28). As seen from the ¹H NMR spectral changes (CD₃CN/DMSO-*d*₆ 9:1, v/v) of **125**, with added TBAF, the NH protons of the pyrroles on the strap, shifted from 5.99–5.96 to 5.57–5.54 ppm, do not interact with the added anions via simple NH–anion hydrogen bonds. This is derived from an anion–π interaction, [109, 110] also supported by the downfield shifts in β-pyrrole CH from 6.54–6.49 and 5.80–5.74 to 6.85–6.80 and 5.92–5.90 ppm. ITC measurement (CD₃CN/DMSO-*d*₆ 97:3, v/v) suggests multiple binding modes, [1 + 1] and [1 + 2], for F[−] with *K*_a values of 3.72 × 10⁸ and 5.0 × 10⁵ M^{−1} and regular [1 + 1] binding for Cl[−], CH₃CO₂[−], and H₂PO₄[−] with *K*_a values of 1.94 × 10⁴, 1.89 × 10⁴, and 1.33 × 10³ M^{−1}, respectively [111].

4.2 Anion-Responsive Aryl-Bridged Bispyrroles

Apart from quinoxaline-bridged bispyrroles, several reports describe the anion-binding properties of aryl-bridged oligopyrroles, for example, 1,3-bis(pyrrol-2-yl) benzenes **126–128** (Fig. 29) synthesized by Sessler et al., which are essential building units of macrocycles; **126** shows *K*_a values at, for example, 2,300, 4,300, 1,100, 190, 290, 1,300, 280, and 32 M^{−1} for F[−], Cl[−], Br[−], I[−], HSO₄[−], H₂PO₄[−], NO₃[−], and ClO₄[−], respectively, estimated from ¹H NMR spectral changes in CD₂Cl₂. These *K*_a values are larger than those of dimethyldipyrromethane **52**, possibly because the bite angle present in **126** provides a better structural match to Cl[−] (and likely most other anions) [78]. Eichen and coworkers reported 1,3-dipyrrol-2-ylazulene **129** (Fig. 29), which binds F[−] (11,000 M^{−1}), Cl[−] (110 M^{−1}), Br[−] (100 M^{−1}), and I[−] (50 M^{−1}) in CH₂Cl₂ and F[−] (>1,000 M^{−1}) in DMSO. F[−] enhances fluorescence by more than tenfold in DMSO presumably via conformational changes from the fairly coplanar structure of core azulene and two

Fig. 29 Aryl-bridged bispyrrole derivatives **126–129**

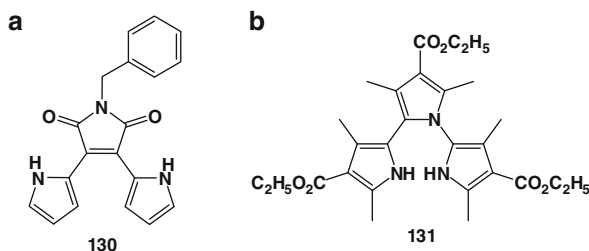
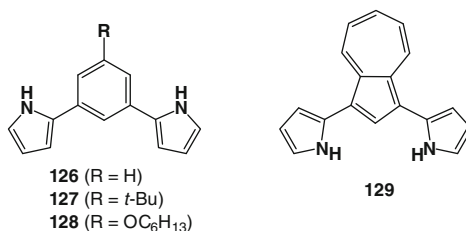


Fig. 30 (a, b) Pentacycle-bridged bispyrrole derivatives **130** and **131**

pyrrole rings, elucidated by single-crystal X-ray analysis, to that with partially disrupted π -conjugation between azulene and pyrroles [112].

Maleimide-bridged bispyrrole **130** (Fig. 30a), prepared by Sun, Hsu, Chow, and coworkers, has K_a values of 18,500 and 36,300 M⁻¹ for F⁻ and CN⁻ in CH₂Cl₂, respectively. The significant fluorescence quenching and red-shift caused by F⁻ and CN⁻ exposure stems from deprotonation of a pyrrole NH [113]. The terpyrrole isomer **131** (Fig. 30b), an analog of **130** and DPQs, synthesized by Sessler and coworkers, shows color changes upon the addition of anions such as F⁻ and H₂PO₄⁻ in CH₂Cl₂. The K_a values of **131** are estimated as 1,82,000, 160, 60, and 17,500 M⁻¹ for F⁻, Cl⁻, Br⁻, and H₂PO₄⁻, respectively, which are higher than those of DPQ **72** [114].

Metal-mediated changes to the preorganized conformation are observed in the metal complexes of bipyridine-bridged bispyrrole **132**. Ru(II) and Rh(III) complexes **132-Ru** and **132-Rh** (Fig. 31a) prepared by Sessler and coworkers exhibit anion binding in DMSO, e.g., **132-Ru** has been reported to have K_a values of 7,000, 370, and 104,000 M⁻¹ for F⁻, Cl⁻, and H₂PO₄⁻, respectively. In particular, the K_a value for H₂PO₄⁻ is ca. 2,600-fold greater than for the DPQ-Ru(II) complex **81-Ru**. And compared with **132-Ru**, higher affinities of triply charged **132-Rh** (870 M⁻¹ for Cl⁻) lead to precipitates upon H₂PO₄⁻ binding. Single-crystal X-ray structures of Cl⁻ complexes of **132-Ru** and **132-Rh** elucidate C–H \cdots Cl interactions (C \cdots Cl: 3.65 and 3.59 Å on average for **132-Ru** and **132-Rh**, respectively) along with N–H \cdots Cl interactions [115]. In addition, monomeric pyrrole building subunits can be incorporated into metal complexes by substituting the metal ligand moiety. Gale and coworkers prepared Pt(II) complexes **133** and **134** (Fig. 31b) from 3- and 4-(pyrrol-2-yl)pyridines. The single-crystal X-ray structure of a BF₄⁻ salt of **133**

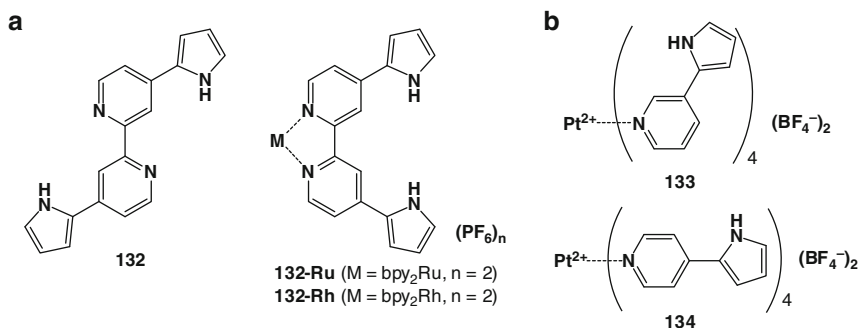
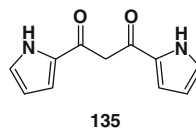


Fig. 31 (a) Bipyridine-bridged bispyrrole **132** and metal complexes; (b) Pt(II)-bridged pyrrole-based anion receptors **133** and **134**

Fig. 32 1,3-Dipyrrolyl-1,3-propanedione **135**



shows the 1,2-alternate conformation and binding of two BF_4^- anions via N–H···F and C–H···F hydrogen bonds. The anion-binding behavior of **133** and **134** upon the addition of TBA salts in $\text{DMSO-}d_6$ reflects 1:1 stoichiometry, except in the case of CH_3CO_2^- binding by **133** with K_2 ($2,400 \text{ M}^{-1}$) $>$ K_1 (216 M^{-1}). This suggests that an allosteric effect exists that preorganizes the second binding site upon complexation of the first equivalent of CH_3CO_2^- . In DMSO , in contrast to **134**, which binds anions using pyridyl *o*-CH sites and not pyrrole NH, **133** uses pyrrole β -CH and not NH to show large K_a values, for example, 960 (**133**) and 216 (**134**) M^{-1} for Cl^- and 1,115 (**133**) and <10 (**134**) M^{-1} for CH_3SO_3^- . In contrast to the binding mode in solution, **133** forms the CH_3SO_3^- complex via an N–H···O hydrogen bond; this suggests that the hydrogen-bonding acceptor DMSO molecules drive the pyrrole rings to invert and face the “outside” [116].

In 2005, Maeda and Kusunose found that the key starting molecule necessary to produce useful acyclic oligopyrrole derivatives was 1,3-dipyrrolyl-1,3-propanedione (dipyrrolyldiketone) **135** (Fig. 32), first synthesized by Oddo and Dainotti in 1912 [117] and refined by Battersby and coworkers in 1984 [118]. Dipyrrolyldiketone **135** can be obtained from pyrrole by treatment with malonyl chloride. Therefore, dipyrrolyldiketone derivatives can be prepared from the corresponding substituted pyrroles. On the basis of the “pyrrole library,” thus far, Maeda and coworkers have synthesized various dipyrrolyldiketone derivatives [119–128].

One derivative of dipyrrolyldiketones is the pyrazole-bridged bispyrrole. Following the first example reported by Oddo and Dainotti [117], dipyrrolylpyrazoles (DPPs, **136–140**, Fig. 33a) were synthesized by Maeda and coworkers by the condensation of excess hydrazine monohydrate with the corresponding dipyrrolyldiketones. *N*-Methyl-substituted **131–133** were obtained similarly from diketones

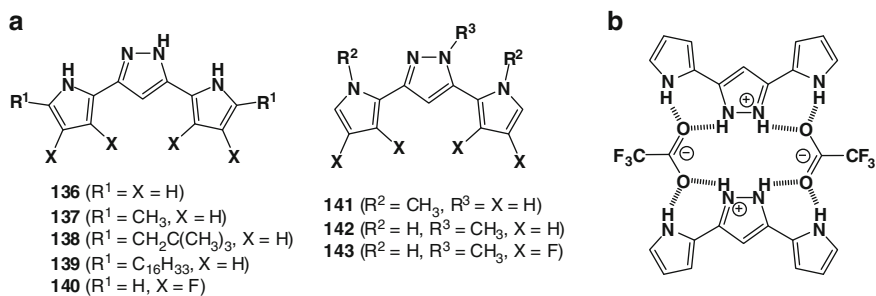


Fig. 33 (a) Dipyrrolylpyrazoles **136–143**; (b) [2 + 2] assembly of **136**₂·TFA₂

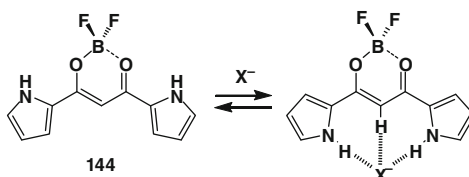
or from the methylation of the corresponding DPPs. Based on the anion-binding ability of the pyrrole NH sites, as observed in **132** and **133** ($K_a = 1,600$ and $28,000\text{ M}^{-1}$ for $CH_3CO_2^-$ in CH_2Cl_2 , respectively), the planar [2 + 2]-binding structures (As one of the other examples [129]) with TFA (Fig. 33a) were elucidated by single-crystal X-ray analyses of **136**₂·TFA₂, **137**₂·TFA₂, and **140**₂·TFA₂ complexes. SEM measurements on a silicon substrate showed that micrometer- and nanometer-scale morphologies of TFA complexes of DPPs via intermolecular interactions such as π - π stacking. In sharp contrast to unsubstituted **136**₂·TFA₂ and α -methyl **137**₂·TFA₂ that yield crystalline objects, TFA complexes **137**₂·TFA₂ and **138**₂·TFA₂ with neopentyl and hexadecyl chains form petal-like objects with widths of ca. 500 nm and assembled sheet structures with thicknesses <100 nm. Further, β -fluorinated **140**₂·TFA₂ exhibits rod-like morphologies with widths of ca. 100–200 nm and small amounts of microcrystals [130].

5 Boron Complexes of Dipyrrolyldiketones as Acyclic Anion Receptors with Planar Geometries

5.1 Boron Complexes of Dipyrrolyldiketones

Supramolecular assemblies built from planar pyrrole-based anion receptors also have the potential to show anion-responsive behavior and, under the appropriate conditions, form functional organized structures comprising cationic and anionic species. To explore this potential, however, it is essential to first design and synthesize fairly planar π -conjugated systems comprising pyrrole rings that can efficiently bind anions. In 2005, Maeda and Kusunose reported that the BF_2 complex **144** of dipyrrolyldiketone **115** (Fig. 34) was a candidate π -conjugated acyclic anion receptor with the potential in forming stacked structures. The molecule **144** consists of two pyrrole rings and a boron-bridged 1,3-propanedione

Fig. 34 BF₂ complex of dipyrrolyldiketone **144** and anion-binding mode



moiety. The pyrrole rings, which exist even in the acyclic structure, are stabilized by the neighboring electron-withdrawing carbonyl unit; therefore, the skeleton structure could be appropriate for various uses such as sensors, functional materials, etc. The absorption and emission maxima of the receptor **144** are observed at 432 and 451 nm in CH₂Cl₂, respectively; these electronic properties of a single molecule could be applied to the potential photonic and electronic materials such as supramolecular assemblies, as mentioned. The solid-state assembly of **144** has been revealed by single-crystal X-ray analyses. Planar **144**, wherein the pyrrole nitrogens are on opposite sides of the molecule as observed in solution state, forms stacked structures with an offset arrangement¹ [119]. The BF₂ complex **144** does not form a preorganized conformation because the two pyrrole NH are not located at the appropriate positions for anion binding. Upon the addition of anions, receptor **144**, as a “molecular flipper,” exhibits inversions of the two pyrrole rings and binds anions using the pyrrole NH and bridging CH to form a planar receptor–anion complex (Fig. 34). N–H···X[−] and bridging C–H···X[−] interactions are implicated from the ¹H NMR chemical shifts of other molecular flippers (instead of **144**, vide infra) upon the addition of anions as TBA salts. Further, the discrete resonances of the two species – free receptor and anion complex – suggest that the equilibrium between these forms is too slow to be detected on the NMR timescale, possibly because of the requirement for pyrrole inversions prior to anion binding. The absorption and emission spectra of **144** change in the presence of anions as TBA salts, suggesting its potential as a colorimetric anion sensor. The UV/vis absorption spectral changes of **144** in CH₂Cl₂ indicate K_a values of 15,000, 2,100, 930,000, and 270,000 M^{−1} on binding with Cl[−], Br[−], CH₃CO₂[−], and H₂PO₄[−], respectively [119, 124]. Thus, clearly, receptor **144** is more efficient at anion binding than DPQ **72** [90] and 1,3-bis(pyrrol-2-yl)benzene **126** (in CH₂ClCH₂Cl) [115].

The available library of pyrrole derivatives reported so far shows that the introduction of substituents to the receptor framework of **144** yields a variety of molecular flippers, **145–152** (Fig. 35). Maeda et al. reported the α-alkyl-substituted receptors **145-n** and **146** from α-alkylpyrroles [119, 124]. Maeda et al. also prepared β-alkyl- and β-fluorine-substituted receptors **147–149**, which can act as

¹Maeda et al. discovered the formation of multicrystalline systems of **144** and have since been investigating the photophysical and electric conductive properties of the single-crystal state with the aim of discovering the unique properties possible because of the ordered assembly of π-conjugated molecules [131].

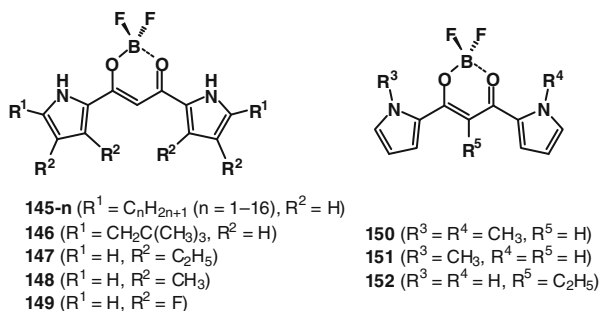


Fig. 35 BF_2 complexes of dipyrrolyldiketones **145–152**

building blocks for covalently linked oligomers due to their free α -positions [120, 122, 126]. In addition, receptor molecules **150–152**, whose binding sites are (partially) protected, were also synthesized [121]. Further, single-crystal X-ray analysis of some receptors revealed stacked structures similar to **144**. The interaction between NH and BF, which is essential for specific assembling modes such as a hydrogen-bonding dimer, is observed in other receptors including the parent **144**. The binding constants (K_a) of **144**, **145-n**, and **146–149** for Cl^- , Br^- , $CH_3CO_2^-$, $H_2PO_4^-$, and HSO_4^- were determined from UV/vis absorption spectral changes upon the addition of anions [119, 120, 122, 124, 126]. Enhanced values were obtained for unsubstituted **144** because of the less steric hindrance at the pyrrole α -positions and for β -fluorinated derivative **149** because of the polarized NH and CH binding sites. The K_a values of α -alkyl-substituted receptors **145-n** are smaller in receptors with longer alkyl chains and their binding kinetics are also dependent on the alkyl chain lengths. All the receptors **144–149** shown here except for **148** bind $CH_3CO_2^-$ more efficiently than the other anions. Upon the addition of $CH_3CO_2^-$ to **149** (2×10^{-3} M) in CD_2Cl_2 at $-50^\circ C$, both the NH and CH peaks (at 9.02 and 6.65 ppm, respectively) in the 1H NMR spectrum disappear and new signals appear downfield at 12.09 and 8.23 ppm, respectively. Similar downfield shifts are observed upon the addition of other anions to these acyclic receptors. The anion-binding behaviors of the sterically “blocked” derivatives **150–152** suggest the essential role of the bridging CH site in anion binding. Thus, from these experimental and theoretical data, the affinity for anions can be determined from the following factors: (a) electronic effects of the peripheral substituents, (b) steric effects of the α -substituents, and (c) relative stabilities of the preorganized conformation. The solid-state structures of the receptor–anion complexes of **144**, [119] **149**, [120] and **145-2** [124] prepared from TBA salts, as revealed by single-crystal X-ray analyses, show anion-bridged 1-D chains (**144** and **149**) and regular [1 + 1] complex (**145-2**).

The replacement of fluorine substituents in a boron moiety of molecular flippers by 1,2-diol units such as catechol derivatives enables the attachment of acyclic anion receptors to the π -conjugated “backbone.” Maeda et al. synthesized catechol-substituted receptors **153–156** (Fig. 36a) from the corresponding dipyrrolyldiketones [119, 122] by treatment with BCl_3 and then with excess catechol

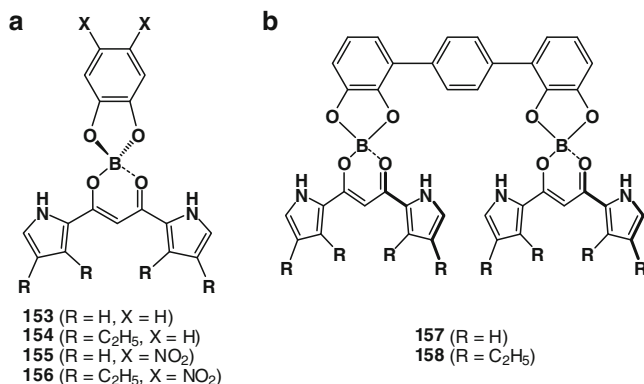


Fig. 36 (a) Catechol-substituted boron complexes of dipyrrolyldiketones **153**–**156**; (b) terphenyl-bridged dimers **157** and **158**

derivatives in refluxing CH₂Cl₂. The UV/vis absorption spectra of “BO₂” complexes **153** and **154** in CH₂Cl₂ exhibit absorption maxima (λ_{max}) at 435 and 454 nm, respectively, which are red-shifted by 2–3 nm in comparison with the maxima of the corresponding BF₂ complexes **144** and **147**. Further, compared with the high-intensity fluorescence of **147** at 471 nm (λ_{em} excited at 420 nm; emission quantum yield: $\Phi_{\text{F}} = 0.98$), the weak fluorescent emission of **154** at 474 nm (λ_{em} excited at 420 nm; $\Phi_{\text{F}} = 0.001$) can be attributed to the quenching path of the intramolecular electron transfer. The binding constants (K_{a}) of **154** for anions in CH₂Cl₂ are lower than those of **147** due to the fact that the catechol oxygens (**154**) are less electronegative than fluorines (**147**). The K_{a} values of **156** for anions are higher than those of **154**, because of the electron-withdrawing effect of the nitro groups [132]. The substitution at a boron unit by neighboring hydroxyl groups of various functional units enables the formation of covalently linked dimers. In fact, Maeda et al. prepared the ditopic receptors **157** and **158** (Fig. 36b) by the treatment of intermediate BCl₂ complexes with *p*-phenylene-bridged dicatechol. These receptors are extended systems bridged by “spacer” moieties between the acyclic anion receptor. Single-crystal X-ray analysis of **158** suggests that both the receptor units are oriented in the same direction so that a Π -shaped *syn* conformation is generated with an intramolecular B–B distance of 8.68–9.17 Å. The locations of the two receptor units in **158** lead to [1 + 1] binding for linear dicarboxylates (–O₂C(CH₂)_{*n*}CO₂–, *n* = 2–6); the K_{a} values for succinate (*n* = 2), glutarate (*n* = 3), adipate (*n* = 4), pimelate (*n* = 5), and suberate (*n* = 6) in their TBA salt forms in CH₂Cl₂ are 19,000, 72,000, 810,000, 2,600,000, and 440,000 M^{–1}, respectively. This observation suggests that the distance between the receptor units (ca. 9 Å) is crucial in the determination of the selectivity of the dianions² [132].

²Emission quantum yield (ϕ_{F}) of **154** is under further validation. Further, other elements besides fluorine and oxygen can also be introduced at the boron moiety [133].

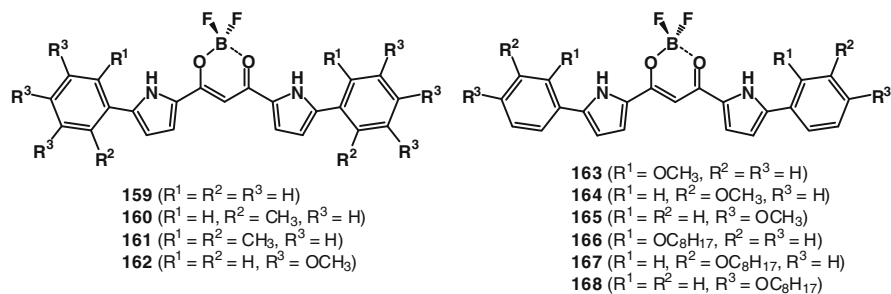


Fig. 37 Aryl-substituted derivatives **159–168**

5.2 Aryl-Substituted Anion Receptors

Tunable electronic properties and stacking abilities requires extension of the π -conjugation of the molecular flippers. Thus, Maeda et al. attempted to synthesize α -aryl-substituted derivatives of dipyrrolyldiketone BF_2 complexes. Initially, α -aryl-substituted **159–162** (Fig. 37) were obtained from the α -aryl-substituted pyrroles, which were synthesized by cross-coupling reactions via the corresponding α -aryl-substituted dipyrrolyldiketones. The absorption maxima (λ_{max}) of **159**, **160**, and **162** in CH_2Cl_2 appear at 500, 480, and 516 nm in CH_2Cl_2 , respectively, which are red-shifted as compared to **144** (432 nm), **145–16** (457 nm), **146** (457 nm), **147** (452 nm), **148** (449 nm), and **149** (421 nm). Conversely, λ_{max} for **161** appears at 456 nm, which is blue-shifted by 46, 24, and 60 nm as compared to **159**, **160**, and **162**, respectively, as a result of the distortion of the aryl rings [123]. Maeda and Eifuku also prepared receptors bearing mono-alkoxy-substituted phenyl moieties **163–168** (Fig. 37). The UV/vis absorption maxima (λ_{max}) of **163**, **164**, and **165** in CH_2Cl_2 were observed at 513, 501, and 518 nm, respectively, suggesting that alkoxy-substitution at the *ortho* and *para* positions affords a red-shift whereas similar substitution at the *meta* position has almost no effect in comparison with the λ_{max} value of α -phenyl **159** (500 nm), and that the length of the alkoxy chain has almost no effect on the electronic state [127]. Single-crystal X-ray analysis of α -aryl-substituted receptors also demonstrates stacked structures.

Selective iodination at the α -pyrrole positions of β -ethyl-substituted **147** on treatment with *N*-iodosuccinimide (NIS) in CH_2Cl_2 is found to be a key step in synthesizing the mono-**169** and bis-iodinated derivative **170**, which are essential starting materials in the coupling reactions used for various functional molecules and covalently linked oligomer systems. Suzuki cross-coupling of **169** or **170** and phenylboronic acid afford monophenyl- **171** and bisphenyl-substituted **172** [134]. Using the corresponding aryl boronic acids under similar conditions, the bis-iodinated derivative **170** can be transformed into pyrrolyl-, furyl-, and thienyl-substituted derivatives **173–175** (Fig. 38a) [135]. Mono- **169** and bis-iodinated **170** are also converted into the receptors **176–179**, which possess a formyl functionality [136]. The covalently linked dimer **180** (Fig. 38b) was synthesized by the coupling of

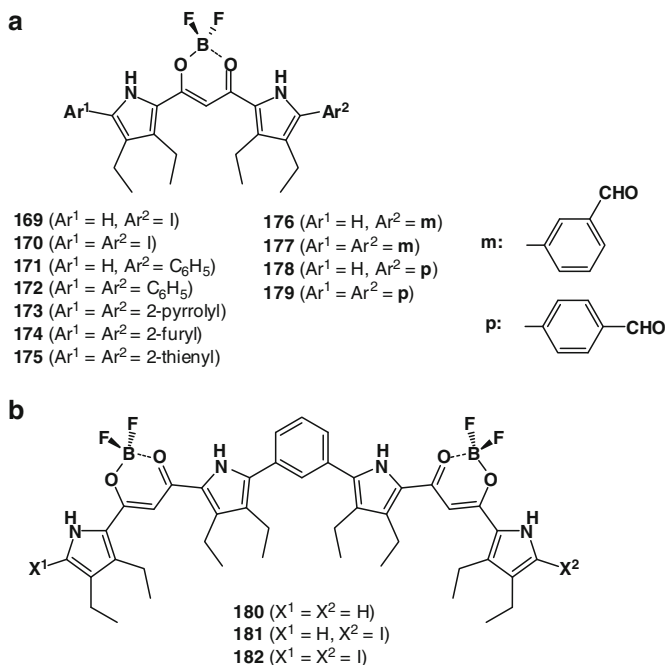


Fig. 38 (a) Iodinated **169** and **170** and β -ethyl-substituted aryl-substituted receptors **171–179**; (b) phenylene-bridged dimers **180–182**

mono-iodinated **169** with 1,3-benzenediboronic acid bis(pinacol)ester. Further iodination of phenylene-bridged dimer **180** affords bis-iodinated and mono-iodinated dimers (**181** and **182**) [134]. The UV/vis absorption bands of **172–175** in CH_2Cl_2 are observed at 499, 551, 538, and 527 nm, respectively, suggesting red-shifts that are comparable to that of α -unsubstituted **147** (451 nm). Those of formyl-substituted **176–179** in CH_2Cl_2 are observed at 474, 495, 482, and 510 nm, respectively. Dimer **180**, whose λ_{max} value is 489 nm due to the incomplete π -conjugation at the *meta*-phenylene linkage, together with iodinated derivatives, is a potential subunit for the formation of anion-responsive oligomers. In the solid state, the receptors **170** and **172–179** form stacked dimers or higher-order stacked structures [134–136].

Compared with unsubstituted **144**, α -phenyl **159** has augmented K_a values, especially for halides (ca. 2.0 and 1.3-fold enhancement for Cl^- and Br^- , respectively), possibly via pentacoordination (Fig. 39) in contrast to oxoanion binding. In contrast, doubly and totally *o*-C-blocked **160** and **161** exhibit smaller K_a values (ca. 1/10 and 1/30 for Cl^- binding), possibly due to steric hindrance and electrostatic repulsion of the anions by the π -plane. The K_a values of *meta*-substituted **164** and **165** and *para*-substituted **167** and **168** are almost comparable with those of **159**. There are no significant differences between methoxy- and octyloxy-substituted receptors. In contrast, the intramolecular hydrogen bonding in *ortho*-substituted **163** and **166** affords complicated binding modes with low affinities for anions; this suggests that

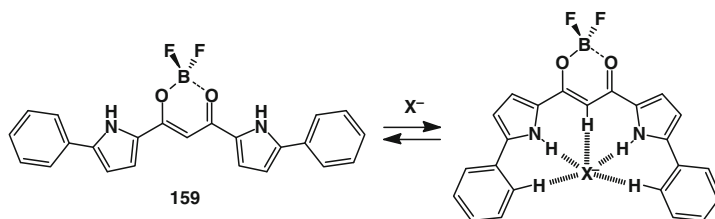


Fig. 39 Anion-binding mode of aryl-substituted receptor **159**

ortho-substituents can interfere with anion binding. Further, compared with **159**, β -ethyl **172** shows similar and smaller K_a values for oxoanions and halides, respectively [123, 127, 134]. Proton NMR spectral changes of α -aryl-substituted receptors upon anion binding provide valuable insights into the binding behaviors of aryl-*o*-CH along with those of core pyrrole NH and bridging CH. In addition, at lower temperatures with a small amount of Cl^- , a new NH signal appears between that of the free receptor and the [1 + 1] complex. This is attributed to the [2 + 1] binding complex $\mathbf{159}_2 \cdot \text{Cl}^-$; formation of the [2 + 1] complex is also supported by DOSY NMR and electrospray ionization time-of-flight mass spectrometry (ESI-TOF-MS) [123]. However, even in CHCl_3 containing 0.5% EtOH, pyrrolyl **173** shows considerably larger K_a values, $>10^6 \text{ M}^{-1}$ for Cl^- , H_2PO_4^- , and CH_3CO_2^- , than those of **172**, **174**, and **175** and α -unsubstituted **147** because of the presence of multiple polarized NH sites [135]. Note that smaller K_a values are expected with an increase in the number of phenyl-substituents in **147**, **171**, and **172** because of the steric hindrance between the α -phenyl and β -ethyl moieties. But in contrast, the bisformyl-substituted receptor **177** exhibits augmented K_a values compared with those of the corresponding monoformyl **176**, while **179** shows larger K_a values for halide and CH_3CO_2^- anions than that for **178**. This tendency in the formylphenyl-substituted receptors **176**–**179** may stem from the increased affinity of the *o*-CH sites due to the electron-withdrawing formyl moiety [134, 136]. Maeda et al. reported single-crystal X-ray structures of the anion complexes of α -aryl-substituted receptors, $\mathbf{159} \cdot \text{Cl}^-$, $\mathbf{162} \cdot \text{Cl}^-$, and $\mathbf{173} \cdot \text{Cl}^-$, which form pentacoordinated geometries as the building components of the electrostatically mediated alternatively stacking structures consisting of “planar anions (receptor–anion complexes)” and tetraalkylammonium cations (Fig. 40) [123, 135]. These “charge-by-charge” columnar structures, observed so far only in the crystal states as 3-D organized structures, allow the formation of dimension-controlled organic salts by using planar anions under appropriate conditions.

5.3 Supramolecular Structures Consisting of Acyclic Anion Receptors

Peripheral modifications to receptor molecules allow stabilization of the stacked structures not only in the solid state but in soft materials such as supramolecular

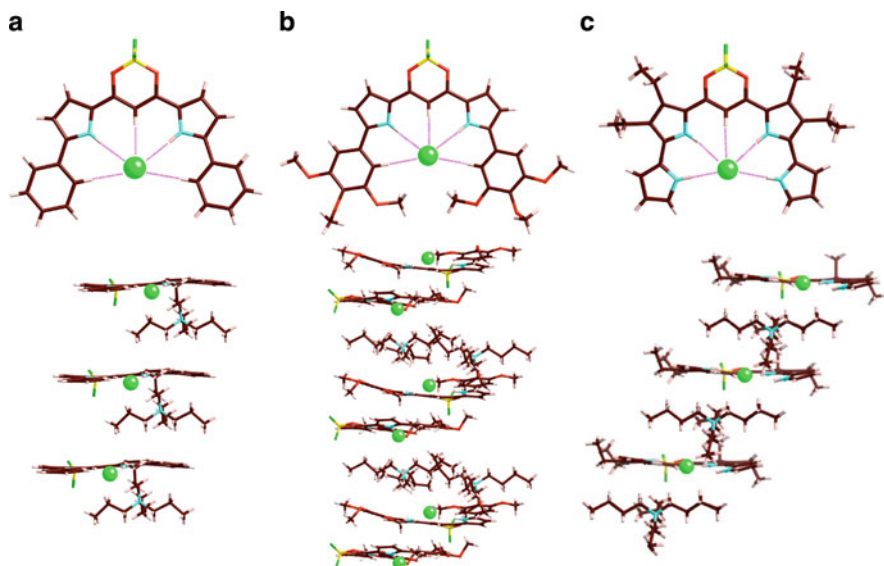


Fig. 40 Solid-state single molecules and “charge-by-charge” assemblies of receptor–anion complexes: (a) **159**·Cl[−]; (b) **162**·Cl[−]; (c) **173**·Cl[−]. Tetraalkylammonium cations are omitted for clarity in the top views

gels [137–142] that are responsive to anions [143–145]. Maeda et al. prepared derivatives with aliphatic chains at the aryl rings (**183–185**, Fig. 41) by procedures similar to those used for **159–168**. These anion receptors **183–185** gelate octane (10 mg mL^{−1}); the transition temperatures between the gel and solution states are −8.5 (**183**), 4.5 (**184**), and 27.5°C (**185**, Fig. 42a), suggesting that the longer alkyl chains afford more stable gels. The octane gel of hexadecyloxy-substituted **185** (10 mg mL^{−1}) exhibits split absorption bands with absorption maxima at 525 and 555 nm along with a shoulder at 470 nm due to the formation of stacked structures; this is in contrast to the single peak at 493 nm exhibited in a diluted solution containing dispersed monomers. This supramolecular organogel formation is achieved for the ordered structures via noncovalent interactions between the π -conjugated moieties and their substituents; this is supported by AFM (Fig. 42b), SEM, and XRD observations. The addition of anions (10 equiv) in the solid form (TBA salts) to the fluorescent octane gel results in a transition to the solution state; the gels are gradually transformed into solutions beginning from areas close to where the solid salts have been added (Fig. 42c). In this process, once the receptor (gelator) molecules in the gel bind to the anions, the counter TBA cations concertedly approach the receptor–anion complexes to form soluble ion pairs and afford the octane solution. In the case of the gel of **185**, these transitions are quite distinct from the crystal states mentioned previously (e.g., **162**·Cl[−]; Fig. 40b), which are

Fig. 41 BF_2 complexes **183**–**185** with 3,4,5-trialkoxy-substituted aryl rings

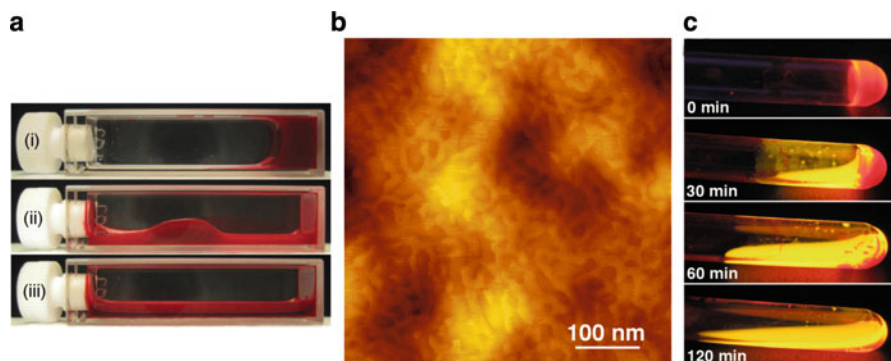
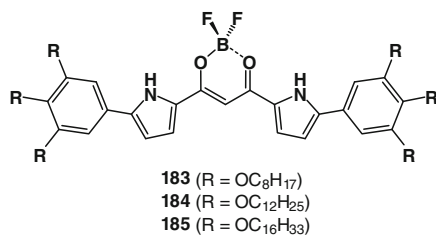


Fig. 42 (a) Phase transition of **185** in octane (10 mg mL⁻¹) between solution and gel at (i) 25.0, (ii) 27.5, and (iii) 30.0°C; (b) AFM 2-D image in a tapping mode of **185** (from octane gel) cast by spin-coating on a silicon substrate; (c) transition of supramolecular organogel of **185** in octane (10 mg mL⁻¹) at 20°C upon the addition of Cl^- (10 equiv) added as a solid TBA salt (under UV (365 nm) light)

due to the insolubility of the TBA salt of $\mathbf{162}\cdot\text{Cl}^-$ in apolar hydrocarbon solvents³ [123].

Condensation of formyl-substituted **176**–**179** with hexadecylamine or 3,4,5-trihexadecyloxyaniline and following reduction by $\text{NaBH}(\text{OAc})_3$ affords **186**–**193** (Fig. 43). In contrast to **185**, bis-substituted **191** and **193** in octane (10 mg mL⁻¹) appear to have fairly dispersed, and not gel-like, states at r.t. When the solutions are cooled, **191** and **193** form opaque solutions below ca. 1 and ca. -10°C , respectively, and form gel-like materials below ca. -10 and ca. -30°C , respectively. UV/vis and NMR analyses and DLS support the formation of assembled structures. In these systems, the connection of three π -conjugated moieties, a core π -plane and two side aryl units, by sp^3 methylene bridges is the basis for the formation of supramolecular assemblies that are not very rigid but

³Anion additives may not always act simply as inhibitors but may also be exploited as building units in soft materials. From this point of view, structural modifications to anion receptors and the choice of appropriate combinations of anions, cations, receptors, and solvents are currently being investigated in order to harness the fascinating properties of supramolecular gels that are sensitive to chemical stimuli [146].

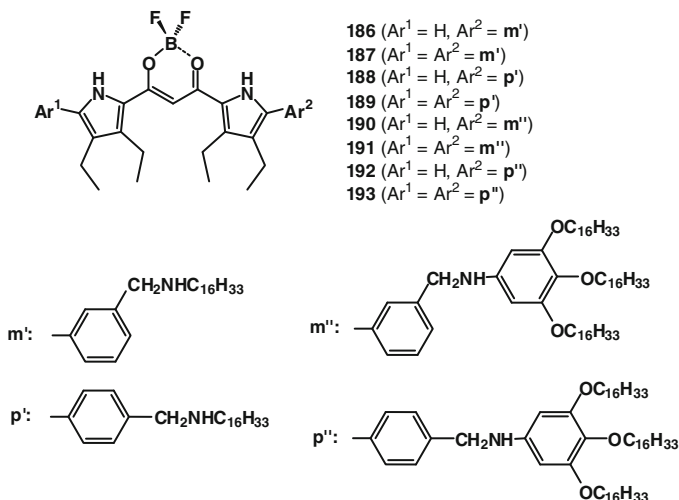


Fig. 43 BF_2 complexes **186–193** derived from formyl-substituted receptor molecules

yield soft materials by fairly ordered organization under the appropriate conditions. Further, addition of 1 equiv of Cl^- as a TBA salt can modulate the nature of the assembled structures, along with their optical and electronic properties [136].

Organized structures can be formed in aqueous solutions by exploiting the interactions between hydrophobic moieties inside the assemblies and the association of hydrophilic sites with water molecules [147, 148]. For example, Maeda et al. synthesized poly(ethylene glycol) (PEG)-substituted amphiphilic π -conjugated acyclic oligopyrroles (type A: **194–197**; type B: **198–201**, Fig. 44) by procedures similar to those for **159–168** and **183–185**. While amphiphiles **194**, **200**, and **201** precipitate from water, their derivatives **195–199** are soluble. Their λ_{max} values are observed at 460, 496, 506, 462, and 481 nm (1×10^{-5} M), respectively, in water; these values are blue-shifted as compared with those in MeOH (498, 510, 512, 510, and 512 nm). This suggests the formation of H-aggregates in aqueous solutions. The fluorescence spectra of **195–199** in aqueous solutions are observed as each monomer's fluorescence peak at 546, 571, 572, 672, and 671 nm with low emission quantum yields (Φ_F , determined at λ_{ex} values that are equal to the respective λ_{max} values) of 0.01, 0.01, 0.09, 0.02, and 0.02, respectively, which are characteristic aspects of H-aggregates. The solid films cast from the aqueous solutions of **195–199** exhibit almost the same red-shifted UV/vis absorption profiles ($\lambda_{max} = 526, 540, 530, 548, \text{ and } 531$ nm, respectively) as those cast from CH_2Cl_2 solutions; this result suggests that the removal of water molecules by slow evaporation at r.t. or by freeze-drying disrupts the H-aggregate formations, which are supported by water molecules and instead leads to other assembled structures (J-type aggregates). Cryo-TEM analysis of **198** (1×10^{-5} M) shows vesicular structures [149] with diameters of 30–80 nm (Fig. 45), which are consistent with the results of DLS measurements. The wall thickness (dark part) of capsules is estimated to be ca.

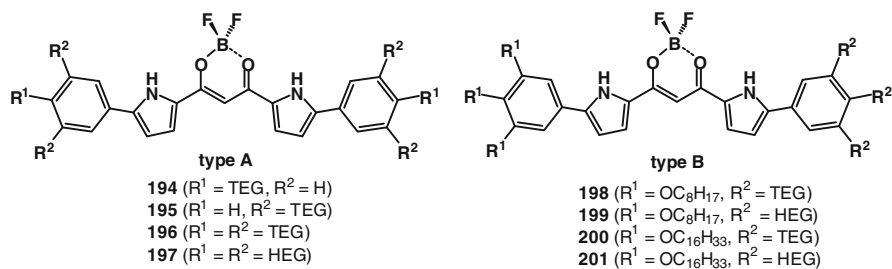


Fig. 44 Amphiphilic derivatives of acyclic anion receptors **194–201**

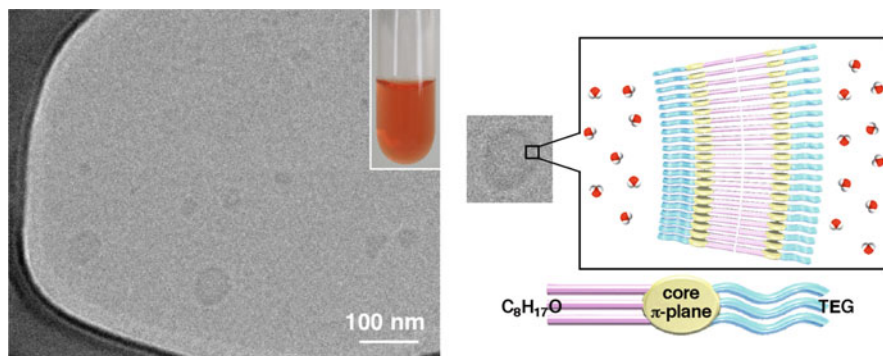


Fig. 45 Cryo-TEM image of **198** from an aqueous solution (1×10^{-5} M) without staining along with the photograph of the aqueous solution (1×10^{-4} M; inset) and possible assembly mode of **198** in vesicles

5 nm, which indicates hydrophobic segments consisting of bilayers of amphiphilic molecules (ca. 3.9 nm from AM1 calculations). In contrast to amphiphiles with only hydrophilic chains (type A), **198** (type B) possibly forms bilayers such as biotic lipids by exploiting the hydrophobic interactions of the aliphatic chains and locating the hydrophilic TEG chains on the outside to form water-soluble vesicles [125].

6 Summary

This chapter briefly described recent progress in the guest-binding and supramolecular chemistry of anion-responsive acyclic oligopyrroles⁴. The salient features of such systems are the fact that they exhibit dynamic conformation changes and, more importantly, can be incorporated into various macromolecules and complexes as

⁴Recently, liquid crystal properties of BF_2 complexes of dipyrrolyldiketerones have been revealed [150].

subunits by means of covalent and noncovalent interactions – metal coordination, hydrogen bonding, π – π stacking, etc. And from the potential for forming planar anionic species, anion binding by π -conjugated acyclic oligopyrroles is indeed a fascinating area of study. What is necessary is appropriate molecular design and accurate synthetic procedures for the subunits that will allow the formation of soft materials such as gels, liquid crystals, colloids, micelles, etc., consisting of both negative- and positive-charged species.

Acknowledgments The contributions of the Maeda group reported herein were supported by Grants-in-Aid for Young Scientists (B) (No. 17750137, 19750122, 21750155) and Scientific Research in a Priority Area “Super-Hierarchical Structures” (No. 18039038, 19022036) from the Ministry of Education, Culture, Sports, Science and Technology (MEXT), Izumi Science and Technology Foundation, Iketani Science Technology Foundation, Mitsubishi Chemical Corporation Fund, Kumagai Foundation for Science and Technology, Nissan Science Foundation, Saneyoshi Scholarship Foundation, the Japan Securities Scholarship Foundation, the Science and Technology Foundation of Japan, Shorai Foundation for Science and Technology, and the Kao Foundation for Arts and Sciences, the matching fund subsidies for private universities from the MEXT, 2003–2008 and 2009–2014, and the Ritsumeikan Global Innovation Research Organization (R-GIRO) project, 2008–2013.

References

1. Miller C (2006) *Nature* 440:484
2. Pusch M (2010) In: Kew J, Davies C (eds) *Ion channels from structure and function*. Oxford University Press, New York, p 172, references therein
3. Dutzler R, Campbell EB, Cadene M, Chait BT, MacKinnon R (2002) *Nature* 415:287
4. Bianchi A, Bowman-James K, García-España E (eds) (1997) *Supramolecular chemistry of anions*. Wiley-VCH, New York
5. Singh RP, Moyer BA (eds) (2004) *Fundamentals and applications of anion separations*. Kluwer Academic/Plenum, New York
6. Stibor I (ed) (2005) *Anion sensing*. Topics in current chemistry, vol 255. Springer, Berlin, pp 238
7. Sessler JL, Gale PA, Cho WS (2006) *Anion receptor chemistry*. RSC, Cambridge
8. Vilar R (ed) (2008) *Recognition of anions. Structure and bonding*, vol 129. Springer, Berlin, pp 252
9. Schmidtchen FP, Berger M (1997) *Chem Rev* 97:1515
10. Beer PD, Gale PA (2001) *Angew Chem Int Ed* 40:486
11. Sessler JL, Camiolo S, Gale PA (2003) *Coord Chem Rev* 240:17
12. Martínez-Mañez R, Sancenón F (2003) *Chem Rev* 103:4419
13. Gale PA (2005) *Chem Commun*:3761
14. Gale PA (2006) *Acc Chem Res* 39:465
15. Gale PA, Quesada R (2006) *Coord Chem Rev* 250:3219
16. Kang SO, Begum RA, Bowman-James K (2006) *Angew Chem Int Ed* 45:7882
17. Bolondeau P, Segura M, Perez-Fernandez R, de Mendoza J (2007) *Chem Soc Rev* 36:198
18. Gale PA, García-Garrido SE, Garric J (2008) *Chem Soc Rev* 37:151
19. Caltagirone C, Gale PA (2009) *Chem Soc Rev* 38:520
20. Maeda H (2010) In: Kadish KM, Smith KM, Guillard R (eds) *Handbook of porphyrin science*. Vol 8. World Scientific, New Jersey, chap 38

21. Fischer H, Orth H (1934) *Die Chemie des Pyrrols*. Akademische Verlagsgesellschaft M. B. H, Leipzig
22. Kadish KM, Smith KM, Guillard R (eds) (2000) *The porphyrin handbook*. Academic, San Diego
23. Gale PA, Sessler JL, Král V, Lynch V (1996) *J Am Chem Soc* 118:5140
24. Gale PA, Sessler JL, Král V (1998) *Chem Commun*:1
25. Sessler JL, Gross DE, Cho WS, Lynch VM, Schmidtchen FP, Bates GW, Light ME, Gale PA (2006) *J Am Chem Soc* 128:12281
26. Lee CH, Miyaji H, Yoon DW, Sessler JL (2008) *Chem Commun*:24
27. Jasat A, Dolphin D (1997) *Chem Rev* 97:2267
28. Sessler JL, Seidel D (2003) *Angew Chem Int Ed* 42:5134
29. Chandrashekar TK, Venkatraman S (2003) *Acc Chem Res* 36:676
30. Shimizu S, Osuka A (2006) *Eur J Inorg Chem*:1319
31. Sessler JL, Cyr MJ, Lynch V, McGhee E, Ibers JA (1990) *J Am Chem Soc* 112:2810
32. Shionoya M, Furuta H, Lynch V, Harriman A, Sessler JL (1992) *J Am Chem Soc* 114:5714
33. Sessler JL, Davis J (2001) *Acc Chem Res* 34:989
34. Seidel D, Lynch V, Sessler JL (2002) *Angew Chem Int Ed* 41:1422
35. Maeda H (2007) *Eur J Org Chem*:5313
36. Maeda H (2009) *J Incl Phenom* 64:193
37. Coles SJ, Gale PA, Hursthouse MB (2001) *CrystEngComm* 53:1
38. Best MD, Tobey SL, Anslyn EV (2003) *Coord Chem Rev* 240:3
39. Houk RJT, Tobey SL, Anslyn EV (2005) In: Stibor I (ed) *Anion sensing. Topics in current chemistry*, vol 255. Springer, Berlin, p 119
40. Schmuck C (1999) *Chem Commun*:843
41. Schmuck C (1999) *Eur J Org Chem*:2397
42. Schmuck C (2006) *Coord Chem Rev* 250:3053
43. Schmuck C (2000) *J Org Chem* 65:2432
44. Schmuck C, Dudaczek J (2007) *Eur J Org Chem*:3326
45. Schmuck C, Rehm T, Gröhn F, Reinhold F (2006) *J Am Chem Soc* 128:1430
46. Schmuck C, Rehm T, Klein K, Gröhn F (2007) *Angew Chem Int Ed* 46:1693
47. Gunther H, Anslyn EV (2002) *Chem Eur J* 8:2218
48. Schmuck C, Schwegmann M (2005) *J Am Chem Soc* 127:3373
49. Schmuck C, Schwegmann M (2006) *Org Biomol Chem* 4:836
50. Ciferri A (ed) (2000) *Supramolecular polymers*. Marcel Dekker, New York
51. Brunsveld L, Folmer BJB, Meijer EW, Sijbesma RP (2001) *Chem Rev* 101:4071
52. Sauvage JP (ed) *Transition metals in supramolecular chemistry*. Wiley, Chichester
53. Manners I (2004) *Synthetic metal-containing polymers*. Wiley-VCH, Weinheim
54. Schubert US, Newkome GR, Manners I (eds) (2006) *Metal-containing and metallocsupramolecular polymers and materials*. ACS, Washington, DC
55. Gröger G, Stepanenko V, Würthner F, Schmuck C (2009) *Chem Commun*:698
56. Gale PA, Camiolo S, Chapman CP, Light ME, Hursthouse MB (2001) *Tetrahedron Lett* 42:5095
57. Gale PA, Camiolo S, Tizzard GJ, Chapman CP, Light ME, Coles SJ, Hursthouse MB (2001) *J Org Chem* 66:7849
58. Gale PA, Navakhun K, Camiolo S, Light ME, Hursthouse MB (2002) *J Am Chem Soc* 124:11228
59. Light ME, Gale PA, Navakhun K (2005) *Acta Cryst E* 61:o1300
60. Navakhun K, Ruangpornvisuti V (2006) *J Mol Struct Theochem* 772:23
61. Navakhun K, Ruangpornvisuti V (2009) *J Mol Struct Theochem* 907:131
62. Sessler JL, Pantos GD, Gale PA, Light ME (2006) *Org Lett* 8:1593
63. Sessler JL, Barkey NM, Pantos GD, Lynch VM (2007) *New J Chem* 31:646
64. Zhang Y, Yin Z, Li Z, Hea J, Cheng JP (2007) *Tetrahedron* 63:7560
65. Yin Z, Li Z, Yu A, He J, Cheng JP (2004) *Tetrahedron Lett* 45:6803

66. Chen CL, Chen YH, Chen CY, Sun SS (2006) *Org Lett* 8:5053
67. Chen CL, Lin TP, Chen YS, Sun SS (2007) *Eur J Org Chem*:3999
68. Zyryanov GV, Palacios MA, Anzenbacher P Jr (2007) *Angew Chem Int Ed* 46:7849
69. Falk H (1989) *The chemistry of linear and oligopyrroles and bile pigments*. Springer, Vienna
70. Wood TE, Thompson A (2007) *Chem Rev* 107:1831
71. Becker W, Sheldrick WS, Engel J (1978) *Acta Cryst B* 34:1021
72. Sessler JL, Eller LR, Cho WS, Nicolaou S, Aguilar A, Lee JT, Lynch VM, Magda DJ (2005) *Angew Chem Int Ed* 44:5989
73. Shin JY, Dolphin D, Patrick BO (2004) *Cryst Grow Des* 4:659
74. Huggins MT, Musto C, Munro L, Catalano VJ (2007) *Tetrahedron* 63:12994
75. Vega IED, Camiolo S, Gale PA, Hursthouse MB, Light ME (2003) *Chem Commun*:1686
76. Vega IED, Gale PA, Hursthouse MB, Light ME (2004) *Org Biomol Chem* 2:2935
77. Guo Y, Shao SJ, Xu J, Shi YP, Jiang SX (2004) *Inorg Chem Commun* 7:333
78. Sessler JL, An D, Cho WS, Lynch V, Marquez M (2005) *Chem Eur J* 11:2001
79. Renić M, Basarić N, Mlinarić-Majerski K (2007) *Tetrahedron Lett* 48:7873
80. Chauhan SMS, Bisht T, Garg B (2009) *Sens Act B* 141:116
81. Denekamp C, Suwinska K, Salman H, Abraham Y, Eichen Y, Ben Ari J (2007) *Chem Eur J* 13:657
82. Sessler JL, An D, Cho WS, Lynch V (2003) *J Am Chem Soc* 125:13646
83. Lin CI, Selvi S, Fang JM, Chou PT, Lai CH, Cheng YM (2007) *J Org Chem* 72:3537
84. Fürstner A (2003) *Angew Chem Int Ed* 42:3582
85. Davis JT (2010) In: Gale PA, Dehaen W (eds) *Anion complexation by heterocycle based receptors. Topics in heterocyclic chemistry*. Springer, Berlin DOI 7081_2010_29
86. Sessler JL, Weghorn SJ, Lynch V, Fransson K (1994) *J Chem Soc Chem Commun*:1289
87. Morosini P, Scherer M, Meyer S, Lynch V, Sessler JL (1997) *J Org Chem* 62:8848
88. Oddo B, Dainotti C (1911) *Gazz Chim Ital* 41:248
89. Behr D, Brandänge S, Lindström B (1973) *Acta Chem Scand* 27:2411
90. Black CB, Andrioletti B, Try AC, Ruiperez C, Sessler JL (1999) *J Am Chem Soc* 121:10438
91. Sessler JL, Andrioletti B, Anzenbacher P Jr, Black C, Eller L, Furuta H, Jursikova K, Maeda H, Marquez M, Mizuno T, Try A (2004) In: Singh RP, Moyer BA (eds) *Fundamentals and applications of anion separations*. Kluwer Academic/Plenum, New York, p 71
92. Anzenbacher P Jr, Try AC, Miyaji H, Jursiková K, Lynch VM, Marquez M, Sessler JL (2000) *J Am Chem Soc* 122:10268
93. Mizuno T, Eller L, Wei WH, Sessler JL (2002) *J Am Chem Soc* 124:1134
94. Kirkovits GJ, Zimmerman RS, Huggins MT, Lynch VM, Sessler JL (2002) *Eur J Org Chem*:3768
95. Sessler JL, Maeda H, Mizuno T, Lynch VM, Furuta H (2002) *Chem Commun*:862
96. Sessler JL, Maeda H, Mizuno T, Lynch VM, Furuta H (2002) *J Am Chem Soc* 124:13474
97. Sessler JL, Pantos GD, Katayev E, Lynch VM (2003) *Org Lett* 5:4141
98. Ghosh T, Maiya BG, Smanta A (2006) *Dalton Trans*:795
99. Aldakov D, Anzenbacher P Jr (2003) *Chem Commun*:1394
100. Aldakov D, Palacios MA, Anzenbacher P Jr (2005) *Chem Mater* 17:5238
101. Aldakov D, Anzenbacher P Jr (2004) *J Am Chem Soc* 126:4752
102. Anzenbacher P Jr, Jursikova K, Aldakov D, Marquez M, Pohl R (2004) *Tetrahedron* 60:11163
103. Pohl R, Aldakov D, Kubát P, Jursiková K, Marquez M, Anzenbacher P Jr (2004) *Chem Commun*:1282
104. Anzenbacher P Jr, Palacios MA, Jursiková K, Marquez M (2005) *Org Lett* 7:5027
105. Palacios MA, Nishiyabu R, Marquez M, Anzenbacher P Jr (2007) *J Am Chem Soc* 129:7538
106. Ghosh T, Maiya BG, Wong MW (2004) *J Phys Chem A* 108:11249
107. Wu CY, Chen MS, Lin CA, Lin SC, Sun SS (2006) *Chem Eur J* 12:2263
108. Szydło F, Andrioletti B, Rose E (2006) *Org Lett* 8:2345
109. Ballester P (2008) In: Vilar R (ed) *Recognition of anions. Structure and bonding*, vol 129. Springer, Berlin, p 127

110. Schottel BL, Chifotides HT, Dunbar KR (2008) *Chem Soc Rev* 37:68
111. Yoo J, Kim MS, Hong SJ, Sessler JL, Lee CH (2009) *J Org Chem* 74:1065
112. Salman H, Abraham Y, Tal S, Meltzman S, Kapon M, Tessler N, Speise S, Eichen Y (2005) *Eur J Org Chem*:2207
113. Lin Z, Chen HC, Sun SS, Hsu CP, Chow TJ (2009) *Tetrahedron* 65:5216
114. Shevchuk SV, Lynch VM, Sessler JL (2004) *Tetrahedron* 60:11283
115. Plitt P, Gross DE, Lynch VM, Sessler JL (2007) *Chem Eur J* 13:1374
116. Vega IED, Gale PA, Light ME, Loeb SJ (2005) *Chem Commun*:4913
117. Oddo B, Dainotti C (1912) *Gazz Chim Ital* 42:716
118. Stark WM, Baker MG, Leeper FJ, Raithby PR, Battersby AR (1988) *J Chem Soc Perkin Trans* 1:1187
119. Maeda H, Kusunose Y (2005) *Chem Eur J* 11:5661
120. Maeda H, Ito Y (2006) *Inorg Chem* 45:8205
121. Fujimoto C, Kusunose Y, Maeda H (2006) *J Org Chem* 71:2389
122. Maeda H, Kusunose Y, Mihashi Y, Mizoguchi T (2007) *J Org Chem* 72:2621
123. Maeda H, Haketa Y, Nakanishi T (2007) *J Am Chem Soc* 129:13661
124. Maeda H, Terasaki M, Haketa Y, Mihashi Y, Kusunose Y (2008) *Org Biomol Chem* 6:433
125. Maeda H, Ito Y, Haketa Y, Eifuku N, Lee E, Lee M, Hashishin T, Kaneko K (2009) *Chem Eur J* 15:3709
126. Maeda H, Haketa Y, Bando Y, Sakamoto S (2009) *Synth Met* 159:792
127. Maeda H, Eifuku N (2009) *Chem Lett* 38:208
128. Maeda H, Kusunose Y, Terasaki M, Ito Y, Fujimoto C, Fujii R, Nakanishi T (2007) *Chem Asian J* 2:350
129. Sanchez-Quesada J, Seel C, Prados P, de Mendoza J (1996) *J Am Chem Soc* 118:277
130. Maeda H, Ito Y, Kusunose Y, Nakanishi T (2007) *Chem Commun*:1136
131. Maeda H, Bando Y, Haketa Y, Honsho Y, Seki S, Nakajima H, Tohna N (submitted)
132. Maeda H, Fujii Y, Mihashi Y (2008) *Chem Commun*:4285
133. Maeda H, Takayama M, Kobayashi K, Shinmori H (submitted)
134. Maeda H, Haketa Y (2008) *Org Biomol Chem* 6:3091
135. Maeda H, Mihashi Y, Haketa Y (2008) *Org Lett* 10:3179
136. Maeda H, Fujii R, Haketa Y (2010) *Eur J Org Chem*:1468
137. Terech P, Weiss RG (1997) *Chem Rev* 97:3133
138. Abdallah DJ, Weiss RG (2000) *Adv Mater* 12:1237
139. Fages F (ed) (2005) *Low molecular mass gelators. Topics in current chemistry*, vol 256. Springer, Berlin, pp 283
140. Weiss RG, Terech P (eds) (2006) *Molecular gels: materials with self-assembled fibrillar networks*. Springer, Dordrecht
141. Ishi-i T, Shinkai S (2005) In: Würthner F (ed) *Supramolecular dye chemistry. Topics in current chemistry*, vol 258. Springer, Berlin, p 119
142. Smith DK (2007) In: Atwood JL, Steed JW (eds) *Organic nanostructures*. Wiley-VCH, Weinheim, p 111
143. Maeda H (2008) *Chem Eur J* 14:11274
144. Lloyd GO, Steed JW (2009) *Nat Chem* 1:437
145. Piepenbrock MOM, Lloyd GO, Clarke N, Steed JW (2010) *Chem Rev* 110:1960
146. Maeda H, Haketa Y, Sasaki S, Masunaga H, Ogawa H, Mizuno N, Araoka F, Takezoe H (to be submitted)
147. Hamley IW (2000) *Introduction to soft matter – polymers, colloids, amphiphiles and liquid crystals*. Wiley, Chichester
148. Israelachvili JN (1992) *Intermolecular and surface forces*. Academic, London
149. Luisi PL, Walde P (eds) (2000) *Giant vesicles*. Wiley-VCH, Chichester
150. Maeda H, Terashima Y, Haketa Y, Asano A, Honsho Y, Seki S, Shimizu M, Mukai H, Ohta K (2010) *Chem Commun* 46: (in press)

Anion Binding and Transport by Prodigiosin and Its Analogs

Jeffery T. Davis

Abstract The red-colored prodiginines, exemplified by prodigiosin **1**, are secondary metabolites produced by a number of microorganisms, including the bacterium *Serratia marcescens*. These tripyrrole natural products and their synthetic analogs have received renewed attention over the past decade, primarily because of their promising immunosuppressive and anticancer activities. One of the hallmarks of prodiginin chemistry is the ability of the monoprotonated ligand to bind anions, including the essential chloride and bicarbonate ions. The resulting lipophilic ion pair is then able to diffuse across the hydrophobic barrier presented by phospholipid bilayers. Thus, prodiginines have been found to be potent transmembrane anion transporters and HCl cotransporters. In this chapter, the author reviews what is known about the solid-state structure of prodiginins and their anion complexes, the solution conformation of prodiginines, and the biochemical evidence for the ability to bind anions and to transport HCl across cell membranes. Recent progress in making synthetic models of prodiginines and recent results on the ability of prodigiosin to transport HCO_3^- across lipid membranes are discussed.

Keywords Anion binding · Membrane transport · Prodiginine · Prodigiosin · Tripyrrole

Contents

1	Introduction	146
2	Structural Studies of the Prodiginines and Their Anion Complexes	150
3	Further Insight into Prodiginine Conformation from X-Ray and Computational Studies	154

J.T. Davis
Department of Chemistry and Biochemistry, University of Maryland, College Park, MD 20742,
USA
e-mail: jdavis@umd.edu

4	Solid-State Structural Studies on Prodiginine•HCl and Prodiginine–Metal Ion Complexes	156
5	X-Ray Structures of Prodiginine–Metal Complexes	158
6	Proton Transport: Early Studies Showing That Prodiginines Alter Intracellular pH	159
7	Prodiginines Alter pH by Facilitating Transmembrane H ⁺ Cl ⁻ Symport (or the Functionally Equivalent OH ⁻ /Cl ⁻ Exchange)	161
8	HCl Transport Mediated by Prodiginines Has Biological Consequences	163
9	Prodiginines, H ⁺ Cl ⁻ Cotransport and Apoptosis	164
10	Synthetic Prodiginine Analogs Shown to Bind Cl ⁻ in Solution, Transport Cl ⁻ Across Lipid Membranes and Possess Anticancer Activity	167
11	Prodiginines Can Also Facilitate Anion Exchange (Antiport) Across Phospholipid Membranes	167
12	H ⁺ Cl ⁻ Transport by Synthetic Receptors Designed to Mimic Prodiginine Function ...	170
13	Prodigiosin 1 Facilitates Transmembrane Transport of Bicarbonate Anion	171
14	Conclusions and Outlook	173
	References	174

1 Introduction

The prodiginines (prodigiosenes) are heterocyclic natural products with a truly colorful history. Different terrestrial and marine bacteria produce these secondary metabolites. The most well-known microorganism that produces prodiginines is *Serratia marcescens* (*Bacillus prodigiosis*), a bacterium that grows well in damp and warm conditions (Fig. 1).



Fig. 1 *Serratia marcescens* (with permission from the American Society for Microbiology)

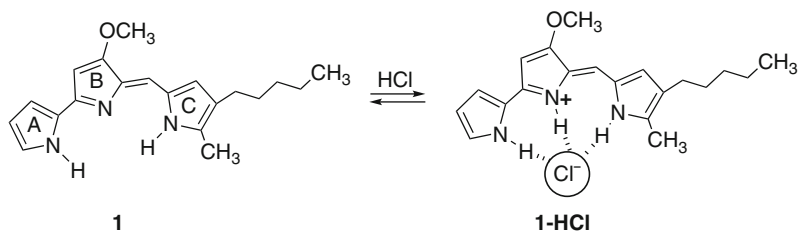


Fig. 2 The structure of prodigiosin **1** and the complex **1•HCl**

Serratia marcescens owes its name to Bartolomeo Bizio, an Italian microbiologist. Bizio, in an 1823 letter to a Venetian priest, explained the scientific origins of the bloody red color that had appeared on polenta, a corn meal produced annually by the Padua locals [1, 2]. At the time of this occurrence, during the wet and hot year of 1818, the polenta's strange coloring alarmed the community. As we know now, the polenta's red color did not arise because of any witchcraft. On the basis of his observations and experiments, Bizio suspected that microorganisms growing on the corn meal had caused the pigmentation. Indeed, it was later shown that the red color was due to the conjugated structure of the prodiginines, exemplified by the parent compound prodigiosin **1** (Fig. 2) (the UV-vis spectrum of prodigiosin **1** was reported in the following paper, although the proposed structure for **1** was incorrect at the time: [3]). There are a number of excellent reviews and book chapters that provide many interesting stories about the rich history and the religious and cultural impact of *S. marcescens* and their prodiginine metabolites [4–6].

Prodigiosin **1** was first isolated in pure form from *S. marcescens* in 1929 [7], and its correct structure was established by partial and total synthesis in the early 1960s [8, 9]. In addition to prodigiosin **1**, there are many other naturally occurring prodiginines. Some other natural products **2–5** that will be discussed in this chapter are shown in Fig. 3. Early studies on the prodiginine natural products indicated that they were extremely cytotoxic and therefore they were not initially developed as drug candidates. However, over the last 15 years there has been a renewed interest in the chemistry and biochemistry of natural and synthetic prodiginines, in large part because some derivatives have promising anticancer and immunosuppressive activities at concentrations below which they are cytotoxic [10–13].

As depicted in Fig. 2 the protonated prodigiosin **1•H⁺** has a binding pocket for Cl[−], using hydrogen bonds and electrostatic interactions to coordinate the anion. As discussed later in this chapter, one hypothesis to explain how prodiginines trigger apoptosis, or programmed cell death, is due to their ability to transport HCl across plasma and intraorganellar membranes and to thus alter intracellular pH [14, 15]. In addition to binding anions, prodiginines also form complexes with transition metal ions [10]. It has been proposed that the redox chemistry of prodiginine–metal complexes may induce apoptosis. Thus, Manderville and colleagues have shown that prodiginines can bind tightly to double-stranded DNA and that prodiginine•Cu²⁺ complexes can trigger oxidative cleavage of DNA [16, 17]. A description of the metal binding and redox chemistry of the prodiginines is outside the scope of this chapter;

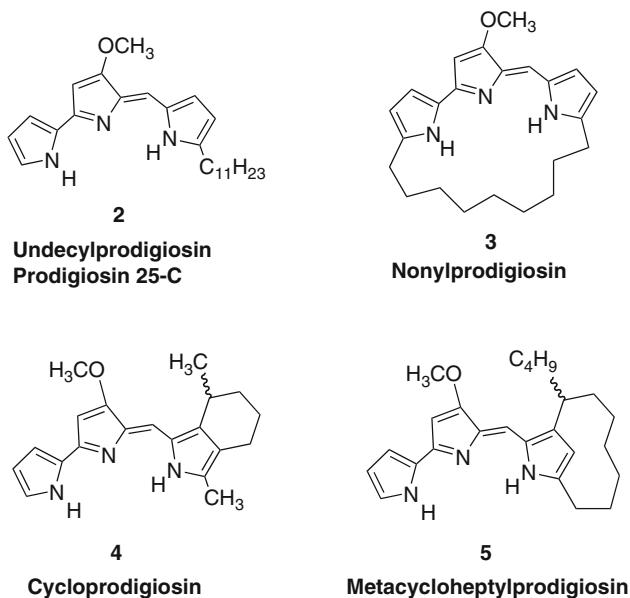


Fig. 3 Structures of four naturally-occurring prodiginines 2–5

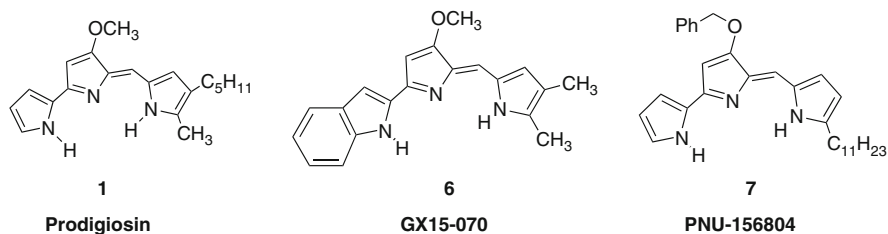


Fig. 4 Structures of some prodiginines that are being developed as pharmaceuticals

the interested reader should refer to Manderville's 2001 review article on the subject [10]. This chapter's focus is to review that which is known about the binding and transmembrane transport of anions by prodigiosin **1** and analogs.

One ongoing and important effort is to produce prodiginines that are less toxic than the natural products but that are effective as immunosuppressive and/or anticancer agents. This goal has inspired the chemical syntheses of many new prodiginines [6, 18–22]. A search of the *SciFinder* database returns structures for hundreds of analogs, many of which are found in an extensive patent literature. Notably, some prodiginines have gone into preclinical and clinical trials (Fig. 4). For example, Aida Pharmaceuticals has prodigiosin **1** in preclinical trials for the treatment of pancreatic cancer [12, 23]. The analog, obatoclax mesylate (GX15-070) **6**, [24] developed by Gemin Pharmaceuticals, has undergone Phase I clinical

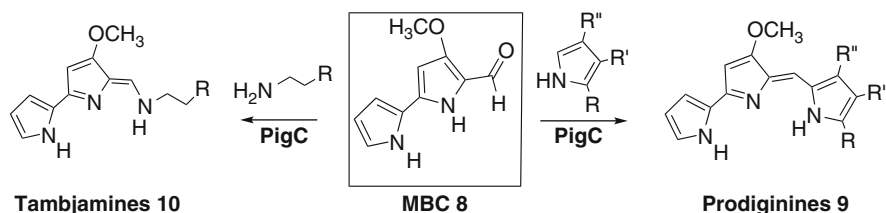


Fig. 5 A key intermediate in prodiginine biosynthesis is 4-methoxy-2,2'-bipyrrole-5-carbaldehyde (MBC) **8**. Using the biosynthetic enzyme *PigC*, compound **8** can react with pyrroles and amines to make new prodiginines **9** and tambjamines **10**

Table 1 Key review articles on prodiginosin

Title	Author(s)	Year	Ref
Prodiginosin-like pigments	N.N. Gerber	1975	[30]
Seeing red: the story of prodiginosin	J.W. Bennett, R. Bentley	2000	[5]
Synthesis, proton-affinity and anticancer properties of the prodiginosins	R.A. Manderville	2001	[10]
Chemistry and biology of prodiginosins	A. Furstner	2003	[6]
The prodiginosins, proapoptotic drugs with anticancer properties	Perez-Tomas et al.	2003	[11]
The biosynthesis and regulation of bacterial prodiginines	G.P.C. Salmond et al.	2006	[28]
Anticancer and immunosuppressive properties of bacterial prodiginines	G.P.C. Salmond et al.	2007	[12]
Red to red-prodiginosins for mitigation of harmful algal blooms	D. Kim et al.	2008	[31]
Prodiginosins as anti cancer agents	R. Pandey et al.	2009	[13]

trials for patients suffering from lymphocytic leukemia [25]. The analog PNU-156804 (**7**), because of its immunosuppressive properties, [26] has been used as an antirejection compound in organ transplants [27].

On another front, there has also been a major effort in understanding the biosynthesis of prodiginine natural products. This approach, led by researchers at the University of Cambridge, [28] holds promise for making new analogs by manipulating the biosynthetic machinery. For example, one key intermediate in prodiginine biosynthesis is 4-methoxy-2,2'-bipyrrole-5-carbaldehyde (MBC) **8**, which is also often an intermediate in chemical syntheses. As depicted in Fig. 5 condensation of this aldehyde MBC **8** with a variety of pyrroles and amines in the presence of the biosynthetic enzyme *PigC* can give rise to new prodiginines **9** and a group of derivatives of related natural products known as the tambjamines **10** [29].

The chemistry and biochemistry of the prodiginines, like their history, is quite fascinating. Table 1 lists some of the key review articles that have been written about the prodiginines. The focus of this current chapter is the anion binding and anion transmembrane transport properties of the prodiginines. After a brief review of the structure of the prodiginines, we will focus on the biochemical and chemical

data that has been accumulated to show how prodiginines are able to bind anions and to transport anions, especially chloride and bicarbonate, across phospholipid bilayer membranes.

2 Structural Studies of the Prodiginines and Their Anion Complexes

Despite the potent biological activities of many prodiginines, there are surprisingly few structural and computational studies reported in the literature, on either the natural products or their synthetic analogs. Issues concerning tautomeric and rotameric equilibria, solution conformation, and proton affinities of the prodiginines make their structural analysis not at all straightforward. As shown below in Fig. 6, the free base form of prodiginosin **1** may exist in solution as a mixture of tautomers. For example, structures **I** and **II** are tautomers that differ in the location of a pyrrole NH proton and the azafulvene's exocyclic C–C double bond. Indeed, the tautomeric state of the free base has been a point of some contention in the

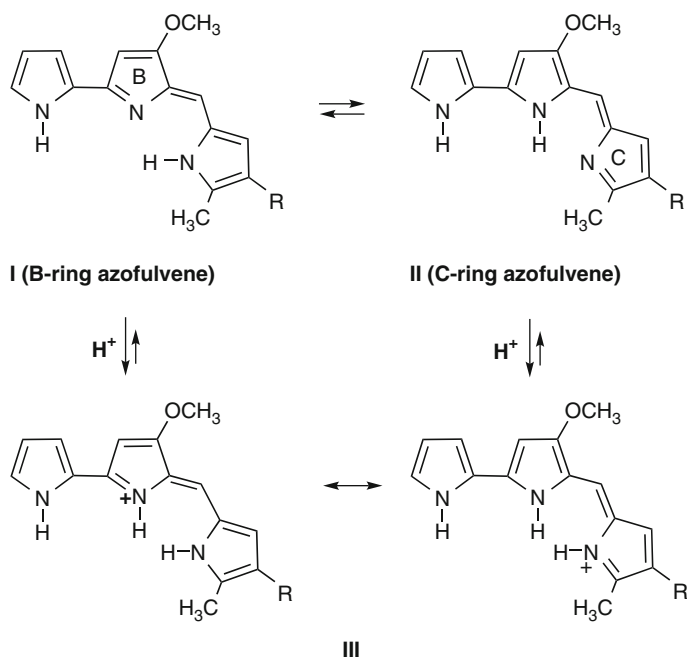


Fig. 6 Structures **I** and **II** represent different tautomers for the prodiginine's free base. Tautomers **I** and **II** differ in the location of the pyrrole NH and in the location of the azofulvene's C–C double bond. Protonation of tautomers **I** and **II** gives **III**, which can be depicted as either one of two major resonance forms

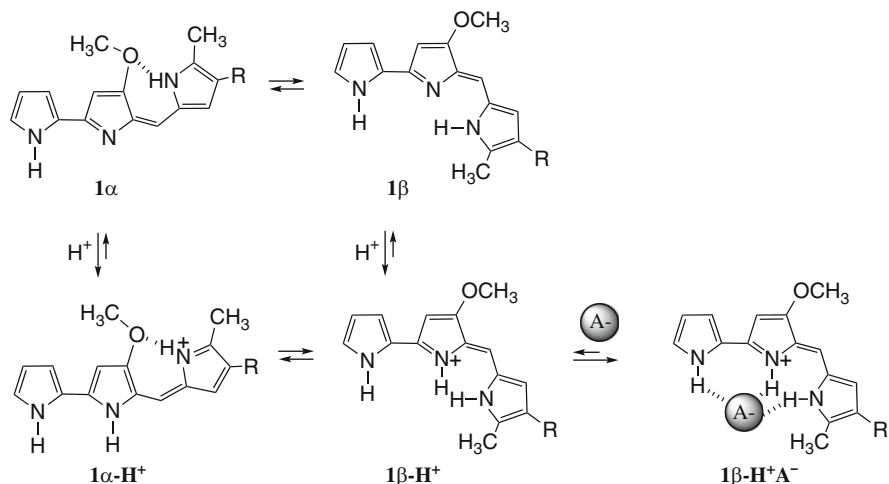


Fig. 7 Prodiginines, both in their free-base and protonated forms, can exist as so-called α - and β -isomers. The α -isomer is stabilized by an intramolecular hydrogen bond between the B-ring methoxy group and the C-ring NH proton. The monoprotinated β -isomer is stabilized by hydrogen bonds from three NH protons to the bound anion

prodiginine literature, with the azafulvene structure being drawn sometimes for the B-ring (tautomer **I**) and sometimes for the C-ring (tautomer **II**). As discussed below, X-ray crystal structures of synthetic prodiginines support the contention that isomer **I**, with the azafulvene located on the B-ring, is the favored tautomer (at least in the solid state). It should be emphasized, however, that protonation of either prodiginine tautomer **I** or **II** gives conjugate acids that are simply resonance forms of one another (see structure **III**).

In addition to issues regarding different tautomers and protonation sites, there is even more potential for structural complexity with the prodiginines because of different conformations about the methyne linkage connecting the B- and C-rings. As shown in Fig. 7, both the free base and the protonated form of prodigiosin can adopt either the α -isomer or the β -isomer. The α -isomer 1α is stabilized by a hydrogen bond between the NH proton of the C-ring and the oxygen atom of the B-ring's methoxy group. For the β -isomer 1β pictured in Fig. 7, which is the conformation that is usually drawn in the literature, the three pyrrole rings are all "cis" to one another, with each nitrogen atom oriented toward the center of a cleft. Transformation of the two isomers 1α and 1β corresponds to a *cis*–*trans* isomerization about the double bond connecting the B- and C-rings. While 1α is stabilized by hydrogen bonding between the B- and C-rings, one might well expect that binding an anion into the "all-*cis*" tripyrrole cleft would shift the equilibrium to favor the β -isomer, especially for the protonated prodiginine cation where each of the three NH protons could hydrogen bond to the anion to give the lipophilic ion pair $1\beta\text{-H}^+A^-$. As described below, both X-ray and NMR data show that anions are indeed bound by the prodiginine β -isomer.

Rizzo and colleagues used solution NMR spectroscopy to study the rotamer populations of the synthetic prodiginine **7** (PNU-156804), a drug developed in the 1990s by the Pharmacia & Upjohn company [32]. In their study, Rizzo and colleagues used the distinct UV-vis absorption bands for the prodiginine free base ($\lambda_{\text{max}} = 460$ nm) and for its protonated form ($\lambda_{\text{max}} = 525$ nm) to conduct a spectrophotometric titration that provided them with a $\text{p}K_{\text{a}}$ value of 7.20 for the equilibrium mixture of the α - and β -geometric isomers of **7**. Significantly, Rizzo and colleagues found that **7** gave two separate peaks in an HPLC trace when the separation was done under acidic conditions. They assigned these separate peaks to two slowly interconverting conformers, namely **7 α** and **7 β** . NMR analysis also showed two sets of resonances that varied in their relative ratios depending on the pH or solvent. Using HPLC data, they measured the interconversion rates for the two isomers which enabled them to calculate the $\text{p}K_{\text{a}}$ values for the two conformers, with $\text{p}K_{\alpha} = 8.23 \pm 0.03$ for **7 α** and $\text{p}K_{\beta} = 5.4 \pm 0.2$ for **7 β** . This analysis indicated that the α -isomer of the prodiginine free base is much more basic than is the β -isomer, presumably because protonation of the **7 α** results in the formation of the stabilizing intramolecular hydrogen bond as shown in Fig. 6.

The ^1H NMR spectra of **7** in CDCl_3 showed a dramatic influence on the nature of the counter-anion, as the **7 β •HCl** salt gave a single set of resonances that were consistent with the β -isomer. This result is significant because it demonstrated that the Cl^- anion could influence ligand conformation in a nonpolar solvent. Thus, in water, the protonated prodiginine **7 α •H $^+$** adopted the “open” α -isomer, presumably because it was stabilized by the intramolecular hydrogen bond between the B- and C-rings. But in the nonpolar solvent, CDCl_3 , the Cl^- anion can hydrogen bond with the cleft formed by the three pyrrole rings in **7 β •H $^+$ Cl $^-$** . NOE interactions between the three NH-exchangeable protons (NH-1A to NH-1B and NH-1B to NH-1C) and the H-4C to H-1'' NOE confirmed the double-bond geometry for the β -isomer of PNU-156804•HCl in CDCl_3 . Similar conclusions were obtained in a recent NMR structure determination of the HCl salt of heptylprodigiosin, which also forms the pure β -isomer in CDCl_3 [33].

Changing the counter-anion from chloride to the less basic methanesulfonate had a significant influence on the ^1H NMR spectra of the ligand. Thus, the PNU-156804• $\text{CH}_3\text{SO}_3\text{H}$ salt was found to be a mixture of conformers ($\alpha/\beta = 1/2$) in CDCl_3 . This result allowed Rizzo and colleagues to assign the NMR resonances for both isomers and to carry out a detailed conformational analysis. NOESY data indicated that the two geometrical isomers of PNU-156804 **7** differed mainly in the torsion angles about the C-2b-C-1'' bonds. For the β -rotamer, this torsion angle was close to 0° , whereas the angle was near 180° for the α -isomer (see Fig. 6). The authors noted that the α -isomer's geometry coincided nicely with a previous crystal structure of a synthetic prodiginine [34]. Rizzo and colleagues explained that the α -isomer was stabilized by a hydrogen bond between the protonated nitrogen of ring C and the B-ring's exocyclic oxygen. Importantly, the NMR studies showed NOEs between the CH_3 group of the methanesulfonate anion and multiple NH and CH protons on the PNU-156804 core, indicating ion pairing and hydrogen bonding of the CH_3SO_3^- anion with the prodiginine receptor, especially for the β -rotamer

Fig. 8 Structure of the β -conformer of the monoprotonated form of PNU-156804, $7\beta\cdot\text{H}^+\text{CH}_3\text{SO}_3^-$, as deduced from NOESY data in CDCl_3 . The strong NOESY cross-peaks, indicated with *double arrows*, include a cross-peak from the A-ring NH to the bound CH_3SO_3^- anion

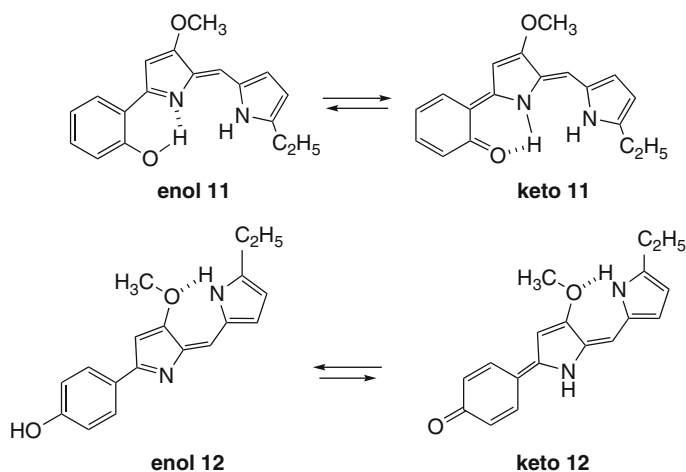
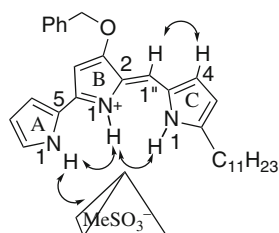


Fig. 9 A-Ring phenol derivatives **11** and **12** exist in equilibrium as enol or keto tautomers

(see Fig. 8). The authors noted that their observations of distinct α - and β -isomers merited a detailed theoretical study of the prodiginine's electronic properties. However, a decade later, little computational work on prodiginines has been published.

Recently, Manderville and colleagues published a study describing the conformation, protonation state and metal-binding affinity of synthetic prodiginines **11** and **12** (Fig. 9) analogs that contained isomeric phenols as their A-ring components [35]. These analogs had some unique properties, as compared to natural prodiginines. Thus, **11** and **12** underwent tautomerization in protic solvents to give mixtures of keto tautomers with $\lambda_{\text{max}} = 530 \text{ nm}$ and enol tautomers with $\lambda_{\text{max}} = 460 \text{ nm}$, with the keto tautomers predominating in protic solvents. Conversely, the enol isomers were the exclusive tautomers observed in aprotic solvents. Manderville and colleagues proposed that the special properties for the *o*-phenol **11** arose because of formation of an intramolecular hydrogen bond between the A-ring's phenol OH and N1 of the B-ring. They measured a $\text{p}K_{\text{a}}$ of 6.0 for the protonated analog $11\cdot\text{H}^+$, a value that was 1.4 $\text{p}K_{\text{a}}$ units below that determined for *p*-phenol **12**. They

rationalized that this difference in acidity for analogs **11** and **12** was due to the stabilization provided by the intramolecular hydrogen bond formed by the β -form of **11**. They also noted that since the α - and β -forms of natural prodiginines likely have different biological activities, *o*-phenol **11** may well be a useful model for understanding how prodiginine β -isomers bind to DNA and/or proteins.

3 Further Insight into Prodiginine Conformation from X-Ray and Computational Studies

In 1999, Furstner and colleagues published a study on the total synthesis and structural proof of the macrocyclic nonylprodigiosin **3** (see Fig. 3) [36]. They presented solid-state evidence that a synthetic intermediate on the way to **3** adopted the β -conformation with the B-ring existing as the azafulvene moiety. It should be emphasized that nonylprodigiosin **3** is constrained to adopt a β -conformation because of the carbon chain that links the A- and C-pyrrole rings.

A 2002 study by Manderville and colleagues described a prodiginine **13** that formed a hydrogen-bonded dimer in the solid state (Fig. 10) [37]. Within this dimer, the free base **13** was fixed in the β -conformation with all three pyrrole rings “*cis*” to one another. Once again, the B-ring of **13** existed as the azafulvene tautomer, which allowed for intermolecular hydrogen bonds between the B-ring nitrogen of one prodiginine **13** and the pyrrole NH atoms on the A- and C-rings of its partner. As described in more detail below, Parr et al. also observed a hydrogen-bonded dimer in the solid-state structure of a similar prodiginine analog [38]. Crystal-packing forces, which facilitate formation of hydrogen-bonded dimers, are the likely reason for the β -isomer being adopted in the solid state. As described below, calculations

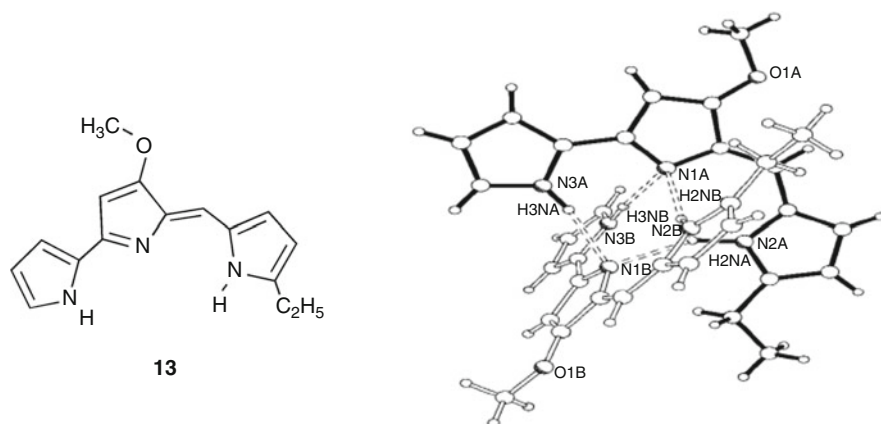


Fig. 10 Prodiginiosin analog **13** and depiction of the solid-state structure of its free base form. The X-ray structure shows a noncovalent dimer (**13**)₂ formed by intermolecular hydrogen bonds. Reprinted with permission from [37]

by Parr and colleagues indicated that the more extended prodiginine α -isomer should be lower in energy than the β -isomer [38].

There has been little reported about computational analysis of prodiginines and, to our knowledge, no reports on calculations for prodiginine–anion complexes. The most detailed computational work on prodiginine conformation was reported in 2008 [39]. In that study, Cole and colleagues conducted density functional theory (DFT) calculations on neutral and protonated compounds in order to better understand the mass spectra and fragmentation patterns of protonated prodiginines. These authors noted that prodiginine structures are typically drawn in the β -configuration as depicted in Fig. 6. But, Cole's DFT calculations showed that the β -isomers are not the lowest-energy structures in the gas phase. Instead, they found that the lowest-energy conformation has the prodiginine A- and C-rings rotated 180° relative to the central B-ring (Fig. 11). They rationalized that this geometry allows the molecule to maintain planarity while placing the lone pairs of electrons on the three nitrogen atoms as far apart as possible, so as to minimize electrostatic repulsion. Ab initio

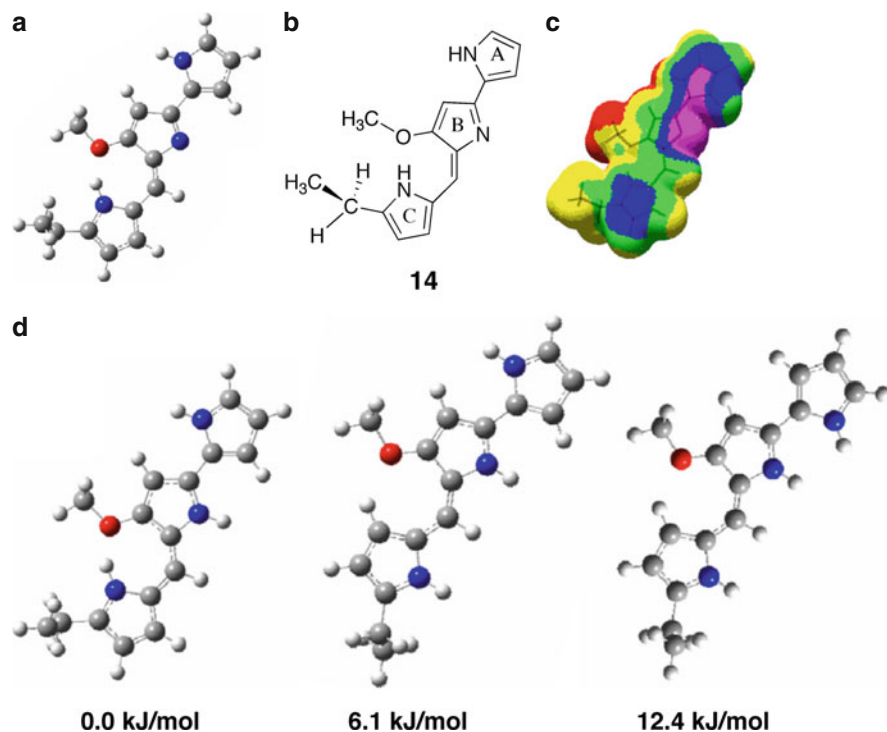


Fig. 11 (a) Optimized geometry of the neutral prodiginine model system **14** at the B3PW91/6-31G* level; (b) chemical structure for **14**; (c) electron density map (order of decreasing electron density is *purple* > *blue* > *green* > *yellow* > *red*) indicating highest electron density at the nitrogen atom of the central B-ring; (d) the optimized prodiginine conformations and their relative energies calculated by DFT. Reprinted with permission from [39]

calculations on 2,2'-bipyrrole (a model for the prodiginine A- and B-rings) indicate that the compound's global energy minimum is a nonplanar conformation that is twisted about 40° out of plane [40]. As reported by Cole, Fig. 11a (I) shows the low-energy geometry of the neutral model compound **14**, Fig. 11b (II) shows the chemical structure of this conformation and Fig. 11c (III) shows the compound's electron density map. Figure 11c (III) indicates that the B-ring's nitrogen has the highest electron density, suggesting that this nitrogen atom is the preferred site of protonation. These authors also calculated the relative energies of three stable conformers of the $[M + H]^+$ species that resulted from protonation of the neutral **14**. As indicated in Fig. 11d, the lowest-energy conformation for **14** contained an intramolecular hydrogen bond between the C-ring's NH proton and the B-ring's methoxy group, namely, the α -isomer observed by Rizzo and colleagues in their NMR investigations [32]. In a recent study, DFT calculations by Parr and colleagues also showed that the free base's lowest-energy conformation had an "all-*trans*" arrangement for the three pyrrole rings that make up the α -isomer [38]. But, they stressed that this α -isomer conformation was just 4 kJ/mol lower in energy than the β -conformation that had been experimentally observed in their X-ray crystal structure. Parr and colleagues suggested that the ability to form hydrogen bonds, to either a Cl^- anion or to another potential electron-rich partner, could readily provide the energy needed to switch the conformation favored by the prodiginine's tripyrrole unit. Calculations on the related tambjamine natural products (see structure **10** in Fig. 5) also indicate that an intramolecular H-bond is formed between an NH donor and the B-ring's exocyclic oxygen atom [41]. It would seem that theoretical computations on the structure and dynamics of prodiginines and their complexes with anions and metal cations is one area that is ripe for exploration, especially given these compounds' growing importance in drug development.

4 Solid-State Structural Studies on Prodiginine•HCl and Prodiginine–Metal Ion Complexes

There are only a few X-ray crystal structures available for complexes of protonated prodiginines with anions or for complexes of deprotonated prodiginines with metal cations. In this section, we describe what is known about the solid-state structures of prodiginines and their complexes. While exploring the chemistry of acyclic oligopyrroles Sessler and colleagues synthesized a linear hexapyrrole **15** that is essentially two prodiginine units connected together [42]. Indeed, the structure of the bis-HCl salt of this hexapyrrole **15** can be considered to be a harbinger for understanding how prodiginines bind anions. Thus, the X-ray structure of the bis-HCl salt of **15** showed two chloride anions bound to a planar S-shaped conformation (Fig. 12). Both of the clefts formed by the protonated tripyrrole units had three $NH \cdots Cl^-$ hydrogen bonds that fixed the anions in their respective binding sites. This early result, as later described by Sessler and Gale, provided "...direct structural conformation for the mode of binding presumed to be operative in prodigiosin and its analogues" [43].

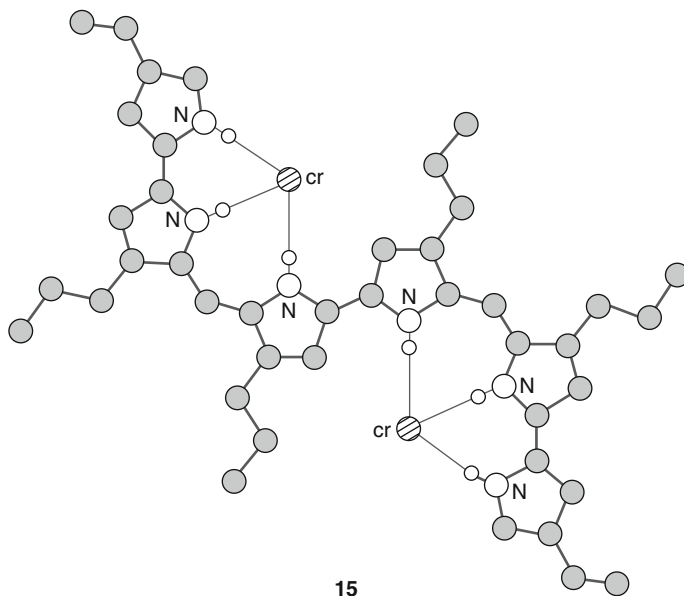


Fig. 12 The X-ray structure of the bis-HCl salt of hexapyrrole **15** shows two chloride anions bound to a planar S-shaped conformation. Reprinted with permission from [42]

Indeed, the Sessler group later obtained solid-state data that confirmed the manner in which prodiginines bind chloride ions [18]. An X-ray crystal structure of the complex **16**•HCl showed a chloride anion bound in the prodiginine's tripyrrole cleft, held there by hydrogen bonds and, presumably, by electrostatic interactions with the protonated ligand (Fig. 13). The prodiginine analog clearly adopts the β -isomer in this structure. The tripyrrole unit in **16**•HCl is relatively flat with the C-ring showing a small deviation from planarity. This conformation for **16**•HCl is similar to that found in the solid state for the HCl salt of a derivative of nonylprodigiosin, **3**•HCl, although as previously mentioned the chain connecting the A- and C-rings in that macrocycle helped to constrain the tripyrromethane's β -isomer conformation [36].

Parr, Wasserman and colleagues recently reported the X-ray crystal structures of both the free base and the HCl salt of a synthetic prodiginine **17**, a compound with a 2,5-dimethyl pyrrole as the C-ring [38]. The X-ray structure of the HCl salt of **17** (Fig. 14) shows a planar tripyrromethane cation with all three N–H hydrogens pointing toward the bound chloride anion. Again, it is these 3 N–H \cdots Cl $^-$ hydrogen bonds that stabilize the β -conformation for **17**•HCl. This study also revealed the predominant tautomer favored by the free base in the solid state. The X-ray structure of free base **17** showed that the B-ring was not protonated and that this B-ring contained the azafulvene unit. Thus, the C8–C9–C10 methyne linker had a shorter C8–C9 bond (1.350(7) Å), as compared to a C9–C10 bond length of 1.407(7) Å. Crystallized from CH₂Cl₂, the free base form of **17** forms a noncovalent

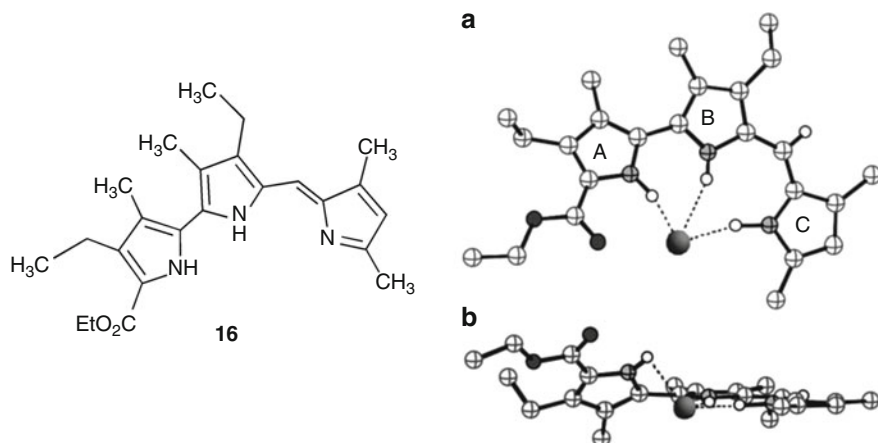


Fig. 13 Left panel: Structure of the prodiginine **16**. Right panel: Views of the X-ray structure of the complex formed between the protonated prodiginine **16** and chloride ion; Reprinted with permission from [18]

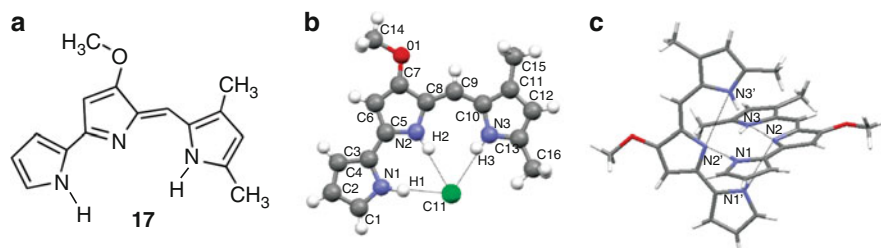


Fig. 14 The structure of prodiginine **17** and solid-state structures of the complex **17**•HCl and the free base form, which forms a noncovalent dimer (**17**)₂. Reprinted with permission from [38]

dimer that is held together by intermolecular H-bonds between NH protons on the A- and C-rings of one molecule of **17** and the B-ring's nitrogen of the other molecule. This structure is reminiscent of the noncovalent dimer observed in the solid-state structure of analog **13** by Manderville and colleagues [37]. In both of the solid-state dimers formed by **13** and **17**, the prodiginine free base adopts the β conformer.

5 X-Ray Structures of Prodiginine–Metal Complexes

Manderville has provided compelling evidence that prodiginosin (**1**) can bind to DNA and cleave double-stranded DNA in the presence of transition metals [16, 17]. They have proposed that prodiginosin's ability to cleave dsDNA may be important for its potent anticancer activity. In a 2003 communication, they reported on the

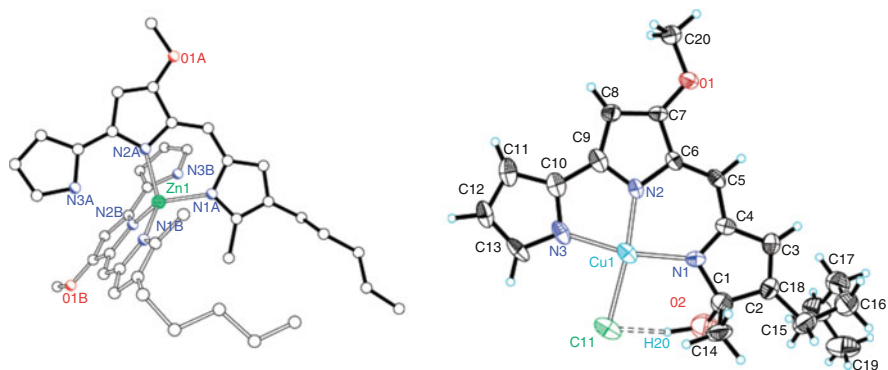


Fig. 15 *Left Panel:* Perspective drawing of the solid-state structure of $\text{Zn}\bullet(\mathbf{1})_2$. The Zn atom is represented by a *green sphere*. *Right Panel:* ORTEP plot (50% probability thermal ellipsoids) of the solid-state structure from the reaction of prodigiosin **1** with CuCl_2 . The observed structure has an $-\text{OH}$ group added to the C1 position on prodigiosin's C-ring. Reprinted with permission from [44]

coordination chemistry of prodiginine anions with Zn (II) and Cu (II) [44]. Treatment of prodigiosin **1** with strong base deprotonated the pyrrole NH protons, which then enabled reaction with transition metal salts. Deprotonated prodigiosin **1** bound Zn (II) to generate a 2:1 complex, $\text{Zn}\bullet(\mathbf{1})_2$. A solid-state structure of this complex showed it to be a 4-coordinate, neutral species with the B- and C-rings of two prodiginines bound to the metal cation to give a distorted tetrahedral geometry. The ^1H NMR spectra of the complex $\text{Zn}\bullet(\mathbf{1})_2$ indicated that this structure was maintained in CDCl_3 solution. In contrast to the structure obtained with Zn (II), reaction of deprotonated prodigiosin with $\text{CuCl}_2\bullet 2\text{H}_2\text{O}$ gave a 1:1 complex with a distorted square planar geometry, wherein the Cu (II) cation was coordinated to all three pyrrole nitrogen atoms. Remarkably, the C-ring of this prodigiosin•Cu (II) complex was oxidized at its C1 position. Solution NMR experiments indicated that this OH group attached to the prodiginine C-ring was derived from H_2O . Manderville and colleagues noted that understanding how prodigiosin was oxidized under these conditions might provide insight into the mechanism of DNA cleavage that was catalyzed by the prodiginine•Cu (II) system (Fig. 15).

6 Proton Transport: Early Studies Showing That Prodiginines Alter Intracellular pH

In retrospect, the first indication that prodiginines could move HCl across membranes came during the studies on their influence on the activity of vacuolar H^+ -ATPase (V-ATPase), a highly conserved enzyme found in eukaryotes. The V-ATPases are responsible for the acidification of certain cell types and intracellular organelles by pumping protons, against their chemical potential, across plasma and intracellular

membranes [45]. ATPases catalyze the hydrolysis of adenosine triphosphate (ATP) into adenosine diphosphate (ADP) and phosphate ion. The reaction is highly exergonic and the V-ATPases use the energy from ATP hydrolysis to transport protons across intracellular and plasma membranes. The effect of V-ATPase proton transport activity is the acidification of certain cellular organelles, including lysosomes, Golgi apparatus and other vacuoles. Thus, the V-ATPases are often necessary for proper regulation of intracellular and/or intraorganellar pH and for regulation of numerous cellular functions.

There were two reports in 1995 that prodiginines could destroy the pH gradients that existed across the membranes of certain cellular organelles, and thus serve as de facto inhibitors of V-ATPase [50, 51]. As detailed below, this ability to alter transmembrane pH gradients was later shown to be due to the ability of these natural products to facilitate the cotransport of $H^+ Cl^-$ (or alternatively to enable exchange of OH^- and Cl^- anions) ([46, 47]; for a similar study as that described in [47], see also [48, 49]). In the first of their 1995 papers, Kataoka and colleagues showed that prodigiosin 25-C (undecylprodigiosin) **2** was able to neutralize acidic organelles that were located within cytotoxic T cells and, by so doing, negate the cytotoxicity of these T cells [50]. These authors demonstrated that prodigiosin 25-C **2** and the ATPase inhibitor, concanamycin B (CMB), were potent immunosuppressants, both *in vitro* and *in vivo*. Thus, they proposed “. . .because PrG and CMB showed similar immunosuppressive effects *in vivo* as well as *in vitro*, it is most likely that the inhibition of intra-organellar acidification is responsible for suppression of CTL *in vivo*” [50].

In their second 1995 publication, Kataoka and colleagues demonstrated that **2** was able to neutralize the proton-translocation activity of V-ATPase, without inhibiting the enzyme's ATP hydrolysis activity [51]. They found that prodigiosin 25-C **2** inhibited the accumulation of pH-sensitive dyes, such as acridine orange, in the acidic compartments of baby hamster kidney (BHK) cells. In addition, **2** inhibited the proton pump activity of V-ATPase with an IC_{50} value of ca. 30 nM (see Fig. 16a), but the compound did not alter the ATPase enzyme activity, even at ligand concentrations of up to 1 μ M (see Fig. 16b). In marked contrast to the properties displayed by prodigiosin 25-C **2**, bafilomycin A, a known inhibitor of V-ATPase, inhibited both the protein's proton pump activity and its ATP hydrolysis activity. Another group later published similar findings that the immunosuppressant, cycloprodigiosin hydrochloride (cPrG•HCl) **4**, inhibited the proton-translocation mediated by V-ATPase without influencing the enzyme's ATPase activity [52].

Significantly, Kataoka and colleagues also used transmission electron microscopy to show that **2** caused a significant swelling of the Golgi apparatus and mitochondria within the BHK cells [51]. These results supported the hypothesis that prodigiosin 25-C **2** raised the pH of acidic compartments through the inhibition of the proton pump activity of V-ATPase, thereby causing the observed morphological changes to the Golgi apparatus and mitochondria. The authors proposed that inhibition of the ATPase's proton-translocation activity resulted in osmotic imbalances that led to water influx and consequent swelling of the intracellular organelles.

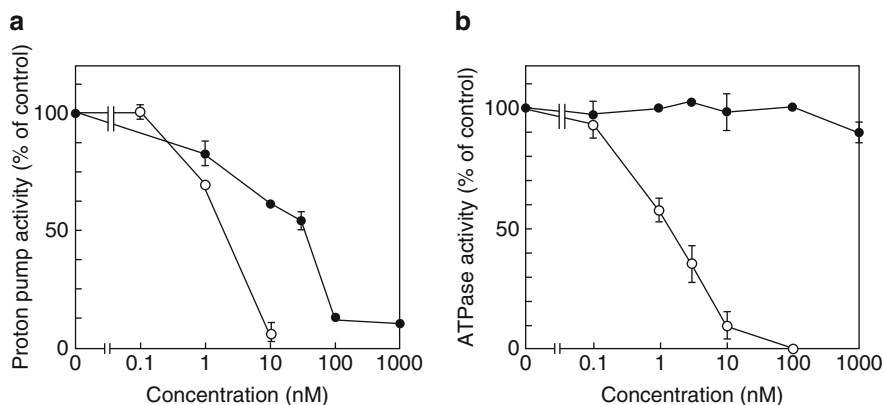


Fig. 16 Proton pump and ATPase activities in rat liver lysosomes. (a) FITC ~ dextran containing lysosomes were incubated with prodigiosin 25-C filled circle or bafilomycin AI open circle, and fluorescence quenching was measured after the addition of ATP. (B) V-ATPase activity was measured by the release of inorganic phosphate from ATP. The reaction mixture was incubated with prodigiosin 25-C filled circle or bafilomycin A, open circle. Reprinted with permission from [51]

In these 1995 papers, Kataoke and colleagues did not offer any specific molecular mechanism for how prodiginine **2** might disrupt the proton pump activity of V-ATPase, but they later demonstrated how the proton transport properties of prodiginines can have key biological consequences. Thus, Nagai, Kataoka and colleagues showed that both prodigiosin 25-C **2** and metacycloprodigiosin **5** suppressed bone resorption by osteoclasts, cells that are responsible for breaking down bone tissue by digesting minerals and matrix proteins [53]. The osteoclasts require an acidic microenvironment in order to carry out bone digestion and resorption. That acidic pH is regulated by the osteoclast's V-ATPase, found in the cell's outer membrane. Nagai and coauthors demonstrated that bone tissue treated with prodiginines had a dramatic decrease in the amount of digestion observed, probably because "...inhibition of the acidification of vacuolar organelles causes the destruction of the acidic microenvironment of osteoclasts and results in significant damage to the osteoclastic function in bone resorption" [53].

7 Prodiginines Alter pH by Facilitating Transmembrane H^+ Cl^- Symport (or the Functionally Equivalent OH^-/Cl^- Exchange)

In 1998, two seminal papers in the field were published by Ohkuma, Wasserman and colleagues wherein they demonstrated that prodiginines uncouple the proton-translocation activity of V-ATPase by functioning as transmembrane H^+Cl^- cotransporters [46, 47]. In these two papers, Ohkuma, Wasserman and colleagues demonstrated that

three different members of the prodiginine family, prodigiosin **1**, prodigiosin 25-C **2** and metacycloprodigiosin **5** all inhibited the proton-translocation activity of bovine V-ATPase in a process that depended on the presence of chloride anion [46, 47]. They also showed that prodiginines did not cause the formation of a membrane potential across the lysosomes. These two results suggested that the H^+ translocation was electroneutral and that chloride was moved across membranes by the prodiginines. On the basis of these observations, they proposed that prodiginines facilitate the cotransport, or symport, of H^+Cl^- across vesicular membranes. The authors also pointed out that H^+Cl^- symport was functionally equivalent to OH^-/Cl^- anion exchange, and that their results could not unequivocally distinguish between the two possible mechanisms. Nonetheless, over the years the prodiginines have been consistently described as transmembrane H^+Cl^- symporters.

Having demonstrated a Cl^- dependence in lysosomal membrane preparations, these authors carried out key experiments that investigated Cl^- transport across liposomal membranes, systems devoid of any ion channel proteins that might contribute to anion transport or to proton translocation [46]. First of all, they discovered that the prodiginines could modulate the internal pH of liposomes depending on the Cl^- anion gradient that exists across the membrane. Thus, if the extravesicular solution contained excess Cl^- , then they found that the addition of the prodiginines would lower the internal pH, presumably by moving H^+Cl^- into the liposome interior. Conversely, if the intravesicular solution were higher in Cl^- concentration, relative to the bulk solution, then the prodiginines would cause an increase in the intra-liposomal pH, again because they cotransported H^+Cl^- out of the vesicle (or alternatively they promoted transmembrane OH^-/Cl^- exchange). In another indirect method of demonstrating chloride anion transport, these authors showed that prodiginines were able to induce the Cl^- -dependent swelling of liposomes and erythrocytes [47]. In this case, chloride anion permeability was estimated by measuring the swelling of vesicles in buffers containing iso-osmotic ammonium salts. Thus, addition of any of the three prodiginines (namely **2**, **3** and **5**) caused swelling of phospholipid liposomes, as determined by a reduction in the absorbance of liposomes suspended in 0.2 M NH_4Cl , but not in ammonium gluconate [47].

The results described above, although convincing, provided only indirect evidence that prodiginines could transport Cl^- anion across lipid membranes. Thus, Ohkuma, Wasserman and colleagues designed an experiment that provided direct proof for transmembrane Cl^- transport as mediated by the prodiginines [46]. They demonstrated that prodiginines **2**, **3** or **5** each promoted the uptake of radioactive ^{36}Cl from external buffer, with concomitant acidification of the internal compartment, when the initial pH of the extravesicular buffer was more acidic than the liposome's interior. This was clear evidence that prodiginines could transport H^+Cl^- when confronted with a transmembrane pH gradient.

Ohkuma, Wasserman and colleagues concluded that the ability of the prodiginines to uncouple the V-ATPase's proton-translocation activity was due to their ability to facilitate $H^+ Cl^-$ symport (or OH^-/Cl^- antiport) across membrane barriers [46–49]. As depicted in Fig. 17, they proposed that prodiginines could

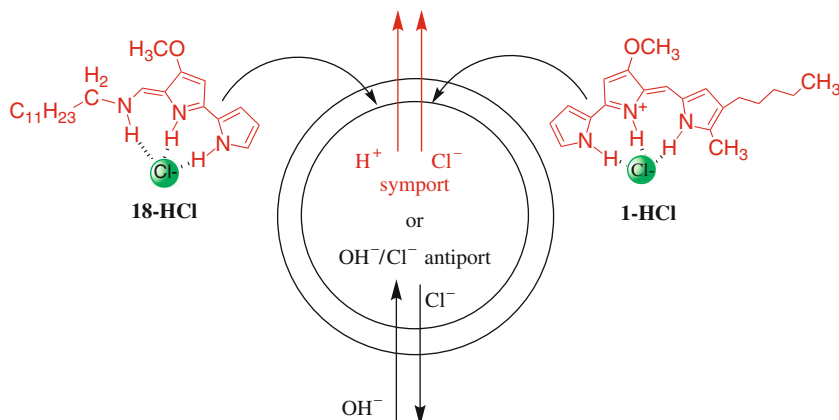


Fig. 17 Proposed mechanism for how prodiginosin **1** and the related tambjamine **18** alter the intravesicular pH within a liposome. The lipophilic ion pair **1**•H⁺Cl⁻ formed by prodiginosin **1** and HCl can be transported across the membrane (a symport process shown in red). An alternative to explain the change in intravesicular pH change would be if the monoprotinated form of prodiginosin **1** were able to catalyze exchange of the Cl⁻ and OH⁻ anions (antiport process shown in black)

form lipophilic ion pairs upon binding H⁺ Cl⁻ via electrostatic, charge-transfer and hydrogen-bonding interactions. These lipophilic ion pairs would then enable the proton-coupled movement of chloride across a phospholipid membrane. In a recent paper, Ohkuma and colleagues demonstrated that a member of the tambjamine antibiotic family, BE-18591 (**18**), also uncoupled V-ATPases through its H⁺Cl⁻ symport activity [54]. As shown in Fig. 17, prodiginines and tambjamins have similar structures. Ohkuma and colleagues found that 4-methoxy-2,2'-bipyrrole-5-carboxyaldehyde **8** (see Fig. 5), the synthetic precursor of BE-18591 (**18**), did not inhibit the proton pump activity of V-ATPase in membrane vesicles. This finding indicated that at least three nitrogen atoms, with two of the nitrogen atoms in pyrrole rings, are required for H⁺Cl⁻ symport activity.

8 HCl Transport Mediated by Prodigines Has Biological Consequences

Plant vacuoles contain two distinct proteins that function as H⁺ pumps: H⁺-ATPase and an H⁺-translocating pyrophosphatase (H⁺-PPase) [55]. Pyrophosphatase is an enzyme that converts one molecule of pyrophosphate into two phosphate ions in an exergonic reaction ($\Delta G = -34$ KJ). This reaction, when coupled to the translocation of protons across the membrane, enables an acidic pH to be maintained within the plant vacuole. Shimmen et al. showed that nanomolar concentrations of cycloprodiginosin hydrochloride (cPrG•HCl) **4** blocked acidification of vacuolar vesicles

by H^+ -PPase [56]. At the time of this study, there were no known inhibitors of this H^+ -PPase pump. Significantly, this inhibition of vacuolar acidification by cPrG•HCl **4** was anion-specific, as it occurred in buffers containing chloride anion but not in media containing the more hydrophilic sulfate anion (SO_4^{2-}). Shimmen's paper provided one of the first reports about the attenuated activity of a prodiginine as a function of the anion (Cl^- vs. SO_4^{2-}).

These authors prepared isolated vesicles from vacuolar membranes that contained the H^+ -PPase proton pump enzyme, but that had other plasma and ER membrane components removed. They used cPrG•HCl **4** purified from *Pseudoalteromonas denitrificans* to show that this compound markedly suppressed the H^+ transport activity of the H^+ -PPase without influencing the enzyme's phosphatase activity. This ligand-mediated inhibition of acidification occurred only in buffers containing chloride anion, but not in the sulfate buffers lacking chloride. In solutions containing 50 mM KCl, the prodiginosin cPrG•HCl **4** (10 nM) inhibited the effects of the proton transport activity of H^+ -PPase. In a separate experiment, these authors also showed that cPrG•HCl **4** rapidly destroyed any pH gradient that had been previously generated across the vacuolar membrane by the action of H^+ -PPase. In marked contrast, cPrG•HCl **4** showed no effect on the intravacuolar pH in an assay medium that lacked chloride anion, but instead contained 25 mM K_2SO_4 . These observations supported the earlier proposal made by Sato et al. that prodiginines function as H^+/Cl^- symporters [46, 47]. Presumably, sulfate anion was too hydrophilic for cPrG **4** to be able to bind and move across the vacuolar membrane. These authors noted that the concentration of Cl^- is high enough in plant cells that cPrG•HCl **4** should be able to destroy any pH gradients that are built up across the vacuolar membrane within plant cells. Thus, they suggested that the H^+ uncoupling activity of cPrG•HCl **4** might ultimately be useful for studying the physiology of vacuoles in living plants. Indeed, one year later these same authors showed that cPrG•HCl **4** could promote acidification of vacuoles in living plant cells in the presence of Cl^- anion [57].

9 Prodiginines, H^+Cl^- Cotransport and Apoptosis

Cell shrinkage, membrane blebbing, condensation of nuclear chromatin and fragmentation of DNA characterize apoptosis, or programmed cell death. Various studies indicate that intracellular acidification can induce apoptosis in cancer cells [58]. The intracellular pH (pH_i) of cancer cells is often more alkaline than that of normal cells, and maintenance of this alkaline pH_i is required for growth, transformation, and metabolism of these cancer cells. Therefore, a potential antitumor therapy would be to trigger apoptosis of cancer cells by perturbing the mechanisms that control the pH_i of cancer cells. As described above, prodiginines have recently been shown to deacidify lysosomes and, thus, negate the proton-translocation activities of V-ATPase without any measurable inhibition of ATP hydrolysis [50, 51]. This uncoupling of V-ATPase by prodiginines was attributed to the

compounds' ability to promote H^+/Cl^- symport (or the functionally equivalent OH^-/Cl^- antiport) across vesicular membranes that experienced a transmembrane pH gradient.

In this study, Yamamoto and colleagues examined the impact of cycloprodigiosin hydrochloride (cPrG•HCl) **4** on cancer cell lines both *in vitro* and *in vivo* [14]. They found that cPrG•HCl **4** inhibited the growth of six different liver cancer cell lines in a dose- and time-dependent fashion. In sharp contrast, treatment of normal rat hepatocytes with cPrG•HCl **4** had no effect on cell growth. In one case, *in vitro* treatment of Huh-7 liver cancer cells with cPrG•HCl **4** caused apoptosis. This group also showed that cPrG•HCl **4** raised the pH of acidic organelles within these Huh-7 cancer cells and also lowered the intracellular pH_i (below $pH_i = 6.8$). Figure 18 shows Huh-7 cells loaded with the pH-sensitive dye, acridine orange, before and after treatment of these cells with cPrG•HCl **4**. In the upper frame, the orange fluorescence is due to acridine orange located within the acidic lysosomes. As seen in the lower frame, after treatment with cPrG•HCl **4** for 1 h the characteristic orange fluorescence was not observed, indicating deacidification of the lysosomes. These authors also used flow cytometry to determine that the intracellular pH of the Huh-7 cells decreased from $pH_i = 7.3$ to $pH_i = 6.8$ after treatment with cPrG•HCl **4** for

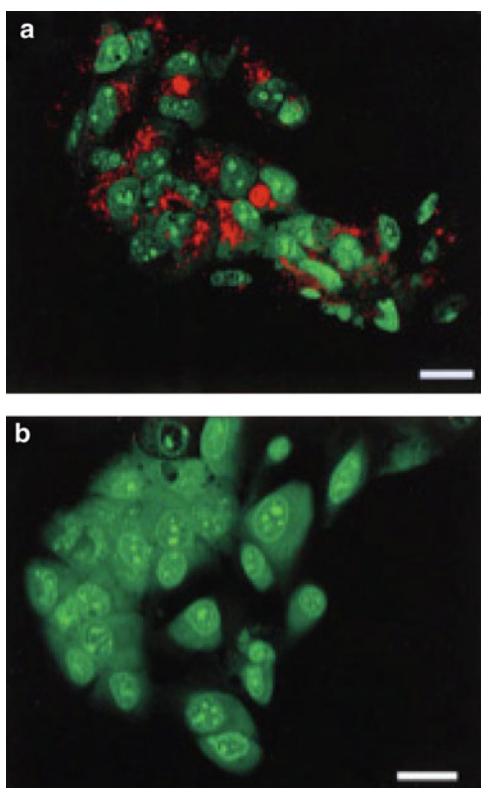


Fig. 18 Acridine orange staining of (a) untreated Huh-7 liver cancer cells and (b) Huh-7 cells treated with 276.5 nmol/L of cPrG•HCl **4** for 1 h. The red color in (a) is indicative of the acid form of the pH-sensitive acridine dye. Treatment of the cells with cPrG•HCl **4** results in neutralization of the acidic compartments within these cells. Reprinted with permission from [14]

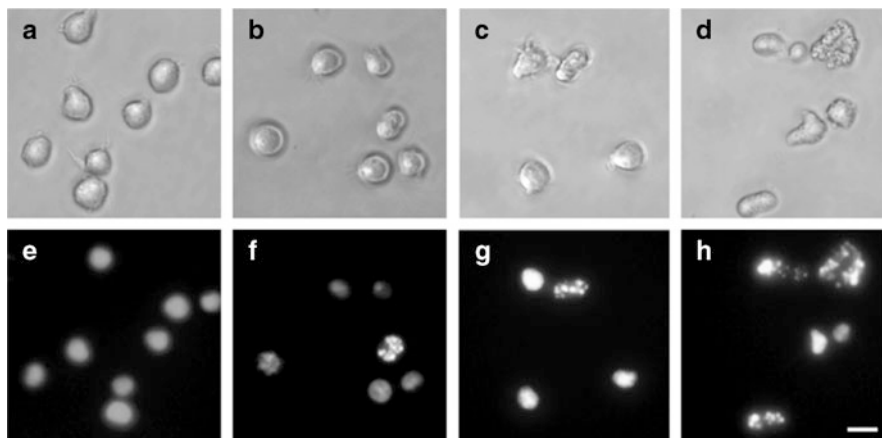


Fig. 19 Effect of prodiginine **PG-L-1** on cellular and nuclear morphology in U937 cells. Cells (6×10^5 cells/dish) were treated with 0 mg/mL (A, E), 0.1 mg/mL (B, F), 1.5 mg/mL (C, G), and 50 mg/mL (D, H) of **PG-L-1** and then the cells were observed under a phase contrast microscope (A, B, C, D), or a fluorescence microscope (E, F, G, H) after being stained with Hoechst 33258 (40 mM) for 10 min. The bar indicates 10 mm. Reprinted with permission from [15]

24 h. For the *in vivo* experiments, nude mice containing xenografted Huh-7 cells received 2 weeks of treatment with cPrG•HCl **4**. After 8 days of treatment with compound **4**, they observed that tumor growth was significantly inhibited. Importantly, a histological examination showed that apoptosis had occurred in the tumor cells treated with cPrG•HCl **4**. Although these authors cautioned that the molecular mechanisms underlying the effects of cPrG•HCl **4** on tumor cells needed further attention, they suggested that prodiginine analogs had much potential to be effective anticancer drugs¹ [59].

In a later paper, Nakashima and colleagues showed that a bacterial prodiginine, one that they dubbed **PG-L-1**, was cytotoxic to human myeloid leukemia (U937) cells [15]. This compound caused the typical increase in acidity in intracellular compartments, presumably because of $H^+ Cl^-$ symport. The authors proposed that this acidification of the cytoplasm triggered apoptosis. As shown in Fig. 19, incubation with the prodiginosin **PG-L-1** caused significant morphological changes in the U937 cells. Fluorescent staining of these treated U937 cells showed that **PG-L-1** caused diagnostic changes in the nuclear material that was typical of apoptosis.

For more details about the ability of prodiginines to trigger cellular apoptosis and on the use of prodiginines as anticancer therapeutics, the interested reader should consult recent reviews and primary articles [10–15, 59–61].

¹The same group later reported similar studies as described in [14].

10 Synthetic Prodiginine Analogs Shown to Bind Cl^- in Solution, Transport Cl^- Across Lipid Membranes and Possess Anticancer Activity

An important study regarding the potential anticancer properties of synthetic prodiginines was reported by Sessler, Magda and colleagues in 2005 [18]. In that paper, they reported that the transmembrane rate of Cl^- transport correlated with the compound's *in vitro* anticancer activity. As mentioned earlier, X-ray crystal structures showed that some of these synthetic analogs bound Cl^- in the solid state (see compound **16** in Fig. 13). Sessler, Magda and colleagues also used isothermal titration calorimetry (ITC) to demonstrate that the protonated forms of the prodiginines had a strong affinity for binding chloride in CH_3CN solution. While the free base forms of the tripyrroles bound Cl^- only weakly, even below the limits of detection by ITC, the protonated forms of the prodiginine analogs showed substantial affinities for Cl^- . Thus, the apparent binding constants were in the range of $K_a = 5.9 \times 10^5 \text{M}^{-1}$ to $1.0 \times 10^5 \text{M}^{-1}$ for the formation of Cl^- adducts by these protonated tripyrroles.

These authors also measured the prodiginines' efficiency for transmembrane transport of chloride ions across synthetic phospholipid membranes, using an ion-selective electrode to monitor Cl^- efflux from the liposomes. They discovered that the synthetic analog **13** (see Fig. 10) with the structure closest to that of the natural product **1** showed the fastest rate of Cl^- efflux from liposomes. The authors concluded, from a series of transport experiments using different transmembrane pH gradients, that these synthetic compounds operated via the H^+/Cl^- cotransport mechanism.

The *in vitro* anticancer activity of these synthetic analogs was determined from a cell proliferation assay using both A549 human lung cancer and PC3 human prostate cell lines. All of the tested compounds, including **13** (Fig. 10) and **16** (Fig. 13), exhibited significant cytotoxic activity, with 100% of the cancer cells killed using concentrations of 40 mM of the analogs. In examining the combined data, the authors noted that the *in vitro* anticancer activity correlated best with the Cl^- transport rates, rather than with the association constant (K_a) for Cl^- binding. These results led Sessler, Magda and colleagues to conclude that "... the strong correlation between transport rates and anticancer activity *in vitro*, in conjunction with evidence for anion binding in the solid state and solution phase, lead us to suggest that the H^+/Cl^- ion symport mechanism proposed by Ohkuma, Wasserman, and co-workers is chemically reasonable" [18].

11 Prodiginines Can Also Facilitate Anion Exchange (Antiport) Across Phospholipid Membranes

On the basis of the pioneering studies of Ohkuma, Wassermann and colleagues, prodigiosin **1** has typically been described in the literature as an H^+/Cl^- cotransporter. However, Ohkuma et al. indicated that the observed pH changes in vesicles

caused by the addition of **1** could also be due to a Cl^-/OH^- anion exchange mechanism [46, 47]. A 2005 study by Seganish and Davis showed that prodigiosin **1** could indeed move Cl^- anions across phospholipid membranes via an anion exchange, or antiport, mechanism [62]. Thus, these authors showed that prodigiosin **1** was able to exchange Cl^- anion for NO_3^- anions during transmembrane transport, without any observed change in the internal pH of the liposomes, a result that was entirely consistent with prodigiosin **1** functioning as an antiporter.

In their study, Seganish and Davis began by showing that prodigiosin **1** operates as an anion carrier, rather than as an ion channel. To distinguish a carrier mechanism from channel formation, they measured Cl^- influx into liposomes made from dipalmitoyl-phosphatidylcholine (DPPC) at temperatures that included those that were above and below DPPC's gel-to-liquid crystalline transition temperature (41°C). These DPPC liposomes contained a fluorescent dye, lucigenin, that is selective for interaction with Cl^- anion [63]. Previous studies have shown that an ion carrier's efficiency is limited by diffusion through the membrane and that the transport rate is greatly diminished in the "frozen" gel state [64]. Ion channel activity, on the other hand, is not as sensitive to the lipid phase and the observed transport rate for channels is not as temperature-dependent as for mobile carriers. Indeed, the transmembrane transport of Cl^- by prodigiosin **1** across the DPPC liposomes was quite sensitive to the lipid phase. Thus, the influx of Cl^- was rapid at 43°C , a temperature above DPPC's phase transition, whereas little Cl^- influx was observed at 37°C , a temperature at which DPPC exists in its gel state (Fig. 20). The authors indicated that these transport results were consistent with prodigiosin **1** functioning as a chloride anion carrier.

Seganish and Davis also discovered that the ability of prodigiosin **1** to transport Cl^- into phospholipid vesicles depended greatly on the nature of the anion that was initially inside the liposome. In experiments with vesicles that contained either Na_2SO_4 or NaNO_3 , they measured both the internal pH of the liposomes (using the pH-sensitive dye pyranine) [65] and Cl^- influx (using the lucigenin dye). When the liposomes were filled with the hydrophilic sulfate anion ($\Delta G_{\text{hyd}} = -1,080 \text{ kJ/mol}$), the authors found that the addition of prodigiosin **1** resulted in immediate

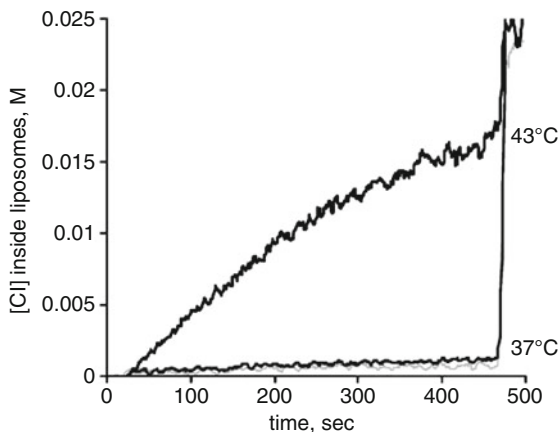


Fig. 20 Chloride influx into DPPC liposomes at 43°C and 37°C . The data at each temperature is the average of three runs using 0.004 mol% of prodigiosin **1**. The trace shown in *gray* represents a DMSO blank at 37°C . Reprinted with permission from [62]

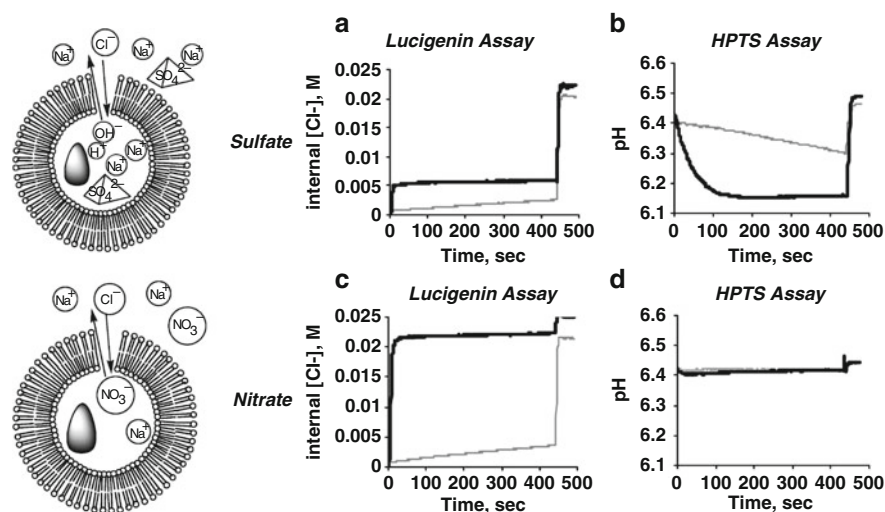


Fig. 21 Chloride gradient assays on 100 nm EYPC liposomes in 10 mM sodium phosphate (pH 6.4) containing either 75 mM Na_2SO_4 (a and b) or 100 mM NaNO_3 (c and d). The chloride gradient was initiated by adding NaCl to give an external concentration of 25 mM. Chloride concentration inside the vesicles (panels a and c) was calculated from the fluorescence of entrapped lucigenin dye. The pH (panels b and d) is calculated from the fluorescence ratio of HPTS dye emitted at 510 nm when excited at 403 and 460 nm in a dual wavelength assay. The trace shown in *gray* represents DMSO blanks. Reprinted with permission from [62]

acidification inside the liposomes but Cl^- influx occurred to only 20% of the value that would be expected for complete equilibration. In contrast, when similar experiments were conducted with liposomes that were loaded with the less hydrophilic nitrate anion ($\Delta G_{\text{hyd}} = -300$ kJ/mol) the authors observed rapid and complete exchange of Cl^- and NO_3^- , but with no concomitant change in intravesicular pH (Fig. 21). Seganish and Davis concluded that prodigiosin **1** was able to facilitate $\text{Cl}^-/\text{NO}_3^-$ anion exchange (antiport) in the experiments with nitrate-loaded liposomes. In contrast, prodigiosin **1** was able to promote some initial H^+/Cl^- symport (or OH^-/Cl^- exchange) when the hydrophilic sulfate anion was present in the liposomes. Thus, this paper was important because it showed, for the first time, that prodigiosin **1** could facilitate transmembrane anion exchange. Moreover, the study also demonstrated that prodigiosin's mechanism for Cl^- transport might well change from Cl^-/A^- antiport to H^+/Cl^- symport, depending on the environmental conditions.

Thompson, Davis and colleagues later used this $\text{Cl}^-/\text{NO}_3^-$ transmembrane exchange assay, with the lucigenin dye, to investigate the ability of a series of synthetic prodiginines to transport chloride ions across liposomal membranes made from egg yolk L-phosphatidylcholine (EYPC) [66]. They found that most of these synthetic prodiginines retained significant chloride ion transport ability at low ligand: lipid concentrations (0.1 mol%). For example, the β -substituted prodiginines **19** and **20**, shown in Fig. 22, while less active than prodigiosin **1**, still retained a significant ability to move Cl^- anion across EYPC lipid membranes. The authors

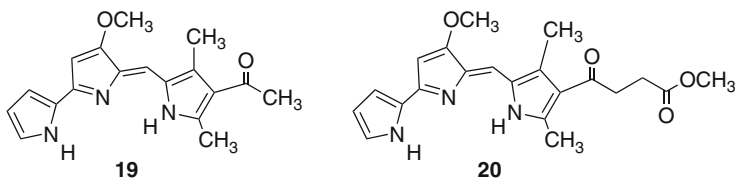


Fig. 22 Structures of C-ring modified analogs **19** and **20**. Both compounds were shown to facilitate transmembrane transport of Cl^- anion

noted that the modest decreases in Cl^- transport rates exhibited by these synthetic prodiginines may be due to either a reduced ability to partition into the lipid membrane, a reduced rate of diffusion across the bilayer or because of a change in binding affinity for Cl^- anion. Nonetheless, the most important finding of these transport experiments was that different side chains could be attached to the prodiginine's tripyrrole unit core without losing the ability to transport chloride ions across phospholipid membranes.

12 $\text{H}^+ \text{Cl}^-$ Transport by Synthetic Receptors Designed to Mimic Prodiginine Function

Recently, the groups of Gale and Smith reported intriguing studies on neutral ligands designed to mimic prodiginosin's ability to transport HCl across bilayer membranes [67, 68]. Thus, compound **21** in Fig. 23 contains two hydrogen bond donors, a pyrrole NH and an amide NH, for interaction with anions. Moreover, compound **21** has a basic imidazole side chain that can be protonated and then enhance hydrogen bond interactions with a bound Cl^- anion. In this way, receptor **21** was designed so that it might cotransport $\text{H}^+ \text{Cl}^-$ across a bilayer that is experiencing a pH gradient. The working hypothesis was that compound **21** should be able to move HCl from an acidic solution into a more basic solution where ligand deprotonation and Cl^- decomplexation would then be favored. An X-ray crystal structure of **21**•HCl showed a [2 + 2] dimer, with each chloride involved in three hydrogen bonds. Two of the $\text{NH} \cdots \text{Cl}$ hydrogen bonds involved the pyrrole NH and amide NH of one molecule and the third hydrogen bond was with the imidazolium unit of another molecule of **21**. The authors noted that HCl bound within such a [2 + 2] dimer would be protected by the structure's lipophilic exterior. If the solid-state structure were relevant to function, then such an organization would provide a nice way to sequester HCl for transport across the hydrophobic membrane.

Using a Cl^- electrode, the authors found that **21** transported Cl^- across vesicles made from 1-palmitoyl-2-oleoyl-sn-glycero-3-phosphocholine (POPC) and cholesterol. The authors showed that the rates of Cl^- transport were pH-dependent. The greatest rate of Cl^- efflux from the NaCl-filled liposomes occurred when the intravesicular solution was acidic (pH 4.0) and the extravesicular buffer was near neutral (pH 6.7). In biomimetic fashion, the synthetic compound **21** could also deacidify liposomes, a property that is a hallmark of the prodiginines. Thus,

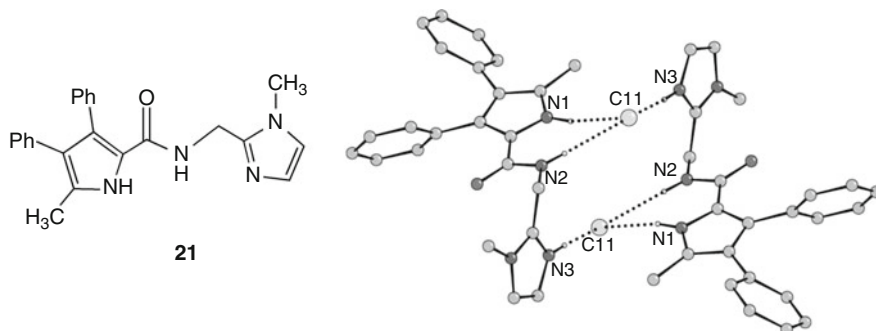


Fig. 23 A synthetic prodiginine mimic **21** and the crystal structure of its HCl complex showing formation of a “2 + 2” hydrogen-bonded dimer. Reprinted with permission from [67]

addition of compound **21** to liposomes loaded with the acid-sensitive dye, Oregon Green 514, destroyed the initial pH gradient across the membrane. Gale and Smith proposed that the free base of **21** that partitioned into the membrane could diffuse across the bilayer where it bound HCl at the interface of the lipid membrane and the intravesicular solution. The resulting lipophilic ion pair could then move back across the bilayer to deposit HCl into the more basic external solution.

13 Prodigiosin 1 Facilitates Transmembrane Transport of Bicarbonate Anion

Recently, Davis, Gale, Quesada and colleagues showed that prodigiosin **1** can facilitate the transmembrane exchange of Cl^- and HCO_3^- anions [69]. These authors suggested that prodigiosin's specific pattern of hydrogen-bond donors and acceptors might well allow it to function as a complementary receptor for binding and membrane transport of bicarbonate (Fig. 24). Indeed, it was reported over 50 years ago that prodigiosin **1** reacts with carbonic acid to give a protonated adduct, $\mathbf{1}\cdot\text{HCO}_3^-$ [70]. Davis and colleagues showed, using NMR spectroscopy, that prodigiosin **1** can bind HCO_3^- anion in the nonpolar solvent CD_2Cl_2 . Significantly, the ^1H NMR signals for **1** that were most influenced upon addition of tetraethyl-ammonium bicarbonate were the H_2 proton on the A-ring and the methyl group on the C-ring. The authors noted that these would be the protons closest to the anion-binding cleft formed by the “all-*cis*” β -isomer of prodigiosin **1** (Fig. 1). Although the authors did not report a stability constant for the $\mathbf{1}\cdot\text{HCO}_3^-$ complex, their ^1H NMR data demonstrated that the free base form of prodigiosin **1** could bind HCO_3^- in solution.

In addition to showing evidence for binding, Davis and colleagues also demonstrated that prodigiosin **1** was a potent transmembrane transporter of HCO_3^- using independent assays. Earlier studies by Seganish and Davis had shown that prodigiosin **1** could facilitate the anion exchange of nitrate and bicarbonate in phospholipid membranes [62]. Although nitrate and bicarbonate anions have similar sizes and

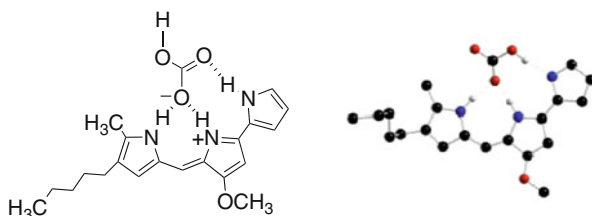


Fig. 24 Possible structure of a complex of HCO_3^- with the protonated prodigiosin $1 \cdot \text{H}^+$

shapes, bicarbonate is more hydrophilic than nitrate and thus it is more challenging to transport bicarbonate across a lipid bilayer [71]. In the first set of experiments, phospholipid vesicles filled with NaCl solution were suspended in a sulfate-containing buffer and prodigiosin **1** was added to the solution (see Fig. 25). The efflux of Cl^- anion from the liposomes was monitored using a Cl^- -selective electrode and under these conditions there was no significant movement of Cl^- from within the liposomes. After 2 min, a solution of sodium bicarbonate was added to the extravesicular solution and it was immediately evident that this addition turned on chloride efflux, suggesting that prodigiosin **1** could facilitate $\text{Cl}^-/\text{HCO}_3^-$ antiport exchange across these liposomal membranes.

The experiments depicted in Fig. 25 provided strong, yet indirect, evidence that prodigiosin **1** could transport bicarbonate across lipid membranes, since it was the Cl^- and not the HCO_3^- anion that was being monitored. The authors next used ^{13}C NMR spectroscopy to verify the prodigiosin-mediated transmembrane transport of HCO_3^- . In these NMR assays, the paramagnetic Mn^{2+} ion was used to bleach any ^{13}C NMR signal that originated from extravesicular $\text{H}^{13}\text{CO}_3^-$ anion, whereas the ^{13}C NMR signals for intravesicular $\text{H}^{13}\text{CO}_3^-$ would be unaffected by the membrane-impermeable Mn^{2+} . Thus, these NMR experiments allowed for the direct discrimination of extravesicular and intravesicular $\text{H}^{13}\text{CO}_3^-$ and enabled the transmembrane movement of this anion to be firmly established (Fig. 26).

Figure 26 shows data that illustrates prodigiosin-mediated $\text{HCO}_3^-/\text{Cl}^-$ exchange. EYPC liposomes (5 mM) filled with 450 mM NaCl were suspended in a sulfate solution and 50 mM $\text{NaH}^{13}\text{CO}_3$ was added to this solution. A sharp ^{13}C NMR signal for the extravesicular $\text{H}^{13}\text{CO}_3^-$ was observed at δ 161 ppm. Addition of Mn^{2+} to this solution caused complete broadening of the ^{13}C NMR signal for extravesicular bicarbonate. After the addition of prodigiosin **1**, a sharp ^{13}C NMR signal for $\text{H}^{13}\text{CO}_3^-$ reemerged due to ligand-mediated transport of bicarbonate into the liposome.

In this paper, the authors demonstrated that “small” molecules such as the natural product prodigiosin **1** could facilitate $\text{Cl}^-/\text{HCO}_3^-$ anion exchange, a process that is typically mediated by membrane proteins. The authors noted that this demonstration of $\text{Cl}^-/\text{HCO}_3^-$ antiport “...may well present an alternative mechanism by which prodigiosin **1** can influence biological systems” [69]. Furthermore, they proposed that synthetic $\text{Cl}^-/\text{HCO}_3^-$ antiporters based on prodigiosin’s tripyrrole framework might prove to be useful tools for biomembrane research.

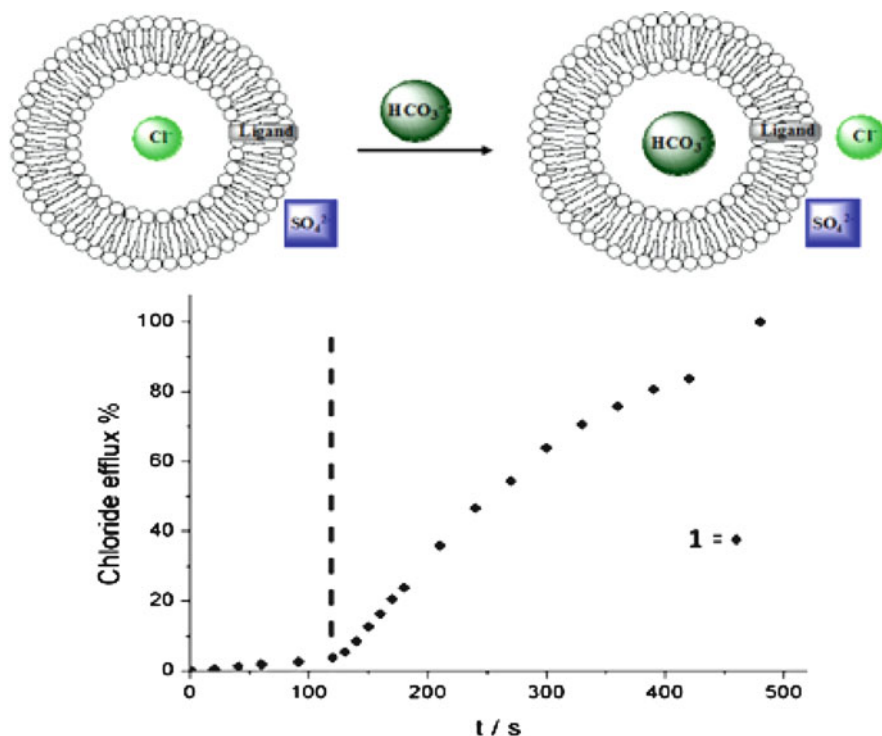


Fig. 25 Results of chloride transport (measured using a chloride-selective electrode) that commenced when a bicarbonate pulse was added to the external solution. Below $t = 120$ s (i), chloride efflux is promoted by the addition of prodigiosin **1** (diamond) (0.04% molar carrier to lipid) to unilamellar POPC vesicles loaded with 451 mM NaCl and 20 mM phosphate buffer, pH 7.2, dispersed in 150 mM Na_2SO_4 and 20 mM phosphate buffer, pH 7.2. At $t = 120$ s, a solution of NaHCO_3 was added to give a 40 mM external concentration. At $t = 420$ s, the vesicles were lysed with detergent and the final reading at $t = 480$ s was considered to equal 100% chloride efflux. Figure modified from [69]

14 Conclusions and Outlook

It is now clear from both the biochemical literature and from a variety of solid-state and solution studies that the protonated prodiginines are able to bind to anions. The resulting lipophilic ion pairs are also able to diffuse across the hydrophobic barrier that makes up phospholipid bilayer. In this way, the prodiginines are able to function as transmembrane anion transporters and, depending on the conditions, they can also function as de facto H^+Cl^- transporters. In particular, the ability to coordinate and transport both Cl^- and HCO_3^- anions makes the prodiginines potentially valuable for mediating important biological processes that depend on the proper balance of these two essential anions. The author believes that the combination of organic synthesis and the use of biosynthetic machinery will, in

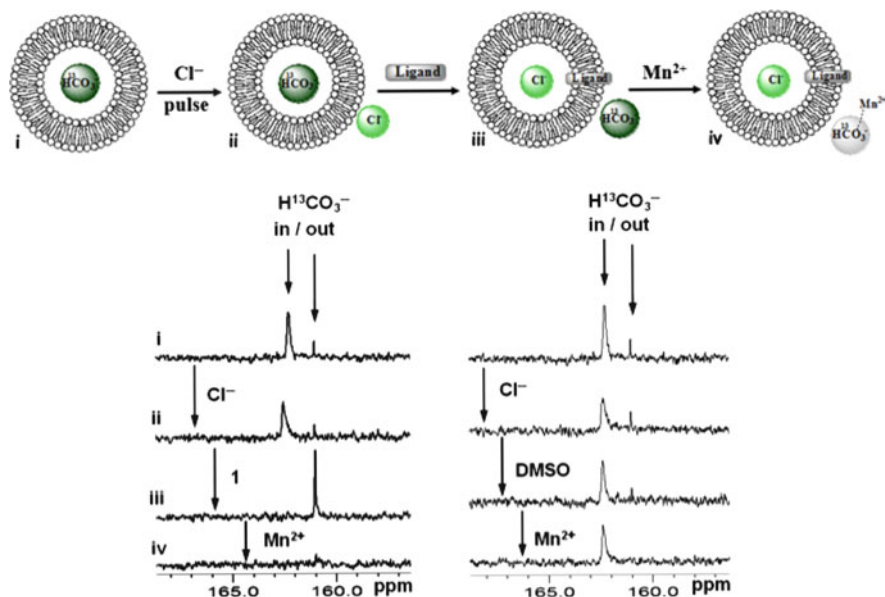


Fig. 26 ^{13}C -NMR experiments demonstrate that prodiginosin **1** is able to facilitate chloride/bicarbonate antiport. (a) Titration sequence for monitoring the transmembrane transport of bicarbonate ions in $\text{H}^{13}\text{CO}_3^-$ loaded EYPC liposomes by prodiginosin **1** and DMSO. (b–d) ^{13}C -NMR spectra (i) before and (ii) after the addition of the 50 mM NaCl pulse to EYPC vesicles loaded with 100 mM $\text{NaH}^{13}\text{CO}_3$, 20 mM HEPES buffer, pH 7.5, and dispersed in 75 mM Na_2SO_4 , 20 mM HEPES buffer, pH 7.5; (iii) after the addition of prodiginosin **1** or DMSO (**1**, 0.1 mol%; DMSO, 870 mol%); (iv) after the addition of 0.5 mM Mn^{2+} (1:100 $\text{Mn}^{2+}/\text{Cl}^-$ ratio). Figure modified from [69]

the future, continue to produce new prodiginine analogs that are less cytotoxic but better able to be used as anticancer agents and other pharmaceuticals. The coming decade will undoubtedly reveal more about the mechanism of action of these pyrrole-based natural products and also reveal more about how their anion binding and anion transport abilities is translated into a biological function.

References

1. Bizio B (1823) *Biblioteca Italiana o sia Giornale di Letteratura, Scienze e Arti* Tomo 30: 275–295
2. Merlino CP (1924) *J Bacteriol* 9:527–543
3. Hubbard R, Rimington C (1950) *Biochem J* 46:200–225
4. Gaughran ER (1969) *Trans NY Acad Sci* 31:3–24
5. Bennett JW (2000) *Adv Appl Microbiol* 47:1–32
6. Fürstner A (2003) *Angew Chem Int Ed* 42:3582–3603
7. Wrede IF, Hettche O (1929) *Ber Deut Chem Ges* 62:2678–2687
8. Wasserman HH, McKeon JE, Smith L, Forgiione P (1960) *J Am Chem Soc* 82:506–507

9. Rapoport H, Holden KG (1962) *J Am Chem Soc* 84:634–642
10. Manderville RA (2001) *Curr Med Chem Anticancer Agents* 1:195–218
11. Perez-Tomas R, Montaner B, Llagostera E, Soto-Cerrato V (2003) *Biochem Pharm* 66:1447–1452
12. Williamson NR, Fineran PC, Gristwood T, Chawrai SR, Leeper FJ, Salmond GPC (2007) *Future Microbiol* 2:605–618
13. Pandey R, Chander R, Sainis KB (2009) *Curr Pharm Design* 15:732–741
14. Yamamoto C, Takemoto H, Kuno K, Yamamoto D, Tsubaru A, Kamata K, Hirata H, Yamamoto A, Kano H, Seki T, Inoue K (1999) *Hepatology* 30:894–902
15. Nakashima T, Tamura T, Kurachi M, Yamaguchi K, Oda T (2005) *Biol Pharm Bull* 28:2289–2295
16. Melvin MS, Ferguson DC, Lindquist N, Manderville RA (1999) *J Org Chem* 64:6861–6869
17. Melvin MS, Tomlinson JT, Saluta GR, Kucera GL, Lindquist N, Manderville RA (2000) *J Am Chem Soc* 122:6333–6334
18. Sessler JL, Eller LR, Cho WS, Nicolaou S, Aguilar A, Lee JT, Lynch VM, Magda DJ (2005) *Angew Chem Int Ed* 44:5989–5992
19. Baldino CM, Parr J, Wilson CJ, Ng SC, Yohannes D, Wasserman HH (2006) *Bioorg Med Chem Lett* 16:701–704
20. Fürstner A, Radkowski K, Peters H, Seidel G, Wirtz C, Mynott R, Lehmann CW (2007) *Chem Eur J* 13:1929–1945
21. Diaz RIS, Bennett SM, Thompson A (2009) *Chem Med Chem* 4:742–745
22. Clift MD, Thomson RJ (2009) *J Am Chem Soc* 131:14579–14583
23. For more information on Aida Pharmaceuticals and their development of prodigiosin **1** as an anti-cancer agent, see the website: <http://www.crunchbase.com/company/aida-pharmaceuticals>
24. Dairi K, Yao Y, Faley M, Tripathy S, Rioux E, Billot X, Rabouin D, Gonzalez G, Lavallee JF, Attardo G (2007) *Org Process Res Dev* 11:1051–1054
25. O'Brien SM, Claxton DF, Crump M, Faderl S, Kipps T, Keating MJ, Viallet J, Cheson BD (2009) *Blood* 113:299–305
26. D'Alessio R, Bargiotti A, Carlini O, Colotta F, Ferrari M, Gnocchi P, Isetta A, Mongelli N, Motta P, Rossi A, Rossi M, Tibolla M, Vanotti E (2000) *J Med Chem* 43:2557–2565
27. Stepkowski SM, Erwin-Cohen RA, Behbod F, Wang ME, Qu X, Tejpal N, Nagy ZS, Kahan BD, Kirken RA (2002) *Blood* 99:680–689
28. Williamson NR, Fineran PC, Leeper FJ, Salmond GPC (2006) *Nat Rev Microbiol* 4:887–899
29. Chawrai SR, Williamson NR, Salmond GPC, Leeper FJ (2008) *Chem Commun*:1862–1864
30. Gerber NN (1975) Prodigiosin-like pigments. *CRC Crit Rev Microbiol* 3:469–485
31. Kim D, Kim J, Yim JH, Kwon SK, Lee CH, Lee HK (2008) *J Microbiol Biotech* 18:1621–1629
32. Rizzo V, Morelli A, Pinciroli V, Sciangula D, D'Alessio R (1999) *J Pharm Sci* 88:73–78
33. Sertan-de Guzman AA, Predicala RZ, Bernardo EB, Neilan BA, Elardo SP, Mangalindan GC, Tasdemir D, Ireland CM, Barraquio WL, Concepcion GP (2007) *FEMS Microbiol Lett* 277:188–196
34. Blake AJ, Hunter GA, McNab H (1990) *Chem Commun*:734–736
35. La JQH, Michaelides AA, Manderville RA (2007) *J Phys Chem B* 111:11803–11811
36. Fürstner A, Grabowski J, Lehmann CW (1999) *J Org Chem* 64:8275–8280
37. Melvin MS, Tomlinson JT, Park G, Day CS, Saluta GR, Kucera GL, Manderville RA (2002) *Chem Res Toxicol* 15:734–741
38. Jenkins S, Incarvito CD, Parr J, Wasserman HH (2009) *CrystEngComm* 11:242–245
39. Chen K, Rannulu NS, Cai Y, Lane P, Liebl AL, Rees BB, Corre C, Challis GL, Cole RB (2008) *J Am Soc Mass Spectrom* 19:1856–1866
40. Duarte HA, Duani H, De Almeida WB (2003) *Chem Phys Lett* 369:114–124
41. Skawinski WJ, Venanzi TJ, Venanzi CA (2004) A molecular orbital study of tambjamine E and analogues. *J Phys Chem A* 108:4542–4550
42. Sessler JL, Weghorn SJ, Lynch V, Fransson K (1994) *J Chem Soc Chem Commun*:1289–1290
43. Sessler JL, Camiolo S, Gale PA (2003) *Coord Chem Rev* 240:17–55

44. Park G, Tomlinson JT, Melvin MS, Wright MW, Day CS, Manderville RA (2003) *Org Lett* 5: 113–116
45. Nelson N, Perzov N, Cohen A, Hagai K, Padler V, Nelson H (2000) *J Exp Biol* 203:89–95
46. Sato T, Konno H, Tanaka Y, Kataoka T, Nagai K, Wasserman HH, Ohkuma S (1998) *J Biol Chem* 273:21455–21462
47. Ohkuma S, Sato T, Okamoto M, Matsuya H, Arai K, Kataoka T, Nagai K, Wasserman HH (1998) *Biochem J* 334:731–741
48. Konno H, Matsuya H, Okamoto M, Sato T, Tanaka Y, Yokoyama K, Kataoka T, Nagai K, Wasserman HH, Ohkuma S (1998) *J Biochem* 124:547–556
49. Matsuya H, Okamoto M, Ochi T, Nishikawa A, Shimizu S, Kataoka T, Nagai K, Wasserman HH, Ohkuma S (2000) *Biochem Pharm* 60:1855–1863
50. Lee MH, Kataoka T, Magae J, Nagai K (1995) *Biosci Biotechnol Biochem* 59:1417–1421
51. Kataoka T, Muroi M, Ohkuma S, Waritani T, Magae J, Takatsuki A, Kondo S, Yamasaki M, Nagai K (1995) *FEBS Lett* 359:53–59
52. Kawauchi K, Shibutani K, Yagisawa H, Nakatsuji S, Anzai H, Yokoyama Y, Ikegami Y, Moriyama Y, Hirata H (1997) *Biochem Biophys Res Commun* 237:543–547
53. Woo JT, Ohba Y, Tagami K, Sumitani K, Kataoka T, Nagai K (1997) *Biosci Biotech Biochem* 61:400–402
54. Tanigaki K, Sato T, Tanaka Y, Ochi T, Nishikawa A, Nagai K, Kawashima H, Ohkuma S (2002) *FEBS Lett* 524:37–42
55. Rea PA, Poole RJ (1993) *Annu Rev Plant Physiol Plant Mol* 44:157–180
56. Maeshima M, Nakayasu T, Kawauchi K, Hirata H, Shimmen T (1999) *Plant Cell Physiol* 40:439–442
57. Nakayasu T, Kawauchi K, Hirata H, Shimmen T (2000) *Plant Cell Physiol* 41:857–863
58. Lagadic-Gossman D, Huc L, Lecureur V (2004) *Cell Death Differ* 11:953–961
59. Yamamoto C, Takemoto H, Kuno K, Yamamoto D, Nakai K, Baden T, Kamata K, Hirata H, Watanabe T, Inoue K (2001) *Oncology* 8:821–824
60. Francisco R, Pérez-Tomás R, Giménez-Bonafé P, Soto-Cerrato V, Giménez-Xavier P, Ambrosio S (2007) *Eur J Pharmacol* 572:111–119
61. Kawauchi K, Tobiume K, Iwashita K, Inagaki H, Morikawa T, Shibukawa Y, Moriyama Y, Hirata H, Kamata H (2008) *Biosci Biotechnol Biochem* 72:1564–1570
62. Seganish JL, Davis JT (2005) *Chem Commun*:5781–5783
63. McNally BA, Koulov AV, Smith BD, Joos JB, Davis AP (2005) *Chem Commun*:1087–1089
64. Krasne S, Eisenman G, Szabo G (1971) *Science* 174:412–414
65. Kano K, Fendler JH (1978) *Biochim Biophys Acta* 509:289–299
66. Sáez Díaz RI, Regourd J, Santacrose PV, Davis JT, Jakeman DL, Thompson A (2007) *Chem Commun*:2701–2703
67. Gale PA, Light ME, McNally B, Navakhun K, Sliwinski KE, Smith BD (2005) *Chem Commun*:3773–3775
68. Gale PA (2005) *Chem Commun*:3761–3772
69. Davis JT, Gale PA, Okunola OA, Prados P, Iglesias-Sánchez JC, Torroba T, Quesada R (2009) *Nat Chem* 1:138–144
70. Stefayne D (1960) *J Org Chem* 25:1261–1262
71. Davis AP, Sheppard DN, Smith BD (2007) *Chem Soc Rev* 36:348–357

Indoles and Related Heterocycles

Hemraj Juwarker, Jae-min Suk, and Kyu-Sung Jeong

Abstract Indole and the related heterocycles have emerged as efficient building blocks for the creation of novel anion receptors. This chapter focuses on the employment of indoles, carbazoles, and indolocarbazoles in the creation of molecular clefts, macrocycles, oligomers, and sensors. The majority of these structures utilize the heterocyclic NH as a hydrogen bond donor in binding to anions of various sizes and geometries. These heterocycles are often connected by amides and ureas which also function as hydrogen bond donors in anion binding. Finally, molecular sensors based on indoles and carbazoles have been described, showing color or fluorescence changes upon anion binding or deprotonation of the heterocyclic NH by basic anions.

Keywords Anion recognition · Carbazole · Hydrogen bond · Indole · Indolocarbazole · Macrocycle · Molecular cleft · Molecular sensor · Oligomer

Contents

1	Introduction	178
2	Molecular Clefts	180
2.1	Indole–Amide Hybrids	180
2.2	Indole–Urea Hybrids	183
2.3	Carbazoles	186
2.4	Indolocarbazoles	187
2.5	Others	190
3	Macrocycles	191
3.1	Anion Receptors	192
3.2	Ion Pair Receptor	193
4	Acyclic Oligomers	193
4.1	Oligoindoles	195

4.2	Oligoindolocarbazoles	196
5	Molecular Sensors	198
5.1	Indole-Based Sensors	198
5.2	Carbazole-Based Sensors	200
6	Conclusions	202
	References	203

Abbreviations

AcO	Acetate
Bz	Benzyl
BzO	Benzoate
CD	Circular dichroism
CIC	Chloride ion channel
CIS	Complexation induced shift
DABCO	1,4-Diazabicyclo[2.2.2]octane
DMSO	Dimethyl sulfoxide
K_a	Association constant
K_d	Dissociation constant
NMR	Nuclear magnetic resonance
NrtA	Nitrate-binding protein
phen	Phenanthroline
SBP	Sulfate-binding protein
Ser	Serine
TBA	Tetrabutylammonium
THF	Tetrahydrofuran
Trp	Tryptophan
UV/Vis	Ultraviolet/visible

1 Introduction

Molecular or ionic recognition is a fundamental event in biochemical processes which include transport, signaling, transcription, and catalysis. Over the last four decades, chemists have devoted their efforts toward the creation of synthetic molecules that can imitate and reproduce the molecular recognition phenomenon observed in biological systems. In the design of synthetic receptors, the most important task is choosing the noncovalent interactions to be employed in the binding between a receptor and a substrate. This is controlled by the careful selection of functional groups in the synthesis of the receptor. In particular, hydrogen bonding has been proven as a prevalent and powerful noncovalent interaction employed by synthetic receptors for anion binding, as anions serve as good hydrogen bonding acceptors.

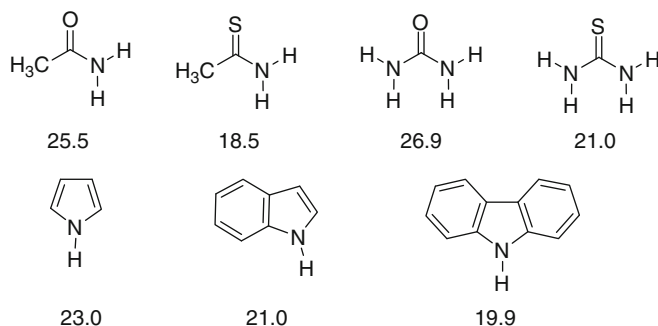


Fig. 1 pK_a values in DMSO of representative molecules used as hydrogen bond donors in synthetic anion receptors [3, 4]

The hydrogen bond has been known to be strongly electrostatic in nature [1]. It is also viewed as an incipient proton transfer reaction, and more advanced proton transfer gives rise to stronger hydrogen bonds [2]. In this context, hydrogen bonding strength has often been correlated to the acidity and basicity of the interacting partners; in general, the more acidic proton serves as the better hydrogen bonding donor, and the more basic atom functions as the better acceptor. Figure 1 shows the pK_a values in DMSO of the representative molecules containing the functional groups that serve as good hydrogen bond donors.

Indole is a heterocyclic aromatic compound with a good hydrogen bond donor NH. Since indole is a key component of the amino acid tryptophan, it is not surprising to find some examples of proteins that employ the indole NH for anion binding. For example, sulfate-binding protein (SBP) of *Salmonella typhimurium* sequesters sulfate dianion with a dissociation constant (K_d) of 0.17 μM by a total of seven hydrogen bonds, formed with five amide NHs of the backbone, one indole NH of Trp¹⁹² side chain, and one OH of Ser¹³⁰ [5, 6]. The next example is nitrate-binding protein, NrtA from *Synechocystis* sp. PCC 6803. The nitrate ion binds with $K_d = 0.3$ mM by electrostatic interactions and six hydrogen bonds including one hydrogen bond with the indole NH of Trp¹⁰² [7, 8] (Fig. 2).

It is evident that several hydrogen bond donors are present in the anion binding sites of proteins, which operate together in a convergent and cooperative manner to achieve strong and selective binding to a specific anionic substrate. In this regard, chemists have designed and prepared anion receptors that contain multiple functional groups capable of hydrogen bonding with anions. While indoles are prevalent in the synthesis of natural products and pharmaceuticals, they have only recently been recognized as useful building blocks for the construction of synthetic anion receptors. Since 2004, anion receptors containing indole, carbazole and indolocarbazole moieties have been described, but this field is still in its infancy [9]. Details studied to date will be described in this chapter by classifying the type of anion receptors as molecular clefts, macrocycles, acyclic oligomers, and molecular sensors.

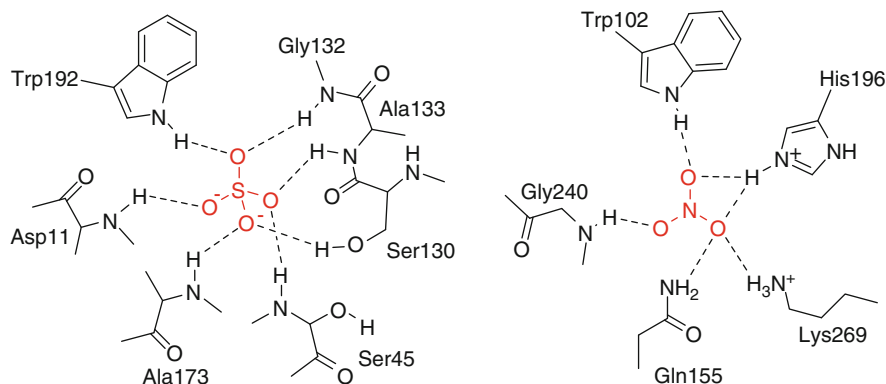


Fig. 2 Hydrogen-bonding modes of two anion binding proteins utilizing the indole NH: sulfate-binding protein (*left*) and nitrate-binding protein (*right*). Hydrogen bonds are marked as *dotted line* [5–8]

2 Molecular Clefts

A general class of anion receptors is molecular clefts. These can be defined as acyclic, concave molecules with cavities or indentations in the molecular surface, into which a guest can fit but is not completely encapsulated [10, 11]. They are often, if not always, characterized by convergent functional groups directed toward each other, but separated by an appropriate linker, thus providing the space for anion binding. Molecular clefts are more synthetically feasible than macrocycles, and serve as platforms on which to modulate key structural elements before synthetic expansion into more complex structures. In the following examples, it can be noticed that indoles and related heterocycles are linked together by amides and ureas that afford additional hydrogen bonding sites for anions, thus increasing binding strength and selectivity.

2.1 Indole–Amide Hybrids

Amides have been the most popular functional group employed in the creation of synthetic receptors for anions. They have found utility in linking together indole units while simultaneously providing additional NHs for anion binding, thus maximizing interactions with anions.

Anion receptors **1** and **2** containing two indole groups attached to pyridine-2, 6-carboxamide and isophthalimide cores were synthesized by Gale and coworkers in 2007 [12]. Receptor **1** possesses a binding cavity preorganized by intramolecular N(pyridine)•••HN(amide) hydrogen bonds. **1** binds anions in the order of fluoride ($K_a > 10^4 \text{ M}^{-1}$) \gg acetate (250 M^{-1}) $>$ dihydrogen phosphate (70 M^{-1}) $>$ chloride ($< 10 \text{ M}^{-1}$) with 1:1 stoichiometry in 0.5% water/DMSO. Crystal structures

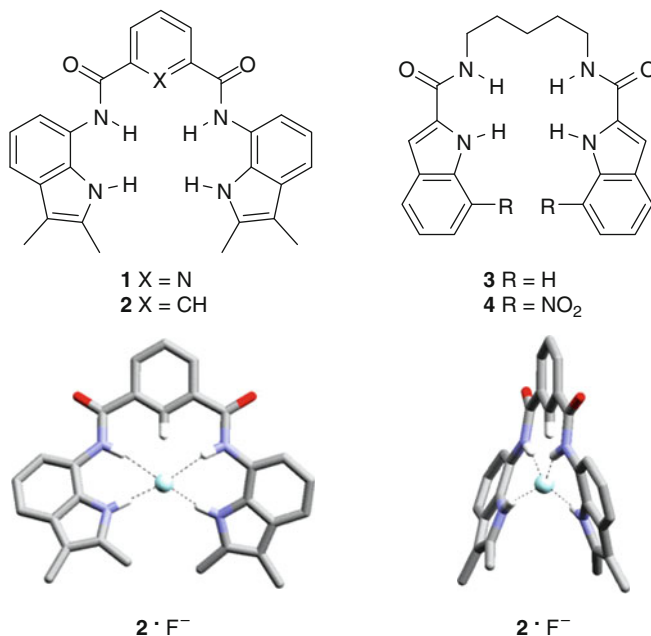


Fig. 3 Structures of indole–amide hybrid clefts **1–4** and top and side views of X-ray crystal structures of **2** with fluoride [12, 13]

of complex **1**•TBA⁺F⁻ show a “twisted” conformation where fluoride forms four hydrogen bonds with all the receptor NHs. Relative to **1**, receptor **2** showed slightly higher binding affinities; the association constants (K_a , 0.5% water/DMSO) for acetate, dihydrogen phosphate and benzoate were 880, 1,140, and 120 M⁻¹, respectively. **2** formed 1:1 complexes with these anions but formed 1:2 complexes with fluoride ($K_1 = 940$ M⁻¹, $K_2 = 21$ M⁻¹ in 5% water/DMSO). The same group also prepared anion receptors **3** and **4** with flexible alkyl spacers that showed low binding affinities for anions (fluoride, acetate, benzoate, chloride) in 0.5% water/DMSO ($K_a = 10$ –150 M⁻¹) with a slight selectivity towards dihydrogen phosphate (260 M⁻¹) [13] (Fig. 3).

In 2008, Jurczak and coworkers reported anion receptors **5–7** which contain rigid aromatic spacers, pyrrole, azulene and pyridine, respectively [14]. They examined the binding properties of **5–7** with benzoate and dihydrogen phosphate in 0.5% water/DMSO-*d*₆. The relative binding affinities (K_a) with benzoate were in the order of **6** (526 M⁻¹) > **5** (33 M⁻¹) > **7** (28 M⁻¹) based on changes in the chemical shifts of the indole or amide NHs, while those with dihydrogen phosphate were in the order of **6** (2,400 M⁻¹) > **7** (164 M⁻¹) > **5** (35 M⁻¹). Although **5** possesses an additional hydrogen bond donor of the pyrrole NH, **6** showed the highest binding affinities. Authors rationalized that electrostatic repulsions between the pyrrole and amide NH groups in **5** destabilize the *syn–syn* conformation required for anion binding. Despite possessing a more preorganized binding cavity,

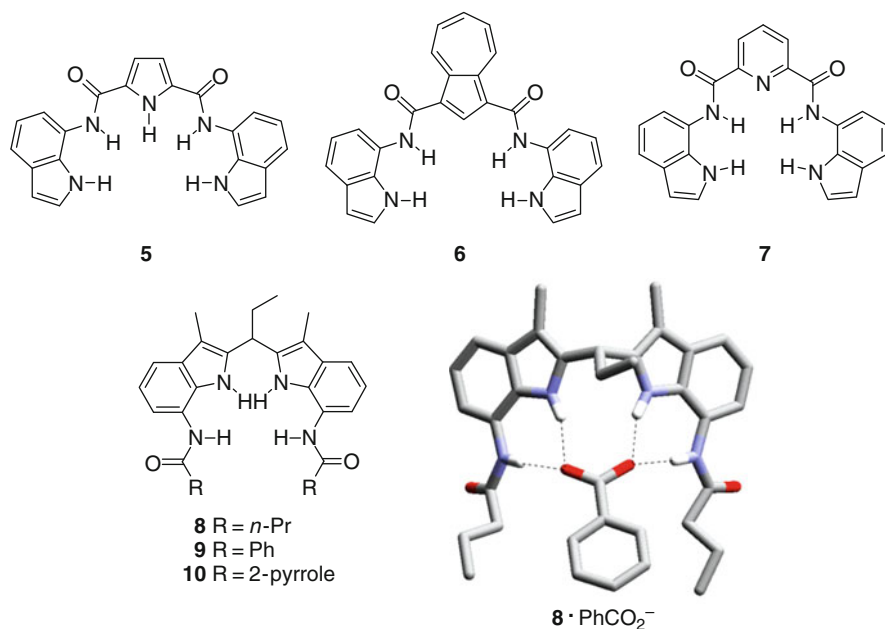


Fig. 4 Anion receptors **5–10** based on indole–amide clefts and a crystal structure of **8** with benzoate [14, 15]

7 showed lower binding affinities than **6**, possibly due to electrostatic repulsions between the bound anion and the pyridine nitrogen.

In 2009, the same group reported receptors **8–10** in which two amidoindoles were linked via methylene units to yield curved conformations [15]. Receptor **8** strongly bound anions with 1:1 stoichiometry: dihydrogen phosphate ($K_a > 10^4 \text{ M}^{-1}$) > benzoate ($1,970 \text{ M}^{-1}$) > chloride (150 M^{-1}) > bromide (10 M^{-1}) in 5% water/DMSO. Receptor **8** was able to bind dihydrogen phosphate in a more competitive medium, 25% v/v water/DMSO (210 M^{-1}). On the other hand, **9** and **10** showed surprisingly lower binding affinities towards the anions other than **8**; association constants of **9** and **10** with dihydrogen phosphate were determined to be only 990 and 215 M^{-1} , compared to that ($K_a > 10^4 \text{ M}^{-1}$) of **8**. Authors explained that the pendant groups (phenyl in **9**, pyrrole in **10**) may give rise to steric hindrances, thus leading to the decreased affinities. X-ray crystallographic analysis of complex **8**•PhCO₂⁻ clearly demonstrated that benzoate was bound by four hydrogen bonds with two indole NHs and two amide NHs (Fig. 4).

Caltagirone and coworkers reported receptor **11** containing two indole units linked to a bipyridyl unit [16]. **11** is a heteroditopic receptor comprising two different binding sites for hydrogen bonding and metal coordination. Receptor **11** bound anions with 1:1 stoichiometry by adopting a *s-cis* conformation of the 2,2'-bipyridyl unit: dihydrogen phosphate ($K_a = 90 \text{ M}^{-1}$) > acetate (58 M^{-1}) > benzoate (35 M^{-1}) > chloride ($< 10 \text{ M}^{-1}$) in 0.5% water/DMSO-*d*₆. Coordination of

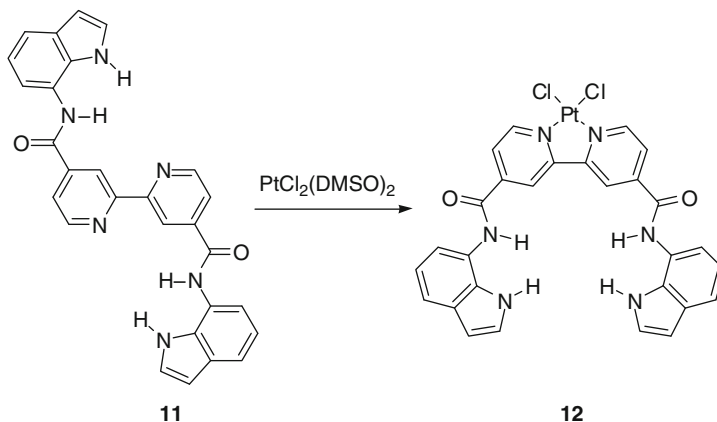
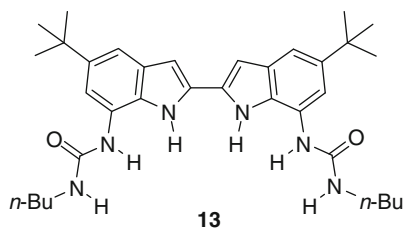


Fig. 5 Heteroditopic receptors **11** and **12** [16]

Pt (II) to the bipyridyl induced a conformational switch from an open ended structure (*s-trans*) to a convergent cleft (*s-cis*). Relative to **11**, the preorganized receptor **12** now displayed much increased affinities under identical conditions; dihydrogen phosphate ($K_a = 3,644 \text{ M}^{-1}$), benzoate (280 M^{-1}), acetate (189 M^{-1}), chloride (37 M^{-1}). The enhanced binding affinities of **12** are due to the higher degree of preorganization induced by Pt (II) coordination which locks the free rotation of the bipyridyl units. Unlike in solution, crystal structures of **11** showed 1:2 complexes with acetate and chloride, adopting the *s-trans* conformation where each of the bound anions was held by two hydrogen bonds to the indole and amide NHs (Fig. 5).

2.2 Indole–Urea Hybrids

The utility of urea in synthetic anion receptors stems directly from its ability to simultaneously donate two hydrogen bonds, and offers a hydrogen-bonding motif complementary to bidentate oxoanions (e.g., carboxylates) [17]. Combining urea and thiourea groups with indoles is therefore, a feasible strategy to further increase the number of NH donors in the binding cavity of an anion receptor.



In 2007, Jeong and coworkers reported receptor **13** containing a 2,2'-biindolyl scaffold and urea groups [18]. Receptor **13** has two indole NHs and four urea NHs,

and displayed strong binding affinities towards oxoanions such as acetate, dihydrogen phosphate and pyrophosphate in DMSO ($K_a = \sim 10^5 \text{ M}^{-1}$). According to ^1H NMR spectra, the two indole NHs and two inner urea NHs participated in hydrogen bonding with these oxoanions, but the two terminal urea NHs did not. On the other hand, all six NH protons in **13** were simultaneously involved in hydrogen bonding with alkyl dicarboxylates such as malonate, succinate, glutarate and adipate. **13** bound these dicarboxylates strongly in a highly polar medium 10% v/v MeOH/DMSO with association constants ranging from $1.6 \times 10^5 \text{ M}^{-1}$ (malonate) to $8.1 \times 10^5 \text{ M}^{-1}$ (adipate).

A series of anion receptors based on an indole scaffold functionalized with amide and urea in the 2- and 7-positions have been reported by the Gale group [19–22]. As a representative example, amide–urea hybrid **14** bears four hydrogen bond donors of two urea NHs, one indole NH and one amide NH. **14** binds oxoanions strongly such as acetate ($K_a = 10^4 \text{ M}^{-1}$), dihydrogen phosphate ($4,950 \text{ M}^{-1}$) and benzoate ($4,460 \text{ M}^{-1}$) in 0.5% $\text{H}_2\text{O}/\text{DMSO}$. ^1H NMR titrations caused large downfield shifts (>1 ppm, e.g., acetate) for all NHs of the indole, urea and amides. Titration curves showed that complexation induced shifts (CIS) for urea and indole NHs reached a plateau upon addition of 1 equivalent of an anion, but the amide NH signal continued to shift downfield when excess of an anion was added. Authors suggest that the amide NH points out of the binding cavity to accommodate further binding in the presence of excess anion. A crystal structure of complex **14**• TBA^+Cl^- supports this claim by showing one chloride anion tightly hydrogen bonded to the indole and urea NHs and a second bound to the amide NH out of the cavity (Fig. 6).

Gale and coworkers reported 1,3-diindolylureas **15**–**18** containing four convergent hydrogen bond donors; two indole NHs and two urea NHs [23]. According to ^1H NMR titrations, receptor **15** strongly bound oxoanions such as acetate, benzoate and dihydrogen phosphate with $K_a > 10^4 \text{ M}^{-1}$, but weakly bound chloride ($K_a = 128 \text{ M}^{-1}$) in 0.5% water/DMSO- d_6 . It was also observed that while receptors **15** and **16** formed 1:1 complexes with anions in solution, diverse stoichiometries were observed in the solid state. For example, crystallization of **15** in the presence of excess bicarbonate (HCO_3^-) provided the crystal structure of complex $(\text{15})_2 \cdot \text{CO}_3^{2-}$ in which carbonate, not bicarbonate, was held by two molecules of

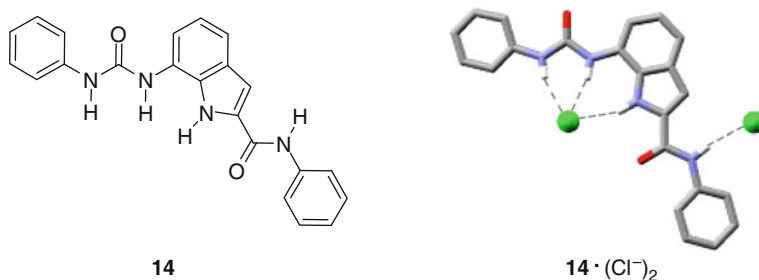


Fig. 6 Urea–amide hybrid **14** and its crystal structure with chloride [19–22]

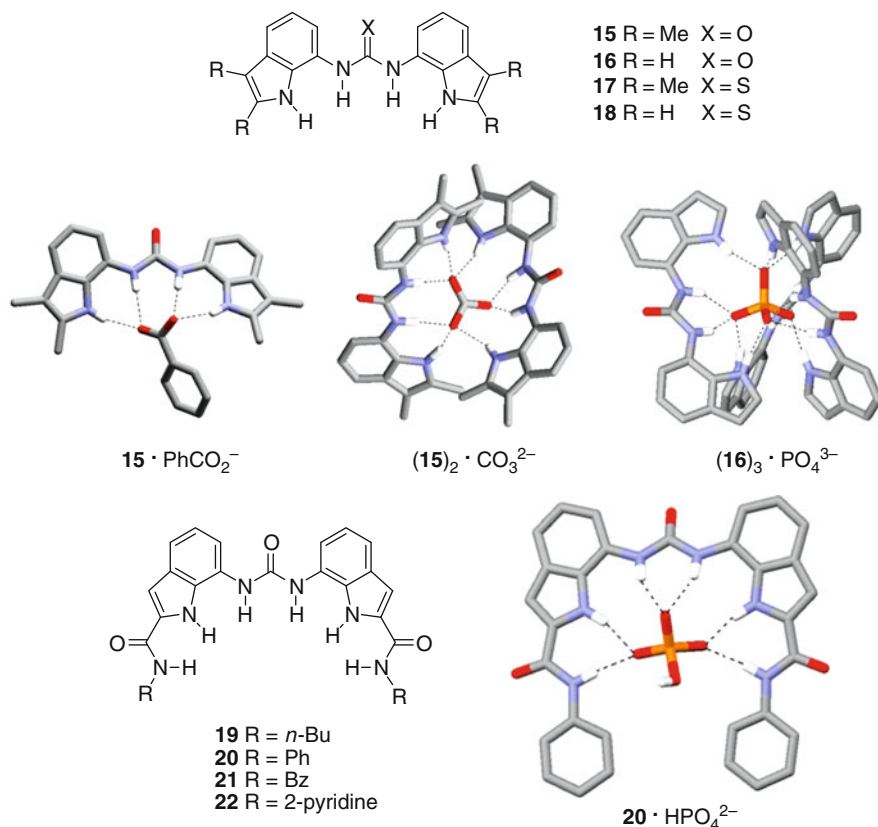


Fig. 7 Indole–urea hybrids **16–25** and X-ray crystal structures of their complexes with anions [23, 24]

15 with eight hydrogen bonds (Fig. 7). Furthermore, when receptor **16** was crystallized in the presence of excess dihydrogen phosphate (H₂PO₄⁻), the crystal contained a fully deprotonated phosphate (PO₄³⁻) which was complexed by three molecules of **16** stabilized by twelve hydrogen bonds. These results show that deprotonation occurs during crystallization as a result of increased acidity of the bound anion upon forming multiple hydrogen bonds.

The same group reported modified diindolylurea receptors **19–22** with additional amide groups at both ends [24]. These receptors bind oxoanions by six hydrogen bonds. The association constants (*K*_a) of **20** were >10⁴ M⁻¹ (BzO⁻, AcO⁻), 2,250 M⁻¹ (HCO₃⁻) and 107 M⁻¹ (H₂PO₄⁻) in 0.5% water/DMSO-*d*₆. As mentioned earlier, deprotonation of dihydrogen phosphate was observed during the crystallization with **20**, resulting in the formation of the monohydrogen phosphate complex. Again, multiple hydrogen bonding interactions with the bound oxoanion reduces its p*K*_a, resulting in proton transfer from the bound anion to the unbound

species in solution. These results parallel certain enzymatic behaviors, where biocatalytic transformations involving oxoanionic substrates are initiated upon significant increases in substrate acidity upon hydrogen bonding in the active site [25].

2.3 Carbazoles

Carbazole contains one hydrogen bond donor NH that is slightly more acidic than the indole NH. As a consequence, carbazole can serve as a suitable building block for synthetic anion receptors, as demonstrated for the first time by Jurczak and coworkers in 2004 [26]. They reported carbazole-based receptors **23** and **24** with amide functionalities that bind anions by three hydrogen bonds. ^1H NMR titrations of **23** yielded association constants: dihydrogen phosphate ($K_a = 1,910 \text{ M}^{-1}$) > benzoate ($1,230 \text{ M}^{-1}$) > chloride (13 M^{-1}) in 5% $\text{D}_2\text{O}/\text{DMSO-}d_6$. Relative to **23**, the aliphatic analog **24** unexpectedly displayed much larger association constants: dihydrogen phosphate ($19,800 \text{ M}^{-1}$), benzoate ($8,340 \text{ M}^{-1}$) and chloride (115 M^{-1}) under identical conditions. A X-ray crystal structure of complex **23**• Cl^- showed that chloride is held by three $\text{NH}\cdots\text{Cl}^-$ and by an aromatic $\text{CH}\cdots\text{Cl}^-$ hydrogen bond (Fig. 8).

Gale and coworkers reported dicarbazolyl urea **25** [27], analogous to the diindolyl ureas described in Sect. 2.2. Receptor **25** binds oxoanions via four $\text{NH}\cdots\text{O}^-$ hydrogen bonds, and shows comparable binding affinities with the diindolyl urea analogs **15** and **16**. The association constants (K_a) of **25** were determined to be $>10^4 \text{ M}^{-1}$ (acetate and bicarbonate), $5,670 \text{ M}^{-1}$ (benzoate) and 102 M^{-1} (chloride) in 0.5% water/DMSO. A crystal structure of complex **25**• PhCO_2^- clearly demonstrated four hydrogen bonds between benzoate and the carbazole and urea NHs (Fig. 9).

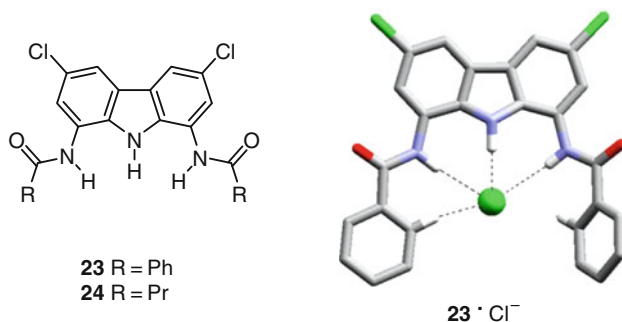


Fig. 8 Carbazole–amide hybrid **23** and **24** and a crystal structure of **23** with chloride [26]

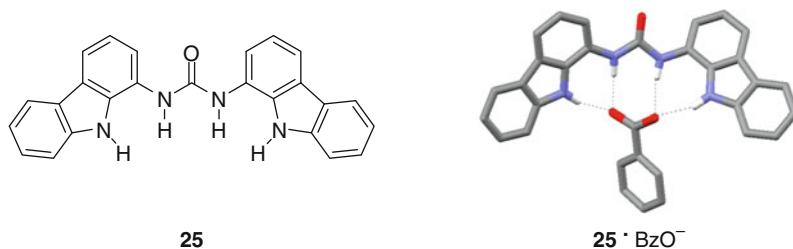


Fig. 9 A carbazole–urea hybrid **25** and its X-ray crystal structure with benzoate [27]

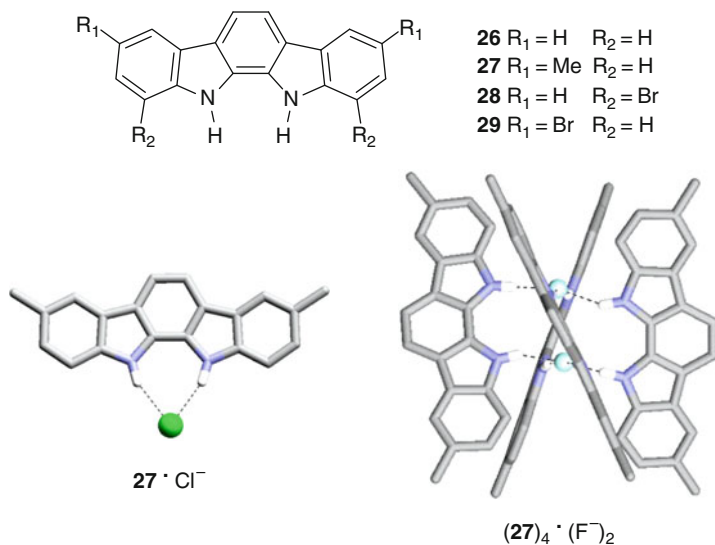


Fig. 10 Indolocarbazole receptors **26–29** and X-ray crystal structures of **27**·Cl⁻ and **(27)**₄·(F⁻)₂ [28]

2.4 Indolocarbazoles

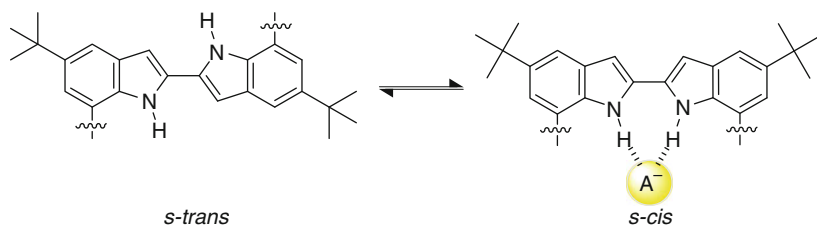
Indolocarbazoles contain two hydrogen bond donor NHs which are preorganized to simultaneously participate in hydrogen bonding with anions. As a result, the indolocarbazole scaffold has emerged as a useful building block for anion receptors (Fig. 10).

Indolocarbazoles were first utilized as anion receptors by Beer and coworkers in 2005 [28]. A series of synthetically feasible indolocarbazole derivatives **26–29** were prepared and their anion binding properties were described. As a representative example, **27** was shown to hydrogen bond to anions in the trend of PhCO₂⁻ (log K_a = 5.4 M⁻¹) > H₂PO₄⁻ (5.2) > F⁻ (4.7) > Cl⁻ (4.1) in acetone. Receptor **26** showed similar affinities, while **29** with bromo substituents displayed slightly

higher binding affinities in the same trend of PhCO_2^- ($\log K_a = 5.9 \text{ M}^{-1}$) > H_2PO_4^- (5.3) > F^- (5.0) > Cl^- (4.9) due to the electron-withdrawing effect. A crystal structure of $\mathbf{27}\cdot\text{Cl}^-$ demonstrates that the chloride ion is held by two equal hydrogen bonds with NHs. Additionally, an interesting crystal structure of a 2:1 complex between $\mathbf{27}$ and TBA^+F^- was obtained in which four indolocarbazole molecules self-assembled in a helical fashion around two fluoride anions by $\text{NH}\cdots\text{F}^-$ hydrogen bonds.

Jeong et al. prepared receptors $\mathbf{30}$ and $\mathbf{31}$ to reveal the effect of preorganization on anion binding affinities [29]. Owing to dipole–dipole repulsions, the biindole unit in $\mathbf{30}$ exists in an *s-trans* conformation. In the presence of an anion, however, the conformation switches to an *s-cis* enabling both NHs to simultaneously hydrogen bond to the same anion. On the contrary, two NHs in indolocarbazole receptor $\mathbf{31}$ are covalently locked to donate hydrogen bonds in the same direction. This difference was proven to have a large effect on the magnitude of the binding affinity (Fig. 11).

In detail, the binding constants K_a of receptor $\mathbf{30}$ were $1.4 \times 10^5 \text{ M}^{-1}$ (acetate), $5.1 \times 10^3 \text{ M}^{-1}$ (chloride), $2.1 \times 10^2 \text{ M}^{-1}$ (bromide), 77 M^{-1} (hydrogen sulfate) and 6 M^{-1} (iodide) in acetonitrile. Meanwhile, $\mathbf{31}$ displayed much higher binding affinities: $>2 \times 10^6 \text{ M}^{-1}$ (acetate), $1.1 \times 10^5 \text{ M}^{-1}$ (chloride), $8.7 \times 10^3 \text{ M}^{-1}$ (bromide), $2.1 \times 10^3 \text{ M}^{-1}$ (hydrogen sulfate) and $1.8 \times 10^2 \text{ M}^{-1}$ (iodide). It is evident that $\mathbf{31}$ binds anions 20–40 times more strongly than $\mathbf{30}$, corresponding to the additional stabilization of $\Delta\Delta G = \sim 2 \text{ kcal mol}^{-1}$.



Receptor $\mathbf{32}$, containing both hydrogen bond donors (NHs) and acceptors (pyridyl nitrogen), was prepared for selective binding of dihydrogen phosphate [30]. The association constant (K_a) of $\mathbf{32}$ with H_2PO_4^- was determined to be $1.1 \times 10^5 \text{ M}^{-1}$ in CH_3CN which is higher than those obtained with other anions: $2.2 \times 10^4 \text{ M}^{-1}$ (AcO^-), $5.0 \times 10^3 \text{ M}^{-1}$ (Cl^-), $2.1 \times 10^3 \text{ M}^{-1}$ (CN^-), $1.6 \times 10^3 \text{ M}^{-1}$ (HSO_4^-), $5.6 \times 10^2 \text{ M}^{-1}$ (Br^-) and 40 M^{-1} (I^-). Authors explain that the high binding affinity for dihydrogen phosphate stems from two additional hydrogen bonds between the pyridyl nitrogens and the hydroxyl groups of dihydrogen phosphate. Using reference molecules without pyridyl moieties, these hydrogen bonds were proven to additionally stabilize the complex by $\Delta\Delta G = \sim 3.2 \text{ kcal mol}^{-1}$.

In addition to NHs, the hydroxyl groups of serine, tyrosine, and threonine have also been found to participate in anion binding in biological systems. Examples include phosphate-binding protein [31, 32] and a CIC chloride channel [33, 34].

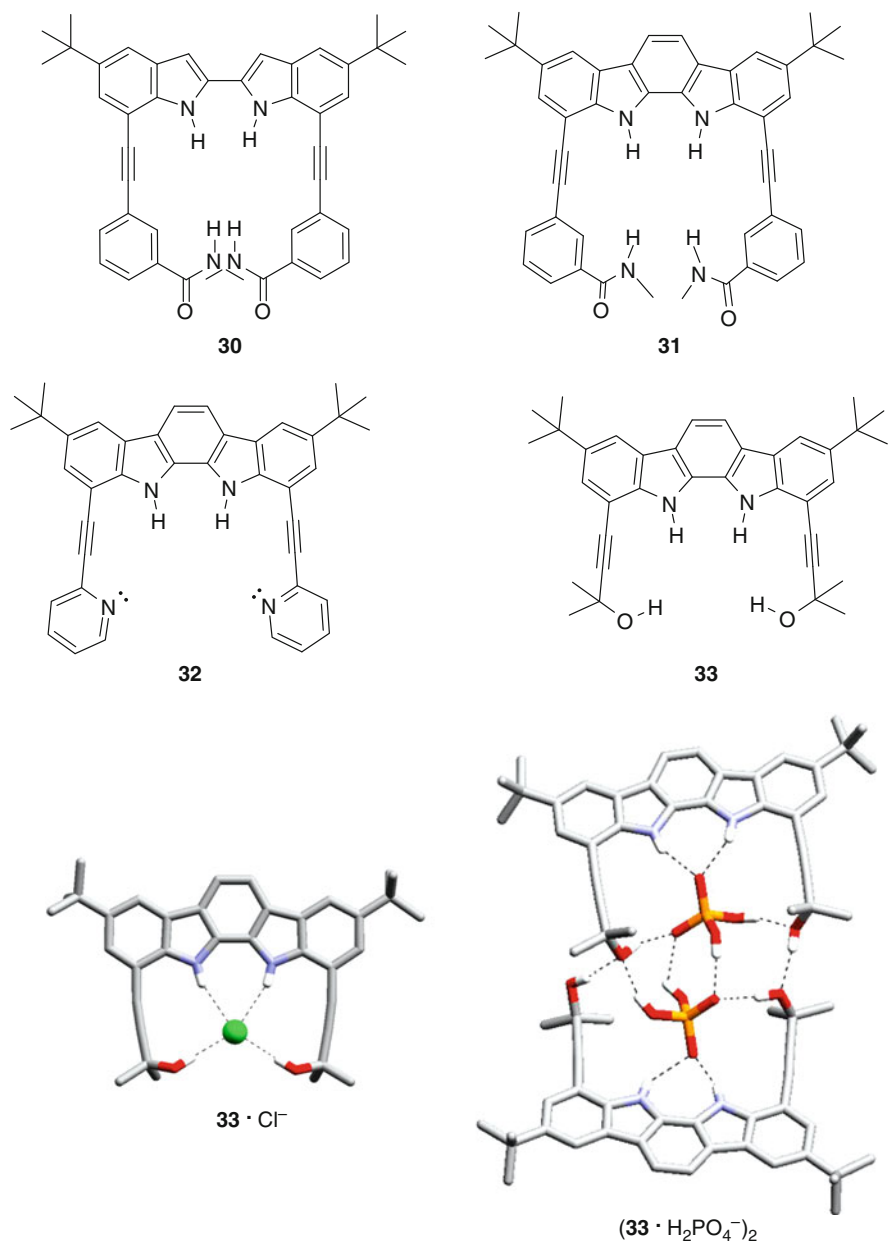


Fig. 11 Indolocarbazole-based clefts as anion receptors **30–33** and X-ray crystal structures of **33·Cl⁻** and **(33·H₂PO₄⁻)₂** [29–30]

However, only limited examples of synthetic anion receptors have been described that utilize the hydroxyl group in anion binding. Jeong et al. prepared receptor **33**

containing two NH and two OH groups [35]. It was demonstrated in two crystal structures that two hydroxyl groups were involved in hydrogen bonding with chloride and hydrogen phosphate. In the solid state, **33** formed a 1:1 complex with chloride, while a 2:2 complex with dihydrogen phosphate was observed. Two hydroxyl groups in **33** were measured to greatly increase the binding affinities towards anions by forming two additional hydrogen bonds, stabilizing the complex up to $\Delta\Delta G = \sim 5 \text{ kcal mol}^{-1}$ in 1% $\text{H}_2\text{O}/\text{CH}_3\text{CN}$.

2.5 Others

Beer et al. employed indolocarbazole **26** in creating an anion-templated pseudorotaxane **34** [36]. The sulfate anion is dianionic and tetrahedral and has been known to form multiple hydrogen bonds. For example, sulfate is effectively bound by two molecules of **26**, as demonstrated in the crystal structure of complex **34**, which shows each of the two indolocarbazoles binding one pair of oxygen atoms of sulfate. By replacing one of the indolocarbazoles with isophthalamide-containing crown ether, a pseudorotaxane type complex **34** self-assembled upon hydrogen bonding to sulfate (Fig. 12).

Indole based tripodal receptors were reported by Ito and coworkers in 2007 [37]. Triindolylmethane **35** contains three indolyl NHs suitably positioned to collectively hydrogen bond to anions. **35** was shown to possess a binding selectivity for chloride in CDCl_3 ($K_a = 1,200 \text{ M}^{-1}$) over other anions tested: Br^- (105 M^{-1}), I^- (27 M^{-1}), HSO_4^- (34 M^{-1}) and NO_3^- (36 M^{-1}). Authors claimed the selectivity for chloride is due to a complementary size of the binding pocket for chloride over other larger anions.

Browning et al. reported anion binding properties of **36**, a C_3 -symmetric phosphine with three indolyl substituents [38]. Receptor **36** was designed to form three hydrogen bonds with anions and the phosphine core was able to coordinate to transitional metals. ^1H NMR spectroscopy titrations in CD_2Cl_2 yielded association constants (K_a): $3,920 \text{ M}^{-1}$ (Cl^-), $2,730 \text{ M}^{-1}$ (AcO^-), 320 M^{-1} (Br^-) and 150 M^{-1} (BF_4^-). Crystal structures of complex **36**• F^- demonstrated a 1:1 binding stoichiometry by three $\text{NH}\cdots\text{F}^-$ hydrogen bonds. Authors also reported a crystal structure of a **36** (as a copper–phenanthroline complex) with BF_4^- . Despite the weak hydrogen bonding nature of BF_4^- in solution [40], the crystal structure shows that upon coordination to Cu(I), three fluorides of BF_4^- can form hydrogen bonds with each of the three indolyl NHs in the receptor.

Jang and coworkers prepared a ditopic receptor **37** that possessed a biindolyl core and Zn porphyrin arms. The biindolyl unit served as an anion binding site while the porphyrin units allowed for the coordination of neutral ligands, e.g., 1,4-diazabicyclo[2.2.2]octane (DABCO) [39]. Receptor **37** bound a chloride ion with an association constant (K_a) of $4.93 \times 10^4 \text{ M}^{-1}$ in THF, which was enhanced in the presence of DABCO (1 equiv) to $7.10 \times 10^5 \text{ M}^{-1}$. Likewise, the presence of chloride (1 equiv) also increased the binding affinity of **37** with DABCO from

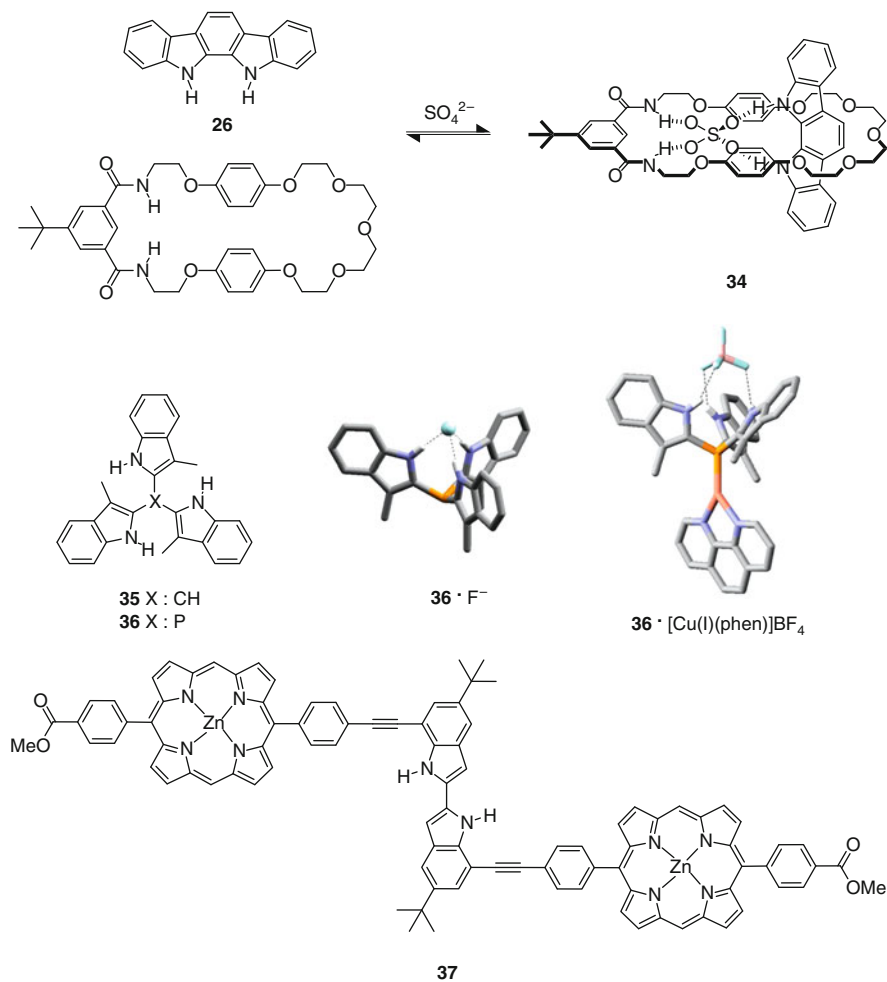


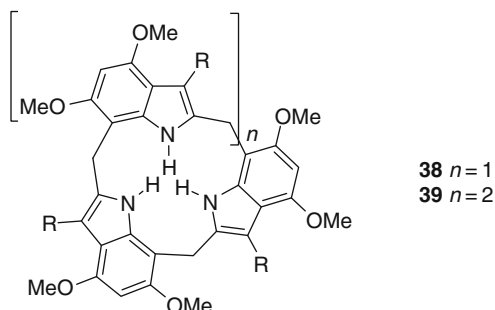
Fig. 12 Sulfate-templated pseudorotaxane **34**, tripodal indoles **35** and **36**, and crystal structures of **36** complexed with anions, and a ditopic receptor **37** [36–39]

$K_a = 2.02 \times 10^6 \text{ M}^{-1}$ to $2.48 \times 10^7 \text{ M}^{-1}$ in THF. The results clearly prove allosteric binding events with positive cooperativity.

3 Macrocycles

Macrocycles have been extensively studied as synthetic receptors for a variety of molecular and ionic guests despite their synthetic challenge. In particular, macrocycles that function as anion receptors typically possess a well-defined cavity in which multiple NH hydrogen bond donors are presented in a convergent manner.

While a large number of cyclic oligopyrroles such as calix[n]pyrrole and sapphyrins have been reported [41], indole based macrocycles are extremely rare. Although not studied as anion receptors, Black and coworkers first reported the synthesis of calix[n]indoles **38** and **39**, macrocycles comprising three or four indole rings connected by methylene groups [42, 43].



3.1 Anion Receptors

Jeong and coworkers reported macrocycles **40** and **41** in which two indolocarbazoles were connected by linear ethynyl and butadiynyl bridges [44, 45]. Each macrocycle possesses a rigid, planar cavity with four NHs that converge to form strong hydrogen bonds with anions. Macrocycle **40** contains a small cavity with the dimension of $2.6 \text{ \AA} \times 2.6 \text{ \AA}$ between NH protons, to which only a single atoms of small ionic radius (e.g., F^- , O^-) can coordinate. This is evident in the crystal structure of complex **40**• $\text{Bu}_4\text{N}^+\text{Cl}^-$ where chloride is held by four $\text{NH}\cdots\text{Cl}^-$ hydrogen bonds and sits above the cavity, but is not inserted due to the limited space for the large chloride ion. It is worthwhile noting that tetrabutylammonium is placed on the aromatic surface near the bound chloride ion owing to cation- π and electrostatic interactions. The association constants (K_a) of **40** with halides were determined to be in the order of F^- ($5.6 \times 10^8 \text{ M}^{-1}$) > Cl^- ($2.1 \times 10^6 \text{ M}^{-1}$) \gg Br^- ($1.9 \times 10^3 \text{ M}^{-1}$) > I^- ($3.0 \times 10^2 \text{ M}^{-1}$) in acetonitrile. **40** also showed strong binding to polyatomic anions: AcO^- ($6.5 \times 10^6 \text{ M}^{-1}$) > H_2PO_4^- ($3.2 \times 10^6 \text{ M}^{-1}$) > N_3^- ($9.1 \times 10^5 \text{ M}^{-1}$) > HSO_4^- ($6.8 \times 10^5 \text{ M}^{-1}$) > NO_3^- ($3.9 \times 10^5 \text{ M}^{-1}$) > CN^- ($7.5 \times 10^4 \text{ M}^{-1}$) in same solvent. The ^1H NMR spectra showed two interesting features; first, anion induced changes ($\Delta\delta$) in chemical shifts of the NH signals correlated linearly to the binding affinities. Secondly, two sets of the ^1H NMR signals were observed when less than 1 equivalent of an anion was added at room temperature due to slow exchange between free macrocycle and its complex on the ^1H NMR (500 MHz) time scale.

Compared to **40**, macrocycle **41** contains a larger cavity ($2.6 \text{ \AA} \times 5.1 \text{ \AA}$) and can accommodate more than one atom simultaneously. The crystal structure of complex **41**• $\text{Bu}_4\text{N}^+\text{N}_3^-$ clearly shows both end nitrogen atoms of the azide simultaneously bound within the cavity in a bridged manner, each forming two hydrogen bonds. In contrast, the crystal structure of complex **40**• $\text{Bu}_4\text{N}^+\text{N}_3^-$ displays that only

one nitrogen atom is coordinated to the cavity. This structural difference between **40** and **41** was manifested in their relative binding affinities with anions. According to UV/Vis titration experiments, **41** formed more stable complexes with polyatomic anions such as azide and oxoanions in 10% v/v methanol/acetone. For example, the association constants (K_a) of **40** and **41** were determined to be 2,300 and 81,000 M^{-1} for azide, 4,300 and 2,20,000 M^{-1} for dihydrogen phosphate, 94 and 15,000 M^{-1} for nitrate, and 81 and 13,000 M^{-1} for hydrogen sulfate. These results prove that for polyatomic anions, a bridged (end-to-end) hydrogen bonding mode like in $41 \cdot N_3^-$ is more stable than an end-on mode as seen in $40 \cdot N_3^-$, despite forming the same number of hydrogen bonds (Fig. 13).

Sessler et al. reported a pyrrole–carbazole hybrid macrocycle **42** in which two carbazole moieties were incorporated into a previously studied calix[4]pyrrole [46] to create an extended binding cavity containing six hydrogen bond donor NHs [47]. A crystal structure of $42 \cdot PhCO_2^-$ revealed that binding of benzoate occurred primarily from the four pyrrolic NH groups resulting in a folded, “wing-like” conformation of the macrocycle. Association constants (K_a) in dichloromethane were determined for acetate ($2.3 \times 10^5 M^{-1}$), benzoate ($7.7 \times 10^4 M^{-1}$), oxalate ($3.1 \times 10^4 M^{-1}$), succinate ($9.5 \times 10^3 M^{-1}$), dihydrogen phosphate ($7.2 \times 10^4 M^{-1}$) and chloride ($3.5 \times 10^4 M^{-1}$). Authors suggested that the contribution from the carbazole NHs was minor as the groups are not oriented in plane with the oxygens of benzoate (Fig. 14).

3.2 Ion Pair Receptor

Jeong et al. also reported an ion pair receptor **43** containing both cation- and anion-binding sites [48]. By attaching a diazacrown unit to an indolocarbazole scaffold, two heterotopic binding sites are placed in close proximity, able to form a contact ion pair which is crucial to minimize unfavorable energy required for charge separation. In a polar medium (10% v/v DMSO/ CD_3CN), receptor **43** weakly binds chloride with an association constant (K_a) of 7 M^{-1} . However, the binding affinity significantly increased in the presence of an alkali metal cation. For example, addition of 1 equivalent of Li^+ , Na^+ and K^+ yielded association constants of 120 M^{-1} , 14,000 M^{-1} and 6,200 M^{-1} , respectively. Sodium ion showed the largest enhancement (2,000-fold), attributed to favorable electrostatic interactions between the bound halide and alkali metal cation (Fig. 15).

4 Acyclic Oligomers

The use of oligomers in anion recognition is closely related to the field of foldamer research. Foldamers are synthetic molecules in which noncovalent forces guide the folding into ordered secondary structures such as α -helices and β -turns [49–51]. Foldamers have recently been developed as novel receptors for molecules and ions

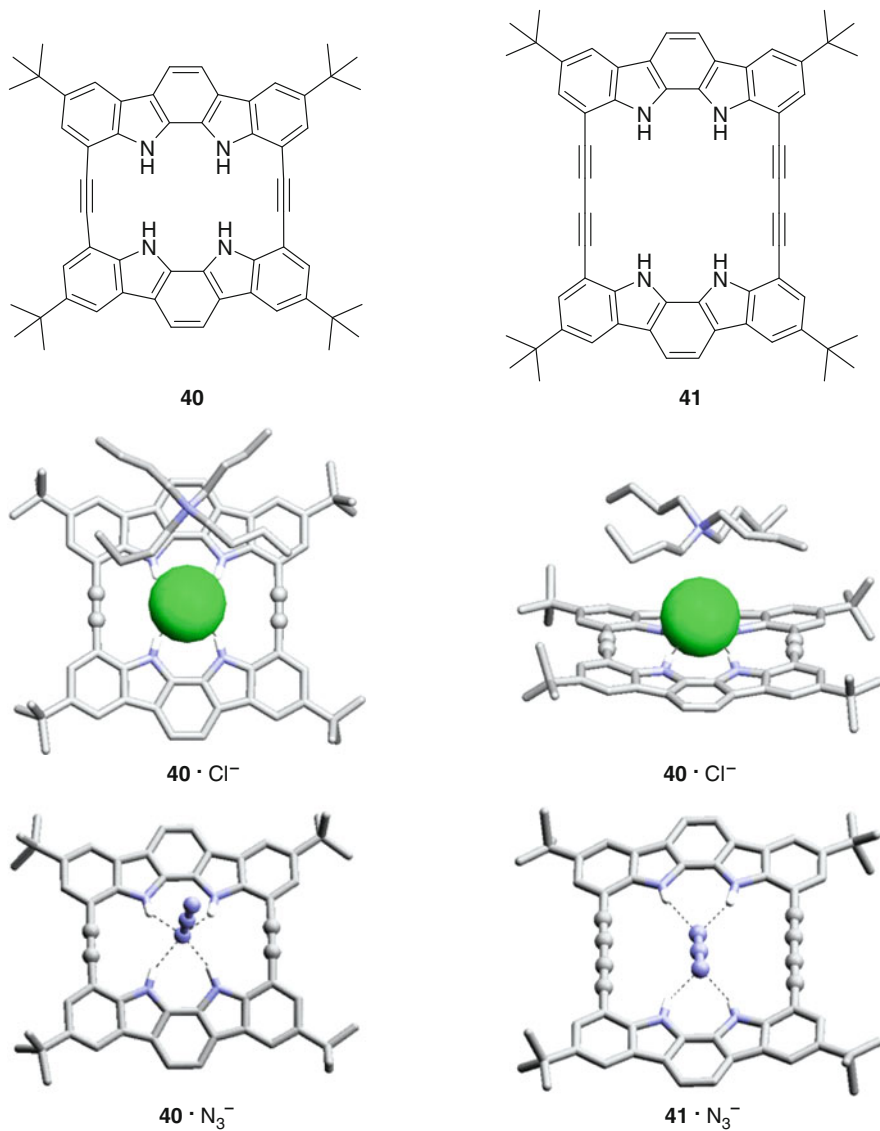


Fig. 13 Indolocarbazole-based macrocycles **40**, **41** and top and side views of X-ray crystal structures of **40**·Cl⁻, and X-ray crystal structures of **40** and **41** with N₃⁻ [44, 45]

as folding often results in a helical cavity which is isolated from the outer environment [52]. Anion binding foldamers are created by synthetic extension of monomer units containing hydrogen bond donor groups into longer oligomeric strands. Jeong's group, in particular, has reported examples of indole based foldamers used as anion receptors.

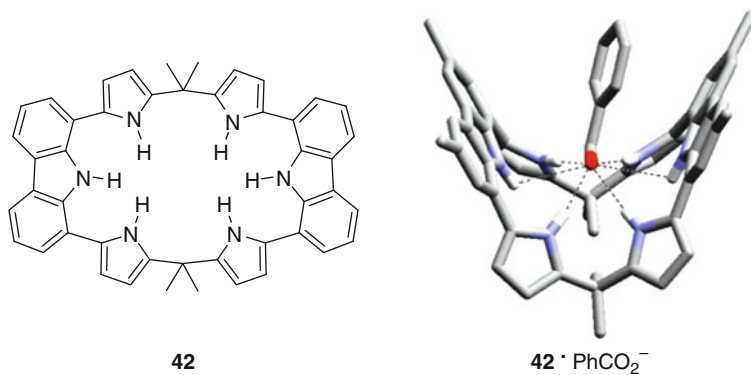


Fig. 14 Carbazole-pyrrole hybrid macrocycle **42** and its crystal structure with benzoate [47]

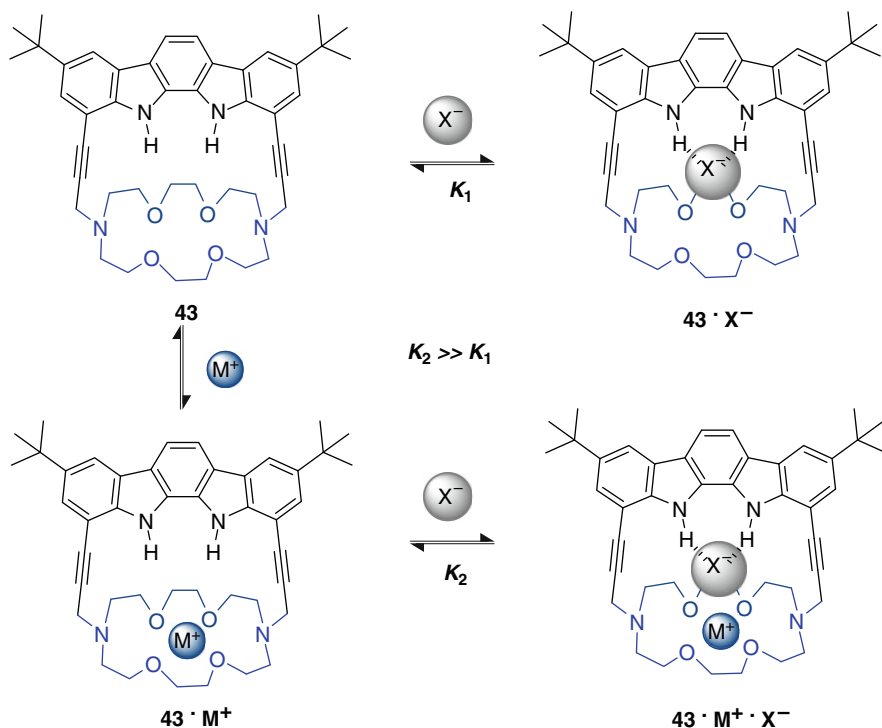


Fig. 15 Indolocarbazole-based macrocycle **43** as an ion pair receptor [48]

4.1 Oligoindoles

Anion binding by oligoindoles **44–46** was first reported in 2005 [53]. Synthetic extension of indole monomers by sequential Sonogashira coupling reactions result

in oligomeric strands containing multiple indole donor NH groups. The oligoindoles exist in an extended stair-like conformation in the absence of anion where the biindole unit maintains an *s-trans* conformation to minimize dipole–dipole repulsion as previously discussed in the Sect. 2.4. However, upon addition of tetrabutylammonium chloride, the biindoles adopt an *s-cis* conformation enabling the indole NH protons to simultaneously participate in hydrogen bonding with chloride. In turn, the oligoindoles fold into helical structures with one turn comprising four indole rings, proved by ^1H NMR spectroscopy. The association constants between oligoindoles and tetrabutylammonium chloride were $1.3 \times 10^5 \text{ M}^{-1}$ for **44**, $1.2 \times 10^6 \text{ M}^{-1}$ for **45**, and $>10^7 \text{ M}^{-1}$ for **46**. In a more competitive medium for hydrogen bonding (10% v/v $\text{H}_2\text{O}/\text{CH}_3\text{CN}$), the association constants were determined to be 210 M^{-1} and $23,000 \text{ M}^{-1}$ for **45** and **46**, respectively. The binding affinities greatly increased with longer chain lengths of the oligomers, supporting the formation of helical complexes (Fig. 16).

Authors found that the fluorescent properties of the oligoindoles were strongly dependant on the nature of the terminal groups; an oligoindole **47** containing benzoate termini was the most fluorescent [54]. Addition of an anion led to dramatic hypochromic and bathochromic shifts ($\Delta\lambda$ up to 65 nm) of the emission band, changing the solution color from bright blue to dim bluish green. The authors rationalized this effect as excimer formation between the π -stacked aromatic planes in a helical conformation. Fluorescence titrations afforded the association constants with moderate selectivity in the range of 10^3 – 10^6 M^{-1} for anions ($\text{I}^- \approx \text{NO}_3^- < \text{Br}^- < \text{AcO}^- < \text{N}_3^- \approx \text{CN}^- < \text{Cl}^- < \text{F}^-$) in 20% v/v $\text{MeOH}/\text{CH}_2\text{Cl}_2$.

Oligoindoles **44–47** possess no chiral component and therefore fold to give a racemic mixture of right- and left-handed helices in the presence of an anion [55, 56]. In order to induce the preferential formation of one particular helix, a chiral oligoindole **48** capped with 1-(*S*)-phenylethylamido units was synthesized. Circular dichroism (CD) spectroscopy of **48** alone displayed no appreciable Cotton effect. Addition of tetrabutylammonium chloride, however, led to strong induced CD signals in CH_2Cl_2 , which gradually intensified and saturated upon addition of approximately 1 equivalent of chloride. The association constant between **48** and tetrabutylammonium chloride ion was determined to be $2.9 \times 10^5 \text{ M}^{-1}$ in 1% v/v $\text{MeOH}/\text{CH}_2\text{Cl}_2$. Finally, the enantiomer of **48** with 1-(*R*)-phenylethylamido units showed the same CD behaviors but the opposite Cotton effect. These results demonstrate that anion binding can induce the preferential formation of one racemic helix over another.

4.2 Oligoindolocarbazoles

Hydrogen bonding between synthetic receptors and molecular/ionic guests in water is almost negligible owing to strong competition with solvent molecules. In general, synthetic anion receptors employing hydrogen bonds bind anions strongly in organic solvents but not in water. However, proteins utilize hydrogen bonds to

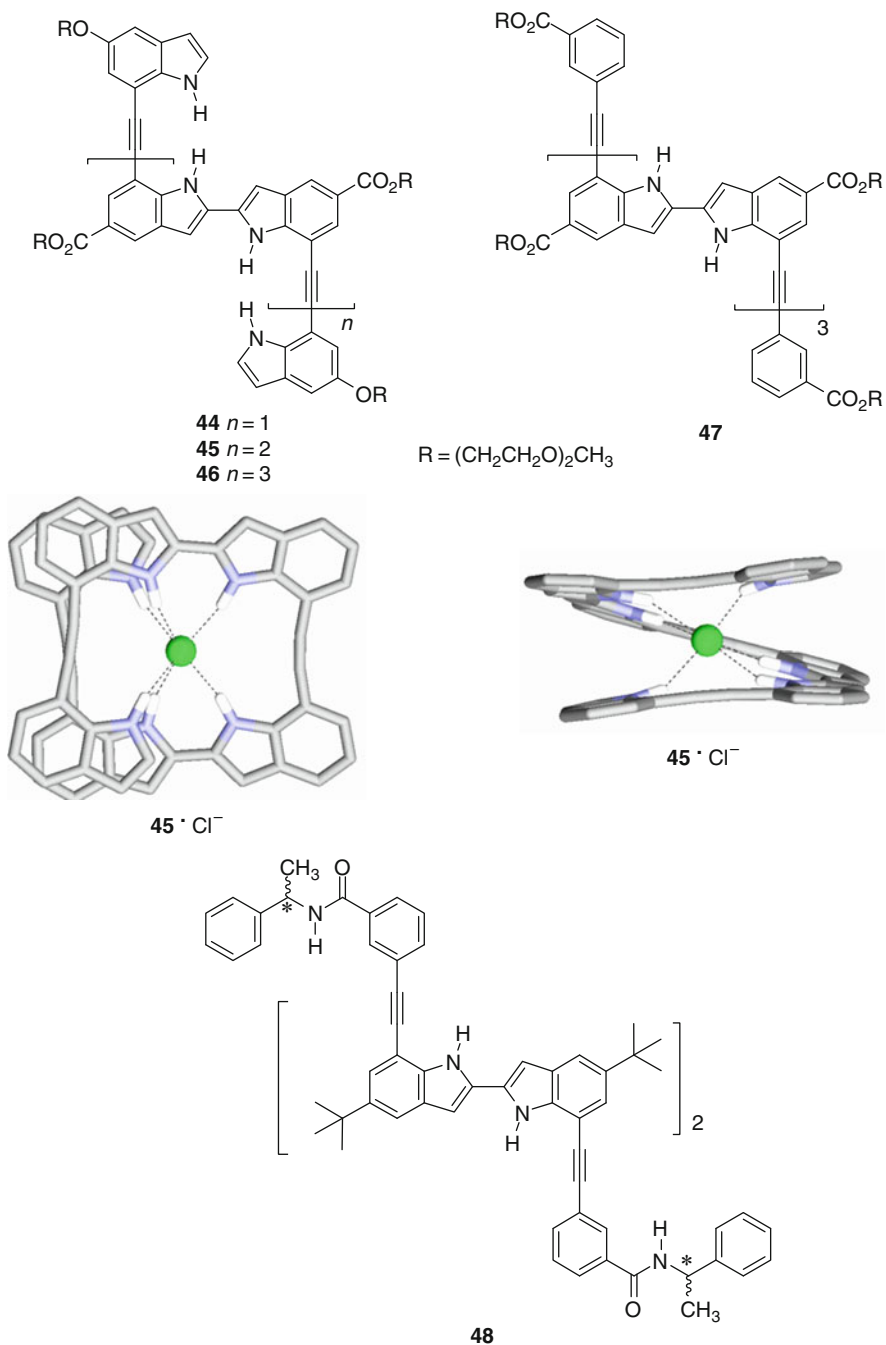


Fig. 16 Oligoindoles **44–48** and top and side views of an energy-minimized structure of complex **45** $\cdot\text{Cl}^-$ (side chains of diethylene glycol esters and ethers are replaced with hydrogen atoms) [53–56]

bind anions efficiently in water. A plausible explanation is that the binding site is surrounded by hydrophobic organic fragments, and in part segregated from bulk water, thus rendering an organic solvent-like microenvironment.

Oligo(indolocarbazole) **49** was designed to encapsulate anions in water by hydrogen bonds, similar to proteins [57]. Oligomer **49** is soluble in water under basic conditions and folds into a helical conformation to generate an internal cavity surrounded by six NH protons. The ^1H NMR spectrum of **49** changes noticeably upon addition of sodium fluoride, chloride, and bromide, but no change was observed with sodium iodide and perchlorate. The association constants of **49** with sodium fluoride, chloride, and bromide were determined to be 46, 65, and 19 M^{-1} , respectively. Lithium, sodium and potassium chloride afforded an identical association constant, implying no cation effect. Moreover, binding affinities between a methyl ester derivative of **49** and halides decreased in the order of F^- ($1,83,000 \text{ M}^{-1}$) > Cl^- ($36,800 \text{ M}^{-1}$) > Br^- ($1,350 \text{ M}^{-1}$) > I^- (86 M^{-1}) in an organic medium, 4:1 v/v DMSO/MeOH. As demonstrated here, fluoride binds more strongly than chloride in an organic medium, but less strongly in water. Authors rationalized this difference by the solvation energy; the fluoride ion solvates much more strongly in water than the chloride ion does, which reduces net binding energy (Fig. 17).

5 Molecular Sensors

Molecular sensors that yield distinct color or fluorescence changes upon anion binding are extremely useful in that they allow for naked-eye detection of analytes. These features are advantageous for prompt, qualitative detection of anionic analytes that are toxic (e.g., pertechnetate, fluoride), or that may cause environmental pollution (e.g., nitrate, phosphate). Molecular sensors in general consist of binding and signaling sites [58]. Upon binding, chromophores or fluorophores in the signaling units are electronically perturbed which typically results in a color or fluorescence change. In this regard, a number of indole-based molecular sensors have been prepared. Furthermore, the acidity of the indole NH can result in deprotonation by basic anions (e.g., fluoride, carboxylate) that also induce distinct color changes.

5.1 Indole-Based Sensors

Shao and coworkers have reported an oxidized bis(indolyl)methane **50**; a simple chromophore containing an acidic hydrogen bond donor moiety and a basic hydrogen bond acceptor moiety [59]. Deprotonation of the indole NH by basic anions induced a color change. For example, deprotonation by fluoride in acetonitrile led to a color change from yellow to red. Protonation of the basic indole component also resulted in a color change. Addition of acidic HSO_4^- to a 4:1 v/v $\text{CH}_3\text{CN}/\text{H}_2\text{O}$

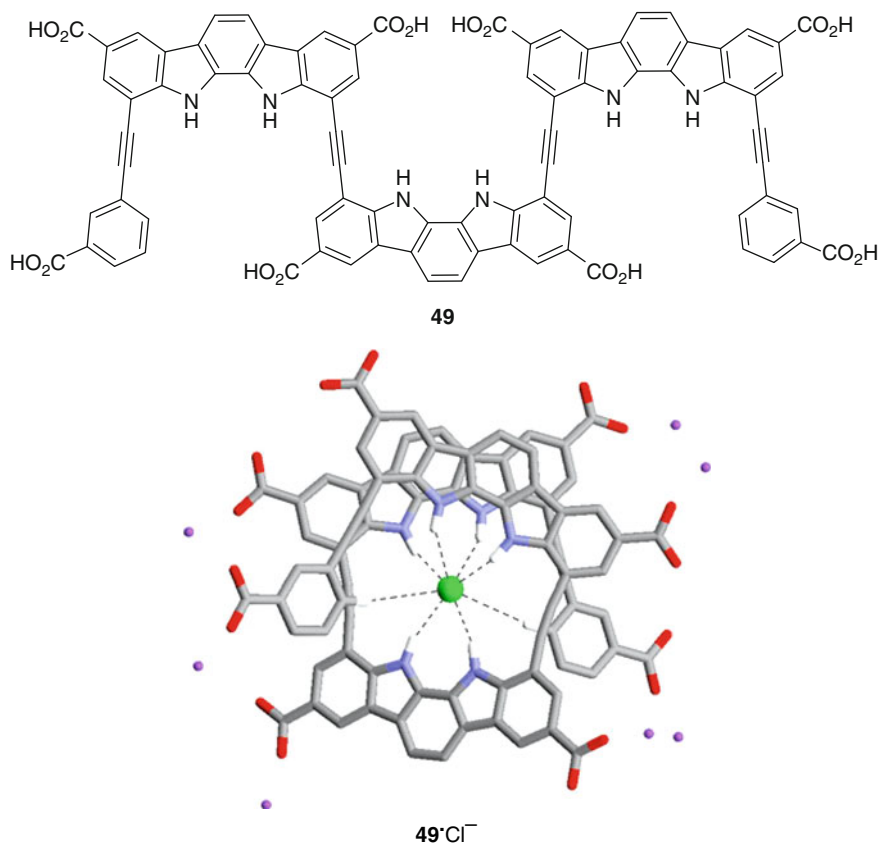


Fig. 17 Indolocarbazole oligomer **49** and an energy-minimized structure of its complex with chloride [57]

solution of **50** caused a color change from yellow to pink by protonation. This molecule was shown to act as a selective colorimetric sensor either for F⁻ in aprotic solvents or for HSO₄⁻ and other weakly acidic species in water-containing solvents.

Pfeffer et al. developed anion sensors by tethering indole to urea or thiourea groups [60]. The indole and urea NHs of **51** and **52** were deprotonated by fluoride, evident by disappearance of the corresponding proton resonances after the addition of 1.2 equivalents of fluoride during ¹H NMR titration. Importantly, addition of fluoride to **53** induced a visible color change from colorless to yellow–orange by deprotonation of the NH protons. The association constants (*K*_a) of these receptors with chloride, acetate and dihydrogen phosphate were determined to be in the range of 10²–10⁴ M⁻¹ in DMSO.

Pyrene derivatized indoles **54** and **55** were studied by Fang, Chou and coworkers as selective molecular sensors for the fluoride ion [61]. In DMSO, a visible color change from colorless to green was observed only upon titration with fluoride and corresponding absorption spectra confirmed that only fluoride causes a spectral

change. A characteristic new band appearing in the visible region was attributed to extended π -conjugation in **54**⁻, formed by deprotonation by fluoride. Similarly, a color change (greenish-yellow to bright red) was only noticed upon the addition of F⁻ to a DMSO solution of **55** (Fig. 18).

Lin and coworkers reported phenylhydrazone-indole based receptors **56** and **57** as molecular sensors for acetate [62, 63]. **56** and **57** were shown to bind to acetate with good selectivity in DMSO solution. Furthermore, a visible color change from orange to purple was observed, presumably due to the transformation of the indolehydrazone form to the azo form upon hydrogen bonding to acetate.

The Sessler group synthesized and studied the anion binding properties of 2,3-diindol-3-yl quinoxalines (DIPs) **60** and **61** [64]. The molecules displayed anion binding properties that follow the trend: H₂PO₄⁻ \gg F⁻ > BzO⁻ > Cl⁻ > HSO₄⁻. Importantly, distinct color changes were seen upon the addition of fluoride and dihydrogen phosphate; dichloromethane solutions turn from yellow to brown (F⁻) and orange (H₂PO₄⁻) upon the addition of 10 equivalents of the anions. The high selectivity for dihydrogen phosphate ($K_a = 20,000 \text{ M}^{-1}$ in dichloromethane) shown by **61** is in contrast to the previously studied and structurally related 2,3-dipyrrol-2-yl quinoxalines [67] that demonstrated a significantly lower affinity for the dihydrogen phosphate ($K_a = 80 \text{ M}^{-1}$).

Analogous versions of DIPs were investigated by Yan and coworkers [65]. The species **62** and **63** showed high affinities for basic anions such as fluoride, acetate and dihydrogen phosphate in DMSO. In addition, the receptors were also shown to operate as colorimetric sensors for optical detection of fluoride and acetate. For example, addition of excess fluoride to a DMSO solution of **62** induces a color change from yellow to orange. Similarly, addition of fluoride and acetate to **63** both induced color changes from bright yellow to gray.

For selective detection of fluoride ion, Shiraishi and coworkers prepared 1,4-bis(3-indolyl)-2,3-diaza-1,3-butadiene **64** by a one-step condensation of indole-3-carbaldehyde and hydrazine [66]. Addition of F⁻ to a DMSO solution of **64** induced fluorescence change from colorless (0 equiv) to bright green (30 equiv) as well as a color change to yellow (50 equiv). Negligible changes in the UV/Vis and fluorescence spectra were observed with other anions (Cl⁻, Br⁻, I⁻, AcO⁻, ClO₄⁻, H₂PO₄⁻, HSO₄⁻, NO₃⁻, and SCN⁻), implying that compound **64** functions as a colorimetric and fluorometric probe for selective fluoride ion sensing.

5.2 Carbazole-Based Sensors

Amendola and coworkers have reported a pyridium-carbazole-based trifurcate receptor **65** that formed 1:1 complexes with oxoanions and halides in acetonitrile [68]. Spectrophotometric and ¹H NMR experiments described selective recognition of chloride (log $K_a > 7$) even in the presence of fluoride and bromide. Addition of excess of anions of higher basicity (F⁻ and AcO⁻) caused deprotonation of the NHs which induced a color change to bright yellow.

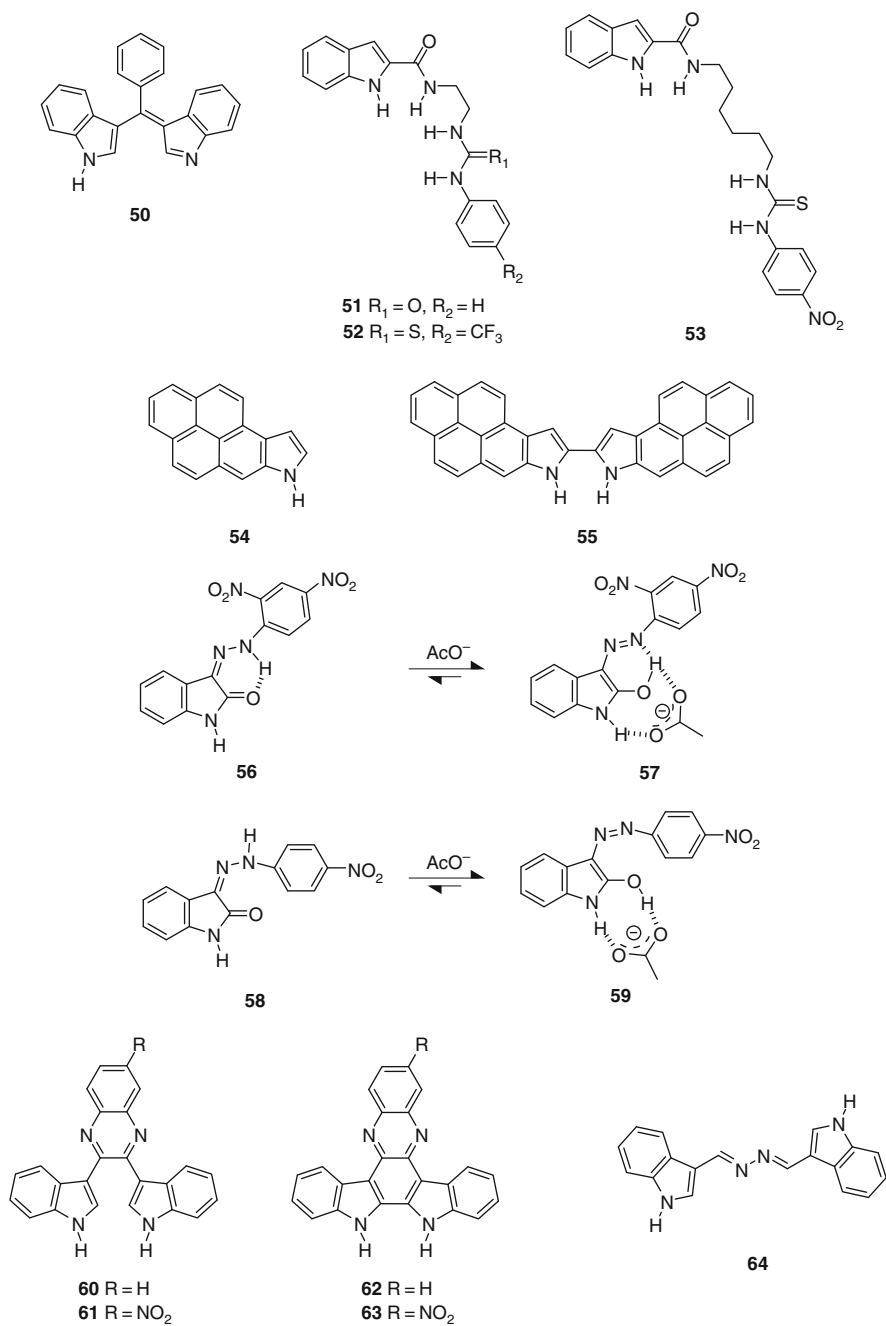


Fig. 18 Indole- and related heterocycle-based molecular sensors **50–64** [59–66]

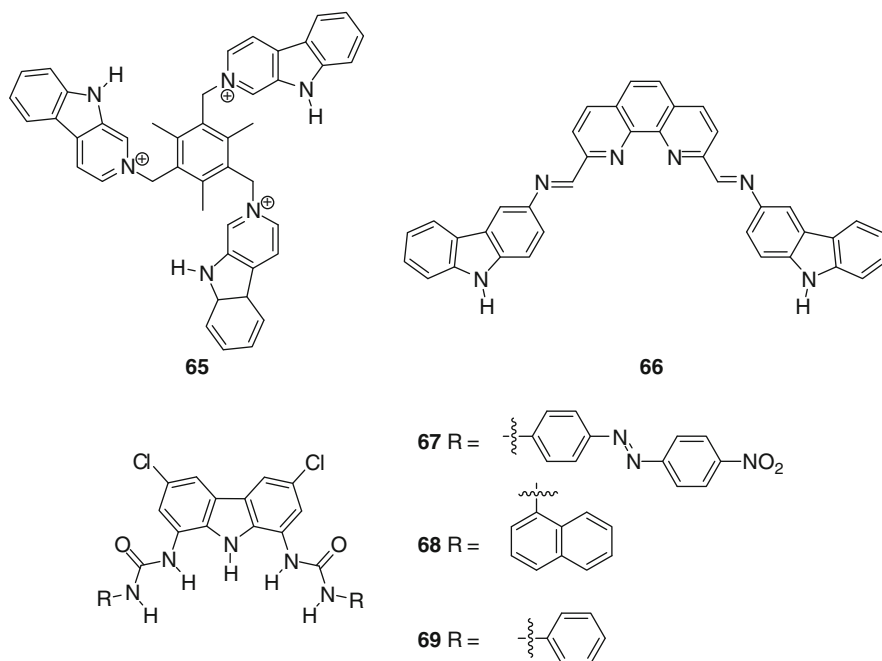


Fig. 19 Carbazole-based molecular sensors **65–69** [68–70]

A carbazole–phenanthroline based anion receptor **66** was reported by Lin et al. in which two carbazole groups were attached to a phenanthroline core by imine linkages [69]. ^1H NMR and UV/Vis titration experiments demonstrated a high selectivity for iodide ($K_a = 5 \times 10^4 \text{ M}^{-1}$) while not having any affinity for other halides. Authors attributed this selectivity to a complementary fit of the large anion.

Carbazole was also utilized by Kim and coworkers in developing fluorescent receptors **67–69** [70]. These compounds were demonstrated to function as “dual-channel” anion sensors, displaying both a colorimetric and fluorescent output upon anion binding. By linking urea moieties to the carbazole scaffold, the molecular sensors were synthesized having both chromogenic and fluorogenic signaling subunits. By plotting fluorescence intensity vs. absorption shift of the UV/Vis spectrum in the presence of many anions, diverse sets of anions could be identified as each signaling subunit demonstrated a different optical response upon binding to a specific anion (Fig. 19).

6 Conclusions

In the last five years, the anion binding ability of indoles and related heterocycles has been realized. Structurally diverse anion receptors based on indoles, carbazoles, and indolocarbazoles have been reported, attributed to the hydrogen bonding donor

ability of their NHs. Molecular clefts are a good starting point to validate the utility of these heterocycles in anion binding. Often, linking multiple indoles by other NH donor groups offers stronger binding to anions. Indoles have also been incorporated into preorganized macrocycles containing cavities of fixed sizes where hydrogen bonding from convergent NHs results in specificity towards complementary anions. Furthermore, acyclic oligomers based on the indole scaffold were designed to fold into discrete structures by encapsulating anions in helical cavities. Finally, the anion binding properties of indoles and related heterocycles have been applied toward the creation of molecular sensors that yield specific color and fluorescence changes upon complexation. It is clear that indoles and related heterocycles are suitable building blocks for the construction of novel receptors and functional devices. As the molecular toolbox expands to generate more sophisticated structures and functions, we expect to see these heterocycles utilized further.

References

1. Morokuma K (1977) *Acc Chem Res* 10:294
2. Steiner T (2002) *Angew Chem Int Ed* 41:48
3. Bordwell FG, Druker GE, Fried HE (1981) *J Org Chem* 46:632
4. Bordwell FG, Ji G-Z (1991) *J Am Chem Soc* 113:8398
5. Pflugrath JW, Quioco FA (1985) *Nature* 314:257
6. He JJ, Quioco FA (1991) *Science* 251:1479
7. Koropatkin NM, Pakrasi HB, Smith TJ (2006) *Proc Natl Acad Sci* 103:9820
8. Okunola OA, Santacroce PV, Davis JT (2008) *Supramol Chem* 20:169
9. Gale PA (2008) *Chem Commun*:4525
10. Rebek J Jr (1987) *Science* 235:1478
11. Harmata M (2004) *Acc Chem Res* 37:862
12. Bates GW, Gale PA, Light ME (2007) *Chem Commun*:2121
13. Caltagirone C, Gale PA, Hiscock JR, Hursthouse MB, Light ME, Tizzard GJ (2009) *Supramol Chem* 21:125
14. Zielinski T, Dydio P, Jurczak J (2008) *Tetrahedron* 64:568
15. Dydio P, Zielinski T, Jurczak J (2009) *Chem Commun*:4560
16. Caltagirone C, Mulas A, Isaia F, Lippolis V, Gale PA, Light ME (2009) *Chem Commun*:6279
17. Choi K, Hamilton AD (2003) *Coord Chem Rev* 240:101
18. Lee JY, Lee MH, Jeong K-S (2007) *Supramol Chem* 19:257
19. Bates GW, Triyanti, Light ME, Albrecht M, Gale PA (2007) *J Org Chem* 72:8921
20. Makuc D, Triyanti, Albrecht M, Plavec J, Rissanen K, Valkonen A, Schalley CA (2009) *Eur J Org Chem*:4854
21. Caltagirone C, Hiscock JR, Hursthouse MB, Light ME, Gale PA (2008) *Chem Commun*:3007
22. Makuc D, Lenarcic M, Bates GW, Gale PA, Plavec J (2009) *Org Biomol Chem* 7:3505
23. Caltagirone C, Hiscock JR, Hursthouse MB, Light ME, Gale PA (2008) *Chem Eur J* 14:10236
24. Gale PA, Hiscock JR, Moore SJ, Caltagirone C, Hursthouse MB, Light ME (2009) *Chem Asian J* 5:555
25. Taylor MS, Jacobsen EN (2006) *Angew Chem Int Ed* 45:1520
26. Chmielewski MJ, Charon M, Jurczak J (2004) *Org Lett* 6:3501
27. Hiscock JR, Caltagirone C, Light ME, Hursthouse MB, Gale PA (2009) *Org Biomol Chem* 7:1781
28. Curiel D, Cowley A, Beer PD (2005) *Chem Commun*:236

29. Chang K-J, Chae MK, Lee C, Lee J-Y, Jeong K-S (2006) *Tetrahedron Lett* 47:6385
30. Kwon TH, Jeong K-S (2006) *Tetrahedron Lett* 47:8539
31. Copley RR, Barton GJ (1994) *J Mol Biol* 242:321
32. Hirsch AKH, Fisher FR, Diederich F (2007) *Angew Chem Int Ed* 46:338
33. Dutzler R, Campbell EB, Cadene M, Chait BT, Mackinnon R (2002) *Nature* 415:287
34. Dutzler R, Campbell EB, Mackinnon R (2003) *Science* 300:108
35. Ju J, Park M, Suk J-M, Lah MS, Jeong K-S (2008) *Chem Commun*:3546
36. Chmielewski MJ, Zhao L, Brown A, Curiel D, Sambrook MR, Thompson AL, Santos SM, Felix V, Davis JJ, Beer PD (2008) *Chem Commun*:3154
37. Oi W, Nishiki M, Ito K (2007) *Lett Org Chem* 4:112
38. Yu JO, Browning CS, Farrar DH (2008) *Chem Commun*:1020
39. Lee C-H, Yoon H, Jang W-D (2009) *Chem Eur J* 15:9972
40. Restorp P, Berryman OB, Sather AC, Ajami D, Rebek Jr, J (2009) *Chem Commun*:5692
41. Sessler JL, Gale PA, Cho W-S (2006) *Anion receptor chemistry*. RSC, Cambridge
42. Black DS, Bowyer MC, Kumar N, Mitchell PSR (1993) *J Chem Soc Chem Commun*:819
43. Black DS, Craig DC, Kumar N (1995) *Tetrahedron Lett* 36:8075
44. Chang K-J, Moon D, Lah MS, Jeong K-S (2005) *Angew Chem Int Ed* 44:7926
45. Kim NK, Chang K-J, Moon D, Lah MS, Jeong K-S (2007) *Chem Commun*:3401
46. Gale PA, Sessler JL, Kral V, Lynch VM (1996) *J Am Chem Soc* 118:5140
47. Piatek P, Lynch VM, Sessler JL (2004) *J Am Chem Soc* 126:16073
48. Chae MK, Lee J-I, Kim N-K, Jeong K-S (2007) *Tetrahedron Lett* 48:6624
49. Gellman SH (1998) *Acc Chem Res* 31:173
50. Hill DJ, Mio MJ, Prince RB, Jughes TS, Moore JS (2001) *Chem Rev* 101:3893
51. Hecht S, Huc I (eds) (2007) *Foldamers: structure, properties, and applications*. Wiley-VCH, Weinheim
52. Juwarker H, Suk J, Jeong K-S (2009) *Chem Soc Rev* 38:3316
53. Chang K-J, Kang B-N, Lee M-H, Jeong K-S (2005) *J Am Chem Soc* 127:12214
54. Kim U-I, Suk J-M, Naidu VR, Jeong K-S (2008) *Chem Eur J* 14:11406
55. Naidu VR, Kim MC, Suk J-M, Kim H-J, Lee M, Sim E, Jeong K-S (2008) *Org Lett* 10:5373
56. Naidu VR, Suk J-M, Lee GW, Jeong K-S (2009) *Bull Korean Chem Soc* 30:482
57. Suk J-M, Jeong K-S (2008) *J Am Chem Soc* 130:11868
58. de Silva AP, Nimal Gunaratne HQ, Gunnlauugsson T, Huxley AJM, McCoy CP, Rademacher JT, Rice TE (1997) *Chem Rev* 97:1515
59. He X, Hu S, Liu K, Guo Y, Xu J, Shao S (2006) *Org Lett* 8:333
60. Pfeffer FM, Lim KF, Sedgwick KJ (2007) *Org Biomol Chem* 5:1795
61. Lin C-I, Selvi S, Fang J-M, Chou P-T, Lai C-H, Cheng Y-M (2007) *J Org Chem* 72:3537
62. Wang Y, Lin H, Shao J, Cai Z-S, Lin H-K (2008) *Talanta* 74:1122
63. Shao J, Wang Y, Lin H, Li J, Lin H (2008) *Sens Actuators B* 134:849
64. Sessler JL, Cho D-G, Lynch VM (2006) *J Am Chem Soc* 128:16518
65. Wang T, Bai Y, Ma L, Yan X-P (2008) *Org Biomol Chem* 6:1751
66. Shiraishi Y, Maehara H, Hirai T (2009) *Org Biomol Chem* 7:2072
67. Sessler JL, Maeda H, Mizuno T, Lynch VM, Furuta H (2002) *J Am Chem Soc* 124:13474
68. Amendola V, Boiocchi M, Fabbri L, Palchetti A (2005) *Chem Eur J* 11:5648
69. Yu M, Lin H, Lin H (2008) *Supramol Chem* 20:357
70. Thangadurai TD, Singh NJ, Hwang I-C, Lee JW, Chandran RP, Kim KS (2007) *J Org Chem* 72:5461

Pyrrole-Based Anion Sensors, Part I: Colorimetric Sensors

Pavel Anzenbacher Jr.

Abstract This chapter focuses on chemo-sensing aspects of pyrrole and oligopyrrole-based colorimetric receptors for anions. Since pyrroles can play the role of a receptor as well as a signal transducer very efficiently and because of the focus on anion sensing, they can be organized following the modes of signal transduction such as colorimetry, fluorescence, and electrochemistry rather than structural features of the receptors. This chapter focuses on colorimetric sensors and in particular those based on pyrrole, polypyrrole, and pyrrole benzo-analogs, i.e., indole and carbazole-based sensors for anions.

Keywords Anions · Electrochemistry · Fluorescence · Luminescence · Sensor

Contents

1	Introduction	205
2	Colorimetric Sensors	208
3	Calix[4]pyrroles	215
4	Calixpyrrole-Based Colorimetric Displacement Assays	223
5	2,3-(Dipyrrol-2-yl)quinoxaline	229
6	Miscellaneous Colorimetric Sensors	229
7	Concluding Remarks	233
	References	233

1 Introduction

Pyrrole and its derivatives occupy a spot close to the hearts of many chemists focusing on anion sensing, and as a result pyrrole-containing receptors and sensors have emerged as among the most versatile and useful in anion sensor materials. Not surprisingly, pyrrole and oligopyrrole-based receptors for anions have been reviewed [1–3]. This and the following chapter, however, differ from the previous ones [4–7] by its focus on chemo-sensing aspects of such materials. Thus, receptors that do not provide an output signal useful for a potential chemosensor development are not discussed here. Also, because of the focus on anion sensing, this chapter and the next are organized in a different way and use the modes of signal transduction such as colorimetry, fluorescence, and electrochemistry as the main criterion. This means that one receptor may appear in two places if it was, for example, used to generate an optical as well as an electrochemical sensor. Part I is focused on the colorimetric anion sensors and Part II on the fluorescence and electrochemical anion sensors.

Apart from pure affection, there are also many rational reasons for this continuing fascination and use of this simple five-membered heterocycle in the synthesis of anion sensors. In this chapter, pyrrole, polypyrrole and pyrrole benzo-analogs, i.e., indole and carbazole based sensors for anions will be reviewed. From the perspective of sensors, one should consider two features that make a successful anion sensor. Traditionally, sensors are considered to comprise a receptor moiety and signal transducer that provides the output signal recorded or observed and evaluated. The successful sensing event is then largely determined by a synergy between the anion–receptor interaction, usually binding, and generating the changes in an observable property such as color, luminescence, redox properties, conductivity, etc. Most interestingly, pyrroles can play both roles – the role of a receptor and a signal transducer – very efficiently, which also explains their popularity in the anion sensing science.

Among the reasons for the extensive use of pyrroles as recognition motifs in anion receptors [2, 3] and sensors is that pyrroles, unlike other moieties that comprise the functionalities capable of forming $\text{C}=\text{O} \cdots \text{HN}$ intra- and inter-molecular bridges (e.g., amides, ureas, and thioureas), do not self-associate. Pyrroles, similar to amides, are frequently used to prepare electroneutral anion receptors and sensors that operate, i.e., bind anions, using hydrogen bonding. Pyrroles are weak acids; the unsubstituted pyrrole has a $\text{p}K_{\text{a}}$ of 23 which means it can form hydrogen bonds with anions, but can also be deprotonated by strong bases such as LDA, NaH, Bu-Li, etc. Compared to other hydrogen bond donors also favored by supramolecular chemists, $\text{p}K_{\text{a}}$ of pyrrole ($\text{p}K_{\text{a}} \sim 23$ in DMSO) is comparable or slightly higher compared to most of the primary and secondary amides (acetamide $\text{p}K_{\text{a}} \sim 25$ in DMSO; benzamide ~ 23 in DMSO; *N*-methylbenzamide ~ 21.5 ; *N*-phenylbenzamide ~ 19 , etc.). Within the realm of acidic heterocycles, pyrrole acidity is lower than that of imidazole (~ 18.6), indole (~ 21), carbazole (~ 20), benzimidazole (~ 16.4), pyrazole (20), benzotriazole (~ 12), or 1,2,3-triazole (~ 14) (<http://www.chem.wisc.edu/areas/reich/pkatable/index.htm>). Thus, the pyrrole is a conservative choice of a hydrogen

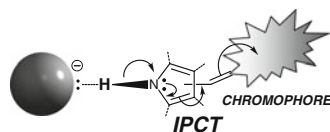
bond donor: reasonably available for hydrogen bonding, but still not too likely to be easily deprotonated. In fact, in most cases, pyrrole does not get deprotonated by most anions, including the basic anions such as fluoride or carboxylates. Depending on the substitution and solvent, however, some basic anions such as, for example, fluoride and tribasic phosphate, cause pyrrole deprotonation. This ability to undergo deprotonation is in some cases a liability because some pyrrole derivatives, particularly at high anion excess, can display a continuum of behavior between hydrogen-bonding and deprotonation. Needless to say, for the preparation of anion sensors deprotonation is an undesirable event that relegates such compounds and materials to the realm of pH sensors rather than anion sensors.

What further distinguishes pyrroles and analogs from other hydrogen-bond donors is the ability of pyrroles to play an active role in signal transduction. This is due to the fact that pyrrole is a π -excessive – and therefore electron-rich – heterocycle, graciously willing to let go a part of its electronic density to suitable acceptors. As a result, pyrroles act as donors in intramolecular partial charge-transfer (IPCT) schemes utilizing π -conjugated moieties capable of accepting the excess of electron density. With respect to signal transduction, the role of pyrroles as donors is usually further augmented by anion binding (Fig. 1). As the anion attracts the acidic proton involved in hydrogen bonding, the electronic density of the H–N bond shifts toward nitrogen and causes further polarization of the pyrrole electronic cloud. An acceptor attached through a bridge capable of transferring the excess charge from the pyrrole accommodates the excess partial charge, thus completing the partial charge transfer (IPCT) cascade.

As a direct result of IPCT, in most cases the HOMO–LUMO gap is narrowed compared to the resting state, predominantly due to rising HOMO-levels. However, both actual HOMO/LUMO energy levels usually increase upon anion binding. In general, this suggests that in optical sensors we are likely to observe red-shifted (a bathochromic shift) absorption spectra and a decrease in the luminescence intensity.

From this perspective it seems that pyrroles have it all: they are good receptors and they are capable of aiding in signal transduction. This together with the relative ease of synthesis and derivatization makes pyrroles favored moieties for the anion sensor design. In the following paragraphs, the pyrrole-based anion sensors will be organized into sub-chapters following the signal transduction rather than structural features. Some compounds display two different signal transduction modes, for

Fig. 1 Hydrogen bonding between an anion and pyrrole NH induces an intramolecular partial charge-transfer (IPCT) process that results in a changed distribution of electron density in the sensor. Such change in electron density further results in change of color, fluorescence or electrochemical properties



example, change in color and fluorescence. In such cases, they will be included into a sub-chapter corresponding to the application proposed by the authors of the respective articles.

2 Colorimetric Sensors

Perhaps the oldest category in this otherwise relatively young field of molecular sensing is formed by the porphyrins and their expanded congeners [8, 9] such as sapphyrins [10, 11], calixphyrins [12, 13], cyclo[n]pyrroles [14, 15], and other derivatives. Conjugated oligopyrroles and pyrrole macrocycles in particular, appear to have the advantage of having large π -delocalized chromophores that serve as chromophores. An early example in this respect are porphyrins and their interaction with DNA, dating to the late 1970s [16–19], and nucleotides [20], in which the first reports on potential hydrogen bonding were proposed.

An interesting example of a classical porphyrin binding fluoride was recently described by Swager and coworkers [21] (Fig. 2). According to this 2001 report a “doubly strapped” porphyrin comprising four bi-thiophene fragments in the straps **1** was found to bind two fluoride anions in dichloromethane in a cooperative binding mode involving both the “straps” and the pyrrole NH protons in a sandwich-like pattern. While this interesting binding mode was not confirmed by solid-state structural analyses, an indirect proof for the proposed complex came from the strong selectivity for the small fluoride anion. The narrow cleft between the straps and the porphyrin plane was found to accommodate fluoride while the larger anions, such as chloride, bromide, iodide, acetate, cyanide, and dihydrogen phosphate, fail to induce a change in the UV spectrum. This material can be electro-polymerized to form a conductive polymer. Interestingly, the treatment of the polymer poly-**1** with a F^- anion shifted the redox waves associated with the porphyrin moiety to lower potentials. Interestingly, the electrochemical behavior of the conjugated polymer was largely unaffected (Fig. 2).

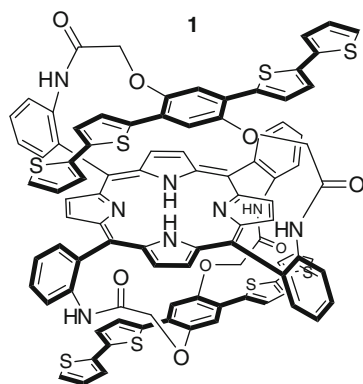


Fig. 2 A porphyrin triple-decker-like sensor shows a dramatic selectivity for fluoride, presumably because the small fluoride anion can fit between each of the conjugated thiophene oligomers and the opposite face of the porphyrin macrocycle

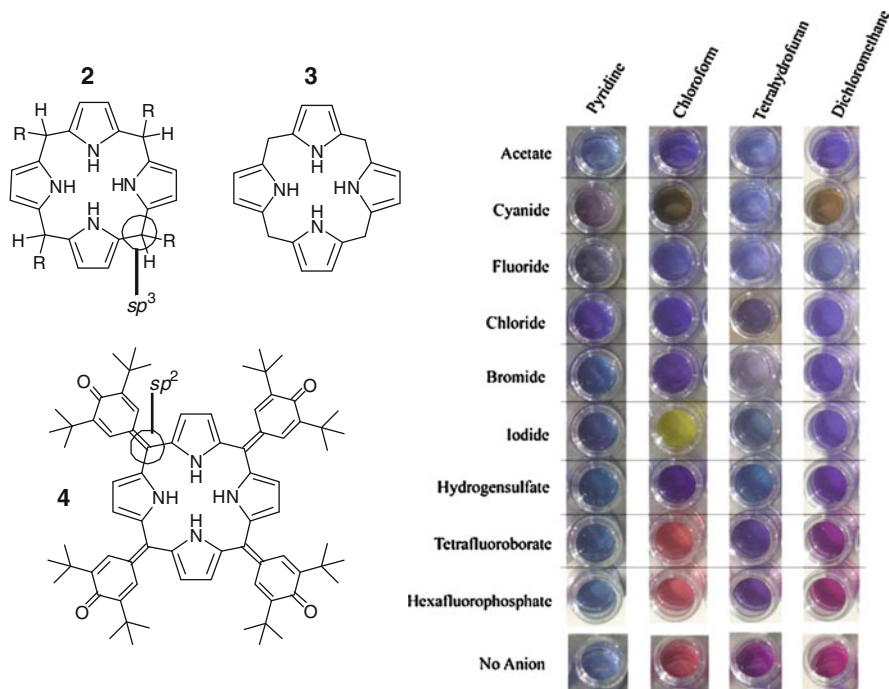
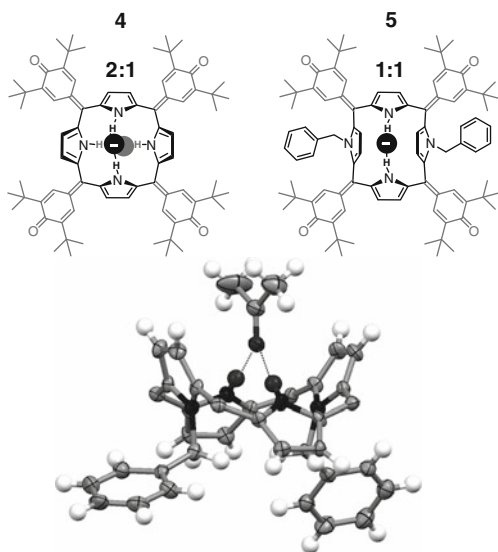


Fig. 3 Schematic drawing of a porphyrinogen **2**, porphyrinogen core **3**, and porphyrinogen-like colorimetric sensor **4**. Original photographs of solutions of **4** in the stated solvents in the presence of excesses of the respective anions as their tetra-*n*-butylammonium salts

A precursor to porphyrins, known as a porphyrinogen is a reduced tetrapyrrolic macrocycle with four *meso*-carbons. Each *meso*-carbon bears two substituents, where at least one of the two substituents per *meso*-carbon is hydrogen (Fig. 3). Figure 3 shows a porphyrinogen **2** and porphyrinogen core **3**. While all of the *meso*-carbons in a porphyrinogen are in sp^3 hybridization and none of the 1H-pyrroles is in its oxidized form, it is clear that the derivative **4** is a compound in its own class. Compound **4** comprises the porphyrinogen core, none of the four pyrrole moieties is in an oxidized form, yet, the *meso*-carbons display sp^2 hybridization. In some ways, this compound is a missing link between a porphyrin, porphyrinogen, and calix[4] pyrrole. From the perspective of sensing, compound **4** and its N_{21},N_{23} -dibenzylated congener display strong solvatochromism as well as an ability to form hydrogen bonds to Lewis bases via NH-moieties of the pyrrole fragments. The combination of hydrogen bonding to anions and the solvatochromism yielded an interesting colorimetric signal transduction scheme (Fig. 3).

While compound **4** displays very intense color transitions, perhaps even more interesting is the fact that this compound appears to bind to anions in an unusual binding mode (Fig. 4). The stoichiometry of the complex appears to be 1:2 (receptor:anion), one anion is presumably bound above, and the second anion below the

Fig. 4 *Top*: Proposed binding modes for anions by porphyrinogen **4** and the N_{21} , N_{23} -dibenzylated congener **5**. *Bottom*: A part of the X-ray structure of the **5**•O=C(CH₃)₂ complex showing that the porphyrinogen core (*meso*-substituents are omitted for clarity) shows a 1,3-alternate conformation with 1,3-*syn*-binding mode and 1:1 stoichiometry



macrocyclic plane. This binding mode corresponds to two association events, each characterized by an association constant. Most interestingly, this binding mode appears to display cooperativity and the association constants are calculated from the changes in UV–Vis spectra. Perhaps, this is due to the distortion of the macrocycle conformation as a result of the first binding event. This notion is further indirectly supported by the observation that the compound **5** displays only one binding event. It is conceivable that the structure of the anion complexes with compound **5** is similar to the structure of the **5**•O=C(CH₃)₂ complex (Fig. 4).

In all anions, the second association constant is ca. one half of the magnitude of the constant describing the first binding event. The magnitudes of K_a values suggest stable anion binding by both porphyrinogens **4** and **5**, which for halides follows the trend: fluoride > chloride > bromide > iodide, quite similar to the binding order observed for similar porphyrinogen-like receptors, calix[4]pyrroles. However, for polyatomic anions, no clear trend was observed. Most of the association constants (K_a) are in the order of 10^4 M^{-1} . Only the notoriously hard-to-bind anions such as hexafluorophosphate, perchlorate, and iodide display association constants of $\sim 10^3 \text{ M}^{-1}$. On a qualitative level, the spectral changes correlate well with the magnitude of the affinity constants. The correlation appears to be much better for the compound N_{21}, N_{23} -dibenzyl porphyrinogen **5**, which appears to form a 1:1 complex with analytes (Fig. 5).

The changes in color displayed by both compounds **4** and **5** are visually striking. Because both compounds display strong solvatochromism, it appears that the combination of the solvent, its dielectric properties, acidity or basicity as well as the ability to form hydrogen bonds play a role in the resulting output color (Fig. 5). In some instances, fluoride, iodide, and cyanide appear to undergo an irreversible

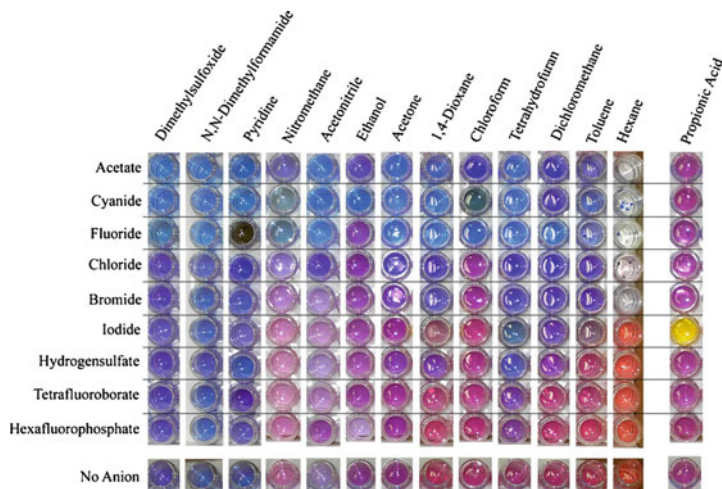


Fig. 5 Striking changes in color observed for compound **5** in various solvents in the presence of anions. Similar color changes were also observed for compound **4**

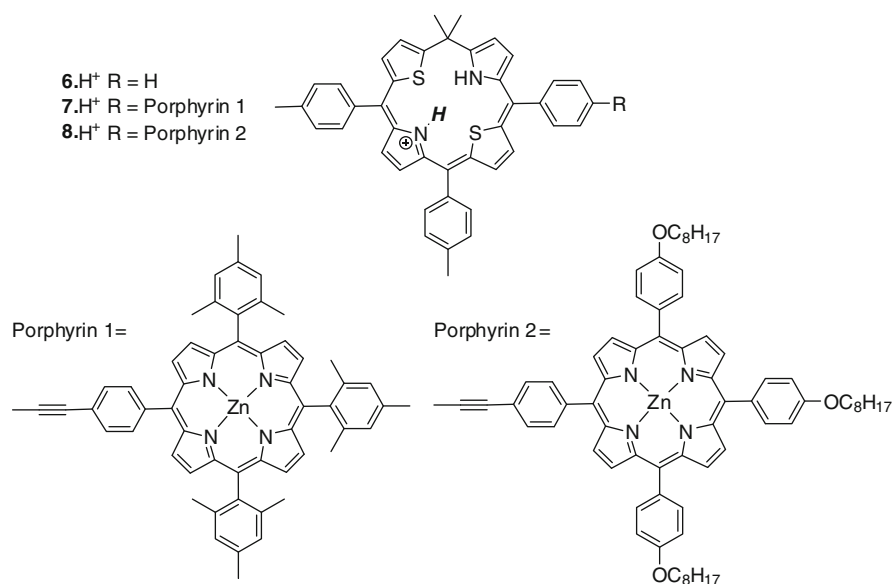


Fig. 6 Structures of the protonated 21,23-dithiaphlorin $6.H^+$, $7.H^+$, and $8.H^+$

reaction with the sensor. Compound **5** was also used as an electrochemical sensor [22].

In 2008, the protonated 21,23-dithiaphlorin $6.H^+$, $7.H^+$, and $8.H^+$ (Fig. 6) were synthesized and their affinity for anions studied [23].

The respective association constants recorded in CH_2Cl_2 for $6.\text{H}^+$ with common anions were estimated as follows: for Cl^- ($K_a = 4.8 \times 10^3 \text{ M}^{-1}$), Br^- ($K_a = 2.1 \times 10^4 \text{ M}^{-1}$), I^- ($K_a = 1.5 \times 10^4 \text{ M}^{-1}$), HSO_4^- ($K_a = 3.3 \times 10^3 \text{ M}^{-1}$), SCN^- ($K_a = 1.8 \times 10^3 \text{ M}^{-1}$). Similarly, the compounds $7.\text{H}^+$ showed association constants for bromide an iodide $K_a = 4.6 \times 10^4$ and $2.3 \times 10^4 \text{ M}^{-1}$, respectively. The compound $8.\text{H}^+$ was found to display $K_a = 6.2 \times 10^3 \text{ M}^{-1}$ for iodide, which was determined by fluorescence titration. In the absence of an X-ray structure it is, however, somewhat unclear if perhaps the protonated 21,23-dithiaphlorin $6.\text{H}^+$, $7.\text{H}^+$, and $8.\text{H}^+$ do not act as simple acid–base indicators that change color when the proton is transferred from the protonated 21,23-dithiaphlorin onto the anion.

The fact that polypyrrolic macrocycles, rich in NH hydrogen bond donor groups, can act as strong anion complexing agents in their protonated forms is now well established [24–30]. To date, anion binding in the solid state has been observed for many types of pyrrolic macrocycles, namely sapphyrin **9** (Fig. 7), which has been studied most extensively. As described in detail below, it was indeed with this system (sapphyrin) that pyrrole-based anion binding was first noted and appreciated.

Sapphyrin, a pentapyrrolic macrocycle discovered by Woodward and his group [31], contains five pyrroles and four *meso*-carbons conjugated to form an aromatic 22 π -electron framework. The free-base form of sapphyrin has three pyrrolic NH and two sp^2 -hybridized imine-type nitrogens. The latter nitrogen atoms are relatively basic, with $\text{p}K_a$ values of ca. 4.8 and 8.8 as recorded for the corresponding conjugate acids in water [32, 33]. This basicity has the consequence that sapphyrins exist in mono- or di-protonated forms, depending on the conditions and it is these species that are important as anion chelating agents. Thus, depending on the size and the geometry of the anion, several binding modes were recognized using X-ray diffraction: First, a fluoride was found to bind inside the sapphyrin core, being held there via a regular array of five $\text{N-H}\cdots\text{F}$ hydrogen bonds (ca. 2.7 Å), while the two larger chloride anions were bound above and below, to opposite faces of the sapphyrin ring via a combination of hydrogen bonding and electrostatic interactions (Fig. 8). This out-of-plane binding mode reflects the fact that anionic chloride is larger than anionic fluoride and that only the latter is of an appropriate size to fit within the relatively small sapphyrin core. Furthermore, a third binding mode was

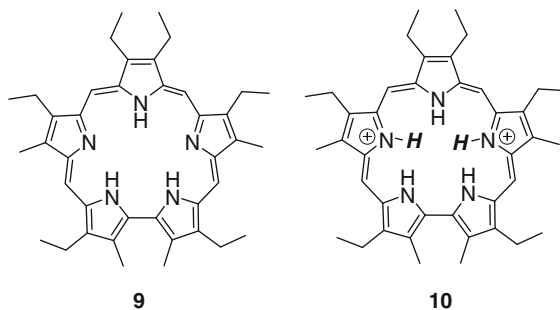


Fig. 7 Structure of sapphyrin **9** and its doubly protonated form **10**

Fig. 8 X-ray structures of sapphyrin-anion complexes: complex of **10** with fluoride (*top*), two chloride anions (*center*). Complex of **11** with phosphate (*bottom*)

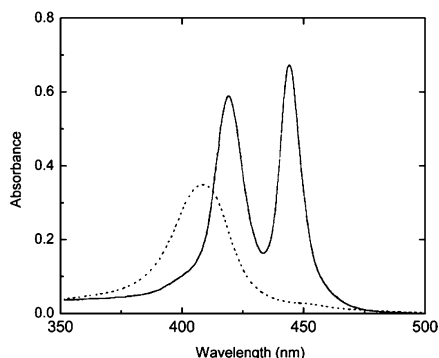
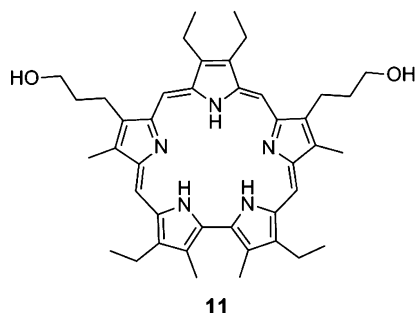
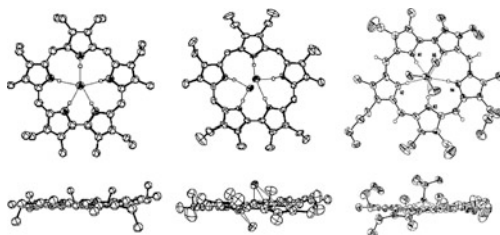
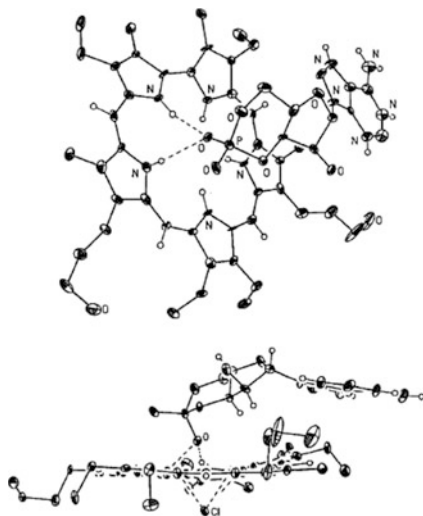


Fig. 9 Visible spectra of 3 μM sapphyrin **11** in 5 mM PIPES, pH 7.0 (*dashed line*), and in the presence of a 50% (v/v) solution of CH_3CN in 5 mM PIPES, pH 7.0 showing clearly the aggregate, dimer and monomer absorption

found for inorganic phosphate where one negatively charged oxygen is found almost inside the sapphyrin cavity while the rest of the anion is suspended above the macrocycle plane.

In aqueous media, depending on the substitution of the macrocycle, sapphyrin derivatives are protonated at a range of pH, from mildly acidic to neutral conditions (pH \sim 5–7) [10, 11]. Furthermore, owing to their organic nature, similar to porphyrins, sapphyrins are found to aggregate in aqueous solutions. The degree of aggregation is changed in the presence of anions, a feature which is exploited in UV–Vis titration measurements in the visible region as well as in fluorimetric sensing experiments [11, 32]. Because sapphyrins bind phosphates strongly over chlorides, this selectivity was exploited in phosphate sensing in biological environment where the chloride anions abound. As Fig. 9 shows, the colorimetric output in sapphyrin sensors is predominantly based on the dramatic shift of the Soret-like maxima of the sapphyrin aggregates at ca. 400 nm to form a new intensive maximum at 425 nm attributed to stable dimers (dimerization constant of $1.2 \times 10^4 \text{ M}^{-1}$) [11]. Strong association or addition of detergent may also result in the formation of a monomeric form characterized by a strong Soret-type maximum at ca. 450 nm. Similar changes are also observed for Q-type bands and absorption in the 750–850 nm region [10, 11]. This process appears to be due to dissociation of aggregates into dimers and monomers. This ratiometric behavior

Fig. 10 Two views showing selected heteroatoms of the solid-state complex formed between monobasic cAMP, chloride anion, and $[11H\bullet 2]^{2+}$. The *top view* shows the details of the interaction between monobasic cAMP and $[11H\bullet 2]^{2+}$. The *bottom view* shows an edge-on view of the complex. The bound oxyanion of cAMP and the chloride anion are found to be 1.376 and 1.820 Å, respectively, above the root-mean square plane of the pyrrolic nitrogens. The phosphorus atom is 2.667 Å from this same plane. Reproduced with permission from [33]



may be easily leveraged as a signal output from sapphyrin sensors. While the aggregation and attendant difficulties in the determination of equilibrium constants preclude accurate estimation of the binding constant, the sapphyrin-phosphate affinity is described by an apparent stability constant of ca. $30,000 \text{ M}^{-1}$ [10, 11, 33].

Perhaps more important is the discovery that sapphyrins can bind phosphate esters including nucleotides such as cyclic as well as non-cyclic nucleotide mono-phosphates while showing a high variability of the proportion of the aggregate: dimer:monomer ratios [3, 33, 34]. This is likely due to the synergy between the coordination of the negatively charged phosphate by the sapphyrin and the π - π stacking interaction of the nucleobase with the sapphyrin macrocycle (Fig. 10). Thus, sapphyrins can not only be used for sensing of simple inorganic anions and namely phosphates but also for nucleotides and nucleic acids [33].

Interestingly, similar behavior of sapphyrins was also found for pertechnetate anion showing a respectable association constant of $3,900 \text{ M}^{-1}$, which is, however, almost an order of a magnitude lower than the one estimated for sodium phosphate [35].

Furthermore, UV-Vis spectroscopy in the visible region was also used to study the ability of sapphyrin dimers to complex carboxylates corresponding to *N*-CBZ-protected aspartic and glutamic acids. The corresponding association constants recorded were relatively weak despite the multitopic nature of the dimeric sapphyrin receptor ($K_a = 4 \times 10^3$ – $2 \times 10^4 \text{ M}^{-1}$ in 5% methanol in dichloromethane) and did not encourage a further development as sensors for carboxylates [36].

As mentioned above, a number of pyrrolic macrocycles follow a similar trend in properties, i.e., their ring systems undergo protonation and the large macrocyclic cations then bind anions. Depending on the ring size, delocalization, topology and

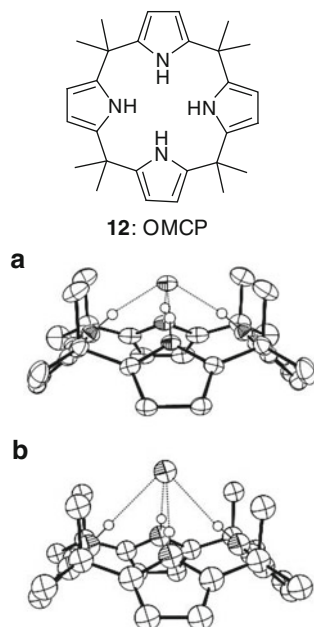
other factors, such materials display varying anion binding capabilities, while their electronic properties determine the degree of color and/or fluorescence change to serve as a signal transduction pathway. While many of these newer materials could find their way into anion sensing applications, they have not been studied as vigorously as sapphyrins yet. It is, therefore, quite likely that new sensor materials will emerge from the family of the expanded protonated porphyrins in the near future.

3 Calix[4]pyrroles

Calixpyrroles, with the most known calix[4]pyrrole (Fig. 11) are among the most widely studied examples of electroneutral oligopyrrolic macrocycles that bind anions via an array of hydrogen bonds. The calix[4]pyrrole was first prepared by Baeyer [37] in 1886 and was only recently recognized as an anion receptor [39]. While calix[4]pyrrole itself has only weak UV-absorption and does not display appreciable fluorescence, its value is in the fact that the *meso*-alkyl substituents in the *meso*-octaalkylcalix[4]pyrrole make the pyrrole even more electron rich and an even more effective IPCT donor. Furthermore, the electron-rich nature of the pyrrole moieties makes the calix[4]pyrrole derivative easy-to-modify to generate a wide variety of chemosensor materials. Figure 11 shows the structure of calix[4]pyrrole and its complex with fluoride (a) and chloride (b).

In a CD_2Cl_2 solution, octamethylcalix[4]pyrrole (OMCP) **12** was found to bind fluoride and chloride anions (studied in the form of their tetrabutylammonium salts) with affinities, K_a , of 1.7×10^4 and $3.5 \times 10^2 \text{ M}^{-1}$, respectively, as judged from

Fig. 11 Octamethylcalix[4]pyrrole (OMCP) **12** binds both fluoride, chloride and other anions in the solid state [38, 39]. While these two structures are similar, in the case of the fluoride anion complex, the average $\text{N}\cdots\text{F}$ distance is 2.767 Å, while for the corresponding chloride complex the $\text{N}\cdots\text{Cl}$ distance is 3.303 Å. Thus, fluoride anion appears to be more tightly bound in the solid state. This is also confirmed by other solid state structures of calix[4]pyrrole-fluoride complexes, namely the structure of the octamethylcalix[4]difluoropyrrole[40]. Reproduced with permission from [39]



$^1\text{H-NMR}$ experiments. Later it turned out that the actual values of the association constants depend on many factors and are highly tunable. Thus, halogenation of the pyrrole-beta positions improved dramatically the anion binding affinity. Furthermore, the solvent and counter-cation are also important factors affecting the affinity and the magnitudes of the respective binding constants. Recently, the combined efforts of Schmidtchen, Gale and Sessler utilizing largely isothermal titration calorimetry (ITC) yielded a unifying treatment of the issue [41]. From the perspective of chemosensor development, the data obtained from spectral measurements, particularly the UV-Vis and fluorescence titrations appear to be more meaningful.

The first calix[4]pyrrole derivative displaying easily discernible change in color was compound **15** [42]. Compound **15** allowed naked-eye observation of the anion-induced color changes in the conjugated chromophores. This is the first report on the naked-eye detection of anions by a chromogenic calix[4]pyrrole. Here, the IPCT from the pyrrole to the electron-deficient anthraquinone moiety is mediated by the ethynylene bridge. It should be noted that the high excess of anions in the CD_2Cl_2 solution might also have induced *N*-deprotonation of the pyrrole involved in the IPCT dyad or deprotonation of the phenolic hydroxyl-group in compound **14**, both of which could lead to the observed changes in color in **13** and **14**. Needless to say, compound **15**, which does not comprise the electron-withdrawing anthraquinone moiety, does not display IPCT despite the fact that the calix[4]pyrrole receptor binds the anions. Even though the actual association constants for anions and the chemosensors **13–15** were not determined, the UV-Vis spectral changes observed for **13–15** suggest that the anion affinity follows the order of fluoride > chloride > dihydrogen phosphate \gg bromide \sim iodide \sim hydrogen sulfate, as evidenced by a clearly observable yellow-to-red color change (Fig. 12).

The following work on the IPCT sensors by Nishiyabu and Anzenbacher [43] building on the formyl-calix[4]pyrrole derivative [44] resulted in improved calix[4]pyrrole sensors obtained in a one- or two-step transformation of the calix[4]pyrrole receptor. Sensors **16–18** show increased IPCT signaling in the presence of anions,

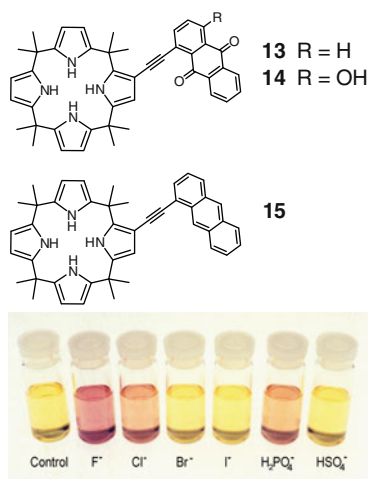


Fig. 12 *Top*: OMCP derivatives **13** and **14** were the first naked-eye colorimetric sensors for anions. *Bottom*: Color changes in **13** in CH_2Cl_2 (50 μM) before (control) and after the addition of 100 equivalents of representative anions as tetrabutylammonium salts

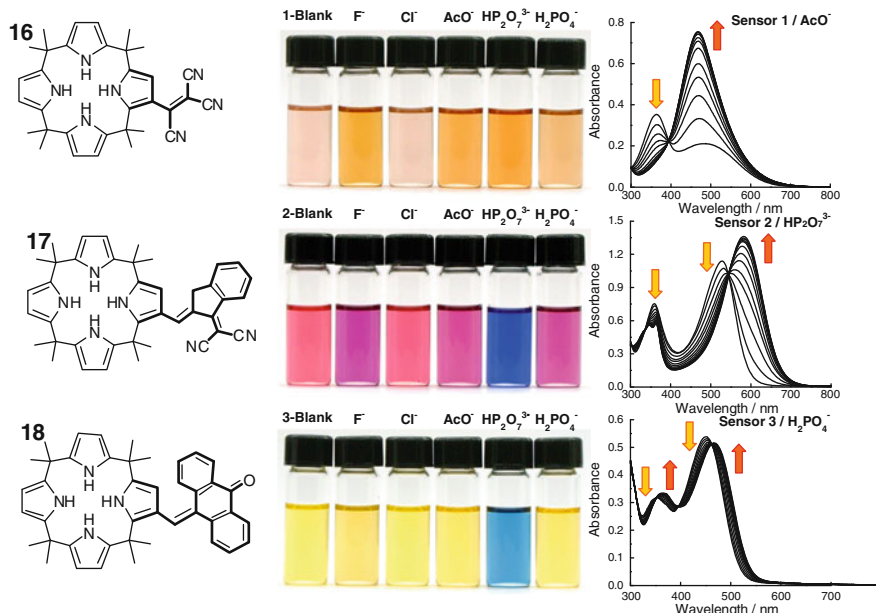


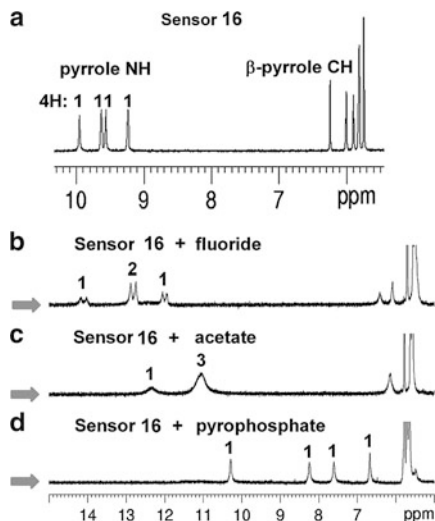
Fig. 13 Colorimetric calix[4]pyrrole chemosensors developed by Anzenbacher and coworker [43] showed a dramatic response to the presence of anions in wet DMSO. Reproduced with permission from [43]

which is easy to observe by the naked eye, UV–Vis as well as NMR spectroscopy (Fig. 13).

These compounds not only showed increased affinity for anions (determined in wet DMSO), but did not undergo deprotonation as shown in the proton NMR spectra even in the presence of basic anions such as fluoride, acetate or hydrogen pyrophosphate trianion, which are strong bases (Fig. 14).

The actual values of the association constants recorded in DMSO follow the general trend fluoride > hydrogen pyrophosphate > acetate > dihydrogen phosphate > chloride. Particularly compound **16**, the tricyanovinyl-calix[4]pyrrole shows strong anion binding for fluoride ($K_a > 10^6 \text{ M}^{-1}$), hydrogen pyrophosphate ($K_a = 5.8 \times 10^5 \text{ M}^{-1}$), acetate ($K_a = 2.42 \times 10^5 \text{ M}^{-1}$), dihydrogen phosphate ($K_a = 5.2 \times 10^3 \text{ M}^{-1}$), and chloride ($K_a = 1.4 \times 10^3 \text{ M}^{-1}$). From the strong binding of acetate and weak binding of chloride and dihydrogen phosphate it was suggested that similar calix[4]pyrrole derivatives might be potentially useful for sensing of carboxylates in biological environment at physiological conditions, in the presence of 0.1 M Cl^- and 2 mM HPO_4^{2-} [45, 46]. Thus, binding of acetate was explored in a blood plasma-like electrolyte solution (0.1 M Cl^- , 2 mM HPO_4^{2-} , 0.1 M Na^+ , 4 mM K^+ , pH 7.4) and also the same electrolyte solution containing bovine serum albumin, BSA (0.1 M Cl^- , 2 mM HPO_4^{2-} , 0.1 M Na^+ , 4 mM K^+ , 46 g/L BSA, pH 7.4). It was found that the sensors respond equally well when the carboxylates are added in the electrolyte comprising BSA. An array chip

Fig. 14 $^1\text{H-NMR}$ spectra of sensor **16** (a) and complexes **16**/ F^- (b), **16**/ AcO^- (c), and **16**/ $\text{HP}_2\text{O}_7^{3-}$ (d) recorded in $\text{DMSO-}d_6$ (0.5% water)



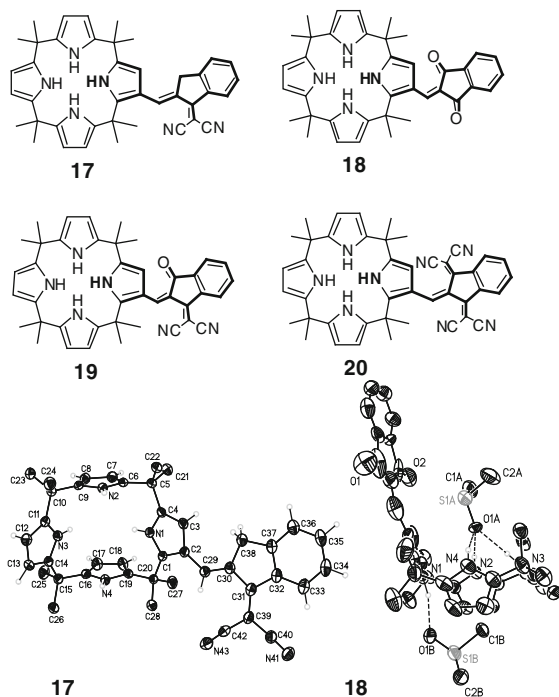
comprising sensors embedded in a polymer matrix was then used to sense antipyretic carboxylate, namely salicylic acid, ibuprofen and naproxen. It was found that neither real blood plasma nor BSA interferes with the carboxylate sensing. Lipophilic carboxylates such as ibuprofen and naproxen yielded a strong response compared to hydrophilic carboxylates (salicylate, acetate, hydrogen carbonate), presumably due to the coextraction of the carboxylate by the polymer sensor-matrix optode material [43].

The same authors further expanded the set of IPCT calix[4]pyrrole chemosensors for another three 1,3-indanedione-calixpyrrole derivatives **17–20** with the structures shown in Fig. 15.

The sensors **16–20** do not show signs of significant deprotonation in the proton NMR spectra in wet $\text{DMSO-}d_6$. However, in the UV–Vis spectra where a lower concentration of the sensor is used and larger excess of the anion is easier to achieve, at high anion concentration partial deprotonation was observed. This is, obviously, an issue with basic anions such as fluoride or hydrogen pyrophosphate. This feature is illustrated in Fig. 16.

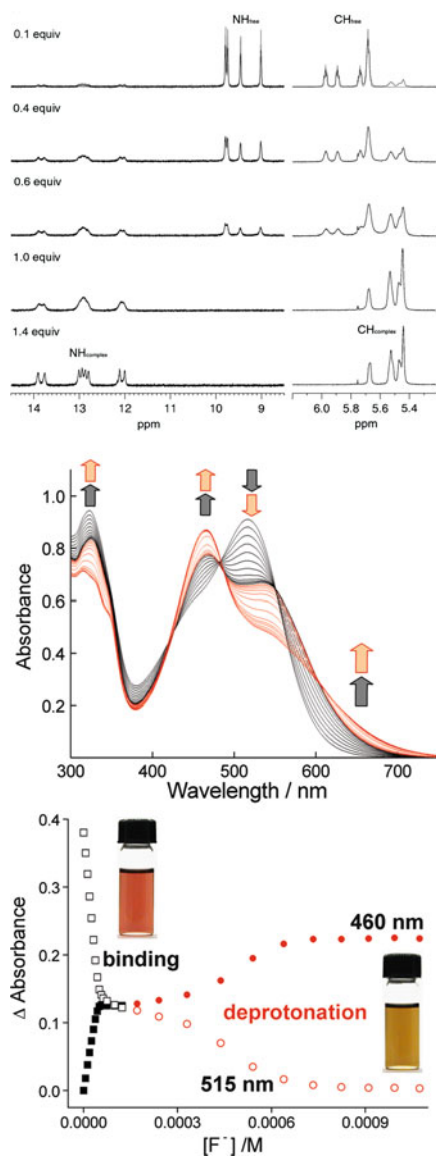
Continuing in the similar vein, Lee and coworkers utilized the same formyl-OMCP derivative for condensation with malononitrile and synthesized an OMCP-dicyanovinyl chemodosimeter [47] that with anions yields a yellow color while with cyanide it undergoes an addition reaction and becomes colorless. The corresponding association constants (K_a) for halides are in the range of $6.24 \times 10^5 \text{ M}^{-1}$ for fluoride to $9.8 \times 10^4 \text{ M}^{-1}$ for chloride, and $2.8 \times 10^3 \text{ M}^{-1}$ for bromide. Surprisingly, acetate was bound strongly ($K_a = 2.8 \times 10^5 \text{ M}^{-1}$) in acetonitrile with 3% DMSO. Lee et al. also continued the research in colorimetric anion sensors using strapped calix[4]pyrroles [48] by combining the effect of the strap with the formyl-calixpyrrole condensation product 1*H*-indene-1,3(2*H*)-dione to form

Fig. 15 *Top*: Structure of the 1,3-indanedione-calixpyrrole colorimetric chemosensors **17–20**. *Bottom*: X-ray structures of chemosensor **17** and **18**



2-([1*H*-pyrrol-3-yl]methylene)-1*H*-indene-1,3(2*H*)-dione featured in the sensor **18**. This strapped 1,3-indanedione also binds various anions and suffers the irreversible addition of the cyanide to the pyrrole vinyl substituents. This sensor, presumably due to the strap, shows high association constants for fluoride ($K_a = 1.25 \times 10^6 \text{ M}^{-1}$), chloride ($K_a = 4.0 \times 10^5 \text{ M}^{-1}$), acetate ($K_a = 4.1 \times 10^5 \text{ M}^{-1}$) and hydrogen pyrophosphate ($K_a = 2.53 \times 10^6 \text{ M}^{-1}$) anions [49]. Another strapped OMCP derivative by Lee and coworkers [50] utilizes the 2,3-di(1*H*-pyrrol-2-yl)quinoxaline moiety as a colorimetric and fluorescent sensor for anions. The signal transduction in this derivative is particularly interesting. The association constants suggest preferential binding of fluoride ($K_a = 9.0 \times 10^6 \text{ M}^{-1}$) and chloride ($K_a = 1.1 \times 10^4 \text{ M}^{-1}$) over dihydrogen phosphate ($K_a = 1.1 \times 10^3 \text{ M}^{-1}$) and acetate ($K_a = 8.1 \times 10^3 \text{ M}^{-1}$) using UV–Vis spectroscopy titrations in CH_3CN -DMSO (93:7), despite the fact that the degree of the apparent change in color is in the order of fluoride > phosphate > chloride > acetate. Thus, the sensor, perhaps due to the smaller binding cavity as a result of the steric limitation by the strap, binds preferentially fluoride and chloride. It is, however, not entirely clear why the response is so strong for a weakly bound dihydrogen phosphate. The calix[4]pyrroles isomerism was employed by Anzenbacher and Dehaen to generate colorimetric anion sensors utilizing this unique feature [51, 52]. During the synthesis of OMCP **12**, an inverted or confused calix[4]pyrrole **21** is also synthesized (Fig. 17) [53].

Fig. 16 *Top*: ^1H NMR spectra (selected regions) of sensor **18** (10 mM) in $\text{DMSO-}d_6$ titrated by fluoride. The NH and β -pyrrole CH proton resonances in a free and complexed sensor **18** are labeled as follows: NH_{free} , CH_{free} , $\text{NH}_{\text{complex}}$, and $\text{CH}_{\text{complex}}$. The integrals and splitting of the pyrrole NH resonances show that the calix[4]pyrrole receptor is not deprotonated by the basic fluoride anions. *Center*: Absorption spectra of sensor **18** (50 μM in DMSO) titrated by fluoride. *Bottom*: Binding isotherms derived from absorbance at 460 and 515 nm



The chemosensors **16** and **22–24** were used for anion sensing. Because the *N*-confused calix[4]pyrrole binds anions via three NH bonds and one C β H bond, the anion binding properties of the corresponding sensors were expected to be different. While both types of chemosensors bind anions, sensors **23** and, to a lesser degree, also **24** display significant deprotonation of the pyrrole NH, to which the electron-withdrawing chromophore is attached. In these cases, the binding and

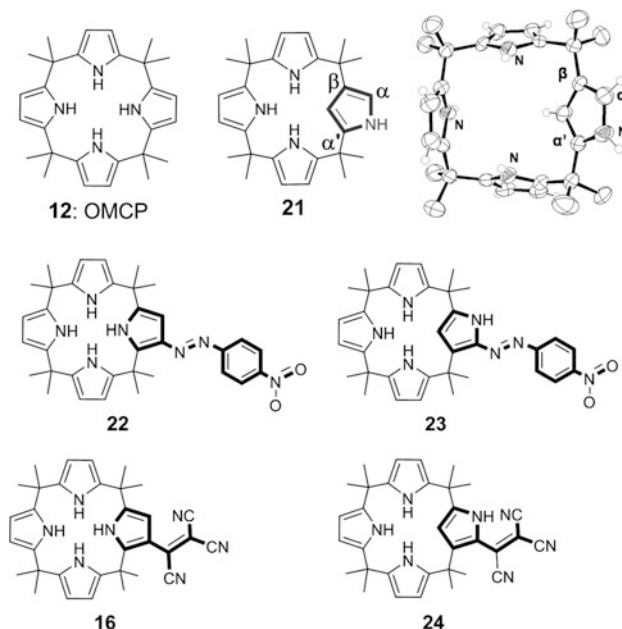
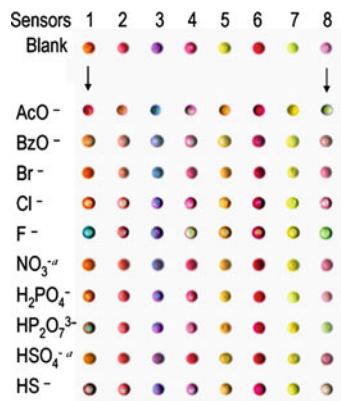


Fig. 17 Structure of OMCP, the *N*-confused congener **21**, and the corresponding X-ray structure. Colorimetric sensors **22** and **23** as well as **16** and **24** were synthesized using both regular OMCP and its *N*-confused analog via electrophilic substitution with diazonium salts or tetracyanoethene, respectively

deprotonation cannot be easily distinguished. The color changes associated with the IPCT are quite striking, from yellow to red and blue, the latter presumably due to deprotonation. In general, the association constants are of a similar magnitude as OMCP derivatives, but show higher affinity to acetate, which was bound strongly ($K_a = 2.4 \times 10^5 \text{ M}^{-1}$ and $9.0 \times 10^3 \text{ M}^{-1}$ in the case of **16** and **22**, respectively). Compounds **22** and **23** showed a combination of binding and deprotonation. Similarly, the association constants for phosphate and pyrophosphate were also found to exceed those of the corresponding calix[4]pyrrole receptors **12** and **21**, respectively.

The relative lack of anion selectivity by the above calixpyrrole-based chemosensors was an inspiration for using these derivatives in a cross-reactive differential sensor array by Anzenbacher and coworkers [54]. The cross-reactive chemosensor elements are not selective toward specific analytes and the analytical information comes from recognition of the response pattern derived from an output signal (e.g., optical [55, 56], electrical [57, 58] signals) generated by a large number of non-selective sensors. Here, a large number of sensors with a different degree of interactions result in the formation of a pattern specific for a given analyte mixture.

Fig. 18 A digital photograph of a glass slide with micro-wells filled with sensor-polymer films after application of aqueous analytes (200 nL, 5 mM). The anion concentration is 20 mM. The change in color is easy-to-observe even by the naked eye



Such pattern recognition approaches could be powerful enough to circumvent the need for difficult-to-make analyte-specific sensors.

Anzenbacher et al. designed an array sensor using the colorimetric anion sensors distributed in a hydrogel and applied into wells (0.95 mm in diameter, 0.25 mm deep) micro-machined in glass slide. In these micro-wells, the hydrogels were applied as a solution, which upon drying formed a 10- μ m thick polymer film, coating the surface of the wells. Into these polymer-coated wells aqueous analytes (0.2 μ L) were applied, and the change in color was recorded using a flatbed scanner (Fig. 18).

The array composed mostly of calixpyrroles **16–24** is capable of recognition of anions in water. Interestingly, an array of eight cross-reactive chemosensors was capable of differentiating between eight aqueous anions, as well as samples of toothpastes. Overall, the colorimetric sensor array for anion detection was found to differentiate between more than 20 analytes including multianalyte samples such as toothpaste [54]. Because the chemosensors in the array consisted mostly of calix[4] pyrrole derivatives described above, the array showed a selectivity bias toward major components of toothpastes such as fluoride and pyrophosphate while still displaying a cross-reactive response to other anionic analytes. The data recorded from the array consists of RGB values of each of the eight sensors to generate a total of 24 variables (8 sensors \times 3 colors). Hierarchical clustering analysis (HCA) was used to show the clustering of the responses of the sensors to 20 different analytes, 10 anions in water as well as identification of toothpastes, based on their anion content (Fig. 19).

Perhaps the most important aspect of this work was the comparison of association constants recorded in solution using NMR or UV–Vis spectroscopy with the array response, which showed that a solid-state array fabricated using polymer matrices doped with chemosensors (see above) correlates with the solution studies. Therefore, supramolecular studies published in the literature may be used directly to design array sensors biased toward an analyte of choice.

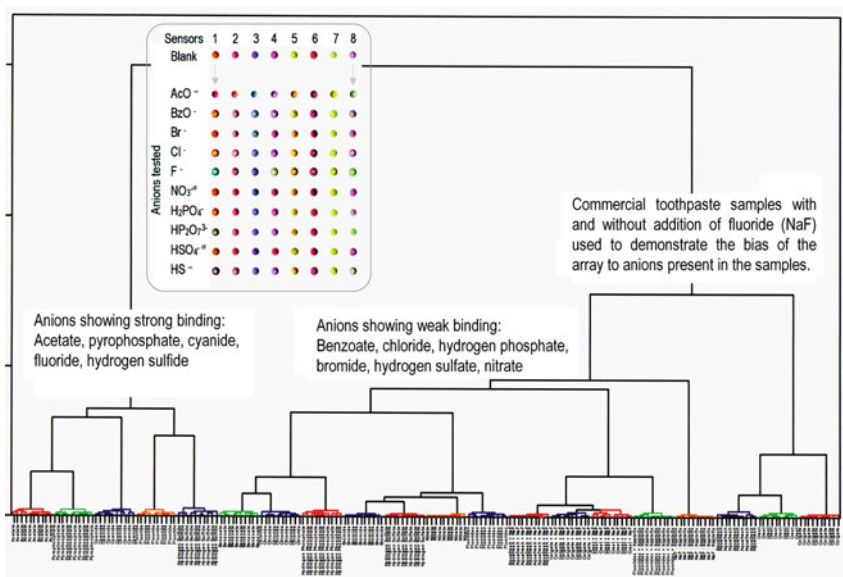


Fig. 19 Hierarchical clustering analysis (HCA) dendrogram with Ward linkage showing Euclidean distance between 200 samples (11 anions, 4 toothpaste brands and control experiments, 10 trials each analyte). More details are provided in the literature [54]. *Inset* shows the section of the 8-sensor element array used to recognize ten different anions

4 Calixpyrrole-Based Colorimetric Displacement Assays

In general, the displacement assay is a competitive assay utilizing a receptor, in this case OMCP, and a dye capable of weak binding to the receptor while displaying a change of color as it forms the receptor–dye complex. When a competing anion displaces the dye in the calixpyrrole complex, the receptor–anion complex is colorless while the dye displays its original color corresponding to the free state of the dye. The first dye-displacement assay using OMCP was demonstrated by Gale et al. using 4-nitrophenol as a dye (Fig. 20) [59].

The dye-displacement approach is quite popular within the community, perhaps due to the high variability and, of course, because it is easy to do. Thus, OMCP displacement assays were performed with chloranil [60], Brooker's merocyanine [61], while Saki and Akkaya used the 4-nitrophenolate displacement in the binding cavity of a dimeric calix[4]pyrrole derivative [62].

5 2,3-(Dipyrrol-2-yl)quinoxaline

2,3-(Dipyrrol-2-yl)quinoxaline (DPQ) **25**, known in the literature since 1911 [63], is another potential anion sensor re-discovered by Sessler as an anion receptor and sensor following the examples of sapphyrin and OMCP. DPQ is easily made in high

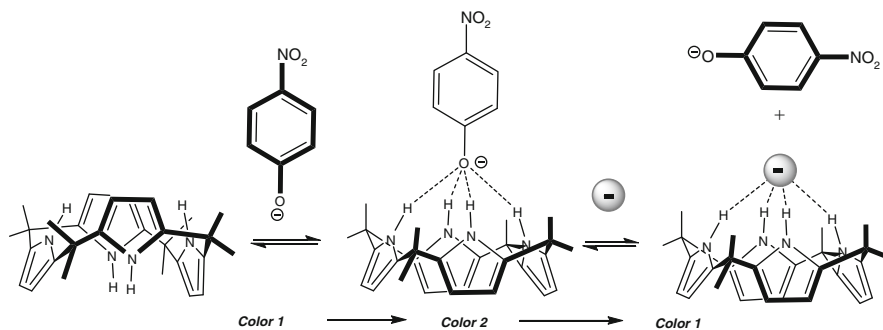
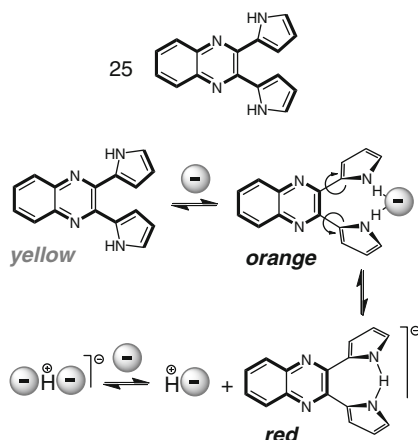


Fig. 20 The dye-displacement by Gale et al. uses brightly yellow nitrophenolate anion, which in the presence of OMCP becomes nearly colorless. Upon addition of a competitive, i.e., more strongly binding, anion the nitrophenolate is released and the yellow color is regenerated [59]

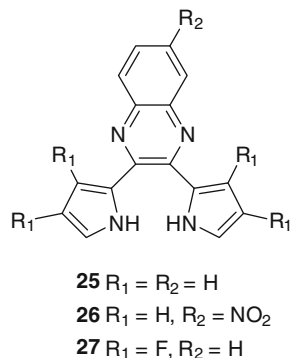
Fig. 21 The structure of 2,3-(dipyrrol-2-yl)quinoxaline (DPQ) **25**, the anion binding by DPQ and possible deprotonation



yield by a condensation reaction between 1,2-di(1*H*-pyrrol-2-yl)ethane-1,2-dione [63, 64] and 1,2-phenylenediamine or a suitably substituted analog thereof [65]. DPQ comprises two pyrrole NH groups capable of hydrogen bonding to the anions, while a built-in quinoxaline ring serves as a colorimetric and/or fluorimetric reporter of any binding events. As illustrated in Fig. 21, this putative sensing system is expected to operate through a combination of electronic and conformational effects. Interestingly, while some anions are bound by DPQ sensors via hydrogen bonding, more basic anions such as fluoride deprotonate the parent DPQ system to form a hydrogen-bridged DPQ anion (Fig. 21) [66]. The deprotonation is augmented in the presence of an excess of anion, as the protonated anion often forms a proton bridged dianion X–H–X⁽⁻⁾.

The first two derivatives, **25** and **26**, investigated by Sessler and coworkers [65] respond to the presence of anion by quenching of the fluorescence intensity and a

Fig. 22 Structure of the first generation DPQ sensors

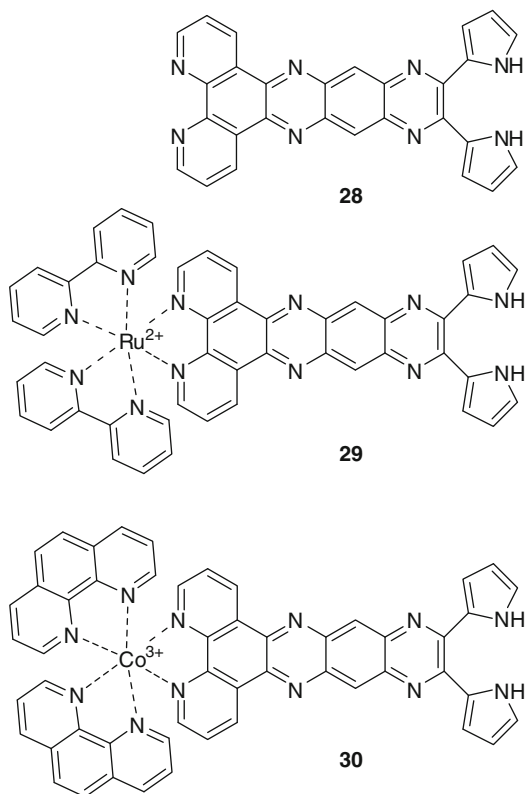


dramatic color change from yellow to orange-red in the case of **25** and **27**, and from yellow to dark purple in the case of **26** (Fig. 22). By contrast, the addition of chloride or phosphate anion did not induce appreciable fluorescence quenching or a noticeable change in color except in the case of sensor **27** [65, 66].

In the case of **27**, phosphate anion induced a similar color change as seen with fluorides, but only at a considerably higher anion concentration. Quantitative measurements of the anion binding affinities were made using standard fluorescence quenching or UV–Vis absorbance titration techniques. These analyses helped confirm that the observed colorimetric change did indeed reflect an anion binding process. For instance, as would be expected based on its colorimetric behavior, receptor **27** showed a significantly enhanced affinity for $H_2PO_4^-$ anion ($K_a = 1.73 \times 10^4 M^{-1}$ for **27** vs. $80 M^{-1}$ for **26** in CH_2Cl_2) [41, 65]. Further, the more dramatic color changes seen for **26** and **27** in the presence of fluoride anion (tetrabutylammonium salt) are also reflected in higher K_a values (1.2×10^5 and $6.2 \times 10^4 M^{-1}$ for **26** and **27**, respectively, in CH_2Cl_2 vs. $1.8 \times 10^4 M^{-1}$ for **25**). This is rationalized in terms of an increased NH hydrogen bond donor ability in the case of **26** and **27** that results from the electron withdrawing groups present on the DPQ skeleton, however, also the deprotonation or a combination of deprotonation and binding cannot be ruled out (Fig. 23).

The success of these initial systems led to the synthesis of the fused DPQ and other analogs and derivatives. For example, DPQ derivatives with a fused phenanthroline moiety **28** were synthesized and used to prepare (bis(BiPy)) complexes with Co(III) and Ru(II) [67]. Here, the phenanthroline ligand **28** displayed only moderate affinity for fluoride ($K_a = 440 M^{-1}$ in DMSO). In contrast, the metallocomplexes **29** and **30** displayed strong affinity for fluoride as reflected by the values of the corresponding association constants $K_a = 540,000$ and $120,000 M^{-1}$ in DMSO, respectively. In all of the cases, the affinity constants for chloride and dihydrogen phosphate were lower than $50 M^{-1}$. The trend observed for fluoride binding confirms the hypothesis that the electron-deficient metal ions render the ligand more electron-deficient and the pyrrole NH moieties more acidic and available for hydrogen bonding. Also, more electron-deficient trivalent Co(III) should impart to

Fig. 23 Structure of the phenanthroline-fused DPQ and the corresponding Ru(II) and Co(III) complexes



the corresponding complex **29** higher affinity for fluoride compared to the divalent Ru(II). Independently, a similar approach was used by Anzenbacher et al. [68]; however, their sensor utilized fluorescence for signal transduction, and will be described in the following section on fluorescence-based sensors.

Because the DPQ-based receptors and sensors feature simple “unidirectional” binding, three-dimensional receptor architectures were pursued in a hope that larger and more complex anions could be sensed. Thus, sensors **31–34** feature three-dimensional binding cavities, in which the additional pyrrole moieties are separated from the signaling unit and cannot be easily deprotonated (Fig. 24) [69, 70].

In the case of DPQ derivatives **31** and **33**, UV–Vis titration studies revealed that the absolute fluoride and phosphate anion affinities recorded in CH₂Cl₂ were increased relative to the unsubstituted DPQ **25** ($K_a(\text{F}^-) = 18,200 \text{ M}^{-1}$) to $K_a(\text{F}^-) = 32,000 \text{ M}^{-1}$ and $K_a(\text{F}^-) = >1,000,000 \text{ M}^{-1}$ for **31** and **33**, respectively, while the association constants for dihydrogen phosphate increased from $K_a(\text{H}_2\text{PO}_4^-) = 60 \text{ M}^{-1}$ for the unsubstituted **25** to $K_a(\text{H}_2\text{PO}_4^-) = 4,300$ and $300,000 \text{ M}^{-1}$ for **31** and **33**, respectively) [69]. More recently, the dicyanopyrazine analogs **32** and **34** (Fig. 24) were also synthesized. Here, the colorimetric studies carried out in CH₂Cl₂ confirmed that the dicyanopyrazine **34** binds

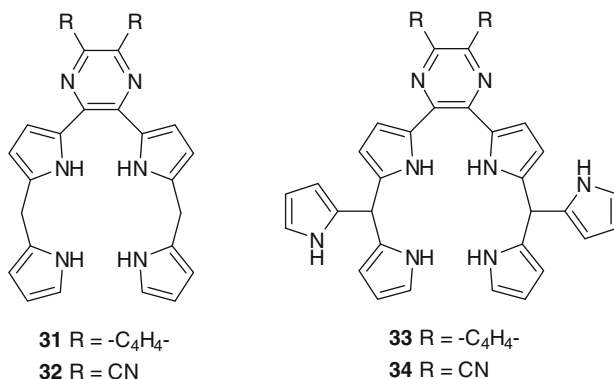
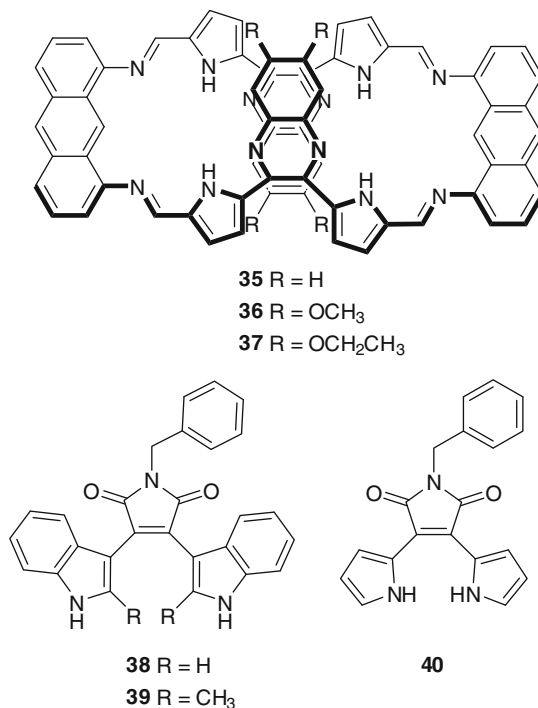


Fig. 24 Structures of DPQ derivatives with three-dimensional binding cavity **31** and **33** and their dicyanopyrazine analogs **32** and **34**

preferentially acetate ($K_a = 175,000 \text{ M}^{-1}$) compared to DPQ-based sensor **33** ($K_a = 46,000 \text{ M}^{-1}$). Conversely, dihydrogen phosphate is bound preferentially by **33** ($K_a = 300,000 \text{ M}^{-1}$) compared to **34** ($K_a = 30,000 \text{ M}^{-1}$). Also, dicarboxylates such as oxalate, malonate and succinate are bound preferentially by **33** ($K_a \sim 20,000\text{--}53,000 \text{ M}^{-1}$) compared to **34** ($K_a = 2,000\text{--}24,000 \text{ M}^{-1}$) [70]. It is clear that relatively small changes in the sensor structures lead to significant perturbations in anion-sensing properties. Sadly, these changes are difficult to rationalize at this time. Another three-dimensional DPQ series of derivatives are macrocycles **35–37b** (Fig. 25), which display a deep yellow color and an absorption spectrum dominated by two bands at 367 and 427 nm, respectively [71]. Upon the addition of fluoride, new peaks at 329 and 480 nm were seen to grow in. It was also found that the color of **35** in CH_2Cl_2 solutions changed from yellow to orange or dark yellow in the presence of fluoride and dihydrogenphosphate anions, respectively. The quantitative analysis of these spectral changes suggest a cooperative 2:1 binding mode, which is a reasonable conclusion given the fact that **35** in the solid state displays two-binding moieties. Structurally, it is possible that the anions such as fluoride are bound within the macrocyclic cavities formed by Fig. 8-like shape of the sensor or via an out-of-the macrocycle binding mode. On a quantitative level, **35** binds fluoride and phosphate anions in a cooperative 2:1 fashion corresponding to association constants $K_a = 3 \times 10^5$ and 80 M^{-1} for fluoride and phosphate, respectively [71]. Another interesting class of DPQ analogs are diindolylquinoxalines by Sessler et al. [72]. These sensors display interesting binding selectivity for dihydrogen phosphate ($K_a = 6,800$ and $20,000 \text{ M}^{-1}$ in CH_2Cl_2 solutions), but biphasic behavior for fluoride suggesting a partial deprotonation. The yellow-to-orange color change is also reminiscent of the parent DPQ.

Another intriguing structural analogs of DPQ are maleimide sensors **38–40** [73]. The sensors **38** and **39** (Fig. 25) appear to display a unique anion affinity and selectivity to fluoride and dihydrogen phosphate in CH_2Cl_2 solutions. Here, the usual affinity order is reversed and dihydrogen phosphate is bound more strongly

Fig. 25 Structure of colorimetric sensors structurally related to DPQ: macrocyclic sensors **35–37**, maleimide analogs of DPQ **38–40**



than fluoride. This is, by no means, a small feat considering that fluoride is the anion with the highest surface charge density, and as such is in most cases bound the most strongly by hydrogen bond donors. Thus, binding of fluoride and dihydrogen phosphate by sensor **38** is characterized by association constants of $K_a = 3,910$ and $3,990 \text{ M}^{-1}$, respectively. Similarly, binding of fluoride and dihydrogen phosphate by the sensor **39** corresponds to constants of $K_a = 620$ and $1,530 \text{ M}^{-1}$, respectively. It should be noted that treatment of **38** and **39** with high concentration of hydroxide anion also resulted in the sensor deprotonation. The corresponding spectral features, however, do not resemble the signatures observed while treating the sensors with fluoride and cyanide ions, and it is concluded that the interactions of **38** and **39** with anions are not acid–base in nature, but rather anion binding. Other anions such as cyanide, chloride, bromide, iodide, nitrate, and hydrogen sulfate were not bound with an appreciable affinity ($K_a < 50 \text{ M}^{-1}$). It is conceivable that the more electron-rich indole moieties are harder to deprotonate, particularly when electron-donating methyl substituents in position 2 of the indole moiety are present as it is in the case of sensor **39**. In contrast, sensor **40** is deprotonated by fluoride and hydroxide in CH_2Cl_2 solutions. This behavior is not entirely dissimilar to DPQ [66]. Similar to the parent DPQ, sensors **38–40** display also appreciable fluorescence, which is quenched during the anion binding process, which suggests that sensors **38–40** may also be used in fluorescence-based sensing.

6 Miscellaneous Colorimetric Sensors

These are colorimetric sensors that do not appear to belong to any distinctive class of pyrrole-based anion sensors described previously. A curious case of 2,5-diamidopyrrole sensors **41** and **42** (Fig. 26) containing 4-nitrophenyl or 3,5-dinitrophenyl groups appended to the amide positions was developed by Gale and coworkers [74]. While in the design of sensors for anions, we generally try to shy away from deprotonation because deprotonation could simply relegate a potential anion sensor to the realm of expensive pH sensor; in the following case the receptor deprotonation and anion binding appear to take place at the same. It is particularly interesting when we consider that the deprotonation of the central pyrrole moiety generates a negative charge at the heart of the sensor, which could simply repel anions. The 3,5-dinitrophenyl derivative has been shown to deprotonate in the presence of fluoride, which in acetonitrile solution gives rise to a deep blue color, which appears to correspond to a sensor dimer rather than sensor-anion. However, the 2,5-diamidopyrrole appears fully capable of maintaining the complex with chloride even though there is a deprotonated pyrrole moiety in the relatively close vicinity (Fig. 26) [74].

Jeong and coworkers have led the way in the use of indole as an anion complexation motif [75]. This group has recently described the biindole sensors **43** and **44** and shown that these compounds bind oxoanions in wet DMSO (0.1–0.2% water). Specifically, anion affinity measurements for receptors **43** and **44** with acetate, dihydrogen phosphate and pyrophosphate have been determined by UV–Vis spectroscopy and the anion selectivity for both the receptors was found to be $\text{AcO}^- < \text{H}_2\text{PO}_4^- < \text{HP}_2\text{O}_7^{3-}$ with compound **44** showing a higher binding affinity ($K_a > 5 \times 10^6 \text{ M}^{-1}$) for pyrophosphate than **43** ($K_a > 5.2 \times 10^5 \text{ M}^{-1}$) [76]. Other non-macrocyclic biindolyl clefts were investigated by Jeong and coworkers [77]. While their anion binding was investigated mostly by NMR spectroscopy, the UV–Vis titration experiments showed the association constants having an increase

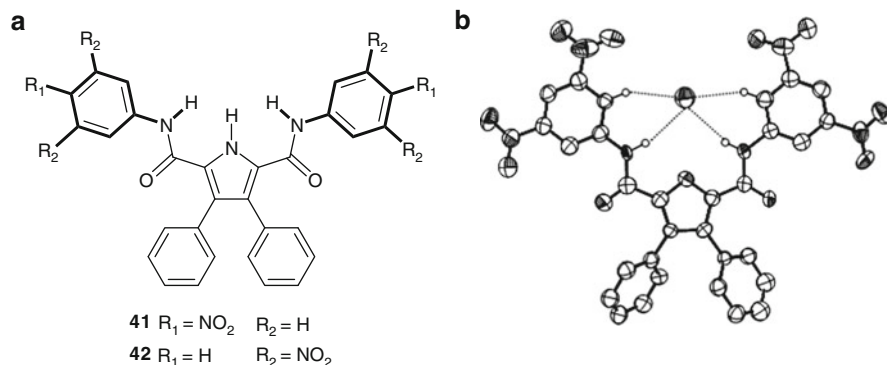


Fig. 26 Structures of 2,5-diamidopyrrole sensors **41** and **42** (a). Single crystal X-ray structure of the chloride anion complex of the deprotonated form of the linear pyrrole-based anion receptor **42** (b)

in the affinity order of $\text{CH}_3\text{CO}_2^- > \text{Cl}^- > \text{Br}^- > \text{HSO}_4^- > \text{I}^-$, and an overall preference for chloride ($K_a = 110,000 \text{ M}^{-1}$) and acetate ($K_a > 10^6 \text{ M}^{-1}$).

Jeong et al. have also continued their work on macrocyclic sensors comprising the indole moiety with the studies of the indolocarbazoles **45** and **46** [78]. Indolocarbazoles have previously been shown to be effective anion complexation moieties [79]. The macrocycles are characterized by a lack of conformational flexibility and possess well-defined anion-binding cavities of different sizes. The smaller macrocycle **45** has been shown to bind azide anions “end-on”, i.e., all the NH groups form hydrogen bonds to a single terminal nitrogen in azide, while compound **46**, which possesses a larger cavity, encapsulates the azide anion with each indolocarbazole unit forming hydrogen bonds to the terminal nitrogens of the azide in an “end to end” fashion (Fig. 27). UV–Vis titrations in a 10% methanol–acetone solution revealed that the end-to-end binding mode results in a more stable complex compared to the “end-on” arrangement with the association constants for azide to be $K_a = 2,300 \text{ M}^{-1}$ for **45** and $81,000 \text{ M}^{-1}$ for **46**, respectively. The highest ratio K_a (**46/45**) was found with iodide which interacts only very weakly with compound **45** ($K_a < 10 \text{ M}^{-1}$) but is bound strongly by compound **46** ($K_a = 2,400 \text{ M}^{-1}$). Compound **46** is a particularly good receptor for dihydrogen phosphate binding this anion with a stability constant $K_a = 220,000 \text{ M}^{-1}$.

Sessler and Katayev have reported the synthesis of three new bipyrrrole- or dipyrromethane-based amido-imine hybrid macrocycles, **47–49**, based on substituted

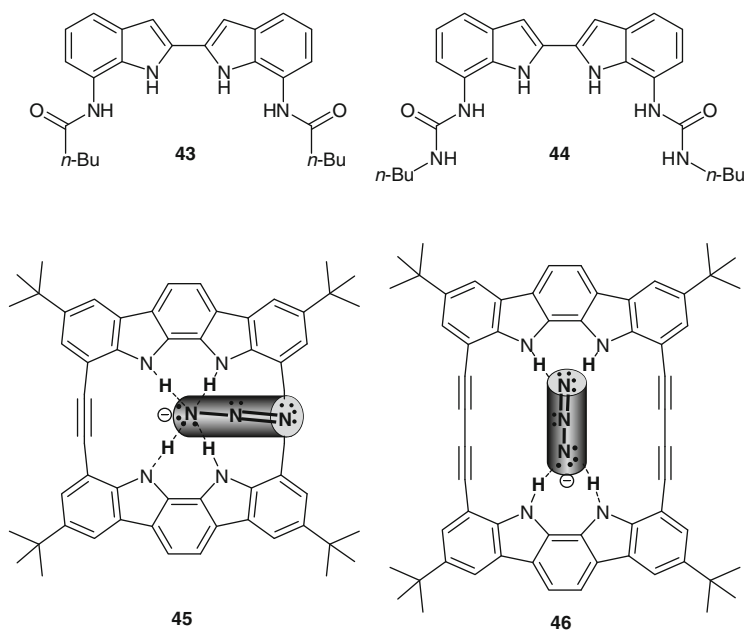


Fig. 27 Structures of biindole sensors **43** and **44** (top) and indolocarbazole sensors **45** and **46** (bottom)

pyrrole units (Fig. 28) [80]. The three receptors display very high affinities for oxoanions with stability constants determined by UV–Vis titrations in acetonitrile in the order of 10^7 M^{-1} . Only receptor **47** is able to bind the large perrhenate anion ($K_a = 124,000 \text{ M}^{-1}$), while the most structurally rigid receptor **49** shows a preference for chloride ($K_a = 281,000 \text{ M}^{-1}$). This unusual preference for a spherical halide was rationalized on the basis of X-ray diffraction studies, which showed that in the chloride complex all pyrrole rings and the two amide groups point into the cavity and are available for hydrogen bonding. As a consequence, the size of the cavity is almost circular and relatively small and accommodates best spherical anions such as chloride or bromide.

The three large oligopyrrolic macrocyclic sensors **50**, **51**, and **52** (Fig. 28) have been reported by the same authors [81, 82]. The anion binding properties of the sensors **50–52** were investigated by UV–Vis titrations in acetonitrile using a variety of anions including Cl^- , Br^- , NO_3^- , CH_3COO^- , ClO_4^- , ReO_4^- , HSO_4^- , and H_2PO_4^- . All three compounds display a strong preference for HSO_4^- and H_2PO_4^- ($K_a > 10,000 \text{ M}^{-1}$ in all cases and in a few instances approaching $10 \times 10^6 \text{ M}^{-1}$). Interestingly, compounds **50** and **51** bind H_2PO_4^- with a 1:2 receptor:anion stoichiometry in solution while compound **52** was shown to bind H_2PO_4^- with a 1:3 stoichiometry. Receptor **50** interacts strongly with acetate ($K_a = 25,700 \text{ M}^{-1}$) while compound **51** shows only moderate affinity toward both acetate ($K_a = 2,400 \text{ M}^{-1}$) and chloride ($K_a = 2,430 \text{ M}^{-1}$), presumably due to the presence of the flexible

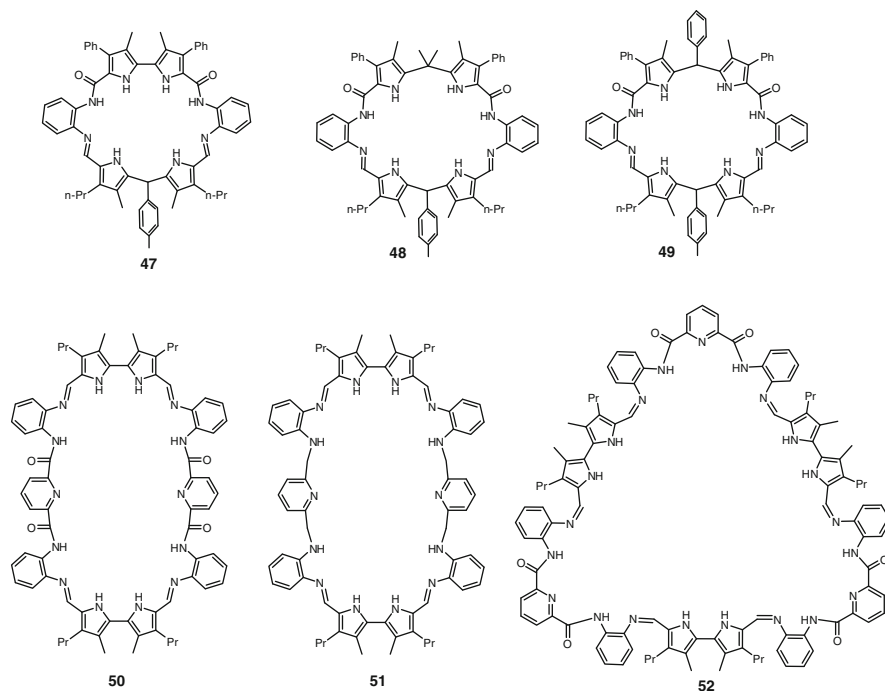


Fig. 28 Structures of sensors 47–52

methylamino linkers, which enables a wider range of conformations, but also reduces slightly the preorganization of the receptor. Macrocycle **52** is unique amongst the compounds studied as it is capable of binding perrhenate ReO_4^- ($K_a = 2,240 \text{ M}^{-1}$), an anion frequently used as a model for radioactive pertechnetate. Interestingly, upon addition of one equivalent of H_2PO_4^- to **52**, the solution becomes slightly orange turning back to yellow when an excess of anion is added. This is presumably due to the fact that the receptor can complex three equivalents of this anion in the solution with the red color generated by complexes of lower stoichiometry. All in all, the macrocycles **47–52** could be interesting anion sensors as they display interesting anion-binding profiles, are not prone to deprotonation, and are capable of clearly observable signal transduction. However, their synthesis – like in most expanded porphyrinoids – is among the most difficult presented in this section, and may present an obstacle for the future use of these materials.

A relatively large number of potential anion sensors were prepared and studied while displaying anion binding with concomitant change in color that also display significant propensity toward deprotonation. This is not to say that these sensors do not bind anions, but rather that both processes, i.e., binding and deprotonation, take place at the same time, and often the association constant and the deprotonation equilibrium constant are not significantly different. Such a situation results in complex equilibria that are difficult to analyze and quantify. A very insightful account on anion-sensor deprotonation was recently published by Fabbrizzi and coworkers [83]. While such materials are not necessarily disqualified as anion sensors, the conditions during the anion sensing experiments must be set up in such a way that what is observed is indeed anion sensing, not a simple deprotonation. It is then even more difficult to set up experimental conditions for sensing and reduce such sensors to practice in a way that would result in unambiguous qualitative and quantitative information. While this depends on the actual sensors and anions, it appears that perhaps the best way is to carry the anion-sensing experiments in an excess of aqueous buffer (e.g., 50–100 mM HEPES pH=7.0 and DMSO 1:1). Here, the DMSO enables the solubilization of the sensor while the aqueous HEPES provides conditions at which a potentially deprotonated sensor is immediately reprotonated, and the concentration of the HEPES prevents substantial changes in the pH even in the presence of relatively high anion concentration.

Examples of colorimetric sensors that also show deprotonation are numerous. Perhaps, one of the best examples are the 4,4'-dicarboxamidoindole-2,2'-bipyridine and the corresponding Pt(II)Cl_2 complex by Caltagirone et al. [84], which can act as a colorimetric sensor for fluoride. The NMR titrations with fluoride show a formation of a hydrogen-bonded complex in a slow exchange regime, which at higher fluoride concentration suffers deprotonation. Both hydrogen-bonding and deprotonation and the corresponding equilibrium constants are distinctive enough that they can be observed by NMR and UV-Vis spectroscopy. Not always, however, is the situation as clear as in the case of pyrrole carboxamide-based sensors [85] or diazo-substituted pyrrole sensors [86], for example, which display a prominent effect of deprotonation.

7 Concluding Remarks

This chapter, sadly, presents only highlights from work of many groups active in the field of pyrrole-based receptors and sensors. This chapter did not cover receptor chemistry, sensing of electroneutral analytes, metal ions, gasses, and others. It appears that the field of pyrrole sensors has flowered over the years, building on a solid background studies devoted to pyrrole receptor chemistry. Pyrrole as a receptor-generating “building block” has the further advantage that it can be functionalized readily and thus incorporated into an almost infinite number of very elaborate receptor systems. While the structural diversity is obvious, upon reading these paragraphs the reader can see that there are also patterns: patterns that can be followed like a red thread to more and more new sensors. Soon, yesterday’s receptors will pop-up as sensors in various sensing ensembles, with chromophores attached to provide new knowledge and serve the scientific community, and, perhaps, drive new products to markets to serve people. It is safe to predict that pyrrole-based systems will continue to play a prominent part in the evolving story of anion recognition and anion sensing.

References

1. Sessler JL, Gale PA, Cho W (2006) *Anion Receptor Chemistry*; Monographs in Supramolecular Chemistry; The Royal Society of Chemistry: Cambridge, 2006
2. Cho WS, Sessler JL (2005) Artificial pyrrole-based anion receptors. In: Schrader T, Hamiltonz AD (eds) *Functional synthetic receptors*. Wiley-VCH, Weinheim
3. Sessler JL, Camiolo S, Gale PA (2003) *Coord Chem Rev* 240:17–55
4. Gale PA, Quesada R (2006) *Coord Chem Rev* 250:3219–3244
5. Gale PA, Garcia-Garrido SE, Garric J (2008) *Chem Soc Rev* 37:151–190
6. Caltagirone C, Gale PA (2009) *Chem Soc Rev* 38:520–563
7. Beer PD, Gale PA (2001) *Angew Chem Int Ed* 40:486–516
8. Sessler JL, Weghorn SJ (1997) Expanded, contracted & isomeric porphyrins. *Tetrahedron organic chemistry series*, vol 15. Pergamon, Oxford, UK
9. Sessler JL, Seidel D (2003) *Angew Chem Int Ed*, Oxford, UK, 42:5134–5175
10. Sessler JL, Davis JM, Král V, Kimbrough T, Lynch V (2003) *Org Biomol Chem* 1:4113–4123
11. Sessler JL, Davis JM (2001) *Acc Chem Res* 34:989–997
12. Král V, Sessler JL, Zimmerman RS, Seidel D, Lynch V, Andrioletti B (2000) *Angew Chem Int Ed* 39:1055–1058
13. Sessler JL, Zimmerman RS, Bucher C, Král V, Andrioletti B (2001) *Pure Appl Chem* 73:1041–1057
14. Koehler T, Seidel D, Lynch V, Arp FO, Ou Z, Kadish KM, Sessler JL (2003) *J Am Chem Soc* 125:6872–6873
15. Seidel D, Lynch V, Sessler JL (2002) *Angew Chem Int Ed* 41:1422–1425
16. Carvlin MJ, Fiel RJ (1983) *Nucl Acids Res* 11:6121–6139
17. Fiel RJ, Howard JC, Mark EH (1979) Datta Gupta N. *Nucl Acids Res* 6:3093–3118
18. Fiel RJ, Munson BR (1980) *Nucl Acids Res* 8:2835–2842
19. Pasternack RF, Gibbs EJ, Villafranca JJ (1983) *Biochem* 22:5409–5417
20. Pasternack RF, Antebi A, Ehrlich B, Sidney D, Gibbs EJ, Bassner SL, Depoy LM (1984) *J Mol Catal* 23:235–242

21. Takeuchi M, Shioya T, Swager TM (2001) *Angew Chem Int Ed* 40:3372–3376
22. Schumacher AL, Hill P, Ariga K, D'Souza F (2007) *Electrochem Commun* 9:2751–2754
23. Gupta I, Frohlich R, Ravikanth M (2008) *Eur J Org Chem* 11:1884–1900
24. Sessler JL, Cyr MJ, Lynch V, McGhee E, Ibers JA (1990) *J Am Chem Soc* 112:2810–2813
25. Shionoya M, Furuta H, Lynch V, Harriman A, Sessler JL (1992) *J Am Chem Soc* 114: 5714–5722
26. Furuta H, Cyr MJ, Sessler JL (1991) *J Am Chem Soc* 113:6677–6678
27. Sessler JL, Ford DA, Cyr MJ, Furuta H (1991) *J Chem Soc Chem Commun* 1733–1735
28. Sessler JL, Cyr MJ, Burrell AK (1991) *Synlett* 127–134
29. Sessler JL, Mody TD, Ford DA, Lynch VM (1992) *Angew Chem Int Ed* 31:452–455
30. Sessler JL, Morishima T, Lynch VM (1991) *Angew Chem Int Ed* 30:977–980
31. Bauer VJ, Clive DLJ, Dolphin D, Paine JB III, Harris FL, King MM, Loder J, Wang SWC, Woodward RB (1983) *J Am Chem Soc* 105:6429–6436
32. Král V, Furuta H, Shreder K, Lynch VM, Sessler JL (1996) *J Am Chem Soc* 118:1595–1607
33. Iverson BL, Shreder K, Král V, Lynch VM, Sessler JL (1996) *J Am Chem Soc* 118:1608–1616
34. Král V, Sessler JL (1995) *Tetrahedron* 51:539–554
35. Gorden AEV, Davis J, Sessler JL, Král V, Webster KD, Schroeder NL (2004) *Supramol Chem* 16:91–100
36. Sessler JL, Andrievsky A, Král V, Lynch VM (1997) *J Am Chem Soc* 119:9385–9392
37. Baeyer A (1886) *Dtsch Chem Ges* 19:2184–2185
38. Gale PA, Sessler JL, Král V, Lynch VM (1996) *J Am Chem Soc* 118:5140–5141
39. Camiolo S, Coles SJ, Gale PA, Hursthouse MB, Sessler JL (2001) *Acta Cryst* E57:o816–o818
40. Anzenbacher P Jr, Try AC, Miyaji H, Jursíková K, Lynch VM, Marquez M, Sessler JL (2000) *J Am Chem Soc* 122:10268–10272
41. Sessler JL, Gross DE, Cho WS, Lynch VM, Schmidtchen FP, Bates GW, Light ME, Gale PA (2006) *J Am Chem Soc* 128:12281–12288
42. Miyaji H, Sato W, Sessler JL (2000) *Angew Chem Int Ed* 39:1777–1780
43. Nishiyabu R, Anzenbacher P Jr (2005) *J Am Chem Soc* 127:8270–8271
44. Anzenbacher P Jr, Jursíková K, Shriver JA, Miyaji H, Lynch VM, Sessler JL, Gale PA (2000) *J Org Chem* 65:7641–7645
45. Marshall WJ, Bangert SK (2004) *Clinical chemistry*, 5th edn. Elsevier, Edinburg
46. Schmidt RF, Thews G (1989) *Human physiology*, 2nd edn. Springer, Berlin
47. Hong SJ, Yoo J, Kim SH, Kim JS, Yoon J, Lee CH (2009) *Chem Commun* 189–191
48. Lee CH, Miyaji H, Yoon DW, Sessler JL (2008) *Chem Commun* 24–34
49. Kim SH, Hong SJ, Yoo J, Kim SK, Sessler JL, Lee CH (2009) *Org Lett* 11:3626–3629
50. Yoo J, Kim MS, Hong SJ, Sessler JL, Lee CH (2009) *J Org Chem* 74:1065–1069
51. Nishiyabu R, Palacios MA, Dehaen W, Anzenbacher P Jr (2006) *J Am Chem Soc* 128: 11496–11504
52. Gu R, Depraetere S, Kotek J, Budka J, Wagner-Wysiecka E, Biernat JF, Dehaen W (2005) *Org Biomol Chem* 3:2921–2923
53. Depraetere S, Smet M, Dehaen W (1999) *Angew Chem Int Ed* 38:3359–3361
54. Palacios MA, Nishiyabu R, Marquez M, Anzenbacher P Jr (2007) *J Am Chem Soc* 129: 7538–7544
55. Lavigne JJ, Savoy S, Clevenge MB, Ritchie JE, McDoniel B, Yoo SJ, Anslyn EV, McDevitt JT, Shear JB, Neikirk D (1998) *J Am Chem Soc* 120:6429–6430
56. Goodey A, Lavigne JJ, Savoy SM, Rodriguez MD, Currey T, Tsao A, Simmons G, Wright J, Yoo SJ, Sohn Y, Anslyn EV, Shear JB, Neikirk DP, McDevitt JT (2001) *J Am Chem Soc* 123:2559–2570
57. Legin A, Smirnova A, Rudnitskaya A, Lvova L, Suglobova E, Vlasov Y (1999) *Anal Chim Acta* 385:131–135
58. DiNatale C, Davide F, Brunink JAJ, D'Amico A, Vlasov YG, Legin AV, Rudnitskaya AM (1996) *Sens Actuators B* 34:539–542
59. Gale PA, Twyman LJ, Handlin CI, Sessler JL (1999) *Chem Commun* 1851–1852

60. Shao S, Guo Y, He L, Jiang S, Yu X (2003) *Tetrahedron Lett* 44:2175–2178
61. Linn MM, Poncio DC, Machado VG (2007) *Tetrahedron Lett* 48:4547–4551
62. Saki N, Akkaya EU (2005) *J Inclusion Phenom Macrocycl Chem* 53:269–273
63. Oddo B (1911) *Gazz Chim Ital* 41:248–255
64. Behr D, Brandänge S, Lindström B (1973) *Acta Chem Scand* 27:2411–2414
65. Black CB, Andrioletti B, Try AC, Ruiperez C, Sessler JL (1999) *J Am Chem Soc* 121:10438–10439
66. Pietrzak M, Try AC, Andrioletti B, Sessler JL, Anzenbacher P Jr, Limbach HH (2008) *Angew Chem* 120:1139–1142
67. Mizuno T, Wei WH, Eller LR, Sessler JL (2002) *J Am Chem Soc* 124:1134–1135
68. Anzenbacher P Jr, Tyson DS, Jursíková K, Castellano FN (2002) *J Am Chem Soc* 124:6232–6233
69. Sessler JL, Maeda H, Mizuno T, Lynch VM, Furuta H (2002) *Chem Commun* 862–863
70. Sessler JL, Pantos DL, Katayev E, Lynch VM (2003) *Org Lett* 5:4141–4144
71. Sessler JL, Maeda H, Mizuno T, Lynch VM, Furuta H (2002) *J Am Chem Soc* 124:13474–13479
72. Sessler JL, Cho DG, Lynch V (2006) *J Am Chem Soc* 128:16518–16519
73. Lin Z, Chen HC, Sun SS, Hsu CP, Chow TJ (2009) *Tetrahedron* 65:5216–5221
74. Camiolo S, Gale PA, Hursthouse MB, Light ME (2003) *Org Biomol Chem* 1:741–744
75. Chang KJ, Moon D, Lah MS, Jeong KS (2005) *Angew Chem Int Ed* 44:7926–7929
76. Lee JY, Lee MH, Jeong KS (2007) *Supramol Chem* 19:257–263
77. Chang KJ, Chae MK, Lee C, Lee JY, Jeong KS (2006) *Tetrahedron Lett* 47:6385–6388
78. Kim NK, Chang KJ, Moon D, Lah MS, Jeong KS (2007) *Chem Commun* 3401–3403
79. Curiel D, Cowley A, Beer PD (2005) *Chem Commun* 236–238
80. Katayev EA, Boev NV, Khrustalev VN, Ustynyuk YA, Tananaev IG, Sessler JL (2007) *J Org Chem* 72:2886–2896
81. Katayev EA, Sessler JL, Khrustalev VN, Ustynyuk YA (2007) *J Org Chem* 72:7244–7252
82. Sessler JL, Katayev EA, Pantos GD, Reshetova MD, Khrustalev VN, Lynch VM, Ustynyuk YA (2005) *Angew Chem Int Ed* 44:7386–7390
83. Amendola V, Esteban-Gomez D, Fabbrizzi L, Licchelli M (2006) *Acc Chem Res* 39:343–353
84. Caltagirone C, Mulas A, Isaia F, Lippolis V, Gale PA, Light ME (2009) *Chem Commun* 6279–6281
85. Chen CL, Lin TP, Chen YS, Sun SS (2007) *Eur J Org Chem* 3999–4010
86. Chauhan SMS, Bisht T, Garg B (2009) *Sens Actuators B Chem* B141:116–123

Pyrrole-Based Anion Sensors, Part II: Fluorescence, Luminescence, and Electrochemical Sensors

Pavel Anzenbacher Jr.

Abstract This review focuses on fluorescence and luminescence-based sensors as well as electrochemical sensors based on the pyrrole moieties. The fluorescence sensors include porphyrins and expanded porphyrins such as sapphyrins, calixpyrroles with covalently attached fluorophore moieties, and are – together with the colorimetric sensors – the largest growing group of pyrrole-based sensors. Similarly, the electrochemical sensors comprising pyrrole moieties are also becoming popular. They include calixpyrrole, porphyrin, and calixphyrin receptors combined with metallocene, as well as dipyrrolylquinoxalines and others. While the electrochemical signal transduction is at times difficult to interpret, they hold a promise for the development of sensitive ion-selective electrodes (ISEs) and other devices in the future.

Keywords Anions · Electrochemistry · Fluorescence · Luminescence · Sensor

Contents

1	Introduction	237
2	Fluorescence-Based Sensors	238
3	Pyrrole-Based Electrochemical Anion Sensors	257
4	Concluding Remarks	264
	References	264

1 Introduction

In the last two decades there has been a dramatic increase in the development of luminescence-based sensor for anions. In the realm of optical sensors [1, 2], the luminescence-based methods show unique potential for high sensitivity at low analyte concentration. With the development of inexpensive strong and monochromatic sources of excitation light such as LEDs or solid state lasers and sensitive detectors the luminescence methods become routinely available in small dimensions (and battery powered modules), which make them available for field operation. Hence, the luminescence-based methods of sensing are now widely accessible to all scientific community, and while the luminescence methods are, perhaps, still little under-utilized in supramolecular chemistry, their superior features such as sensitivity and ability to operate in intensity as well as lifetime and other modes compared to colorimetric methods will make them increasingly popular in the near future. The first luminescence-based sensors for anions date to 1980s and early 1990s to works of Beer, Balzani, Czarnik, and others [3–5]. It should be noted that a large portion of optical sensors with large pi-delocalized chromophores, typically oligo-acenes, are both chromophores as well as fluorophores, and it is not surprising that a number of compounds introduced in previous paragraphs can act both as colorimetric and fluorimetric sensors. Even though the division is somewhat arbitrary, in this review the sensors are listed based on their use as it appears in chemical literature.

2 Fluorescence-Based Sensors

In the fluorescence- and luminescence-based sensors, pyrroles and their congeners also act as donors in the intramolecular partial charge-transfer (IPCT) cascade to transfer the excess of electronic density. The frequently observed decrease in luminescence intensity, albeit more difficult to attribute, is commonly due to several effects including direct quenching by the anion, or due to red-shifted luminescence, which is easier to deactivate via nonradiative processes. In the case that the luminescence does not shift, because of a generally small Stokes shift in organic molecules, the overlap between absorption and emission results in luminescence self-absorption, which also usually decreases the emission intensity. In rare cases, when the formation of the sensor-anion complex dramatically reduces the rotational and vibrational motion, the deactivation pathways for nonradiative processes are limited, and a turn-on sensor may be realized. Finally, combinations of both IPCT and increased rigidity of the system may result in a combination of both effects, which then often leads to a ratiometric-type response. Needless to say, turn-on signaling and ratiometric response are highly useful and desirable features, as they are easily distinguished from nonspecific kinetic quenching, and provide output easier to harness in applications.

In electrochemistry, the smaller increase in LUMO energy levels are likely to increase the reduction potential because the electron-rich sensor–anion complex would be more difficult to reduce, while the relatively larger increase in HOMO-levels is likely to result in a dramatic change in oxidation potentials. However, in pyrrole-based sensors the sensor oxidation is frequently irreversible and results in the formation of polypyrrole-type coatings on the working electrode. While the optical processes are easier and more reliable to interpret, the perhaps too simple predictions and interpretations of the electrochemistry data need to be evaluated quite carefully. Needless to say, electronic effects associated with anion hydrogen bonding to pyrroles, IPCT, and associated changes in the HOMO-LUMO gap are important for signal transduction and generating the output signal.

The first luminescence studies on pyrrole-based sensors are, once again, dated back to the porphyrin literature. Among the first successful fluorescence-based sensors are therefore porphyrins and expanded porphyrins, particularly sapphyrins.

Another method, one that is widely available for use with various receptors involves the covalent attachment of a fluorophore to the polypyrrole skeleton. Perturbation of the electronic properties of these attached groups upon anion complexation then produces a response detectable by the naked eye or via changes in the fluorescence spectrum or both. Here, the first systems reported in the literature were covalently linked, calixpyrroles bearing anthracene subunits (i.e., calix[4]pyrroles **1**) [6]. These systems were obtained from the coupling of a calixpyrrole aminoacids and various aminoanthracenes (Fig. 1).

The fluorescence of these sensors **1–3** was shown to be quenched significantly in the presence of certain anionic guests, with the degree of quenching depending on the bound anion. Two aspects were explored in this study. First, the direct amide-connection between the OMCP and the anthracene fluorophore in **1**, which provides not only electron-withdrawing effect on the pyrrole making it more acidic and available for hydrogen bonding but also cross-conjugation with the anthracene. Second, in **2** the OMCP receptor is separated from the carboxamide functionality by a methylene bridge, thus largely removing the possibility of a direct through-the-bond electronic communication between the pyrrole and the signaling fluorophore. Finally, in sensor **3** both the OMCP and the anthracene fluorophore were separated by a methylene bridge from the carboxamide moiety, separating both the receptor and the fluorophore from the amide. The affinity was determined from the quenching of the blue anthracene fluorescence (390–520 nm). All three sensors showed a

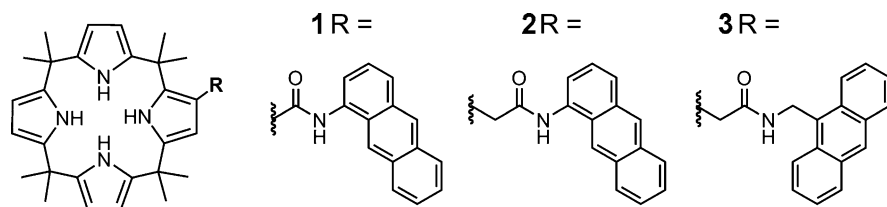


Fig. 1 Structures of the first generation calix[4]pyrrole fluorescent sensors for anions

similar trend in their anion-sensing behavior, albeit the association constants were the highest for the direct carboxamide compound **1**. Thus, for fluoride the $K_a = 148,000 \text{ M}^{-1}$ in case of **1** (**2**: $K_a = 48,980 \text{ M}^{-1}$, **3**: $K_a = 48,980 \text{ M}^{-1}$), for chloride the $K_a = 74,130 \text{ M}^{-1}$ in case of **1** (**2**: $K_a = 6,460 \text{ M}^{-1}$, **3**: $K_a = 5,130 \text{ M}^{-1}$), and for dihydrogen phosphate the $K_a = 91,200 \text{ M}^{-1}$ in case of **1** (**2**: $K_a = 7,940 \text{ M}^{-1}$), all the constants were determined in acetonitrile.

Following the same concept, the second generation calix[4]pyrrole anion sensors **4–6** were produced by Anzenbacher et al. [7]. In this case, dansyl, Lissamine-rhodamine B, or fluorescein moieties were attached to the calix[4]pyrrole framework to serve as the fluorescent reporter groups, while an amide or thiourea residue was used as the covalent linker between these fluorophores and the calix[4]pyrrole backbone (Fig. 2). This choice of a linker serves to provide the second anion binding site. Most importantly, sensors **5** and **6** require the presence of water and neutral-to-basic pH to hydrolyze the lactone of the rhodamine and fluorescein labels. Therefore, a small amount of buffered water was added into the acetonitrile (94:4 water, pH 7.0). Once again, the anion binding was monitored using the decrease in fluorescence emission intensity observed when sensor **5** was titrated with an increasing concentration of anions. It was found that sensors **4–6** show considerable selectivity for dihydrogen phosphate and pyrophosphate anions relative to chloride anions. This selectivity was explained by the presence of the second anion binding group, namely the amide or thiourea link, and the favorable interactions it permits with nonspherical anions. These same ancillary interactions permit sensors **5–6** to operate successfully in the presence of a small amount of water at physiological pH.

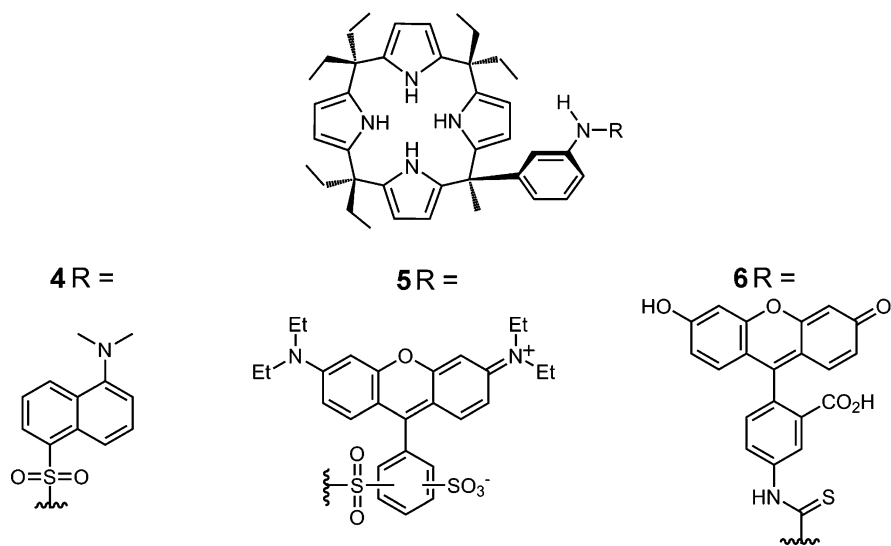


Fig. 2 The second generation of calix[4]pyrrole fluorescent sensors **4–6** was found to operate in acetonitrile in the presence of water at pH 7.0

Quantitative assessments of the anion-induced spectral changes were used to determine the affinity constants for this and other representative anions and were as follows. Thus, for fluoride the sensor **4** showed $K_a = 148,000 \text{ M}^{-1}$ while for both **5** and **6** the respective K_a were $> 10^6 \text{ M}^{-1}$. For chloride, however, the values of association constants were found significantly lower: $K_a = 10,500 \text{ M}^{-1}$, $K_a = 18,200 \text{ M}^{-1}$, and $K_a < 10,000 \text{ M}^{-1}$ for **4–6**, respectively. The recorded association constants for dihydrogen phosphate were as follows: $K_a = 168,300 \text{ M}^{-1}$, $K_a = 446,000 \text{ M}^{-1}$, and $K_a = 682,000 \text{ M}^{-1}$ for **4–6**, respectively. Finally, the association constants for hydrogen pyrophosphate (or rather dihydrogen pyrophosphate due to equilibrium) the constants were $K_a = 131,000 \text{ M}^{-1}$, $K_a = 170,000 \text{ M}^{-1}$, and $K_a > 10^6 \text{ M}^{-1}$ for **4–6**, respectively.

As part of their work on strapped calix[4]pyrroles, Lee et al. also developed a coumarin-strapped calix[4]pyrrole, in which the fluorescence intensity can be controlled by the dual “input parameters” of cation and anion; the added cation (Na^+) “switches on” the signal, generating a high intensity state, whereas the anion (Cl^-) “switches off” the signal, producing a low intensity state [8]. Thus, while the association constants were $K_a = 1.9 \times 10^6 \text{ M}^{-1}$, $K_a = 3.7 \times 10^4 \text{ M}^{-1}$, and $K_a = 8.9 \times 10^5 \text{ M}^{-1}$, for chloride, bromide and acetate in wet acetonitrile, respectively, in the presence of sodium hexafluorophosphate the same association constants were found to be higher. In the presence of a sodium ion, the corresponding constants were $K_a = 2.3 \times 10^6 \text{ M}^{-1}$, $K_a = 1.0 \times 10^5 \text{ M}^{-1}$, and $K_a = 1.3 \times 10^5 \text{ M}^{-1}$ for chloride, bromide, and acetate, respectively.

Another strongly represented group of pyrrole containing fluorescence-based anion sensors are DPQ derivatives. Because the DPQ derivatives display both colorimetric and fluorimetric response, a number of DPQ derivatives were utilized for fluorescence-based anion sensing. Anzenbacher et al. published several works on DPQ derivatives useful as fluorescence-based sensors [9–11]. For example, two series of DPQ derivatives with extended conjugated substituents attached in the 5,8-positions of the quinoxaline ring were synthesized and their anion-sensing properties tested (Fig. 3). In the first series, sensors **7–10** and **11–14** with extended conjugated moieties help to establish brightly fluorescent chromophores with tunable fluorescent output. In general, the anion affinities did not change significantly compared to the parent DPQ derivatives [9]. However, what changed dramatically was the wavelength at which these sensors emit light (Fig. 3 bottom), a feature important in practical applications. The photograph in Fig. 3 also shows a comparison with the fluorescence output of the parent DPQ, which shows blue-shifted emission in the near-UV region.

Perhaps more important is the demonstration of the fluorescence sensitivity. Figure 4 shows sensor **9**, solutions in CH_2Cl_2 illuminated with black light. Sensor **9** displays a response to fluoride and hydrogen pyrophosphate anions, $K_a = 25,600 \text{ M}^{-1}$ and $K_a = 57,300 \text{ M}^{-1}$ for fluoride and pyrophosphate, respectively. The same sensor displays affinity for chloride and dihydrogen phosphate lower than 100 M^{-1} . Yet, when one examines carefully the photograph in Fig. 4, it is obvious that compared to the control (Blank) sample, the weakly binding anions such as chloride and phosphate also quench the strong fluorescence in **9**. It should

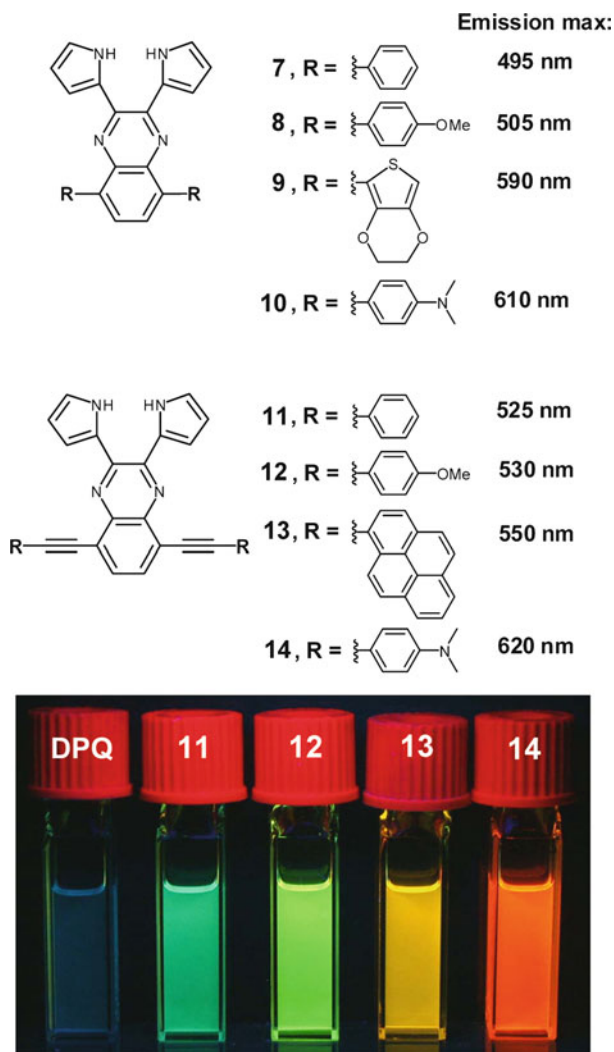


Fig. 3 Structures of DPQ derivatives with improved fluorescence properties 7–14

be noted that a large excess of weakly binding anion is required to achieve a clearly observable quenching.

Sun and coworkers have synthesized a series of dipyrrolylquinoxaline (DPQ)-containing monomer **11** and polymers (**15** and **16**) which were employed as chromogenic and fluorescent chemosensors for inorganic anions [12]. Anion binding studies were conducted using UV–Vis, fluorescence and ^1H NMR spectroscopic techniques in CH_2Cl_2 and $\text{DMSO}-d_6$ solution, respectively, and the following binding affinity order for all compounds examined was found: $\text{F}^- > \text{HP}_2\text{O}_7^{3-} > \text{CN}^- > \text{AcO}^- > \text{H}_2\text{PO}_4^- \approx \text{Cl}^- \approx \text{Br}^- \approx \text{I}^- \approx \text{NO}_3^-$. The sensitivity of the

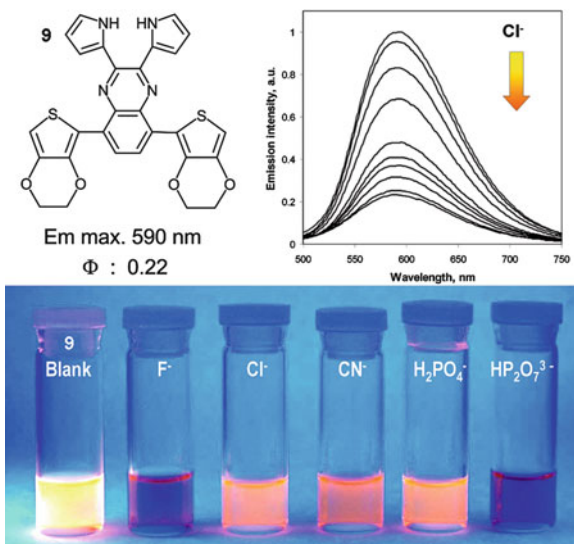
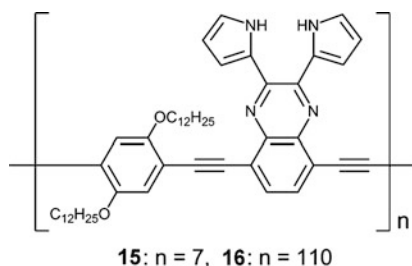


Fig. 4 DPQ-based fluorescence sensor **9**. The sensor fluorescence can be largely quenched by adding weakly binding anions such as chloride, cyanide, or dihydrogen phosphate.

Note: the anions in vials are in 100 equivalent excess

Fig. 5 Structure of DPQ-based poly(phenylene ethynylene) sensors **15** and **16** that display amplified quenching



DPQ-based chemosensor was found to display a 34-fold enhancement by incorporation into the conjugated polymer. However, a careful UV-Vis spectroscopic study concluded that in the presence of fluoride or pyrophosphate, the colorimetric responses and fluorescence quenching observed in chemosensors **11**, **15**, and **16** were found to be due to a complex behavior that includes both anion binding and deprotonation of the N-H proton of the pyrrole units, so the anion selectivity is primarily determined by the relative basicity of the anions (Fig. 5).

As was mentioned above, the fluorescence-based signal transduction offers a number of possibilities, including various signal transduction modes such as intensity, lifetime, anisotropy, etc. Signal transduction utilizing emission lifetimes (lifetime-based chemical sensing) is particularly attractive, because it is unaffected by the sample's emission intensity, thereby circumventing many limitations of intensity-based methods. Anzenbacher et al. demonstrated a long-lifetime Ru(II)

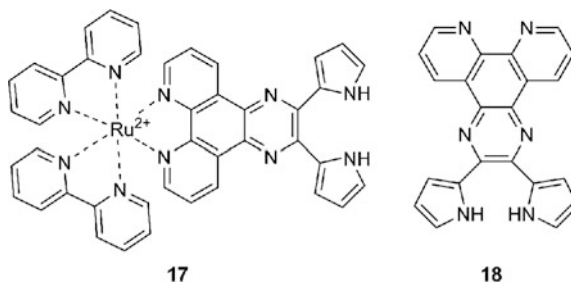


Fig. 6 Structure of sensor **17** and the DPQ-ligand **18**

(Bipy)₂DPQ complex **17** and the phenanthroline-DPQ ligand **18** to demonstrate the possibility of lifetime-based anion sensing [13] (Fig. 6).

Similar to the sensors **29** and **30** discussed in the Part I, the sensor **17** displays higher affinity for anions over the ligand **18**. The association constants in dichloromethane with 2% acetonitrile were fluoride: $K_a = 640,000 \text{ M}^{-1}$; cyanide: $K_a = 428,000 \text{ M}^{-1}$; chloride: $K_a = 3.7 \times 10^4 \text{ M}^{-1}$; and dihydrogen phosphate: $K_a = 8.9 \times 10^5 \text{ M}^{-1}$.

Prior to cyanide addition, this complex exhibits a single exponential lifetime ($\tau = 377 \pm 20 \text{ ns}$). With increasing cyanide concentrations, the intensity decays are composed of two exponentials: long τ (320–370 ns) and short τ (13–17 ns). These data suggest that there are at least two distinct luminescent species, consisting of anion-bound **17** (short τ) and free **17**, the sum of which results in the observed lifetime quenching in Fig. 7. The shift in fractional intensity makes **17** a suitable lifetime-based sensor for anions since the fractional intensity shifts from an initial dominant long lifetime component to the short lifetime component [13]. This work represents the first example of a direct method for the luminescence lifetime-based sensing of anions.

The following sensors **19** and **20** are examples of an approach according to which the quinoxaline moiety in DPQ sensors is replaced by different chromophores. This idea is important because various moieties bearing the pyrrole affinants will not only provide different signal output, but also because their electronic properties determine to which degree they participate in the IPCT as acceptor of the excess electron density on the pyrrole affinants. This, in turn, partly determines the acidity of the pyrrole NHs and on the binding-or-deprotonation equilibria in the sensor. The sensor **19** is a DPQ analog comprising a bridging moiety [14]. In the presence of fluoride CH_2Cl_2 , the color of solutions containing compound **19** changed from pale brown to yellow. While compound **19** displays a fluoride anion affinity ($K_a = 1.8 \times 10^5 \text{ M}^{-1}$) that is circa 10 times higher than that of the parent DPQ ($K_a = 1.8 \times 10^4 \text{ M}^{-1}$), its dihydrogenphosphate anion affinity is dramatically enhanced (by a factor of ca. 220; $K_a = 1.8 \times 10^4 \text{ M}^{-1}$ for **9** vs. 80 M^{-1} for DPQ, respectively). It is presumed that the presence of three electron-withdrawing ester substituents improves the anion affinities in a general way, while the geometry changes caused by replacing the quinoxaline moiety with a pyrrole serves to augment the dihydrogenphosphate anion selectivity (Fig. 8).

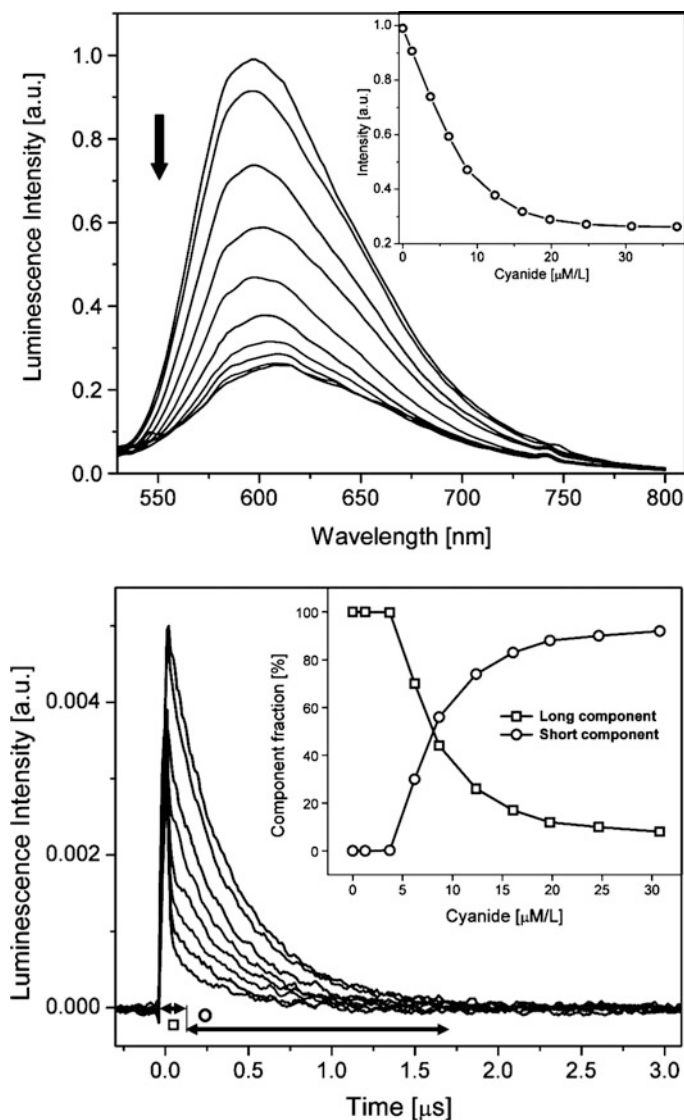
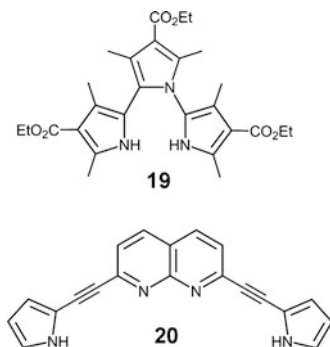


Fig. 7 *Top*: the quenching of the steady state photoluminescence spectrum of **17** measured throughout the cyanide titration and the corresponding response isotherm (*inset*). *Bottom*: changes in the time-resolved photoluminescence decay of sensor **17** upon the addition of cyanide (0–32 μM), obtained with 458 nm excitation. *Inset*: shifts in fractional intensity of the two lifetime components obtained from bi-exponential analysis. Reproduced with permission from [13]

Another recently reported system that could also be considered a DPQ analog is 2,7-bis(1*H*-pyrrol-2-yl)ethynyl-1,8-naphthyridine (BPN) **20** that contains two hydrogen bonding donors (pyrrolic NH) attached to naphthyridine chromophore via a dialkynyl spacer [15] (Fig. 8). In contradistinction to DPQ, sensor **20** has the

Fig. 8 Structures of sensors **19** and **20**

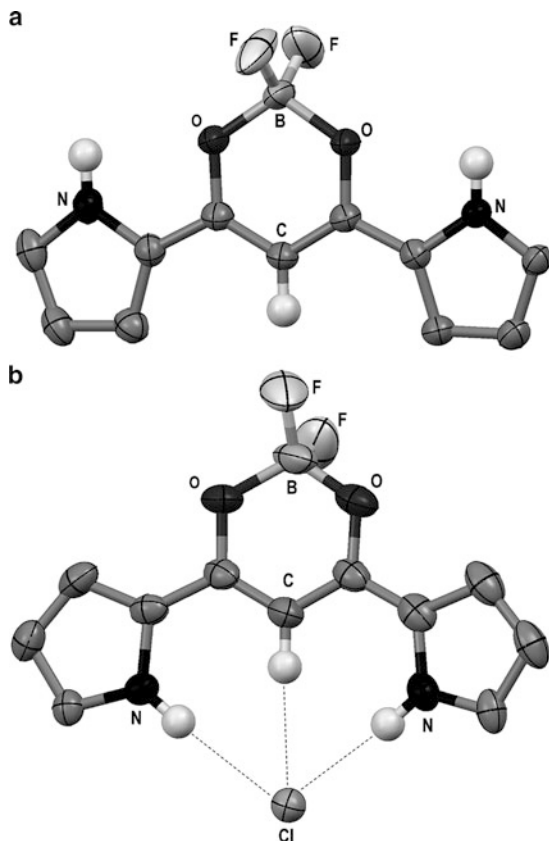


naphthyridine nitrogens exposed in the binding cavity so they could participate in creating an array of hydrogen-bond donors (pyrrole NHs) and acceptors (naphthyridine nitrogens), a feature that makes BPN an efficient saccharide receptor and sensor in CH_2Cl_2 . Upon binding of octylglycosides, the BPN fluorescence changes from cyan (emission maximum 475 nm) to yellow–green (maximum 535 nm). While the octylglycosides are not anionic, considering the similarity with DPQ receptors and sensors, it is more than likely that **20** is capable of binding and most likely also sensing sugar-phosphate analytes.

Maeda and coworkers have continued their work on BF_2 complexes of dipyrrolylpropanediones [16, 17] and have reported the synthesis and the anion binding properties of BF_2 complexes of β -tetraethyl-substituted pyrrolylpropanediones (**21**, and also **36** shown in the Part I). This type of acyclic fluorescence (and colorimetric) sensors displays interesting conformation change in the presence of anion. Figure 9 shows the dipyrrolylpropanedione- BF_2 moiety in the resting state (Fig. 9a) and in the presence of anions (Fig. 9b). In essence, at least three hydrogen atoms take part in the formation of the anion complex. These are the pyrrole NH moieties and the C–H of the propanedione- BF_2 ring. In the resting state, all three rings of the sensor are in one plane and both pyrrole NHs are in position *anti*- to the C–H. In the anion complexes, the three rings are also in one plane, but the pyrrole rings are turned for 180° and are *syn*- with the CH. Thus, the anion is surrounded by a pyrrole-dipyrrolylpropanedione- BF_2 -pyrrole cleft with all three hydrogen bond donors pointing to the anion (Fig. 9). The anion is also found in the same plane with the three rings.

The first generation sensors **21**–**25** display both a clearly observable change in color and fluorescence, and their anion binding properties were studied by UV–Vis titration techniques with a variety of putative anionic guests (F^- , Cl^- , Br^- , CH_3CO_2^- , H_2PO_4^- , and HSO_4^-). Most importantly, however, strong fluorescence was also observed, and a number of studies also employed fluorescence titration. It was found that upon addition of anions, the emission of sensors is almost completely quenched by fluoride and more modestly suppressed by oxoanions, possibly due to intramolecular electron transfer. The addition of chloride or bromide had little effect on the intensity of the fluorescence emission. Actually, it was

Fig. 9 Conformational transition in the dipyrrolylpropanedione- BF_2 moiety from the resting state (a) to an anion complex (b). Atoms that are not part of the dipyrrolylpropanedione- BF_2 or are not involved in hydrogen bonding were omitted



found that in some sensors such as **22**, the emission is completely quenched by addition of acetate and brought back to 80% of the original level by addition of chloride into the **22**-acetate complex (Fig. 10).

Sadly, the sensor **21** is not soluble enough for accurate quantitative studies. Therefore, the affinity for anions was determined only for sensors **22–25** [18]. In the dipyrrolylpropanedione- BF_2 sensors **22–25**, the overall anion binding affinities in CH_2Cl_2 were acetate > fluoride > dihydrogen phosphate > chloride > bromide > hydrogen sulfate. Among the sensors, the general trend in affinities was **24** < **25** < **22** < **23** suggesting that the electron-withdrawing effect of β -fluoro-substituents, previously observed in calix[4]pyrroles and DPQs, is at play in dipyrrolylpropanedione- BF_2 sensors as well [19] (Part I). Similarly, it appears that the electron-donating alkyl substituents decrease the acidity of hydrogens involved in the anion binding. Thus, the sensor **24** with two β -alkyl-substituents displays lowest affinity for anions. Sensor **22** with only one alkyl substituents which is attached in α -position displays higher affinity for the anions tested. The authors suggest that the sensor **25** with the high-electron density ethoxycarbonyl substituents might repel the negatively charged anions, thus contributing to surprisingly low affinity for

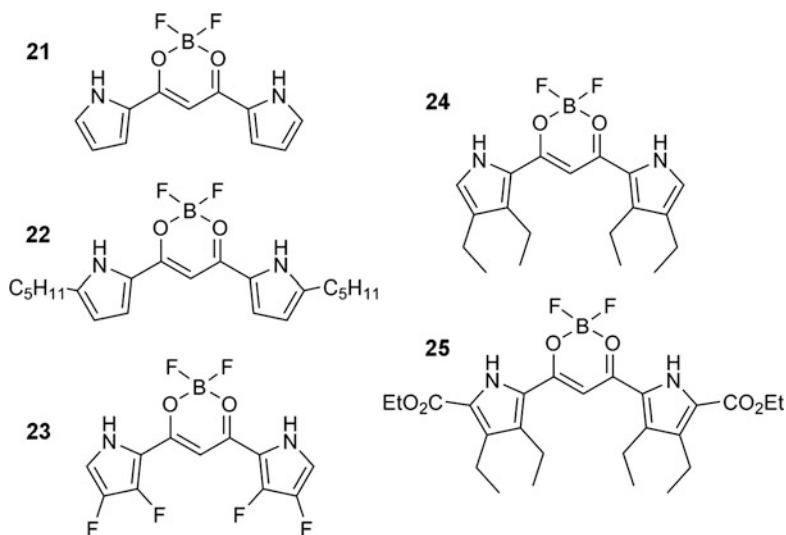


Fig. 10 Structure of the first generation dipyrrolylpropanedione-BF₂ sensors **21–25**

anions. From the pairs of two derivatives with electron-withdrawing groups in α - and β -position (**23** and **25**) and electron-donating alkyl substituents in α - and β -position (**22** and **24**) it appears that the electronic effects imparted by the α -substituents are weaker than the effects due to β -substituents. How much this is due to the fact that the β -substituents always appear in pairs compared to only one α -position per pyrrole moiety is not entirely clear. Regarding the selectivity for anions, the sensors **24** and **23** show the most interesting selectivity order of acetate > dihydrogen phosphate > fluoride and corresponding affinity constants. Sensor **23**: Acetate $K_a = 960,000 \text{ M}^{-1}$; dihydrogen phosphate $K_a = 190,000 \text{ M}^{-1}$; and fluoride $K_a = 160,000 \text{ M}^{-1}$. Sensor **24**: Acetate $K_a = 210,000 \text{ M}^{-1}$; dihydrogen phosphate $K_a = 91,000 \text{ M}^{-1}$; and fluoride $K_a = 42,000 \text{ M}^{-1}$. Thus, the binding constants for **24** display a ratio acetate:phosphate:fluoride of 4:2:1, which is quite remarkable selectivity.

The same authors reported another class of dipyrrolylpropanedione-BF₂ sensors **26–32** with aryl-substitution on dipyrrolyldiketone skeleton (Fig. 11) [20, 21]. Series of organogelators that contain long alkoxy chains at the 3-, 4- and 5-positions of the pendant aromatic ring labeled by a common number **30** but carrying different alkyl residues R were also synthesized. Finally, a last sub-series **30–32** comparing phenyl to thien-2-yl and pyrrole-2-yl in the α -position of the pyrrole substituents was also studied.

The binding constants for the 1: 1 complexes of receptors **26–28** for various anions (Cl^- , Br^- , CH_3CO_2^- , H_2PO_4^- , and HSO_4^-) in CH_2Cl_2 involves hydrogen bonding following the outline above (Fig. 9b) with the *ortho*-CH hydrogen providing additional hydrogen-bond donors (Fig. 12a). This explains the decrease in the order **26** > **27** > **28** possibly as a result of decreasing availability of the

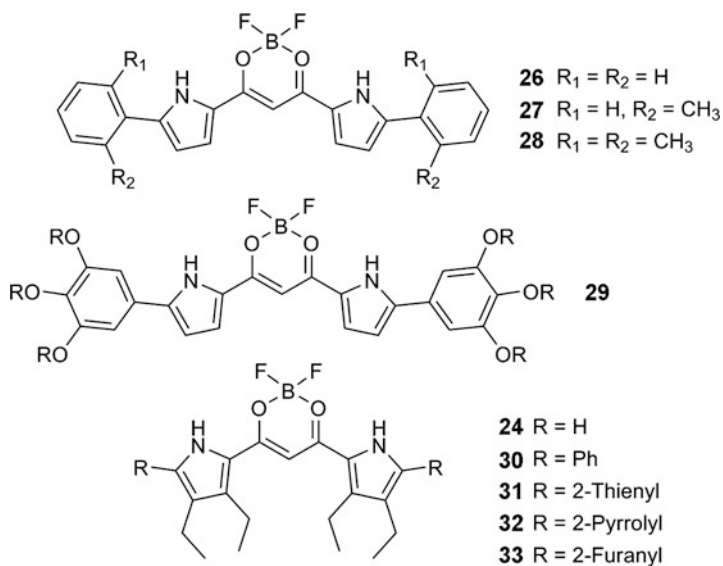


Fig. 11 The second generation of dipyrrolylpropanedione- BF_2 sensors **26–33**

ortho-CH moieties due to methyl substitution in **27** and **28**. Interestingly, the organogelators **30** display sol–gel phase transitions accompanied by a change in fluorescence in the presence of anions [20]. Derivative **30** with $R = \text{hexadecyl}$ affords a transparent gel in octane which shows a fluorescent emission at 654 nm. Upon heating above 27.5°C ($T_{\text{sol-gel}}$) a sol–gel transition occurs and a solution is formed which returns to the gel state upon cooling below $T_{\text{sol-gel}}$. Addition of chloride to the organogel of this compound at 20°C effected a gradual decomposition of the gel in ca. 2 h, yielding an orange-colored highly emissive solution. In the case of bromide and acetate, the transition time was found to be 2–3 days and 3 h, respectively. The authors have suggested that the slow gel collapse observed upon addition of these anions can be correlated with the pyrrole ring inversion process required for formation of a convergent array of hydrogen bond donors for anion binding.

The series of sensors with extended conjugated substituents was extended from phenyl derivative **30** to thienyl, pyrrolyl, and furanyl derivatives **31–33**, and their fluorescence and anion-binding properties were investigated. Figure 12b shows the extended pyrrole sensor **32**, which possesses four NH-type and one CH-type hydrogen bond donors. Not surprisingly, sensor **32** shows the highest affinity for anions observed within the series. The binding constants for the 1:1 complexes of sensor **32** in $\text{CHCl}_3\text{--}0.5\% \text{ EtOH}$ are as follows: Acetate $K_a = 3.0 \times 10^6 \text{ M}^{-1}$; dihydrogen phosphate $K_a = 1.8 \times 10^6 \text{ M}^{-1}$; chloride $K_a = 1.2 \times 10^6 \text{ M}^{-1}$; bromide $K_a = 1.8 \times 10^5 \text{ M}^{-1}$; and hydrogen sulfate $K_a = 1.7 \times 10^5 \text{ M}^{-1}$. It should be noted, that the anion affinity in CH_2Cl_2 was too high to record reliable values of the association constants using optical methods which was the reason for

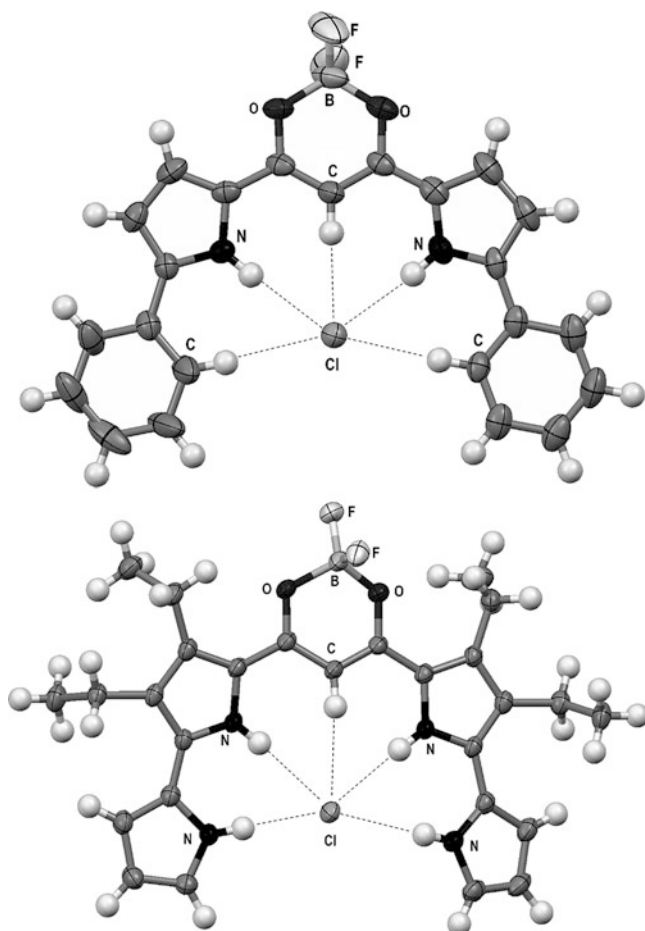


Fig. 12 The X-ray structures of the second generation of dipyrrolylpropanedione- BF_2 sensors **26** and **32** showing the additional hydrogen bonds $\text{CH}-\text{Cl}$ and $\text{NH}-\text{Cl}$ in **26** and **32**, respectively

the unusual $\text{CHCl}_3-0.5\% \text{ EtOH}$ mixture. Using ITC the authors were able to estimate the association constants in CH_2Cl_2 for chloride ($1.7 \times 10^8 \text{ M}^{-1}$) and acetate ($2.2 \times 10^7 \text{ M}^{-1}$). Finally, Fig. 13 shows examples of the colorimetric and fluorescence response second generation dipyrrolylpropanedione- BF_2 sensors **21**, **22**, **26**, **27**, and **28** to the presence of chloride and fluoride [20].

Currently, “extended pyrroles” such as indole, carbazole or indolocarbazole are undergoing a certain renaissance in the anion-sensing field as alternatives of pyrrole [22]. An example of the use of indole fragment in a porphyrin-type sensor is a compound called oxyindolporphyrin **34**, an N-confused corrole, by Furuta, Maeda, and Osuka (Fig. 14) [23].

Perhaps the most interesting aspect of sensor **34** is that due to the rigid narrow and 13-membered ring structure afforded two optical isomers that showed the

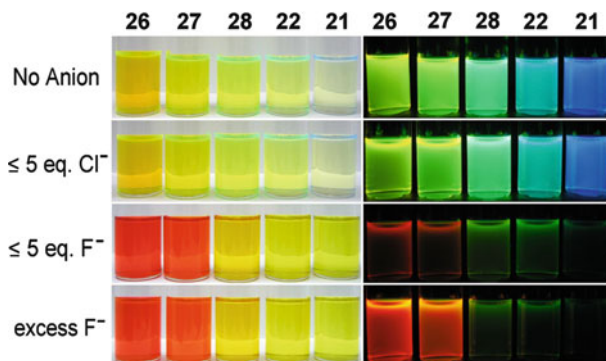
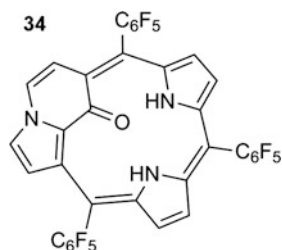


Fig. 13 Colorimetric and fluorescence response of dipyrrolylpropanedione- BF_2 sensors **21**, **22**, **26**, **27**, and **28** to the presence of chloride and fluoride

Fig. 14 Structure of oxyindolopyrin **34**



distinct circular dichroism (CD) at 281, 318, 365, 429, and 443 nm. These isomers were stable, and the racemization was not detected by chiral HPLC even after heating in DMSO at 150°C over 2 days. Interestingly, compound **34** binds fluoride anion via hydrogen-bonding interactions with the inner pyrrolic NHs. The anion binding is specific for F^- , and other halide anions, Cl^- , Br^- , and I^- , did not induce any spectral change in optical behavior of **34**. In the case of fluoride in CHCl_3 the Soret band at 425 nm was shifted to 431 nm, and the emission band at 631 nm was suppressed progressively by increasing fluoride concentration. Assuming 1:1 stoichiometry, the fluoride affinity is characterized by an association constant of $K_a = 1.4 \times 10^4 \text{ M}^{-1}$, which is quite close to the fluoride affinity for unsubstituted calix[4]pyrrole ($\sim 1.7 \times 10^4 \text{ M}^{-1}$ in CH_2Cl_2). The fluorescent nature of the receptor **34** would be attractive for F^- anion sensing, while the chiral nature of the sensor could make this a chiroptical sensor in the future.

In 2005, Beer and coworkers reported the first anion complexation studies with indolocarbazole [24]. Indolocarbazoles are structurally related to bisindolylmaleimides are a currently popular class of chemicals originally isolated 1970s from natural sources.

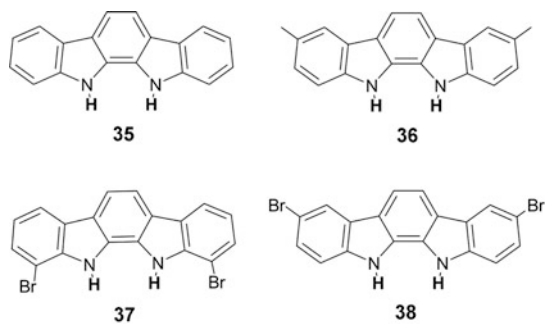
Compounds **35–38** were synthesized via a modification of the Fischer indolization a corresponding hydrazine and 1,2-cyclohexanedione. Binding studies conducted by UV-Vis titrations in acetone showed that under these conditions, the

compounds were very effective benzoate receptors ($K_a = 25,120\text{--}795,000\text{ M}^{-1}$ in acetone), with all four indolocarbazoles **35**–**38** forming the strongest complex with this anion. Sadly, the observed selectivity was relatively low with none of the anions being bound more than an order of a magnitude weaker than benzoate. Interestingly, fluorescence spectroscopy was used to assess whether compounds **35** and **36** could be used as fluorimetric sensors for anions. Significant fluorescence enhancement was observed with fluoride, chloride and dihydrogen phosphate, whilst the addition of benzoate quenched the fluorescence and hydrogen sulfate had little effect. The X-ray crystallographic structure of the sensor **36** revealed that four indolocarbazoles surround two fluoride anions in a helical arrangement (Fig. 15).

Jeong and coworkers have emerged as one of the leading groups in the area of indolocarbazole-based anion receptors. In addition to the colorimetric sensors described above (see Part I, Fig. 27, **43**–**46**) Jeong and coworkers used alkynyl-linked biindole oligomers as anion-templated foldamers **38**–**42** [25]. A series of compounds were synthesized (Fig. 16a, b), containing four, six and eight indole groups, respectively. The single bond between the two indoles forming the biindole moiety appears to undergo a conformational change to achieve a maximum degree of hydrogen bonding with the anion (Fig. 16a). ^1H NMR studies with these compounds in the absence and in the presence of one equivalent of chloride showed significant upfield shifts of the aromatic protons in these foldamers that can be attributed to the fact that these compounds fold-up around the chloride template (Fig. 16c), resulting in stacking of the indole rings.

The anion binding and associated conformational changes can be observed in CH_2Cl_2 -20% MeOH as a dramatic emission color transition from blue to cyan, thus providing a ratiometric output as the maximum at 428–433 nm is quenched and a new broad maximum located between 490–505 nm. The association constants recorded for the biindole hexamer **41** and octamer **42** show strong anion binding in the order: Fluoride > chloride > cyanide \sim azide > acetate > while bromide, iodide and nitrate displayed similar affinities and their relative order varied among sensors. Clearly, a preference for spherical anions (smaller halides) and tubular anions (cyanide, azide) prevails in these sensors. The highest affinity constants recorded in 20% MeOH in CH_2Cl_2 for **42** were as follows: Fluoride $K_a = 1.2 \times 10^6\text{ M}^{-1}$; chloride $K_a = 2.9 \times 10^5\text{ M}^{-1}$; cyanide $K_a = 1.1 \times 10^5\text{ M}^{-1}$; azide $K_a = 1.2 \times 10^5\text{ M}^{-1}$; acetate $K_a = 9.4 \times 10^4\text{ M}^{-1}$; nitrate $K_a = 8.0 \times 10^4\text{ M}^{-1}$; bromide $K_a = 5.0 \times 10^4\text{ M}^{-1}$; and iodide $K_a = 2.1 \times 10^4\text{ M}^{-1}$. The magnitude of these association constants is very high, particularly if one considers that they have been recorded in protic solvents where traditionally sensors utilizing hydrogen bonding are at disadvantage. The high affinity for anions is most likely due to the cooperative nature of the binding in the folded sensors.

The same group extended the foldamer sensor concept further by utilizing indolocarbazole [26, 27] hydrogen bond donors instead of biindole. While the biindoles must undergo a conformational change in the presence of anions (Fig. 16a), the indolocarbazole sensor **43** (Fig. 17a) is already preorganized in *syn*-like fashion and upon anion-induced receptor folding all the hydrogen bond



36-F solid state structure
(side and top view)

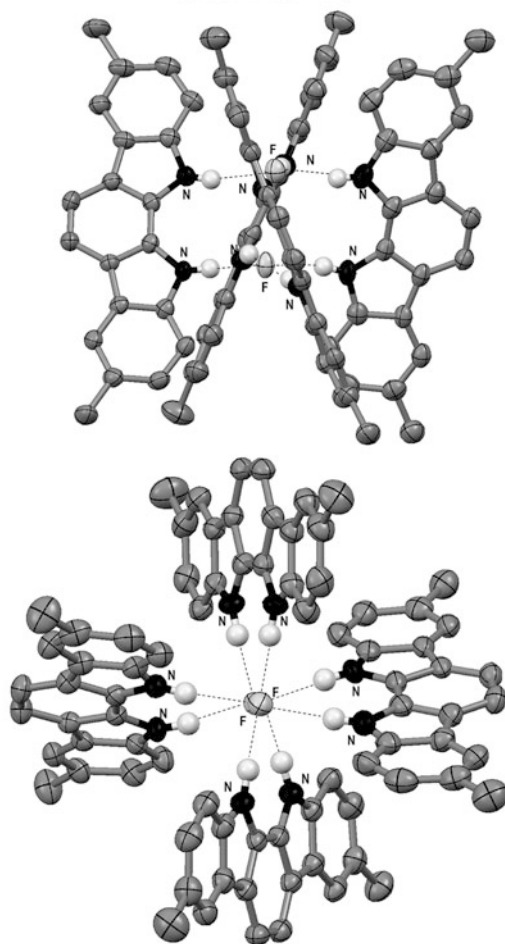


Fig. 15 *Top*: structures of indolocarbazole sensors 35–38. *Center*: solid-state structure of the complex of 36 with fluoride (*side-view*). *Bottom*: complex of 36 with fluoride (*top-view*)

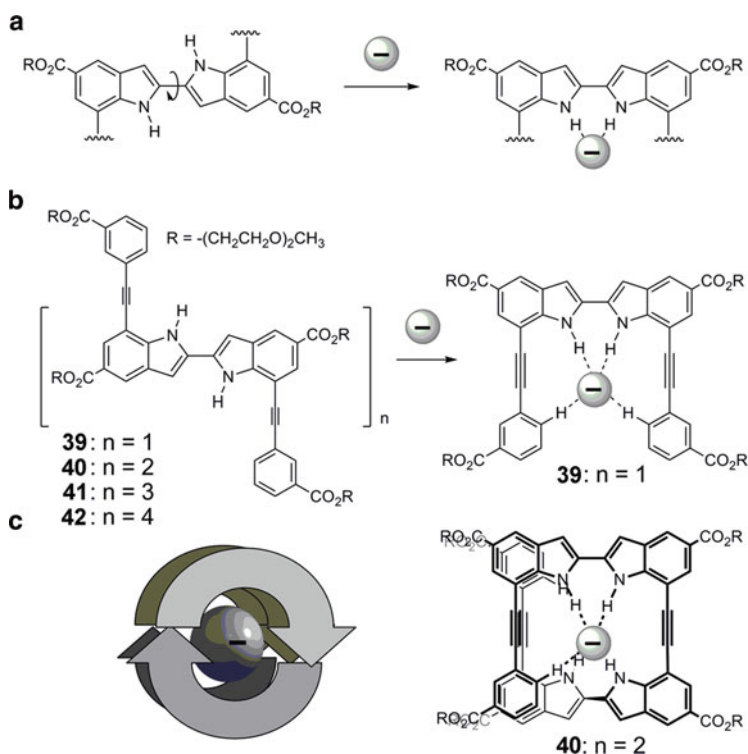
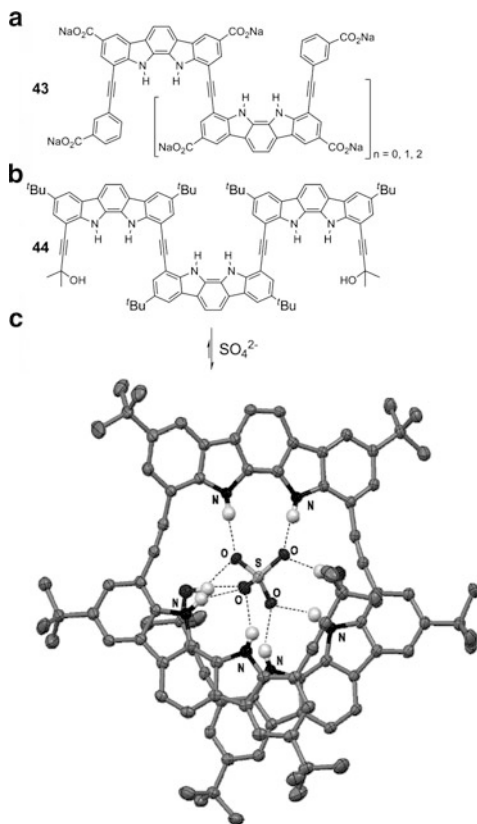


Fig. 16 Biindole foldamers and the principle of their folding to maximize hydrogen bonding to the anions

donors point in one direction, ready for anion binding. For comparison, the association constants were determined for the ester precursors in protic medium, 4:1 (v/v) DMSO/MeOH. The association constants decrease in the order F^- ($K_a = 183,000 \text{ M}^{-1}$) > Cl^- ($K_a = 36,800 \text{ M}^{-1}$) > Br^- ($K_a = 1,350 \text{ M}^{-1}$) > I^- ($K_a = 86 \text{ M}^{-1}$). Most importantly, the sodium salt of the trimer foldamer **43**: $n = 2$ binds anions in pure water: The corresponding association constants for sodium salts were Cl^- ($K_a = 65 \text{ M}^{-1}$) > F^- ($K_a = 46 \text{ M}^{-1}$) > Br^- ($K_a = 20 \text{ M}^{-1}$) while I^- and ClO_4^- did not show appreciable binding. Finally, the binding selectivity for chloride ion was found to be independent on the counterion; LiCl, NaCl, and KCl gave an identical association constant [26]. In another report by the same authors [27], a selective sulfate binding was observed. Hydrogen bonding to anions drives helical folding of an indolocarbazole oligomer **44**, thus resulting in an internal cavity with six NHs and two OHs for binding sulfate with high selectivity (Fig. 17b). Figure 17c shows the solid-state structure of the sensor **44** in the complex with sulfate. Quantitative studies of anion binding were in 10% MeOH in CH_3CN . The corresponding association constants for tetra-*n*-butylammonium salts were SO_4^{2-} ($K_a = 640,000 \text{ M}^{-1}$) \gg Cl^- ($K_a = 8,800 \text{ M}^{-1}$) > CH_3CO_2^- ($K_a = 5,700 \text{ M}^{-1}$) > H_2PO_4^- ($K_a = 3,600 \text{ M}^{-1}$) > Br^- ($K_a = 2,800 \text{ M}^{-1}$) > CN^- ($K_a = 1,600 \text{ M}^{-1}$)

Fig. 17 Structures of indolocarbazole foldamers **43** (a) and **44** (b). The sulfate-selective foldamer **44** undergoes sulfate-induced helical folding from the linear form (b) to the helical sulfate complex (c)



$> \text{N}_3^-$ ($K_a = 790 \text{ M}^{-1}$). Finally, the success of these materials is crowned by the fact that the biindole and indolocarbazole foldamers are ratiometric fluorescence-based sensors. In the case of **44**, for example, the original intense maximum at 415 nm is partly quenched ($\sim 60\%$) while the new maximum at 455 nm appears (with concomitant increase in the intensity at 480–530 nm). As a result, a deep-blue fluorescence is converted to a beautiful cyan color. From the perspective of the sensor development, two independent channels may be used: Blue to follow the quenching of the blue channel (410–480 nm) while the increase in the intensity in the Green channel (490–550 nm) can be independently used to establish ratiometric response [27].

Anzenbacher and coworkers have continued their research on anion sensing and have demonstrated that simple anion sensors based on hydrogen-bonding interactions can bind and sense anions in hydrophilic polymer matrices, despite their inability to bind anions in water [48, 49]. Moreover, they have reported a series of tripodal sensor molecules **45–48** based on 1,3,5-triaminomethyl-2,4,6-triethylbenzene [28] which can form arrays of six hydrogen-bond donors (Fig. 18) [29].

Fig. 18 *Top*: structures of tripod sensors **45–48** based on 1,3,5-triaminomethyl-2,4,6-triethylbenzene. *Bottom*: turn-on fluorescence behavior of sensor **48** in the presence of various anions

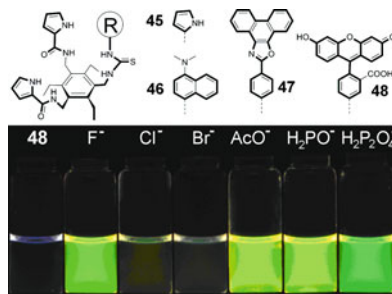
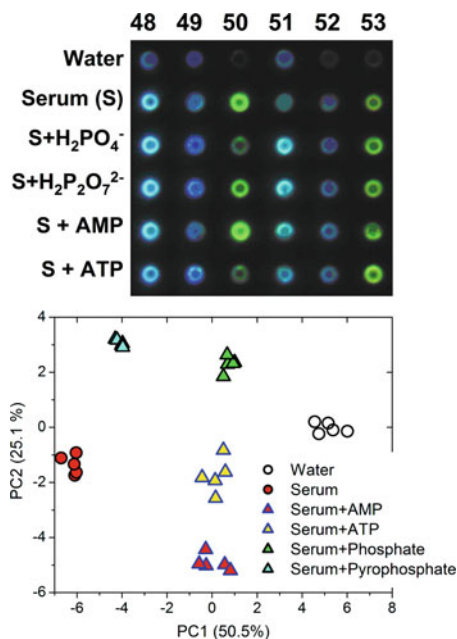


Fig. 19 Turn-on fluorescent sensors **46–48** and their congeners **49–51** are used in a sensor array chip to recognize anions in human blood serum. Fluorescence recorded directly from the array chip analyzed by pattern-recognition methods such as PCA allows for analysis of response patterns from the array for unambiguous recognition of anions



An X-ray crystal analysis of the related receptor showed that these receptors form a complex with phosphate in the solid state where the receptor in the all-up conformation binds up to three phosphate anions. Fluorescent arrays were constructed utilizing **46–48** and **49–51** embedded in hydrophilic polyurethane matrices to detect biological phosphate ions in blood serum. Principal component analysis (PCA) showed that films of **46–48** and **49–51** (not based on pyrrole receptors) allow phosphate, pyrophosphate, AMP and ATP to be distinguished (Fig. 19).

Schmuck et al. [30] utilized their guanidiniocarbonyl pyrrole approach [31, 32] to demonstrate naked-eye sensing displacement ensemble for the selective detection of citrate while typical competitors such as tartarate or malate were not induce significant response. This study was performed in water using the trademark guanidiniocarbonyl pyrrole moieties attached to the 1,3,5-triaminomethyl-2,4,6-triethylbenzene [28] via amide linkages. The tripodal receptor **52** (Fig. 20) forms a

Fig. 20 Fluorescence-based dye-displacement assay utilizes receptor **52** and carboxyfluorescein **53** to form a nonfluorescent ensemble. Upon addition of a competitive carboxylate, the fluorescence is recovered. This ensemble responds to citrate **54**, but not malate **55** or tartarate **56**

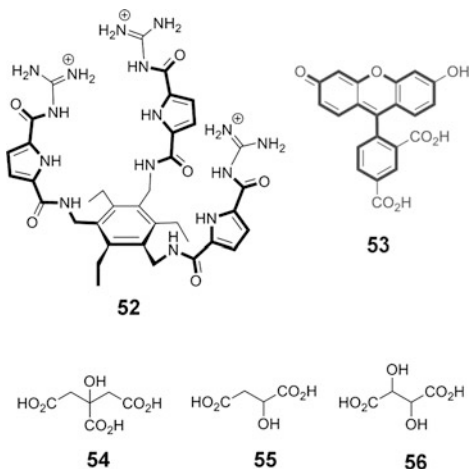
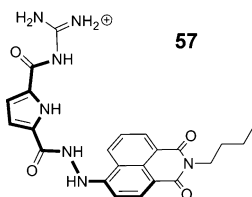


Fig. 21 Fluorescence-based sensor **57** acts as a turn-on sensor for pyrophosphate



nonfluorescent ensemble with carboxyfluorescein **53**. Upon addition of a competitive carboxylate, carboxyfluorescein is released from the receptor and fluorescence recovered. This ensemble responds to citrate **54**, but not malate **55** or tartarate **56**.

Recently, Fu et al. synthesized and tested sensor **57** based on pyrrole-naphthalimide bearing a Schmuck-type guanidiniocarbonyl pyrrole moiety. The sensor displays a selective fluorescent enhancement with pyrophosphate over ATP, ADP, AMP, and other inorganic anions in aqueous solution [29] (Fig. 21).

3 Pyrrole-Based Electrochemical Anion Sensors

In addition to porphyrins, calix[4]pyrroles, and other polypyrrolic systems discussed in the literature, a number of receptors comprising pyrrolic subunits and ferrocene moieties were also designed to elucidate the anion binding using electrochemical signal output [1] (Part I).

A number of efforts were mounted to combine calix[4]pyrrole receptors with metallocene, predominantly ferrocene, to generate electrochemical anion sensors. The early papers by Gale and Sessler [33, 34] suggested that this approach may yield interesting sensors. Thus, the calix[4]pyrrole **58** with ferrocene attached to *meso*-carbon showed that the ferrocene C-H participates in anion binding as

documented by the ^1H NMR experiments in acetonitrile- d_3 /DMSO- d_6 9:1 (v/v) [34]. The anion binding by the ferrocene conjugate has not been compromised as evidenced by ^1H NMR measurements. However, it was found that the CH moiety adjacent to the ferrocene attachment to the *meso*-carbon stabilizes the sensor-anion complex via CH-anion hydrogen bonding. The resulting interaction affects the ferrocene moiety providing a strong electrochemical output signal. The redox potentials from square-wave voltammograms (SWVs) revealed that for halide anions, binding of fluoride induces the largest cathodic shift in the ferrocene/ferrocenium couple (76 mV), which should correspond to strong association. The comparison of association constants and electrochemical data is as follows: Fluoride $\Delta E = -76$ mV ($K_a > 3,380 \text{ M}^{-1}$); chloride $\Delta E = -36$ mV ($K_a > 3,190 \text{ M}^{-1}$); bromide $\Delta E = -12$ mV ($K_a = 50 \text{ M}^{-1}$); dihydrogen phosphate $\Delta E = -100$ mV ($K_a = 300 \text{ M}^{-1}$); and hydrogen sulfate $\Delta E \leq 10$ mV ($K_a < 10 \text{ M}^{-1}$). Similar data, albeit with different electrode were recorded using Osteryoung square-wave voltammetry experiments by Radecka and Gale [35]. Here too, dihydrogen phosphate and fluoride generated the strongest signal, followed by bromide and chloride, both in current and potential.

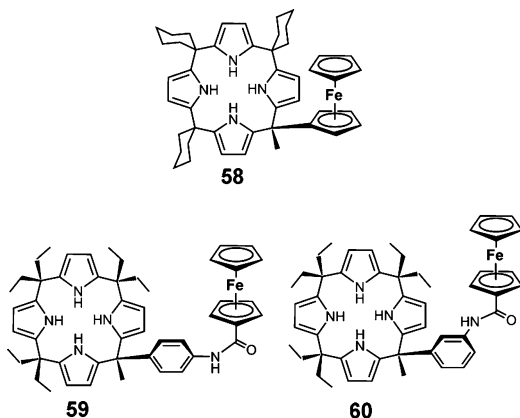
Similarly, Cheng et al. synthesized calix[4]pyrroles **59** and **60** in which the ferrocene moiety was attached to the amino-functionality on the *meso*-aromatic substituents of the scaffold originally used to generate fluorescent calix[4]pyrrole sensors [7] (Fig. 2). Here too, the resulting sensors displayed anion binding as evidenced by both ^1H NMR spectroscopy and SWV measurements. For example, for sensor **59**, the ΔE values for anions in acetonitrile with 0.1 M tetra-*n*-butylammonium perchlorate were recorded as follows: Fluoride $\Delta E = 80$ mV ($K_a > 1,000,000 \text{ M}^{-1}$); chloride $\Delta E = 32$ mV ($K_a = 5,300 \text{ M}^{-1}$); bromide $\Delta E = -4$ mV ($K_a = 150 \text{ M}^{-1}$); dihydrogen phosphate $\Delta E = 132$ mV ($K_a = 1,900 \text{ M}^{-1}$); acetate $\Delta E = 80$ mV ($K_a > 1,000,000 \text{ M}^{-1}$); and hydrogen sulfate $\Delta E = -8$ mV ($K_a < 50 \text{ M}^{-1}$). Combining all of the above data, it appears that dihydrogen phosphate always gives a very strong electrochemical signal, almost regardless of the magnitude of the association constant. Bromide and hydrogen sulfate are very weakly binding and their electrochemical signal while not negligible, is small. The pattern for fluoride and chloride is not easy to summarize or interpret (Fig. 22).

Finally, calix[4]pyrrole was also used and studied in ion-selective electrodes (ISEs) [36–38] and promising results were obtained. However, because these are often complicated sensor systems utilizing membranes, conductive polymers doped with various ion-exchangers, their behavior is often complex, thus a topic generally beyond the scope of this review.

More recent studies by Bucher et al. on metallo-complexes of ferrocene-substituted porphyrin [39] and calixphyrin [40] suggest that these materials also could be used as potential sensors for anions. In these materials, the anion is coordinated to the metal inside the tetrapyrrole-macrocyclic cavity, and does not feature pyrrole-anion interaction.

One of the more interesting materials is the bridged dipyrrole conjugates, the *ansa*-ferrocene **61** containing two pyrrolic NH and two amidic NH groups [41]. Quantitative ^1H NMR spectroscopic titration studies revealed that receptor **61**

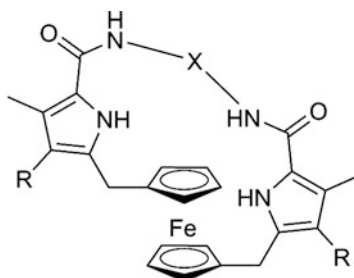
Fig. 22 Calix[4]pyrrole-ferrocene sensors



possessed high affinity for fluoride, chloride, and dihydrogenphosphate ($K_a \geq 105$, 9,030, and 11,300 M^{-1} for F^- , Cl^- , and $H_2PO_4^-$, respectively, in CD_3CN). These results are consistent with the electrochemistry studies and led to the suggestion that this receptor acts as an effective redox-based sensor for F^- (80 mV) and $H_2PO_4^-$ (136 mV) [41]. In order to regulate the $H_2PO_4^-$ anion affinities and modulate the nature of the Fc/Fc^+ – based electrochemical properties, three new *ansa*-ferrocene systems containing bridging arms of different length and nature were synthesized. The affinities for $H_2PO_4^-$ increase in a stepwise fashion as the number of oxygen atoms in the linking bridge increases from 0 to 2 ($K_a = 4,050$, 13,200, 81,400 M^{-1} , respectively, for **62**, **63**, and **64** in CD_2Cl_2 containing 2% $DMSO-d_6$). Such observation is consistent with the ether-type oxygen atoms being involved directly in the anion binding process. On the other hand, the degree of the anion-induced cathodic shift in the Fc/Fc^+ potentials does not fully correlate with the number of oxygen atoms ($\Delta E = 128$, 140, and 140 mV for **62**, **63**, and **64**, respectively) [42] (Fig. 23).

During their studies of pyrrole-amide receptors, Gale and coworker reported two new ferrocene-appended amidopyrroles that show considerable promise as electrochemical anion sensors [19]. The electrochemical behavior of sensors **65** and **66**, in the presence and absence of a variety of anions was determined by CV methods in dichloromethane using a platinum microdisc electrode. Upon the addition of fluoride anion to **66**, a large anodic shift in the Fc/Fc^+ was observed (cf. $\Delta E = -130$ mV). However, in the case of **65**, addition of fluoride anion produces the largest volumetric shifts and yields two waves ($\Delta E = -125$ and -255 mV). Interestingly, receptor **65** was found to display a strong affinity for benzoate anion ($K_a = 1,820 M^{-1}$) and addition of this anion produced a significant shift in the first voltammetric wave ($\Delta E = -120$ mV). In the case of **65**, the most significant shifts in the voltammetric waves were observed with F^- and $C_6H_5CO_2^-$. This is fully consistent with the proposal that the electrochemical oxidation of the receptors is affected by the bound anion (Fig. 24).

Fig. 23 *Ansa*-ferrocenes **61**–**64** are among the oldest pyrrole-based supramolecular receptors for anions



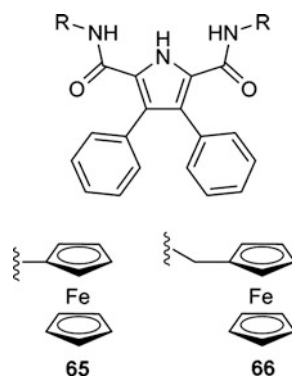
61 X = CH₂(CH₂OCH₂CH₂OCH₂)CH₂, R = C₂H₅

62 X = CH₂(CH₂)₃CH₂, R = CH₃

63 X = CH₂(CH₂OCH₂)CH₂, R = CH₃

64 X = CH₂(CH₂OCH₂)₂CH₂, R = CH₃

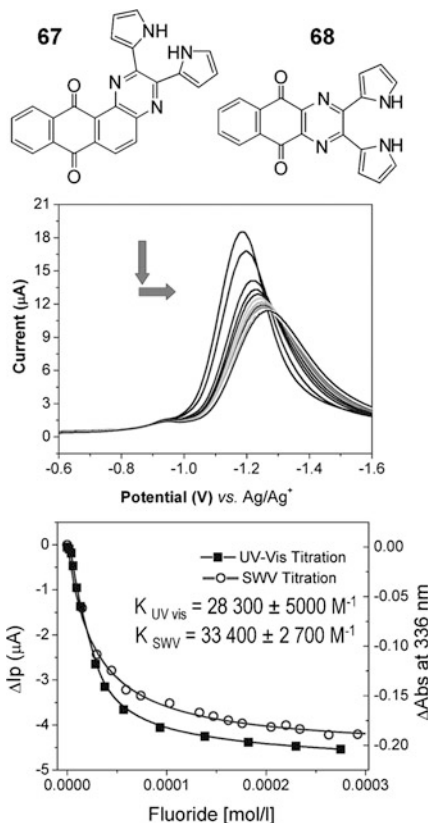
Fig. 24 Structure of electrochemical pyrrole-carboxamide sensors, **65** and **66**



Anzenbacher and coworkers have synthesized DPQ analogs **67** and **68** [43] comprising quinone groups to generate colorimetric and electrochemical responses upon binding of anionic guests into the receptor (Fig. 25). As each receptor has effectively two output channels, comparison of the colorimetric and electrochemical data can be used to determine the nature of the anionic substrate present, as opposed to systems with a single output channel which may not provide a unique response to each anionic guest.

Thus, the conjugated chromophores in **67** and **68** generate an intensive change in color and with a redox-active moiety such as quinone directly fused to the chromophore while displaying a strong change in both colorimetric and electrochemical properties, both current and potential shift (Fig. 25 center), was observed in the presence of inorganic anions. As expected, the association constants derived from UV–Vis and SWV measurements yielded very similar values of association constants (Fig. 25, bottom panel). Unique anion-specific response was observed for fluoride, pyrophosphate and acetate anions. However, even anions that do not bind strongly and thus do generate a dramatic or easy-to-observe change in color can be

Fig. 25 *Top*: structure of sensors **67** and **68**



detected by changes in the electrochemical behavior of the sensors. This is a typical behavior of dihydrogen phosphate, which in most pyrrole-based electrochemical sensors does not display strong binding, but induces strong change in redox potential (see above). DFT (B3LYP/6-31G*) calculations performed for both “on” and “off” state of sensor–fluoride model were found to be in good agreement with the observed electrochemical and spectroscopic data.

A similar approach to combining colorimetric (UV–Vis) measurements with conductivity or electrochemical measurements was demonstrated by Anzenbacher et al. [44, 45]. Here, the DPQ-sensor **9** with electropolymerizable thiophene moieties forms a conductive polymer. Conductivity in such polythiophene is due to positive charge injected to the backbone (hole conductivity). Electrical doping of the polymer results in holes present in the material. The holes are partly stabilized by electrolyte counter-anions such as perchlorate or hexafluorophosphate. In the presence of competing anion, the anion binds to both the DPQ-pyrrole moieties utilizing more specific hydrogen bonding interactions as well to the doped polymer backbone due to nonspecific interactions. Because the doped thiophene polymers

possess deep blue–green color, this color partly changes as a result of anion binding. Furthermore, exchange of the nonspecific counter-anions for more strongly bound analyte anions results in a dramatic change in conductivity (usually decrease), which depends on the strength of the binding. Thus, such a sensor allows for investigating the analyte using two sources of output signal: Colorimetric as well as conductivity. Because the transparent indium tin-oxide (ITO) electrodes can be used, both measurements can be done during one spectro-electrochemistry experiment [44, 45] (Fig. 26).

Jeppesen and Becher incorporated a redox-active tetrathiafulvalene (TTF) unit into a calix[4]pyrrole-like macrocycle. The sensor **69** was designed to permit the detection of anions by binding-induced changes in the electrochemically properties of the TTF unit. ^1H NMR experiments show that the sensor **69** binds anions with high affinity observed in the calix[4]pyrrole field. In fact, the affinities for chloride and fluoride anions were so high that they had to be determined from competitive experiments. Thus, the association constants recorded for sensor **69** and fluoride $K_a = 2,100,000 \text{ M}^{-1}$ ($\Delta E = \text{ND}$); chloride $K_a = 120,000 \text{ M}^{-1}$ ($\Delta E = -43 \text{ mV}$); bromide $K_a = 7,600 \text{ M}^{-1}$ ($\Delta E = -34 \text{ mV}$). The results from the electrochemical experiments reveal that the complexation of the anions inside the cavity of **69** shift the first oxidation of the TTF unit towards more cathodic potentials, which may be due to delocalization of the negative charge to the TTF moiety (Fig. 27).

In another example, Sessler and Jeppesen prepared a series of calix[4]pyrrole-TTF sensors **70–73** with not only all eight *meso*-methyl substituents that prevent the macrocycle oxidation, but also with a different number and position of the TTF-annulated pyrrole moieties within the macrocycle [46]. TTF annulated to the calix[4]pyrrole system serves to enhance the anion binding affinities substantially but at the price of lowered selectivity. Cyclic voltammetry (CV) studies, carried out in 1,2-dichloroethane, provided evidence of an anion-dependent electrochemical response with Cl^- and Br^- ions. This response was particularly dramatic in the case of the monotetrathiafulvalene-calix[4]pyrrole **5**, with a ΔE_{max} of -145 mV

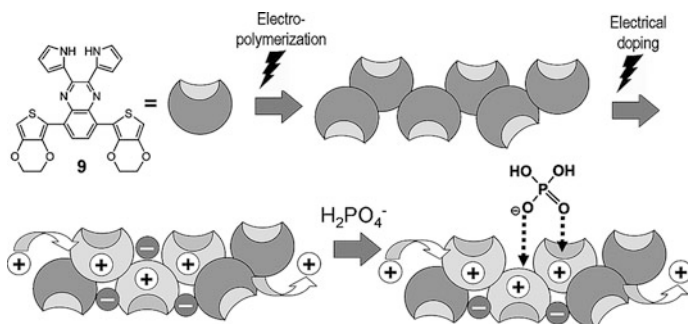


Fig. 26 DPQ-sensor **9** is electro-polymerized to form a conductive polymer. Electrical doping injects positive charges into the polymer. In the presence of anion, synergy between hydrogen-bonding to the DPQ pyrroles and nonselective electrostatic attraction between the anion and the doped polymer results in a strong binding

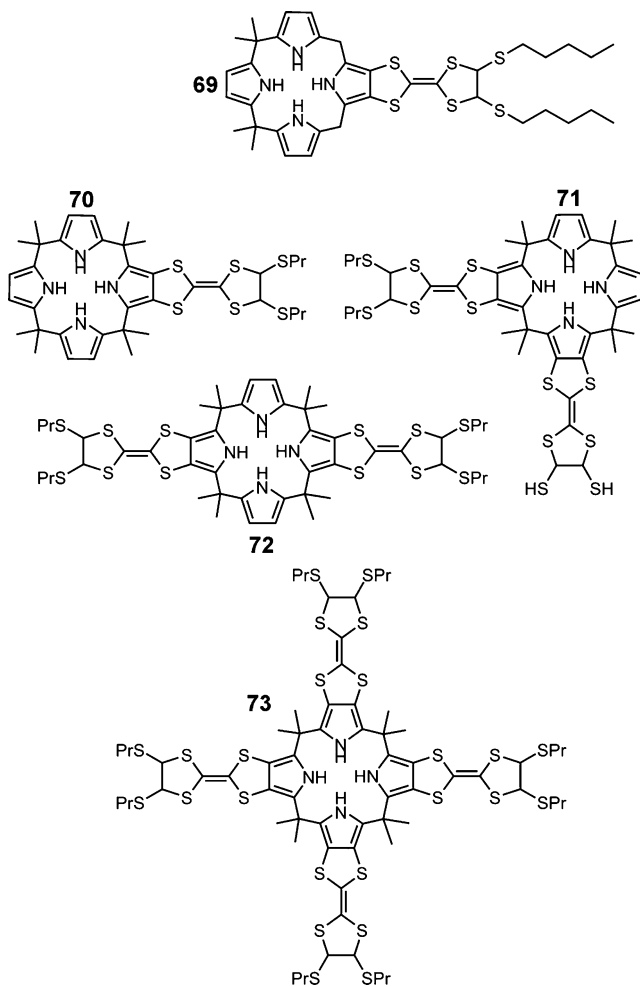


Fig. 27 Calix[4]pyrrole macrocycles with a fused redox-active tetrathiafulvalene moiety

being seen after the addition of approximately one equivalent of Cl^- ion. CV titration experiments were also carried out with solutions containing CN^- , NO_2^- , or CH_3CO_2^- ions. However, in the presence of these anions the redox events become irreversible, thus precluding the recording reliable results. It was also demonstrated that halide anion complexation can be monitored by electrochemical means, in particular by observing the shifts in the TTF-based redox waves as a function of Cl^- or Br^- concentration. This ability to effect electrochemical sensing, along with this increased affinity and selectivity that results, underscores the advantage that accrues from the introduction of TTF subunits into the calix[4] pyrrole scaffold. Sensor compound derived from structure **70** was recently attached to gold electrode for electrochemical sensing of chloride [47]. Furthermore, the

TTF-calix[4]pyrroles turned out to be excellent sensors for electron-poor nitroaromatic compounds including explosives.

4 Concluding Remarks

This chapter also only scratches the surface of the burgeoning field of pyrrole-based receptors and sensors with luminescence or electrochemical signal transduction, and similarly to the previous chapter, this one also focused on anion sensing. There are, however, a large number of pyrrole receptors, to which fluorophores were attached to generate successful sensors. Lately, a number of elegant studies appeared that utilize pyrrole benzo-analogs endowed with intrinsic fluorescence. While the original approach was to synthesize a receptor and attach a reporter, these new derivatives were designed and synthesized with dual purpose of binding and sensing. It is this author's opinion that such materials might be the future of the field. The future of the anion-sensing field will also be populated by electrochemical sensors. Their potential for high sensitivity at low concentrations when coupled to modern electrochemical devices such as various sub-microelectrodes, quartz-crystal microbalances and other signal transduction schemes will make these materials important. Like all good things, they come to he who waits.

References

1. Borisov SM, Wolfbeis OS (2008) *Chem Rev* 108:423–461
2. Oehme I, Wolfbeis OS (1997) *Mikrochim Acta* 126:177–192
3. de Silva AP, Gunaratne HQN, Gunlaugsson T, Huxley AJM, McCoy CP, Rademacher JT, Rice T (1997) *Chem Rev* 97:1515–1566
4. Beer PD, Gale PA (2001) *Angew Chem Int Ed* 40:486–516
5. Martínez-Mañez R, Sancenón F (2003) *Chem Rev* 103:4419–4476
6. Miyaji H, Anzenbacher P Jr, Sessler JL, Bleasdale ER, Gale PA (1999) *Chem Commun*: 1723–1724
7. Anzenbacher P Jr, Jursíková K, Sessler JL (2000) *J Am Chem Soc* 122:9350–9351
8. Miyaji H, Kim HK, Sim EK, Lee CK, Cho WS, Sessler JL, Lee CH (2005) *J Am Chem Soc* 127:12510–12512
9. Aldakov D, Anzenbacher P Jr (2003) *Chem Commun*:1394–1395
10. Pohl R, Aldakov D, Kubát P, Jursíková K, Marquez M, Anzenbacher P Jr (2004) *Chem Commun*:1282–1283
11. Aldakov D, Palacios MA, Anzenbacher P Jr (2005) *Chem Mater* 17:5238–5241
12. Wu CY, Chen MS, Lin CA, Lin SC, Sun SS (2006) *Chem Eur J* 12:2263–2269
13. Anzenbacher P Jr, Tyson DS, Jursíková K, Castellano FN (2002) *J Am Chem Soc* 124: 6232–6233
14. Shevchuk SV, Lynch VM, Sessler JL (2004) *Tetrahedron* 60:11283–11291
15. Liao JH, Chen CT, Chou HC, Cheng CC, Chou PT, Fang JM, Slanina Z, Chow TJ (2002) *Org Lett* 4:3107–3110
16. Maeda H, Kunusose Y (2005) *Chem Eur J* 11:5661–5666
17. Maeda H, Ito Y (2006) *Inorg Chem* 45:8205–8210

18. Maeda H, Kusunose Y, Mihashi Y, Mizoguchi T (2007) *J Org Chem* 72:2612–2616
19. Denuault G, Gale PA, Hursthouse MB, Light ME, Warriner CN (2002) *New J Chem* 26:811–813
20. Maeda H, Haketa Y, Nakanishi T (2007) *J Am Chem Soc* 129:13661–13674
21. Maeda H, Mihashi Y, Haketa Y (2008) *Org Lett* 10:3179–3182
22. Gale PA (2008) *Chem Commun*:4525–4540
23. Furuta H, Maeda H, Osuka A (2001) *J Am Chem Soc* 123:6435–6436
24. Curiel D, Cowley A, Beer PD (2005) *Chem Commun*:236–238
25. Kim UI, Suk J, Naidu VR, Jeong KS (2008) *Chem Eur J* 14:11406–11414
26. Suk J, Jeong KS (2008) *J Am Chem Soc* 130:11868–11869
27. Kim J, Juwarker H, Liu X, Lah MS, Jeong KS (2010) *Chem Commun* 46:764–766
28. Stack TDP, Hou Z, Raymond KN (1993) *J Am Chem Soc* 115:6466–6467
29. Zyryanov GV, Palacios MA, Anzenbacher P Jr (2007) *Angew Chem Int Ed* 46:7849–7852
30. Schmuck C, Schwegmann M (2006) *Org Biomol Chem* 4:836–838
31. Schmuck C (2006) *Coord Chem Rev* 250:3053–3067
32. Schmuck C (2000) *Chem Eur J* 6:709–718
33. Sessler JL, Gebauer A, Gale PA (1997) *Gazz Chim Ital* 127:723–726
34. Gale PA, Hursthouse MB, Light ME, Sessler JL, Warriner CN, Zimmerman RS (2001) *Tetrahedron Lett* 42:6759–6762
35. Szymanska I, Radecka H, Radecki J, Gale PA, Warriner CN (2006) *J Electroanal Chem* 591:223–228
36. Král V, Sessler JL, Shishkanova TV, Gale PA, Volf R (1999) *J Am Chem Soc* 121:8771–8775
37. Shishkanova TV, Sapurina I, Stejskal J, Král V, Volf R (2005) *Anal Chim Acta* 553:160–168
38. Sessler JL, Král V, Shishkanova TV, Gale PA (2002) *Proc Natl Acad Sci USA* 99:4848–4853
39. Bucher C, Devillers CH, Moutet JC, Royal G, Saint-Aman E (2004) *New J Chem* 28:1584–1589
40. Bucher C, Devillers CH, Moutet JC, Pecaut J, Royal G, Saint-Aman E, Thomas F (2005) *Dalton Trans* 22:3620–3631
41. Scherer M, Sessler JL, Gebauer A, Lynch VM (1998) *Chem Commun*:85–86
42. Sessler JL, Zimmerman RS, Kirkovits GJ, Gebauer A, Scherer M (2001) *J Organomet Chem* 637–639:343–348
43. Anzenbacher P Jr, Palacios MA, Jursíková K, Marquez M (2005) *Org Lett* 7:5027–5030
44. Aldakov D, Anzenbacher P Jr (2004) *J Am Chem Soc* 126:4752–4753
45. Anzenbacher P Jr, Jursíková K, Aldakov D, Marquez M, Pohl R (2004) *Tetrahedron* 60:11163–11168
46. Nielsen KA, Cho WS, Lyskawa J, Levillain E, Lynch VM, Sessler JL, Jeppesen JO (2006) *J Am Chem Soc* 128:2444–2451
47. Jensen LG, Nielsen KA, Breton T, Sessler JL, Jeppesen JO, Levillain E, Sanguinet L (2009) *Chem Eur J* 15:8128–8133
48. Nishiyabu R, Anzenbacher P Jr (2005) *J Am Chem Soc* 127:8270–8271
49. Palacios MA, Nishiyabu R, Marquez M, Anzenbacher P Jr (2007) *J Am Chem Soc* 129:7538–7544

Imidazolium-Based Receptors

Ermitas Alcalde, Immaculada Dinarès, and Neus Mesquida

Abstract Imidazolium salts, which constitute a varied pool of charged chemical entities, are situated at the crossroads of multidisciplinary fields in chemistry because of their incorporation in a broad array of molecular systems. Imidazolium functionality has emerged as a privileged structural motif for the design of specifically tailored artificial receptors for anion recognition and sensing. The specific focus of this chapter is to give an overview of these positively charged systems, with a brief discussion of the chemistry of imidazolium quaternary salts. Representative examples of imidazolium-based systems have been ordered according to their molecular frameworks and include cyclophanes, protophanes, and calixarenes as well as a tripodal molecular platform. The final section concerns miscellaneous molecular systems with a variety of coexisting topologies as well as a number of subunits, each with its own specific properties. These systems have applications in anion recognition chemistry leaning toward nanoscience.

Keywords Anion recognition · Charged frameworks · Chemosensors · Heteroaromatic systems · Hydrogen bonds · Imidazolium · Nanostructures · Template synthesis

Contents

1	Introduction	268
2	Imidazolium Quaternary Salts	271
2.1	The Imidazolium Functionality	278
3	Cyclophanes	283
4	Calixarenes	288
5	Tripodal Platform for Anion Receptors	291
6	Miscellaneous Systems and Applications	292

E. Alcalde (✉), I. Dinarès, and N. Mesquida

Departament de Farmacologia i Química Terapèutica, Facultat de Farmàcia, Laboratori de Química Orgànica, Universitat de Barcelona, Avda. Joan XXIII, s/n, 08028 Barcelona, Spain
e-mail: ealcalde@ub.edu

7 Conclusions	296
Addendum	297
References	297

1 Introduction

Imidazolium quaternary salts encompass a pool of charged building blocks with a great potential for chemical diversification. Their incorporation within a broad array of cationic and oligocationic systems situate them at the crossroads of multidisciplinary fields directed toward anion recognition chemistry and room-temperature ionic liquids (RTILs), as well as *N*-heterocyclic carbenes (NHCs), a family of ancillary ligands in organometallic chemistry. Imidazolium units can thus be considered as privileged structural motifs for the conception and design of specifically tailored charged systems in any of these fields dedicated to research and development (R&D), Fig 1.

Against a background of advances in anion recognition leaning toward the domain of nanosciences, imidazolium-based systems have emerged as novel molecular hosts with a wide variety of frameworks and shapes. The specific focus of this chapter is to give a brief overview of these attractive charged systems, giving special emphasis to the chemistry of imidazolium quaternary salts. It should serve as a complement to the reviews covering current developments in anion receptors and anion-templated synthesis [1–8]. Other charged π -deficient heteroaromatic units with anion binding ability have been reported, especially pyridinium-based frameworks, and are discussed in the corresponding chapters.

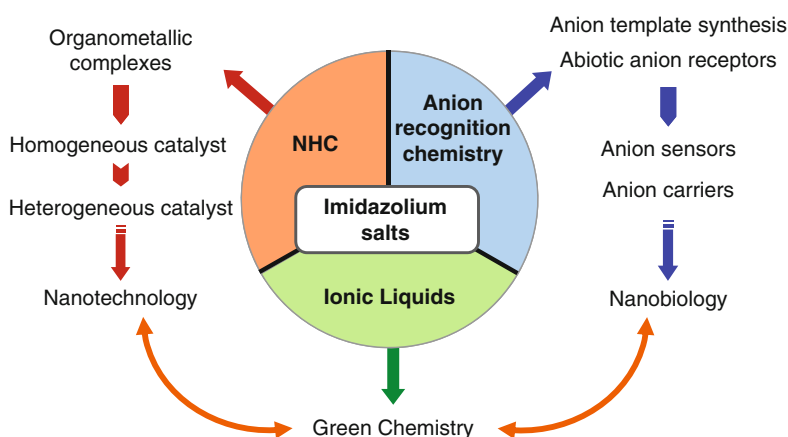


Fig. 1 The imidazolium pool at the crossroads of multidisciplinary fields in chemistry

Simple quaternary imidazolium salts with low melting points have become an alternative to conventional organic solvents, representative examples of ionic liquids being the 1-butyl-3-methylimidazolium salts [bmim][X] and 1,3-dibutylimidazolium salts [bbim][X]. RTILs are currently a fertile area in R&D as green solvents [9–15], and their applications in chemical industry have been reviewed [16]. At the same time, quaternary imidazolium salts are direct precursors of imidazolylidenes, the largest class of NHCs. The number of reported metal–NHC complexes has increased considerably with the emergence of different applications (Fig. 1) [17–23].

Different types of noncovalent interactions are involved in anion recognition depending on the structural features of the synthetic receptor: (1) electrostatic interactions, (2) hydrogen bonds, (3) a combination of electrostatic and hydrogen-bond interactions, (4) the hydrophobic effect, and (5) metal or Lewis acid coordination [24]. When the noncovalent driving forces for anion binding of quaternary salt hosts are examined, two types of control can be considered: electrostatic interactions alone, or combined with hydrogen-bonding interactions. The acidity of the H-bond donor moiety should be relatively weak to hamper deprotonation under physiological conditions.

The earliest examples of quaternary salt moieties functioning mainly through noncovalent (1)-type interactions were the macrotricyclic quaternary ammonium salts of **M·4A** type, with the four cationic groups situated at the vertices of a tetrahedral scaffold [25, 26]. For (3)-type interactions, the imidazolium-based cyclophanes **1·2A** were simple models for intermolecular interactions driven by hydrogen bonds [27], and it is notable that their synthesis exploited their ability to bind chloride anions [28]. Imidazolium units are the main structural motifs for the formation of a novel of charged hydrogen bond (C–H)⁺...anion in dications **1·2A**.

Bis-imidazolium cyclophane prototype **1a·2Cl·2H₂O** has a solid-state structure in which the chloride counteranions are noncovalently bonded to the cyclophane framework through nonclassic (C–H)⁺...Cl[−] hydrogen bonds. Dication **1a**²⁺ adopts a chair-like conformation in contrast to the cone-like arrangement observed for **1b**²⁺ (Fig. 2). Solution studies in polar solvents by ¹H NMR spectroscopy revealed the importance of the hydrogen bonds in controlling anion binding [27].

In the same year, some other imidazolium-based systems were also reported (Fig. 3). A new tripodal imidazolium receptor **2·3X** for chloride anions was studied by ¹H NMR spectroscopy, since the 2,4,6-trimethylbenzene platform favors an optimal geometry of the imidazolium motifs for the interaction with anions [29]. This anion receptor was found to be similar to the tridentate imidazolium salt **3·3Cl**, which had previously been used as a direct precursor to the isolable and stable NHC [30], and was also studied in the gas phase by electrospray mass spectrometry in the positive mode [31].

The triple bridged imidazolium-linked cage **4·3Br** [32] and several *para*-cyclophanes **5·2Br** [32, 33] and **6·2Br** [34] have been reported. X-ray diffraction analysis of the tris-imidazolium cage **4·3Br** reveals that in each molecule the three

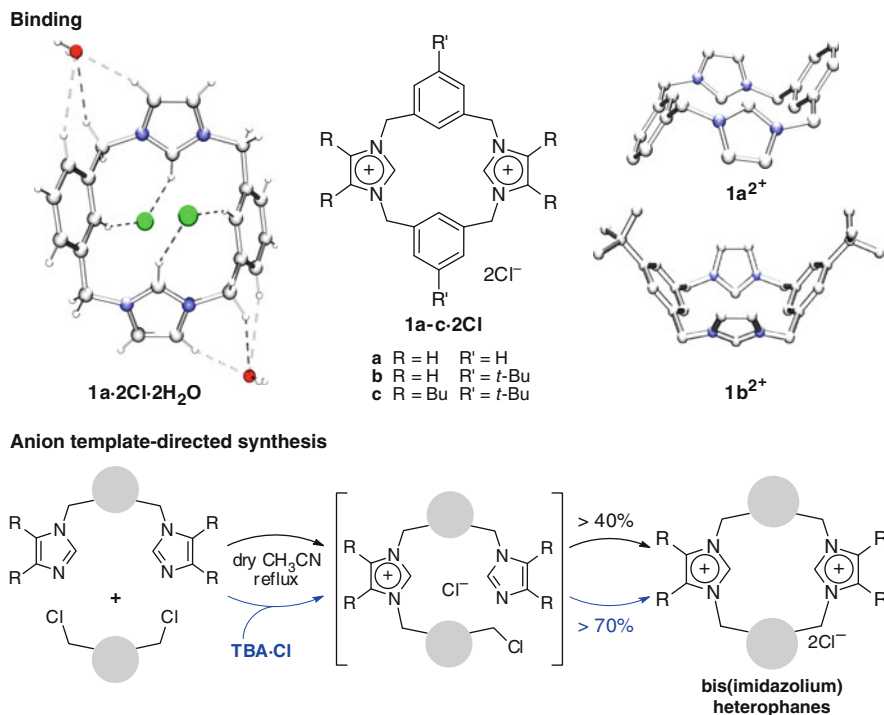


Fig. 2 Hydrogen-bond-driven anion recognition by imidazolium-based cyclophane **1-2A**

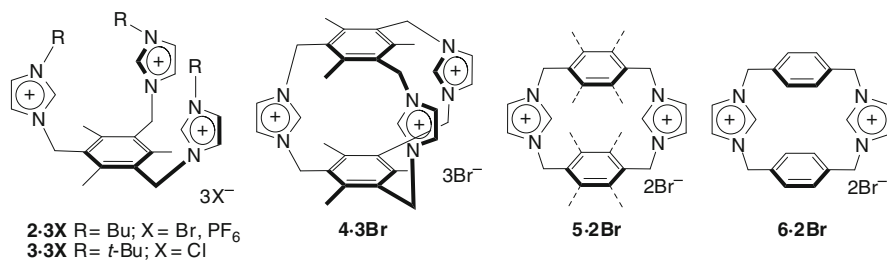


Fig. 3 Early examples of imidazolium-based systems

Br[−] anions stay outside the cavity and form hydrogen bonds with two water molecules rather than with imidazolium C–H moieties of the trication.

Other systems are considered in the corresponding chapters: those containing quaternary π -deficient heteroaromatic moieties with relatively acidic (C–H)⁺, such as pyridinium and azinium rings; and protonated heteroaromatic systems combining both electrostatic interactions and the (N–H)⁺...anion hydrogen bond, for example, the [Sap-2H]-2A-type sapphyrins exhibiting anion-binding properties with excellent phosphate-binding activity [35].

2 Imidazolium Quaternary Salts

The pyridinium quaternary systems and, to a lesser extent, azinium condensed compounds were the most frequently investigated charged heteroaromatic systems until the 1990s. Such studies sought insight into the fundamental topics of heteroaromatic chemistry addressed to structural and physicochemical properties, synthesis, and reactivity. As an example, quaternization reactions of pyridines and dequaternizations of pyridinium salts permitted the examination of basic aspects of a subtype of the Menshutkin reaction, a type of aliphatic substitution, and the use of pyridine as a leaving group in elimination reactions [36, 37]. In contrast, imidazolium quaternary salts are virtually unexplored in this context [38, 39].

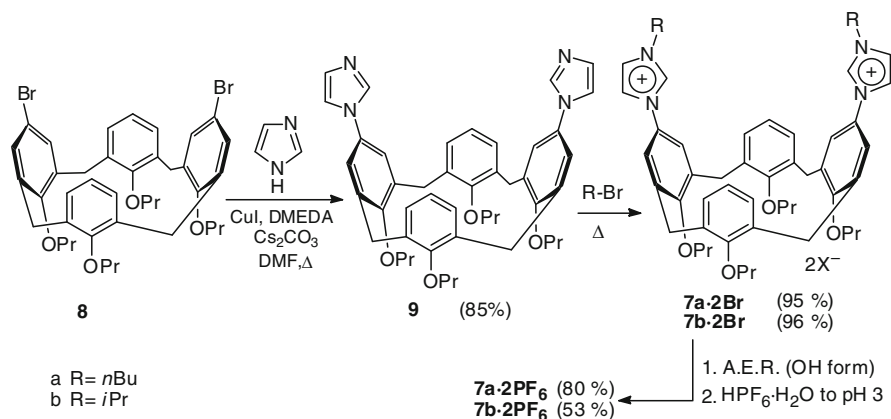
In recent years, imidazolium-based systems have been associated with advances in anion recognition chemistry, NHCs, and RTILs. It is not always sufficiently recognized that the intensive research developed in each of these fields is united by a common denominator: the chemistry of imidazolium salts. Nevertheless, research in imidazolium-based ionic liquids is currently bridging this gap, and several reviews have covered their purity and stability, among other 'neglected issues' [13], their chemical reactivity [12], their chemical stability [9], and the supramolecular organization and networks in ILs [10].

Certain aspects of the quaternary imidazolium salts merit a brief comment:

1. Synthesis
2. Counteranion exchange
3. Chemical stability
4. Structure and physical aspects

Synthesis. In general terms, the synthetic methods for the preparation of quaternary imidazolium cations could be arranged according to the nature of the substituent attached to the nitrogen atoms, either aliphatic and benzylic or aromatic fragments, and their substitution pattern (whether symmetrical or unsymmetrical). Symmetrically substituted imidazolium salts with either aryl or sterically hindered aryl groups have been prepared following a two-step protocol, starting with condensation of glyoxal with two equivalents of arylamine and the cyclization with paraformaldehyde in the presence of a chloride source in the last step [23, 40].

Without doubt, the most common route to the imidazolium-based systems is a subclass of the Menshutkin reaction [41], a nucleophilic substitution reaction carried out under neutral conditions between *N*-substituted imidazoles and an alkylating agent. When planning the preparation of any imidazolium-based system using this neutral *N*-alkylation with an alkyl(benzyl)halide, attention should be paid to the reaction temperature to avoid dequaternization (the reverse of the Menshutkin reaction). Notably, imidazolium salts are among the most robust cationic heteroaromatic compounds [38, 39, 42]. A synthetic option could be the use of an aromatic nucleophilic reaction, but this is limited to aromatic or heteroaromatic halide activated toward S_NAr [42].



Scheme 1 The first imidazolium structural motifs linked to a calix[4]arene scaffold with an (*arene*)C–N(imidazolium) direct bonds

Other methods can be applied to obtain specific compounds and are complementary to the more general procedures. Starting with a copper-catalyzed coupling reaction, an efficient strategy for the synthesis of the novel dicationic imidazolocalixarenes **7a·2PF₆** and **7b·2PF₆** has been reported (Scheme 1), illustrating the first examples of calix[4]arenes containing two imidazolium motifs directly bonded to the scaffold with an (*arene*)C–N(imidazolium) bond type [43]. Thus, a copper-catalyzed Ullmann-type reaction protocol of sterically hindered *N*-arylimidazoles [44] was conveniently applied to transform dibromocalixarene **8** to the bis(imidazolyl)calixarene **9**, and quaternizing the imidazole rings followed by anion exchange gave the targeted dications **7a·2PF₆** and **7b·2PF₆** as anion receptors (see Fig. 8 in Sect. 4). Likewise, dicationic calix[4]arenes **7a·2Br** and **7b·2Br** are precursors of bidentate metal complexes [45].

Among the different aspects of synthetic supramolecular chemistry, template-directed synthesis is a fertile area of research. During the 1990s, advances in efficient template macrocyclization reactions normally involved the use of cations and neutral molecules as templates, while approaches using anion templation were far less common [28, 46]. Recently, strategic anion templation [7], anion-templated assembly [4], and anions as templates in supramolecular chemistry [8] have been reviewed.

The anion template-directed synthesis of dicationic [1₄] heterophanes permits the examination of the anion templation phenomena within simple bis-imidazolium systems and exemplifies how the chemistry of imidazolium salts is fundamental for the design and synthesis of molecular hosts with a capacity for anion recognition. Early studies were centered on dicationic [1₄]heterophanes, e.g. **10a·2Cl** with both π -excessive and highly π -deficient heteroaromatic rings linked in a 1,3-alternating manner, which are immediate precursors of nonclassical quadrupolar [1₄] heterophanes built up from imidazolium methylene triazolate subunits [47]; the positively charged rings were selected due to the recognized chemical stability of the

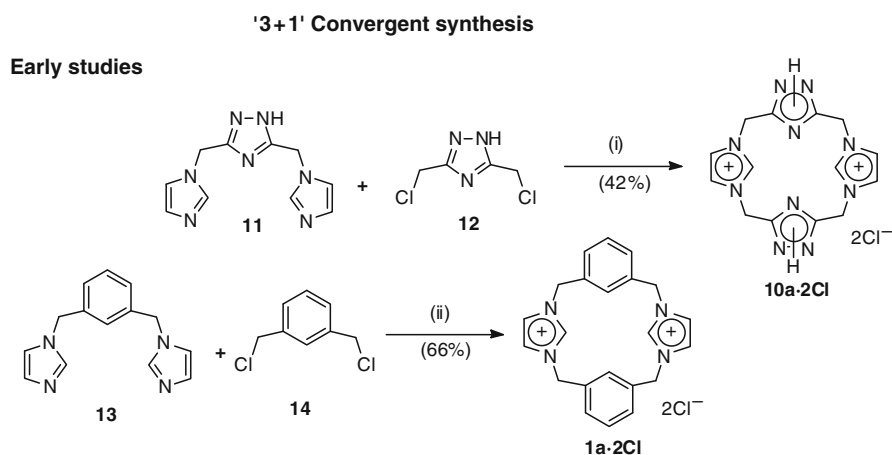
imidazolium moiety located in a variety of azolypyridinium(imidazolium) salts with different interannular spacers [39]. Thus, a straightforward strategy based on a '3 + 1' convergent stepwise synthesis allowed a simple entrance to the dication **10a·2Cl**, which involved joining a trinuclear acyclic system with a bis(halomethyl) monomer (Scheme 2). Quaternization of the protophane **11** with the bis(chloromethyl) compound **12** under neutral conditions produced the dicationic macrocycle **10a·2Cl** in a yield of 42%, a remarkable result for a macrocyclization reaction [47].

In further studies on bis-imidazolium heterophanes, simple model dications **1·2A** were designed to explore their potential for anion complexation. First of all, the application of the '3 + 1' approach was examined: for example, the coupling of protophane **13** with bis(chloromethyl)benzene **14** gave the model **1a·2Cl**, and several examples of **1·2A** were obtained in yields ranging from 48 to 66% (Scheme 2) [27]. The plausible strategic role of the chloride anion in the '3 + 1' convergent stepwise synthesis was then investigated, focusing on the reaction yield and rate:

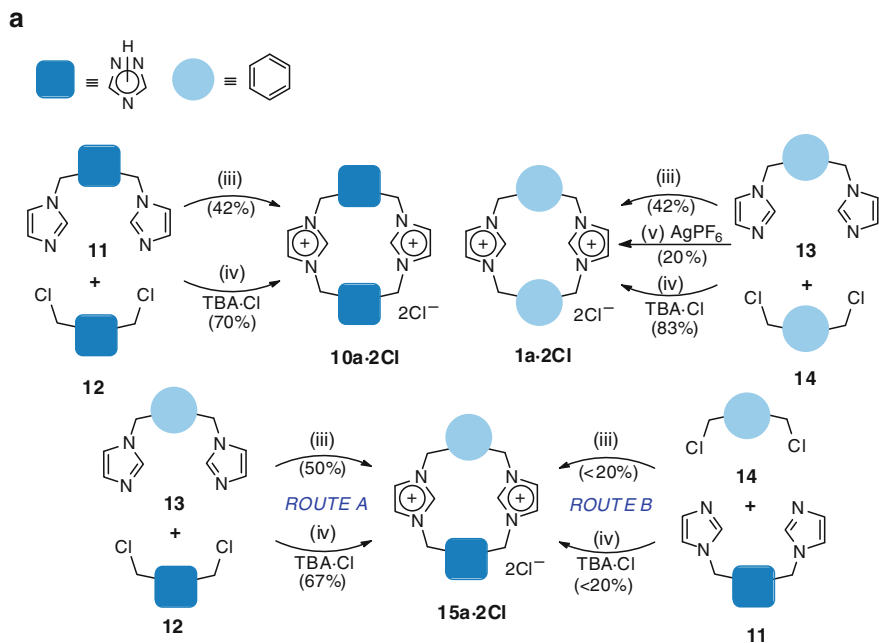
1. The anion template effect in the '3 + 1' macrocyclization process – the yield
2. Competitive experiments
3. Quantification of the chloride template effect – the rate

Anion templation. The anion-controlled formation of dications **10a·2Cl** and **1a·2Cl** demonstrated that chloride anions increased the yield from 42 to 70% and 83%, respectively. Changing to other anions such as hexafluorophosphate lowered the yield to 20%.

Formation of dicationic heterophanes with two *s*-triazole units **10a·2Cl** in the presence of TBA·Cl was less efficient than of those bearing the dicationic prototype **1a·2Cl**. A feasible reason could be the diminished ability of the most abundant 1,2,4-triazole tautomer in the reaction medium, e.g. 1*H*-1,2,4-triazole, to form assisted hydrogen bonds with chloride anions in the best fit conformation geometry



Scheme 2 (continued)



Scheme 2 '3 + 1' Convergent synthesis of bis-imidazolium cyclophanes: (a) anion template-directed '3 + 1' stepwise macrocyclization process; (b) competitive experiments; (c) kinetic study: quantification of the chloride template effect

required for the ring-closure step. Furthermore, the optimal geometry for the cationic tetranuclear acyclic intermediate should be assisted by $\text{NH}\cdots\text{Cl}^-$ hydrogen bonds between the anion and the usually less favored 4*H*-1,2,4-triazole tautomer in solution.

To shed further light on the preferences in the '3 + 1' approach, bis-imidazolium dication **15a·2Cl** was prepared via two alternative pathways, A and B. The '3 + 1' macrocyclization process proceeded more efficiently when the building blocks were protophane **13** and dichloride **12** (via A, 50% yield) than when compounds **14** and **11** were used instead (via B, <20% yield), and moreover, the chloride anion templation functioned in route A but not in B. Thus, the bis(chloromethyl)-*s*-triazole **11** is more reactive and slightly accelerates the quaternization reaction in the condensation step. Likewise, protophanes containing 1,3-disubstituted benzene, i.e. **13**, are more prone to self-templation in the ring-closure step.

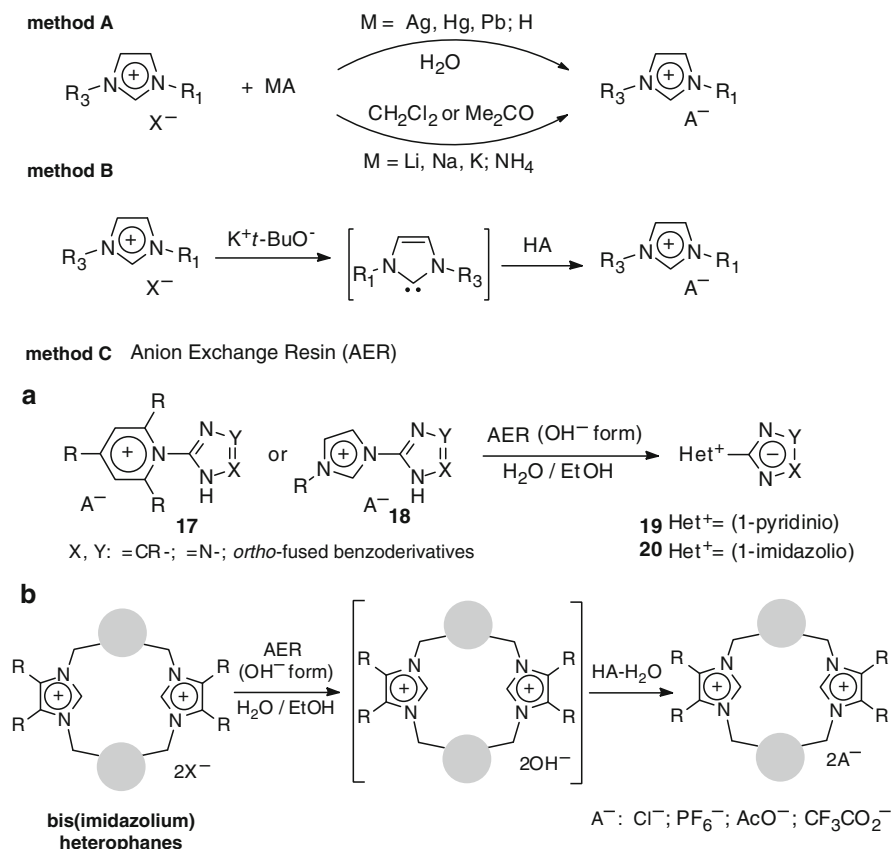
Certain aspects of 1,2,4-triazole chemistry should be noted. The background offered by Kauffmann's arenology principle, both for classification and generation of heteroaromatic systems, permits heteroaromatic fragments to be related to classical functional groups, for a *C*-linked heteroaryl fragment being either a donor group (π -excessive) or an acceptor group (π -deficient) [48]. Accordingly, the decreasing π -excessive nature of an azole nucleus modulates the physical properties and chemical response of a designed system [42, 49–51]. As an example, the electron-withdrawing capacity of the 1,2,4-triazol-5-yl group is much greater than that of the 2-imidazolyl substituent because of the presence of a second pyridine-like nitrogen atom [50, 52]. Among other points to consider are the acidity and basicity of azoles [53] and studies on the tautomerism in heterocycles [54], i.e. *s*-triazoles [55, 56].

Competition experiments. Among the different competitive experiments that have been undertaken, two examples merit comment. The reaction of protophanes **11** and **13** and the bis(chloromethyl) derivatives **12** and **14** showed differences when the macrocyclization protocol proceeded in the absence and presence of a chloride anion source (Scheme 2). Thus, a reaction was set up between protophane containing 1,3-disubstituted benzene **13** and both bis(chloromethyl) derivatives **12** and **14**, which gave dicationic macrocycles **1a·2Cl** and **15a·2Cl** in a 1.2:1.8 ratio, and after adding a chloride anion source, in a ratio of 0.5:2.5 (Scheme 2) [28]. The formation of dication **15a·2Cl** as the major product confirms the importance of both the condensation step and the anion-templated ring-closure step in the '3 + 1' macrocyclization process.

Recapping the results, the structural recognition motifs for anion templation of the bis-imidazolium prototype **1a·2Cl** involve the interaction of a chloride ion with the hydrogen-bond donor source from the charged imidazolium motifs, assisted by the aromatic units. This is corroborated by the data gained in solution by ^1H NMR spectroscopy and in the solid state by X-ray crystallography [27]. The chloride anions generated in situ during the '3 + 1' macrocyclization process act as self-templates through the formation of hydrogen bonds with the reaction intermediate in the ring-closure step. Both the intermolecular condensation and anion-templated intramolecular cyclization play a significant role in the '3 + 1' stepwise macrocyclization reaction [28].

Chloride template effect quantification: a kinetic study. The template effects exerted by chloride anions in the ring-closure reaction of the cationic tetranuclear acyclic intermediate **16a·Pic** to produce bis-imidazolio cyclophane **1a·2Cl** have been quantitatively evaluated using a UV-vis technique. The kinetics of the reaction with model $16a^+ \rightarrow 1a^{2+}$ showed that the rate of the ring closure of $16a^+$ was increased up to ten times in the presence of Bu_4NCl 0.04 M (Scheme 2) [57].

The counteranion exchange. The apparent directness of the anion exchange process does not imply that it is either simple or trivial. The synthesis of imidazolium-based receptors usually involves a quaternization reaction of the imidazole fragment(s) using alkyl or benzyl halides and gives the targeted imidazolium system in which the counteranion(s), ion halide, can be exchanged using different protocols (Scheme 3).



Scheme 3 Counteranion exchange. Method A, classical procedures; method B, via NHC; method C, anion exchange resin (AER) antecedents: (a) early studies, *N*-azolyipyridinium(imidazolium) salts **17** and **18**; (b) application to bis(imidazolium) heterophanes

A general procedure is the classical halide ion exchange with another inorganic salt (MA), which is also commonly used to remove halide ions in ILs (method A). Another reported process to avoid halide impurities in ILs is via NHCs, (method B) [58], an unconventional way for an imidazolium quaternary salt anion exchange.

Isolation of pure imidazolium quaternary salt systems is sometimes difficult and can be a serious problem when the solubility of the different ionic species present in the solution mixture is similar. A comparative study of the transformation of *N*-azolyipyridinium(imidazolium) salts **17** and **18** to the corresponding mesomeric betaines **19** and **20** showed that the method of choice makes use of a strongly basic anion exchange resin (AER) [42, 59]. This protocol was then conveniently applied to a variety of *N*-azolyimidazolium salts with different spacers [39].

Exploiting our standard protocol, the counteranions of bis-imidazolium heterophanes, e.g. **1·2Cl** and **10·2Cl**, were changed by column chromatography packed with a strongly basic AER (OH⁻ form) followed by immediate collection of the eluates in aqueous acid solution to pH = 3 (Scheme 3). The anion exchange proceeded through the corresponding imidazolium hydroxides, e.g. **1·2OH** and **10·2OH** [27, 43, 47, 60, 61].

A simple protocol permits iodide or bromide anions in ILs to be exchanged for a broad range of anions. Selected anions were loaded in an AER using two different procedures and were then used to provide a pure ion pair as shown in Fig. 4 [62].

The preparation of an AER conveniently loaded with a new selected anion by treatment with acid or ammonium salts not only offers an efficient tool to prepare the appropriate ion pair in quantitative yield, including task-specific and chiral ILs, but it is also recyclable and minimizes the formation of toxic by-products, with the corresponding environmental benefits.

Chemical stability. Heteroaromatic imidazolium quaternary salts show high chemical stability in a wide range of chemical processes as reflected in the aforementioned reviews on simple imidazolium salts, i.e. ILs [9, 12, 13]. They resist chemical degradation during thermolysis caused by either the reverse Menschutkin reaction or Hofmann elimination, hydrolysis, and other degradation reactions, which mainly stem from the acidity of the C(2)-H, among others.

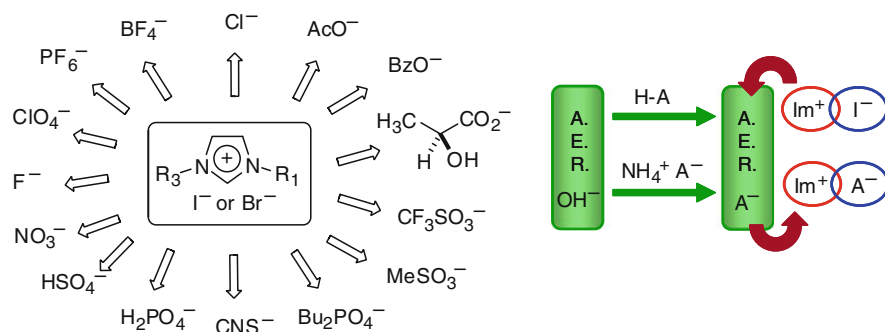


Fig. 4 Anion exchange resin (AER): a simple and efficient counteranion exchange protocol

Structure and physical aspects. The imidazolium-based systems are attractive from the viewpoint of structural chemistry, and the multidisciplinary facets of their characteristic physical and physicochemical properties have significant implications in the fields of anion recognition, ILs, and NHCs, as well as R&D, see Fig. 1.

In the following section, these different perspectives are briefly highlighted.

2.1 The Imidazolium Functionality

Kauffmann's areno-analogy principle relates heteroaromatic fragments with classical functional groups [48]. Hence, the cationic imidazolium quaternary fragments are nonclassical acceptor groups, and the highly π -deficient heteroaromatic character and the C(2)–H flanked by the two heteroatoms are the distinguishing features of these cationic structural motifs for anion recognition. Particularly significant are the following:

1. Brønsted C(2)–H acids and pK_a values
2. Deuterium exchange at C(2)
3. Nonclassical (C–H)⁺...anion hydrogen bonds.

Brønsted C(2)–H acids and pK_a values. There were only three reports on this fundamental property of imidazolium quaternary salts until 2004. These experimental studies were concerned with the basicity of NHCs, the conjugate bases of the imidazolium salts, and the first pK_a value was recorded for the 1,3-diisopropyl-4,5-dimethylimidazolium cation (24.0 in DMSO-*d*₆, entry 14 in Fig. 5) [63]. The 1,3-di-*tert*-butylimidazolium cation was then examined and its pK_a value was found to be 22.7 in DMSO (entry 3) [64]. The deuterium exchange reactions of C(2)–H for other simple imidazolium salts were also studied, and the data were used to obtain a reliable pK_a for cation ionization in water; the carbon acid pK_a of azolium cations in aqueous solution was $pK_a = 23.8$ for the imidazolium cation, $pK_a = 23.0$ for the 1,3-dimethylimidazolium cation (entry 1), and $pK_a = 21.6$ for the 1,3-dimethylbenzimidazolium cation [65].

In the same period, the 'non-innocent' nature of some specific imidazolium ionic liquids was recognized for the first time [15]. The interest in ILs as green solvents has grown spectacularly both in academia and industry in the last few years, as reflected by the aforementioned reviews focused on the chemistry of imidazolium salts [9, 12, 13].

In 2007, a significant study of the equilibrium acidities of 16 imidazolium ILs examined the structural factors and nature of the counteranion in DMSO at 25°C, obtaining the pK_a data gathered in Fig. 5. The steric hindrance to solvation and the electronic effects of the substituents induce differences in the pK_a values in the range of 19.7–23.4, while the pK_a 's of the 1-butyl-3-methyl imidazolium salts were around 22.0, irrespective of the nature of the usual counteranions [66]. Hence, the acidities of 1,3-dialkylimidazolium 'CH heteroaromatic acids' are similar to those of hydrocarbon acids such as indene ($pK_a = 20.1$) and 2-methyl or 3-methylindenes ($pK_a \sim 22$) in DMSO [67, 68].

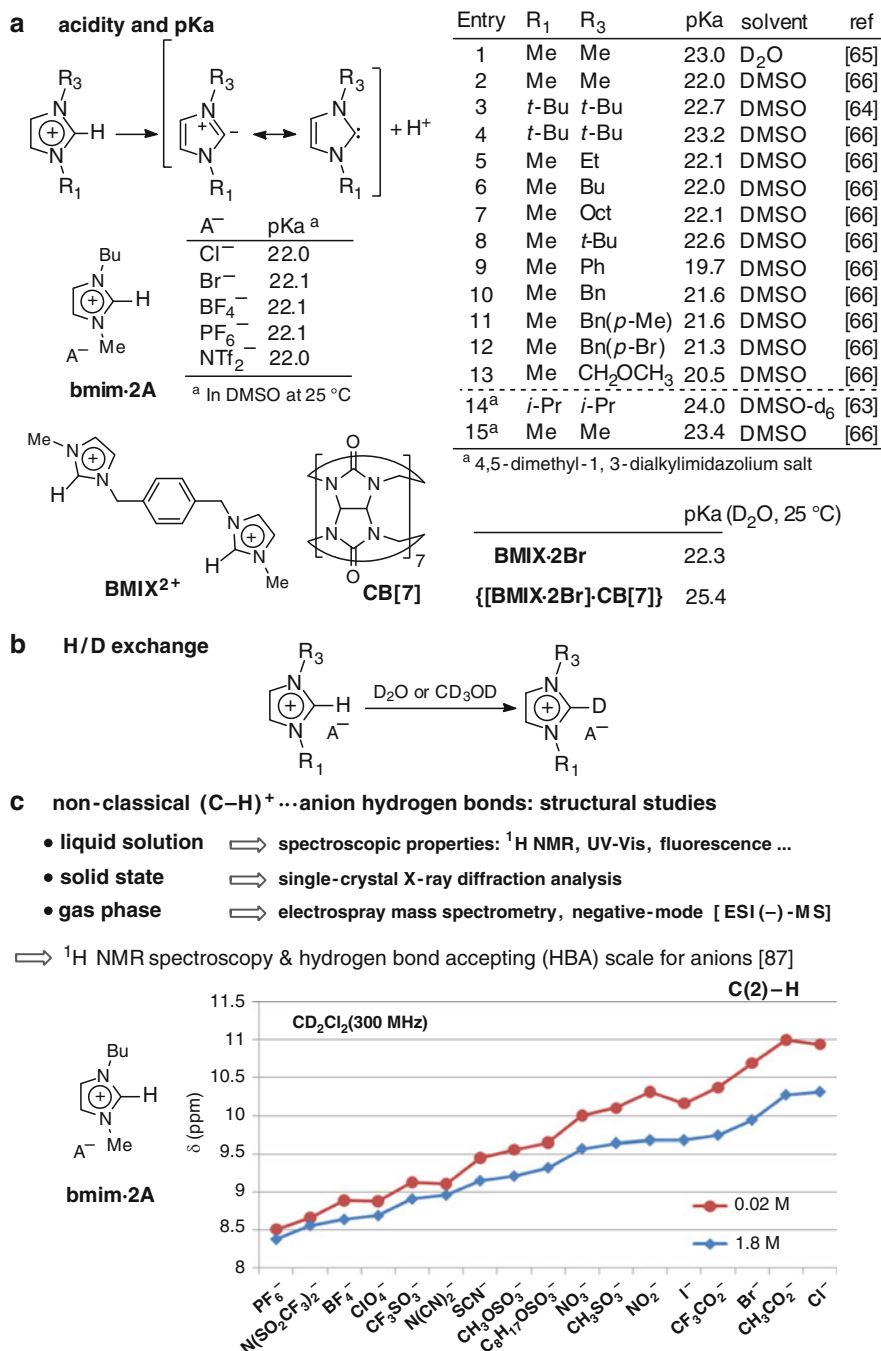


Fig. 5 Distinctive features of imidazolium quaternary salts: (a) 'CH heteroaromatic acids' and pK_a values; (b) deuterium exchange at C(2); (c) structure and (C–H)⁺...anion hydrogen bonds

The tunable imidazolium motif can be adjusted to modulate the acidity of the C(2)–H. Because of the versatility of the imidazolium functionality within host–guest chemistry, the effect of supramolecular inclusion of imidazolium systems on the acidity of the C(2)–H protons is illustrated with the bis-imidazolium cation **BMIX·2Br** ($pK_a = 22.3$, 25°C in D_2O), which forms a 1:1 complex with cucurbit [7]uril. A host molecule of **CB[7]** acts as a hydrogen-bond acceptor for the acidic C(2) hydrogen atoms by adapting the ‘bis-imidazolium guest’ within the cavity for optimal $(\text{C}–\text{H})^+\cdots\text{O}=\text{C}$ hydrogen-bonding interactions and thereby increasing the pK_a value to 25.4 (Fig. 5) [69].

Deuterium exchange at C(2). In imidazoles, the C(2)–H can be isotope-exchanged upon prolonged heating in D_2O , while the π -deficient heteroaromatic 1,3-dialkylimidazolium counterparts can be exchanged under mild reaction conditions. Imidazolium quaternary salts are ‘CH heteroaromatic acids’ and it was recognized as early as 1964 that the C(2)–H proton of the 1,3-dimethylimidazolium salt functioned as a carbon acid since it underwent deuterium exchange under mild conditions [70]. In general, the C(2)–H is more acidic than other ring hydrogen atoms, the reactivity order being $\text{C}(2)–\text{H} \gg \text{C}(5)–\text{H} > \text{C}(4)–\text{H}$. Imidazolium salts bearing a methyl group in the 2-position also undergo isotopic exchange under neutral and mild reaction conditions [38, 71] in a similar way to the better known active methyl groups in 2-methyl and 4-methylpyridinium quaternary salts.

Both the C(2)–H and the C(2)– CH_3 moieties of imidazolium-based systems, especially with halide counteranions, are prone to H/D exchange under neutral conditions, while the 4- and 5-positions require the presence of bases or transition metals. The susceptibility of imidazolium salt systems to H/D exchange can be modulated to promote or even hinder the isotopic exchange process. Very few studies on this topic have been published so far. The isotopic exchange studies on azolium cyclophanes concerned only imidazolium systems [5]. The H/D exchange at C(2)–H of imidazolium species is facile in many cases, and can readily occur when the imidazolium cyclophane is dissolved in a protic deuterated solvent, CD_3OD or D_2O . Thus, the acidic C(2)–H of cyclophanes **1a–c·2Cl** undergo H/D exchange under mild conditions in D_2O or $\text{D}_2\text{O}/\text{CD}_3\text{OD}$ at 35°C overnight in a quantitative yield [31]. An interesting study has shown that the rate of the H/D exchange reactions can vary substantially with the structure of the cyclophane, and different cyclophanes have been examined in detail, e.g. **5·2Br** (Fig. 3) [33].

The C(2)–H isotopic exchange of a homologous series of 1-alkyl-3-methylimidazolium salts (Br^- , BF_4^- and PF_6^-) has been studied by ^1H NMR spectroscopy in D_2O and CD_3OD : longer alkyl chains slowed the rate, while the isotopic exchange of imidazolium BF_4^- and PF_6^- salts was negligible [72]. Because of the propensity of 1,3-dialkylimidazolium salts to undergo deuterium exchange, the H/D exchange has been examined with several examples of C(2)–H and C(2)– CH_3 imidazolium salts with different anions being studied under neutral or moderately basic conditions [73]. Another study was mainly focused on the transition-metal-free synthesis of several perdeuterated 1,3-dialkylimidazolium salts (ILs) along with the deuterium isotopic exchange using different solvents and bases; the presence of small amounts of basic impurities, for instance, traces of starting material such as

1-methylimidazole, favored the isotopic exchange behavior [74]. A kinetic study of the H/D exchange of 14 imidazolium-based systems, cationic and dicationic [1₄]calixarenes as well as 11 open-chain cations in methanol-*d*₄ containing 3% water, showed that mesityl-substituted compounds exhibited the highest rate constants [75].

Non-classical (C–H)⁺...anion hydrogen bonds. The structural properties of the imidazolium functionality can be adapted for precise direct supramolecular assembly: the noncovalent driving forces for anion recognition are the aforementioned combination of electrostatic and hydrogen-bond interactions. Depending on the structural features of the imidazolium systems and the nature of the counteranion, other interactions can also take place between the cations and the anions. Conversely, the usually weaker CH/ π noncovalent interactions are fairly strong for anionic ‘guests’ bearing aromatic units, e.g. tetraphenylborate anions; the structural study of the **bmim**·**B(Ph)₄** ionic liquid has revealed the (C–H)⁺... π hydrogen bonds both in solution and in the solid state [76].

Due to the diversity of imidazolium-based artificial anion receptors, a varied range of physical techniques can characterize the receptor-anion complex, especially those that can define the preferential role of the nonclassical (C–H)⁺...anion hydrogen-bond interactions. While the majority of supramolecular studies have been carried out in solution and to a lesser extent in the solid state, the gas phase has been neglected; the most common techniques used are highlighted in Fig. 5.

Despite the significance of computational methods in chemistry and the ascent of odorless chemistry, already noted in 1992 [77], there are few studies on the applications of computational techniques as complementary tools in the interpretation of experimental data of existing imidazolium-based systems and in the design of new ones. These theoretical studies deal with the design of systems bearing polyarene signaling subunits as fluorogenic chemosensors for anions [6, 78, 79] and with the molecular modeling of simple imidazolium salts–ILs [80].

In the gas phase, electrospray ionization mass spectrometry (ESI-MS) is a powerful analytical technique, which has also been applied in supramolecular chemistry since the 1990s [81–83].

For the characterization of a series of tetracationic catenanes, at both the molecular and supramolecular levels, ESI-MS was found to be better than other soft-ionization techniques such as fast atom bombardment mass spectrometry (FAB-MS) [84]. Exploiting the sensitivity of the ESI technique, we have examined the behavior of bis-imidazolium cyclophanes **1a–c**·**2Cl** and other dications together with the tridentated imidazolium salt **3**·**3Cl** in the gas phase [31, 61]. Two relevant studies of imidazolium ionic liquids deal with the gaseous supermolecules of ILs and the ‘magic numbers,’ using both ESI(+) and ESI(–) experiments [85], and the gas-phase nature of ILs was also examined by Fourier transform ion cyclotron mass spectrometry (FTCIR-MS) [86].

In solution, ¹H NMR spectroscopy has proved to be crucial for providing evidence of the (C–H)⁺...anion interactions, and the choice of the solvents is dictated by the product solubility. At nonaggregating concentrations, the proton

chemical shift of the acidic C(2)–H protons is the most affected by: (a) the nature of the counteranion, (b) structural factors, and (c) the solvent polarity.

The anion effect has been recently studied using a simple imidazolium salt **bmim**·**2A**, and a hydrogen-bond-accepting (HBA) ability scale for varied anions of the cation (**bmim**)⁺ has been determined by means of ¹H NMR spectroscopy and a solvatochromic UV/vis probe in CD₂Cl₂ to minimize solvation. As shown in Fig. 5, the hexafluorophosphate anion is the reference of ‘non-HBA anion,’ and changing the nature of the counteranion causes a significant deshielding of C(2)–H protons from 8.38 ppm for **bmim**·**2PF**₆ up to 10.31 ppm for **bmim**·**2Cl**. The counteranion effect on the chemical shift was correlated for each anion at concentrations of either 0.02 or 1.8 M [87]. Other selected examples of ¹H NMR spectroscopy studies are discussed in the following sections, e.g. for the cyclophane prototypes **1**·**2A**, see Fig. 6.

The palette of hydrogen bonds in the solid state show different types of D–H···A hydrogen bonding, which are the most important of all directional intermolecular interactions. Nevertheless, the definition of terms and categories according the strength of the hydrogen bonds depends on the focus of the field of interest, resulting in the coexistence of different terminologies and classifications [88].

The commonly used are (a) ‘strong’ (quasi-covalent nature), ‘moderate’ (mainly electrostatic), and ‘weak’ (electrostatic/dispersion H-bonds) [89]; and (b) ‘very strong’, ‘strong’, and ‘weak’ H-bonds as proposed from a supramolecular point of view [90].

The tunable imidazolium functionality can be adjusted to modulate the structural organization of the imidazolium-based host system and has different binding sites mainly controlled by unconventional H-bonds and electrostatics along with π -stacking. The self-assembly of simple imidazolium quaternary salt networks shows a typical organization in the solid state, forming networks between the imidazolium cations and the counteranions through ‘weak’ to ‘moderate’ hydrogen-bond forces combined with electrostatic interactions (H···anion bond lengths >2.2 Å, C–H···anion bond angles between 100° and 180°) [10]. Notably, the design of *N,N'*-diaromatic bis(imidazolium) building blocks (‘tectons’) driven by π -stacking and the characteristic interactions of the two imidazolium rings generated supramolecular crystalline structures: here we enter the domain of crystal engineering [91].

In the solid state, the crystalline phase permits an accurate structural study of the nonclassical (C–H)⁺···anion hydrogen-bond interactions present in imidazolium-based anion receptors by single-crystal X-ray diffraction methods.

Selected examples of imidazolium-based anion receptors are discussed in the following sections, although the number of anion hosts mentioned is unavoidably limited by the scope of the chapter, and the literature has been covered up to December 2009. For more information, the recent aforementioned reviews cover anion receptors based on organic frameworks and also containing metal subunits [1–3], and give a comprehensive description of the ‘chemistry of azolium cyclophanes’ from different angles [5] along with a brief review on ‘imidazolium receptors for anion recognition’ [6].

3 Cyclophanes

The molecular diversity present in macrocycles allows the design of new host systems that exhibit more specific properties, such as cyclophanes, phanes, and heterophanes, as well as calixarenes, which are a source of a broad array of molecules and shapes. During the 1990s, the commonly used ring components present in heterophanes were uncharged heteroaromatic moieties and, in the few cases in which they were charged, they were pyridinium(azinium) quaternary rings, for example, the cyclophanes derived from 4,4'-bipyridinium units, like today's classical Stoddart's 'blue box'.

In the chemistry of imidazolium(pyridinium) azolate betaines and the imidazolium-based frameworks developed by our research group, the first macrocyclic systems examined were bis(imidazolium)-[1₄]meta-heterophane prototypes **10·2A** and the novel quadrupolar 'bis-betaines' (Fig. 6). The fact that the imidazolium units were selected due to the recognized stability of the methyleneimidazolium azolate betaine building blocks is noteworthy [47, 92]. Maintaining the two imidazolium moieties present in dications **10·2A**, simple bis(imidazolium) cyclophane prototypes **1·2A** arise as models for intermolecular interactions driven by nonclassical (C–H)⁺⋯anion hydrogen bonds in which the halide counteranion is noncovalently bound to the macrocyclic framework. Notably, the single-crystal X-ray diffraction analysis of dication **1a·2Cl·2H₂O** typified the first example of a non-classical (C–H)⁺⋯Cl[−] hydrogen bond between the imidazolium rings and chloride anions (Fig. 2) [27]. Further studies on the ability of dications **1·2A** to bind chloride anions showed that their '3 + 1' convergent stepwise synthesis is template-controlled by the presence of chloride anions, e.g. **1a·2Cl** and **10a·2Cl** (see Scheme 2 in Sect. 2) [28, 57].

On the whole, the imidazolium functionality represents the main structural motif for the formation of unconventional (C–H)⁺⋯Cl[−] charged assisted hydrogen bonds, which are the noncovalent forces driving the anion interactions exhibited by (bis-imidazolium) cyclophane prototypes **1a–c·2A**. There is a good parallel between the experimental trends observed in the solid state by X-ray crystallography, in solution by ¹H NMR complexation studies, and in the gas phase by electrospray ionization mass spectrometry in the negative mode ESI(−) MS, Fig. 6 [27, 60, 61].

The first single-crystal X-ray diffraction analysis of an imidazolium-based system revealed the unconventional (C–H)⁺⋯Cl[−] hydrogen bonds between the C(2)–H imidazolium rings and halide anions. In the dication **1a·2Cl·2H₂O**, the noncovalent interactions are based in multicentered (C–H)⁺⋯Cl[−] bonds established between the Cl[−] with the aromatic hydrogen atom on the *m*-xylyl spacer and the acidic hydrogen atom of the imidazolium ring, which is the shortest hydrogen-bond interaction (2.54 Å, θ = 157°); there are also weak interactions with water. The chloride anions occupy an outer position above and below the main plane defined by the methylene spacer groups. The hydrogen-bond networks help to sustain the crystal lattice, and the solid-state aggregates revealed that chloride anions and the water molecules were located among the dications in a channel fashion (Figs. 2 and 6).

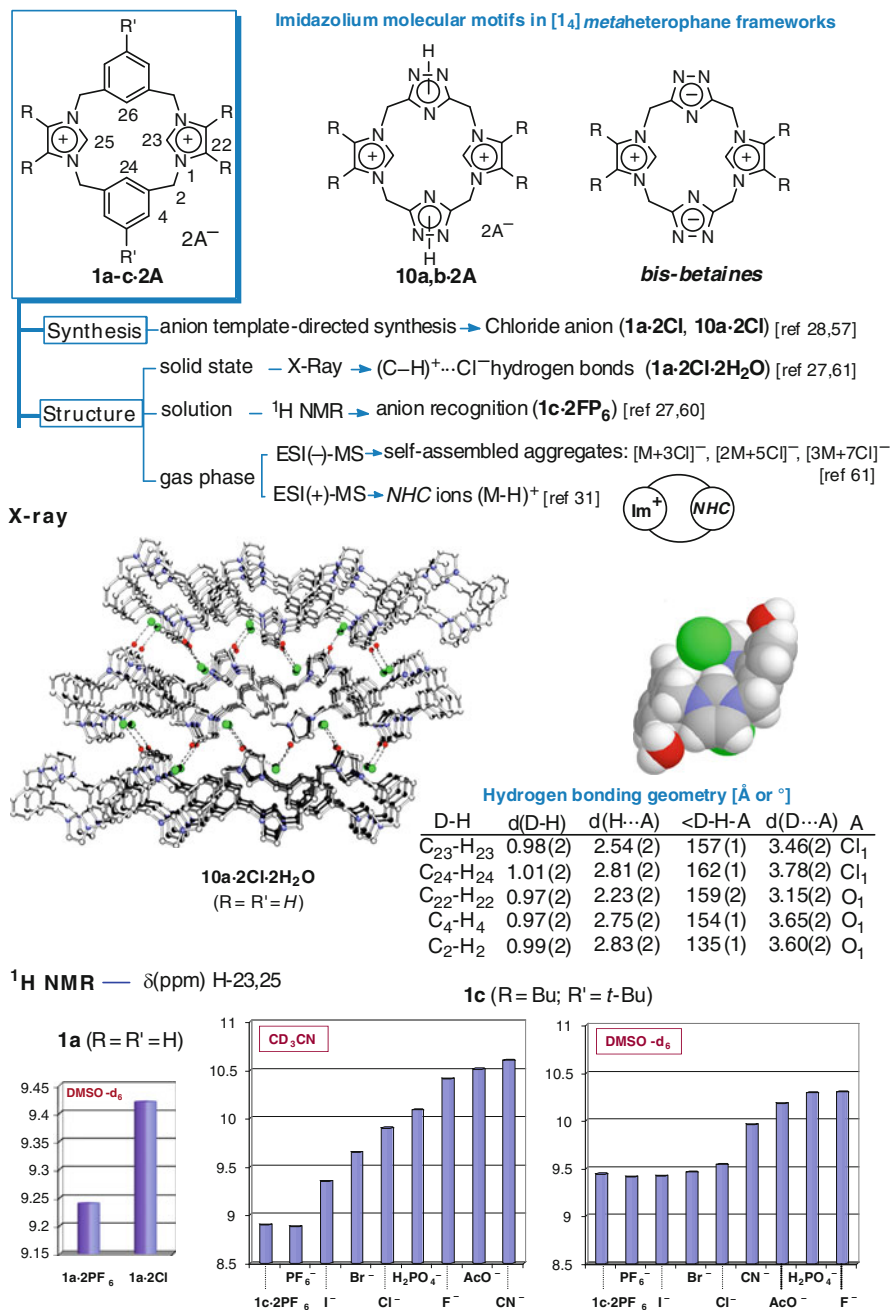


Fig. 6 Imidazolium-based systems as a new family of artificial anion receptors: identification of bis(imidazolium)-cyclophane prototypes **1-2A**

In solution, the anion-binding behavior of the anion receptor prototype **1c·2PF₆** was examined by ¹H NMR in CD₃CN and DMSO-*d*₆, revealing the importance of the imidazolium units as motifs for anion recognition. The acidic H-23 and H-25 hydrogen atoms were then shifted downfield up to ~10 ppm, although the 1:1 complexes, e.g. with AcO[−] anions, exhibited anion-binding affinity with moderate association constants.

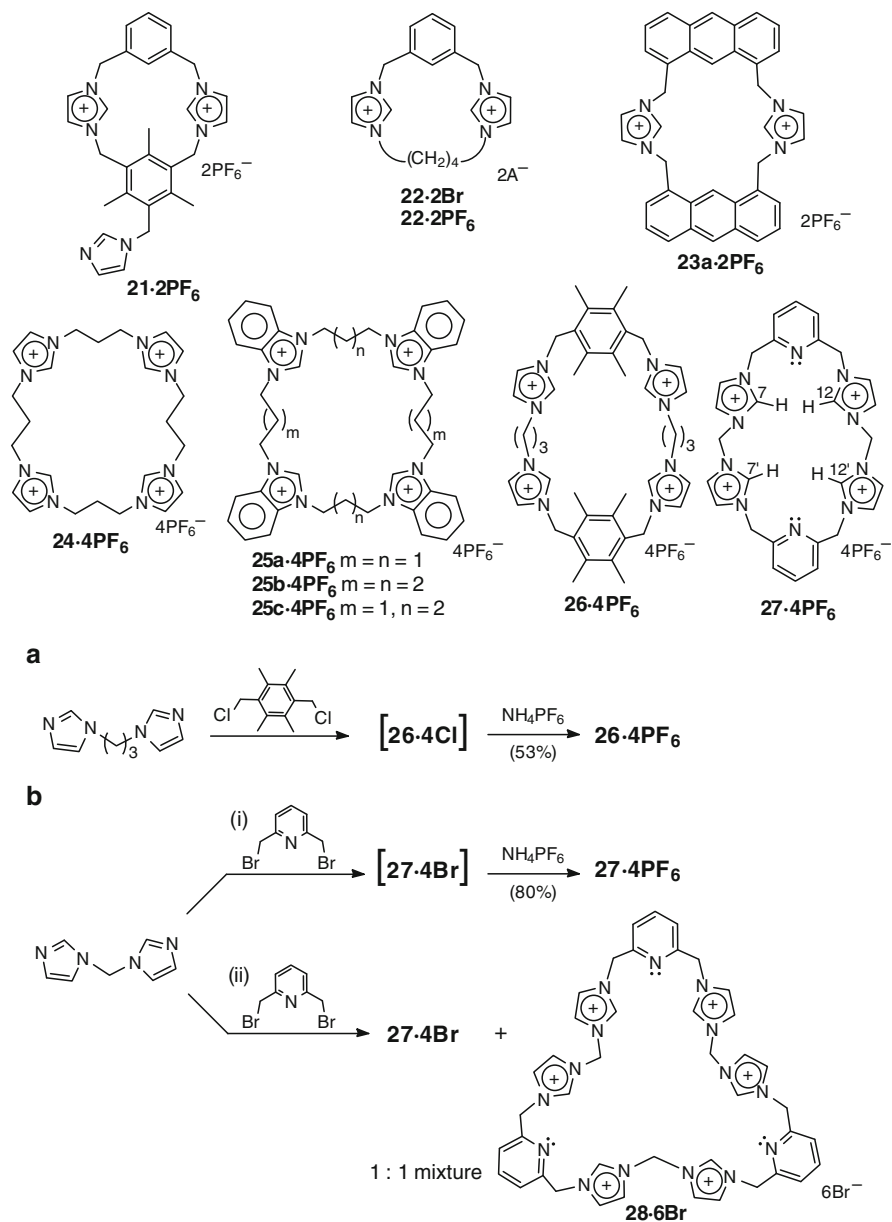
In the gas phase, cyclophanes **1a–c·2Cl** have also been examined by ESI-MS, and the negative-ion mode response showed the formation of self-aggregates as a consequence of the hydrogen-bonded halide anion complexes, e.g. **1a·2Cl**. Yet, when the Cl[−] anion was replaced by PF₆[−], the macrocycle **1a·2PF₆**, exhibited only one peak at *m/z* 145 from [PF₆][−]. Conversely, the ESI(+) MS response showed the singly charged NHC ions among other characteristic peaks.

In 2006, the chemistry of azolium cyclophanes with two or more azolium groups constituting parts of a macrocycle was reviewed, with a comprehensive coverage of their structural diversity. The authors underlined the growing interest in imidazolium-based cyclophanes due to their potential applications in both anion recognition chemistry and as precursors to NHC metal complexes. Other azolium rings have been far less investigated [5].

A parameter playing a crucial role in the scaffold selection process is ‘chemical tractability’, which refers to synthetic accessibility and suitability for chemical modification. Cyclophanes and their open-chain system counterparts, protophanes, are a priori synthetically accessible and considered to be interesting frameworks for anion binding and sensing applications; so a number of groups have been exploring them for their anion recognition properties and particularly as precursors of NHC complexes. In the last few years, the anion recognition chemistry of imidazolium-based cyclophanes and protophanes has continued to generate considerable interest, especially for the design of selective anion chemosensors, which is mentioned in Sect. 6.

Bis-imidazolium [1₄]cyclophane **21·2PF₆**, bearing an additional imidazole ring binds halide anions, and the complexation behavior has been examined by UV–vis spectroscopic titration in acetonitrile, showing a 1:1 binding stoichiometry in each case. The best binding affinity corresponds to Cl[−] ions ($K = 4.06 \times 10^4 \text{ M}^{-1}$) while other halides result in a loss of activity, in the following order: Br[−] (~2-fold) > F[−] (~5-fold) > I[−] (~2,000-fold). The X-ray analysis of dication **22·2Br** with the imidazolium rings interconnected by a rigid *m*-xylyl and a flexible 1,4-butyl shows (C–H)⁺⋯Br[−] hydrogen bonds between the C(2)–H imidazolium rings and bromide anions, 2.66 Å, $\theta = 171^\circ$ and 2.70 Å, $\theta = 165^\circ$, respectively; the bromide ions also form H-bonds with the hydrogen atom of the *m*-xylyl linker and the methylene groups. The host **22·PF₆** binds the halide anions in the order Br[−] > Cl[−] > > F[−] > I[−] but with weaker affinity and selectivity compared to host **21·2PF₆** (Fig. 7) [93].

The anthracene-linked cyclophane host **23a·2PF₆** binds H₂PO₄[−] ($K = 1.3 \times 10^6 \text{ M}^{-1}$) more strongly than halide ions, following the order F[−] (~4-fold) > Cl[−] (~600-fold) > Br[−] (~1,000-fold), and functions as a fluorescent anion sensor for H₂PO₄[−] because the binding of the anion quenches the fluorescence of the



(a) Reagent concentrations and conditions: the reaction was carried out without high-dilution conditions in dry acetonitrile and reflux overnight.

(b) Reagent concentrations and conditions: the two reactions were carried out with equimolar amount of the reagents, 170 nM in dry acetonitrile. (i) Dropwise addition at room temperature for 0.5 h and reflux overnight; (ii) dropwise addition at room temperature for 5 h and reflux overnight.

Fig. 7 Oligocationic imidazoliophanes: bis(imidazolium) and tetrakis(imidazolium) cyclophanes

bis-imidazolium anthracene cyclophane. The selective binding of H_2PO_4^- over other anions has been studied by means of fluorescence and ^1H NMR and rationalized using ab initio theoretical calculations; it should be noted that the association constants were measured using fluorescence titrations [94].

Tetrakis(imidazolium) cyclophane **24·4PF₆** and benzimidazolium analogs of variable cavity size **25a–c·4PF₆** exhibit high binding affinities and selectivity to F^- ions. Host **25c·4PF₆** forms 1:1 stoichiometric complexes with F^- ions with strong stability constants ($K > 10^4 \text{ M}^{-1}$) and, in the case of benzoate, a 1:2 complex was observed with weaker affinities ($K_1 > 2,700 \text{ M}^{-1}$, $K_2 > 600 \text{ M}^{-1}$) from ^1H NMR spectroscopic titration studies [95].

The tetrakis(imidazolium) [1₆]heterophane **26·4PF₆** [96] forms 1:1 complexes with halides and oxoanions in DMSO-*d*₆. From the ^1H NMR titration experiments, the binding affinity of this receptor was reported to be in the order $\text{HSO}_4^- > \text{Br}^- > \text{H}_2\text{PO}_4^- > \text{Cl}^- > \text{I}^- > \text{ClO}_4^-$. Changing the aromatic *p*-arylene fragments in the **26·4PF₆** by a π -deficient heteroaromatic 2,6-pyridiyl ring led to the tetrakis(imidazolium)[1₆]heterophane **27·4PF₆**, which exhibited high binding affinity to F^- ions. In solution, the association constants were calculated using ^1H NMR spectroscopy titrations in DMSO-*d*₆, and the binding studies indicated that the host formed a 1:1 complex with F^- ions, $K = 28,900 \text{ M}^{-1}$, while a 1:2 (heterophane: anion) complex predominated for the other anions examined: Cl^- , Br^- , I^- , AcO^- , and HSO_4^- . In the solid state, the single-crystal X-ray diffraction analysis of the complex **27·F·3PF₆** revealed that the F^- ion was located inside the macrocycle core, with H-bonds involving all four (C–H)⁺ moieties of the imidazolium rings through $\text{H}\cdots\text{F}^-$ interactions, $\text{H}(7)\cdots\text{F}^-$ of 1.99 Å and $\text{H}(12)\cdots\text{F}^-$ 2.08 Å, respectively. In contrast, each chloride ion of the 1:2 complex **27·2Cl·2PF₆** was bound to only two imidazolium C(2)–H hydrogen atoms [97].

The synthesis of tetrakis(imidazolium) cyclophanes **26·4PF₆** and **27·4PF₆** merits a brief comment. The macrocycle **26·4PF₆** is formed by a direct and convenient synthetic approach involving the one-pot reaction of equimolecular amounts of 1,3-di(1*H*-imidazol-1-yl)propane and 1,4-bis(chloromethyl)durene in boiling acetonitrile overnight without high dilution conditions. After anion exchange with NH_4PF_6 , **26·4PF₆** was obtained in 53% yield, which is a remarkable result for a macrocyclization process (Fig. 7) [96]. The macrocyclic analog **27·4PF₆** has also been successfully targeted by applying the efficient one-pot synthetic protocol. Thus, reaction of equimolecular amounts of a solution of 1-(1*H*-imidazol-1-ylmethyl)-1*H*-imidazole and a solution of 2,6-bis(bromomethyl)pyridine, added dropwise during 0.5 h at 170 nM in dry acetonitrile and then refluxed overnight, proceeded cleanly. The tetrakis(imidazolium) cyclophane **27·4Br** formed was isolated as **27·4PF₆** in 80% yield (Fig. 7) [97]. Nevertheless, it would have been interesting if the authors had provided an explanation for such high yield obtained by an extremely simple synthetic pathway. Furthermore, application of the tetracationic cyclophane **27·4Br** has been recently reported in the field of NHC–metal complexes, which is unsurprising since macrocycle **27·4Br** contains four imidazolium motif precursors of NHC species and two 2,6-disubstituted pyridine units with recognized metal complexation abilities. Accordingly, a study on Ag(I) and Au(I)

complexes with tetra- and hexacarbene macrocycles has focused on the already known macrocycle **27·4Br** [97] and the new hexakis(imidazolium) cyclophane **28·6Br**. In their preparation, the synthetic procedure previously employed to obtain macrocycle **27·4Br** underwent ‘a slight modification’: the dropwise addition of a solution of 2,6-bis(bromomethyl)pyridine in acetonitrile was extended from 0.5 to 5 h, which resulted in the formation of a 1:1 mixture of tetrakis **27·4Br** and hexakis **28·6Br** imidazolium cyclophanes. Unfortunately, the authors do not give the experimental details for the preparation and separation of the mixture (Fig. 7) [98].

When considering these results, whatever the charged open-chain intermediates produced during the condensation step, it seems reasonable to think about the self-template role played by the halide ions generated in situ during the stepwise macrocyclization process.

The anion-binding association constants of the aforementioned examples of cyclophanes as well as the imidazolium-based anion receptors discussed in the following sections have usually been determined in solution phase using analytical spectroscopic methods such as ^1H NMR, UV-vis, and fluorescence titrations. Comparative data of K 's, however, seem to be fairly difficult to obtain due to the absence of standard methods of determination of the binding constants, for example, titration protocols, ‘reference’ anion hosts, and computational analysis methods which could permit a reliable correlation of the binding affinities to anions. In this context, a detailed study of the *meso*-octamethylcalix[4]pyrrole anion receptor with several chloride salts in solution revealed that ^1H NMR spectroscopic titrations and isothermal titration calorimetry (ITC) give rise to concordant anion binding affinity constants when the conditions for the measurements are comparable [99].

4 Calixarenes

Calixarenes, which are particularly attractive scaffolds for receptor development, are easily preorganized into a number of topographies and readily functionalized in a selective manner [100–102]. This has given a biological perspective to the rapidly growing field of bionanotechnology, whose aim is to develop new tools for biology, new biomaterials, selective sensors and supramolecular devices for clinical analysis, new therapeutics, and smart drug delivery systems [103]. Despite the use of imidazolium structural motifs as anion recognition elements, there are just five examples describing the incorporation of the imidazolium functionality in organized architectures such as calixarenes or resorcinarenes. A plausible reason is the problematic chemical tractability, that is their accessibility, since a relevant factor is the laborious preparation of the precursors, which implies several synthetic steps, and suitability for chemical modifications of targeted imidazolium-based calixarenes.

Bis(imidazolium) calixarenes **7a·2PF₆** and **7b·2PF₆**, with the imidazolium units directly bonded to the upper rim of the calixarene structure, have been efficiently prepared, as referred to in the previous Section 2 (Scheme 1), and the anion binding

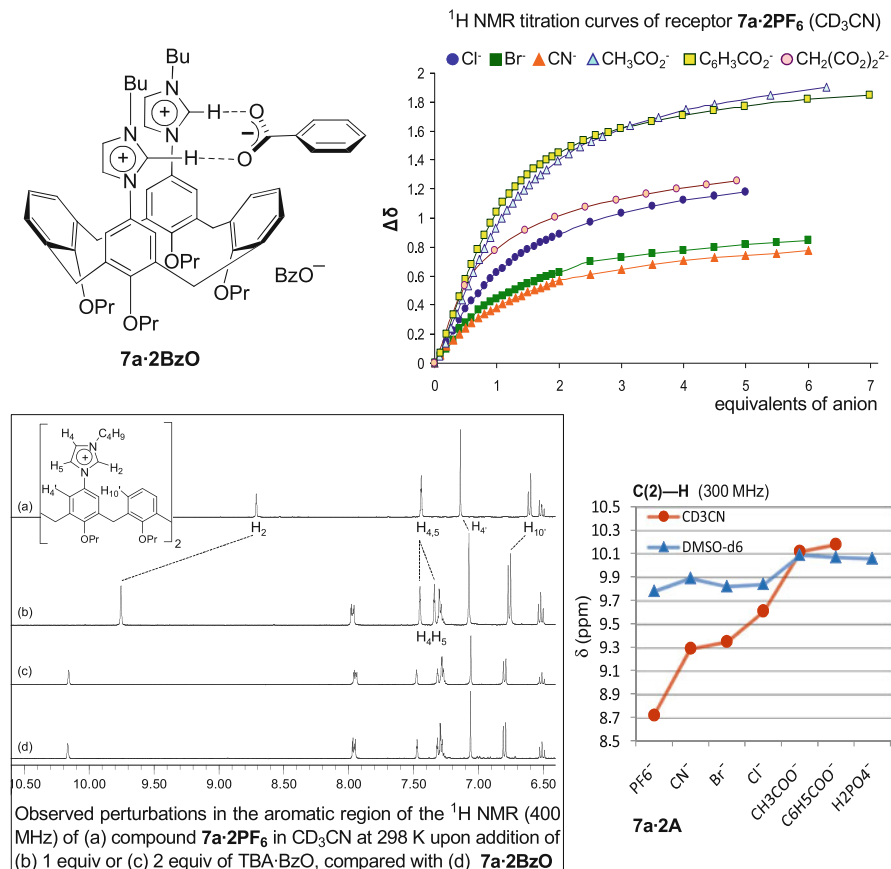
(arene)C–N(imidazolium) direct bond

Fig. 8 Bis(imidazolium)calix[4]arenes: (arene)C–N(imidazolium) direct bond

properties have been studied in solution by ¹H NMR spectroscopy [43]. Several organic and inorganic anions were examined, and bis(*N*-butylimidazolium) dication **7a·2PF₆** exhibited the best recognition properties toward carboxylate anions (BzO⁻ > AcO⁻) together with halides (Br⁻ and Cl⁻) to form a 1:1 complex in CD₃CN, probably in a perched position above the cavity (Fig. 8). Calixarene **7a·2PF₆** binds BzO⁻ ($K = 404 \text{ M}^{-1}$) twice as strongly as the other tested anions. Moreover, precipitation of the dihydrogen phosphate salt during the titration in CD₃CN suggested that the interaction between the receptor and the H₂PO₄⁻ anion is appreciable even though it was not possible to calculate the K -value. A titration in DMSO-*d*₆ showed 1:2 complex (receptor-anion) formation with stability constants in the order BzO⁻ > H₂PO₄⁻ > Cl⁻ and confirmed the affinity of imidazolium motifs toward oxoanions. Host **7a·2PF₆** binds BzO⁻ ($K_1 > 5,800 \text{ M}^{-1}$) and to a lesser extent H₂PO₄⁻ (2.5-fold) > Cl⁻ (3-fold).

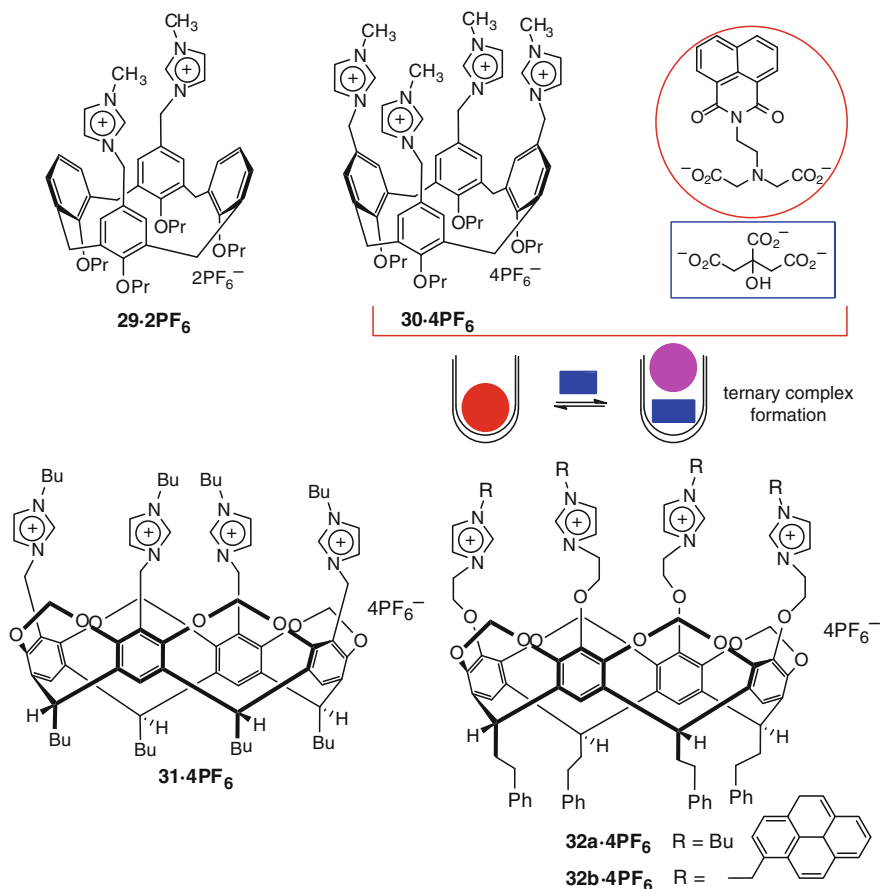
(arene)C–spacer–N(imidazolium) bond

Fig. 9 Tetrakis(imidazolium)calix[4]arenes and resorcinarenes:(arene)C–spacer–N(imidazolium) bond

The incorporation of a methylene linker between imidazolium units and the calixarene scaffold simplifies their preparation and gives flexibility to the recognition motifs (Fig. 9). Thus, bis- and tetrakis-imidazolium calixarenes, **29-4PF₆** and **30-4PF₆**, were easily accessible, and their ability to act as anion receptors for small inorganic anions (H_2PO_4^- , HSO_4^- , Cl^- and Br^-) was evaluated by ^1H NMR titration experiments in $\text{DMSO}-d_6$ [104]. Both calixarenes, **29-4PF₆** and **30-4PF₆**, displayed the same affinity for H_2PO_4^- ($K \sim 1,950$) followed by Cl^- , ~ 2 -times weaker, proving that only two imidazolium motifs were used for binding. Interestingly, the tetrakis(imidazolium) calixarene, **30-4PF₆**, behaved as a selective receptor for the citrate anion in aqueous media by a supramolecular sensing assembly with 1,8-naphthalimide, involving the formation of a ternary fluorophore–host–anion complex and the sequence of pH changes is responsible for differential fluorescence quenching [105].

A cavitand derived from resorcinarene, acting as a basic skeleton, and two examples anchoring quaternary imidazolium salts are described as anion receptors, specifically, molecular systems containing four imidazolium units linked by flexible groups such as methylene **31·4PF₆** [95] or oxyethylene **32a·4PF₆** [106]. These tetracationic structures showed good affinity for inorganic anions (CD₃CN–H₂O 9:1) and dicarboxylates (DMSO-*d*₆), respectively. The cavitand **32b·4PF₆** bearing four pyrene fragments has been described as a selective fluorescent chemosensor for guanosine triphosphate (GTP) [107].

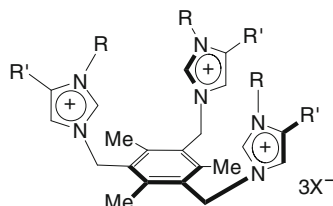
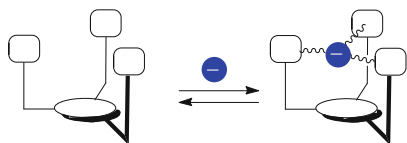
5 Tripodal Platform for Anion Receptors


Tripodal systems constitute a class of hosts where the platform provides three arms to which the anion coordinating functional groups are attached. The resulting tripodal topologies favor the formation of stable host–anion complexes. Tripodal receptors for recognition and sensing of cations and anions have been reviewed, and a limited number have referred to imidazolium systems [108]. Several acyclic tris(imidazolium) tripodal receptors, three imidazolium groups connected through a 1,3,5-trialkylbenzene platform linker, have been reported since 1999 (Fig. 10) [3, 6].

The receptor **2·3PF₆** recognized halide anions, which was confirmed by ¹H NMR titration experiments in CD₃CN (Fig. 10) [29]. Exploiting the tripodal platform, the methyl or ethyl substituent at the phenyl ring favors an arrangement in which the imidazolium subunits point to the same side, thus giving rise to a ‘bowl’, which is suitable for the interaction with anions. Further studies have shown that trication **33·3Br** exhibits good recognition toward the PO₄³⁻ anion in water, as determined by UV–vis spectroscopic titration [109]. To enhance the anion binding stretch of the model system **2·3PF₆**, the host **34·3PF₆**, with a nitro group in the imidazolium side arms was prepared and examined by means of ¹H NMR spectroscopy in DMSO-*d*₆ [110, 111]. In a series of ¹H NMR spectra in aqueous CD₃CN, anionic enantioselective recognition was displayed by the homochiral tripodal imidazolium receptor **35·3PF₆**, which showed selectivity for (*R*)-2 over (*S*)-2-aminopropionate [112, 113].

The complex stability and selectivity of imidazolium tripodands can be improved by moving from an open to a closed cavity, that is, from a tripod to a cage. The tris(imidazolium) cage **4·3Br** was synthesized, but no evidence of the inclusion of an anion into the cavity has been reported (see Fig. 3, Sect. 1) [32]. A novel and elegant approach to a cage-like imidazolium system has been devised with the receptor **36·3PF₆**, in which imidazolium–bipyridine pendant arms are linked to a 1,3,5-triethylbenzene platform. The imidazolium rings act as hydrogen-bond donor structural motifs toward anions, and the 2,2′-bipyridyl groups at the end of the arms can coordinate a cation, thus forming a ‘cage’ [3, 114, 115].

On reaction with an iron(II) salt, the bipyridine subunits coordinated the metal center to give the [**36·Fe(II)**]**5PF₆** complex, which generated a cavity with a six

a directly using non-covalent interactions

- 2-3PF₆** R = Bu; R' = H
33-3Br R = Bn; R' = H
34-3PF₆ R = Me; R' = NO₂
35-3PF₆ R = ; R' = H

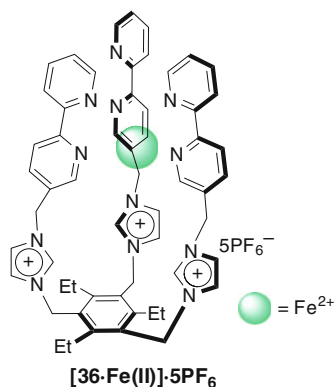
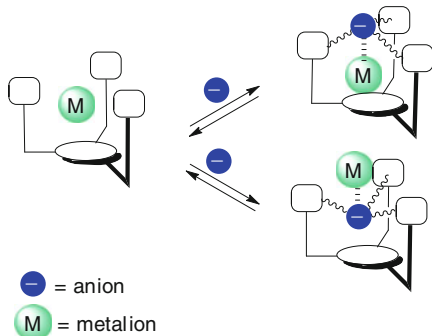
b electrostatic interaction with metal complex

Fig. 10 Imidazolium-based tripodal anion receptors

H-bond donor set suitable for anion encapsulation. X-ray crystallographic studies, ¹H NMR and UV–vis titration experiments in aqueous acetonitrile demonstrated that inclusion complexes were formed of both spherical halides, with decreasing affinity from Cl[−] to I[−], and rodlike N₃[−] ions [114, 115]. Further studies with the tris (imidazolium) cage [36·M(II)]·5PF₆ are described in Sect. 6.

6 Miscellaneous Systems and Applications

The demand for synthetic receptors has been increasing rapidly within the analytical sciences, and these receptors are finding uses in simple indicator chemistry, cellular imaging, and enantiomeric excess analysis, while also being involved in various practical assays of bodily fluids. Thereby, one of the most promising future uses of synthetic receptors is in the area of differential sensing [116, 117]. In the last few years, the development of abiotic sensors for the selective sensing of

biologically important anions has attracted considerable attention due to their potential bioanalytical application. In anion recognition chemistry, when the coordination event is coupled to a suitable signal (optical, electrochemical, etc.), a chemosensor is obtained, and the anion–chemosensor interaction is transduced in simple signals such as changes in color, fluorescence, or oxidation potential shifts, thus opening the door to the sensing/determination (qualitative or quantitative) of target anions [118].

Recent research has developed a number of imidazolium systems bearing signaling unit(s) such as polyarenes as a result of their interest as anion sensors [78, 79]. A common approach to the development of fluorogenic anion chemosensors is the covalent attachment between a receptor and the indicator. The coupling of two moieties exhibits different functions: the binding site, where the anion is coordinated; and the signaling subunit, which has the task of signaling the coordination event via changes in its fluorescence behavior. Accordingly, two anion sensor design strategies have been applied to given imidazolium-based cyclophanes and open-chain polynucleating systems:

1. Those containing polyarene signaling units
2. ‘Pincers’ that bear pendant polyarene groups

Signaling units and their incorporation into protophane and cyclophane frameworks. Two imidazolium moieties were linked to anthracene, acridine, quinoxaline, or binaphthalene through the methylene interannular spacers **37a–e**·**2PF₆**, and their anion binding properties could be easily monitored via fluorescence quenching effects (Fig. 11) [94, 119, 120]. Among the various anions, such as HSO₄[−], CH₃CO₂[−], I[−], Br[−], Cl[−], and F[−], dications **37a–e**·**2PF₆** showed the highest binding affinity with the biologically significant anions H₂PO₄[−], and HP₂O₇^{3−} (PPi) in acetonitrile. It should be noted that PPi is the product of ATP hydrolysis under cellular conditions and is involved in DNA replication. The fluorescent quenching effect upon the addition of the anions was explained by a photo-induced electron transfer (PET) mechanism.

In parallel, two imidazolium motifs were incorporated within a cyclophane framework combined with two anthracene rings (**23a**·**2PF₆**) [94] or quinoxaline rings (**23d**·**2PF₆**) [119], and their association constants are higher than those of open-chain bis(imidazolium) systems, which suggest that a preorganized rigid binding pocket might play an important role in the anion binding. Moreover, fluorescence studies of the receptor **23d**·**2PF₆** show anion-induced excimer formation with almost all the anions studied, except pyrophosphate and acetate, due to intermolecular π – π stacking between antiparallel quinoxaline rings. Chiral bis(imidazolium) protophanes (*S*)-**37e**·**2PF₆** and (*R*)-**38**·**2PF₆**, with a binaphthalene signaling system, have been examined in order to develop chiral anion recognition [121].

Pincers. The bis(imidazolium) open-chain trinucleating systems **39a,b**·**2PF₆** tethered by two fluorogenic polyarene moieties such as (1-pyrenyl)methyl units were studied, and the binding affinities of these hosts could be easily monitored via the changes of pyrene excimer peaks. Moreover, compound **39b**·**2PF₆** is the first

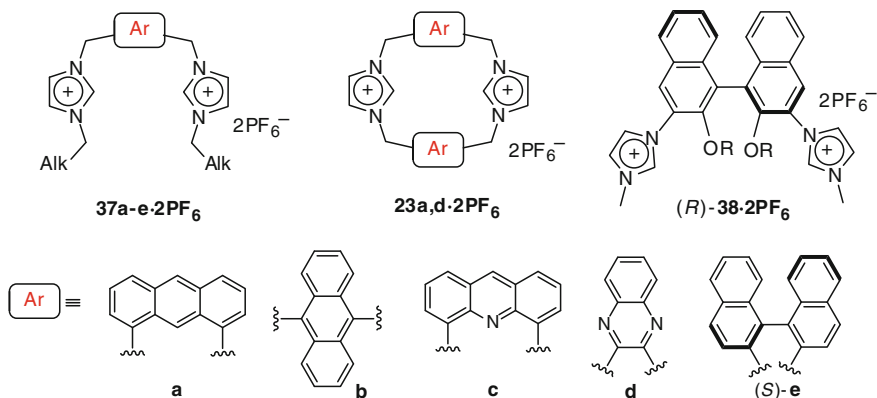
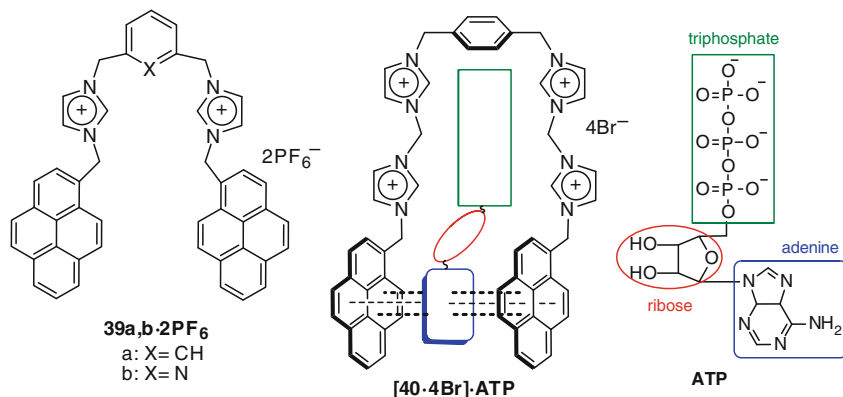
(bis)imidazolium heterophanes and protophanes ...**a** containing polyarene signaling units**b** tethered by polyarene groups

Fig. 11 Fluorogenic anion sensors: imidazolium-based systems bearing polyarene signaling rings

example of a fluorescent logic gate, which used two different anions as inputs, OH⁻ and TFA⁻, Fig. 11 [122]. Recently, the tetracationic imidazolium sensor **40-4Br** was prepared and its recognition properties towards several nucleoside triphosphates were studied in aqueous media [123]. Notably, this tetrakis (imidazolium) open-chain pentanucleating system showed a selective response to adenosine triphosphate (ATP) at the physiological pH (7.4), [40-4Br]·ATP, with a unique switch of excimer *versus* monomer pyrene fluorescence. Due to the characteristic sandwich π-π stacking of pyrene-adenine-pyrene of sufficient intensity to discriminate ATP from ADP and AMP, this fluorogenic receptor could serve as a model for investigations of ATP-relevant biological processes.

Another kind of measurable effect when recognition occurs is the electrochemical response: here we enter the domain of ‘multicomponent supramolecular

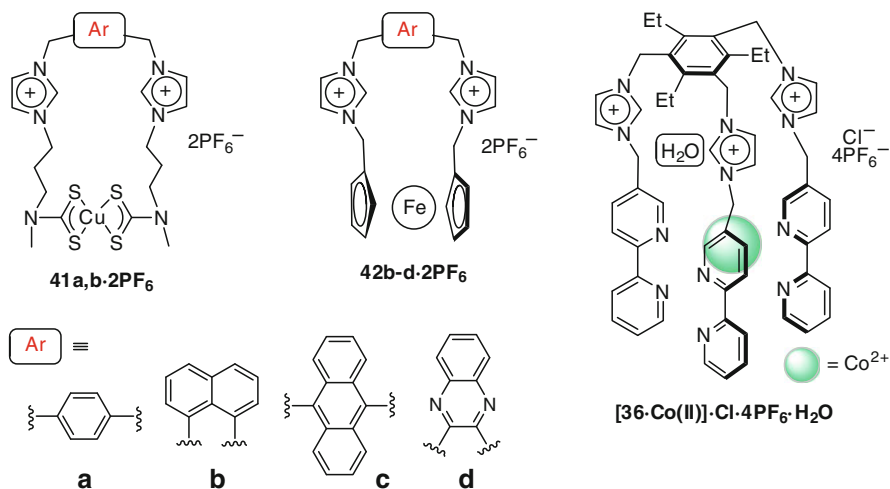


Fig. 12 Electrochemical anion sensors: bis(imidazolium) polynucleating open-chain and cage-like systems

chemistry' directed toward nanoscience and nanotechnology [3, 124]. The reversible metal 'ligand' coordination interaction is a useful control factor for driving a dynamic self-assembly process [125, 126].

Receptors containing positively charged H-bond donors, such as imidazolium, are able to form stable anion complexes even in aqueous media, which makes them compatible with highly positively charged redox fragments such as cationic transition-metal complexes. Thus, bis(imidazolium) salts **41a, b-2PF₆⁻** with Cu(II) dithiocarbamate complexes can electrochemically sense the binding of Cl⁻ and H₂PO₄⁻, and significant cathodic shifts of the respective Cu(II)/Cu(III) were observed (Fig. 12) [127]. On the other hand, the multisignaling chemosensors with the redox-active ferrocene and fluorescence-bearing groups linked to imidazolium rings **42b-d-2PF₆⁻** showed particularly strong electrochemical responses to F⁻ and displayed a 'switched on' behavior in the fluorescent spectra [128].

The novel tris(imidazolium) cage-like **[36-Co(II)]·5PF₆⁻** is able to sense the different tendencies of anions to receive H-bonds in aqueous solution with significant selectivity, acting as a redox-active cage for the electrochemical sensing of anions. The effect of the solvent on the appearance of the voltammetric response will provide effective electrochemical sensors [3, 115].

In parallel, interest has been growing in the blending of supramolecular structures with porous inorganic solids to obtain hybrid organic-inorganic materials. These hybrid materials show enhanced patterns of selectivity and new functional chemical properties. Recent examples have indicated that combining supramolecular models with recognition/sensing procedures and nanoscopic supports can result in new applications of hetero-supramolecular concepts in signaling protocols: not

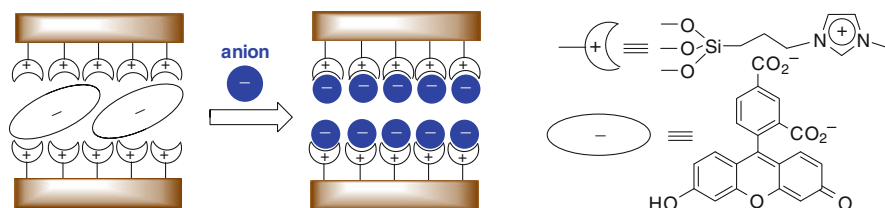


Fig 13 Hybrid organic–inorganic nanoscopic materials

the simple anchoring of chemosensors to a solid support, but the search for new functional outcomes in which the solid scaffolding itself plays a significant role in the recognition/sensing paradigm [129]. Mesoporous solids functionalized with anion binding groups have proved to be suitable anion hosts and have been used in selective colorimetric displacement assays [130]. Thus, hybrid materials containing nanoscopic ‘binding pockets’ functionalized with imidazolium units and loaded with a dye showed their sensing ability towards carboxylates (acetate, citrate, lactate, succinate, oxalate, tartrate, malate, mandelate, glutamate) and certain nucleotides (ATP, adenosine diphosphate (ADP), for guanosine monophosphate (GMP)) in pure water at pH 7.5 (Fig. 13) [131]. This approach is especially attractive because of the emergence of new molecular–solid synergic effects that are difficult to achieve in molecular-based systems or in nanoscopic solids individually.

Continuing in the nanoscale dimension, ILs have recently attracted interest as benign solvent systems for the synthesis of nanomaterials and they are emerging as alternative liquid templates for the generation of a plethora of size- and shape-controlled nanostructures. The morphologies of the metal products are more sensitive to the nature of the anions compared to the cations of the ILs [132, 133]. Furthermore, the use of ‘ionophilic’ ionic liquids based on bis(imidazolium) aromatic systems can be used as a components in solar cells or organic electroluminescent diodes (OLEDs), exhibiting efficiency enhancement with respect to similar aromatic systems without imidazolium moieties [134].

7 Conclusions

In the past few years, the imidazolium functionality has gained a place among the classical anion binding functional groups and has emerged as an attractive starting point for the design of abiotic anion receptors and selective molecular sensors. Imidazolium-based systems are still taking shape, but their basic outline shows that imidazolium is a versatile structural motif for supramolecular assembly. The present pace of development is expected to continue in the coming years, with applications directed toward nanoscience.

Addendum

Since the submission of this chapter, imidazolium based systems have continued their progress in different fields in chemistry, in particular ionic liquids (ILs) have been featured widely in recent chemical open literature. Significant advances have been made in a fundamental aspect of imidazolium functionality by Ludwig and co-workers, who have reported direct spectroscopic evidence of an enhanced cation–anion interaction driven by non-classical (C–H)⁺... anion hydrogen bonding in pure imidazolium ILs [135]. Notably, Sessler and co-workers have revealed the conception and design of a ‘Texas-sized’ molecular box that allows anion-induced assembly of novel interlocked systems [136]. This flexible tetracationic imidazolium-based macrocycle opens fascinating perspectives for molecular devices in nanoscience.

Acknowledgements The authors express their thanks to the AGAUR (Generalitat de Catalunya), Grup de Recerca Consolidat 2005SGR158 and 2009SGR562.

References

1. Caltagirone C, Gale PA (2009) *Chem Soc Rev* 38:520–563
2. Gale PA, García-Garrido SE, Garric J (2008) *Chem Soc Rev* 37:151–190
3. Amendola V, Fabbri L (2009) *Chem Commun* 513–531
4. Vickers MS, Beer PD (2007) *Chem Soc Rev* 36:211–225
5. Baker MV, Brown DH (2006) *Mini Rev Org Chem* 3:333–354
6. Yoon J, Kim SK, Singhb NJ, Kim KS (2006) *Chem Soc Rev* 35:355–360
7. Lankshear MF, Beer PD (2006) *Coord Chem Rev* 250:3142–3160
8. Gimeno N, Vilar R (2006) *Coord Chem Rev* 250:3161–3189
9. Sowmiah S, Srinivasadesikan V, Tseng M-Ch, Chu Y-H (2009) *Molecules* 14:3780–3813
10. Leclercq L, Schmitzer AR (2009) *Supramol Chem* 21:245–263
11. Imperato G, König B, Chiappe C (2007) *Eur J Org Chem* 1049–1058
12. Chowdhury S, Mohan RS, Scott JL (2007) *Tetrahedron* 63:2363–2389
13. Scammells PJ, Scott JL, Singer RD (2005) *Aust J Chem* 58:155–169
14. Welton T (2004) *Coord Chem Rev* 248:2459–2477
15. Dupont J, Spencer J (2004) *Angew Chem Int Ed* 43:5296–5297
16. Plechkova NV, Seddon KR (2008) *Chem Soc Rev* 37:123–150
17. Arduengo AJ, Bertrand G (2009) *Chem Rev* 109:3209–3210
18. Poyatos M, Mata JA, Peris E (2009) *Chem Rev* 109:3677–3707
19. Homden DM, Redshaw C (2008) *Chem Rev* 108:5086–5130
20. Gade LH, Bellemin-Laponnaz S (2007) *Coord Chem Rev* 251:718–725
21. Enders D, Niemeier O, Henseler A (2007) *Chem Rev* 107:5606–5655
22. Liddle ST, Edworthy IS, Arnold PL (2007) *Chem Soc Rev* 36:1732–1744
23. Arduengo AJ (1999) *Acc Chem Res* 32:913–921
24. Beer PD, Gale PA (2001) *Angew Chem Int Ed* 40:486–516
25. Schmidtchen FP (1981) *Chem Ber* 114:597–607
26. Schmidtchen FP, Berger M (1997) *Chem Rev* 97:1609–1646
27. Alcalde E, Alvarez-Rúa C, García-Granda S, García-Rodríguez E, Mesquida N, Pérez-García L (1999) *Chem Commun* 295–296

28. Alcalde E, Ramos S, Pérez-García L (1999) *Org Lett* 1:1035–1038
29. Sato K, Arai S, Yamagishi T (1999) *Tetrahedron Lett* 40:5219–5222
30. Dias HV, Jin W (1994) *Tetrahedron Lett* 35:1365–1366
31. Alcalde E, Mesquida N, Vilaseca M (2000) *Rapid Commun Mass Spectrom* 14:1443–1447
32. Baker MV, Bosnich MJ, Williams CC, Skelton BW, White AH (1999) *Aust J Chem* 52:823–825
33. Baker MV, Bosnich MJ, Brown DH, Byrne LT, Hesler VJ, Skelton BW, White AH, Williams CC (2004) *J Org Chem* 69:7640–7652
34. Cabildo P, Sanz D, Claramunt RM, Bourne SA, Alkorta I, Elguero J (1999) *Tetrahedron* 55:2327–2340
35. Král V, Furuta H, Shreder K, Lynch V, Sessler JL (1996) *J Am Chem Soc* 118:1595–1607
36. Zoltewicz JA, Deady LW (1978) *Adv Heterocycl Chem* 22:71–121
37. Gallo R, Roussel C, Berg U (1988) *Adv Heterocycl Chem* 43:173–299
38. Grimmett MR (1980) *Adv Heterocycl Chem* 27:241–326
39. Alcalde E (1994) *Adv Heterocycl Chem* 60:197–259
40. Hintermann L (2007) *Beilstein J Org Chem*. doi:10.1186/1860-5397-3-22
41. Bini R, Chiappe C, Pomelli CS, Parisi B (2009) *J Org Chem*. doi:10.1021/jo9009408
42. Alcalde E, Dinarès I, Frigola J, Jaime C, Fayet J-P, Vertut M-C, Miravittles C, Rius J (1991) *J Org Chem* 56:4233–4238
43. Dinarès I, Garcia de Miguel C, Mesquida N, Alcalde E (2009) *J Org Chem* 74:482–485
44. Alcalde E, Dinarès I, Rodríguez S, Garcia de Miguel C (2005) *Eur J Org Chem* 1637–1643
45. Dinarès I, Garcia de Miguel C, Font-Bardia M, Solans X, Alcalde E (2007) *Organometallics* 26:5125–5128
46. Fyfe MCT, Stoddart JF (1997) *Acc Chem Res* 30:393–401
47. Alcalde E, Alemany M, Gisbert M (1996) *Tetrahedron* 52:15171–15188
48. Kauffmann T (1979) *Angew Chem Int Ed* 18:1–19
49. Alcalde E, Gisbert M, Pérez-García L (1994) *Chem Commun* 981–982
50. Abbotto A, Bradamante S, Facchetti A, Pagani GA (1999) *J Org Chem* 64:6756–6763
51. Pérez-García L, Mesquida N, Alemany M, Fernández I, Vilaseca M, Alcalde E (2002) *Eur J Org Chem* 2691–2698
52. Barlin GB (1967) *J Chem Soc B* 641–647
53. Catalán J, Abboud JLM, Elguero J (1987) *Adv Heterocycl Chem* 41:187–274
54. Elguero J, Marzin C, Katritzky AR, Linda P (1976) *Advances in heterocyclic chemistry, supplement 1: the tautomerism of heterocycles*. Academic, New York
55. Claramunt RM, López C, García MA, Otero MD, Torres MR, Pinilla E, Alarcón SH, Alkorta I, Elguero J (2001) *New J Chem* 25:1061–1068
56. Oziminski WP, Dobrowolski JC, Mazurek AP (2004) *J Mol Struct* 680:107–115
57. Ramos S, Alcalde E, Doddi G, Mencarelli P, Pérez-García L (2002) *J Org Chem* 67:8463–8468
58. Earle MJ, Seddon KR (2001) *Preparation of imidazole carbenes and the use thereof for the synthesis of ionic liquids*. World Patent WO 2001077081 A1
59. Alcalde E, Dinarès I, Elguero J, Fayet JP, Vertut MC, Miravittles C, Molins E (1987) *J Org Chem* 52:5009–5015
60. Alcalde E, Mesquida N, Pérez-García L (2006) *Eur J Org Chem* 3988–3996
61. Alcalde E, Mesquida N, Vilaseca M, Alvarez-Rúa C, García-Granda S (2007) *Supramol Chem* 19:501–509
62. Dinarès I, Garcia de Miguel C, Ibáñez A, Mesquida N, Alcalde E (2009) *Green Chem* 11:1507–1510
63. Alder RW, Allen PR, Williams SJ (1995) *Chem Commun* 1267–1268
64. Kim YJ, Streitwieser A (2002) *J Am Chem Soc* 124:5757–5761
65. Amyes TL, Diver ST, Richard JP, Rivas FM, Toth K (2004) *J Am Chem Soc* 126:4366–4374
66. Chu Y, Deng H, Cheng JP (2007) *J Org Chem* 72:7790–7793
67. Bordwell FG, Fried HE (1991) *J Org Chem* 56:4218–4223

68. For Bordwell pKa table (acidity in DMSO), see the following website: <http://www.chem.wisc.edu/areas/reich/pKatable/index.htm>
69. Wang R, Yuan L, Macartney DH (2006) *Chem Commun* 2908–2910
70. Olofson RA, Thompson WR, Michelman JS (1964) *J Am Chem Soc* 86:1865–1866
71. Buncel E, Clement O, Onyido I (2000) *Acc Chem Res* 33:672–678
72. Lin ST, Ding MF, Chang CW, Lue SS (2004) *Tetrahedron* 60:9441–9446
73. Handy ST, Okello M (2005) *J Org Chem* 70:1915–1918
74. Giernoth R, Bankmann D (2008) *Eur J Org Chem* 2881–2886
75. Fahlbusch T, Frank M, Schatz J, Schühle DT (2006) *J Org Chem* 71:1688–1691
76. Dupont J, Suarez PAZ, De Souza RF, Burrow RA, Kintzinger JP (2000) *Chem Eur J* 6:2377–2381
77. Amato I (1992) *Science* 256:306–308
78. Kim SK, Kim HN, Xiaoru Z, Lee HN, Lee HN, Soh JH, Swamy KMK, Yoon J (2007) *Supramol Chem* 19:221–227
79. Kim SK, Lee DH, Hong JI, Yoon J (2009) *Acc Chem Res* 42:23–31
80. Yan S, Lee SJ, Kang S, Lee JY (2007) *Supramol Chem* 19:229–241
81. Baytekin B, Baytekin HT, Schalley CA (2006) *Org Biomol Chem* 4:2825–2841
82. Di Tullio A, Reale S, De Angelis F (2005) *J Mass Spectrom* 40:845–865
83. Oshovsky GV, Verboom W, Fokkens RH, Reinhoudt DN (2004) *Chem Eur J* 10:2739–2748
84. Ashton PR, Brown CL, Chapman JR, Gallagher RT, Stoddart JF (1992) *Tetrahedron Lett* 33:7771–7774
85. Gozzo FC, Santos LS, Augusti R, Consorti CS, Dupont J, Eberlin MN (2004) *Chem Eur J* 10:6187–6193
86. Leal JP, Esperança JMSS, Minas da Piedade ME, Lopes JNC, Rebelo LPN, Seddon KR (2007) *J Phys Chem A* 111:6176–6182
87. Lungwitz R, Spange S (2008) *New J Chem* 32:392–394
88. Steiner T (2002) *Angew Chem Int Ed* 41:48–76
89. Jeffrey GA (1997) *An introduction to hydrogen bonding*. Oxford University Press, Oxford
90. Desiraju GR, Steiner T (1999) *The weak hydrogen bond*. Oxford University Press, Oxford
91. Leclercq L, Noujeim N, Schmitzer AR (2009) *Cryst Growth Des* 9:4784–4792
92. Alcalde E, Alemany M, Pérez-García L, Rodríguez ML (1995) *Chem Commun* 1239–1240
93. Yuan Y, Gao G, Jiang Z-L, You J-S, Zhou Z-Y, Yuan D-Q, Xie R-G (2002) *Tetrahedron* 58:8993–8999
94. Yoon J, Kim SK, Singh NJ, Lee JW, Yang YJ, Chellappan K, Kim KS (2004) *J Org Chem* 69:581–583
95. Wong WWH, Vickers MS, Cowley AR, Paul RL, Beer PD (2005) *Org Biomol Chem* 3:4201–4208
96. Sato K, Onitake T, Arai S, Yamagishi T (2003) *Heterocycles* 60:779–784
97. Kavitha Chellappan K, Singh NJ, Hwang I-C, Lee JW, Kim KS (2005) *Angew Chem Int Ed* 44:2899–2903
98. Hahn JE, Radloff C, Pape T, Hepp A (2008) *Chem Eur J* 14:10900–10904
99. Sessler JL, Gross DE, Cho W-S, Lynch VM, Schmidtchen FP, Bates GW, Light ME, Gale PA (2006) *J Am Chem Soc* 128:12281–12288
100. Gutsche CD (1998) *Calixarenes revisited*. The Royal Society of Chemistry, Cambridge
101. Mandolini L, Ungaro R (2000) *Calixarenes in action*. Imperial College Press, London
102. Matthews SE, Beer PD (2005) *Supramol Chem* 17:411–435
103. Baldini L, Casnati A, Sansone F, Ungaro R (2007) *Chem Soc Rev* 36:254–266
104. Fahlbusch T, Frank M, Schatz J, Schmaderer H (2006) *Eur J Org Chem* 1899–1903
105. Koner AL, Schatz J, Nau WM, Pischel U (2007) *J Org Chem* 72:3889–3895
106. Kim SK, Kang B-G, Koh HS, Yoon YJ, Jung SJ, Jeong B, Lee K-D, Yoon J (2004) *Org Lett* 6:4655–4658
107. Kim SK, Moon B-S, Park JH, Seo YI, Koh HS, Yoon YJ, Lee KD, Yoon J (2005) *Tetrahedron Lett* 46:6617–6620

108. Kuswandi B, Nuriman, Verboom W, Reinhoudt DN (2006) *Sensors* 6:978–1017
109. Yuan Y, Jiang Z-L, Gao G, Zhang G-L, You J-S, Xie R-G (2002) *Chin J Chem* 20:447–452
110. Ihm H, Yun S, Kim HG, Kim JK, Kwang K, Kim KS (2002) *Org Lett* 4:2897–2900
111. Yun S, Ihm H, Kim HG, Lee C-W, Indrajit B, Oh KS, Gong YJ, Lee JW, Yoon J, Lee HC, Kim KS (2003) *J Org Chem* 68:2467–2470
112. Howarth J, Al-Hashimy NA (2001) *Tetrahedron Lett* 42:5777–5779
113. Alhashimy N, Brougham DJ, Howarth J, Farrell A, Quilty B, Nolan K (2007) *Tetrahedron Lett* 48:125–128
114. Amendola V, Boiocchi M, Colasson B, Fabbrizzi L, Rodriguez Douton M-J, Ugozzoli F (2006) *Angew Chem Int Ed* 45:6920–6924
115. Amendola V, Boiocchi M, Colasson B, Fabbrizzi L, Monzani E, Douton-Rodriguez MJ, Spadini C (2008) *Inorg Chem* 47:4808–4816
116. Wiskur SL, Ait-haddou H, Lavigne JJ, Anslyn EV (2001) *Acc Chem Res* 34:963–972
117. Anslyn EV (2007) *J Org Chem* 72:687–699
118. Martínez-Máñez R, Sancenón F (2003) *Chem Rev* 103:4419–4476
119. Singh NJ, Jun EJ, Chellappan K, Thangadurai D, Chandran RP, Hwang I-C, Yoon J, Kim KS (2007) *Org Lett* 9:485–488
120. Kim SK, Seo D, Han SJ, Son G, Lee I-J, Lee C, Lee KD, Yoon J (2008) *Tetrahedron* 64:6402–6405
121. Lu Q-S, Dong L, Zhang J, Li J, Lu L, Huang Y, Qin S, Hu C-W, Yu X-Q (2009) *Org Lett* 11:669–672
122. Lee HN, Singh NJ, Kim SK, Kwon JY, Kim YY, Kim KS, Yoon J (2007) *Tetrahedron Lett* 48:169–172
123. Xu Z, Singh NJ, Lim J, Pan J, Kim HN, Park S, Kim KS, Yoon J (2009) *J Am Chem Soc* 131:15528–15533
124. Langner A, Tait SL, Lin N, Rajadurai C, Ruben M, Kern K (2007) *Proc Natl Acad Sci USA* 104:17927–17930
125. Lehn JM (2007) *Chem Soc Rev* 36:151–160
126. Northrop BH, Zheng YR, Chi KW, Stang PJ (2009) *Acc Chem Res* 42:1554–1563
127. Wong WWH, Phipps DE, Beer PD (2004) *Polyhedron* 23:2821–2829
128. Niu H-T, Yin Z, Su D, Niu D, He J, Cheng J-P (2008) *Dalton Trans* 3694–3700
129. Descalzo AB, Martínez-Máñez R, Sancenón F, Hoffmann K, Rurack K (2006) *Angew Chem Int Ed* 45:5924–5948
130. Coll C, Martínez-Máñez R, Marcos MD, Sancenón F, Soto J (2007) *Angew Chem Int Ed* 46:1675–1678
131. Comes M, Aznar E, Moragues M, Marcos MD, Martínez-Máñez R, Sancenón F, Soto J, Villaescusa LA, Gil L, Amorós P (2009) *Chem Eur J* 15:9024–9033
132. Vidinha P, Nuno MT, Lourenço MT, Pinheiro C, Brás AR, Carvalho T, Santos-Silva T, Mukhopadhyay A, Romão MJ, Parola J, Dionisio M, Cabral JMS, Afonso CAM, Susana Barreiros S (2008) *Chem Commun* 5842–5844
133. Ren L, Meng L, Lu Q, Fei Z, Dyson PJ (2008) *J Colloid Interface Sci* 323:260–266
134. Martín R, Teruel L, Aprile C, Cabeza JF, Álvaro M, García H (2008) *Tetrahedron* 64:6270–6274
135. Wulf A, Fumino K, Ludwig, R (2010) *Angew Chem Int Ed* 49:449–453
136. Gong H-Y, Rambo BM, Karnas E, Lynch VM, Sessler JL (2010) *Nature Chem* 2:406–409

Pyridine and Pyridinium-Based Anion Receptors

Nathan L. Kilah and Paul D. Beer

Abstract Pyridine and pyridinium heterocycles play an important role in anion receptor chemistry. Hydrogen bond arrays are frequently preorganized by the presence of the pyridine nitrogen lone pair of electrons, whilst the positively charged pyridinium group is capable of interacting with anions via a number of polarized noncovalent interactions. This review describes the development of pyridine and pyridinium-based anion receptors, separated into topologically distinct acyclic, macrocyclic, macrobicyclic and interlocked host systems.

Keywords Anion · Pyridine · Pyridinium · Receptor

Contents

1	Introduction	302
2	Pyridine-Based Anion Receptors	303
2.1	Acyclic Receptors	303
2.2	Macrobicyclic and Cryptand Receptors	319
3	Pyridinium-Based Anion Receptors	323
3.1	Acyclic Receptors	323
3.2	Macrocyclic Receptors	326
3.3	Macrobicyclic Receptors	328
3.4	Interpenetrated and Interlocked Receptors	330
4	Conclusion	338
	References	338

N.L. Kilah and P.D. Beer (✉)
Department of Chemistry, Inorganic Chemistry Laboratory, University of Oxford, South Parks
Road, Oxford OX1 3QR, UK
e-mail: paul.beer@chem.ox.ac.uk

Abbreviations

ADP	Adenosine 5'-diphosphate
Ala	Alanine
AMP	Adenosine 5'-monophosphate
ATP	Adenosine 5'-triphosphate
Boc	<i>tert</i> -Butoxycarbonyl
CD	Circular dichroism
DFT	Density functional theory
FT	Fourier transform
Gln	Glutamate
Gly	Glycine
HEPES	4-(2-Hydroxyethyl)-1-piperazineethanesulfonic acid
IR	Infrared
ITC	Isothermal titration calorimetry
MOPS	3-(<i>N</i> -morpholino)propanesulfonic acid
NMR	Nuclear magnetic resonance
NOESY	Nuclear Overhauser effect spectroscopy
Phe	Phenylalanine
Pic	Picrate
ROESY	Rotational frame nuclear Overhauser effect spectroscopy
TBA	Tetra(<i>n</i> -butyl)ammonium
Trp	Tryptophan
Val	Valine

1 Introduction

Many important developments have occurred in the area of anion coordination chemistry over recent decades. This is in no small part due to the ubiquitous nature of anions across biological, medical and environmental chemistry. DNA is a polyanion, almost 70% of enzymatic substrates are anionic [1], and ATP, a major energy source within cells, is also negatively charged. Anions have been implicated in diseases such as cystic fibrosis, which is thought to be caused by the misregulation of chloride channels [2], while bromide was historically used as an anticonvulsant for the treatment of epilepsy [3]. The excessive use of nitrate, phosphate and sulfate anions in fertilizers has led to the increased risk of eutrophication in rivers and lakes which disrupts aquatic life cycles [4]. Additionally, the reprocessing of nuclear fuel results in the discharge of the radioactive pertechnetate anion $^{99}\text{TcO}_4^-$ and its safe disposal is of continuing environmental concern [5]. As a result, the challenge of the coordination and sensing of anions is becoming increasingly important and merits the creative construction of new anion coordinating moieties.

The binding of anions by synthetic receptors poses a unique challenge due to the varied geometry and charge density of the guest anions. Heterocycles play a crucial role in the design and functionality of anion receptors, with pyridine and pyridinium frequently utilized for their rigidity, influences on the binding of anions, and their straightforward incorporation into the anion receptor structure. Pyridine-based anion receptors commonly exploit the hydrogen bonding ability of the pyridine nitrogen lone pair of electrons for either the preorganization of hydrogen bonding 2,6-amide functional groups on the receptor or for complementary hydrogen bond acceptance from a protic anionic guest such as H_2PO_4^- . Protonation or quaternization of pyridine generates cationic pyridinium groups capable of interacting with anions through a range of noncovalent interactions such as electrostatics, increasingly polarized hydrogen bonds (including $\text{CH}\cdots\text{A}^-$) and electrostatic aryl–aryl stacking interactions. The development of simple acyclic receptors has been followed by the investigation of macrocyclic and, more recently, mechanically interlocked host molecules for the binding of anions. This chapter discusses the recognition of anions by pyridine and pyridinium-based molecular probes, in which a number of noncovalent interactions result in selectivity based on size, geometry and charge density of the anionic guest. An incredible array of anion selectivity has been observed and receptors of particular note have been highlighted. Particular emphasis has been given to receptors capable of sensing anions via electrochemical, luminescence or UV–visible methods. Although pyridine can also function as a ligand to metals capable of binding anions via inner or outer coordination spheres, we have limited our review to noncoordinated systems. Readers seeking an outline of metal-based anion receptors are encouraged to consult recent reviews [6, 7].

2 Pyridine-Based Anion Receptors

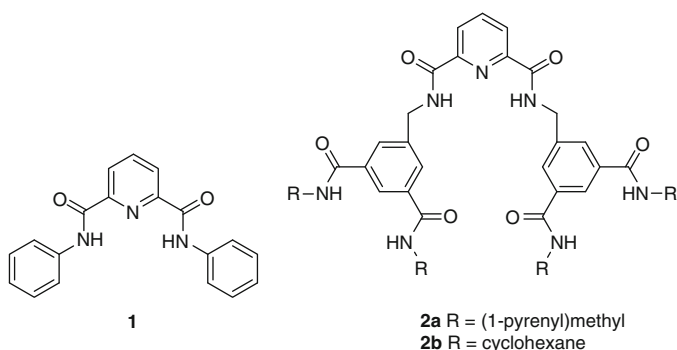
2.1 *Acyclic Receptors*

A large number of pyridine-based acyclic receptors have been developed for the binding of anions. These anion receptors frequently employ additional substituents capable of interacting with the anion via hydrogen bonding or electrostatic interactions. The incorporation of chiral groups (such as amino acids) in the receptor framework can assist in the binding of the enantiomers of chiral anionic substrates.

2.1.1 Neutral Acyclic Receptors

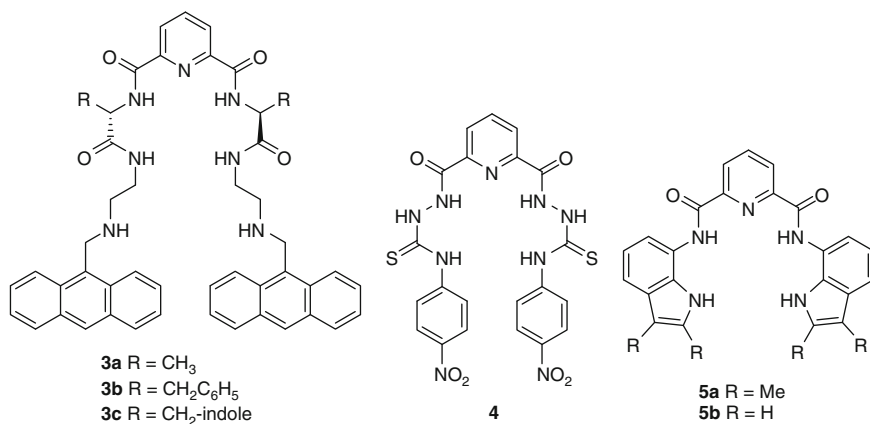
The majority of pyridine-based anion receptors utilize the pyridine-2,6-dicarboxamide group. The pyridine nitrogen lone pair of electrons serves to preorganize the

amide substituents into the *syn-syn* conformation, ideal for the binding of anions [8, 9]. The receptor *N,N*-diphenylpyridine-2,6-dicarboxamide **1** was shown to bind halide ions and acetate in CD_2Cl_2 , with greatest efficacy shown in the order F^- ($K_a = 24,000 \text{ M}^{-1}$) > Cl^- ($K_a = 1,500 \text{ M}^{-1}$) > OAc^- ($K_a = 525 \text{ M}^{-1}$) > Br^- ($K_a = 57 \text{ M}^{-1}$) > I^- ($K_a < 20 \text{ M}^{-1}$) [10]. The significantly stronger binding of fluoride was attributed to increasing electrostatic repulsion between the nitrogen lone pair and the larger halides.



Further application of the bisamide preorganization has been shown for the tetrapyrrene appended receptor **2a**, observed to preferentially sense H_2PO_4^- through six hydrogen bonds in a pseudo-tetrahedral cleft [11]. The *syn-syn* preorganization of the receptor was confirmed by X-ray structural analysis of the tetracyclohexane-substituted receptor **2b**. Receptor **2b** was shown to bind anions of tetrahedral geometry (H_2PO_4^- and PO_4^{3-}) preferentially, but not spherical (Br^-), linear (N_3^-) or planar (NO_3^-) anions. Association constants for H_2PO_4^- ($K_a = 549 \text{ M}^{-1}$) and OAc^- ($K_a = 159 \text{ M}^{-1}$) were determined by ^1H NMR titrations in $\text{DMSO}-d_6$. The pyrene-appended receptor **2** showed increased 1:1 association constants for H_2PO_4^- ($K_a = 1,374 \text{ M}^{-1}$) and OAc^- ($K_a = 239 \text{ M}^{-1}$), with high selectivity for PO_4^{3-} shown by fluorescence measurements in the presence of 50 equivalents of acetate.

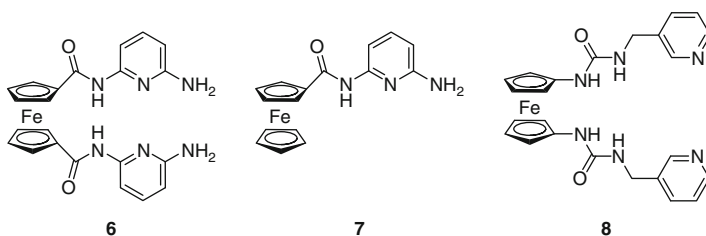
The three anthracene-functionalized receptors **3a-c** were demonstrated to bind the TBA salts of D- and L-phenylalanine in DMSO, resulting in quenching of fluorescence [12]. ^1H NMR titrations in $\text{DMSO}-d_6$ revealed a small preference of **3a** and **3b** for D-phenylalanine ($K_{\text{ad}} = 5.94 \times 10^3 \text{ M}^{-1}$, $7.64 \times 10^3 \text{ M}^{-1}$ and $K_{\text{al}} = 1.86 \times 10^3 \text{ M}^{-1}$, $3.00 \times 10^3 \text{ M}^{-1}$, respectively) whilst the larger **3c** showed the strongest preference for TBA L-phenylalanine ($K_{\text{ad}} = 1.24 \times 10^3 \text{ M}^{-1}$ and $K_{\text{al}} = 2.49 \times 10^3 \text{ M}^{-1}$, respectively). Colorimetric sensing of biologically significant anions has been achieved using the 4-nitrophenyl functionalized receptor **4** [13]. Superior binding of AMP over ADP and ATP in aqueous solution was observed, with naked-eye detection of anions in DMSO and a 4:1 DMSO/water mixture. In addition to hydrogen bonding–anion interactions, deprotonation of the thiourea protons adjacent to the amides were implicated in the anion recognition process.



The sensing of anions in partially aqueous media was studied for the bis-pyrrole appended anion receptor **5a**, shown to bind fluoride with greater affinity than chloride in DMSO–0.5% water and DMSO–5% water mixtures [14]. X-ray crystallographic determination of the fluoride and chloride adducts of **5a** as their TBA salts revealed twisted conformations of the receptors with very different binding modes: the fluoride anion was encapsulated by hydrogen bonds from the central bisamide with the two indole units hydrogen bonding from above and below the pyridine aromatic plane, while the larger chloride anion was perched above the receptor receiving four hydrogen bonds from the receptor. The closely related receptor **5b** was observed by ¹H NMR titrations in DMSO-*d*₆ to display significantly higher binding of H₂PO₄[–] over benzoate and chloride [15]. DFT calculations (B3LYP/6-31G) on receptor **5b** revealed a planar structure of the anion-free host with the expected *syn–syn* conformation of the amide substituents with internal hydrogen bonding between the pyrrole NH and the amide oxygens. DFT analysis of the chloride adduct revealed the formation of a nonplanar structure with the chloride anion perching above the receptor as observed in the related crystal structure of **5a**.TBACl.

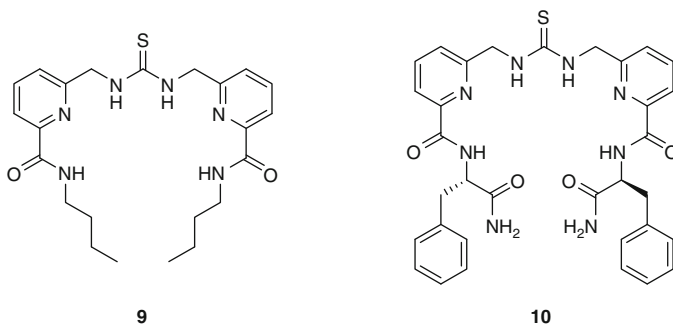
A number of acyclic pyridine-based anion receptors incorporating redox-active ferrocene moieties as potential electrochemical sensors have been prepared [16]. Receptor **6** demonstrated varied binding modes upon the addition of HSO₄[–] or H₂PO₄[–]. Dramatic shifts in the ¹H NMR resonances of the pyridine aryl protons were observed for the addition of HSO₄[–], whilst the addition of H₂PO₄[–] caused large shifts in the ferrocene proton resonances for the hydrogen atoms proximal to the amides. The variable anion-binding modes were confirmed by UV–visible spectroscopy as the addition of H₂PO₄[–] to a solution of **6** was observed to give a hypsochromic shift in the d–d absorption band, a change which was not observed for the addition of HSO₄[–]. Although **6** displayed an irreversible ferrocene redox couple in acetonitrile, the addition of H₂PO₄[–] gave a significant cathodic shift in the redox potential ($\Delta E = 240$ mV at 25°C) corresponding to the stabilization of the ferrocenium cation by the anionic guest. The cathodic shift observed for **6** was

significantly larger than the perturbation observed for the monofunctionalized receptor **7**. The large cathodic shift was attributed to the increased communication between the two amide substituents and the ferrocene redox center.



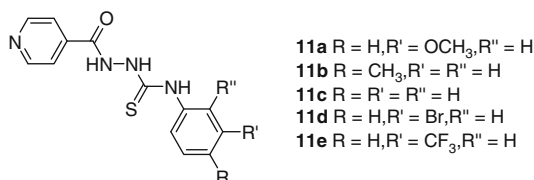
Ferrocene-functionalized anion sensing has also been examined for receptor **8**, which was shown to sense fluoride and H_2PO_4^- by electrochemical and ^1H NMR spectroscopic methods [17]. An electrochemical response to fluoride was observed between 0.1 and 6 equivalents (becoming irreversible at greater equivalents), whilst the receptor was responsive to H_2PO_4^- between 0.25 and 3 equivalents. No electrochemical response was observed upon the addition of Cl^- , Br^- , AcO^- , NO_3^- or HSO_4^- . ^1H NMR titrations in $\text{DMSO}-d_6$ indicated strong binding of fluoride ($K_a = 9.0 \times 10^6 \text{ M}^{-1}$) and H_2PO_4^- ($K_a = 3.9 \times 10^3 \text{ M}^{-1}$) in 1:2 and 1:1 stoichiometry, respectively.

Pyridine groups have also been utilized in the preorganization of mixed thio-urea–bisamide anion receptors incorporating chiral substituents for the recognition of amino acids [18]. Initial investigations with the achiral derivative **9** with TBA phenylacetate revealed downfield shifts of the urea and amide protons, with $K_a = 420 \text{ M}^{-1}$ in 10% $\text{DMSO}-d_6/\text{CDCl}_3$. The chiral anion receptor **10** was shown to bind a range of *N*-protected amino acid carboxylate salts, favoring those with hydrogen bonding (*N*-Ac-Gln- CO_2^-) or electron-rich (*N*-Ac-Trp- CO_2^-) side chains. Diastereoselectivity of the receptor was limited, with *N*-Ac-Gln- CO_2^- giving the greatest differentiation (L:D \approx 2:1). In addition to its use as an anion receptor, compound **10** was shown to function as a ^1H NMR shift reagent for the differentiation of racemic amino acids.



Thio-urea anion receptors **11a–e** incorporating terminal pyridyl and phenyl groups were shown to bind OAc^- , H_2PO_4^- and F^- in acetonitrile by UV–visible

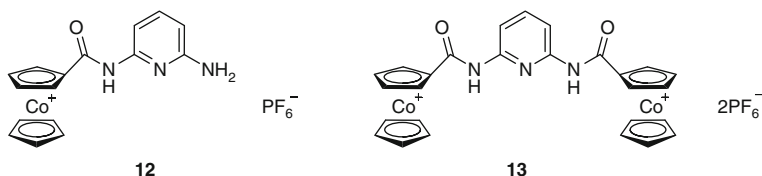
absorption spectroscopy as 1:1 adducts with association constants in the range 10^5 – 10^7 M^{-1} (beyond the accurate determination limit of the technique) [19]. An absorption band at ca. 360 nm developed upon the addition of OAc^- , $H_2PO_4^-$ and F^- with large association constants observed for titrations in mixtures of water and acetonitrile, and also pure water. Analysis of the 1H NMR spectra of **11c** in $MeCN-d_3$ upon the addition of OAc^- indicated significant downfield shift of the thiourea proton resonances. DFT calculations (B3LYP/6-31G* functional) indicated a preference of the terminal pyridine and phenyl rings to associate in polar solution, generating a hydrophobic microenvironment around the thiourea favoring hydrogen bonding with anions.



2.1.2 Charged Acyclic Receptors

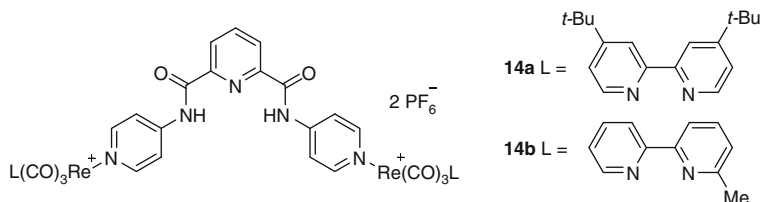
Binding affinities of acyclic pyridine-based anion receptors can be increased by the incorporation of positively charged substituents into the framework. These substituents increase the potential for electrostatic interactions between the receptor and the target anion.

The cobaltocenium hexafluorophosphate anion receptors **12** and **13** were observed by 1H NMR spectroscopy to bind chloride with association constants of $60 M^{-1}$ ($MeCN-d_3$) and $30 M^{-1}$ ($DMSO-d_6$), respectively [20]. Receptor **12** was also shown to bind $H_2PO_4^-$ in $DMSO-d_6$ ($K_a = 250 M^{-1}$), but precipitation prevented the determination of an association constant for the biscobaltocenium **13**. The stronger binding of $H_2PO_4^-$ over chloride was attributed to a repulsive interaction between the pyridine nitrogen lone pair of electrons and the approaching halide. Hydrogen bond formation between the pyridine nitrogen lone pair of electrons and the hydrogen atoms of the $H_2PO_4^-$ may potentially assist in the binding. Very small cathodic shifts were observed for both receptors in the presence of a large excess of chloride ($\Delta E = 5$ mV).

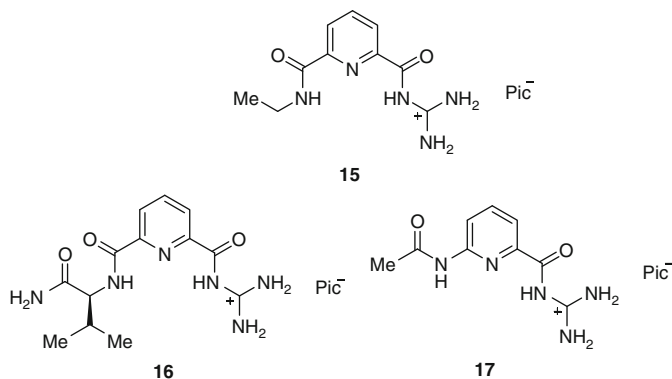


The *syn-syn* preorganized N,N' -di(4-pyridyl)pyridine-2,6-dicarboxamide ligand was complexed to two rhenium(I) centers to give receptors **14a** and **14b** [21]. Anion

binding to the receptors was indicated by luminescence quenching with increasing concentration of anion. Association constants were determined from the luminescence data with a 1:1 binding stoichiometry. Preference for CN^- was observed for both receptors ($K_a = 8.8 \times 10^5$ and $1.4 \times 10^5 \text{ M}^{-1}$) with strong binding for the halides and OAc^- ($\sim 10^4$).



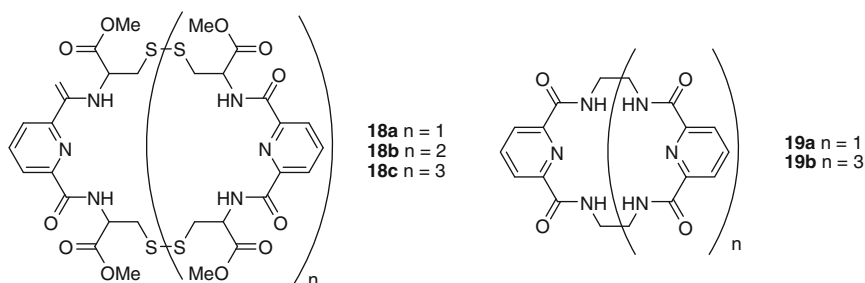
More recently, the binding of amino acid carboxylates to a series of guanidino-carbonylpyridine anion receptors were reported [22]. ^1H NMR titrations were conducted in 40% $\text{D}_2\text{O}/\text{DMSO}-d_6$, revealing significant changes in the chemical shift of the amide protons of the three receptors upon the addition of TBA salts of the amino acid carboxylates (Gly, Ala, Val, Phe) corresponding to a 1:1 binding model. The association constants were observed to increase in the order $17 < 16 < 15$, with general preference given to alanine. Repulsive interactions between the pyridine nitrogen lone pair and the anionic carboxylate were stated to lower the binding ability of the receptors compared to the corresponding pyrrole or benzene-based receptors.



2.1.3 Neutral Macrocyclic Receptors

Many macrocyclic anion receptors have been prepared as the reduced degrees of freedom and increased preorganization of the binding site can enhance the affinity

of the acyclic receptor for anions. A number of examples have been selected which make further use of the pyridine-2,6-dicarboxamide group in the preorganization of the anion-binding site(s). Amino acid functionalized anion receptors **18a–c** were prepared in one step via the condensation of a cysteine methyl ester dimer with 2,6-pyridinedicarbonyl chloride [23]. Preorganization of the macrocycles for anion binding was confirmed by FT-IR measurements and by the absence of cross-peaks between the amide protons and the pyridyl aromatic proton resonances in their ROESY ^1H NMR spectra. ^1H NMR spectroscopy titrations of **18a** ($n = 1$) with 1, ω -dicarboxylic acids $((\text{CH}_2)_m(\text{COOH})_2, m = 1, 2, 3, 4)$ in CDCl_3 revealed the highest affinity for glutaric acid ($m = 3$; $K_a = 3.69 \times 10^2 \text{ M}^{-1}$), attributed to the anion spanning the macrocyclic cavity with four hydrogen bonds formed between the carboxylic acids and the four amide groups.



Condensation of dimethyl 2,6-pyridinedicarboxylate with 1,2-diaminoethane gave the macrocycle **19a**, which when crystallized with tetraphenylphosphonium fluoride was shown to completely encapsulate the fluoride anion [24]. Crystallization with the larger chloride ion revealed that the anion was held outside of the macrocyclic cavity. Solution studies of anion binding in $\text{DMSO-}d_6$ confirmed the preference of the macrocycle for fluoride over chloride ($K_a = 830$ and 65 M^{-1} , respectively). The largest association constants were observed with acetate and dihydrogen phosphate, attributed to numerous complementary hydrogen bonding interactions. In addition to the desired macrocycle **19a**, the very large [2 + 2] macrocycle **19b** was prepared as a side product in low yield [25]. Crystallization of **19b** in the presence of TBA chloride gave a complex encapsulating two chloride ions and two water molecules within the cavity, with two additional waters of crystallization making up the asymmetric unit (Fig. 1). This binding mode is usually energetically unfavorable because of the incorporation of two repulsive chloride ions within the cavity. Multiple hydrogen bonding interactions between the macrocyclic amides and the coincluded water molecules assist in the stabilization of the $(\text{H}_2\text{O} \cdots \text{Cl}^-)_2$ structure.

The effects of the preorganization of the pyridine-2,6-dicarboxamide unit on the conformation of the macrocycle and subsequently the influence on anion binding has been studied in detail by comparison of the pyridine-based macrocycles **20** and **21** with the bisisophthalamide **22** [26–28]. The isophthalamide moiety is generally

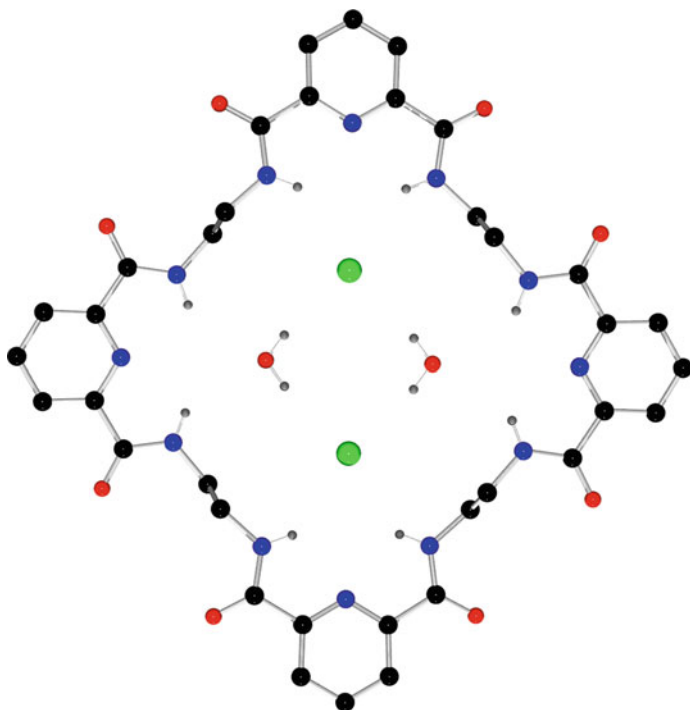
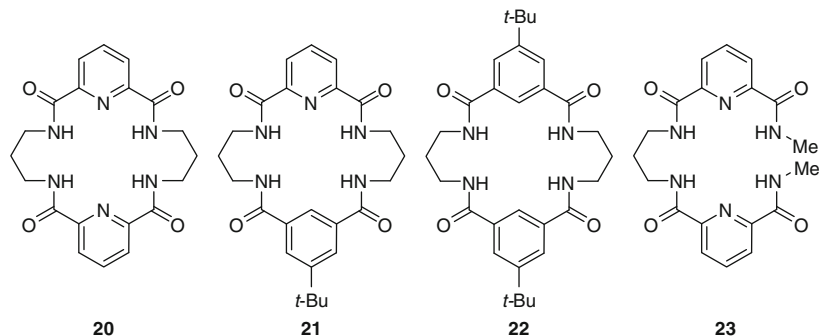


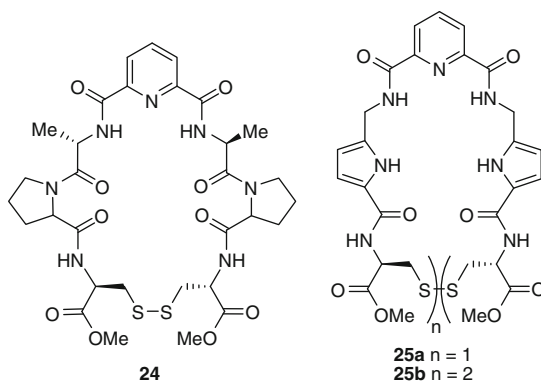
Fig. 1 X-ray structure of **19b** showing coincluded 2Cl.2H₂O

considered superior to the pyridine-2,6-dicarboxamide group for the binding of anions, as the repulsive interaction between the pyridine nitrogen lone pair of electrons destabilizes the approach of anions such as chloride to the amide hydrogen bond donors. Contrary to expectation, the chloride association constants in DMSO-*d*₆ for the bispyridine macrocycle **20** were significantly larger ($K_a = 1,930 \text{ M}^{-1}$) than those obtained for the bisisophthalamide macrocycle **22** ($K_a = 378 \text{ M}^{-1}$) [26, 27]. Additionally, the mixed receptor **21** was observed to bind chloride, benzoate and H₂PO₄⁻ more strongly than either **20** or **22** in 5% water/DMSO-*d*₆ [28]. The weak anion-binding properties of **22** arise from internal hydrogen bond formed between the complementary amide groups, which must be overcome in the anion-binding step, while the preorganized bispyridine macrocycle **20** provides a more open conformation more capable of accepting anions. The mixed receptor retains the preorganization of **20**, whilst simultaneously enforcing the *syn-syn* conformation of the isophthalamide group as identified by NOESY NMR spectroscopy. X-ray crystallographic analysis of the mixed receptor **22** (as the tris TBACl hemi-1,2-dichloroethane solvate) revealed a chloride ion held by four hydrogen bonds within the macrocyclic cavity. The anion was unexpectedly bound closest to the pyridine amides.



Variation in the alkyl spacer of **20** revealed the propyl to be the best for the binding of a range of anions [29]. The influence of the macrocyclic effect on the binding of anions to **20** was examined with the use of the acyclic anion receptor **23**, revealing approximately 20 times reduction in the association constants obtained for Cl^- , OAc^- and H_2PO_4^- in $\text{DMSO}-d_6$.

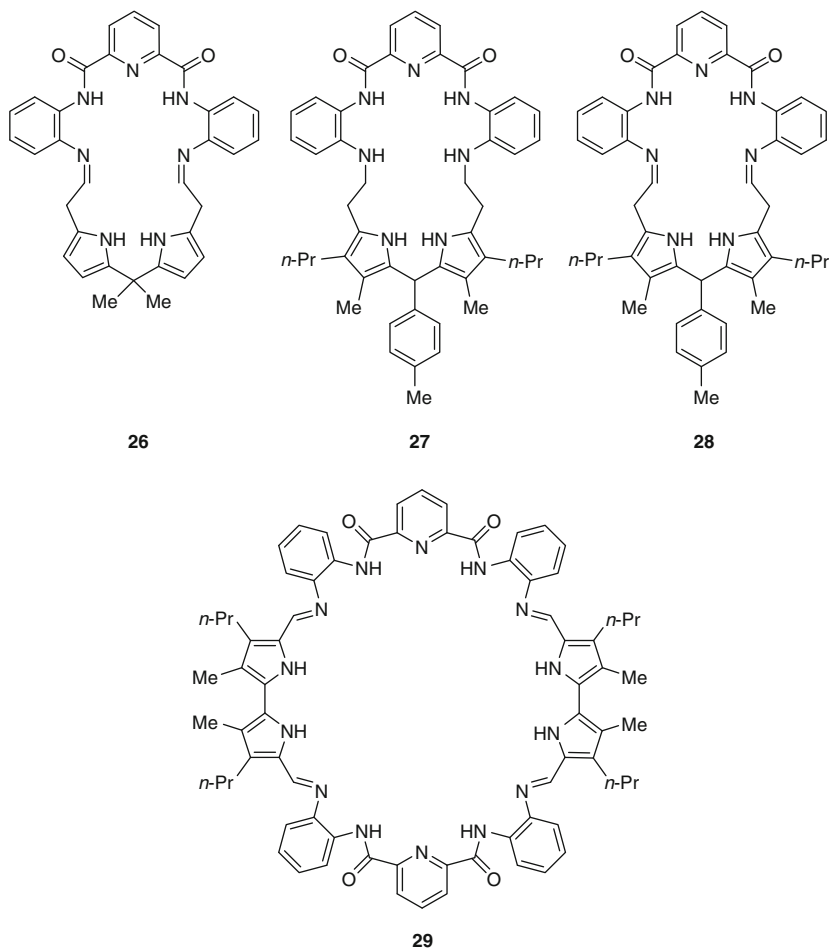
A pyridine-2,6-dicarboxamide modified cyclic peptide **24** was investigated for its ability to bind both cations and anions [30]. A NOESY spectrum of the neutral receptor indicated that the Ala amide does not interact with the pyridine aryl protons, indicative of the *syn-syn* bisamide conformation. Association constants were determined in MeCN for TBA salts by CD spectroscopy through the analysis of the changes in the Cotton effect at 235 nm. Strongest binding was observed for F^- ($K_a = 418 \text{ M}^{-1}$) with further association constants determined for H_2PO_4^- (155 M^{-1}), Br^- (144 M^{-1}), OAc^- (112 M^{-1}), NO_3^- (46 M^{-1}) and Cl^- (30 M^{-1}).



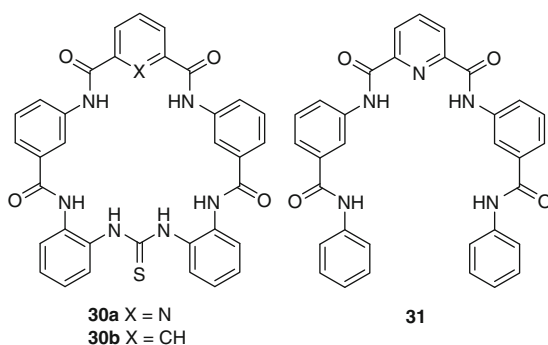
Related cyclic peptide based macrocycles **25a** and **25b** were isolated as [1 + 1] and [2 + 2] macrocycles in 18% and 6.2% yield, respectively [31]. Initial analysis by ^1H NMR spectroscopy in $\text{DMSO}-d_6$ indicated downfield shifts for the amide resonances upon the addition of small aliquots of fluoride and acetate, while the addition of excess quantities of both anions resulted in loss of the amide protons from the spectra. Association constants were obtained by UV-visible titrations in acetonitrile. The addition of fluoride to a solution of **25a** resulted in a decrease in the absorption band (266 nm), with no further changes observed after the addition

of one equivalent ($K_a = 1.43 \times 10^7 \text{ M}^{-1}$). Changes in the UV–visible spectra were also observed for chloride ($K_a = 1.25 \times 10^4 \text{ M}^{-1}$) and acetate ($K_a = 6.87 \times 10^6 \text{ M}^{-1}$). UV–visible titration of **25b** with fluoride, acetate and chloride indicated 1:2 stoichiometry of binding with association constants of 7.84×10^9 , 1.06×10^{10} and $4.13 \times 10^8 \text{ M}^{-2}$, respectively.

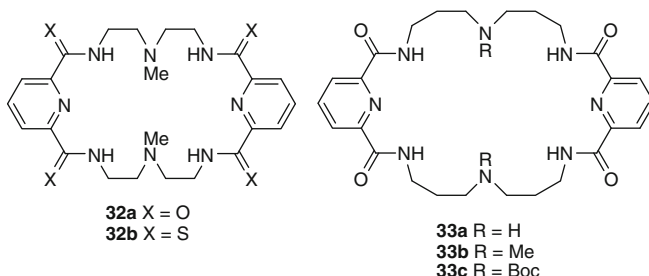
The mixed pyrrole–pyridine macrocycle **26** was shown to be highly selective for H_2PO_4^- and HSO_4^- relative to NO_3^- , as determined by UV–visible titrations in acetonitrile solution [32]. A 1:1 association constant was determined for HSO_4^- ($K_a = 6.4 \times 10^4 \text{ M}^{-1}$), whilst stepwise 1:2 binding was observed for H_2PO_4^- ($K_{11} = 3.42 \times 10^5 \text{ M}^{-1}$, $K_{12} = 2.6 \times 10^4 \text{ M}^{-1}$). Because of this selectivity, the receptor **26** was envisaged as a possible extractant for the removal of hydrogen sulfate from nitrate-rich nuclear waste. Further tuning of the macrocycle cavity was undertaken through the synthesis and analysis of macrocycles **27** and **28** [33]. Receptor **27** was found to favor tetrahedral anions similarly to **26** whilst the larger cavity of **28** gave the greatest association constant with the spherical chloride anion. Sulfate templation was used for the preparation of the [2 + 2] macrocycle **29**, found to rearrange in the presence of H_2PO_4^- or HSO_4^- to the [3 + 3] macrocycle [34, 35]. Synthetic attempts for templation with HCl or HBr led to mixtures of higher oligomers.



In addition to the benefits of preorganization provided by the pyridine-2,6-dicarboxamide unit, a stabilizing influence was observed for the macrocycle **30a** as the corresponding isophthalamide macrocycle **30b** underwent amide hydrolysis in neutral 5% water/DMSO solution [36]. The receptor **30a** was demonstrated by ^1H NMR titrations in the same solvent mixture to strongly bind acetate ($K_a = 16,500 \text{ M}^{-1}$) and benzoate ($K_a = 6,430 \text{ M}^{-1}$) and was found to be superior to the association constants observed for acyclic analog **31**.



Additional pyridine-2,6-dicarboxamide/amine based macrocycles **32a–b** and **33a–c** have been shown to be selective for a range of anions. Macrocycle **32a** exhibited selectivity for H_2PO_4^- ($\log K_a = 4.05$) as determined by ^1H NMR titrations in $\text{DMSO-}d_6$ with weaker association constants observed for HSO_4^- ($\log K_a = 2.03$), F^- ($\log K_a = 2.61$), Cl^- ($\log K_a = 2.69$), Br^- ($\log K_a = 2.71$) and I^- ($\log K_a < 1.0$) [37]. Reaction of **32a** with Lawesson's reagent gave the thioamide macrocycle **32b**, which displayed a surprising increase in affinity for HSO_4^- ($\log K_a = 4.99$) [38]. Increased affinity was also observed for H_2PO_4^- ($\log K_a = 4.63$) and F^- ($\log K_a = 4.11$) whilst the halides were all bound with lower affinity. The enhanced binding of the tetrahedral oxo anions (HSO_4^- and H_2PO_4^-) was attributed to the acid–base properties of the receptors rather than the geometry of the anion as no significant binding was observed for ClO_4^- .



The expanded macrocycles **33a–c** were shown to exhibit selectivity for the oxo anions whilst also showing affinities for the halides [39]. X-ray crystallographic

analysis of the receptors **33a** and **33b** with SO_4^{2-} revealed differing modes of anion binding; the former included the anion within the macrocycle, whilst the latter adopted a folded conformation with the anion located outside of the macrocyclic cavity. Association constants determined by ^1H NMR titrations in $\text{DMSO}-d_6$ for HSO_4^- were observed to be *significantly* larger for **33a** ($K_a = 6.4 \times 10^4 \text{ M}^{-1}$) than either **33b** ($K_a = 73 \text{ M}^{-1}$) or **33c** ($K_a < 10 \text{ M}^{-1}$). A similar trend was observed for H_2PO_4^- : **33a** ($K_a = 4.4 \times 10^3 \text{ M}^{-1}$); **33b** ($K_a = 500 \text{ M}^{-1}$) and **33c** ($K_a = 430 \text{ M}^{-1}$).

The binding of anions in aqueous media is a significant challenge in anion receptor chemistry. Competition of protic solvent for the noncovalent interactions and the necessity of overcoming the solvation of the anion can restrict the binding capabilities and selectivity of anion receptors. A number of cyclic polypeptides have been demonstrated to bind anions selectively in highly polar, protic media [40–43]. Macrocyclic anion receptor **34a** composed of three L-proline and three 6-aminopicolinic acid subunits was demonstrated to bind halides and sulfate in aqueous solution. ^1H NMR spectroscopy titrations in 80% $\text{D}_2\text{O}/\text{CD}_3\text{OD}$ revealed the binding of benzenesulfonate in a 1:1 stoichiometry ($K_a = 44 \text{ M}^{-1}$), whilst a 2:1 host:anion binding stoichiometry was observed for the addition of TBA iodide ($K_a = 1.79 \times 10^5 \text{ M}^{-1}$) and sodium sulfate ($K_a = 1.22 \times 10^5 \text{ M}^{-1}$) [40]. X-ray crystallographic analysis of the iodide complex confirmed the 2:1 host/anion stoichiometry, with the iodide anion held by three hydrogen bonds from each of the two hexapeptide receptors (Fig. 2). Incorporation of hydroxyl groups onto the

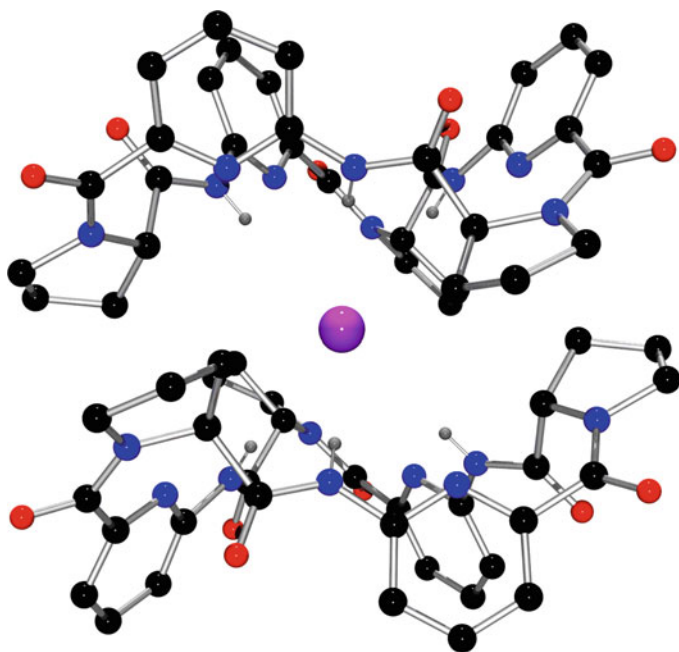
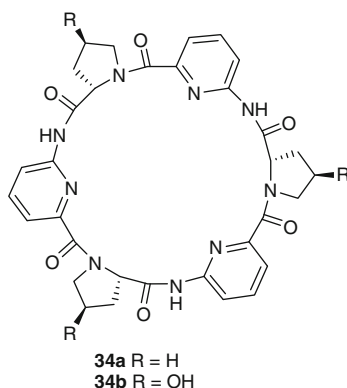


Fig. 2 X-ray crystal structure of **34a₂.I**

proline framework of macrocycle **34b** resulted in the formation of 1:1 complexes with halide and sulfate ions, with the additional functionality thought to inhibit the anion-assisted aggregation of the macrocycles in solution [41].



Further investigations were made into the linked bismacrocycle **35a** to exploit the 2:1 receptor to anion ratio observed for **34a** [42]. Strong selectivity was observed for sodium sulfate, with an association constant of $3.5 \times 10^5 \text{ M}^{-1}$ determined by ^1H NMR titrations in 1:1 $\text{D}_2\text{O}/\text{CD}_3\text{OD}$ [42]. Iodide was also bound strongly by **35a** ($K_a = 3.5 \times 10^5 \text{ M}^{-1}$), with the association constants found to be significantly lower for bromide and chloride.

Further optimization of sulfate and iodide binding was examined through the use of a dynamic combinatorial library containing various disulfide linkers (Fig. 3) [44]. A reaction mixture including disulfide **35b** (a poor anion receptor), K_2SO_4 and the compounds in the disulfide library was monitored by HPLC until complete equilibration had occurred, which corresponded to the amplification of receptors **35c** and **35d**. No amplification was detected in the presence of NaCl or KI . Binding studies on receptors **35c** and **35d** by isothermal titration microcalorimetry (ITC) indicated that the binding was an order of magnitude larger than the precursor **35b** [43, 45]. Further modification of the linker has enabled the sensing of sulfate by luminescence methods [46].

The triazole–pyridine based macrocycles **36a** and **36b** were demonstrated to show diverse binding properties with the halides [47]. UV–visible titrations in dichloromethane revealed absorbance decreases upon the addition of TBA salts of F^- , Cl^- and Br^- to 20 μM solutions of **36a**, with the minimum absorbance corresponding to the addition of 0.5 equivalents and the formation of a 2:1 host–guest complex in solution. The concentration of the host was observed to influence the stoichiometry of anion binding, with the direct formation of the 1:1 complexes observed for F^- , Cl^- and Br^- in 1 μM solutions of **36a**. The iodide complex displayed remarkable stability ($K_a = 8.6 \times 10^{10} \text{ M}^{-2}$), remaining as the 2:1 complex in the presence of 150 equivalents of I^- . Preliminary X-ray crystallographic investigations of the iodide complex of **36b** also revealed the 2:1 host-to-anion binding stoichiometry.

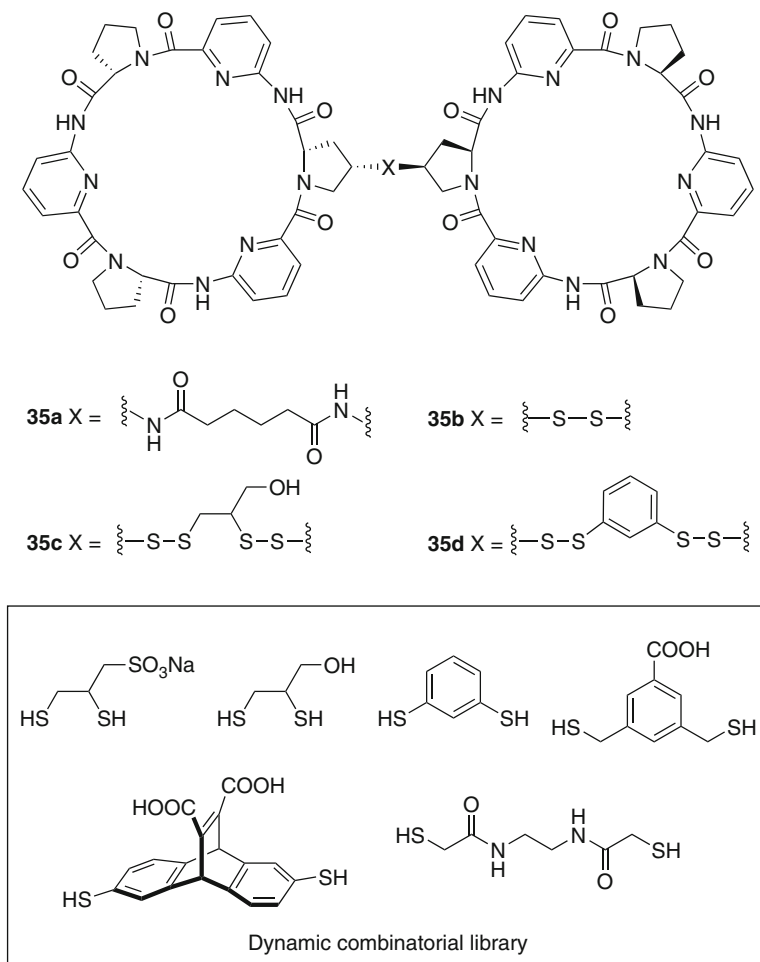
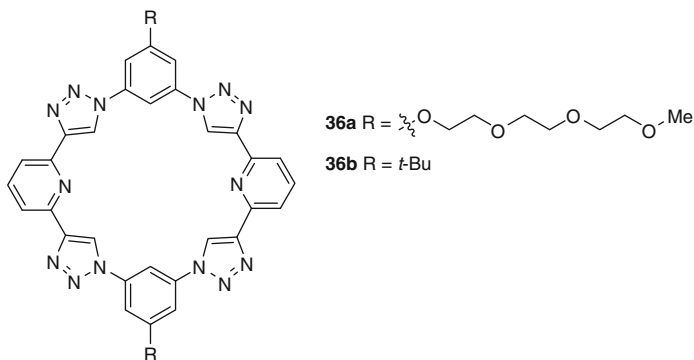
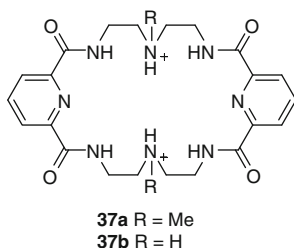


Fig. 3 Dynamic combinatorial library of anion chelates



2.1.4 Charged Macrocyclic Receptors

Similarly to the acyclic receptors, the incorporation of positive charge into the macrocyclic receptor framework can have a significant influence on anion binding through electrostatic interactions. Methylation of the secondary amine spacer of **32a** increased the association constants for all of the anions investigated (with the exception of fluoride) due to enhanced electrostatic interactions, for example, the binding of H_2PO_4^- in $\text{DMSO}-d_6$ where $\log K_a = 4.04$ for **32a** and $\log K_a = 5.32$ for **37a**. $(\text{PF}_6)_2$ [37]. X-ray crystallographic analysis of **37a**. 2I^- revealed the macrocycle in a folded conformation suitable for the binding of larger anions. The basicity of the amine spacers was also utilized in the bisprotonated **37b** [48]. X-ray crystallographic analysis of the $\text{Cr}_2\text{O}_7^{2-}$ adduct of **37b** indicated a folded conformation of the macrocycle where the preorganized bisamides are hydrogen bonded to the anion and the ammonium protons are internally hydrogen bonded to the carbonyl oxygen. X-ray crystallographic analysis of **37b**. $2\text{ReO}_4^- \cdot 3\text{H}_2\text{O}$ revealed a very similar binding mode to the **37b**. $\text{Cr}_2\text{O}_7^{2-}$ structure.



A range of imidazolium- and benzimidazolium-functionalized macrocycles have also taken advantage of the preorganizing effects of the pyridine nitrogen lone pair of electrons on the conformation of the macrocycle.

The tetraimidazolium macrocycle **38** was examined as a receptor for halides and oxoanions [49]. ^1H NMR titrations of tetrabutylammonium fluoride into solutions of the macrocyclic host **38** in $\text{MeCN}-d_3$ and $\text{DMSO}-d_6$ showed significant shifts for the imidazolium hydrogen atoms, with Job-plot analysis indicating a 1:1 binding stoichiometry. The association constant of fluoride binding in $\text{DMSO}-d_6$ was determined as $28,900 \text{ M}^{-1}$. ^1H NMR titrations in $\text{DMSO}-d_6$ with TBACl gave a 2:1 binding stoichiometry, with association constants of $K_{11} = 2,030 \text{ M}^{-1}$ and $K_{12} = 2,790 \text{ M}^{-1}$. X-ray crystallographic analysis of the fluoride and chloride salts of **38** confirmed the binding stoichiometry determined by NMR spectroscopy as the fluoride is bound within the macrocyclic cavity (**37**. $\text{F}(\text{PF}_6)_3$) (Fig. 4a), whilst the larger chloride anions were perched outside of the macrocyclic cavity (**38**. $\text{Cl}_2(\text{PF}_6)_2$) (Fig. 4b). The ferrocene bisimidazolium receptor **39** was prepared for the electrochemical sensing of anions [50]. The addition of fluoride to an acetonitrile solution of the receptor resulted in a cathodic shift ($\Delta E = -214 \text{ mV}$) in the redox potential, whilst the addition of HSO_4^- , Cl^- and Br^- gave much smaller responses ($\Delta E < 100 \text{ mV}$). ^1H NMR titrations in $\text{MeCN}-d_3$ indicated complexation of the anions by the 2-imidazolium C–H anion hydrogen bonds in 1:1 stoichiometry

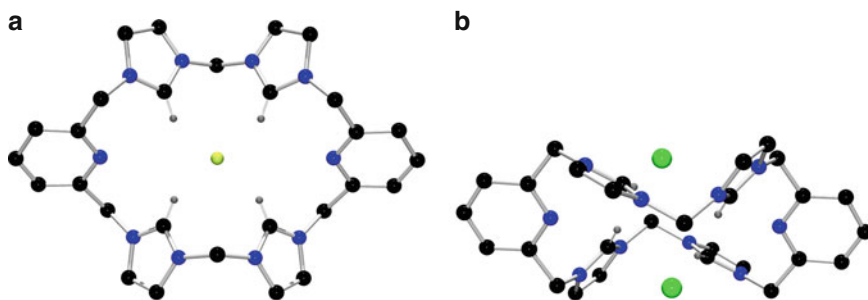
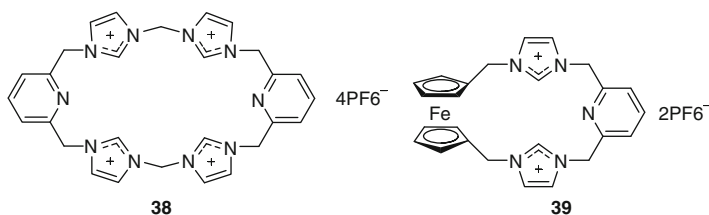
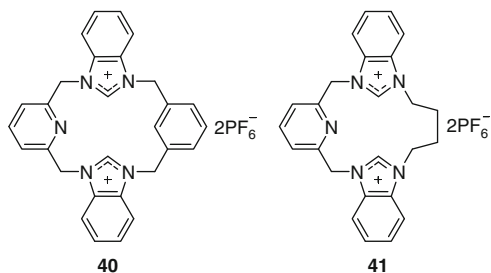


Fig. 4 (a) X-ray crystal structure of **38.F** (b) X-ray crystal structure of **38.Cl₂**

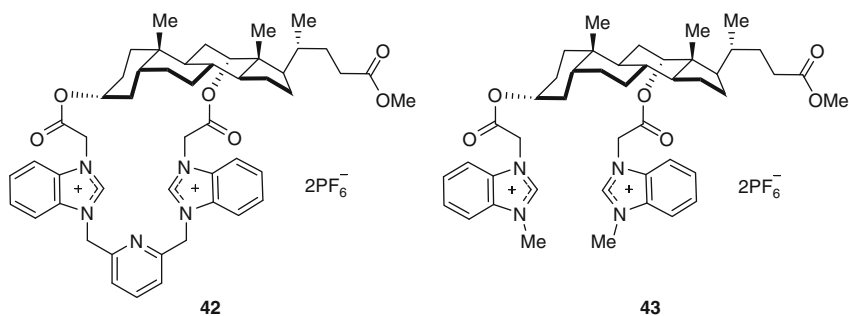
for Cl^- ($K_a = 3.2 \times 10^3 \text{ M}^{-1}$), Br^- ($K_a = 1.2 \times 10^3 \text{ M}^{-1}$), I^- ($K_a = 2.9 \times 10^3 \text{ M}^{-1}$) and OAc^- ($K_a = 4.2 \times 10^3 \text{ M}^{-1}$).



The benzimidazolium macrocycles **40** and **41** were prepared by cyclization with 1,3-bis(bromomethyl)benzene and dibromobutane, respectively, under high-dilution conditions in acetonitrile [51]. The hexafluorophosphate salts of both receptors were observed by UV-visible titrations in acetonitrile to bind Br^- with association constants of $\sim 6,000 \text{ M}^{-1}$.



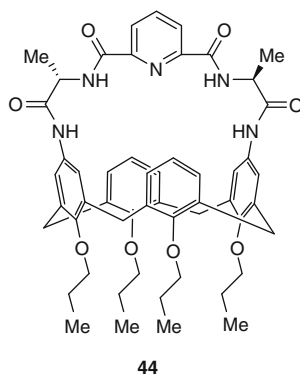
A bile acid based bisbenzimidazolium/2,6-dimethylpyridine macrocyclic receptor **42** was demonstrated to bind anions with high selectivity, but with low affinity compared to non-pyridyl receptors [52]. Interestingly, the association constant for chloride was observed to be lower for **42** ($K_a = 1,400 \text{ M}^{-1}$) than that of the closely related acyclic molecule **43** ($K_a = 2,500 \text{ M}^{-1}$) as determined by ^1H NMR titrations in CDCl_3 . This was postulated to arise from the nitrogen lone pair of electrons interfering with the binding of chloride to the cavity. The association constants for OAc^- , Cl^- , Br^- and I^- with **43** were all determined to be of the order 10^3 M^{-1} .



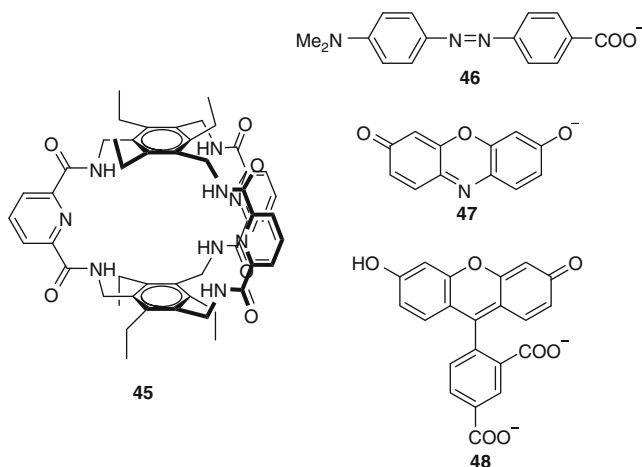
2.2 Macrobicyclic and Cryptand Receptors

2.2.1 Neutral Macrobicyclic and Cryptand Receptors

Additional refinement of anion receptors can be made through greater restriction of the anion-binding site, with macrobicyclic and cryptand receptors placing additional steric constraints on the anion species and potentially increasing the selectivity of the receptor for anions of a particular geometry. The calix[4]arene peptide based macrobicycle **44** was prepared in 40% yield, with 3% of the [2 + 2] macrocycle also observed [53]. X-ray crystallographic analysis of the acetone solvate of **44** revealed preorganization of the 2,6-dicarboxamide and orientation of the additional amide hydrogen atoms toward the center of the chiral cavity. A range of carboxylates (as their TBA salts) were observed to bind to the cavity, as determined by the ^1H NMR spectrometry titration in acetone- d_6 . A preference was shown for D-amino acids $N\text{-Ac-D-PheCO}_2^-$ ($K_a = 10,500 \text{ M}^{-1}$) and $N\text{-Ac-D-AlaCO}_2^-$ ($K_a = 5,700 \text{ M}^{-1}$) over their corresponding enantiomers ($K_a = 7,900$ and $4,900 \text{ M}^{-1}$, respectively). Association constants were also determined to be of the order benzoate ($K_a = 40,100 \text{ M}^{-1}$) > 4-methoxybenzoate ($K_a = 33,300 \text{ M}^{-1}$) > acetate ($K_a = 10,500 \text{ M}^{-1}$) > $N\text{-Ac-GlyCO}_2^-$ ($K_a = 6,200 \text{ M}^{-1}$), with significantly smaller binding of Cl^- ($K_a = 2,800 \text{ M}^{-1}$) and NO_3^- ($K_a = 200 \text{ M}^{-1}$).

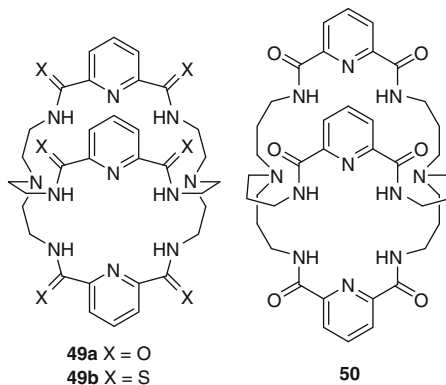


Cryptand receptor **45** forms 1:1 adducts with nitrate and acetate with preorganization of the pyridine-2,6-dicarboxamide groups orienting the six hydrogen atoms toward the center of the cavity [54]. Crystallization of the receptor as the chloride salt showed binding of two equivalents outside the cavity in a 2:1 stoichiometry with the association constant determined for chloride as $K_a = 40 \text{ M}^{-1}$ by $^1\text{H NMR}$ titrations in 25% $\text{CD}_2\text{Cl}_2/\text{MeCN-}d_3$. Acetate was shown to bind within the cavity in a 1:1 complex through hydrogen bonding between two sets of amide hydrogen atoms ($K_a = 770 \text{ M}^{-1}$). Greatest selectivity was observed for nitrate whilst cyanide, chloride, bromide and H_2PO_4^- were bound with lower affinity, presumably because of the size and geometric selectivity of the C_3 cavity for the C_3 nitrate anion. The optical sensing of nitrate was achieved by displacement assays with fluorescent dyes **46**, **47** and **48** [55]. Addition of nitrate to a 40 mM solution of the **45.46** adduct in 1:1 methanol/dichloromethane was sufficient to dissociate the complex, inducing fluorescence. Quantitative analysis was achieved for nitrate, bromide and perchlorate in this solvent system, with determined association constants of 380, 220 and 130 M^{-1} respectively. Increasing the solvent polarity to 3:1, $\text{MeCN}/\text{CH}_2\text{Cl}_2$ required the use of the **45.46** adduct, showing large changes in λ_{max} absorption upon the addition of anions. Nitrate was observed to be the most efficient guest for the **45.46** anion receptor ($K_a = 500 \text{ M}^{-1}$) whilst bromide and perchlorate were bound less strongly ($K_a = 190$ and 70 M^{-1} , respectively).



A range of cryptands have been developed expanding upon the previously described macrocycles **32a**, **32b** and **33a** [38, 56, 57]. The cryptand receptor **49a** was found to bind fluoride in $\text{DMSO-}d_6$ with the highest binding affinity ($\log K_a = 5.90 \text{ M}^{-1}$), whilst the remaining halides, HSO_4^- ($\log K_a = 1.83 \text{ M}^{-1}$) and H_2PO_4^- ($\log K_a = 3.31 \text{ M}^{-1}$) showed lower affinity [38, 56]. Slow exchange of fluoride was observed for both the amide and thioamide receptors with the coupling of the fluoride nuclei to the six degenerate amide hydrogens observed in the ^{19}F NMR spectra as a septuplet [58]. X-ray crystallographic analysis of the fluoride complex of **49a** revealed the cryptand receptor incorporating a single fluoride anion

within the center of the cavity with pseudo- C_3 symmetry [57]. Receptor **49a** was also observed to scavenge DCl from $CDCl_3$, assisted by the protonation of the bridgehead amines [56], whilst the bisprotonated cryptand encapsulated SO_4^{2-} through coordination of the anion by eight hydrogen bonds as determined by X-ray crystallographic investigations [59].



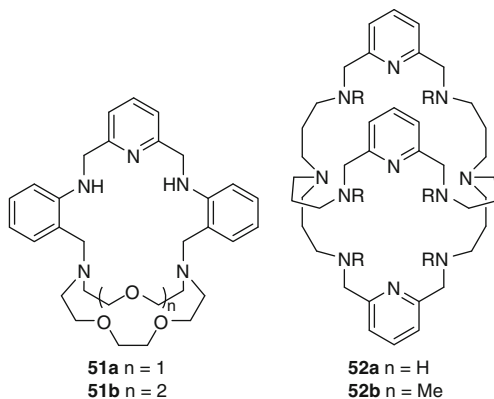
The expanded cryptand **50** was shown to bind anions in $DMSO-d_6$, with the strongest binding observed for fluoride at slow exchange ($K_a > 10^5 M^{-1}$) [60]. X-ray crystallographic analysis of the bis(hydrochloride) complex $H_2\mathbf{50}.Cl_2$ revealed the two cocrystallized chloride anions and a water of crystallization in the macrocyclic cavity, held by a multitude of hydrogen bonding interactions. The sulfate complex $H_2\mathbf{50}.SO_4$ revealed the anion and an additional two water molecules within the cryptand cavity. 1H NMR spectroscopy titrations in $DMSO-d_6$ indicated the preference of **50** for F^- ($K_a > 10^5 M^{-1}$) and HSO_4^- ($K_a = 2,700 M^{-1}$) whilst the halides were bound relatively weakly, viz. Cl^- ($K_a = 180 M^{-1}$).

2.2.2 Charged Macrobicyclic and Cryptand Receptors

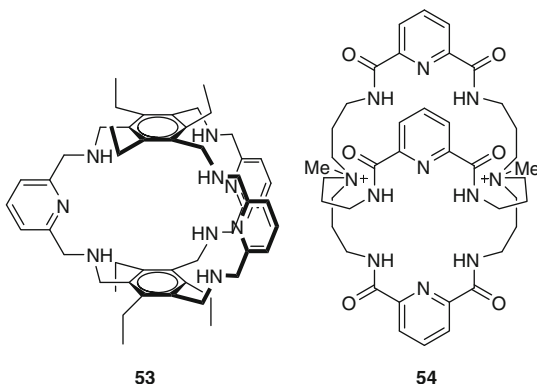
The triprotonated forms of macrobicyclic hosts **51a** and **51b** are capable of reporting anion binding by spectrophotometric titrations [61]. Increase in the absorption maxima were observed upon the addition of halide to a $10^{-4} M$ solution of the receptor in acetonitrile containing 15 equivalents of trifluoroacetic acid. Clear trends were observed for halide binding to $H_3\mathbf{51a}^{3+}$, in the sequence Cl^- ($\log K = 5.15$) $>$ Br^- ($\log K = 4.09$) $>$ I^- ($\log K = 3.82$) $>$ F^- ($\log K = 3.11$) while the larger cavity of $H_3\mathbf{51b}^{3+}$ showed a different trend Cl^- ($\log K = 5.40$) $>$ F^- ($\log K = 4.22$) $>$ I^- ($\log K = 4.09$) $>$ Br^- ($\log K = 3.75$). Interestingly, the selectivity for chloride is retained whilst the preference for bromide and fluoride is reversed in increasing the size of the anion-binding cavity. Association constants were also obtained for $H_3\mathbf{51a}^{3+}$ with oxoanions binding in the sequence HSO_4^- ($\log K = 4.72(1)$) $>$ $H_2PO_4^-$ ($\log K = 3.78(5)$) $>$ ClO_4^- ($\log K = 3.13(4)$) $>$ NO_3^- ($\log K < 1$). Further examination of oxoanion binding with $H_3\mathbf{51b}^{3+}$ showed similar binding for HSO_4^- ($\log K = 4.02(1)$), $H_2PO_4^-$ ($\log K = 3.48(3)$) and ClO_4^-

($\log K = 3.23(2)$) whilst NO_3^- ($\log K = 3.36(1)$) is bound significantly more strongly by the larger receptor. Enhanced NO_3^- binding was attributed to a better fit between the trigonal anion and the protonated amines.

Cryptands have been investigated for the binding of anions with the hexaprotonated cryptand **52a** found to bind hexafluorosilicate (derived from the action of HBF_4 with the glass reaction vessel) within the cryptand cavity [62]. The octaprotonated form was observed to bind three perchlorate anions to the clefts of the cryptand through numerous hydrogen bonds [63]. Receptors **52a** and **52b** were also examined for the extraction of pertechnetate and perrhenate from aqueous solution. X-ray crystallographic analysis of hexaprotonated **52a** as the mixed salt $\text{H}_6\mathbf{52a} \cdot (\text{ReO}_4)_6 \cdot \text{H}_6\mathbf{52a} \cdot (\text{ClO}_4)_2 \cdot 3\text{H}_2\text{O}$ revealed binding of the perrhenate anion to the clefts of the cryptand similar to that observed for the perchlorate structure [64]. The hexamethyl derivative **52b** was demonstrated to show the highest extraction of pertechnetate into chloroform from a buffered aqueous solution at pH 7.4.



The polyaza cryptand receptor **53** was shown to be selective for H_2PO_4^- [65]. The binding of anions to the receptor in its neutral and hexaprotonated states revealed stronger binding for the charged species. Binding of H_2PO_4^- was observed to show little variation in binding strength regardless of the protonation state of the receptor, attributed to favorable hydrogen bonding of the aza hydrogen atoms, with concurrent hydrogen bond acceptance by the pyridyl nitrogen groups.

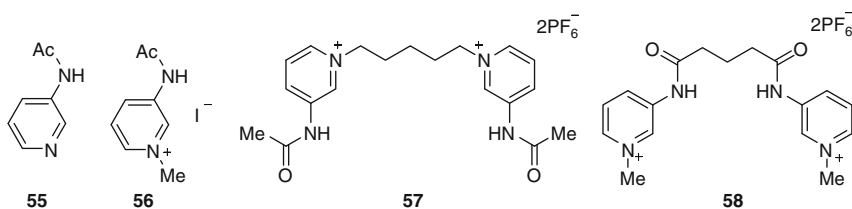


The cationic **54** displayed a preference for H_2PO_4^- ($K_a = 12,000 \text{ M}^{-1}$) whilst lowering the affinity of the receptor for HSO_4^- ($K_a = 340 \text{ M}^{-1}$) and increasing the affinity for Cl^- ($K_a = 3,100 \text{ M}^{-1}$). X-ray crystallography revealed a bowl-shaped conformation for **54**. Cl^- , significantly different from the “Y”-shaped conformers observed for related neutral **50**. Cl^- and **50**. SO_4^{2-} .

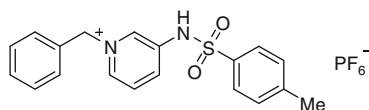
3 Pyridinium-Based Anion Receptors

3.1 Acyclic Receptors

Acyclic pyridinium-based anion receptors make use of enhanced electrostatic interactions between the receptor and the anion to increase the binding affinity. The influence of the pyridinium group on anion binding is illustrated for the binding of benzoate pyridine-amide receptor **55** in $\text{DMSO}-d_6$ was determined to be weak ($K_a = 16 \text{ M}^{-1}$), with methylation of the pyridine significantly increasing the association constant of **56** ($K_a = 300 \text{ M}^{-1}$) [66]. The bispyridinium salts **57** and **58** were observed to bind benzoate with even greater affinity ($K_a > 500 \text{ M}^{-1}$).

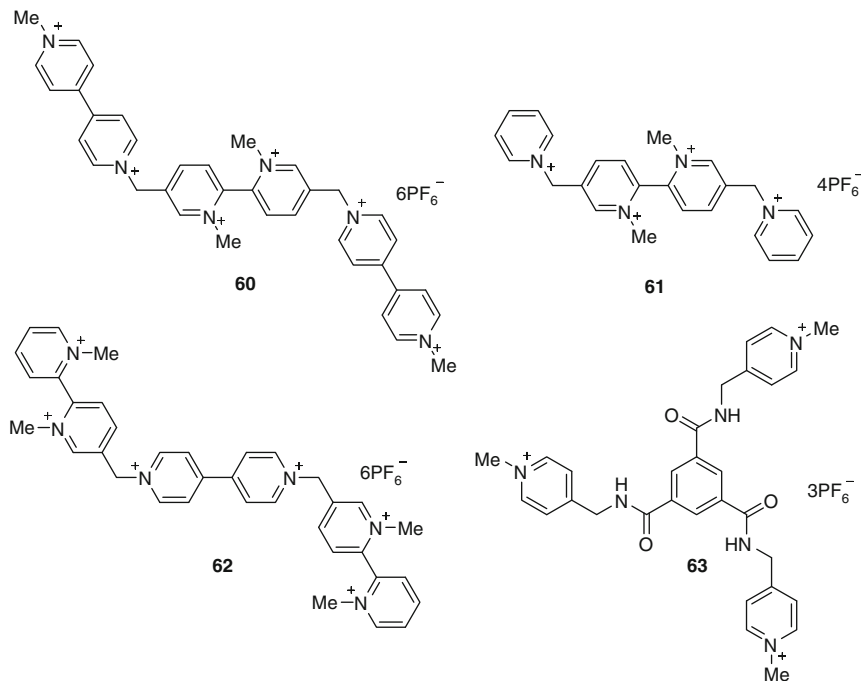


Deprotonation of anion receptors by basic anions (such as fluoride) is frequently implicated in anion receptor chemistry. This deprotonation is given due consideration in the study of the anion-binding properties of **59** [67]. The sulfonamide group of receptor **59** undergoes deprotonation in the presence of F^- , OAc^- and H_2PO_4^- , as observed by UV–visible spectrophotometric titrations in DMSO solution with $\log K_a > 6$ in each case. The absorbance was observed to reach a maximum corresponding to the addition of one equivalent of anion with the deprotonation confirmed by ^1H NMR titrations. The less basic Cl^- , Br^- and NO_3^- anions bind in 1:1 stoichiometry as determined by UV–visible spectrophotometric titrations with association constants of $\log K_a = 4.52$, 3.55 and 2.97, respectively. ^1H NMR titrations indicated a downfield shift of the amide protons with the less basic anions, rather than the previously observed deprotonation.

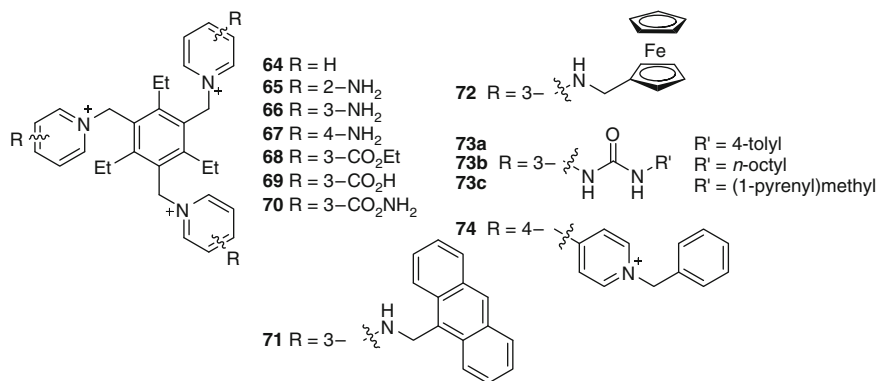


59

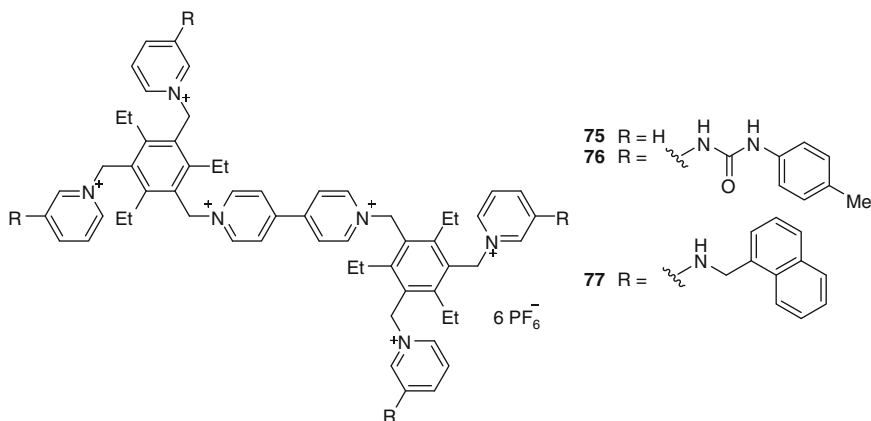
Quaternary bipyridinium and polypyridinium anion receptors were investigated for the recognition of halide anions [68–70]. ^1H NMR spectroscopy titrations in $\text{DMSO-}d_6$ for the structurally related **60–63** showed very similar chloride association constants ($K_a = 30\text{--}40\text{ M}^{-1}$), while the strongest chloride binding was observed for the trisamide-functionalized **63** ($K_a = 110\text{ M}^{-1}$) [69]. Electrochemical investigations of the receptors containing the redox-active 4,4'-bipyridinium moiety by square-wave voltammetric analysis indicated significant cathodic shifts upon the addition of chloride with the largest shift observed for **62** ($\Delta E = 130\text{ mV}$).



Numerous polypyridinium podand anion receptors have been investigated for their binding of the halides and oxoanions (**64–74**). The alternating substitution around the central benzene unit preorganizes the host in a cone conformation suitable for anion binding. The ferrocene-appended **72** showed the most effective binding for halide guests in the sequence Cl^- ($K_{11} = 17,380\text{ M}^{-1}$) $>$ Br^- ($K_{11} = 2,950\text{ M}^{-1}$) $>$ I^- ($K_{11} = 1,860\text{ M}^{-1}$) as determined by ^1H NMR titrations in $\text{MeCN-}d_3$ [71, 72]. Strong binding of acetate to **72** was also observed ($K_{11} = 3,680\text{ M}^{-1}$). ^1H NMR titrations in $\text{MeCN-}d_3$ for the anthracene-appended receptor **71** showed very strong binding of acetate ($K_{11} = 49,000\text{ M}^{-1}$), but significantly weaker halide binding than **72**. The binding of acetate to **71** involves a partial cone conformation of the receptor involving N–H hydrogen bond donation from two arms to the anion. Additional equivalents of anion were bound to the remaining arm through amine and pyridyl CH protons.



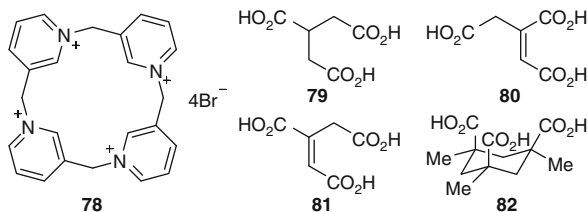
Further tripodal pyridinium anion receptors incorporating urea functionality were investigated for the binding of halides, oxoanions and carboxylic acids [73, 74]. The receptor **73a** was demonstrated by X-ray crystallography to bind in varied conformations to different anions, most visibly manifest in the variations of hydrogen bonding motifs. Of the halides, bromide was shown to bind strongest to **73a** in DMSO-*d*₆ in a 1:1 stoichiometry ($\log K_{11} = 3.46$), with greater affinity than either chloride ($\log K_{11} = 2.64$) or iodide ($\log K_{11} = 1.61$). Further association constants could be obtained for a second and third equivalent of halide, with decreased binding strength due to the association of the anion to the exterior of the receptor. Association constants were also obtained for NO₃⁻ ($\log K_{11} = 2.54$), OAc⁻ (3.21), HSO₄⁻ (1.93) and H₂PO₄⁻ (3.70). Binding studies with the related **73b** in MeCN-*d*₃ showed a marginal preference for chloride over bromide ($\log K_{11} = 3.85$ and 3.62, respectively) and strong binding of NO₃⁻ ($\log K_{11} = 3.46$) and OAc⁻ ($\log K_{11} = 4.61$). Further examples of tripodal anion receptors have been prepared by mechanochemical synthesis via the solvent drop method [75]. Further developments of this class of polypyridinium receptors have focused on the viologen-based receptors **75–77** [74, 76]. The addition of substoichiometric quantities of acetate, malonate and succinate to a solution of **75** in acetonitrile gave rapid formation of an intense purple coloration arising from the formation of a charge-transfer complex in solution. Similar coloration could be observed for receptor **76**, but required the addition of stoichiometric amounts of malonate or succinate and the addition of greater than one equivalent of acetate. Variation in the propensity of **75** and **76** to form the charge-transfer complex was attributed to the urea substituents binding the anion further away from the viologen unit, minimizing the charge-transfer effects. Saturation of the urea-binding sites of **76** allows the third equivalent to approach the viologen center, initiating the color change. Decomposition of the receptor was observed when the anion binding was undertaken in aerobic conditions. ¹H NMR titrations for **75** and **76** with the halides and nitrate revealed downfield shifts for only the *o*-pyridyl protons, indicating direct interaction for the anion with a 1:2 host:guest stoichiometry observed in each case.



A combination tripodal–viologen polypyridinium receptor was recently reported [76]. Halide ions were observed to bind to **74** in a 1:2 stoichiometry, with the first equivalent thought to bind close to the 4,4′-bipyridinium group, while the second occupies a position proximal to the benzyl groups. Chloride was observed to associate most strongly as the 1:1 complex in MeCN-*d*₃ (log K_{11} = 3.98, log K_{12} = 4.86), while bromide (log K_{11} = 3.63, log K_{12} = 6.03) and iodide (log K_{11} = 3.30, log K_{12} = 5.82) were bound less tightly. Colorimetric sensing and decomposition with acetate and malonate were also observed for this receptor.

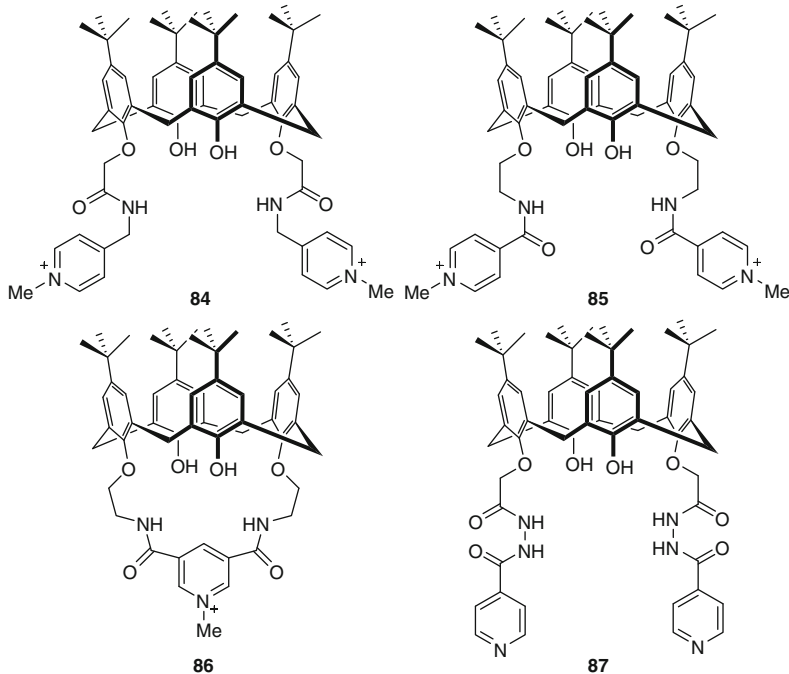
3.2 Macrocyclic Receptors

The macrocyclic effect has been further exploited in pyridinium-based anion receptors. The tetrapyridinium macrocycle **78** was prepared in one step from 3-bromomethylpyridine [77]. X-ray crystallographic analysis of the bromide salt indicated two of the four bromides located within the macrocyclic cavity. The binding of the tricarboxylate anions of **79–82** in D₂O at pH 7–8 was investigated by ¹H NMR spectroscopy titrations with a 1:1 binding stoichiometry determined for all four anions. Significant downfield shifts were observed for the internal pyridinium proton, with smaller upfield shifts observed for the remaining aryl resonances. The association constants were observed in the order **80** (log K_a = 5.1) > **81** (log K_a = 4.5) ≈ **79** (log K_a = 4.4) > **82** (log K_a = 4.1), indicating that the geometry was the determining factor in the binding of the equivalently charged anions to the receptor.



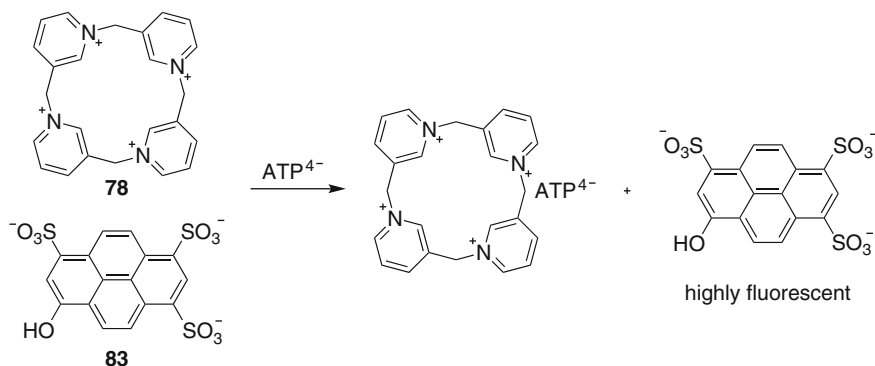
The calixpyridinium macrocycle–pyranine complex **78.83** ($K_a = 3.9 \times 10^5 \text{ M}^{-1}$ at pH 7.5 in MOPS buffer) was exploited in the sensing of ATP^{4-} by a fluorescence displacement assay [78]. Addition of the ATP^{4-} solution gave recovery of the pyranine emission, allowing for determination of the association constant of ATP^{4-} for the receptor **78**, $K_a = 2.87 \times 10^4 \text{ M}^{-1}$. Macrocycle **78** was also found to bind additional biologically relevant anions but with association constants an order of magnitude lower than ATP^{4-} (Scheme 1).

Three related lower rim substituted calix[4]arene receptors were reported to bind anionic guest species [79]. Receptor **84** was demonstrated by ^1H NMR titrations in $\text{DMSO-}d_6$ to bind Cl^- ($K_a = 8,350 \text{ M}^{-1}$), Br^- ($K_a = 170 \text{ M}^{-1}$), H_2PO_4^- ($K_a = 45,225 \text{ M}^{-1}$) and HSO_4^- ($K_a < 20 \text{ M}^{-1}$) with a 1:2 receptor/anion stoichiometry. The selectivity of the receptor for H_2PO_4^- was attributed to the higher basicity of the anion toward the amide groups. The receptor **85** forms a weaker complex with Cl^- ($K_a = 1,150 \text{ M}^{-1}$), whilst forming stronger adducts with Br^- ($K_a = 285 \text{ M}^{-1}$) and HSO_4^- ($K_a = 160 \text{ M}^{-1}$). An association constant could not be determined for H_2PO_4^- because of an unusual titration profile suggesting additional receptor/anion adduct stoichiometry in solution. The macrobicyclic receptor **86** was also shown to bind Cl^- ($K_a = 1,015 \text{ M}^{-1}$) and Br^- ($K_a = 705 \text{ M}^{-1}$) as 1:1 adducts.



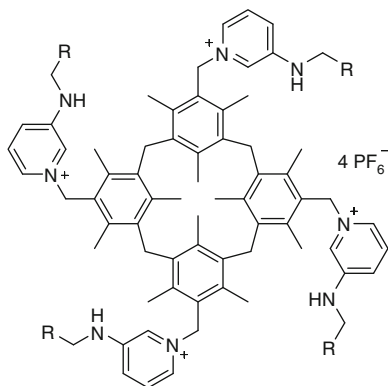
The related calix[4]arene-based anion transport agent **87** transports sodium dichromate from water into dichloromethane most effectively at low pH because of protonation of the pyridine substituents [80]. Two equilibria are in operation, one in which the monoprotonated receptor is paired with HCr_2O_7^- and the other involving the diprotonated receptor with $\text{Cr}_2\text{O}_7^{2-}$.

Following on from the tripodal receptors in Sect. 3.1, the related tetrapodal pyridinium anion receptor **88** was prepared for anion-binding experiments [81].



Scheme 1 Fluorescence displacement assay of ATP^{4-}

Anion-binding studies utilizing UV-visible titrations indicated 1:1 and 1:2 binding stoichiometry, with a preference for dicarboxylic acids. The second equilibrium constants for both malonate ($\log K_{11} = 5.5$, $\log K_{12} = 11.2$) and succinate ($\log K_{11} = 5.2$, $\log K_{12} = 11.2$), were significantly larger than the first, indicating the positive influence of anion binding on the conformation of the receptor in solution for the binding of a second equivalent. Luminescence of the receptor was only observed upon the addition of chloride, arising from a disruption of the self-quenching pyridinium groups.

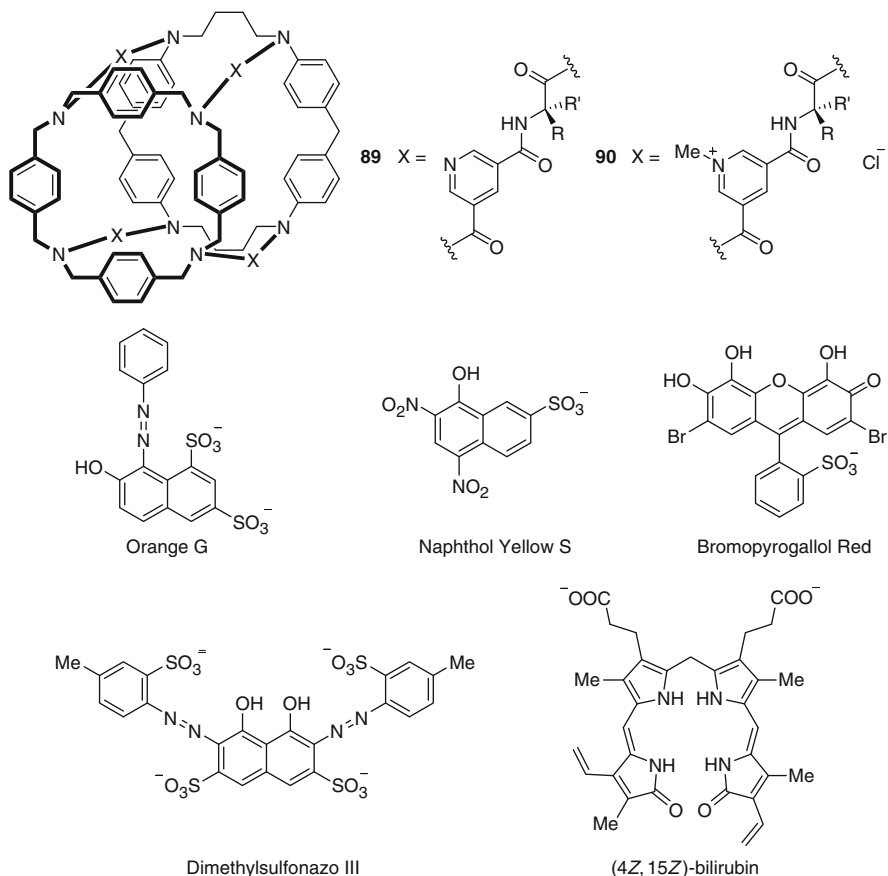


88 R = 1-pyrenyl

3.3 Macrobicyclic Receptors

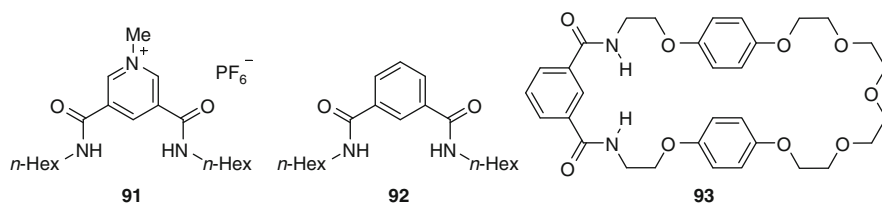
The chiral cyclophane receptor **89** has been investigated for the binding of a range of anions including anionic dyes. Initial anion binding investigations of **89** (R = H, R' = *i*-Pr) were undertaken with 8-anilinoanthalene-1-sulfonate, giving an association constant in 7:3 D_2O - $\text{DMSO}-d_6$ of $K_a = 4.3 \times 10^3 \text{ M}^{-1}$ [82]. Fluorescence

studies for 1:1 mixtures of 8-anilidonaphthalene-1-sulfonate and **89** ($R = H$, $R' = i\text{-Pr}$) in a buffered aqueous solution at pH 4.1 gave an association constant of $K_a = 2.8 \times 10^4 \text{ M}^{-1}$. The pyridinium derivative **90** ($R = H$, $R' = i\text{-Pr}$) was shown to bind anionic dyes with the association constants determined for Orange G ($K_a = 1.2 \times 10^5 \text{ M}^{-1}$), Naphthol Yellow S ($K_a = 3.7 \times 10^5 \text{ M}^{-1}$), Bromopyrogallol Red ($K_a = 2.5 \times 10^5 \text{ M}^{-1}$) and Dimethylsulfonazo III ($K_a = 3.4 \times 10^5 \text{ M}^{-1}$) as 1:1 complexes in an aqueous HEPES-buffered solution [83, 84]. Further investigations with the enantiomers of the pyridinium host **90** showed the ability of the host to discriminate between the conformational enantiomers of the biologically significant dicarboxylate (4*Z*,15*Z*)-bilirubin. Analysis of the circular dichroism spectrum of the host (+)-**90** ($R = H$, $R' = i\text{-Pr}$) upon addition of (4*Z*,15*Z*)-bilirubin revealed the appearance of bands corresponding to the guest chromophore within the chiral environment of the host [85]. The inverse CD spectrum was observed for (–)-**90** ($R = i\text{-Pr}$, $R' = H$). (4*Z*,15*Z*)-bilirubin complex, indicative of the *R*-helical form of (4*Z*,15*Z*)-bilirubin binding within the cavity. Further investigations were made into systems derived from other amino acids, and were shown to possess similar binding properties to those discussed above [86].



3.4 Interpenetrated and Interlocked Receptors

In Nature, strong and highly selective binding of sulfate and phosphate anions in water is achieved by specific proteins possessing a hydrogen bond based anion-binding site buried deep within the three-dimensional structure [87–90]. The majority of the acyclic and macrocyclic receptors discussed previously in this report are limited to operating in aprotic organic solvents, frequently with the bound anion directly exposed to the solvent. Interlocked anion receptors provide a synthetic approach to developing protected anion-binding microenvironments, with total encapsulation of the anion within a hydrophobic binding site. These interlocked species bind anions with significantly greater affinity than their separate components, and generally with greater selectivity. The development of interlocked anion receptors was preceded by the investigation of interpenetrated assemblies. The pyridinium-3,5-bisamide **91** forms a tight ion pair with chloride in acetone- d_6 ($K_a > 10^5 \text{ M}^{-1}$), leaving the remaining coordination hemisphere of the halide anion unsaturated. A 1:1 association constant ($K_a = 100 \text{ M}^{-1}$) was observed for the addition of a solution of **91**.Cl to **92** in acetone- d_6 [91]. No association was observed for **91**.PF₆ with **92** under identical conditions, indicating the necessity of the halide in the templating of the orthogonally coordinated species.



The tight ion pair **91**.Cl was observed to thread through macrocycle **93** to form a pseudorotaxane in solution (**94**). Formation was templated by the chloride anion, and gave rise to a charge-transfer transition at 370 nm as determined by UV–visible spectroscopy, manifest as a pale yellow color. Additional noncovalent interactions between the electron-deficient pyridinium and the electron-rich hydroquinone groups, and the methyl group and the polyether chain, assisted in the threading. No charge-transfer transition was observed with Br[−], I[−] or PF₆[−], further demonstrating the necessity of the chloride anion template in threading. Binding of the ion pair to the macrocycle was also monitored by ¹H NMR spectroscopy titrations, with association constants determined for the macrocycle **93** with **91**.Cl ($K_a = 2,400 \text{ M}^{-1}$), **91**.Br ($K_a = 700 \text{ M}^{-1}$) and **91**.I ($K_a = 65 \text{ M}^{-1}$) in acetone- d_6 . X-ray crystallographic analysis of the adduct **94** showed the halide held by six hydrogen bonds: four from amide N–H forming a pseudotetrahedral cavity, assisted by the adjacent C–H groups (Fig. 5).

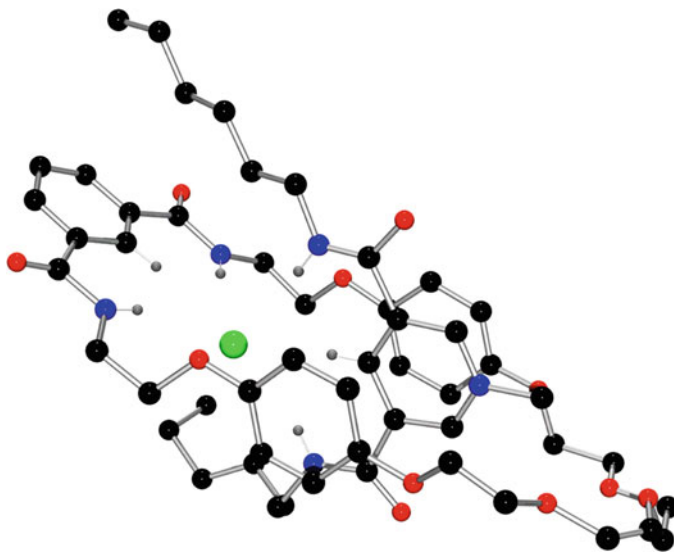
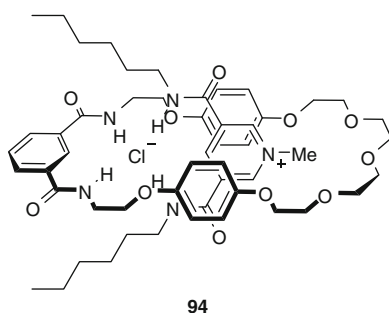
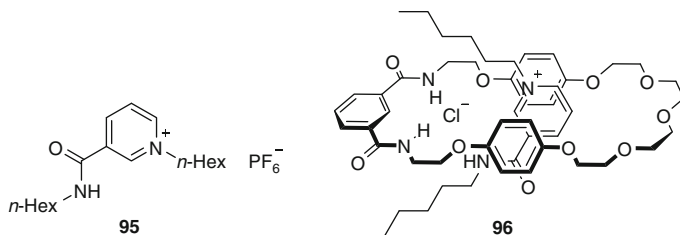
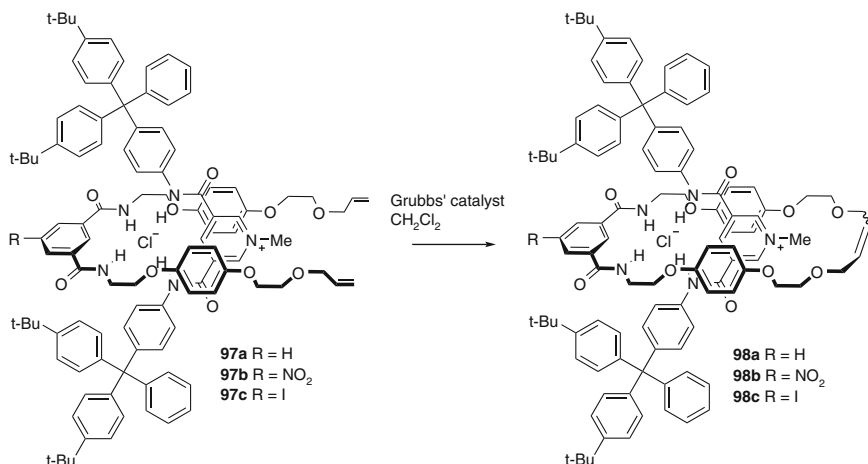


Fig. 5 X-ray crystal structure of **94**



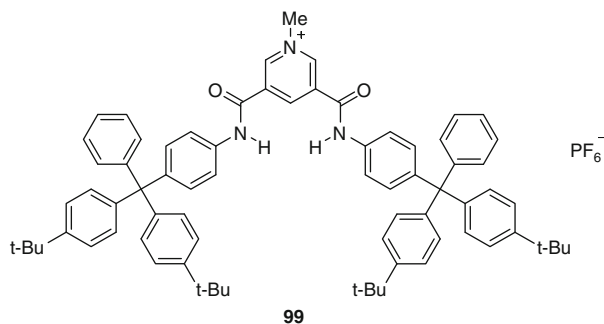
Pseudorotaxane anion binding was also reported for the nicotinamide thread **94** [92]. ^1H NMR titrations in acetone- d_6 showed that the chloride was held between the amide proton and the 2-position of the pyridinium ring with a very large association constant ($K_a > 10^5 \text{ M}^{-1}$). The tight **95**.Cl ion pair was shown to bind with the acyclic isophthalamide **92** ($K_a = 1,100 \text{ M}^{-1}$) and the macrocycle **93** ($K_a = 2,100 \text{ M}^{-1}$) to give the pseudorotaxane **96**. The nicotinamide thread **95**.PF $_6$ did not display any affinity for either **92** or **93**.



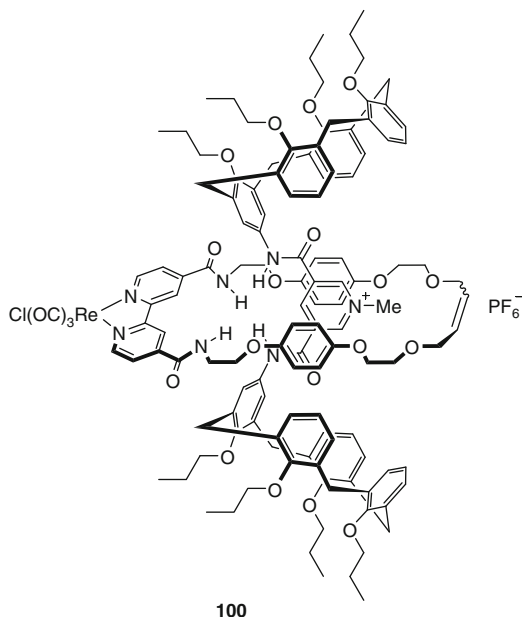


Scheme 2 Grubbs' catalyzed ring-closing metathesis for [2]rotaxane synthesis

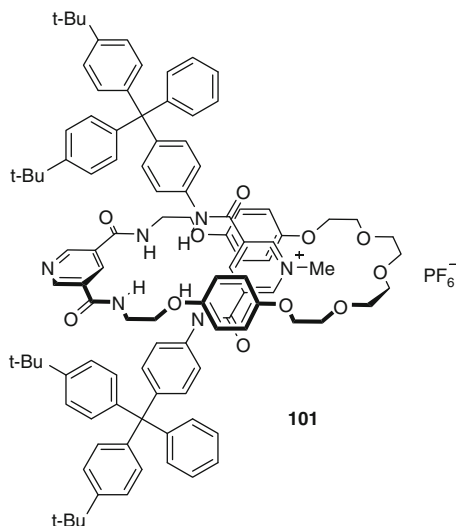
The [2]rotaxane **98a** was prepared by the chloride-templated Grubbs' metathesis of **97a** (Scheme 2) [93]. Exchange of the chloride for hexafluorophosphate gave the interlocked anion receptor **98a**.PF₆. ¹H NMR titrations in 1:1 CDCl₃/CD₃OD indicated a significant preference for Cl⁻ ($K_{11} = 1,130 \text{ M}^{-1}$) over H₂PO₄⁻ ($K_{11} = 300 \text{ M}^{-1}$) and OAc⁻ ($K_{11} = 100 \text{ M}^{-1}$, $K_{12} = 40 \text{ M}^{-1}$). The interlocked structure showed significant differences in anion preference, as the stoppered thread **99** showed a clear preference for the basicity of the anion viz. Cl⁻ ($K_{11} = 125 \text{ M}^{-1}$), H₂PO₄⁻ ($K_{11} = 260 \text{ M}^{-1}$) and OAc⁻ ($K_{11} = 2,200 \text{ M}^{-1}$, $K_{12} = 140 \text{ M}^{-1}$). The reverse order of anion selectivity was attributed to the restricted anion binding site formed by the preorganized tetrahedral cavity of the interlocked species, complementary to the chloride ion. The binding of the larger oxoanions presumably occurs to the exterior of the anion binding site, or results in significant deviation away from the idealized tetrahedral geometry of the cavity. Further functionalization of the macrocycle precursor with nitro (**97b**) or iodo (**97c**) groups dramatically increased the strength of binding of the interlocked structure to the anionic species while maintaining the high selectivity for chloride [94]. The association constants for the nitro-functionalized rotaxane **98b** were determined by ¹H NMR spectroscopy titrations as Cl⁻ ($K_{11} = 4,500 \text{ M}^{-1}$), H₂PO₄⁻ ($K_{11} = 1,500 \text{ M}^{-1}$) and OAc⁻ ($K_{11} = 725 \text{ M}^{-1}$), whilst the iodo-functionalized **98c** gave association constants of Cl⁻ ($K_{11} = 4,500 \text{ M}^{-1}$), H₂PO₄⁻ ($K_{11} = 1,800 \text{ M}^{-1}$, $K_{12} = 180 \text{ M}^{-1}$) and OAc⁻ ($K_{11} = 930 \text{ M}^{-1}$).



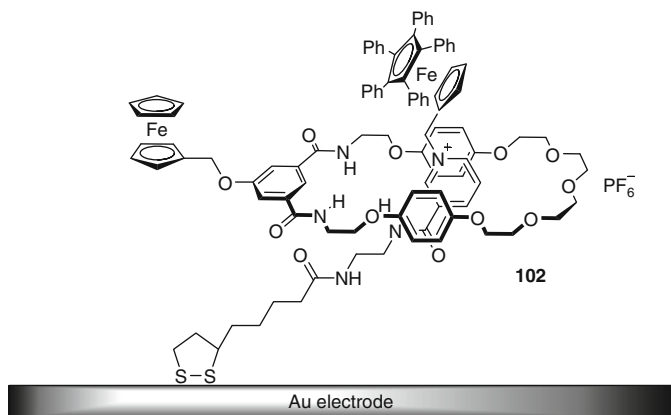
The rhenium(I)bipyridine–calixarene stoppered rotaxane **100** was prepared for the luminescent sensing of anions [95]. Significant enhancement of MLCT transition emission was observed by UV–visible titrations in acetone upon the addition of Cl^- ($K_a = 1.81 \times 10^5 \text{ M}^{-1}$) and NO_3^- ($K_a = 5.13 \times 10^4 \text{ M}^{-1}$), with the largest changes observed for the addition of HSO_4^- ($K_a > 10^6 \text{ M}^{-1}$).



The mixed pyridine–pyridinium interlocked anion receptor **101** was prepared by a novel clipping strategy templated by the chloride ion with the rotaxane isolated in 32% yield [96]. Binding studies were undertaken in 1:1 $\text{CDCl}_3/\text{CD}_3\text{OD}$, analogous to the interlocked species shown above, and indicated preference of the rotaxane for chloride over the oxoanions. The binding of the chloride was too large for determination in this solvent system ($K_a > 10^4 \text{ M}^{-1}$), whilst association constants were determined for the more weakly binding H_2PO_4^- ($K_a = 720 \text{ M}^{-1}$) and OAc^- ($K_a = 520 \text{ M}^{-1}$). Binding studies were undertaken in the more competitive 45:45:10 $\text{CDCl}_3:\text{CD}_3\text{OD}:\text{H}_2\text{O}$ solvent mixture and enabled association constants to be obtained for Cl^- ($K_a = 1,500 \text{ M}^{-1}$), Br^- ($K_a = 780 \text{ M}^{-1}$), H_2PO_4^- ($K_a = 60 \text{ M}^{-1}$) and OAc^- ($K_a = 110 \text{ M}^{-1}$). Observations of the proton resonance changes during the titrations indicated differing modes of binding of Br^- , H_2PO_4^- and OAc^- to that of the Cl^- ion.

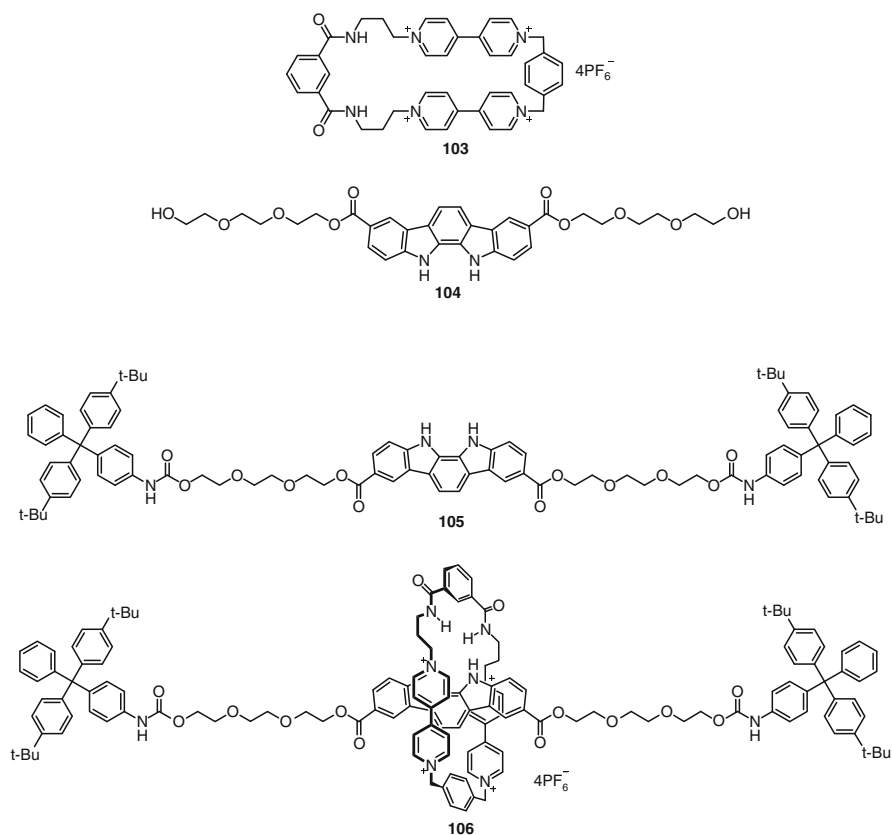


Anion sensing has also been reported for surface-bound rotaxanes via electrochemical methods [97]. The surface-bound rotaxane **102** demonstrated a cathodic shift in the redox potential of the macrocycle-appended ferrocene upon the addition of chloride ($\Delta E = 40 \pm 5$ mV) in acetonitrile. No response ($\Delta E < 8$ mV) was detected for the same ferrocene upon the addition of excess H_2PO_4^- , HSO_4^- , OAc^- , NO_3^- , Br^- and F^- , indicating a marked selectivity of the binding cavity toward the chloride ion.

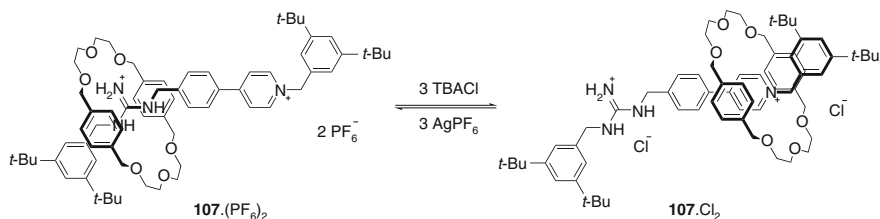


Further pyridinium-based interlocked species were investigated for the tetrapyrrolium macrocycle **103**, which was prepared for the formation of interpenetrated species with the indolocarbazole thread **104** and for rotaxane formation with the axle **105** [98]. The tetrapositive macrocycle gave association constants in

DMSO- d_6 by ^1H NMR titrations for Cl^- ($K_a = 380 \text{ M}^{-1}$), Br^- ($K_a = 150 \text{ M}^{-1}$), I^- ($K_a = 60 \text{ M}^{-1}$) and NO_3^- ($K_a = 40 \text{ M}^{-1}$), whilst the rotaxane **106** gave enhanced association constants for Cl^- ($K_a = 3,000 \text{ M}^{-1}$), Br^- ($K_a = 850 \text{ M}^{-1}$) and I^- ($K_a = 90 \text{ M}^{-1}$). Cooperative binding of the halide ions to the rotaxane was indicated by the increased association constants for the interlocked species with hydrogen bond donation from both the isophthalamide and indolocarbazole moieties. The addition of TBA salts of OAc^- , H_2PO_4^- , F^- and SO_4^{2-} gave decomposition of the macrocycle and rotaxane by one-electron reduction of the bipyridinium groups. Molecular dynamics simulations of anion binding to the rotaxane indicated that anion binding is an enthalpically driven process directed by the hydrogen bond donation. These calculations also indicated a size preference for the smaller Cl^- and Br^- anions compared to the larger I^- and NO_3^- anions.



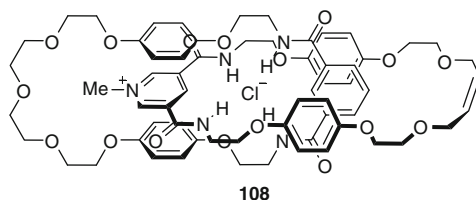
An interlocked anion-responsive molecular switch (**107**) has been developed featuring a polyether macrocycle and a two-station guanidinium/pyridinium axle (Scheme 3) [99]. The macrocycle was observed by ^1H NMR spectroscopy to



Scheme 3 A switchable guanidinium/pyridinium molecular switch

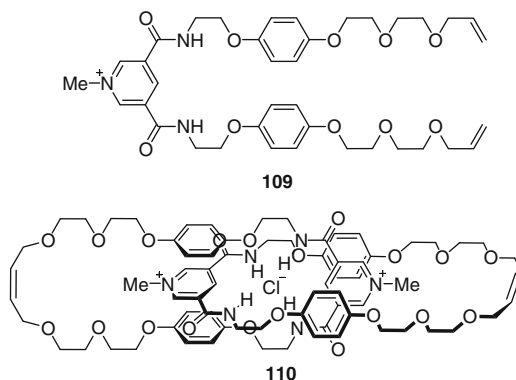
surround the guanidinium station in CDCl_3 , whilst in $\text{MeCN-}d_3$ the macrocycle surrounds the pyridinium site. The macrocycle position could be switched in CD_3NO_2 by the addition of three equivalents of TBACl, resulting in the upfield shifts of the pyridinium proton resonances and the aryl protons of the macrocycle. These changes imply that the macrocycle is present around the pyridinium thread, as confirmed by 2D NOESY spectroscopy. Removal of the chloride anions with three equiv. AgPF_6 in the same solvent resulted in a similar spectrum to the starting material. Anion-initiated switching of the rotaxane could also be undertaken by the addition or removal of bromide or acetate.

The first example of a chloride-templated catenane (**108.Cl**) was prepared in 45% yield by ring-closing metathesis with Grubbs' catalyst, similar to the strategy used for rotaxane **98** [100]. The interlocked receptor showed significant enhancement of chloride binding in 1:1 $\text{CDCl}_3/\text{CD}_3\text{OD}$ ($K_{11} = 730 \text{ M}^{-1}$), with binding significantly stronger than that observed for H_2PO_4^- ($K_{11} = 480 \text{ M}^{-1}$, $K_{12} = 520 \text{ M}^{-1}$) and OAc^- ($K_{11} = 230 \text{ M}^{-1}$), a reversal in trend compared to the acyclic precursors.

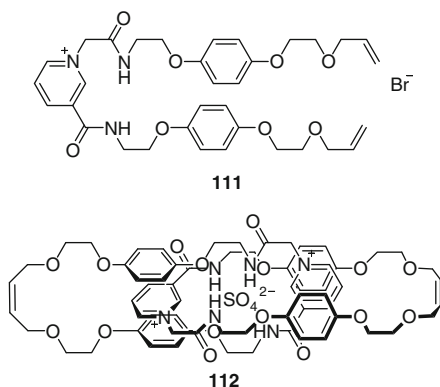


Chloride templation of catenane synthesis was also applied for the double cyclization of the pyridinium precursors **109.Cl** and **109.PF₆** in a remarkably high yield of 80% [101]. Comparison by ^1H NMR spectroscopy of **110**.(PF_6)₂ and **110**.(Cl)(PF_6) indicated significant downfield shifts of the amide protons in the latter, indicative of binding of the chloride anion within the tetrahedral cavity formed between the two pyridinium-bisamide groups. Association constants of anions to **110**.(PF_6)₂ were determined by ^1H NMR titrations in 1:1 $\text{CDCl}_3:\text{CD}_3\text{OD}$, with Cl^- ($K_{11} = 9,240 \text{ M}^{-1}$, $K_{12} = 160 \text{ M}^{-1}$) binding more strongly than Br^- ($K_{11} = 790 \text{ M}^{-1}$, $K_{12} = 40 \text{ M}^{-1}$) and OAc^- ($K_{11} = 420 \text{ M}^{-1}$, $K_{12} = 40 \text{ M}^{-1}$). The bromide was postulated to bind outside of the anion-binding cavity through electrostatic interactions with the pyridinium ring. Further interactions with F^- and H_2PO_4^-

were observed by ^1H NMR spectroscopy; however, no association constants could be determined. Competitive electrospray mass spectrometry experiments further demonstrated the selectivity for chloride as only $\text{M}^+ = \mathbf{110}.\text{Cl}$ was detected from a mixture of the catenane with equimolar amounts of chloride, fluoride, acetate, dihydrogen phosphate, hydrogen sulfate and nitrate. This selectivity is attributed to the topologically constrained anion-binding site.



Sulfate-templated catenation was also undertaken for the nicotinamide precursor **111** with Grubbs' second generation catalyst forming the catenane **112** in 80% yield [102]. ^1H NMR titrations with the hexafluorophosphate salt **112**(PF₆)₂ in 1:1 CDCl₃/CD₃OD indicated downfield shifts of the amide and pyridinium protons upon the addition of anions. Sulfate was shown to bind with greatest affinity ($K_a = 2,200 \text{ M}^{-1}$), with weaker binding for Cl⁻ ($K_a = 780 \text{ M}^{-1}$) and Br⁻ ($K_a = 55 \text{ M}^{-1}$) and with no binding observed for OAc⁻. Significant enhancement of anion binding was observed for the interlocked **112** compared to the acyclic precursor **111** ($K_a = 1,120 \text{ M}^{-1}$). The absence of binding of acetate to **112** was striking, given the strong binding to the acyclic precursor **111** ($K_a = 1,850 \text{ M}^{-1}$).



4 Conclusion

This review highlights recent developments in pyridine and pyridinium-based anion receptors. The synthetic versatility of the heterocyclic framework has allowed for the preparation of a diverse range of receptors, displaying strong affinity to a similarly diverse range of anions. Significant advances have been made in the refinement of the anion-binding sites, with increasing sophistication of interlocked host structures, enabling the binding of anions under increasingly competitive solvent conditions. Future work with pyridine and pyridinium-based anion receptors will continue to refine the selectivity and efficacy of anion receptors through topological restriction of anion-binding sites, striving toward the goal of strong anion binding under aqueous solvent conditions.

Acknowledgments NLK gratefully acknowledges the Royal Commission for the Exhibition of 1851 for a research fellowship.

References

1. Berg JM, Tymoczko JL, Stryer L (2006) *Biochemistry*. W. H. Freeman and Co., New York
2. Berger AL, Randak CO, Ostedgaard LS, Karp PH, Vermeer DW, Welsh MJ (2005) *J Biol Chem* 280:5221
3. Pearce JMS (2002) *J Neurol Neurosurg Psychiatry* 72:412
4. Moss B (1996) *Chem Ind (London)*:407
5. O'Hara MJ, Burge SR, Grate JW (2009) *Anal Chem* 81:1068
6. Rice CR (2006) *Coord Chem Rev* 250:3190
7. Bayly SR, Beer PD (2008) *Struct Bond* 129:45
8. Hamuro Y, Geib SJ, Hamilton AD (1996) *J Am Chem Soc* 118:7529
9. Hunter CA, Purvis DH (1992) *Angew Chem Int Ed* 31:792
10. Kavallieratos K, Bertao CM, Crabtree RH (1999) *J Org Chem* 64:1675
11. Liao J-H, Chen C-T, Fang J-M (2002) *Org Lett* 4:561
12. Xu K-X, Qing G-Y, He Y-B, Qin H-J, Hu L (2007) *Supramol Chem* 19:403
13. Duke RM, O'Brien JE, McCabe T, Gunnlaugsson T (2008) *Org Biomol Chem* 6:4089
14. Bates GW, Gale PA, Light ME (2007) *Chem Commun*:2121
15. Zieliński T, Dydio P, Jurczak J (2008) *Tetrahedron* 64:568
16. Beer PD, Graydon AR, Johnson AOM, Smith DK (1997) *Inorg Chem* 36:2112
17. Otón F, Tárraga A, Espinosa A, Velasco MD, Molina P (2006) *Dalton Trans*:3685
18. Kyne GM, Light ME, Hursthouse MB, de Mendoza J, Kilburn JD (2001) *J Chem Soc Perkin Trans 1*:1258
19. Yang R, Liu W-X, Shen H, Huang H-H, Jiang Y-B (2008) *J Phys Chem B* 112:5105
20. Beer PD, Drew MGB, Graydon AR (1996) *J Chem Soc Dalton Trans*:4129
21. Sun S-S, Lees AJ, Zavalij PY (2003) *Inorg Chem* 42:3445
22. Schmuck C, Machon U (2005) *Chem Eur J* 11:1109
23. Ranganathan D, Haridas V, Karle IL (1998) *J Am Chem Soc* 120:2695
24. Szumna A, Jurczak J (2001) *Eur J Org Chem*:4031
25. Szumna A, Jurczak J (2001) *Helv Chim Acta* 84:3760
26. Chmielewski M, Jurczak J (2004) *Tetrahedron Lett* 45:6007
27. Chmielewski MJ, Szumna A, Jurczak J (2004) *Tetrahedron Lett* 45:8699

28. Chmielewski MJ, Jurczak J (2005) *Tetrahedron Lett* 46:3085
29. Chmielewski MJ, Jurczak J (2005) *Chem Eur J* 11:6080
30. Huang H, Mu L, He J, Cheng J-P (2002) *Tetrahedron Lett* 43:2255
31. Zhang Y, Yin Z, He J, Cheng J-P (2007) *Tetrahedron Lett* 48:6039
32. Sessler JL, Katayev E, Pantos GD, Ustynyuk YA (2004) *Chem Commun*:1276
33. Sessler JL, Katayev E, Pantos GD, Scherbakov P, Reshetova MD, Khrustalev VN, Lynch VM, Ustynyuk YA (2005) *J Am Chem Soc* 127:11442
34. Katayev EA, Pantos GD, Reshetova MD, Khrustalev VN, Lynch VM, Ustynyuk YA, Sessler JL (2005) *Angew Chem Int Ed* 44:7386
35. Katayev EA, Sessler JL, Khrustalev VN, Ustynyuk YA (2007) *J Org Chem* 72:7244
36. Brooks SJ, García-Garrido SE, Light ME, Cole PA, Gale PA (2007) *Chem Eur J* 13:3320
37. Hossain MA, Kang SO, Powell D, Bowman-James K (2003) *Inorg Chem* 42:1397
38. Hossain MA, Kang SO, Llinares JM, Powell D, Bowman-James K (2003) *Inorg Chem* 42:5043
39. Kang SO, Day VW, Bowman-James K (2009) *Org Lett* 11:3654
40. Kubik S, Goddard R, Kirchner R, Nolting D, Seidel J (2001) *Angew Chem Int Ed* 40:2648
41. Kubik S, Goddard R (2002) *Proc Natl Acad Sci USA* 99:5127
42. Kubik S, Kirchner R, Nolting D, Seidel J (2002) *J Am Chem Soc* 124:12752
43. Kubik S, Goddard R, Otto S, Pohl S, Reyheller C, Stüwe S (2005) *Biosens Bioelectron* 20:2364
44. Otto S, Kubik S (2003) *J Am Chem Soc* 125:7804
45. Reyheller C, Hay BP, Kubik S (2007) *New J Chem* 31:2095
46. Reyheller C, Kubik S (2007) *Org Lett* 9:5271
47. Li Y, Pink M, Karty JA, Flood AH (2008) *J Am Chem Soc* 130:17293
48. Ghosh S, Roehm B, Begum RA, Kut J, Hossain MA, Day VW, Bowman-James K (2007) *Inorg Chem* 46:9519
49. Chellappan K, Singh NJ, Hwang I-C, Lee JW, Kim KS (2005) *Angew Chem Int Ed* 44:2899
50. Niu H-T, Yin Z, Su D, Niu D, Ao Y, He J, Cheng J-P (2008) *Tetrahedron* 64:6300
51. Yuan Y, Gao G, Jiang Z-L, You J-S, Zhou Z-Y, Yuan D-Q, Xie R-G (2002) *Tetrahedron* 58:8993
52. Khatri VK, Chahar M, Pavani K, Pandey PS (2007) *J Org Chem* 72:10224
53. Sansone F, Baldini L, Casnati A, Lazzarotto M, Ugozzoli F, Ungaro R (2002) *Proc Natl Acad Sci USA* 99:4842
54. Bisson AP, Lynch VM, Monahan M-KC, Anslyn EV (1997) *Angew Chem Int Ed* 36:2340
55. Niikura K, Bisson AP, Anslyn EV (1999) *J Chem Soc Perkin Trans* 2:1111
56. Kang SO, Llinares JM, Powell D, VanderVelde D, Bowman-James K (2003) *J Am Chem Soc* 125:10152
57. Kang SO, Day VW, Bowman-James K (2010) *J Org Chem* 75:277
58. Kang SO, VanderVelde D, Powell D, Bowman-James K (2004) *J Am Chem Soc* 126:12272
59. Kang SO, Hossain MA, Powell D, Bowman-James K (2005) *Chem Commun*:328
60. Kang SO, Powell D, Bowman-James K (2005) *J Am Chem Soc* 127:13478
61. Esteban-Gómez D, Platas-Iglesias C, de Blas A, Fabbrizzi L, Rodríguez-Blas T (2008) *Chem Eur J* 14:5829
62. Morgan G, McKee V, Nelson J (1995) *J Chem Soc Chem Commun*:1649
63. McKee V, Morgan GG (2003) *Acta Crystallogr Sect C Cryst Struct Commun* 59:o150
64. Farrell D, Gloe K, Gloe K, Goretzki G, McKee V, Nelson J, Nieuwenhuysen M, Pál I, Stephan H, Town RM, Wichmann K (2003) *Dalton Trans*:1961
65. Mateus P, Delgado R, Brandão P, Félix V (2009) *J Org Chem* 74:8638
66. Jeong K-S, Cho YL (1997) *Tetrahedron Lett* 38:3279
67. Amendola V, Boiocchi M, Fabbrizzi L, Palchetti A (2005) *Chem Eur J* 11:120
68. Beer PD, Wheeler JW, Grieve A, Moore C, Wear T (1992) *J Chem Soc Chem Commun*:1225
69. Beer PD, Fletcher NC, Grieve A, Wheeler JW, Moore CP, Wear T (1996) *J Chem Soc Perkin Trans* 2:1545

70. Beer PD, Fletcher NC, Wear T (1996) *Inorg Chim Acta* 251:335
71. Abouderbala LO, Belcher WJ, Boutelle MG, Cragg PJ, Dhaliwal J, Fabre M, Steed JW, Turner DR, Wallace KJ (2002) *Chem Commun*:358
72. Abouderbala LO, Belcher WJ, Boutelle MG, Cragg PJ, Steed JW, Turner DR, Wallace KJ (2002) *Proc Natl Acad Sci USA* 99:5001
73. Turner DR, Paterson MJ, Steed JW (2006) *J Org Chem* 71:1598
74. Dickson SJ, Wallace EVB, Swinburne AN, Paterson MJ, Lloyd GO, Beeby A, Belcher WJ, Steed JW (2008) *New J Chem* 32:786
75. Swinburne AN, Steed JW (2009) *CrystEngComm* 11:433
76. Swinburne AN, Paterson MJ, Fischer KH, Dickson SJ, Wallace EVB, Belcher WJ, Beeby A, Steed JW (2010) *Chem Eur J* 16:1480
77. Shinoda S, Tadokoro M, Tsukube H, Arakawa R (1998) *Chem Commun*:181
78. Atilgan S, Akkaya EU (2004) *Tetrahedron Lett* 45:9269
79. Beer PD, Drew MGB, Gradwell K (2000) *J Chem Soc Perkin Trans* 2:511
80. Tabakci M, Memon S, Yilmaz M, Roundhill DM (2003) *J Inclusion Phenom Macrocyclic Chem* 45:265
81. Filby MH, Dickson SJ, Zaccheroni N, Prodi L, Bonacchi S, Montalti M, Paterson MJ, Humphries TD, Chiorboli C, Steed JW (2008) *J Am Chem Soc* 130:4105
82. Murakami Y, Ohno T, Hayashida O, Hisaeda Y (1991) *J Chem Soc Chem Commun*:950
83. Murakami Y, Ohno T, Hayashida O, Hisaeda Y (1991) *Chem Lett*:1595
84. Murakami Y, Hayashida O, Ito T, Hisaeda Y (1993) *Pure Appl Chem* 65:551
85. Murakami Y, Hayashida O, Nagai Y (1994) *J Am Chem Soc* 116:2611
86. Hayashida O, Ono K, Hisaeda Y, Murakami Y (1995) *Tetrahedron* 51:8423
87. Pflugrath JW, Quioco FA (1985) *Nature* 314:257
88. Luecke H, Quioco FA (1990) *Nature* 347:402
89. He JJ, Quioco FA (1991) *Science* 251:1479
90. Kanyo ZF, Christianson DW (1991) *J Biol Chem* 266:4264
91. Wisner JA, Beer PD, Drew MGB (2001) *Angew Chem Int Ed* 40:3606
92. Wisner JA, Beer PD, Berry NG, Tomapatanaget B (2002) *Proc Natl Acad Sci USA* 99:4983
93. Wisner JA, Beer PD, Drew MGB, Sambrook MR (2002) *J Am Chem Soc* 124:12469
94. Sambrook MR, Beer PD, Lankshear MD, Ludlow RF, Wisner JA (2006) *Org Biomol Chem* 4:1529
95. Curiel D, Beer PD (2005) *Chem Commun*:1909
96. Hancock LM, Beer PD (2009) *Chem Eur J* 15:42
97. Bayly SR, Gray TM, Chmielewski MJ, Davis JJ, Beer PD (2007) *Chem Commun*:2234
98. Brown A, Mullen KM, Ryu J, Chmielewski MJ, Santos SM, Félix V, Thompson AL, Warren JE, Pascu SI, Beer PD (2009) *J Am Chem Soc* 131:4937
99. Lin T-C, Lai C-C, Chiu S-H (2009) *Org Lett* 11:613
100. Sambrook MR, Beer PD, Wisner JA, Paul RL, Cowley AR (2004) *J Am Chem Soc* 126:15364
101. Ng K-Y, Cowley AR, Beer PD (2006) *Chem Commun*:3676
102. Huang B, Santos SM, Félix V, Beer PD (2008) *Chem Commun*:4610

1,2,3-Triazoles and the Expanding Utility of Charge Neutral CH \cdots Anion Interactions

Kevin P. McDonald, Yuran Hua, and Amar H. Flood

Abstract As the field of anion supramolecular chemistry continues to grow in its sophistication and understanding of the noncovalent interactions used to effectively bind anions, there exists new theoretical and experimental evidence for a necessary reexamination of the way in which the field views hydrogen bond donors. The heteroatom based hydrogen-bond donors (e.g., NH and OH) are well-known to provide strong stabilization to negatively charged species. However, new findings point to the untapped stabilization energy that lay dormant in extrinsically-activated CH hydrogen bonds. Computational studies showed that an activated aliphatic or aromatic CH can provide an amount of anion stabilization in the gas phase approaching that of conventional NH based donors. Discovery of the Cu(I)-catalyzed Huisgen 1,3-dipolar cycloaddition to provide 1,2,3-triazoles and the ability to readily “click” this functionality into anion receptors has allowed extensive experimental investigation of the ideas posed by these calculations. This chapter will focus on the evolution of the CH hydrogen bond from being viewed as a weak, secondary interaction to now being utilized as a powerful source of anion stabilization in macrocyclic and oligomeric receptors. In addition, the application of the anion binding power of the 1,2,3-triazole towards the preparation of mechanically interlocked structures will also be discussed.

Keywords Anion complexation · Click chemistry · Hydrogen bonding · Receptor design · Supramolecular chemistry

K.P. McDonald, Y. Hua, and A.H. Flood (✉)
Department of Chemistry, Indiana University, Bloomington, IN 47405, USA
e-mail: aflood@indiana.edu

Contents

1	Introduction	342
1.1	Motivation	342
1.2	Design Aspects of Receptors	344
1.3	CH Hydrogen Bond Donors: Weak and Secondary Interactions or Potentially Strong Sources of Anion Stabilization?	345
1.4	2005: A Computationally Inspired Change in Philosophy	347
1.5	Experimental Exploration of Charge Neutral CH \cdots X $^-$ Interactions in Anion Receptors	348
2	The 1,2,3-Triazole: Experimental and Computational Investigation of Its Anion Binding Affinity in Macrocyclic Triazolophanes	350
2.1	“Click” Chemistry: The Philosophy and the Cu(I)-Catalyzed Huisgen 1,3-Dipolar Cycloaddition	350
2.2	The Functional 1,2,3-Triazole Unit and Macrocyclic Triazolophanes	351
2.3	Calculations on Hydrogen Bond Donor Strength of 1,4-Diaryl-1,2,3-Triazole	353
2.4	Investigating the Tunability of the Phenylene’s CH Hydrogen-Bond Donor Strength	354
2.5	Sandwich Complexes and Positive Cooperativity	355
3	Expanding the Utility of 1,2,3-Triazoles in Anion Supramolecular Chemistry	358
3.1	Triazole Foldamers: The Role of Preorganization	358
3.2	Additional Applications of Triazole CH \cdots X $^-$ in Anion Receptors	359
3.3	Triazolium: A New-Age Surrogate for the Amine-Ammonium Pair?	360
3.4	Triazolium CH \cdots X $^-$ Interactions in Anion Templatation	362
3.5	Triazolophane-Based Ion Selective Electrodes	363
4	Concluding Remarks	363
	References	364

Abbreviations

CD	Circular dichroism
DB24C8	Dibenzo[24]crown-8
DIEA	Diisopropylethylamine
DMF	<i>N,N</i> -dimethylformamide
DMSO	Dimethylsulfoxide
ESI-MS	Electrospray ionization mass spectrometry
TBACl	Tetrabutylammonium chloride

1 Introduction

1.1 Motivation

Anions are ubiquitous. The binding and transport [1, 2] of anions are processes carried out an infinite number of times inside cells every day. They are not only found in enzymatic [3] and other biochemical [4] processes (e.g., chloride,

carbonate, dihydrogen phosphate) but also range from those used in fertilizers (nitrate) [5] to those involved in various industrial processes (perchlorate [6, 7], chromate [8], pertechnetate [8]). On account of the fact that anions are vital to the proper operation of cellular processes, simple fluctuations in their concentration or the presence of toxic anions can lead to health issues. For instance, disruption of chloride transport has been linked to cystic fibrosis. A common route in which humans have been exposed to these toxic anions is from groundwater contamination. Many of these anions possess high thermodynamic stability and environmental mobilities and, as a result, have posed a problem for environmental chemists charged with monitoring and extracting these anions from solution. In particular, a discovery of elevated perchlorate concentration [9] in drinking water has raised concern with the US Environmental Protection Agency, particularly when perchlorate has been found to disrupt proper thyroid function. With this greater understanding of how anions can affect key biological processes, research in the field of anion supramolecular chemistry – anion binding and remediation utilizing noncovalent interactions [10, 11] – has seen exponential growth in the last 20 years. These activities have led to applications in ion selective electrodes [12–14], which can be used for measuring chloride and phosphate concentrations in the human body, as well as to the design of selective receptors for use in environmental anion remediation and liquid-liquid extractions [15, 16]. At the foundation of these advances in anion receptor chemistry lies the application of new synthetic methodologies to allow for the creation of these novel receptors.

Nature has long stood as the main source of inspiration for the development of scientific research programs. Along these lines, the synthetic branches of chemistry have continued to grow in their sophistication and capacity to emulate the complexity illustrated in biological systems, be they natural products or self-assembled supramolecular structures. The target-oriented synthesis of biologically active natural products describes the “classic” field of total synthesis [17], where chemists design synthetic pathways along which construction of the natural product’s framework and molecular complexity can be realized. Supramolecular chemistry, as a new and closely related field, takes its inspiration from the self-organized and hierarchically ordered structures seen in nature. This new field applies nature’s lessons towards the preparation and characterization of novel synthetic compounds that are designed to carry out a useful operation. In the specific case of anion supramolecular chemistry, the intended function of these novel compounds is to effect and utilize complexation as a means for detection and/or remediation of negatively charged guest molecules. The core challenges in both of these fields often lie in the synthetic hurdles to be overcome. Despite the fact that such challenges appear to be fundamentally similar, the ramifications of these transformations are actually quite different. While a total synthetic chemist is focusing on incorporating a key stereocenter at a late stage of a total synthesis to provide the molecule with Nature’s intended function, the supramolecular chemist is focusing on the components (e.g., noncovalent interactions, electronics, ion-pairing) of an artificial receptor to optimize its *designed* function. Where the total synthetic chemist installs a pendant functional group en route to completing the synthesis of the natural product, the supramolecular chemist installs a pendant functional

group to enhance hydrogen bonding to influence the binding event. With these fields aligned toward a common goal, the emulation of nature, often a discovery in one field has the potential to revolutionize the other. This is most clearly illustrated with the advent of “click” chemistry [18]. As total synthetic chemists discover novel methods to prepare previously inaccessible functional groups, the supramolecular chemist examines how new functional groups can be utilized to fully express their inherent *functionality*.

1.2 Design Aspects of Receptors

Schmidtchen wrote that, “the ultimate purpose of host design emerges from the basic strive of chemists to be in command of the chemical and physical behavior of anions” [19]. After years of research in anion supramolecular chemistry, some of the key design factors [11] that have been elucidated through synthetic control include (1) choice of binding moiety, (2) size and shape of the substrate of interest, and (3) synthetic feasibility. While the latter aspect is one of simple practicality, the former aspects are ones that must be carefully investigated by the supramolecular chemist. With inspiration from Nature, many of the first synthetic anion receptors were modeled after proteins [20], utilizing strong NH based hydrogen bond donors (ion-dipole) along with electrostatic-type interactions (ion-ion).

Examples of NH based donors, many of which will be discussed later in this volume, include amine, amide, pyrrole, and urea. Additional NH based donors, which also interact via electrostatic type interactions, involve ammonium and guanidinium. Hydrogen bonding interactions of charge neutral hydrogen bond donors can be approximated as ion-dipole type interactions (Fig. 1). The energy of the ion-dipole interactions depends on the magnitude of the dipole moment, proximity of ion and dipole, and the angle of interaction. The binding moieties listed above each bring a strong bond dipole, yet careful synthetic design must be used to best optimize the latter two parameters. At the same time, consideration needs to be given to the harmony that exists between the size and shape of the receptor cavity with that of the guest. Collectively, these elements must be envisioned by the designer to facilitate strong and/or selective anion complexation.

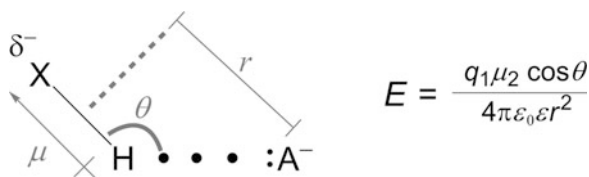
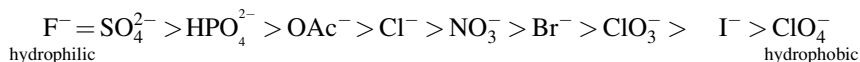


Fig. 1 General representation of hydrogen bonds as an ion-dipole interaction. Equation shows how the energy of an ion(q_1)-dipole(μ_1) interaction relates to dipole (μ_1), $1/r^2$, and directionality ($\cos \theta$)

Reviews [4, 10, 11, 19] have been written discussing these design topics in greater depth.

Two inherent aspects of host-guest chemistry that have gone relatively unexplored for optimizing anion binding are entropy and solvation. Anion binding is considered mainly enthalpically driven, e.g., deriving from the energy of the hydrogen bonding interactions upon association. In opposition, an entropic cost must often be paid to facilitate anion binding, which stems from necessary conformational restrictions of the host and guest molecules [19]. Schmidtchen [19] discusses that the entropic factors that can be taken into consideration regarding molecular design include conformational, vibrational, and configurational entropy. Conformational entropy is described as bond rotations of the receptor to facilitate anion complexation. Configurational entropy describes the various geometrical arrangements that binding partners may adopt leading to differing configurations of host and guest, some of which will not allow for anion binding.

Solvation also plays a role in the overall energetics of binding as a result of the required disordering of solvent (desolvation) of both the host and guest molecules as well as the enthalpic cost of these desolvation events. The degree to which inorganic anions are solvated can be predicted by the Hofmeister series [21]. This series (below) lists the anions from left to right with increasing hydrophobicity. As a result, costs associated with desolvations must be paid to transfer ions against this bias.



Hydrophobicity effects are often utilized in anion receptors designed for the liquid-liquid extraction of anions from polar solvents. Building selectivity into synthetic anion receptors is a means that supramolecular chemists have used to influence this trend. Collaboration between Moyer and Sessler [15, 16] has provided evidence for the selective remediation of nitrate from sulfate-enriched aqueous media utilizing a receptor designed to overcome this bias using built-in size selectivity for the nitrate anion.

1.3 CH Hydrogen Bond Donors: Weak and Secondary Interactions or Potentially Strong Sources of Anion Stabilization?

Heteroatom based donors such as NH and OH are most commonly seen in anion receptors [11] because of the inherent magnitude of the bond's dipole moment, a significant contributing factor to the hydrogen bond donor's strength. The lower electronegativity of the carbon atom as a result, is expected to predetermine CH hydrogen bond donors as weaker compared to NH and OH donors. Nevertheless,

hydrogen bonding interactions from CH donor groups have been observed in the solid-state including $\text{CH}\cdots\text{O}$ and $\text{CH}\cdots\pi$ type interactions. These observations resulted in a landmark investigation of the Cambridge Structural Database [22], culminating in a comprehensive text [23] by Desiraju and Steiner. The authors classified CH based donors as weak, providing $< 4 \text{ kcal mol}^{-1}$ of stabilization in gas phase calculations. The authors also examined haloalkanes as potential donors, which provided early evidence for how CH groups could potentially be activated for hydrogen bonding interactions with electron withdrawing groups. A specific account [24] used hydrogen bond distances to show how the CH in chloroform (CHCl_3) can interact with a bromide anion to the same degree as a secondary amine based donor ($\text{R}_2\text{N-H}$). Alkynyl donors also showed a similar decrease in $\text{CH}\cdots\text{X}^-$ distance on account of the hybridization effect on the CH acidity. Despite these findings, neutral CH hydrogen bond donors were still considered ineffective and impractical throughout the supramolecular community. In the absence of an accessible supramolecular synthon for an activated CH donor, this potentially useful interaction went unnoticed.

The first clear evidence for polarized CH hydrogen bonds affecting anion stabilization was a serendipitous discovery by Farnham and coworkers [25] in 1990 (Fig. 2). The fluorinated macrocyclic ether **1** exhibited a remarkable ability to bind fluoride. Analysis of the crystal structure of $\mathbf{1}\cdot\text{F}^-$ shows four short $\text{CH}\cdots\text{F}^-$ (1.94, 2.06, 2.08, and 2.10 Å) contacts from the CH protons alpha to the vinyl ether and CF_2 moieties. In addition, low temperature ^1H NMR studies in solution confirm $\text{CH}\cdots\text{F}^-$ type interactions based on diagnostic downfield shifts ($\Delta\delta \sim 2.0 \text{ ppm}$) of the methylene proton signals that are hydrogen bonding with fluoride.

This discovery led to similar designs of fluoride receptors [26] utilizing conveniently positioned and activated CH hydrogen-bond donors as secondary stabilizers to inherently stronger OH donors. However, the concept of utilizing highly activated CH groups as significant hydrogen bond donors continued to be unexplored by the supramolecular community as the focus remained on the use of inherently stronger heteroatom-based donors. As research in this field continued to grow, however, more researchers were observing unexpected $\text{CH}\cdots\text{X}^-$ interactions (Fig. 3) as evidenced in crystal structures and ^1H NMR experiments. The

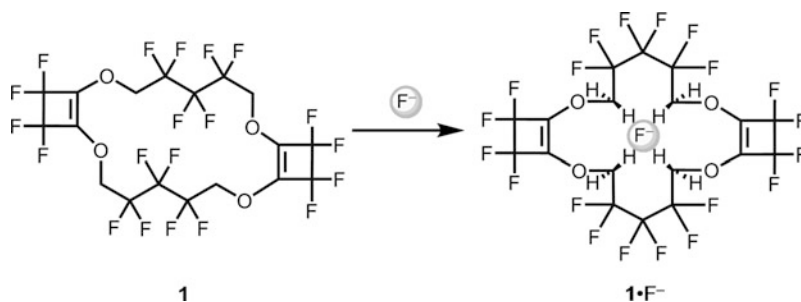


Fig. 2 Polyfluorinated macrocyclic ether **1** developed by Farnham [25] showing unexpected fluoride binding stemming from polarized methylene CH protons

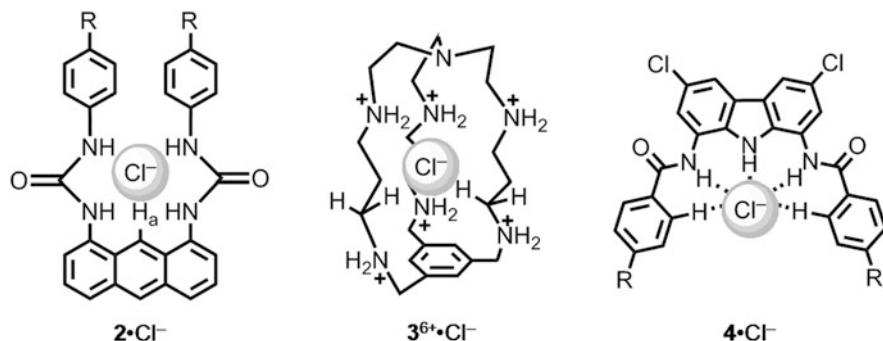


Fig. 3 Receptors **2** [27], **3**⁶⁺ [28], and **4** [31] designed to bind anions via NH hydrogen bond donors show additional $\text{CH}\cdots\text{Cl}^-$ interactions

anthracene-based bis-urea receptor **2** developed by Yoon and coworkers [27] showed a downfield shift ($\Delta\delta = 0.5$ ppm) of proton H_a upon addition of chloride in dimethylsulfoxide (DMSO). The crystal structure of Steed's [28] macrobicyclic azaphane **3**⁶⁺ showed a pseudo-octahedral geometry around the halide defined by three $\text{NH}\cdots\text{X}^-$ and three $\text{CH}\cdots\text{X}^-$ contacts. A so-called "venus-flytrap" receptor [29, 30] developed by Steed also showed prominent $\text{CH}\cdots\text{X}^-$ interactions. Jurczak [31] developed NH donor-rich carbazole **4** utilizing the rigid carbazole scaffold as a means to help preorganize the receptor for binding. An unexpected $\text{CH}\cdots\text{Cl}^-$ contact (2.76 Å) could be clearly seen in the crystal structure. While these observations hinted at the potential importance of $\text{CH}\cdots\text{X}^-$ interactions, the supramolecular community widely classified these phenomena as weak, secondary stabilizing effects.

1.4 2005: A Computationally Inspired Change in Philosophy

Despite all this evidence for the potential power of the CH hydrogen bond donor, the philosophy remained that its inherent donor ability would never approach that of heteroatom based donors. However, Benjamin Hay reported [32] an inspiring computational study investigating the electronic binding energies of complexes between benzene and various inorganic anions. These initial studies illustrated that simple aryl CH donors can provide more than 50% of the stabilization provided by intrinsically stronger heteroatom-based donors (e.g., NH_3 , H_2O). It was also noted that by increasing the acidity of the CH from an alkyl CH (e.g., CH_4) to a phenyl CH, the strength of the hydrogen bonding interaction was increased by nearly threefold, providing >8 kcal mol⁻¹ stabilization in the gas phase. Utilizing this same methodology, Hay demonstrated [33] the tunability (Fig. 4) of the hydrogen bond donor strength of an aromatic CH via inductive and resonance effects utilizing electron withdrawing groups (NO_2 , CN, CF_3) or electron donating groups

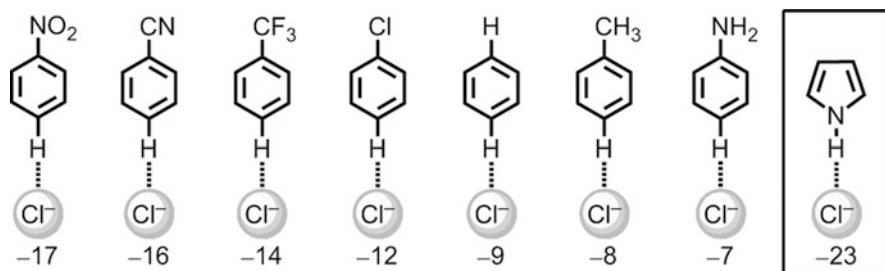


Fig. 4 Computations [33, 34] (MP2/aug-cc-pVDZ) showing substituent effects on hydrogen bond donor energies (kcal mol⁻¹) of aromatic CH and how they compare to the inherently stronger pyrrole NH donor

(NH₂, CH₃) at the *para* position (Fig. 4). According to Hay, an aromatic CH could be activated to the extent that it approaches the donor ability of conventional OH and NH based donors such as NH₃. Such activated hydrogen bonding motifs are distinguished hereafter as being “extrinsic” in character. Nitrobenzene was found to provide more than 70% of the stabilization (−17 kcal/mol) provided by a pyrrole [34] NH donor (−23 kcal/mol)! While his initial study on the hydrogen bond donor ability of aliphatic CH groups found them to be weaker on account of their inherently lower acidity, Hay explored the effects of polarizing the aliphatic CH with various electron withdrawing groups. The results [35] showed that aliphatic CH groups, in a similar fashion as aryl CH groups, can be sufficiently polarized to provide significant hydrogen bond stabilization of a negatively charged ion. For instance, chloroform was calculated to provide −20 kcal/mol of binding energy with chloride in the gas phase. In comparison, water and methanol were calculated to provide −15 and −17 kcal/mol, respectively. With ample *theoretical* evidence for the importance and strength of CH•••X[−] interactions, their presence could no longer go unnoticed.

1.5 Experimental Exploration of Charge Neutral CH•••X[−] Interactions in Anion Receptors

As the theoretical evidence [32, 33, 35] for the potential power of CH•••X[−] interactions grew, experimenters began to systematically and strategically incorporate extrinsic CH hydrogen bond donors into anion receptors (Fig. 5). Sessler, in collaboration with Hay, incorporated a single strap [34, 36] into a calix[4]pyrrole receptor **5** to both preorganize the receptor for binding and investigate the ability of an aromatic CH donor to aid in anion stabilization. The benzodiester-strapped calixpyrrole **5** showed an increase in Cl[−] affinity by a full order of magnitude from 220,000 to 2,200,000 M^{−1} (CH₃CN, 298 K), as determined by UV-Vis

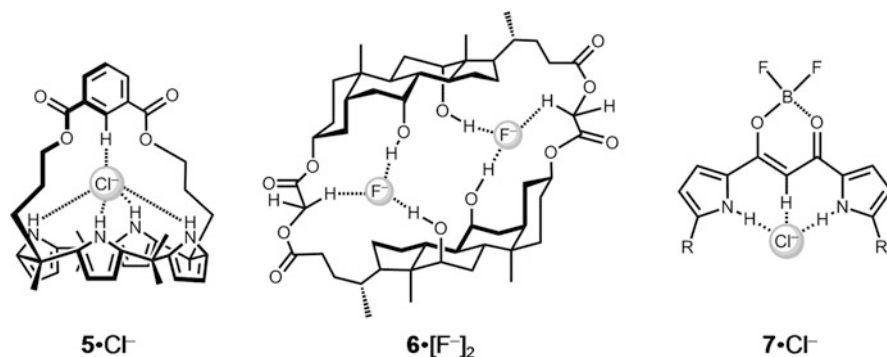


Fig. 5 Receptors **5** [34, 36], **6** [39], and **7** [40–42] designed to utilize polarized CH groups as additional sources of stabilization in anion binding

titration. Researchers have also investigated the ability of calix[4]pyrrole isomers containing internally directed CH hydrogen bond donors [37] to bind anions. In addition, the effects of incorporating nitroaromatic rings into the calix[4]pyrrole backbone to provide additional CH hydrogen bond donors [38] has been studied. Maitra and coworkers [39] developed the cholaphane receptor **6**. The inspiration for its anion binding stems from its facial amphiphilicity with internally oriented hydroxyl groups in addition to its simple preparation from derivatives of bile acid. While the hydroxyl groups are intrinsically stronger hydrogen bond donors, the methylene protons, both activated by the diester functionality and preorganized toward the electropositive cavity of the structurally rigid steroid dimer, showed a diagnostic ¹H NMR downfield shift ($\Delta\delta \sim 0.20$ ppm). Maeda and coworkers developed a dipyrrolyldiketone [40–42] scaffold, which upon addition of excess BF₃•OEt₂ provided chemosensor **7**. ¹H NMR experiments provided evidence for anion complexation via pyrrole NH donors in addition to a strong CH...X⁻ interaction stemming from the CH group bridging the bispyrrole backbone. In support of potential chemosensor applications, fluorescence studies also showed a quenching effect upon fluoride complexation hypothesized to occur on account of polarization of the pyrrole ring and subsequent intramolecular electron transfer.

For further evidence of non-aromatic CH donors, Schalley and coworkers [43] developed resorcinarene **8** (Fig. 6), which was found to bind strongly to anions via the acetal hydrogens. The anion binding properties of **8** were characterized utilizing electrospray ionization mass spectrometry (ESI-MS), which showed the formation of 2:1 complexes with various inorganic anions (SO₄²⁻, PF₆⁻). Johnson, in collaboration with Hay [44], developed a tripodal anion receptor **9** allowing for the first direct comparison between CH...X⁻ and X⁻...π interactions using solution phase measurements. It was determined that receptor **9** bound anions preferentially via CH...X⁻ contacts. What all these investigations have in common is *experimental* evidence that the intrinsic hydrogen bond donor ability of CH based donors can provide significant anion stabilization when sufficiently polarized.

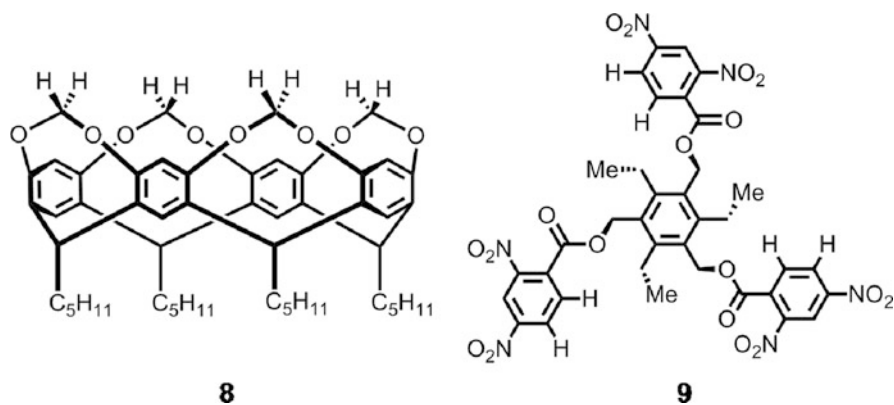


Fig. 6 Receptors **8** [43] and **9** [44] were designed to bind anions selectively via polarized CH hydrogen bond donors

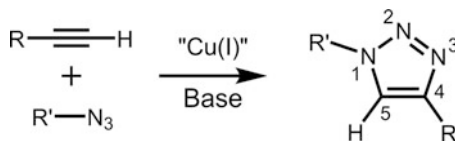
2 The 1,2,3-Triazole: Experimental and Computational Investigation of Its Anion Binding Affinity in Macrocyclic Triazolophanes

2.1 “Click” Chemistry: The Philosophy and the Cu(I)-Catalyzed Huisgen 1,3-Dipolar Cycloaddition

In 2001, Sharpless, Finn, and Kolb developed the chemical philosophy of “click” chemistry [18]. The goal of this philosophy was to follow nature’s lead to “generate substances by joining small units together with heteroatom links” as well as “to develop an expanding set of powerful, selective, and modular “blocks” that work reliably in small- and large-scale applications.” These “click” reactions often involve “spring-loaded” electrophiles, which proceed rapidly to completion while also possessing inherent stereospecificity. The most widely used reaction developed through this philosophy is the Cu(I)-catalyzed Huisgen 1,3-dipolar cycloaddition between a terminal alkyne and an azide (Fig. 7).

The initial discovery of this cycloaddition was by Huisgen [45, 46] in 1967. However, this reaction generally required strong heating and lacked regioselectivity between the 1,4- and 1,5-substituted triazoles. As a result, this transformation was not a practical methodology for the preparation of the triazole functional group. The independent discovery of the Cu(I)-catalyzed reaction, however, by the laboratories of Sharpless [47] and Meldal [48] provided the 1,4-substituted 1,2,3-triazole regioselectively. Not only is regioselectivity key, but its built-in chemoselectivity has also truly given this reaction its click-like nature. The necessary azido [49] and alkynyl substrates can be synthesized in an infinite number of ways from readily available precursors, and these functional groups are orthogonal to many synthetic transformations. In addition, this reaction can be carried out under a host of

Fig. 7 Cu(I)-catalyzed 1,3-dipolar cycloaddition of a terminal alkyne and azide functionality produces a 1,4-disubstituted-1,2,3-triazole in a regioselective fashion



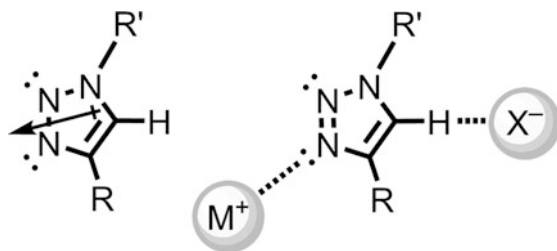
different conditions (pH, solvent, polarity, temperature) as well as in the presence of other functional groups [50]. The mechanism of the Cu(I)-catalyzed reaction is currently under investigation by Finn and coworkers [51, 52]. Various nitrogen based ligands [51] have also been designed for further optimization of this reaction in a wide range of conditions. In biological applications, researches have since replaced cytotoxic Cu catalysts with other transition metals (Ru, Ni, Pd, Pt, and Fe) [53, 54]. Metal-free cycloadditions have also been developed utilizing electron-deficient alkynes in highly strained substrates [55, 56].

2.2 *The Functional 1,2,3-Triazole Unit and Macrocyclic Triazolophanes*

With the advent of click chemistry and related synthetic methodologies towards triazole synthesis, its use has become widespread. Its applications stem from both its unique electronic structure and its favorable sterics evidenced in part through its use in peptide backbones [50]. Its initial application was seen in bio- and peptidomimetics as an amide-bond surrogate [51]. On account of its stability to solvolytic cleavage, there is belief that its incorporation into certain drugs and enzyme inhibitors will show a gain in overall metabolic stability in comparison to its amide containing analogs. Its ability to act as an amide-bond surrogate and β -turn mimic has also been widely studied [50, 57]. The CuAAC (copper-catalyzed azide alkyne cycloaddition) has also seen applications in the fluorescent labeling of peptides and natural products [50, 58, 59]. Its other properties include metal coordination (Fig. 8) [51, 52, 60, 61], use in templated synthesis of interlocked structures [62, 63], and catalysis [52]. The depth and breadth of CuAAC-generated triazoles and their applications provided the lessons necessary to understand its potential functionality as an anion binding moiety.

If the feasibility of any potential anion binding moiety lies in its ease of synthesis, its power arises from its electronic structure. This power comes as a result of providing both an electropositive environment in addition to a polarized bond for halide interaction. The three electronegative nitrogens of the triazole are nested together on one side of the ring providing two key electronic features. Their electron-withdrawing power effectively lowers the electronegativity of the triazole's C₅ carbon, thus increasing the acidity of the CH proton. The orientation of these nitrogens also provides a surprisingly large 5-Debye dipole (Fig. 8) [64]. The nearly collinear arrangement of this dipole with the polarized CH bond provides the

Fig. 8 The strong (5 D) molecular dipole [64] of 1,4-disubstituted-1,2,3-triazoles reinforce the ring's unique multifunctionality as an electron donor for metal binding as well as a hydrogen bond donor for anion coordination



anion binding site. As Hay hypothesized [32, 33, 35], the power of the carbon-based hydrogen bond to act as a strong hydrogen bond donor correlates directly with the proton's acidity. This attribute has been previously observed in facile CH insertion by palladium and other transition metals to prepare "abnormal" carbene triazolium ligands [65]. In addition, the triazole unit's small steric size provides an attribute that can be advantageous in the design of anion receptors. For example, coplanarity akin to phenylene ethynyls [66] can be achieved when a triazole is substituted with two phenyl rings. Such an arrangement can provide the preorganization known to play a large role in receptor design.

Bringing together the potential anion binding power of the triazole with structural design aspects of molecular receptors, triazolophane **14** (Fig. 9) was designed [67, 68]. This design preorganizes eight CH hydrogen bond donors from triazoles and phenylenes toward the internal cavity. The bridging phenylene linkers can be readily tuned to affect solubility, steric control over aggregation, and their hydrogen-bond-donor strength [68]. Macrocyclic **14** was prepared (Fig. 9) from diazide **10** and alkynyl **11** building blocks. Subsequent CuAAC and Sonogashira coupling formed the 5/8 oligomer **13** via **12** in high yields. CuAAC-assisted macrocyclization provided triazolophane **14** in a 70% yield. The intended preorganization of **14** can be further supported by this surprisingly high yield of macrocyclization. Computational modeling and 2-D NMR spectroscopy provided evidence for the preorganized, nearly planar structure of the macrocycle.

¹H NMR titrations of tetrabutylammonium chloride (TBACl) in CD₂Cl₂ showed the ability of triazolophane **14** to interact with anions [67]. Analysis of the UV-Vis spectroscopic data [68] provided a binding constant of 11,000,000 M⁻¹ (CH₂Cl₂, 298 K), which rivaled [69] and, in some cases, exceeded [70] receptors utilizing traditional hydrogen bond donors under the same conditions. The inherent size selectivity built into the macrocyclic receptor through its preorganized structure was mapped through titrations of various halides (F⁻, Br⁻ and I⁻). As a result of their differing sizes and charge densities, differing affinities were observed. The ionic radii of Cl⁻ (1.81 Å) and Br⁻ (1.96 Å) correlated best with the cavity's diameter (~3.8 Å) while F⁻ and I⁻ (1.30 and 2.20 Å, respectively) provided a size mismatch. Simple modeling provides corroborating evidence for this size selectivity of the macrocycle. The smaller size and higher charge density of fluoride is demonstrated by its affinity for the 1,3-bis-*N*-triazole-phenylene triads at the northern and southern points of the macrocycle (Fig. 10b). This spatial selectivity is made evident by a prominent downfield shift of the north *N*-linked phenylene

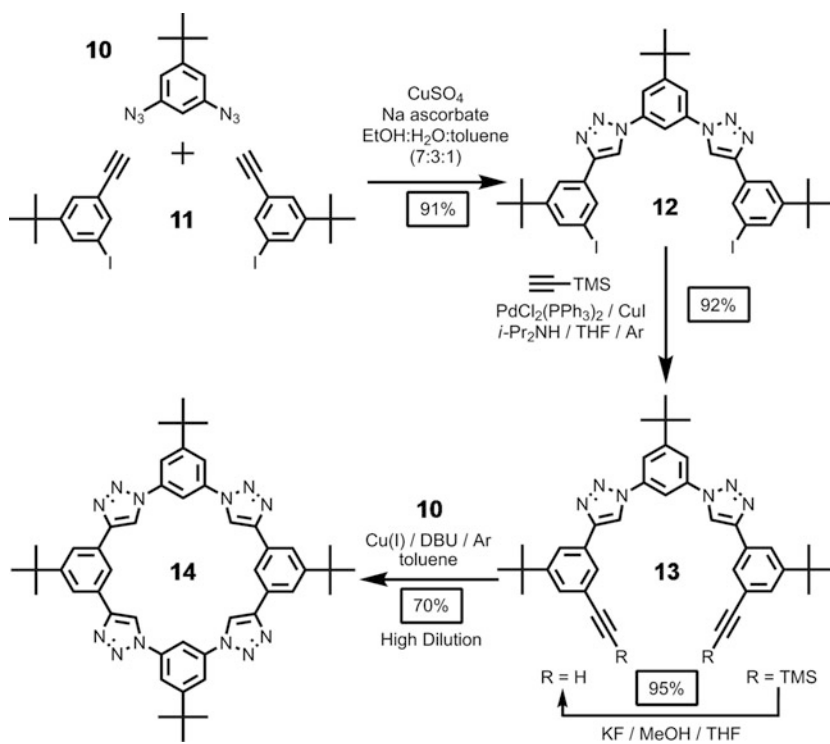


Fig. 9 Modular synthesis of triazolophane **14** [67, 68]

proton and a weak effect on the *C*-linked phenylenes' CH protons. The larger size, more diffuse charge density, and weaker binding of I⁻ is corroborated by the calculated structure (Fig. 10c) showing iodide sitting above the plane of the triazolophane.

2.3 Calculations on Hydrogen Bond Donor Strength of 1,4-Diaryl-1,2,3-Triazole

Calculations [71] showed the lowest energy conformation of the triazolophane to be slightly distorted from planarity in order to minimize intracavity H...H steric interactions. Upon binding with chloride and bromide, the triazolophane undergoes a slight conformational change to a perfectly planar structure (D_{2h}). As a result, only a small deformation energy is paid, consistent with a high degree of preorganization. For the triazoles and the *N*-linked phenylenes, the distances from the CH hydrogen atoms to the cavity's center are observed to shorten upon hydrogen bond formation with chloride.

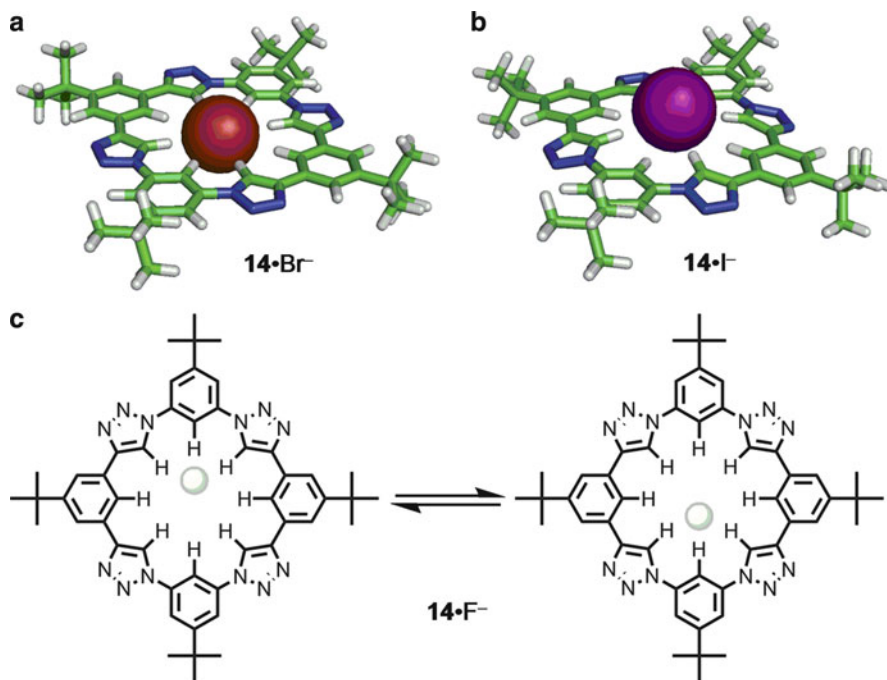


Fig. 10 Graphical representations and models (HF/3–21G) of triazolophane **14** bound with (a) Br^- , (b) F^- , and (c) I^- ions [68]

To fully elucidate the power of the hydrogen bond interactions arising from each type of aryl ring, a deconvolution strategy was carried out. Triads (**15–17**) of the hydrogen bonding groups were used to determine the binding energies of triazoles (T), *N*-phenylenes (N), and *C*-phenylenes (C), respectively. The relative triazole... Cl^- binding energy exceeds (Fig. 11) that of either phenylene unit by a factor of ca. 2.5, confirming the hypothesis that the internally polarized and dipole stabilized triazole ring interacts strongly with anions. In addition, the *N*-linked phenylene CH is slightly more activated (Fig. 11) than the *C*-linked counterpart. This result provides evidence that the anionic guest should experience a stronger interaction with the 1,3-bis-*N*-triazole-phenylene triad of the macrocycle, exactly as was observed with fluoride [68].

2.4 Investigating the Tunability of the Phenylene's CH Hydrogen-Bond Donor Strength

While theoretical calculations [32, 34, 35, 71] have made clear the effects of acidity on the CH hydrogen bond donor, the modular triazolophane synthesis allows for a direct solution-phase investigation of such an effect. By introducing triethyleneglycol substituents into the phenylene linkers [68], the electron donating effects on the

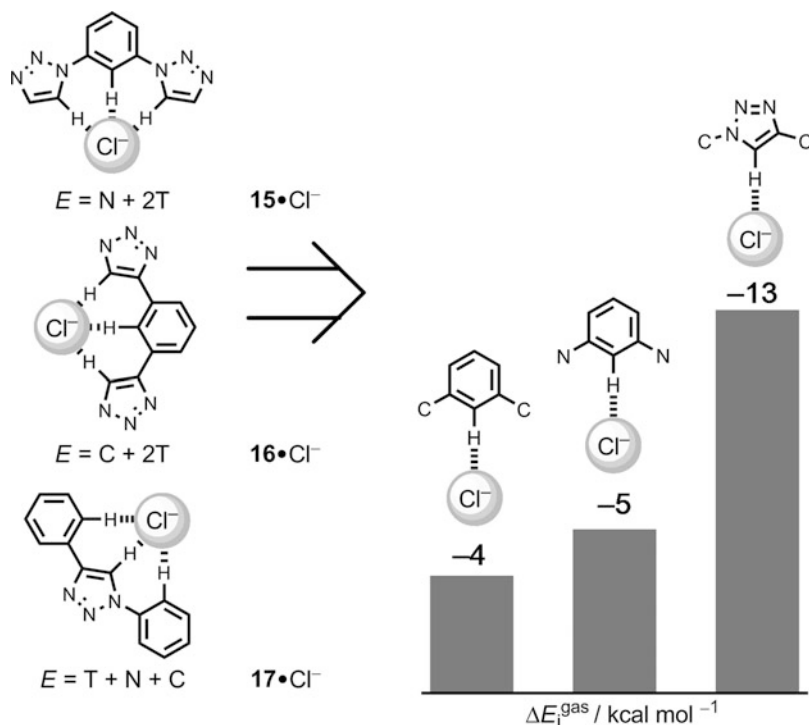


Fig. 11 The binding energy (B3LYP/6–311++G(3df,2p) of the geometry-optimized (B3LYP/6–31+G(d,p)) triazolophane•Cl⁻ complex (**14**•Cl⁻) was decomposed into its constituents [71] via model triads (**15**–**17**) to reveal the rank ordering of the strengths of binding: C-phenylenes (C) < N-phenylenes (N) < 1,2,3-triazoles (T)

internal aromatic protons interacting with the anion can be investigated. The triethylene glycol substituents were systematically added into the macrocycle by incorporating them into the *N*-linked phenylenes, *C*-linked phenylenes, and all four phenylene linkers (**18**–**20**, Fig. 12). As expected, these electron donating groups lowered the binding affinity while maintaining the halide selectivity. This is direct confirmation of the importance of the phenylene $\text{CH}\cdots\text{X}^-$ interaction. Interestingly, placing the ethylene glycol substituents on the *N*-linked phenylenes resulted in a greater loss of binding affinity than when placing them on the *C*-linked phenylenes. This quantitative observation agrees directly with the observed fluoride selectivity for the northern-southern regions and the theoretical data showing that the *N*-linked phenylene CH forms stronger hydrogen bonds.

2.5 Sandwich Complexes and Positive Cooperativity

Size selectivity was made evident with the parent triazolophane **14** showing high affinity for both chloride and bromide. However, it became evident from ESI-MS

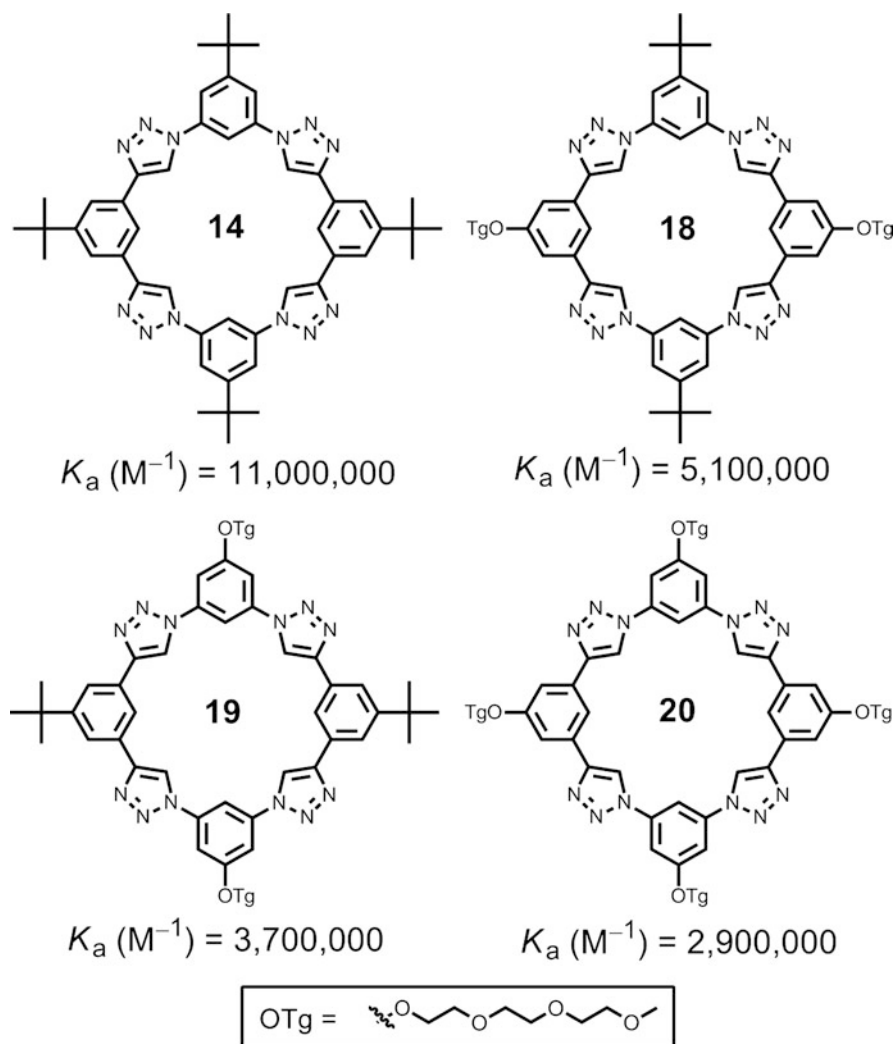


Fig. 12 Incorporation of electron donating triethyleneglycol substituents in **18–20** [68] weaken binding of chloride when compared to triazolophane **14**

and ^1H NMR experiments that triazolophanes can also form 2:1 sandwich complexes in the presence of less than one equivalent of the halide guest. With inspiration coming from the well known sandwich complexes in cation coordination [72] and less well known ones in anion supramolecular chemistry [73, 74], the design of a receptor that would favor the formation of sandwich complexes to bind larger anions (e.g., iodide) was conceived. Elements of its design must include

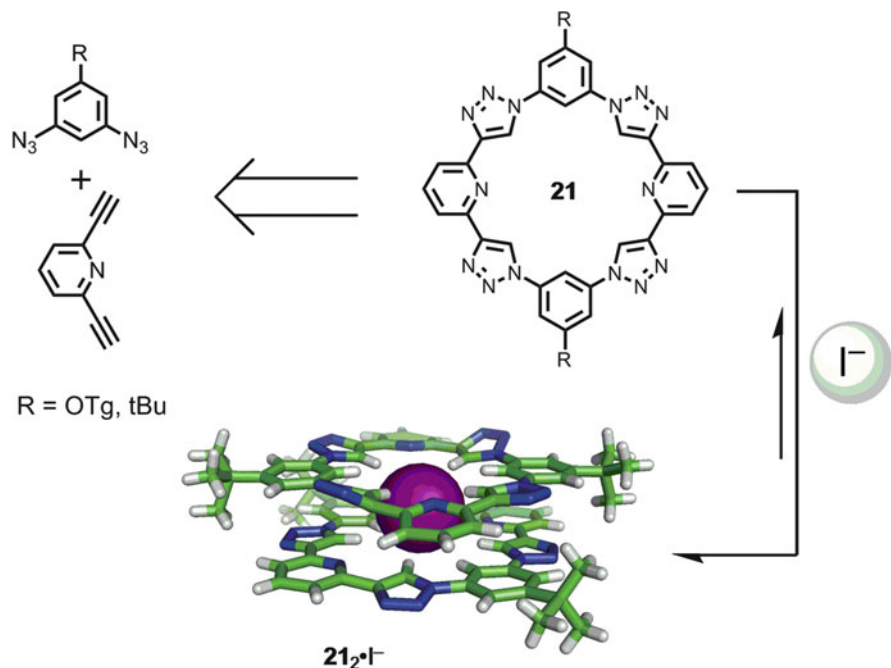


Fig. 13 Triazolophane **21** [75] favors formation of 2:1 complex with iodide utilizing positive cooperativity to further stabilize a sandwich complex

attributes that are able to maximize cooperativity effects. Cooperativity describes the ability of the first binding event to influence the second one. Positive cooperativity allows for direct self assembly of two triazolophanes around the guest of interest. Factors that can favor the second binding event include π - π stacking [74], solvophobic effects [4], and dipole-dipole interactions [75].

Pyridyl-incorporated triazolophane **21** (Fig. 13) was designed [75] in an effort to maximize cooperativity effects as well as to employ the pyridyl lone pairs to destabilize the 1:1 complex. The conveniently modular synthesis of the triazolophane scaffold, through CuAAC of available alkynyl and azido building blocks, allowed for a simple preparation of the macrocycle. In addition, substituents were omitted from the pyridyl linkers to mitigate any steric repulsion between the macrocycles. Copurification and cocrystallization of the *tert*-butyl version of triazolophane **21** allowed for X-ray structural confirmation of a 2:1 sandwich complex showing the iodide being shared between the planar, stacked triazolophanes. ^1H NMR spectroscopy of the OTg-substituted triazolophane provided additional evidence for the 2:1 complex, which was characterized by “extreme” positive cooperativity such that addition of 150 equivalents of TBAI could not drive the formation of a 1:1 complex by mass action.

3 Expanding the Utility of 1,2,3-Triazoles in Anion Supramolecular Chemistry

3.1 Triazole Foldamers: The Role of Preorganization

While it was evident, through calculation and experiment, that the triazole can act as a strong hydrogen bond donor to facilitate anion binding, the effect of preorganization in triazolophanes required additional research. To this end, two groups independently reported 1,4-diaryl oligotriazole foldamers showing an affinity for halide anions [76–78]. Shortly after the publication of macrocyclic triazolophane **14**, Craig and coworkers [76] published the preparation and analysis of oligotriazole foldamers **22** and **23** (Fig. 14). Inspired by previous examples of anion induced folding, the foldamer was designed to provide an electropositive cavity along with triazole-based CH hydrogen bond donors to facilitate the foldamer to wrap itself around the anion. As expected, ^1H NMR titrations of **22** with TBACl in acetone- d_6 showed a significant downfield shift of the internal triazole protons ($\Delta\delta = 1.5, 1.9$ ppm) along with similar shifts in the internal phenylene protons. A solid-state structure of **23**• Cl^- (Fig. 14) makes evident the triazole binding affinity with very short $\text{CH}\cdots\text{Cl}^-$ (2.59, 2.74 Å) contacts along with a significant interaction from the phenylene $\text{CH}\cdots\text{X}^-$ (2.71 Å). Crystallographic characterization of pentad **23**, generated in the absence of Cl^- [77], clearly demonstrates the role of preorganization: the pentad's lowest energy conformation is linear with the two triazole CH groups directed toward opposite sides of the oligomer. In order to facilitate anion binding the receptor must undergo a conformational change in order to generate a binding pocket, which in turn, provides an entropic penalty for complexation. In addition to the effect of preorganization, changing the solvent [77] was found to have a profound effect on the binding event allowing for a strong correlation to be

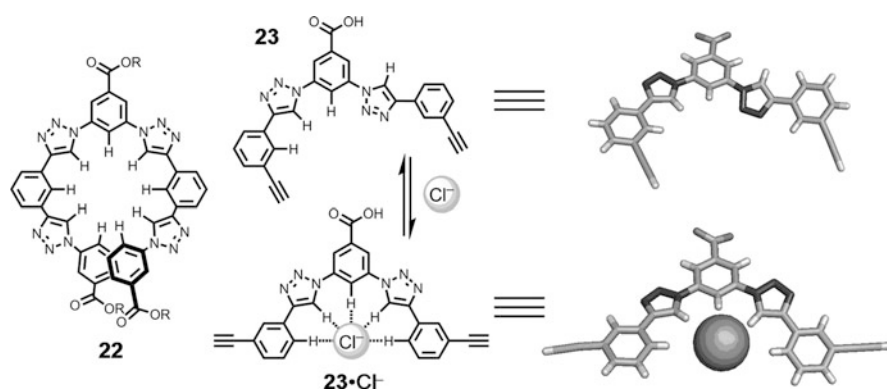


Fig. 14 Foldamers **22** and **23** [76, 77] showed strong Cl^- binding through $\text{CH}\cdots\text{Cl}^-$ interactions. Solid state structures of **23** in absence of chloride shows lack of preorganization of triazole CH donors

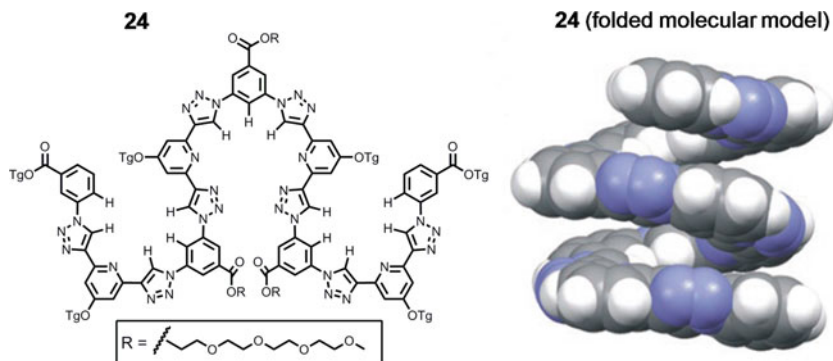


Fig. 15 Foldamer **24** [78] shows a helical preference upon binding of achiral guest halide ion

drawn between the binding affinity and the Gutmann (AN) acceptor number of the solvent. The Gutmann acceptor number gives a quantitative measure for a solvent's ability to accept and/or donate electron density. The triazole CH of foldamer **23** was also found to undergo deuteron exchange in the presence of three equivalents of F^- in D_2O , illustrating the triazole's higher acidity and inherent hydrogen bond donor strength.

Hecht and coworkers then reported on a family of molecules [78] termed "clickamers" (Fig. 15). The helical preferences of these clickamers **24** were enforced using chiral aliphatic side chains and studied using circular dichroism (CD) spectroscopy. Interestingly, the addition of achiral halide guest molecules (Cl^- , Br^- , I^-) in H_2O promoted a helical inversion relative to the neat foldamer. While the binding affinity of **24** was not quantified, this unprecedented chiral response to achiral stimuli opens avenues toward potential applications for foldamers in aqueous sensing in addition, to further illustrating anion binding power of triazoles even in the presence of a highly competitive solvent. More importantly, the foldamers of Craig and an oligomeric version of **14** [68] provide direct evidence that receptor preorganization plays a critical role in the binding power of rigid triazolophanes.

3.2 Additional Applications of Triazole $\text{CH}\cdots\text{X}^-$ in Anion Receptors

With the hydrogen-bond donor ability of the 1,4-disubstituted 1,2,3-triazole becoming clear, it has been incorporated into different types of anion receptors to investigate its ability to aid in anion complexation. One such example is a modification [79] to the strapped calix[4]pyrrole (Fig. 16a) system in which Gale and coworkers introduced a triazole strap to furnish receptor **25**. Its anion binding as well as anion transport properties were investigated. The binding of **25** was studied

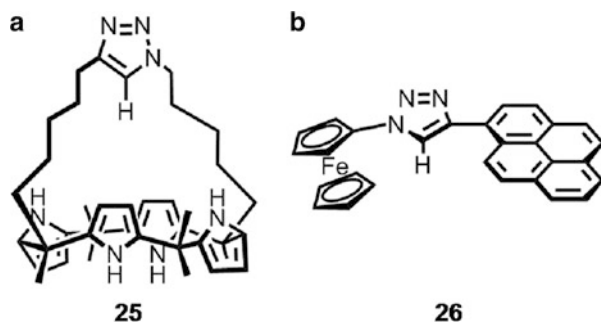


Fig. 16 (a) Triazole-strapped calix[4]pyrrole **25** [79] utilizing an additional $\text{CH}\cdots\text{Cl}^-$ contact to stabilize binding of chloride. (b) "Clicked"-pyrene **26** [80] developed as an electrochemical and fluorescent chemosensor for dihydrogen phosphate

in acetonitrile- d_3 which showed the expected downfield shift of both the pyrrole NH and triazole CH NMR signals correlating to a 1:1 binding stoichiometry. Comparison of the isothermal titration calorimetry data to the parent calix[4]pyrrole showed that receptor **25** bound chloride with a substantially larger enthalpy of complexation as a result of the additional triazole $\text{CH}\cdots\text{Cl}^-$ interaction in addition to the ability of the strap to aid in preorganization of the binding cavity. These attributes combined to provide an increase in chloride binding by nearly two full orders of magnitude. In anion transport studies, **25** was found to be capable of chloride/nitrate antiport-behavior not observed with the parent calix[4]pyrrole.

A dual-mode fluorescence and electrochemical sensor **26** (Fig. 16b) has been developed by Molina and coworkers [80] utilizing the anion binding power of the triazole donor in parallel with the pyrene fluorophore and redox-active ferrocene. This sensor was found to have an affinity for the biologically relevant pyrophosphate anion ($\text{H}_2\text{PO}_7^{2-}$) as made evident by its turn-on fluorescence. For instance, receptor **26** illustrated a 19-fold fluorescence enhancement upon pyrophosphate binding ($\Phi = 6 \times 10^{-3}$ for **26** to $\Phi = 0.111$ for $\text{26}\cdot\text{H}_2\text{PO}_7^{2-}$). In addition to the receptor's fluorescent response, significant cathodic peak shifts of the ferrocene oxidation potential (~ 100 mV) were also observed upon addition of pyrophosphate. ^1H NMR titrations performed in *N,N*-dimethylformamide (DMF) also provided evidence of anion binding through a downfield shift of the triazole CH proton peak (0.11 ppm). Analysis of the ^1H NMR, electrochemical, and UV-Vis titration data all show a 2:1 binding stoichiometry of receptor to pyrophosphate.

3.3 *Triazolium: A New-Age Surrogate for the Amine-Ammonium Pair?*

Recent developments in anion supramolecular chemistry have opened an additional train of thought for the quaternized triazolium and its potential applications.

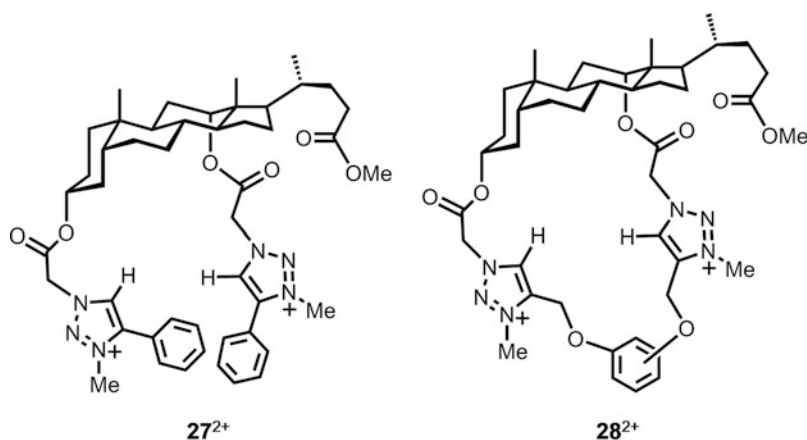


Fig. 17 Steroidal based receptors [82] designed to bind anions via polarized triazolium CH donors

An analogy comes from the amine-ammonium pair, which has found widespread application in anion receptor design as well as in the construction of interlocked structures [81] on account of the increased hydrogen-bonding power upon quaternization. A similar strategy has since been applied to increasing the CH hydrogen bonding ability of the triazole ring. Pandey and coworkers [82] were the first to investigate this idea for anion binding. In the design of cyclic and acyclic bile acid receptors **27**²⁺ and **28**²⁺ (Fig. 17), Pandey utilized pendant methylated triazolium arms along with activated methylene CH groups to provide a hydrogen-bonding environment for anions. Receptors **27**²⁺ and **28**²⁺ showed medium binding affinity for H₂PO₄⁻ with binding constants of 1,100 and 1,920 M⁻¹, respectively, in CDCl₃. The acyclic receptor **28**²⁺ was found to be a stronger binder for the H₂PO₄⁻ on account of its flexibility providing access to a more favorable hydrogen-bonding pocket for the tetrahedral phosphate anion.

The use of the triazolium's anion binding power has since seen application in the functionality of interlocked structures. The first development of this strategy was investigated by Busseron and coworkers [83]. The rotaxane **31**²⁺ incorporated two molecular stations with different affinities for dibenzo[24]crown-8 (DB24C8). The triazolium ion had not previously been described as a molecular station yet inspiration comes from reports of other cationic *N*-heterocyclic systems [84, 85] showing favorable interactions with DB24C8. It was synthesized (Fig. 18) from the CuAAC of glycosidic azide **29** and anilinium alkyne **30**⁺ in the presence of DB24C8 followed by methylation with methyl iodide. ¹H NMR of rotaxane **31**²⁺ showed the crown ether initially positioned over the anilinium center. Upon deprotonation using diisopropylethylamine (DIEA), a downfield shift of 1.16 ppm was observed for the triazolium CH proton in rotaxane **32**⁺ as a result of hydrogen bonding interactions with DB24C8. Additional means by which DB24C8 can interact with the *N*-methyltriazolium are described [83]. Protonation of the aniline moiety and anion exchange facilitated full regeneration of rotaxane **31**²⁺. Busseron has since

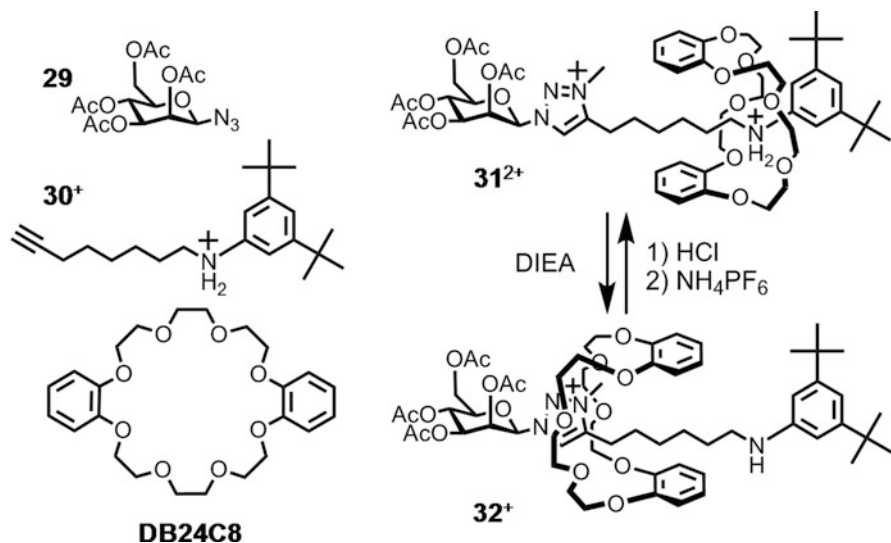


Fig. 18 Glycorotaxane 31^{2+} [83] was designed with dialkylammonium and triazolium binding “stations.” Upon deprotonation, the crown shuttled to the strong triazolium binding station

developed a pH-switchable daisy chain [86] utilizing the same synthetic methodologies allowing for control between an extended and contracted state.

3.4 Triazolium $CH\cdots X^-$ Interactions in Anion Templatation

The synthesis of mechanically interlocked structures has been revolutionized through the art of templated synthesis where, for example, the wheel and axle components of rotaxanes are brought together in a selective fashion prior to covalent bond formation [81]. Leigh has helped to further this methodology [62, 63] with the use of active metal template-directed synthesis of rotaxanes, catenanes, and daisy chains in which the interlocked structure was formed utilizing CuAAC. Anion templated synthesis has also utilized hydrogen bond donors incorporated into the wheel and axle groups allowing for halides to bring the two components together prior to bond formation. Until recently, the ability of a CH hydrogen bond donor to act as a means of accessing anion-templated interlocked structures has gone unexplored. Beer has developed [87] a triazolium based axle 33^+ (Fig. 19) which has shown a very high affinity for Cl^- and Br^- in acetone-*d*₆. Utilizing this halide affinity, it was envisioned that a pseudorotaxane could be formed with isophthalimide macrocycle **34** via anion templation. ¹H NMR studies of pseudorotaxane $35^+ \cdot Cl^-$ identified favorable π - π stacking interactions with the catechol rings of the macrocycle along with strong triazole $CH\cdots Cl^-$ interactions (downfield shift of triazolium signal). Beer has also demonstrated the ability of this

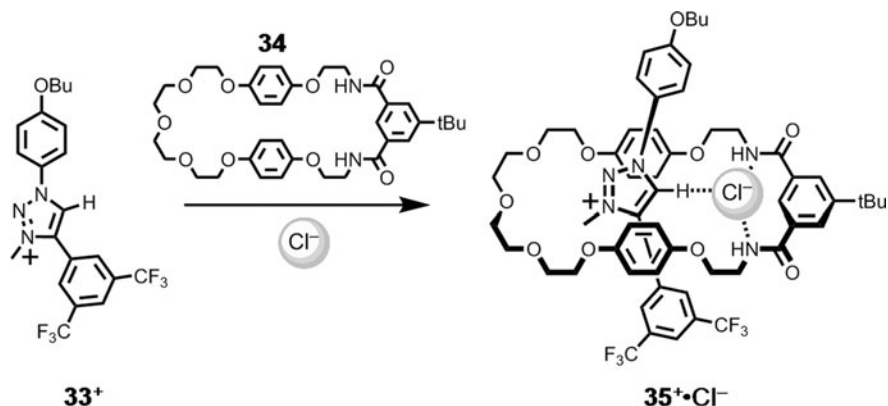


Fig. 19 Chloride-templated self-assembly of pseudorotaxane **35**⁺•Cl⁻ [87] utilizing the affinity of both wheel **34** and triazolium based axle **33**⁺

methodology in a rotaxane synthesis [87] utilizing ring closing metathesis around the triazolium axle, in which the rotaxane has been shown to bind selectively to bromide.

3.5 Triazolophane-Based Ion Selective Electrodes

One way to measure anion concentrations in solution media is with ion-selective electrodes. The selectivity of the commercial cationic ion selective electrodes is dictated by the Hofmeister series [20]. Incorporating anion receptors, or ionophores, into the electrode's membranes can alter the selectivities. Ion selective electrodes with triazolophane **14** as the ionophore were prepared and showed good responses to chloride and bromide [14]. A submicromolar detection limit and a dynamic range of five orders of magnitude toward both halides were found. An anti-Hofmeister selectivity was obtained in one membrane toward salicylate and chloride and the selectivity was sufficient to measure bromide concentrations in a horse serum sample. This positive result illustrates one of the first forays of triazoles into applications in the analytical chemistry of anions.

4 Concluding Remarks

This review has described the utility of charge-neutral, extrinsically-activated CH hydrogen bond donors in anion receptors and the anion templated synthesis of mechanically interlocked structures. In particular, the click-chemistry generated 1,2,3-triazole has recently made a very strong impression on the supramolecular

community for not only its strong coordination to anions but also for its resistance to solvolytic cleavage and metal coordination properties. The 1,2,3-triazole's application as an amide surrogate in bio- and peptidomimetics studies has been well studied, yet its application in anion supramolecular chemistry has only begun to be explored. More importantly, the theoretical studies of Benjamin Hay [32, 33, 35], coupled with experimental investigations of triazole and other extrinsically activated $\text{CH}\cdots\text{X}^-$ contacts, has revolutionized the way in which this community views "strong" hydrogen bond donors. Anion receptors deemed "strong" by the community no longer need to use inherently-activated heteroatom based donors. The NH and OH groups have long been used to coordinate to anions, yet the advent of the CH as a hydrogen bond donor now provides the opportunity for novel and more sophisticated receptor designs. With the gamut of acidity values that carbon-based functional groups can span, there are opportunities for a significant amount of controlled *tunability* to be built into anion receptors. In addition, the simple fact that chemistry at a carbon center is the most fundamental concept in chemical synthesis, there is ample space for further investigations of these acidity concepts in the context of anion supramolecular chemistry. By beginning to change such a fundamental philosophy, researchers must take a new look at supramolecular challenges with a broadened scope. While the CH hydrogen bond donor will never replace NH or OH donors, this newfound "strong" anion coordination ability of CH donors serves to arm supramolecular chemists with additional tools in the pursuit of "control over the physical and chemical behavior of anions" [19].

References

1. Sato T, Konno H, Tanaka Y, Kataoka T, Nagai K, Wasserman HH, Ohkuma S (1998) *J Biol Chem* 273:21455
2. Dutzler R, Campbell EB, Cadene M, Chait BT, MacKinnon R (2002) *Nature* 415:287
3. Christianson DW, Lipscomb WN (1989) *Acc Chem Res* 22:62
4. Kubik S, Reyhelter C, Stuwe S (2005) *J Incl Phenom* 52:137
5. Moss B (1996) *Chem Ind*:407
6. Damian P, Pontius FW (1999) *Environ Prot*:24
7. Urbansky ET (1999) *J Environ Manage* 56:79
8. Langard S, Norseth T (1979) *Handbook on the toxicity of metals*. Elsevier, New York
9. US EPA (2009) *Interim Drinking Water Health Advisory for Perchlorate*. US Environmental Protection Agency, Washington, DC. EPA 822-R-08-025
10. Bianchi A, Bowman-James K, Garcia-España E (1997) *Supramolecular chemistry of anions*. Wiley-VCH, New York
11. Sessler JL, Gale PA, Cho WS (2006) *Anion receptor chemistry*. RSC Cambridge, UK
12. Buhlmann P, Pretsch E, Bakker E (1998) *Chem Rev* 98:1593
13. Oesch U, Amman D, Simon W (1986) *Clin Chem* 32:1448
14. Zahran E, Hua Y, Li Y, Flood AH, Bachas LG (2009) *Anal Chem* 82:368
15. Wintergerst MP, Levitskaia TG, Moyer BA, Sessler JL, Delmau LH (2008) *J Am Chem Soc* 130:4129

16. Fowler CJ, Haverlock TJ, Moyer BA, Shriver JA, Gross DE, Marquez M, Sessler JL, Hossain MA, Bowman-James K (2008) *J Am Chem Soc* 130:14386
17. Nicolau KC, Sorensen EJ (1996) *Classics in total synthesis*. Wiley-VCH Weinheim, Germany
18. Sharpless KB, Finn MG, Kolb HC (2001) *Angew Chem Int Ed* 40:2004
19. Schmidtchen FP (2006) *Coord Chem Rev* 250:2918
20. Luecke H, Quiocho FA (1990) *Nature* 347:402
21. Hofmeister F (1888) *Arch Exp Pathol Pharmacol* 24:247
22. Taylor R, Kennard O (1982) *J Am Chem Soc* 104:5063
23. Desiraju GR, Steiner T (1999) *The weak hydrogen bond*. Oxford University Press Inc, New York
24. Steiner T (1998) *Acta Crystallogr B* 54:456
25. Farnham WB, Roe DC, Dixon DA, Calabrese JC, Harlow RL (1990) *J Am Chem Soc* 112:7007
26. Davis AP, Gilmer JF, Perry JJ (1996) *Angew Chem Int Ed Engl* 35:1312
27. Kwon JY, Jang YJ, Kim SK, Lee K-H, Kim JS, Yoon J (2004) *J Org Chem* 69:5155
28. Ilioudis CA, Tocher DA, Steed JW (2004) *J Am Chem Soc* 126:12395
29. Abouderbala LO, Belcher WJ, Boutelle MG, Cragg PJ, Dhaliwal J, Fabre M, Steed JW, Turner DR, Wallace KJ (2002) *Chem Comm* 4:358
30. Wallace KJ, Belcher WJ, Turner DR, Syed KF, Steed JW (2003) *J Am Chem Soc* 125:9699
31. Chmielewski MJ, Charon M, Jurczak J (2004) *Org Lett* 6:3501
32. Bryantsev VS, Hay BP (2005) *J Am Chem Soc* 127:8282
33. Bryantsev VS, Hay B (2005) *Org Lett* 7:5031
34. Yoon D-W, Gross DE, Lynch VM, Sessler JL, Hay BP, Lee C-H (2008) *Angew Chem Int Ed Engl* 47:5038
35. Pedzisa L, Hay BP (2009) *J Org Chem* 74:2554
36. Lee C-H, Na H-K, Yoon D-W, Won D-H, Cho W-S, Lynch VM, Shevchuk SV, Sessler JL (2003) *J Am Chem Soc* 125:7301
37. Nishiyabu R, Palacios MA, Dehaen W, Anzenbacher P Jr (2006) *J Am Chem Soc* 128:11496
38. Bruno G, Cafeo G, Kohnke FH, Nicolo F (2007) *Tetrahedron* 63:10003
39. Ghosh S, Choudhury AR, Row Tayur NG, Maitra U (2005) *Org Lett* 7:1441
40. Maeda H, Kusunose Y (2005) *Chem Eur J* 11:5661
41. Fujimoto C, Kusunose Y, Maeda H (2006) *J Org Chem* 71:2389
42. Maeda H (2007) *Eur J Org Chem*:5313
43. Zhu SS, Staats H, Brandhorst K, Grunenberg J, Gruppit F, Dalcanale E, Luetzen A, Rissanen K, Schalley CA (2008) *Angew Chem Int Ed* 47:788
44. Berryman OB, Sather AC, Hay BP, Meisner JS, Johnson DW (2008) *J Am Chem Soc* 130:10895
45. Huisgen R, Szeimies G, Mobius L (1967) *Chem Ber* 100:2484
46. Huisgen R (1989) *Pure Appl Chem* 61:613
47. Rostovtsev VV, Green LG, Fokin VV, Sharpless KB (2002) *Angew Chem Int Ed* 41:2596
48. Tornøe CW, Christensen C, Meldal M (2002) *J Org Chem* 67:3057
49. Scriven EFV, Turnbull K (1988) *Chem Rev* 88:297
50. Meldal M, Tornøe CW (2008) *Chem Rev* 108:2952
51. Rodionov VO, Fokin VV, Finn MG (2005) *Angew Chem Int Ed* 44:2210
52. Rodionov VO, Presolski SI, Diaz DD, Fokin VV, Finn MG (2007) *J Am Chem Soc* 129:12705
53. Boren BC, Narayan S, Rasmussen LK, Zhang L, Zhao H, Lin Z, Jia G, Fokin VV (2008) *J Am Chem Soc* 130:8923
54. Golas PL, Tsarevsky NV, Sumerlin BS, Matyjaszewski K (2006) *Macromolecules* 39:6451
55. Baskin JM, Prescher JA, Laughlin ST, Agard NJ, Chang PV, Mille IA, Lo A, Codellia JA, Bertozzi CR (2007) *Proc Nat Acad Sci USA* 43:16793
56. Becer CR, Hoogenboom R, Schuber US (2009) *Angew Chem Int Ed* 48:4900
57. Oh K, Guan Z (2006) *Chem Commun*:3069
58. Patterson AW, Wood WJL, Hornsby M, Lesley S, Spraggon G, Elman JA (2006) *J Med Chem* 49:6298

59. Adam GC, Vanderwal CD, Sorensen EJ, Cravatt BF (2003) *Angew Chem Int Ed* 42:5480
60. Li Y, Huffman JC, Flood AH (2007) *Chem Commun*:2692
61. Muedtner RM, Ostermeier M, Goddard R, Limberg C, Hecht S (2007) *Chem Eur J* 13:9834
62. Aucagne V, Berná J, Crowley JD, Goldup SM, Hänni KD, Leigh DA, Lusby PJ, Ronaldson VE, Slawin AMZ, Viterisi A, Walker DB (2007) *J Am Chem Soc* 129:11950
63. Goldup SM, Leigh DA, Long T, McGonigal PR, Symes MD, Wu J (2009) *J Am Chem Soc* 131:15924
64. Palmer MH, Findlay RH, Gaskell AJ (1974) *J Chem Soc Perkin Trans* 2:420
65. Schuster O, Yang L, Raubenheimer HG, Albrecht M (2009) *Chem Rev* 109:3445
66. Moore JS (1997) *Acc Chem Res* 30:402
67. Li Y, Flood AH (2008) *Angew Chem Int Ed* 47:2649
68. Li Y, Flood AH (2008) *J Am Chem Soc* 130:12111
69. Nielsen KA, Cho WS, Lyskawa J, Levillain E, Lynch VM, Sessler JL, Jeppesen JO (2006) *J Am Chem Soc* 128:2444
70. Chang KJ, Moon D, Lah MS, Jeong KS (2005) *Angew Chem Int Ed* 44:7926
71. Bandyopadhyay I, Raghavachari K, Flood AH (2009) *Chemphyschem* 10:2535
72. Boer FP, Neuman MA, Van Remoortere FP, Steiner EC (1974) *Inorg Chem* 40:2936
73. Choi K, Hamilton AD (2001) *J Am Chem Soc* 123:2456
74. Kubik S, Goddard R, Kirchner R, Nolting D, Seidel J (2001) *Angew Chem Int Ed* 40:2648
75. Li Y, Pink M, Karty JA, Flood AH (2008) *J Am Chem Soc* 130:17293
76. Juwarker H, Lenhardt JM, Pham DM, Craig SL (2008) *Angew Chem Int Ed* 47:3740
77. Juwarker H, Lenhardt JM, Castillo JC, Zhao E, Krishnamurthy S, Jamiolkowski RM, Kim K-H, Craig SL (2009) *J Org Chem* 74:8924–8934
78. Hecht S, Meudtner RM (2008) *Angew Chem Int Ed* 47:4926
79. Fisher MG, Gale PA, Hiscock JR, Hursthouse MB, Light ME, Schmidtchen FP, Tong CC (2009) *Chem Commun*:3017
80. Romero T, Caballero A, Tarraga A, Molina P (2009) *Org Lett* 11:3466
81. Schalley CA, Vögtle F, Dötz KH (2005) *Templates in chemistry I*. Springer, New York
82. Kumar A, Pandey PS (2008) *Org Lett* 10:165
83. Coutrot F, Busseron E (2008) *Chem Eur J* 14:4784
84. Braunschweig AB, Ronconi CM, Han JY, Arico F, Cantrill SJ, Stoddart JF, Khan SI, White AJP, Williams DJ (2006) *Eur J Org Chem*:1857
85. Loeb SJ (2007) *Chem Soc Rev* 36:226
86. Coutrot F, Romuald C, Busseron E (2008) *Org Lett* 10:3741
87. Mullen KM, Mercurio J, Serpell CJ, Beer PD (2009) *Angew Chem Int Ed* 48:4781

Index

A

Amidopyrroles, ferrocene-appended, 259
Amine–ammonium, 360
Amino acids, 16
Aminoanthracenes, 238
Anion binding, 145
Anion complexation, 1, 45, 75, 96, 341
Anion exchange, 167
 resin (AER), 277
Anion receptors, 45, 192
 acyclic, planar geometries, 129
 amidopyrrole-based, 106, 111
 aryl-substituted, 133
 conjugated, 26
 guanidinocarbonylpyrrole-based, 106
 modified polymers, 4
 neutral, 20
 polymer additives, 4
 pyridinium-based, 323
 tripodal platform, 291
Anion recognition, 4, 177
Anion responsive heterocycles, side-chain
 polymers, 14
Anion sensors, pyrrole-based
 electrochemical, 257
Anion stabilization, 345
Anticancer activity, 167
Antiport, 162, 167
Apoptosis, prodiginines, 164
ATPases, 160
Aza-crown ether, 6
Azaethers, cyclic, 5

B

Benziporphomethenes, 92
Benzo-15-crown[5]ether, 24
Benzoate receptors, 252
Bicarbonate anion, transmembrane
 transport, 171
Biindole foldamers, 254
1,4-Bis(3-indolyl)–2,3-diaza-
 1,3-butadiene, 200
Bis(imidazolium) calixarenes, 288
Bis(imidazolium)–cyclophane, 284
Bisamidopyrrole, 113
Bis-betaines, 283
Biscobaltocenium, 307
Bispyrenopyrrole, 118
Bispyrroles, aryl-bridged, 119, 126
Blood plasma protein carboxylates, 10
Boronate anion receptor, 18
Boronate pinacol ester, 18
BPN 246
Bromopyrogallol Red, 329

C

Caesium bromide, 64
Calix[4]pyrrole-ferrocene sensors, 259
Calix[4]pyrrole-*co*-methylmethacrylate, 22
Calix[4]pyrrole[2]thiophene, 21
Calixarenes, 41, 288
Calixphyrins, *N*-confused, 89
 synthesis from acyclic (oligo)pyrrole
 building blocks, 80

synthesis from porphyrins, 77
Calixpyrrole-metalloporphyrin, 62
Calixpyrroles, 9, 21, 39, 215
Carbazoles, 33, 177, 186, 202
 sensors, 200
Carboxyfluorescein, 257
Carboxylate anions, 10
Catalysis, 68
Charged frameworks, 267
Chemosensors, 10, 267
Chlorides, 19, 64
Chloride-templated catenane, 336
Chromophores, 75
Citrate, 256
Click chemistry, 341, 350
Clickamers, 359
Cobaltocenium hexafluorophosphate anion
 receptors, 307
Colorimetric displacement assays, 223
Colorimetric sensors, 208, 229
Cryptand receptors, 319
CuAAC (copper-catalyzed azide alkyne
 cycloaddition), 351
Cyanides, 3, 54
Cyclobis(paraquat-*p*-phenylene), 19
Cyclohexapyrroles, 95
Cyclophanes, 283
Cycloprodiginosin, 148

D

Danishesky's diene, 69
Dialysis membranes, anion-specific, 3
2,5-Diamidopyrrole sensors, 229
1,4-Diaryl-1,2,3-triazole, 353
4,4'-Dicarboxamidoindole-
 2,2'-bipyridine, 232
Dichlorocalix[2]pyrrole[2]pyridine, 9
2,3-Diindol-3-yl quinoxalines (DIPs), 200
Diindolylquinoxaline (DIQ), 21
Diisopinocampheylborane, 18
Dimethylsulfonazo III 329
Dipalmitoyl-phosphatidylcholine
 (DPPC), 168
4,7-Diphenyl-1,10-phenanthroline, 7
N,N-Diphenylpyridine-2,6-
 dicarboxamide, 304
Dipyrins, 115
Dipyrrolyldiketones, boron complexes, 129

Dipyrrolylpropanedione, 246
Dipyrrolylquinoxalines (DPQ), 12, 119,
 223, 237
Dipyrromethanedicarbinols, 86
Dipyrromethanes, 86, 116
Dithiacalixpyrins, 93
Dithiaphlorin, 211
DNA, prodiginines, 147, 158

E

Electrochemistry, 205, 237
1-Ethyl-3-methylimidazolium (EMIM), 46
Ethylenedioxythiophenes (EDOTs), 29
Extraction, 64

F

Ferrocene-viologen, 19
Fluorescein, 239
Fluorescence, 205, 237
 sensors, 238
Fluorides, 3, 25, 208, 309

G

Guanidinium/pyridinium molecular
 switch 336
Guanidinocarbonylpyridine, 308
Guanidinocarbonylpyrrole, 106, 256
GX15-070 148

H

HCl transport, prodiginines, 163
Heteroaromatic systems, 267
Heterophanes, 283
Hexaalkylcalix[4]pyrins, 81
Hofmeister bias, 6
Huisgen 1,3-dipolar cycloaddition, 350
Hydrogen bonds/bonding, 11, 39, 177,
 267, 341
 donors, 345
3-Hydroxybenzoic acid, 49
Hyperphosphatemia, 3

I

Imidazoliophanes, 286
Imidazolium, 17, 267

functionality, 278
quaternary salts, 271
Imidazolium(pyridinium) azolate
betaines, 283
1,3-Indanedione-calixpyrrole, 219
Indole–amide hybrids, 180
Indole–urea hybrids, 183
Indoles, 177, 179
sensors, 198
Indolocarbazoles, 177, 187, 230, 252
Interpenetrated/interlocked receptors, 330
Intramolecular partial charge-transfer
(IPCT), 207, 238
Ion channels, 168
Ion-pair complexation, 45
Ion-pair receptor, 193
Ion-selective electrodes, 5, 237, 258
triazolophane-based, 363
Isophthalate, 50
Isoporphyrin, 77

L
Lipid membranes, 167
Liposomes, 168
Lissamine-rhodamine B 239
Lithocholate ester, 87
Lucigenin, 168
Luminescence, 205, 237

M
Macrobicyclic receptors, 319, 328
Macrocycles, 177, 191
receptors, 326
Membrane transport, 145
Membranes, polyvinyl chloride (PVC), 5
Metacycloheptylprodigiosin, 148
Metacycloprodigiosin, 161
4-Methoxy-2,2'-bipyrrole-5-carbaldehyde
(MBC), 149
5-Methyl-5-(4-nitrophenyl)
dipyrromethane, 48
Methyleneimidazolium azolate betaine, 283
Methyltributylammonium (MTBA)
chloride, 47
Molecular clefts, 177, 180
Molecular sensors, 1, 177, 198
Molecular wire effect, 15

N

Nanostructures, 267
Naphthalimide, 17
Naphthol Yellow S 329
Natural rubber, 2
Neoprene, 2
Nitrate, 3, 172
Nitrate-binding protein, NrtA 179
Nonylprodigiosin, 148
Nylon, 2

O

Obatoclax mesylate, 148
Octaalkylporphyrinogens, 41
Octaethylporphyrin (OEP), 77
Octamethylcalix[4]pyrrole, 9, 23, 215
Oligoindoles, 195
Oligoindolocarbazoles, 196
Oligomers, 177
acyclic, 193
Open-chain systems, 103
Orange G 329
Oxadiazoles, 30
Oxoporphyrinogens, 80
Oxyindolpyrrolin, 250

P

1-Palmitoyl-2-oleoyl-*sn*-glycero-3-
phosphocholine (POPC), 170
Phanes, 283
Phenylene, CH hydrogen-bond donor, 354
Phlorin, 77
Phlorin–dipyrin, 87
Phosphates, 3, 19, 330
Phosphate-selective electrodes, 5, 13
Phospholipid membranes, 167
Pincers, 293
PNU-156804 148
Poly[*ortho*-diaminophenylene-fluorene]-
co-(quinoxaline-fluorene)] 27
Poly[2-(2'-hydroxyphenyl)benzoxazole] 32
Polyamines, cyclic, 6
Polymers, 1
Polyoxymethylene, 2
Polyphenylacetylenes, 15
Polystyrene, 2
Polythiophene, 15

Polyvinyl chloride (PVC) membranes, 5
Porphotetramethenes, 79
Porphyrinogens, 80, 209
Prodiginine–metal complexes, X-ray structures, 158
Prodiginines, 145, 146
 apoptosis, 164
 pH 161
 synthetic, 167
Prodigiosin, 118, 145
Programmed cell death, 164
Proton transport, 159
Pseudoalteromonas denitrificans 164
Pseudorotaxane, 190, 331
Pyridine, 301
Pyridine-2,6-dicarboxamide, 310
Pyridinium, 301
Pyridinium-3,5-bisamide, 330
Pyrophosphate, 30
Pyrophosphosphate, 257
Pyrroles, 39, 75, 103
Pyrrolylcalix[4]pyrrolin, 89

R

Receptors, 39, 75, 301
 acyclic, 303, 323
 design, 341, 344
Renal failure, 3
Resorcinarenes, 290
Room-temperature ionic liquids (RTILs), 268
Rubyrin, 8

S

Saccharide receptor/sensor, 246
Salmonella typhimurium 179
Sandwich complexes, positive cooperativity, 355
Sapphyrins, 7, 212, 270
Serratia marcescens 145

Solvation, 345
Spirocalixpyrins, 84
Steroidal based receptors, 361
Strapped systems, 54
Sulfate, 168, 330, 337
Sulfate-binding protein (SBP), 179
Supramolecular chemistry/assemblies, 3, 103, 341
Synechocystis sp. PCC 6803 179

T

Tambjamines, 149, 163
Template synthesis, 267
Terpyridine, 7
Terpyridine-guanidincarbonylpyrrole, 111
Tetrabutylammonium fluoride (TBAF), 17
Tetrachlorocalix[4]pyridine, 9
Tetrakis(imidazolium) cyclophanes, 287
TetraSpirocyclohexylcalix[4]pyrrole, 40
Tetrathiafulvalene (TTF), 262
Thiacalixpyrins, 93
Thiaphlorin, 98
Thiourea anion receptors, 306
Transmembrane transport, 161, 171
Transport, 64
Tri(decyl)amine, 7
1,2,3-Triazole, 350
 foldamers, 358
Triazolium, 360
Triazolophanes, 350, 352
Triindolylmethane, 190
Triphenylrosarin, 8
Tripyrrane, 87
Tripyrrole, 145

U

Undecylprodigiosin, 148

V

V-ATPase, 159, 164